Stability of Dams Constructed on Problematic Substrates

A thesis submitted in partial fulfilment of the requirements for the degree of Doctor of Philosophy (PhD) to:

Civil Engineering
School of Engineering and Design
Brunel University
United Kingdom

by:

Nihad Bahaaldeen Salih
BSc, MSc

Supervised by:

Dr. Philip Collins

Dr. Stephen Kershaw

March 2013

To: Hazha and Ari

ABSTRACT

Dissolution of soluble substrates such as gypsum presents a major hazard to dams in many parts of the world. This research simulates hypothesised conditions beneath the Mosul Dam, northwest Iraq, where collapse of a karstic system associated with continuous fresh water supply from its massive reservoir water is a recognised problem. The gypsum substrates at Mosul Dam vary in purity and thickness. Experimental work used gypsum rocks and gypseous soils. Gypsum rocks from northern Iraq and similar rocks from Bantycock gypsum mine, UK, were analysed for short-term mechanical response following immersion (5 to 50 weeks) and long-term loading during immersion (maximum 50 weeks). New experimental devices were developed from a conventional oedometer. Cylinder samples (NX, standard diamond drill core size = 54mm diameter, length/diameter ratio equal to 2.5) provided a proxy for massive gypsum strata, while thin samples (NX = 54mm in diameter, 20mm thickness) represented thin layers and lenses. Rectangular bar samples (240 x 40 x 20 mm and 140 x 40 x 20 mm) were tested for short-and long-term mechanical four-point bending behaviour. Samples were permanently submerged at a variety of water pressures, with the influence of groundwater recharge and flow on dissolution simulated by regular changes of water. Stress on each sample was progressively increased to a maximum of 2688 kPa. Small increases in strain were recorded by the end of each test but no failures occurred within 60 days of tests. However, notable failure due to water pressure and axial stress over long time periods of 166 and 238 days occurred. Visible physical changes were observed, notably a decrease in sample mass and volume. Similar change was recorded in ultrasonic velocities. These indicate that gypsum collapse risk beneath dams requires prolonged exposure to dissolution. Gypseous soils from Iraq and similar artificially-prepared soils were also tested. Gypseous soil samples (diameter = 50mm and length = 20mm) and box model strata results showed that gypseous soils are significantly weakened by dissolution over 15 weeks and 50 weeks respectively. Dams built on gypsum substrates are likely to experience ongoing weakening of their foundations, with a progressively increasing risk of failure. This is expected to be enhanced for dams with a large and deep reservoir that induces high ground water pressure.

List of Contents

ACKNOWLEDGMENTS

I feel the need to express my gratitude to all those who contributed directly or indirectly to this thesis and gave me the possibility to complete it.

First of all, I thank my 1st supervisor **Dr Philip Collins** for generous giving of time and guidance whenever needed. Thanks Dr Philip for all those hours in the field, in the labs or in your office, giving me always your valuable advice! You were a wonderful teacher for me all those years in Brunel University. Thank you also for giving immediate feedback on my writing, immediate replies on my uncounted emails and lovely face for my uncounted visits for your office, I feel very lucky that you were my supervisor.

I wish to thank also my 2nd supervisor **Dr Stephen Kershaw**, for his generous giving of time and guidance whenever needed. Thanks Dr Stephen for all those hours in the field, in the labs or in your office and many thanks for your permission to use your lab of geology. Since this thesis would not be the same without your valuable conversations about the research and feedback on my writing.

I would like to express my sincere appreciation to **Ministry of Higher Education and Scientific Research, Scholarship & Cultural Relations Directorate** in Iraq to give me the opportunity to study my PhD in the UK, and also for their help and financially support me to travel to Iraq and bring samples of gypsum rocks and gypseous soils to Brunel University/UK.

Special thanks to the **Cultural Attaché staff/Embassy of Iraq** in London for their significant help for Iraqi students in general and in special, many thanks for their role to get the permissions for my travelling to Iraq, field work in Iraq and samples transportation to Brunel University/UK.

Special thanks to **Bantycock Mine group**, for the great opportunity they offered me to get many large gypsum rock block samples. They really helped me in samples selection and useful information on the gypsum of this mine.

I wish to thank also **Prof John Bull**, Head of Civil Engineering at Brunel University for his great advices on some parts of my research. Thank you Prof John for all that time we spent together and discussed in details on rock bending tests in your office. You were a great teacher and collaborator.

I wish to thank **Prof Mizi Fan**, Head of Research in Civil Engineering at Brunel University for his great help, advices and support. Thank you Prof Mizi for all that time we spent together

and discussed in details on rock bending tests and on gypsum rocks in your office. You were a great teacher and collaborator.

Furthermore I wish to thank **Dr Abdul J. Chaudhary** in Institute for the Environment at Brunel University. Thank you Dr Chaudhary for all that time we spent together in your office and discussed in details on the chemical properties of gypsum salt.

I wish to deeply thank also the great **technician Malcolm Austen** who is one of technicians of Civil Engineering at Brunel University, thanks for being always ready to help in the Civil Engineering labs at Brunel University, thanks for his help to come with me to Imperial College and K4 soil laboratory, thank you Malcolm for your collaboration to achieve my research goals.

I wish to thank also the great **technician Paul Chapman** from Brunel University workshops for being always ready to listen and help in the preparation of developed devices. Thank you Paul for your collaboration to achieve my research developed devices.

Special thanks to President of the University of Sulaimani in Iraq **Ass. Prof Dr Salahalddin Saeed Ali** for his generous giving of time and guidance whenever needed. Thanks Dr Salah for all those hours in your office at college of science/University of Sulaimani in Iraq, talking by telephone, giving me always your valuable advice! You were a wonderful teacher, a great colleague and the best old brother for me.

Furthermore I wish to thank **Prof Namir Al-Saoudi** from the building and construction engineering department at University of Technology in Baghdad/Iraq, my MSc supervisor, who made me love geotechnical engineering! Dr Namir, you have a unique way to share your knowledge and enthusiasm about soil mechanics! Thank you for being always happy to reply my calls and give me voluble advices! Your help is highly appreciated my teacher!

I would also like to thanks **College of Engineering staff at University of Sulaimani** in Iraq for their help; they gave me the permission to international transportation company to transfer my collected gypsum rock and gypseous soils from Iraq.

Last but not least, I thank my great wife **Hazha** whose patience, understanding, love, and support enabled me to complete this project. Thanks my love for everything, really you are great and I will never forget your support. I would like to thank my father, mother, brothers and sisters for their constant loving and supporting during all this time. Great thanks also for my wife family members especially her father and mother for their always being ready to help me, support me and finish all my study requirements in Iraq. To members of both families thank you for your patience and encouragement! I owe you a great debt of gratitude and kindness.

LIST OF SYMBOLS/ABBREVIATIONS

Angle of internal friction (degree) ..... *Φ*

Angle of internal friction-consolidated un-drained direct shear test..... *Φ-CU*

Angle of internal friction-unconsolidated un-drained direct shear test ..... *Φ-UU*

Artificially-prepared gypseous soil..... *AGS*

Aust Cliff gypsum ..... *ACG*

Axial deflection (mm)..... *AD*

Axial modulus (GPa)..... *AM*

Bulk modulus (GPa)..... *BM*

California Bearing Ratio ..... *CBR*

Coarse sand-coarse gypsum-artificial gypseous soil..... *CS-CG-AGS*

Coarse sand-(fine, medium and coarse gypsum)-artificial

Gypseous soil..... *CS-FMCG-AGS*

Coefficient of Gradation ..... C_g

Coefficient of uniformity..... C_u

Cohesion (kN/m^2)..... *C*

Cohesion-consolidated un-drained direct shear test (kN/m2)..... *C-CU*

Cohesion-unconsolidated un-drained direct shear test (kN/m2)..... *C-UU*

Collapse potential (%) ..... C_p

Compression index..... C_c

Compressive strength (MPa) ..... $б_c$

Consolidated un-drained direct shear test ..... *CU-D*

Cylinder-Iraqi gypsum ..... *Cyl-IG*

Cylinder-pink/Bantycock gypsum ..... *Cyl-PBG*

Cylinder-white/Bantycock gypsum ..... *Cyl-WBG*

Dry density (gm/cm^3)..... *DD*

Elastic modulus reduction (Ultrasonic) (%)..... *MR(U)*

Elastic modulus (Ultrasonic) (GPa)..... *EMU*

Expansion index or rebound index ..... C_r

Fine sand-fine gypsum-artificial gypseous soil ..... *FS-FG-AGS*

Fine sand-(fine, medium and coarse gypsum)-artificial

Gypseous soil ..... *FS-FMCG-AGS*

Flexural stress at failure (MPa) ..... $Fб_c$

Food and agriculture organization ..... *FAO*

Gypsum content ..... *GC*

Horizontal deflection (mm) ..... *HD*

Initial void ratio ..... e_o

Iraqi gypsum ..... *IG*

Large four-point bending sample ..... *LFB*

Load at failure (Newton) ..... *LF*

Mass (gm) ..... *wt*

Maximum ..... *Max*

Maximum axial deflection (mm) ..... *MAD*

Maximum depth reduction (%) ..... *MDeR*

Maximum dissolution (US/cm) ..... *MD*

Maximum length reduction (%) ..... *MLR*

Maximum mass reduction (%) ..... *MWtR*

Maximum volume reduction (%) ..... *MVR*

Maximum width reduction (%) ..... *MWR*

Medium sand-(fine, medium and coarse gypsum)-artificial

Gypseous soil ..... *MS-FMCG-AGS*

Medium sand-medium gypsum-artificial gypseous soil ..... *MS-MG-AGS*

Minimum ..... *Min*

Moisture content (%) ..... *MC*

Particle size distribution ..... *PSD*

Particle size for which 10% of the soil sample by weight is finer ..... D_{10}

Particle size for which 30% of the soil sample by weight is finer ..... D_{30}

Particle size for which 60% of the soil sample by weight is finer ..... D_{60}

Path length reduction (Ultrasonic) (%) ..... *PLR (U)*

Pink Bantycock gypsum ..... *PBG*

Pink Bantycock gypsum/Thin layer ..... *PBG/ThL*

Real gypseous soil ..... *RGS*

Resilient Modulus ..... M_R

Scanning Electronic Microscope ..... *SEM*

Shear modulus (GPa) ..... *SM*

Small four-point bending sample ..... *SFB*

Small four-point bending sample-Aust Cliff gypsum ..... *SFB-ACG*

Small four-point bending sample-Iraqi gypsum ..... *SFB-IG*

Small four-point bending sample-pink/Bantycock gypsum ..... *SFB-PBG*

Small four-point bending sample-white/Bantycock gypsum ..... *SFB-WBG*

Small four-point bending sample-white & clay/Bantycock gypsum ..... *SFB-WCBG*

Small four-point bending sample-white & cracks/Bantycock gypsum ..... *SFB-WCrBG*

Small four-point bending sample-white & marl/Bantycock gypsum ..... *SFB-WMBG*

Specific gravity ..... G_s

Standard deviation ..... *SD*

The measure of the strength acid; the measure of the concentration Of hydrogen ions ..... pH

Thin layer-pink/Bantycock gypsum ..... *ThL-PBG*

Thin layer-white & clay/Bantycock gypsum ..... *ThL-WCBG*

Time to failure (second) ..... *TF*

Total dissolved solids ..... *T.D.S*

Transit time reduction (Ultrasonic) (%) ..... *TTR (U)*

Unconsolidated un-drained ..... *UU*

Unconsolidated un-drained direct shear test ..... *UU-D*

Uniaxial compressive strength (MPa) ..... *UCS*

Universal Transverse Mercator (graphical coordinate system, horizontal position representation) ..... *UTM*

Velocity reduction (Ultrasonic) (m/sec) ..... *VR (U)*

Velocity (Ultrasonic) (m/sec) ..... *VU*

Volume (cm^3) ..... *vol*

Wet density (gm/cm^3) ..... *WD*

White Bantycock gypsum ..... *WBG*

White with clay Bantycock gypsum ..... *WBG-C*

White with marl Bantycock gypsum ..... *WBG-M*

X-ray diffraction ..... *XRD*

54 mm diamond bit, use for rocks coring ..... *NX*

CHAPTER ONE: INTRODUCTION

1.1 Background to this study

Soluble rocks underlie more than 20 percent of the earth surface (Dreybrodt et al., 2002) with seven million km^2 underlain by highly soluble gypsum bearing rocks (Maksimovich and Sergeev, 1984). Building dams and reservoirs on soluble rocks can lead to significant problems for the stability of the dams (Maximovich and Meshcheryakova, 2009). Iraq (Figures 1.1 and 1.2) has a large amount of gypsum rocks in addition to gypseous soils, both of which are significant for stability of dams. Iraqi gypsum rock (see Figures 1.3 and 1.4), which occurs with the Mid-Miocene Fatha (Lower Fars) Formation (Jassim and Goff, 2006) (see Figure 1.1) is associated with significant geotechnical problems, most notably at the Mosul Dam, which is severely affected by dissolution and karstification in the bedrock and soils beneath the dam.

Narrow fissures and fractures in gypsum can be enlarged by chemical dissolution. This is particularly the case in sites with high hydraulic gradients such as near dams (Romanov et al., 2003). Cavities (Maximovich and Meshcheryakova, 2009) in dams' foundations can lead to general failure within the gypsum rock body, in turn weakening the dams' foundations as well as inducing subsidence and creating sinkholes in the surrounding areas.

Although some studies have investigated the geotechnical properties of gypsum substrates, little published work on the process of dissolution induced collapse. This project focuses on the Mosul Dam case, which is built on problematic bedrock foundations; the reservoir formed behind the dam adds to the problems (see Figure 1.5). The Mosul Dam area has abundant gypsum substrates with lots of problematic aspects for dam stability, known to engineers for some time. However, there is no systematic study of the detail required to address the issues of dam stability on such substrates, therefore the present research ideas were developed. This thesis investigates gypsum rock and gypseous soil behaviour when exposed to measured loads and measured percolating fresh water over short and long time periods in experimental laboratory apparatus. The context for the research is therefore provided principally by the Mosul Dam, Iraq, which has experienced severe problems associated with gypsum dissolution since its construction in 1980.

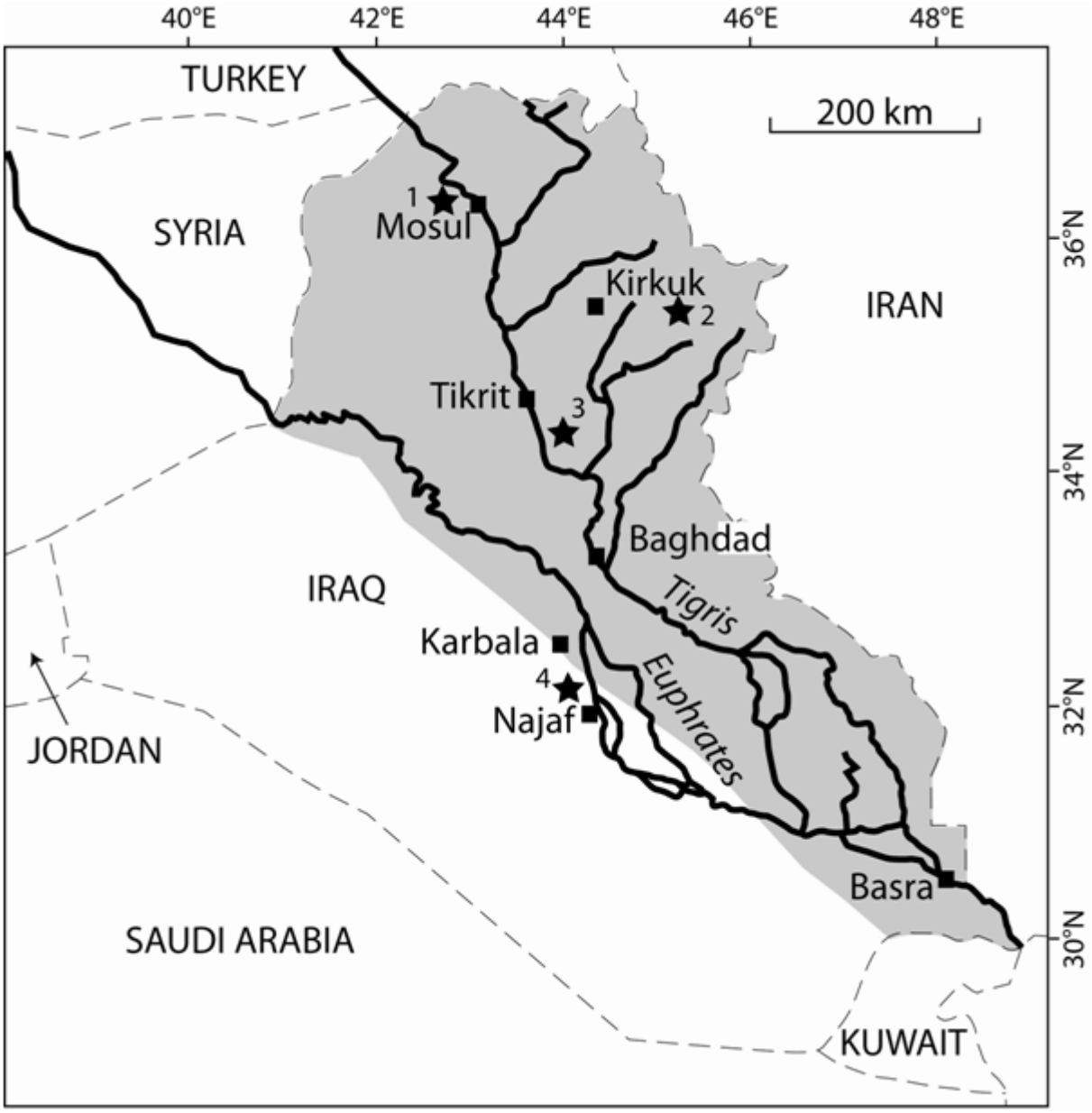

Fig. 1.1: Map of Iraq showing major rivers and settlements. Sampling sites: 1. Badosh; 2. Bazyan; 3. Doz; 4. Tar Al-Najaf. Shaded area indicates the distribution of the Fatha (Lower Fars) Formation in Iraq (modified from Jassim and Goff (2006)).

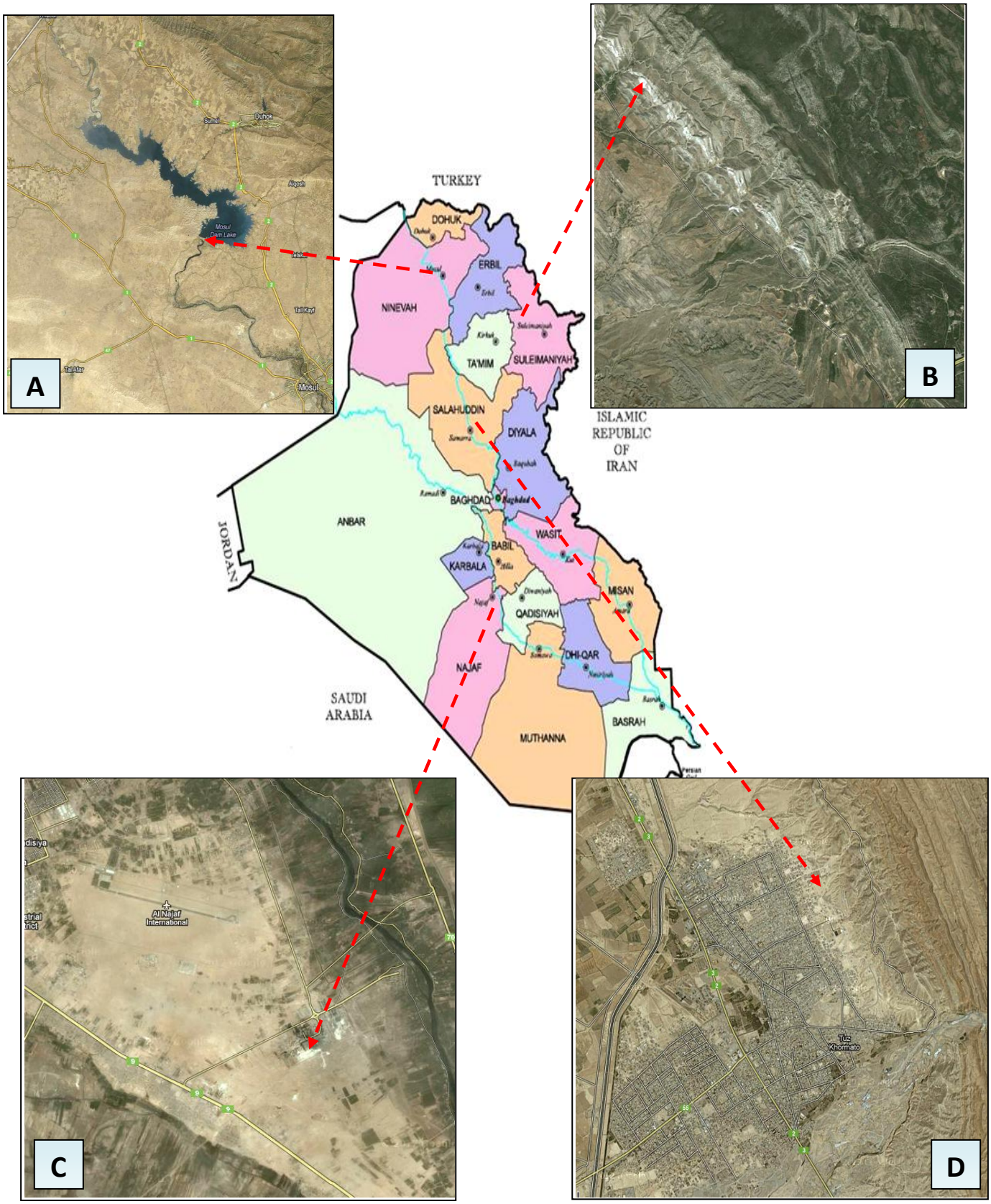

Fig. 1.2: Iraqi samples localities used in this thesis. Iraqi map downloaded from (http://2.bp.blogspot.com/-2kryz1WcG5I/TnSWv5IPwyI/AAAAAAAAA80/Sq3x8o0Tc-g/s1600/iraq_map-political-regional.jpg). A is Badosh sample area (gypseous soil) close to Mosul dam area, B is Bazyan sample area (gypsum rock), C is Tar Al-Najaf sample area (gypseous soil) and D is Doz sample area (gypsum rock and gypseous soil). A, B, C and D photos taken from: www.google.co.uk page, URL: http://maps.google.co.uk/maps?hl=en&tab=wl, accessed at 05-10-2012.

Fig. 1.3: Gypsum layers inter-bedded with soil materials, northern Iraq (Bazyan area in Sulaimani Governorate).

Fig. 1.4: Massive gypsum layer, northern of Iraq (Bazyan area in Sulaimani Governorate, is in part B of Figure 1.2).

1.2 Aim and Objectives of this study

Overall purpose of this thesis:

A. **To understand stability issues of dams built on gypsum-rich substrates in the Mosul area of northern Iraq & other areas.**
B. **To develop new methods to assess impact of dissolution on mechanical properties of gypsum substrates.**
C. **To consider the extent to which the findings presented in this thesis can be applied to other areas.**

1.3 Area of study

Gypsum rock ($CaSO_4.2H_2O$) is a common natural material (see Table 1.1). This project uses the context of Iraqi sites with gypsum rock and gypseous soils. For practical and security reasons, it was not possible to collect large sample volumes. Instead, representative samples were collected from sites in Iraq (Figure 1.2/B). The rock samples were found to be similar to gypsum from the Triassic Period, more than 200 million years old, at Aust Cliff, southern England and, particularly, Bantycock Mine, central England (Figures 1.6 to 1.10) and samples from these sites were used as proxies to simulate conditions in substrates of

Mosul Dam; note that during the time when the English material was deposited, the palaeolatitude and climate of the UK was similar to that of the Middle East at the present day. No gypseous soils similar to those in Iraq are present in the UK because of the present climatic differences but an artificial soil with characteristics similar to Tar Al-Najaf (Figure 1.2/C) was created. Gypseous soil is present in: A) African countries of Somalia, Algeria, Namibia, Libya, Mali, Tunisia, Ethiopia, Morocco, Sudan, Mauritania, Egypt; B) Middle Eastern countries of Iraq, Syria, Yemen, Oman, Kuwait, India, Saudi Arabia, Jordan, Pakistan and Iran; C) Asian countries of India, Pakistan, China and Mongolia; D) countries of the former USSR; E) European countries of Spain and Turkey; F) Southwest USA and parts of central America (FAO, 1990).

Table 1.1: Examples with localities of gypsum rock.

Country	Formation & Place	Author
Italy	Gessos Solfifera Formation	Bonetto et al. (2008)
Mexico	Nacia Mine in Chihuahua	Garcia-Guinea et al. (2002)
Canada	Bow River Forest of the Rocky Mountain Forest/Alberta	Halferdahl (1965)
Egypt	Sinai Peninsula, western and eastern desert	Mancino (2008)
Jordan	Azraq Formation, Lisan region, and Area between Tafila city and Mujib	
Kuwait, Iran, Qatar, Syria and United Arab Emirates	Not given	
USA	Lykins Formation along Colorado front range of the Southern Rocky Mountains	Person and Hurcomb (2002)
Cyprus	Nisou-Pero, Tochni, Aradippou, Maroni, Kalavasos, Pergamos and Mouttagiaka areas	Hadjicharalambous and Michaelides (2007)
Iraq	Fatha Formation-North Eastern part Surdash and Koya basin Kirkuk basin, Jazira Basin, Buzurgan, Abo Ghirab, Nahr Umr, Dujaila Area, Mosul, Euphrates Valley, Hit, South of Ramadi, Tar Al Najaf and Sinjar basin	Ameen and Karim (2007) Stevanovic and Markovic (2003) Jassim and Goff (2006)
UK (see figures 1.6 to 1.10)	Aust Cliff Bantycock Mine	Field visits by the author on November 2009 and April 2010

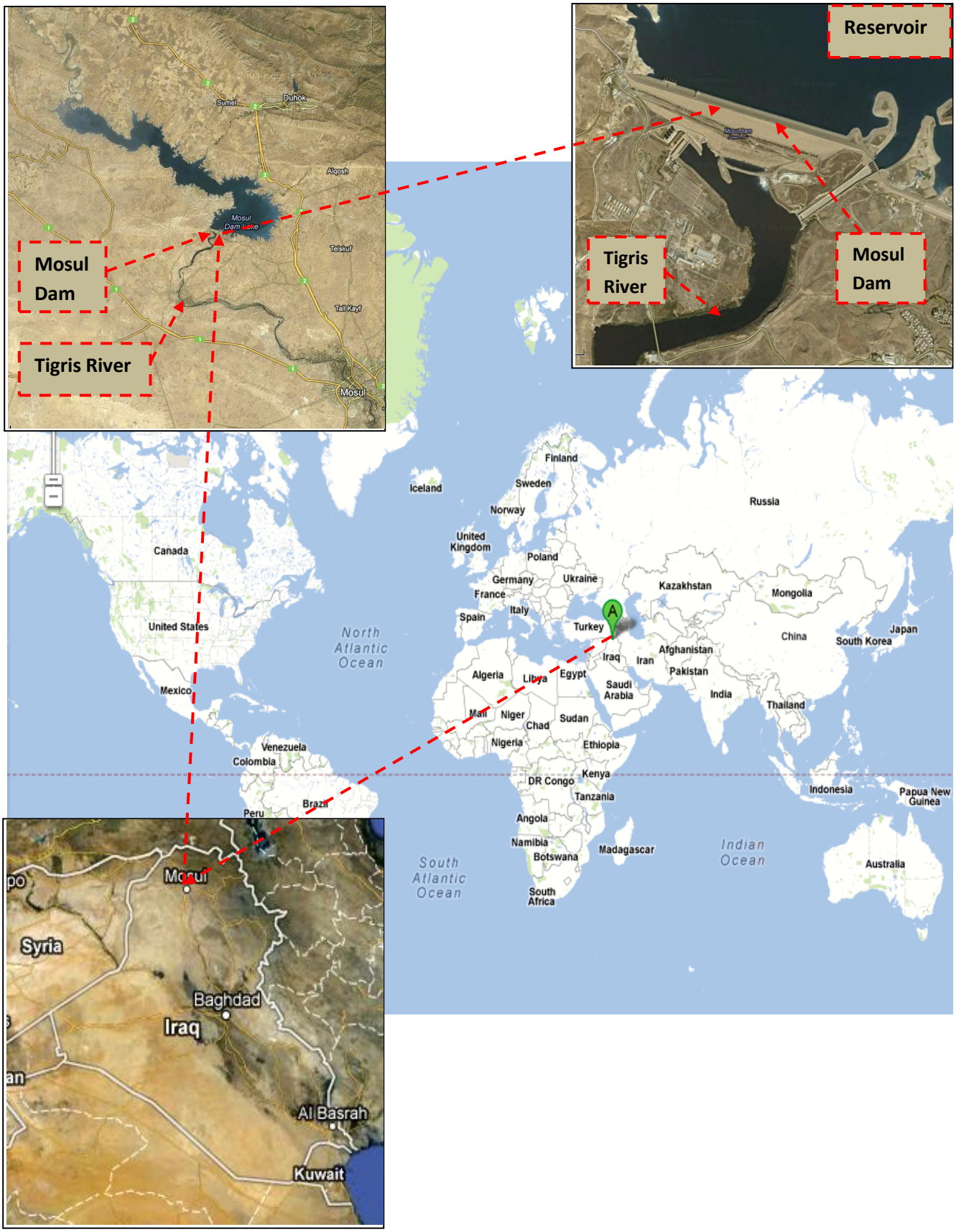

Fig. 1.5: Mosul Dam-Northern Iraq area, all photos taken from: www.google.co.uk page, URL: http://maps.google.co.uk/maps?hl=en&tab=wl, accessed at 05-10-2012.

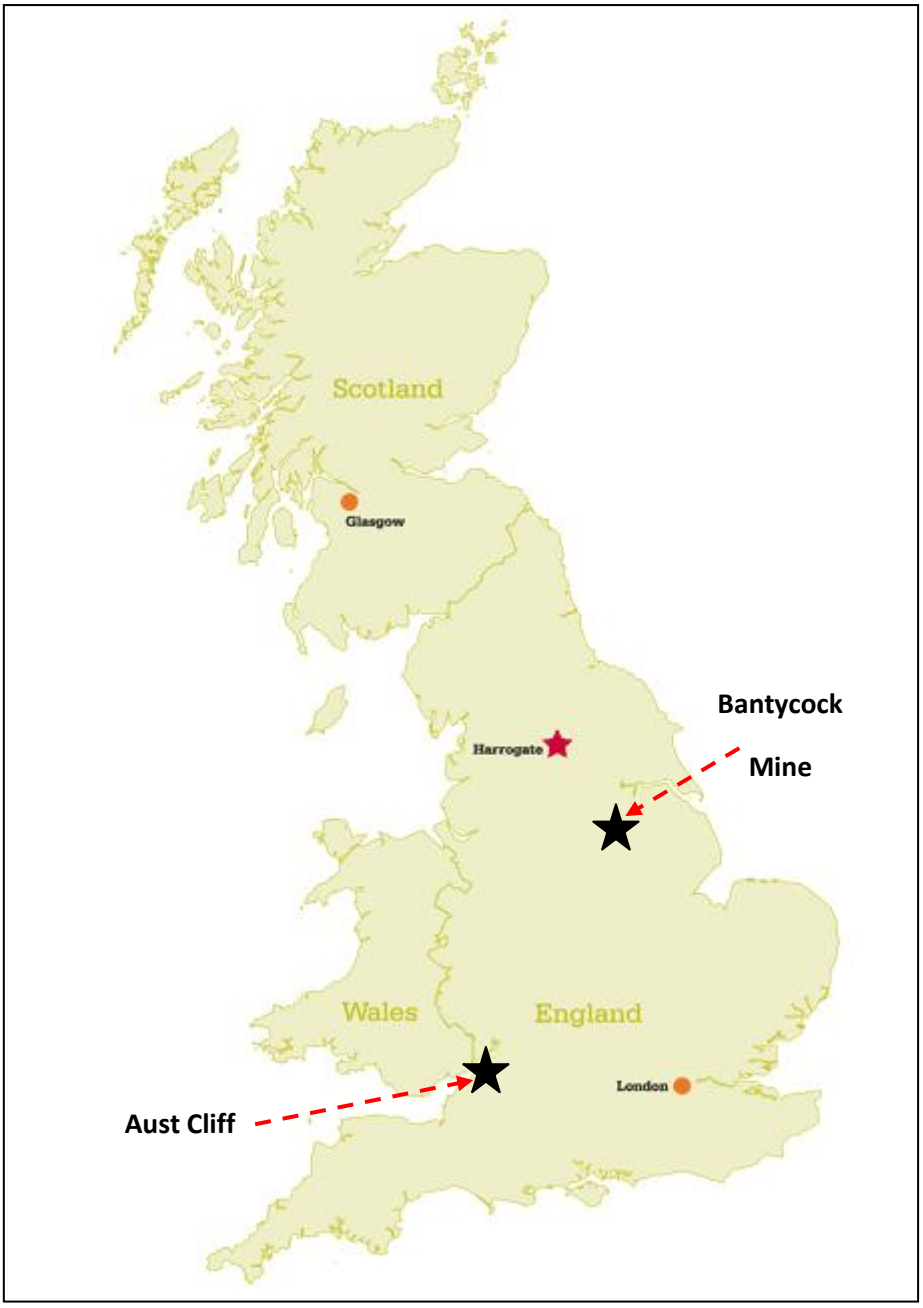

Fig. 1.6: Bantycock Mine and Aust Cliff localities on the UK map (downloaded from: www.hla.co.uk/hla/maps/uk-2.gif)

Fig. 1.7: Bantycock Gypsum-(Nottinghamshire/UK), the general size of collected blocks is 45 cm x 45 cm x 55 cm.

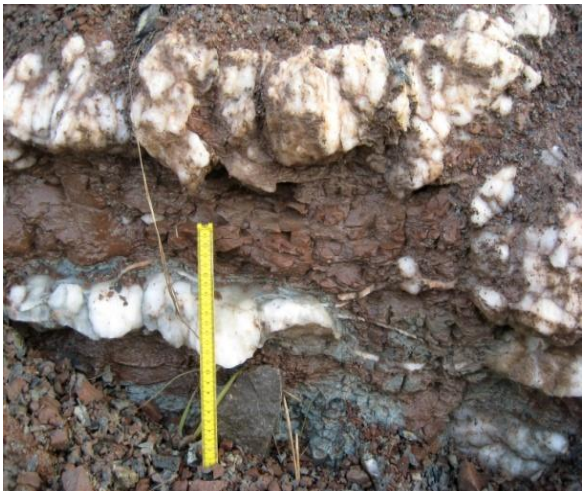

Fig. 1.8: Aust Cliff Gypsum (UK), scale base is about 1 to 15 cm thick. In general gypsum here is inter-bedded with clay and plenty of macro-cracks are distributed within the gypsum itself.

Fig. 1.9: Bantycock Mine in Nottinghamshire, UK**.** Photo 1 taken from: www.google.co.uk page, URL: http://maps.google.co.uk/maps?hl=en&tab=wl, accessed at 05-10-2012, photo 2 was taken by the author at 12-04-2011, and red arrows show some thick layers of gypsum rock.

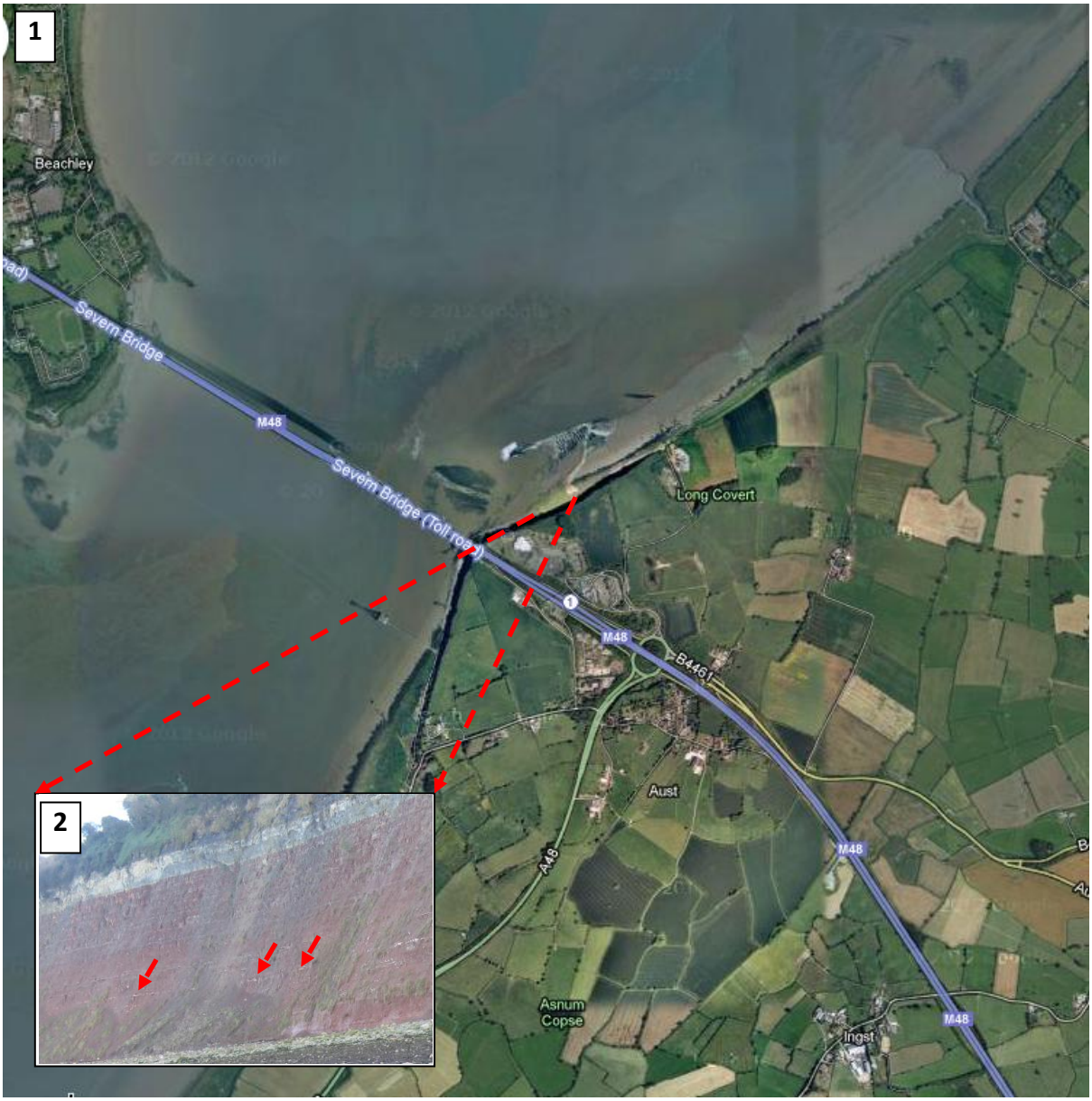

Fig. 1.10: Aust Cliff, UK**.** Photo 1 taken from: www.google.co.uk page, URL: http://maps.google.co.uk/maps?hl=en&tab=wl, accessed at 05-10-2012, photo 2 was taken by the author at 28-11-2009, and red arrows show the gypsum thin layers.

1.4 Gypsum-rich substrates problems

Gypsum salt is a soluble salt; its solubility in pure water is 2.531 g/l at 20^{o}C. Its solubility is about 140 times lesser than halite solubility, which is 360 g/l and 4 times larger than $CaCO_3$ solubility, which is 1.5 mg/l. Increasing of temperature degree impacts on gypsum dissolvability, reaching 2.66 g/l at 43^{o}C (Klimchouk, 1996).

As listed, this salt has the ability to dissolve and leave less volume of gypsum in substrates. Beside this, the leaching process might take place within cracks and fissures inside gypsum body because of ground water variation and surface water infiltration (Fengxiang and Mingiang, 1983; James and Lupton, 1978; Ulker and Gumusolgu, 1982). So, the effective factors for salt dissolution issue are deposit of salt, water unsaturated with $CaSO_4$ or NaCL, a pathway for removal of water containing dissolved gypsum and energy to cause water to flow (Johnson, 2005).

Ground water flow and river water flow can make the gypsum salt dissolve rapidly on contact, dissolving up to 1 metre of gypsum per year (Cooper and Waltham, 1999). According to presented properties of gypsum salt, geological problems and construction failures are found globally, two examples being surface collapse in roads and bridge in Ripon/UK (Cooper and Saunders, 2002) and 400 m^3 sinkhole and 5.5 m land surface drop in North Eastern side of Mosul in Iraq (Al-Layla and Thabet, 1990).

1.5 Scope and Limitation

One year maximum duration experiments were carried out due to the limited time of research (3 years) and available facilities in the Civil Engineering Laboratories. Then, only 5.0 bars applied pressure has been used, which is the maximum allowable pressure in these laboratories. Concerning Iraqi gypsum substrates assessments, a limited number of samples were collected and limited cases of study were conducted because of impossibility of accessing all gypsum rich areas (security issue), regulations of field samples collection and the expensive transportation from Iraq to UK. However, these limitations did not constrict attainment of appropriate quality and amount of data suitable to analyse the problems of gypsum in dams.

1.6 Significance of the study

This study contributes new ideas to the knowledge of gypsum-rich substrates, especially found in dams' sites. The simulation conditions in terms of applied load, massive water influences on long and short term regards are, as far as this author is aware, the first comprehensive detailed analysis of this issue, and forms the first important contribution of this thesis. Then, the comparison between Iraqi and UK gypsum rocks' mechanical properties forms the second contribution. The third contribution to knowledge is the analysis of artificially-prepared gypseous soils based on real Iraqi gypseous soils.

1.7 Layout of thesis

This introduction has presented an overview of gypsum substrates study areas, provided some background information regarding the collected issues of the substrates. The rest of this thesis is designed as below:

Chapter 2 provides a detailed review of dam problems and failures. Background, works and studies on gypsum substrates (soil and rock) are also discussed in this chapter.

Chapter 3 is devoted to methodology of this experimental research work. Field work was carried out in Iraq and UK in order to collect gypsum rock and soil samples. Then the properties of Iraqi and UK collected samples are explored, followed by explanation of formation of artificially-prepared gypseous soil samples properties in addition to all laboratory tests.

Chapter 4 covers the obtained results showing the relationship between the results and the methodology parts.

Chapter 5 presents a detailed discussion of the outcomes of this study and the implementation of this work.

Chapter 6 provides the major outcomes of the thesis and considers the extent to which the aims have been achieved. Thus, recommendations for further works are discussed.

CHAPTER TWO: Literature Review

2.1 Introduction

This thesis analyses stability issues beneath dams built on gypsum-rich substrates. To address this requires an understanding of the origin, properties and types of gypsum-rich substrates, both in the proposed area of study, Mosul Dam, Iraq and at other sites. A brief description of the problem and some associated potential hazards is presented in this chapter. Stability problems associated with dams are considered highlighting the case of the Mosul Dam, and then a summary of gypsum rock and gypseous soil properties and problems is presented. The chapter concludes with some studies on compression and bending on gypsum specifically and on rocks generally, relevant to this study.

2.2 Karst in rocks

Karst develops in areas with soluble rocks, producing characteristic landforms and hydrological systems. It develops due to a combination of well-developed secondary porosity and highly soluble rocks. Karst develops poorly in soluble rocks with high primary porosity, while it may be extensive in soluble rocks with very high secondary porosity (Ford and Williams, 1989). These rock types include solid and fractured limestone, weaker limestones such as chalk, unlithified carbonate sediments and, of particular relevance to this study, gypsum.

Karst processes may involve rapid landscape changes, often and are strongly correlated with the movement of surface and groundwater (Taminskas and Marcinkevicius, 2002). In addition, environmental factors such as temperature, climate, hydrology, vegetation, geology, and the openness of the system to the atmosphere are controlling the direction and intensity of karst processes.

Karst can be: (1) discrete voids, mainly associated with artesian conditions, (2) maze cave, often found in areas of highly entrenched and denuded gypsum karst, (3) vertical breccia-filled pipes, developed downwards from a suitable protective bed at the top of the soluble rock. The size of karstic features ranges from microscopic to landscape scale. Karst occurs in various climatic and ecological zones around the world and occurs principally in solid limestones and fractured rocks, while limited suites of karst features were develop by

weaker limestones, chalk and unlithified carbonate sediments (Ford and Williams, 1989). Gypsum karst is present in many locations: Siberian Platform, Russia; the Eastern-European Plain; North America (Canada, United States and Cuba); South America (Argentina); Europe (Norway, Great Britain, France, Switzerland, Germany, Spain, Italy, Albania, Poland, Ukraine, Romania, Baltic States (Lithuania and Latvia, European Russia); Asia (Asiatic Russia, Siberia, North Caucasus, Turkey, Israel, Syria, Iraq, Iran, General Asiatic countries of the former USSR, Afghanistan, Mongolia and China); Africa (Morocco, Algeria, Libya and Somalia) (see for example Andrejchuk and Klimchouk, 1996; Calaforra and Pulido-Bosch, 1996; Chardon and Nicod, 1996; Cooper, 1996; Forti and Sauro, 1996; Kempe, 1996; Klimchouk et al., 1996; Trzcinski, 1996; Yaoru and Cooper, 1996; Jeschike et al., 2001; Waltham and Fookes, 2005; Liguri e al., 2008; Yilmaz, 2011).

In Iraq many geological problems result from evaporite dissolution in karstic regions. Some of these were recognized by the writer in north-east Iraq (see Figure 2.5). The most common karst forms in Iraq, especially in Mosul area, are sinkholes (dolines), karren, shafts, karst valleys and caves. As a detail on each of these karst forms; (1) sinkholes created either straight in uncovered gypsum or in overlain by limestone, which are up to 20 m in diameter and 1 m – 25 m in depth in gypsum overlain by limestone, (2) lengthened thin holes from karren and shafts are with solution developed in bare gypsum (Jassim et al., 1997). In the UK, visible problems and geological failures were recognized due to the present of gypsum in different places like Ripon in Yorkshire (see Figure 2.8) (Cooper and Saunders, 2002).

2.3 Gypsum properties

Gypsum is a soluble mineral deposited from natural waters that have been concentrated as a result of evaporation, where gypsum is one of several evaporite minerals; evaporite deposits are important sources of gypsum, halite and other minerals (Ingebritsen and Sanford, 1998).

Holiday (1978) showed that gypsum can alter to anhydrite by losing its hydration water, or anhydrite can alter to gypsum by the addition of water. Anhydrite conversion to gypsum may cause 60% increase in the volume of solid phase, which works against litho static pressure of several MN/m^2 and may cause structural damage (James, 1978). This mean that, alteration from state to state can cause volume change, if this happens beneath structures it

might cause structural damage. Papadopoulos et al. (1994) reported on his soaked samples to check their dissolution that in the first hour of saturation early increase of mass was obtained and then with logarithm of time almost regular solubility rate can be noticed. In addition, Papadopoulos et al. (1994) reported on gypsum chemical alteration on heating, continuous mass loss were established and the rate of loss increased after six hour heating.

2.3.1 Gypsum formation

Gypsum forms through crystallization from an aqueous solution or the hydration of anhydrite (FAO, 1990). In marine (lagoon) and epicontinental sea environments, gypsum originates as an evaporitic formation (Klimchouk and Andrejchuk, 1996). An example of this is the Middle Miocene Fatha Formation in Iraq where evaporation in closed or semi-closed marine basins formed thick beds of gypsum, intercalated with carbonates and claystones (Jassim et al., 1997).

2.3.2 Dissolution of gypsum

Gypsum dissolution has been investigated by a large number of researchers so far. Rate of dissolution of gypsum and anhydrite has been studied by James and Lupton (1978). It was noticed to be dependent on the exposed surface area to water, and on the calcium sulphate concentration in sub-saturation solution. Furthermore, it is also associated with flow velocity of water passing over the mineral surfaces and on the salinity of the water.

Water type efficiency to dissolve gypsum was studied by Fengxianga and Mingjiang (1983). It yielded for the same kind of gypsum that the solubility in distilled water is greater than in Yellow River water containing more Ca^{+2} and SO_4^{-2} ions. Due to the efficiency of distilled water to dissolve gypsum, it has been used in many studies on evaporites (especially gypsum rock) (Ali, 1979; Day, 2000; Rauh et al., 2006), in addition to tap and pure water (Razouki and Kuttah, 2004; Razouki et al., 2006; Liang et al., 2008).

Gypsum solubility, a key point for this thesis, is considered by many studies and yielded in valuable information. For instance Ulker and Gumusoglu (1982) found that gypsum solubility is not too high in still water 1.83 gm/litre at 20^oC due to the saturation of this water with $CaSO_4$. Then, Klimchouk (1996) found that gypsum dissolution to be 2.531 gm/l at 20^oC, which is approximately 140 times lower than the solubility of ordinary salt (360

gm/l) and 4 times larger than the solubility of $CaCO_3$ (1.5 mg/l), this agreed with studies of Johnson (2005), Johnson (2008), Bell (2007), Shafiei et al. (2008) and Yilmaz (2011). In addition, the solubility of gypsum in pure water found to be 2.5 kg/cm^3 at 10^{o}C and it has the same solution rate constant and solubility (James and Kirkpatrik, 1980).

Continuous dissolution of gypsum may lead to notable problems such as karstic features such as caves, sinkholes and others (Yilmaz, 2001; Johnson, 2005; Johnson, 2008; Shafiei et al., 2008). Gypsum is susceptible to rapid dissolution whenever there is active motion of ground water that is unsaturated with calcium sulphate. Gypsum solubility is more than limestone and its dissolution causes karst, which result from chemical solution in the existing discontinuities and collapse passages will be expected as a result of karstification. So, Johnson's (2008) study established that karstic gypsum present in dam abutment or a reservoir-impoundment area may cause a number of troubles such as loss of reservoir water or catastrophic loss of the dam itself. Furthermore, gypsum surface karstification has been established to be a result of water percolating down through the overlying strata (Sargent, 2009) using seismic reflection technique. Sargent (2009) also explained that the water flowing through an underlying artesian aquifer causes the dissolution of the gypsum bed, which agreed with Yilmaz (2001) and Johnson (2005) work.

Gypsum dissolution was investigated quantitatively by Al-Dabbagh et al. (1990). Their study yielded that the quantitative estimation of gypsum dissolution is achievable. Velocity of water, the holes diameter (fissure like) and solution constitution were discovered here to be effecting factors on the rate of dissolution. Gypsum tends to dissolve in a steady manner, its dissolution mass increases frequently with an average concentration of 14.5 mg/litre within 30 minutes and average dissolution rate of $3.1*10^{-6}$ m/sec. Similarly, Behnamtalab (2012) showed that increasing fractures in gypsum layer results in the acceleration of the solution process.

Some natural factors such as temperature, quantity of water in contact with gypsum substrates, applied pressure, velocity of water, grain size, etc, may control the process of gypsum dissolution. The paragraphs below include some studies which considered those factors and discovered their influences on gypsum dissolution.

The influence of temperature on gypsum dissolution was considered in the study of Razouki and El-Janabi (1999). It was found that the solubility of gypsum increases by 20 percent with temperature between 0^{o}C and 30^{o}C and reaches a highest dissolution about 2.66 gm/l at 43^{o}C. The solution rate in water depends on temperature, salt concentration in solution and flow rate.

Other environmental factors such as water and overburden pressures have been focused on by Korzhinsky (1953), cited in Klimchouk (1996), that the solubility of minerals increases when the rock fabric experiences pressures higher than that of the ground water. Then, it was reported that the gypsum solubility increase with depth caused by above layers impacts will be about 6 and 14 percent at depth of 50 m and 100 m respectively.

Mineral grain size also has an impact on gypsum dissolution process as established from in the study of Sonnenfeld (1984). Decreasing grain size increases gypsum solubility and gypsum reaches a maximum dissolution when crystals in size range of 0.2 - 0.5 micron.

Applied pressure, a key point for gypsum dissolution, significantly increases dissolution as shown in the experimental study of Zheng et al. (2009) on gypsum solubility at high pressures and ambient temperature. They found that gypsum has a maximal solubility at normal temperature and 6000 MPa pressure inside water. Then, it has a steady solubility at a pressure fewer than 608 MPa and instant dissolution at upper pressure.

Leaching of gypsum, an essential point for dissolution process, has been the focus of some studies such as Azam et al. (1998), and Fengxiang and Mingjiang (1983). Azam et al. (1998) revealed that alteration of calcium sulphate depended on temperature; relative humidity and brine concentration as distilled and brine water were used. The field and laboratory study of Fengxiang and Mingjiang (1983) on the artificial bonds between gypsum seams found that they have not leached out during half of a month, because the well-bonded samples were practically impermeable. In contrast, the un-bonded gypsum seams leached out rapidly due to the water percolating through the fissures at the boundary between gypsum seams and surrounding rock. They also found the intensity of field leaching is much less than laboratory leaching tests.

Gypsum dissolution is also affected by flowing water (Cooper and Waltham, 1999). They studied gypsum at Ripon, North Yorkshire, UK which faced subsidence problems. It was noticed that gypsum dissolution can be very quick in contact with flowing water and a usual river flow, 1 m/sec can dissolve up to one metre of gypsum per year. So, high rates of gypsum dissolution can create an important prospective for a quick enlargement of cave systems, which is through-flow of ground water within the beds of gypsum.

Human activities were considered in the study of Johnson (2005). His study yielded that these activities responsible for some subsidence of evaporites which may let the surface water to run to salt area then dissolve it and might cause sudden ground collapse.

2.4 Gypsum Rock

Gypsum occurs in various colours, due to its mineral content and method of precipitation. Some of its kinds and colours are shown in Figures 2.1, 2.2, 2.3 and 2.4 below.

Fig. 2.1: White gypsum block from Bantycock mine, (from Worley and Reeves, 2007). As listed by them it is "First Grade alabastrine gypsum from the Newark Evaporite).

Fig. 2.2: Gypsum block from Aust Cliff collected on November 2009. See the existing cracks fill with particulate sediment minerals.

Fig. 2.3: Gypsum block from Bazyan, North Iraq, collected on June 2010. See the colour is not pure white which might be due to impurities in the cracks. Geological hammer for scale.

Fig. 2.4: Gypsum block from Koya, North Iraq, collected on June 2010. See the colour is not pure white which might be due to the existing impurities. The block looks like pure gypsum embedded in other mineral.

2.4.1 Distribution of gypsum rock

Gypsum distribution has been studied extensively by many researchers in the world. Gypsum can exist in various conditions of thicknesses and impurities (see Table 2.1). Then, focusing on gypsum rock forms and kinds, Nedriga and Dem'yanova (1986) showed that there are three kinds of gypsinate rocks (gypsum rocks); as beds or large interlayer of gypsum, as individual crystals gypsum is contained in rock and rather uniformly distributed throughout the entire volume of the gypsum rock and large joints of the rock mass fills by gypsum or in soluble coarse-fragmental rock it cements to form conglomerates.

Table 2.1: Gypsum Distribution, it is existing in different conditions of purity and mixed with other minerals.

Author	Country	Characteristics	Formation/Area/Age
Halferdah (1965)	Canada	Layers up to 10 feet (3.048 m) or 11 feet (3.353 m) thick of relatively pure gypsum are separated by impure gypsum, dolomite and shale	Bow River Forest of Rocky Mountain Forest, Alberta
Alphen & Romero (1971)	Spain, Tunisia & Iraq	massive gypsum or anhydrite rocks	Triassic and Cretaceous age
Bell (1981), Cooper (1998) and Cooper (2006)	UK	In both the Middle and Upper Permian Marl of Yorkshire gypsum is found (Bell, 1981). Gypsum occurs only in low ground and natural exposures of gypsum are rare (Cooper, 1998). Up to 10 m of gypsum overlain by red to brown with gypsum for 0-20 m (Roxby Formation), while up to 35m of gypsum for Edlington Formation and also overlain by 0-20 m of red to brown mudstone with gypsum	Permian Strata (Roxby and Edlington Formation) and Triassic Strata
Garcia-Guinea et al (2002)	Spain	1 metre long gypsum crystals, pure gypsum with small and variable Sr, Hg and Miner amount of Zn, Fe, Mg, Mn and Ba	The Jaravias Fe-Pb mine (Pulpi, Almeria) at depth of 50m
Pearson et al (2002)	USA	Gypsum-anhydrite evaporite deposits that outcrops along the Colorado front range of the Southern rocky mountains	Lykins Formation
Ameen et al (2007)	Iraq	Sequence of layers mainly contain gypsum and anhydrite	Fatha (Lower Fars)Formation from Middle Miocene Evaporites Lagoon
Garcia-Ruiz et al (2007)	Mexico	Single crystals of gypsum as long as 11 metre, colorless crystalline Varity of gypsum metre-sized in new galleries and tunnels in the same mine	Nacia mine in Chihuahua, at depth about 290m
Michaelides (2007)	Cyprus	Major sinkholes existing due to gypsum dissolution near river bed	Niso-Pero Chorio, Tochni, Aradippou, Maroni, Kalavasos, Pergamos and Mounttagiaka
Bonetto et al. (2008)	Italy	Gypsum mine, thick beds of coarse and fine grained gypsum (a few decimeters up to 2-3 meter thick) with Marl inter-bedded	Gessos Solfifera Formation in Monferrato Area
Mancino (2008)	Egypt, Iran, Jordan, Saudi Arabia, Kuwait, Qatar	Relatively pure gypsum deposits (Jordan), Large deposits of gypsum (Egypt), Gypsum and anhydrite (10.4% of world crop for Iran)	Southern Sinai (Sinai Peninsula in Egypt), Azraq Formation (Jordan)
	Syria, Turkey and UAE	Phosphogypsum (Syria), Phosphogypsum and FGD and naturally occurring gypsum (Turkey)	Ulas surface mine in Sivas (Turkey)

2.4.2 Problems of gypsum rock

A number of studies on gypsum rock problems showed that it experiences various problems as follows. Gypsum rock forms different karst features with continuous dissolution (see Section 2.2 and Figure 2.5 below). Sinkholes due to gypsum dissolution can reach 400 m^3 in size. The rate of solution of gypsum in field can be between 0.10 and 0.08 m/year by river water. Gypsum dissolution can be countered by ground water, pressure and heat which may be in charge of changing the engineering properties of gypsum like mechanical behaviour, crystal structure and stress-strain with time behaviour (Alphen and Romero, 1971; James et al., 1981; Ulker and Gumusglu, 1982; Al-Layla and Thabet, 1990; Jassim et al., 1997; Klimchouk, 1996; Yilmaz, 2011; Cooper and Saunders, 2002; Johnson, 2005). Figures 2.5, 2.6, 2.7 and 2.8 below show some examples of gypsum rock problematic features.

Fig. 2.5: Karstic features in gypsum rock. Sinkhole formed in gypsum rock at Bazyan, Iraq.

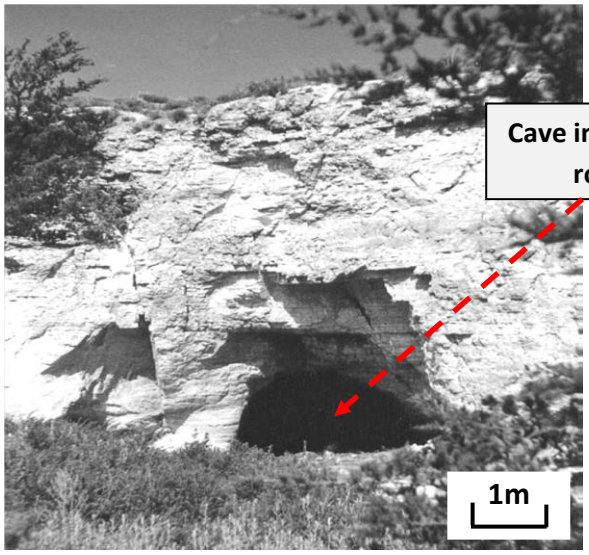

Fig. 2.6: Cave in the Permian Chief Gypsum in western Oklahoma (Cave opening is about 3 m wide) (from Johnson, 2005); evidence on gypsum dissolution caused a cave in the United State.

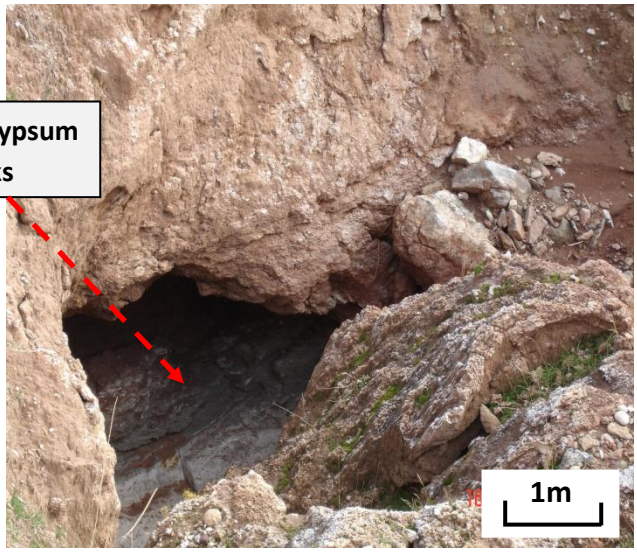

Fig. 2.7: Cave in Fatha Formation Gypsum in North-East Iraq (Cave opening is about 2 m wide) (photo taken on December 2009); evidence on gypsum dissolution caused a cave in Iraq.

Fig. 2.8: Sinkhole at Ure Bank Terrace, Ripon-UK (from Cooper, 2006); the hole formed in April 1997, 10m across and 5.5 m deep. It was caused by collapse of a cave formed in Permian Age gypsum.

2.5 Compression of rocks

Examining rock strength under different loading systems is significant because it shows rock ability to resist external loads and, by inference, can help in risk assessment. Rock strength magnitude can be high or low depending on rock grain size and interaction, and on cementing bonds.

Gypsum resistance to compression is not high. It has been found that the average uniaxial compressive strength for gypsum rock (UCS) is 140 Kg/cm^2, typically varying between 96 Kg/cm^2 to 163 Kg/cm^2; and is very variable, between weak to moderate strength (Karacan and Yilmaz, 1997; Shafiei et al., 2008; Alainachi et al., 2009). However, other studies have found the UCS is medium/moderate strength, varying from 24.1-34.8 and 18-36 MPa generally (Bell, 1994; Karacan and Yilmaz, 2000) (see Table 2.2 for rocks mechanical properties including gypsum).

The compressive strength of rocks (see Table 2.2) and influencing factors on it has been studied extensively. Different kinds of failure have been recognized: shear at angle with the way of axial applied load developing the slip plane; parallel tension to the compression direction. Failed rocks would fracture and lead to powdering of their constituent crystals; ductile or brittle failure depending on the amount of confinement face rocks like: limestone, Stone Mountain granite, Pottsville sandstone and Georgian marble. The failure is fundamentally the same in all cases in uniaxial or triaxial compression (Griggs, 1936; Schwartz, 1964; Bieniawski et al., 1969; Wawersik and Fairhurst, 1970). Other researchers like Ali (1979) and Elizzi (1976) have another view, rock strength and ductility increase in a non-linear relationship with confining pressure.

Poisson's ratio and Young's modulus have been shown to change due to compression. Typically, Young's modulus decreases and Poisson's ratio increases with compressive loads and samples saturation (Ali, 1979; Yilmaz, 2007; Liang et al., 2008; Shafiei et al., 2008) (see Table 2.2)**.** However, Yu et al., 2005 showed that both Young's modulus and Poisson's ratio remained constant or increased. This may be because of the differences in materials used in different studies.

Several studies considered the role of rock sample size and found that increasing length to diameter ratio caused strength to decrease and that deformation in a lateral direction was less than that in the longitudinal direction (Lundborg, 1967; Bieniawski, 1967; Ali, 1979). Increasing of test specimen size resulted in decreasing both uniaxial and triaxial compressive strength for both dry and saturated states (Obret et al., 1946; Shih, 1965; Lundborg, 1967; Elizzi, 1976; Ali, 1979; Hawkins, 1998; Tuncay and Hasancebi, 2009) (see Table 2.2).

A number of studies have considered the influence of rock saturation on compression properties. Rock strength in both uniaxial and triaxial tests was found to be decreased with degree of saturation of specimen (Lundborg, 1967; Ali, 1979; Elizzi, 1976; Bell, 1981; Ulker and Gumusoglu, 1982; Karacan and Yilmaz, 2000; Mortimore et al., 2004; Coviello et al., 2005; Vasarhelyi and Van, 2006; Liang et al., 2008; Gao, et al., 2011; Heidari et al., 2011; Padevet et al., 2011).

A number of researchers have studied the impacts of soaking period and it was found to weaken rocks/gypsum (Ulker and Gumusoglu, 1982; Karacan and Yilmaz, 2000; Coviello et al., 2005; Liang et al., 2008; Gao et al., 2011). Fissures were found to be formed by leaching and cause a significant reduction in shear strength of gypsum seams (Fengxiang and Mingjiang, 1983).

The influence of crystal size on rocks' mechanical properties is considered in several studies. The study of Papadopoulos et al. (1994) established that fine crystals in thin layers of 50 mm diameter (see Figure 2.9 below) were stronger than medium and large crystal sizes.

Static stress effects on rocks mechanical properties also considered by several studies such as the study of Zuo et al. (2005). Their study showed that the increase of static compressive stress cause a decrease in rock's peak stress, corresponding strain, elastic modulus and total strain energy.

Relative humidity influences on rock compressive strength are highlighted in few studies and two different opinions were established. The first opinion is that instantaneous gypsum rock behaviour is not very sensitive to variations in relative humidity; however the dilatancy intensity of uniaxial and triaxial creep tests depends on relative humidity (Hoxha et al., 2006). The second opinion is that uniaxial compressive strength, the dilatancy threshold and the static Young's modulus for gypsum rocks found to be increased due to relative humidity (Eslami et al., 2010).

On temperature influence, a number of studies have been carried out such as the study of Liang et al. (2006) on salt rock. Its strength increases while the temperature increases for both uniaxial and direct shear tests. In another study, the Increase of temperature is weakened rock/gypsum and changed its failure style from brittle to ductile (Gao et al.,

2011). Also, visible sensitivity for temperature was found for gypsum in creep test (Padevet et al., 2011).

Brine concentration impacts on rock strength considered in the study of Gao et al. (2011). They found that rock/gypsum soaking in brine with various concentrations weakened it and change its failure style from brittle to ductile.

Table 2.2: Mechanical properties of different rock types.

Rock Type	Sample State	Uniaxial Compressive Strength	Young's Modulus	Shear Modulus	Poisson's Ratio	Reference
Marbles	air-dry	5283 to 11142 N/cm^2	$3.67*10^6$ to $7.808*10^6$ N/cm^2	$1.517*10^6$ to $2.913*10^6$ N/cm^2	0.210 to 0.340	Xeidakis et al. (1996)
Gypsum	air-dry	12.3-52.7 MPa	13 to 35.7 GPa	Not given	0.11 to 0.46	Karacan and Yilmaz (2000)
	after 20-days sat	4.2-28.8 MPa	Not given	Not given	Not given	
	air-dry	15.04-30 MPa	16.02 to 32.41 GPa	Not given	Not given	Yilmaz and Sender (2002)
red sandstone	air-dry	11.88 MPa (Mean)	3.4 Gpa (Mean)	Not given	Not given	Zuo et al. (2005)
sandstone, limestone, siltstone, dolomite and marl	air-dry	9.16 MPa to 101.08 MPa	Not given	Not given	Not given	Akram and Bakar (2007)
Gypsum	Air-dry Saturated	28.7 to 36.2 MPa 16.2 to 19.7 MPa	2.85-3.35 1.57-2.30	Not given	Not given	Yilmaz (2007)
soluble rocks	air-dry saturated	9-79 MPa 8-54 MPa	5-53 GPa 3-16 GPa	Not given	Not given	Shafiei et al. (2008)
salt rock	air-dry saturated	46 MPa 11 MPa	4.6 GPa 0.5 GPa	Not given	Not given	Liang et al. (2008)
	air-dry	25 MPa	Not given	Not given	Not given	Ozkan et al. (2009)
Gypsum	air-dry	20-30 MPa	20 GPa	Not given	Not given	Waltham (2009)
Sulfaset synthetic rock	air-dry	10.6 to 12.6 MPa	2.0-3.0 GPa	Not given	Not given	Cho et al. (2010)
Gypsum	air-dry wet	33.2 MPa 19.7 MPa	Not given	Not given	Not given	Nuri et al. (2012)
Gypsum	air-dry	14.6 MPa	6.8 GPa	Not given	Not given	Liang et al. (2012)
Gypsum	Not given	9.22 to 36.74 MPa	Not given	Not given	Not given	Pando et al. (2012)

Table 2.3: Some rocks' compression tests.

Rock Type	Compression Test	Sample Kind	Sample Size	Reference	Notes
Granite	Unconfined compression	Cylinders	Dia.=2, 3, 4 and 6 cm L/D = 1	Lundborg (1967)	Increases sample size found to decrease strength
Not given	Not given	Cubes	length 20 to 70 mm	Zatonskikh et al. (1965)	Increase sample size increases the strength up to a maximum value, then drops to a constant value
Gypsum Rock	Triaxial and uniaxial tests	Cylinder	25 mm diameter x 75 mm length	Elizzi (1976)	
Rocks-Gypsum	Unconfined compression	Cylinders	NX (52mm) in Diameter and L/D ratio = 2	Bieniawski et al. (1978); Singh (1993); Karacan and Yilmaz (2000); Yilmaz and Sender (2002); Brady and Brown (2004)	Increase of sample size decrease compressive strength
Gypsum Rock	Triaxial and uniaxial tests	Cylinders	25.4 mm Dia. x 76.2 mm height, 31.75 mm Dia. x 95.25 mm height, 38.1 mm Dia. x 114.3 mm height and 50.8 mm Dia. x 152.4 mm height	Ali (1979)	Increase of sample size decrease compressive strength
Gypsum	In situ & laboratory shear	Thin Layers/seams	50cm x 50cm x 50cm	Fengxiang and Mingjiang (1983)	No given notes on sample size
Amphibole feldspathic quartiz and feldspathic quartz	Unconfined compression	Cylinders	Dia.= NX size	Singh and Singh (1993)	No given notes on sample size
Rocks	Lab Tests	Cylinders	Dia. not less than 50 mm x L/D=2	BS ENV 1997-2 (1999)	Height to diameter ratio between 2.0 and 3.0 and a diameter not less than 50 mm
Common Rocks	Unconfined & Brazilian	Cylinders	50 mm Dia. & L/D=1-3	Thuro et al. (2001)	Length/Diameter ration should equal or greater than 2.0 because of the elastic zone will be with enough length and minimize its effects on modulus of elasticity determination
Salt Rock	Uniaxial compression	Cylinders	50 mm Dia. x 100 mm height	Liang et al. (2006)	No given notes on sample size
Sandstone	Triaxial, uniaxial and tensile tests	Cylinders	25.5 mm Dia. x 50 mm height	Whittles et al. (2006)	No given notes on sample size
Sandstone and siltstone	Uniaxial compression	Cylinders	54 mm Dia. & L/D=1.6-2.5	Agustawijaya (2007)	When length/diameter ratio is between 1.6-2.5 no significant indications has been found that the unconfined compressive strength is influenced by this ratio

Rocks		Cylinders	Dia.=51 mm x L/D=2.0-2.5	MP (2007)	Diameter should not be less than 1.88_in (47_mm)
Various Rocks	Unconfined compression	Cylinders	Dia.=25 and 50 mm x L/D=2	Aoki and Matsukura (2008)	No given notes on sample size
Sediments	Unconfined compression	Cylinders	Not given	Alainachi and Alobaidy (2009)	No given notes on sample size
Three natural soft rocks and artificial one	Oedometric tests	Thin Layers/Discs	Not given	Castellanza et al. (2009)	No given notes on sample size
Rock salt	Uniaxial compression	Cubic and prismatic Core (cylinder)	width=25, 50, 75, 100, 125 mm & H/W=0.5, 1.0, 1.5, 2.0, 2.5 Dia.= 2-93 mm, H/D= 0.5-2.7	Ozkan et al. (2009)	The sample diameter should be preferably be greater than 50_mm for all rock types, the critical H/D and H/W ratios are 1.5 for cores and 2.0 for prismatic samples
Sulfaset synthetic rock	Uniaxial compression	Cylinders	55 mm Dia. x 110 mm height	Cho et al. (2010)	
gypsum	Uniaxial compression	Prismatic	6 in (152.4 mm) x 3 in (76.2 mm) x 1.25 in (31.75 mm)	Janeiro and Einestein (2010)	No given notes on sample size
Gypsum mortar	Short and long term compression tests	Cylinders	10 mm Dia. x 70 mm height	Padevet et al. (2011)	No given notes on sample size
Evaporates; halite, thenardite, glauberite and gypsum	Uniaxial compression	Cylinders	50 mm Dia. X 100 mm height	Liang et al. (2012)	No given notes on sample size

From the details (above Table 2.3) on the variety of sample size for compression tests and from the influences of increased samples size to decrease compressive strength (Obret et al., 1946; Shih, 1965; Zatonskikh et al., 1965; Lundborg, 1967; Bieniawski, 1967; Elizzi, 1976; Ali, 1979; Hawkins, 1998; Tuncay and Hasancebi, 2009), Bieniawski et al. (1978)/ISRM and ASTM (2010) suggested ranges of sample size of uniaxial compression testing, cylindrical sample with diameter not less than 54 mm (NX size) and length/diameter ratio should be 2.5-3.0 (ISRM) or 2.0-2.5 (ASTM). These suggested ranges are in agreement with some researchers' studies on the same regards like Ozkan et al. (2009) and Thuro et al. (2001).

Fig. 2.9: Gypsum rock discs in 50 mm diameter tested; (1) alabaster, (2) medium-sized crystals, (3) coarse-sized crystals (from Papadopoulos et al., 1994, Figure 1). (Note: the samples size and shape are very similar to the thin-layer samples of this research).

2.6 Bending of rocks

As mentioned in Section 2.2, the stability of cave roof slabs might be due to the transformed load of overlying rocks and other structures. Rock failure in the roofs of tunnels and mines often happens in bending states (Ali, 1979). Therefore, examining the mechanical properties of rock beams simulating field conditions might be useful. In order to do so, a beam bending testing in four-point mode is an appropriate test to apply.

Both of Elizzi (1976) and Ali (1979) focused their studies on the difference between compression and tension strain in bending tests. Their studies showed that the calculated compressive strain from four-point bending test was greater than tension strain.

Saturation, a key point for bending issue, has been studied by Ali (1979). He studied saturation influences on bending bars mechanical properties of gypsum rock and discovered that the calculated compressive and tension strain increase with specimen saturation.

Xeidakis et al. (1996), in a study on artificial crack present in bending bar, found that a quite brittle behaviour and the fissure propagation was almost immediate when allocate the crack at a distance from centre. Other researchers such as Aliha et al. (2009) discovered weaker respond in in-plane sliding compare with crack opening state, which done via symmetric four-points bending test.

Kourkoulis et al. (1999), in a study on marble, found the stress-strain behaviour was linear for the zone between 20 and 30 percent of stress failure. While after 30 percent becomes strongly non-linear. In addition, the impacts of rocks' (marble) microstructure, which cause strain gradient, is found to be significant.

Shape and size of bending sample are key factors in bending bar tests. Biolzi et al. (2001) found that size is more significant for bending strength than tensile strength. Cardani and Meda (2004) discovered that bending bar strength has to be decreased with Increases of bar size. While, Coviello et al. (2005) found that specimen slenderness and shape were powerfully responsible for experimental outcomes.

Emfimov (2009) highlighted on the method of bending testing. His study revealed that the bending test method cause some impacts on rock's mechanical behaviours. Also, his study results suggested that the three-point bending test showed higher tension compare to four-point bending test.

Particle orientation, a key point, also influences bending bar resistance to compression. On this point, the Pires et al. (2011) study established that the position of the sample has some impact on compressive strength of bending bars' in both three and four point bending tests.

Some mechanical properties of tested rock bending samples are shown in Table 2.4 below; bending bars sizes and types also can be found in Section 3.6.1.

Table 2.4: Examples of mechanical properties of three and four points bending tests.

Rock Type	Bending Test	Sample Size	Compressive Strength	Young's Modulus	Peak Load	Reference
Marble, three types of granite, gabbro-diorite, gabbride and dolerite	Three point	2400 x 400 x 60mm and 1200 x 200 x 60mm	Not given	20 GPa	Not given	Biolzi et al. (2001)
Sandstone	Three point-centre notched	146.8 mm span x 60 x 26 and 110 mm span x 60 x 26mm	Not given	Not given	0.723 to 1.568 kN	Lin et al. (2009)
	Off-centred notch-three point	146.8 span x 60 x 26 mm and 110 span x 45 x 26mm	Not given	Not given	0.685 to 1.507 kN	
Pre-heated sandstone	Three point	180 x 40 x 40 mm, 450 x 100 x 40 mm and 900 x 200 x 40 mm	4.33 to 17.01 MPa	Not given	1.93-8.14 kN	Biolzi et al. (2011)
Slate	Three and four points	150 x 50 x 30 mm for Three-point and 150 x 30 x 25 mm for Four-Point	0.49 MPa for sample cut parallel to the wide face	Not given	Not given	Pires et al. (2011)
			32.3 MPa for sample cut parallel to the longer side	Not given	Not given	
			42.5 MPa for sample cut parallel to the shorter side	Not given	Not given	

2.7 Creep of rocks

Creep is defined as: "the slow deformation of solids under small loads acting over long periods of time" (Griggs, 1939 Page no. 225). Creep of rocks is found to happen typically in three stages: primary, secondary and tertiary (Griggs, 1940; Robertson, 1960; Price, 1964; Wawersik, 1972; Mirza, 1974; Singh, 1975; Dusseault and Fordham, 1993; Li and Xia, 2000; Maranini and Brignoli, 1999; Ma and Daemen, 2006; Swift and Reddish, 2005; Fabre and Pellet, 2006; Zhao et al., 2012). Furthermore, it was found on rocks creep stages that the tested rocks in uniaxial can face all three stages of creep in both axial and lateral directions: primary, secondary and tertiary (Singh, 1975). Similar behaviour for four-point bending

creep failure was noticed by Fu et al. (2008), with an oscillating stage as a first stage, then stable stage as a second stage and attenuating stage as a third stage.

Many studies have considered the issue of compression and bending creep of rocks, but the processes are still not fully understood. Environmental issues and level of stresses application (for example overburden and/or construction weight), shown below, have a notable role to act on creep phenomena and yield in weaker structure of rocks.

Saturation of rocks, a key point, has been highlighted in many studies. Dry specimen creep has been found to be greater than wet specimen. So, the recorded lateral creep strain was more than the longitudinal creep strain during bending creep tests on shale and uniaxial compression of siltstone (Kanagawen and Nakaari, 1970; Elizzi, 1976).

Degree of saturation and the nature of the saturating fluids influence on creep rate have been considered in some studies. They probably reflect solution, ionic mobility and re-crystallization to effect on the creep behaviour of rock/gypsum. Creep rate increases noticeably for rock saturated in pure water, which is larger than saturated rocks in calcium chloride solution. Axial, lateral and volumetric Instantaneous and creep rate increase due to saturation present (Griggs, 1939; Griggs, 1940; Misra, 1962; Afrouz and Harvey, 1974; Elizzi, 1976; Varo and Passaris, 1977; Ali, 1979).

So, the nature of saturation fluids impacts on creep such as brine water also influences rock creep. It noticed generally to reduce rock's resistance to creep deformation. Evaporites established to be the first and foremost under dilatant conditions and in the presence of brine. This is due to the development of fractures during selective dissolution for the stressed areas in the rock (Griggs, 1940; Lee and De Souza, 1998).

Humidity impact on creep was also investigated in many studies such as the study of Mirza (1974), Varo and Passaris (1977), Hoxha et al. (2006) and Auvray et al. (2008). Humidity was found to cause significant fluctuations in the strain rate. So, strength decreases and deformation characteristics decrease due to increase in humidity. In addition, creep strain rate is strongly dependant on the relative humidity for gypsum rock.

Other environmental factors such as temperature are a key point in creep test. Griggs (1940) found that higher temperature increases creep strain.

Not only external factors influence creep properties, rock internal characteristics also notably impact the creep phenomena. Both Griggs (1940) and Misra (1962) found that rock creep strain rate is affected by impurities and average crystal size. Furthermore, the study of Stacey (1963) showed that a weak spot in a rock body becomes weaker during continuous creep and may lead to catastrophic increase in creep rate.

Application of constant stresses on rocks causes both instantaneous and creep strain. Many studies have been conducted in this regard. For instance, Price (1964) found the instantaneous strain to be significant from the total creep. It was at 24-72% of the instantaneous strain for beams of Pennant sandstone and at 65-85% of the instantaneous load of failure for beams of Wolstanton sandstone, which have exhibited primary and secondary creep. A linear correlation between the applied stress and the creep rate of the secondary stage for both sandstone samples was also obtained. Moreover, increasing applied stress increased creep strain and creep speed was established to be a function of applied stress (Misra, 1962; Peng, 1973; Padevet et al., 2011).

Time also has a great role in controlling the creep process and, with the applied stress, may lead to failure. On this matter, Bradshaw (1964) study revealed that the creep rate decreased with time at invariable stress level**.**

Other researchers calculated creep formula for creep tests (shown in Table 2.5 below).

Table 2.5: Creep properties of different experimented rocks in compression and bending tests [for Lomnitz (1956), $\epsilon(t)$ is the total shear strain in radian, σ is a constant shear stress in any suitable units, q is (μ log e)/slope of creep curve, t is time in seconds, a is a coefficient represents a frequency and μ is the rigidity modulus in same unit of shear stress], [for Robertson (1960), ϵ is the creep rate, t is time in seconds, S is the differential stress in bars and K, $K1$ and $K2$ are constants], [for Hobbs (1970), σ is stress level, t is time in minutes, E_c is mean incremental modulus and g and K are constant], [for Hofer and Knoll (1971), ϵ is the creep rate, t is time and K, $C1$ and $C2$ are constants] and [for Mirza (1974), $\epsilon(t)$ is the creep rate, t is time, $\dot{\epsilon}$ is the strain rate, and C_o, C, B, n, $A1$, $A2$, B_o and $B1$ are constants].

Rock Type	Test Type	Creep Formula	Duration of Test	Applied Pressure	Reference
Granodiorite and gabbro	Torsion	$\epsilon(t) = \{\sigma [1 + q \ln (1+at)]\}/\mu$	1 week	Not given	Lomnitz (1956)
Solenhofen limestone, Danby marble, Rutland White marble and calcite	Triaxial	$\epsilon = t/K$ and $\epsilon = K1\ S - K2$	17 to 167 minutes	Not given	Robertson (1960)
Siltstone, shale, mudstone, and sandstone	Uniaxial, torsion and four point bending	$\epsilon = (\sigma/E_c) + g\ \sigma^n t + K\ \sigma \log (t+1)$	4000 minutes	compressive stresses from 26.4 to 41.4 MPa	Hobbs (1970)
Carnallite	Uniaxial compression	$\epsilon = C1 + C2 \ln t$ at low stress and heat; $\epsilon = K\ t^n$ at high stress and heat	Not given	Not given	Hofer and Knoll (1971)
Evaporitic rocks	Uniaxial compression	Transient creep followed the form of $\epsilon(t) = C_o + C \ln (t + 1)$	48 Days	3000 to 3750 psi	Mirza (1974)
		Creep rate-stress followed a power law as $\epsilon(t) = B\ t^n$			
		Strain rate-time relationship for low stresses described by $\epsilon = A2 + A1/t$			
		High stresses by $\epsilon = B_o + B1nt^{n-1}$			
Gypsum and Anhydrite	Bending, uniaxial & triaxial compression	At low stresses and confining pressure the creep data expressed by the logarithmic relationship and by power law at higher stresses and confining pressure	10 Days-Bending; 30 Days for Uniaxial & Triaxial	30, 40, 60 & 80% of Flexural Strength/Bending; 30, 50, 65 & 80% Comp. Strength/Uniaxial	Elizzi (1976)
Gypsum	Bending, uniaxial & triaxial compression	The creep data expressed by the logarithmic relationship and by power law at higher stresses and confining pressure	30 Days	30, 50, 60 & 80% of Flexural Strength/Bending	Ali (1979)

2.7.1 Methods used for rock creep testing

It has been previously established that a lever system can be used to apply creep stress on rock sample (Griggs, 1939; Griggs, 1940; Price 1964; Li and Xia, 2000; Drescher and Handley, 2003). Other devices, systems and focused areas for creep testing of rocks include:

- A conventional triaxial device to examine creep behaviour of rocks (Bieniawski et al., 1969; Wawersik and Fairhurst, 1970; Martin et al., 1997; Zhao et al., 2012).

- A servo-controlled hydraulic system to apply creep stress and calculate its behaviour (Peng, 1973; Zhao et al., 2012; Li and Xia, 2000).
- A gas hydraulic/hydraulic system to examine rock response for creep (Singh, 1975; Cogan, 1976; Elizzi, 1976; Varo and Passaris, 1977).
- Application of different temperature degree with uniaxial creep device (Hofer and Knoll, 1971).

2.8 Gypseous Soils

Soils of arid and semi-arid regions are rich with sulphates, commonly gypsum (Mitchell and Saga, 2005; Bashour and Sayegh, 2007). Gypsum-rich soil occurs in dry lands, reflecting both of geological and climatic factor (Herrero and Porta, 2000). Gypsum mineral greatly affects substrates in their mechanical behaviour when present as a result. It will be difficult to apply the regular soil tests in order to get gypseous soil physical or chemical properties (Arakelyan, 1986). Due to gypsum's sensitivity to external factors such as temperature, water and loading systems, many researchers have examined its behaviour under various conditions (Mulder, 1969; Alphen and Romero, 1971; Petrukhin and Boldyrev, 1978; Arakelyan, 1986; Al-Ani and Saleam, 1993; Azam, 2000; Salih, 2003; Razouki and Kuttah, 2004; Fattah et al., 2008; Razouki et al., 2008; Al-Farok et al., 2009). The solubility property of gypsum mineral has an impact on voids. Gypsum soil can experience voids after dissolution and thus substrate strength is reduced. However, gypseous soil behaviour under natural and artificial conditions need refinement (Herrero and Porta, 2000).

2.8.1 Formation of gypseous soils

Gypsum in gypseous soil can be pedogenic or geological. The geological origin is in the formation of gypsum deposits. The pedogenic phenomenon is the translocation and deposition of gypsum in a soil profile, which is a result of percolating rainwater or capillary rise and evaporation (Alphen and Romero, 1971).

Gypsum origin in soil is considered in some studies such as FAO (1990). It reported that irrigation and/or weathering of land rich with parent materials cause an accumulation of gypsum in the subsurface horizon. So, it may actually relate to a brackish water-table, in

river beds and lagoons. These locations are ideal for the formation of secondary gypsum deposits.

Similarly, Khademi and Merut's (2003) study showed that during the downward movement of water, a gypsum-rich horizon in the deep colluvial soils could be developed. The outcomes of a rising movement of salt-loaded brine are exterior gypsic and salic horizons in the alluvial plain.

In contrast, the study of Boyadgiev and Verheye (1996) showed that gypsum formation in soil is connected with the weathering of gypsum-bearing rocks which easily dissolve under the action of penetrating water. After this, weathering of parent materials, secondary gypsum accumulates in soil in poor drainage situations. A portion of the original gypsum in the rock is dissolved, the non-gypsiferous (calcium carbonate) fraction increase in good drainage situations and sulphate ions precipitated as $CaSo_4.2H_2O$ at depth.

2.8.2 Distribution of gypseous soils

Gypseous soils are common in arid regions with a yearly rainfall below 400mm (Boyadgiev and Verheye, 1996), also Table 2.6 from FAO (1990), Table 2.7 and Figure 2.10 from Boyadgiev and Verheye (1996) below.

Table 2.6: Distribution of gypseous soils (Modified from FAO 1990, Table 1.2 distribution of gypsiferous soils by countries).

Continent	Country	Km^2	% of total area of country	% of area of gypseous soils
Africa	Somalia	10161.2	16.2	15.5
	Algeria	7966.3	3.3	12.2
	Namibia	5327.7	6.5	8.2
	Libya	3956.8	2.2	6
	Mali	2818.3	2.3	4.3
	Tunisia	1439.8	9.3	2.2
	Ethiopia	1423.4	1.3	2.2
	Morocco	1114.3	2.5	1.7
	Sudan	785	0.3	1.2
	Mauritania	396	0.4	0.6
	Egypt	382.2	0.4	0.6
Southern Asia	Iraq	4779.2	11	7.3
	Syria	3966.6	21.6	6
	Yemen A.R.	2931	8.8	4.5
	Oman	471.6	Not given	0.7
	Kuwait	354.6	Not given	0.5
	India	182	0.06	0.3
	Saudi Arabia	82.5	0.04	0.1
	Jordan	80.5	0.8	0.1
	Pakistan	9.5	0.01	Not given
	Iran	4.2	Not given	Not given
Central Asia	China	11484	1.2	17.5
	USSR	5074.1	0.2	7.7
	Mongolia	60.9	0.04	0.1
Europe	Spain	165.5	0.3	0.3
	Turkey	64.2	0.08	0.1
North America	New Mexico	78	Not given	0.1

Table 2.7: Distribution of gypseous soils in the world.

Country	Remarks	Formation	Author
Iraq	Mainly associated with a geological substrate contain gypsum and anhydrite inter-layers or with Pleistocene terraces associated with such deposits	Derived from sedimentary rock units	Buringh (1960)
	Gypseous soil in Iraq forms 7.3% to 10% of the total world gypsiferous area and 11% to 15% of the area of Iraq	Not given	Fattah et al. (2008)
Spain, North Africa, the middle east and Southwest Siberia	Solid deposits of gypsum and gypsum deposits inter-bedded in marls or clays, silt and sandstones	Eocene and Oligocene, but mainly during the Miocene	Alphen and Romero (1971)
Tunisia and the Central Namib	Crusts usually include 50% to 80% gypsum by weight, the other components are fundamentally quartz grains and calcium carbonate	Not given	Watson (1985)
Erevan	White earths of Erevan contain 5% to 47% gypsum and occur in the air-dried state	Not given	Arakelyan (1986)
Different regions of the former USSR	Clay gypsum soils (ordinary and sandy loams)		
-	See Table 2.6 in page no. 36 of Chapter 2	-	FAO (1990)
America, Spain and the Middle East	In arid and semi-arid regions gypseous soils cover more than 20% of the total country area	Not given	Al-Ani and Saleam (1993)
Kuwait	In association with Dibdiba gravel deposits, gypcrete is mainly present in a layer of 3.0m from ground level	Dibdiba Formation	El-Sayed (1993)
Central Iran	Gravelly and extremely gypsiferous (> 50% gypsum in gypsic horizons)	Sedimentary origin	Khademi and Mermut (2003)
Georgia	Humus sulphate and salt (gypsisols, solonetz and solonchaks)	Not given	Urushadze and Urushadze (2011)

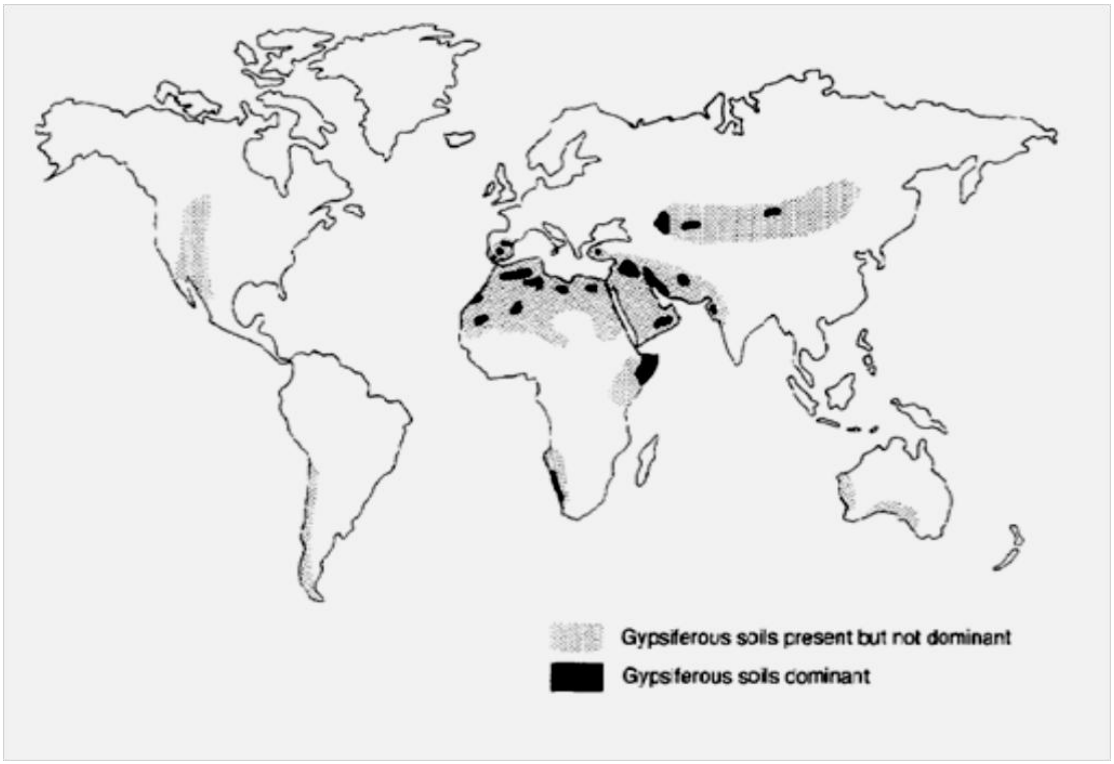

Fig. 2.10: Global Distribution of Gypsiferous Soils (modified from Boyadgiev and Verheye, 1996, Figure 1, adapted from (FAO, 1993), FAO World Soil Resource Report 66, Rome).

2.8.3 Properties and Problems of gypseous soils

Gypsum can break down and mix with other minerals (Mulders, 1969). When it dissolves or broken to particles with a river water, it can be transported as dissolved matter in water a vast distance from its source and then deposit along with sand, silt and clay.

Al-Dabbas et al (2010) have proposed a gypseous soil classification system based on mechanical properties Iraqi gypseous soils (see Table 2.8 below).

Table 2.8: Recent proposed classification, applied for gypsiferous soils (modified from Al-Dabbas et al., 2010). This table shows some geotechnical properties of: Najaf, Karbala, Falluja and Samarra/Iraq gypseous soils, e.g. particles distribution, collapsibility, voids, strength in addition to solubility properties.

Gypsum (%)	Class	Initial void ratio	Coefficient of curvature	Uniformity coefficient	Collapse Potential (%)	Compressive strength (MN/m^2)	Cohesion (kN/m^2)	Plasticity index (%)	Fine grained soil (%)	TDS of soil water extract (ppm)
0.5-25	**Gypsiferous soil**	**<0.45**	**<2.5**	**<25**	**<1.5**	**<1**	**<15**	**<10**	**<50**	**<350**
25-50	**Highly gypsiferous soil**	**>0.45**	**>2.5**	**>25**	**>1.5**	**>1**	**>15**	**>10**	**>50**	**>350**

The study of Fattah et al. (2008) on some Iraqi gypsiferous soils showed that they are problematic from both agricultural and engineering points of view. Various problems have been recognized when structures are built on them such as soil failing, rising of seepage of water throughout the soil, soil softening and sulphate serious effects on concrete. Slow and continuous dissolution of gypsum by seeping water through the gypsum-rich soil were thought to be important in these problems.

The study of Alphen and Romero (1971) on gypseous soils problems established that some damages in large irrigation canals built on gypseous soil were noticed. So, they explained that any gypsiferous soil with more than 2% gypsum content is unsuitable for foundations of hydraulic structures.

2.9 Compression of gypseous soils

Gypseous soils are not very compressible on brief flooding. Long-term flooding can cause localised settlement, depending on; the type of soil, initial gypsum content, relative amount of leached salts, soil properties and the acting load. The soil's piping settlement can be equal to 76.2-93.5% of total settlement of the soil (Petrukhin and Boldyrev, 1978). Similar results were found in preliminary work by the author of this thesis (Salih, 2003) during tests on real and stabilized gypseous soils in which a maximum 12 mm settlement occurred. So, increasing applied pressure on gypseous soil in long-term loading can cause an increase in the recorded settlement.

The influence of seepage of flooding water has been considered in some studies such as Salih (2003). His results showed that the reduction of gypsum content is increased with depth, gravel percent is not affected, sand percent decreased, while silt and clay percents showed an appreciable increase. A decrease in cohesion in the first 50 cm of 150 cm depth was found, while for 125 to 150 cm depth a marginal increase was observed. The angle of internal friction was fairly constant with depth and 24% reduction was obtained due to dissolution.

Soaking period influences on gypseous soil properties have been studied by Razouki and Kuttah (2004) and Razouki et al. (2008). A drop in gypsum and total soluble salt content were obtained, in addition to a significant progressive decrease in the *CBR* (*CBR* is California Bearing Ratio) and M_R (M_R is Resilient Modulus) due to an increase in soaking period.

Brine water influences on gypseous soil properties were studied by Azam (2000). His study revealed that the collapse potential increased when gypseous soil soaking in brine water twice that when soaking in distilled water**.** In contrast, Al-Farok et al. (2009) noticed gypsum dissolution to be decreased with soaking in brine.

Soaking/inundation pressure was noticed by some studies to influence gypseous soil geotechnical properties (e.g. Al-Ani and Seleam, 1993; Razouki et al., 2008 and Fattah et al., 2008). An increase of soaking/inundation pressure was found to increase collapse potential. Maximum shear strength, apparent cohesion and angle of internal friction in *UU* direct shear test, rebound index $C_{r,}$ compression index C_C, volumetric strain and collapse potential on undisturbed and re-compacted gypseous soils also discovered to be decreased when Initial water content increases.

Gypsum salt percent, a key point, has been considered in some studies on gypseous soil geotechnical properties e.g. Fattah et al. (2008) who showed that an increase in gypsum content increases collapse potential. Azam (2000) showed that the compressibility of a soil increases with the addition of clay to calcium sulphate (gypsum salt percent decrease). Similar conclusions were reported in the study of Tran et al. (2012); however they found the compressibility decreased with the addition of sand on soluble salts. Tran et al. (2012) also showed that a gypsum content increase decreases peak shear strength, angle of internal

friction and void ratios. Moreover, the study of Azam (2008) showed that a linear trend has been established with an increase in clay content followed by all calculated swelling properties for a clay-bearing calcium sulphate.

Some physical property like porosity plays an essential role on gypseous soils behaviour since it changes during leaching of gypseous soil due to gypsum dissolution (Al-Farok et al., 2009). Also, they discovered that the large displacement is happening in the tested gypseous soil sample surface, displacement increases continuously over time and reduces with depth and dissolution of gypsum reduces with depth.

2.10 Laboratory Models on gypseous soils

This section considers experimental studies on gypseous soil physical behaviours using real and artificial soils.

The impact of gypsum and limestone on water movement and drainage of costal alluvial soils was considered in the study of Saini (1971). A plexiglass tank (tank size is 125 cm x 10 cm x 52 cm) was used. A layer of 49 cm soil in a column was prepared for various conditions of prepared soil. Experiments were carried out on soil alone and two soils mixed thoroughly with gypsum and limestone. Sodium and chloride leachate contents were recorded over 21 days. The results showed that the addition of gypsum and limestone improved soil drainage, which was accompanied by a greater removal of sodium for treated soil compare with untreated. More sodium was removed after gypsum addition compared with limestone addition, due to the property of sodium to exchange with calcium of gypsum.

Time and heating influences on geotechnical properties of artificially-prepared gypseous soil were highlighted by AlNouri and AlQaissy (1990). The soil samples were with 1%, 9%, 18% and 38% gypsum content. Columns of gypseous soils prepared in plastic pipes with 150mm diameter and 600mm height. Then, these samples were put in distilled water and gypsiferous solution with heating applied on the top of soil columns for different durations. The study yielded that the compression index (C_C), swelling index (C_r), Cohesion (C) decreased while angle of internal friction (Φ) and collapse potential (C_p) increased on increasing of gypsum content. So, negligible time progression effect was observed on C_r. Also, leaching process is examined and found to increase the C_p and C_C. Gypsum

precipitation within the soil reduced C_C, increased C_p for very low and low gypsum content, while it reduced C_p for moderate and high gypsum content soil.

Oedometer and permeability-leaching equipments have been used to calculate soaking and washing properties of real Iraqi gypseous soils by Al-Neami (2006). Long-term experiments for 30 to 180 days were carried out. The results showed that wetting and solution of gypsum caused soil softening and decreased the number and amount of contact areas among soil particles. Soil settlement linearly increased due to washing time. Volumetric strain-time curves consist of sudden collapse and creep occurrence. Most of the compression process occurred at the first weeks of washing period and the secondary compression at the later stages.

Fluctuation of water table and its influences on gypseous soil geotechnical properties, a key point, is reported by Al-Emami (2007). Tar Al-Najaf gypseous soil from South West of Iraq was tested through a laboratory model. The model was a steel container with size of 600_L x 600_W x 500_H mm. A 50 mm layer of well graded sand was put inside the container bottom to act as a lower free draining layer and six layers (60 mm each) of prepared soil was compacted equally to the required density. The model outcomes revealed that gypsum amount decreased gradually with the fluctuation of water. Total dissolved solids, *T.D.S*, also decreased within increasing fluctuation cycles number of water table. Soil particle specific gravity increased due to washing process.

Finally, stabilization/treatment of gypseous soil was also studied through using laboratory model technique. The technique worked successfully as in the study of Al-Alawee (2001) and Abid-Awin (2004). Al-Alawee (2001) studied the impacts of width and thickness of treated layer with soaking process through a steel container (400 mm x 400 mm x 400 mm). Abid-Awin (2004) studied gypseous soil reinforcement through a laboratory model as a cylindrical box with size of 580 mm diameter x 650 mm height.

2.11 Dams

Dams can be of a wide variety of sizes and made from a diverse range of materials, though they are most frequently constructed from concrete or earth. Earth dams are widespread globally due to reasons of low costs and simplicity of construction (Gutierrez et al., 2003),

while concrete dams are expensive and difficult to construct for structural reasons (Agarwalk and Joshi, 1979). Each kind of dam needs to be durable and safe for a long time rather than serving to achieve the main goal of design.

Agarwalk and Joshi (1979) reported on some of highest dams globally, which are earth dams, for example; Nurek Dam (300 m, USSR), Tehri Dam (260 m, India), Mica (244 m, Canada) and Oreville (234 m, USA). Generally, dams are subject to a huge challenge during their life, principally environmental problems such as seasonal temperature variations and surface water movement.

Some dams are facing internal problems within their foundations and surrounding areas rather than their external environment. Examples on those dams include: the Mosul Dam/North West of Iraq (CENWD, 2003; Al-Taiee and Rasheed, 2009; Woodward, 2005), the San Fernando-Olive Hills and Rattlesnake Dams in California and the Hondo-Maximilian and Red Rock dams in Oklahoma (Maximovich and Meshcheryakova, 2009). Each external and internal factor can impact on dam life, which must be carefully considered in order to or find appropriate, cheap and sustainable solutions. The most common problems facing dams are presented in the next section.

2.12 Problems associated with dams

Dam instability and loss of function can result from deterioration of the superstructure, inadequate design of the foundations or from seismicity. Many examples of deterioration are found globally and brief descriptions on some concern associated with dams' stability are presented below.

Soluble rocks is an important key issue if found in a dam's foundation. Spiegel's (1969) study, for example some collapse features were attributable to the solution of rocks, such as the dissolution of Permian rocks underlying dams at sites in Mexico. The magnitude of possible problems related to solution collapse and leakage decreased with increasing depth of Permian beds.

Studies on earth dams' problems show that the differential settlement or a deep tension crack may cause failure of the embankment of an earth dam (Agarwalk and Joshi, 1979;

Maximovich and Meshcheryakova, 2009). So, substrate collapse can occur through piping and karstification (Sherard, 1992).

A significant number of reservoirs around the globe have been damaged by gypsum karstification and demonstrate that leakage below the dam site is the most widespread problem (Cooper and Calow, 1998). Soluble substrates clearly increase the risk of dam failure (Calvino et al., 1981). They can present some geological problematic features such as springs in the Keban Dam Reservoir, and a recognizable leak, 10 m^3/sec seepage quantities, when reservoir level reached 517 m for Ataturk Dam in Turkey (Ertunce, 1999).

Gypsum dissolution issue in the foundation of dams is considered in some studies such as Calvino et al. (1981), who found significant impacts for this dissolution. They proposed that gypsum in a dam's foundation should be protected against temporary contact with reservoir water, which is not saturated with calcium sulphate. So, the presence of gypsum in the foundations of hydraulic structures in the former USSR was investigated by Maximovich and Meshcheryakova (2009). They concluded that such soluble rocks are at risk of enhanced dissolution and karst development that can threaten the structures. Similar impacts of soluble substrates in a dam's site were noticed by Dreybrodt et al. (2002), Romanove et al. (2003) and Shafiei et al. (2008).

Not only can massive layers of soluble substrates cause problems related to collapse, thin layers or lenses also may establish some notable influences on the structures built on them after their dissolution. The field and laboratory study of Fengxiang and Mingjiang (1983) on Longman dam site in China showed that gypsum seams may cause significant shear reduction due to leaching process.

Dissolution of soluble substrates is one of the problematic factors influencing the stability of dams. Uplift pressure is also essential and may cause dams collapse. Uplift pressure, which is water pressure vertically acting in horizontal cracks within the dam itself or its foundation layers, was investigated by Woodward (2005) who established that this pressure tend to destabilize the dam. It is a water pressure acting vertically upwards in horizontal cracks within rather the dam wall or the foundation rock. This factor is taken into account because of its importance in destabilize dams (Woodward, 2005).

2.13 Dam failure mechanisms

Dam failures can be summarized into five types as follows. 1) Overtopping failure due to insufficient spillway discharge capacity during floods, which is considered to be one of the most frequent causes of dam collapse. 2) Dam construction problems, internal deterioration or piping failures of embankment dams, for example the Teton Dam failure in Idaho, USA in 1976 which failed because of some faults in construction methods including using the wrong type of construction materials and methods, e.g. silt and weak compaction of fill; 3) Landslides problems which may cause a concrete dam to survive from falling into the reservoir, a landslide induced flood wave may damage the dam, or overtop it, as happened at Vaiont Dam in Italy in 1960 where 1900 people were killed. 4) Earthquake problem can certainly damage dams, complete failure of a large dam appears to be unusual because of earthquake damage, though the 1971 earthquake in California, USA caused the Lower San Fernando Dam to collapse. 5) Geological problems with dam foundation, existing of problematic materials beneath a dam might cause serious stability issues, for example substrate losing strength as happened in St. Francis Dam and bed rock dissolution beneath two dams, the Tbilisi Dam, USSR and the Saint Francis Dam, USA (Nedriga and Dem'yanova, 1986).

2.14 Dams on gypsum-rich substrates

The presence of gypsum in dam sites has been examined by many researchers such as Calcano and Alzura (1967). They showed that gypsum may cause some problems/difficulties associated with structures stability built on it. These problems/difficulties vary considerably from seepage increase across the abutment to settlement of the structures.

The existence of gypsum can be one of the unfavorable engineering-geological situations if present in the foundations of hydraulic structures (Maksimovich and Sergeev, 1984). There are dams built on gypsum-rich substrates globally, some of them still in use but are experiencing the impact of daily gypsum dissolution, such as leakage from Horsetooth Reservoir, Carter Lake Reservoir in North-central Colorado and from Anchor Dam in Northwest Wyoming in US. Some proposed places for dams were abandoned before construction, such as Upper Mangum Dam site in Southwest Oklahoma-US (Johnson, 2008). Other dams with reported gypsum dissolution issues include the Kamskaya Dam and Bratsk

Reservoir in Eastern Siberia, Russia; EL isiro in Venzuela; Alloz San Loren, Estremera and San Juan Dam in Spain; Mosul Dam in Iraq; Poechos Dam in Peru; Huoshipo Reservoir, Yangmazhai and Mahuangtian Reservoir in China, Baypazinsk Dam in Tajakistan, Tange-Duk Reservoir in Iran and the Yerevan Dam in Armenia. In order to know more on this condition, some of these dams are presented here.

The possible factors facing the stability of dams constructed on soluble substrates were studied by Noneveiller (1982). He listed them as percolation and seepage of impounded water from reservoirs and through the foundations of dams, bearing capacity stability and deformation of foundation of heavy structures. After that, the study of Yilmaz (2001) on gypsum and anhydrite properties revealed more factors influencing the stability issue of dams. He showed factors such as temperature, time and percolating water are the factors controlling gypsum dissolution and lead to chemical effects on cracks, which are significant in dams' sites. Increased dissolution in cracks can cause karst and might result in dam collapse.

Time, as an important key point for a dam on soluble substrates, has been investigated by James and Lupton (1978). They found that gypsum and anhydrite solution with time in the foundation of Poechos Dam, China can cause various problems. These problems can increase seepage flow rates, unacceptable settlement and formation of caverns and disintegration of calcium sulphate cemented conglomerates.

Gypsum karst is an important factor influencing the stability of dams if found in their abutments or foundation. It can compromise a dam's capability for water holding in its reservoir, allowing water to pass through, around or under the dam (Johnson, 2008). Because of the significant role of gypsum karst, a variety of studies have been conducted as shown below.

Pearson and Hurcomb (2002) studied some US dams constructed on soluble layers and their reservoirs in order to discover their problematic existing features. Some important features were discovered such as sinkholes formed at the south end of Horsetooth reservoir, and seepage increased dramatically and 4 cubic feet per second of seepage is nearly saturated with dissolved gypsum at Carter Lake Dam.

Johnson (2008) showed that unnoticed karstified gypsum occurred underneath the Quail Creek Dike in South West Utah, USA, causing the terrible failure of this embankment. The failure happed in 1989 because of water flowing. The mathematical models done by Dreybrodt et al. (2002) showed that gypsum dissolution in the high hydraulic gradient formed by dams can be as fast as 1 cm/year. So, clay-fill cavities if found in pre-existing karstic zones may weaken and fail, which permit water to pour through karstic zones (as shown in Figure 2.11, which is similar to some of the locations in Iraq where samples were collected for this research as shown in Figure 2.12 below).

The degree of salinity of the saturation water has also been examined in some studies such as Kaveh et al. (2011). They calculated the saline water effects on gypsum dissolution process. NaCl was added to the water of saturation in order to test its impact on gypsum dissolution. They modified the experimental method used by James and Lupton (1978). Their study showed that: increase of solvent chloride salinity increases the dissolution of gypsum and decreases the dissolution rate constant until cycle 4. After cycle 4 dissolved NaCl increase leads to a decrease in the quantity of dissolved gypsum, which results in gypsum precipitation.

Precautions before construction of a dam on soluble substrates might be useful. On this matter, Nedriga and Dem'yanova (1986) mentioned in their study some precautions to be done to control the dissolution process of dams' foundation contain soluble rocks. With these precautions, the dams' stability can be safe. These precautions were: 1) providing an inspection gallery and 2) an extensive network of monitoring equipment in order to observe the seepage flow and detect the centers' of leaching.

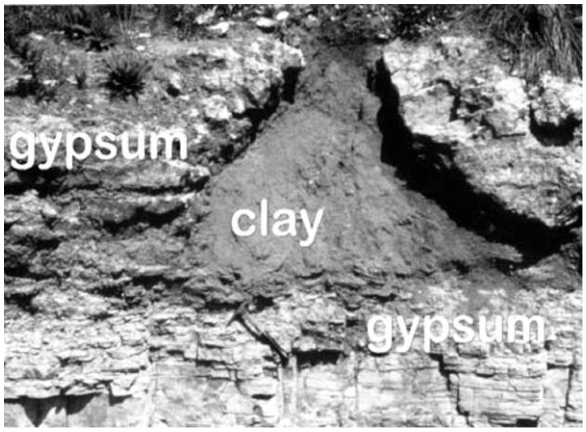

Fig. 2.11: Gypsum-karst opening, filled with clay deposits (taken from Johnson, 2008, Image area is 2 m wide; hammer is at bottom of clay, center).

Fig. 2.12: Gypsum-karst opening, filled with clay deposits (Picture taken in December 2009, Northern Iraq Gypsum-rich substrates; ruler is in the centre of photo).

2.15 Mosul Dam-North West of Iraq

Iraq has seven on-river dams in service, including the Mosul Dam (Al-Faraj, 2005). The dam was constructed in 1980 on the Tigris River near Mosul City, north Iraq. It provides flood control, hydro-electric power generation and most of the major irrigation works in the country. The Mosul Dam is the biggest Iraqi on-river dam, which has an 11.11 billion cubic metre storage capacity with a live storage of 8.16 billion cubic metres.

The Mosul Dam, Iraq (Figure 2.13) provides a case example of a massive dam built on gypsum-rich substrates. As with water-retaining structures found on similar substrates elsewhere, dissolution threatens the stability of the dam.

The Mosul Dam Safety Inspection Team, CENWD, was chosen in order to investigate on it. They showed that the main features of the Mosul Dam are: an approximately 3.4 kilometre long earth filled dam, powerhouse, bottom outlet, concrete-lined spillway and fuse-plugged secondary spillway (CENWD, 2003).

The embankment of Mosul Dam is 113 metres high contains graded filters in the upstream and downstream shells and the total volume of material in the embankment is reported to be approximately 37.7 cubic metres. The embankment has a crest elevation of 340 m and upstream and downstream slopes measuring 1V:2.5H. One metre thick riprap covers the

entire upstream slope. The minimum operating pool elevation is 300 m, maximum operating pool elevation at spillway invert is 330 metre, active storage is over 8.1 billion cubic metres and total storage at maximum operating pool volume is 11.1 billion cubic metres (CENWD, 2003; Al-Faraj, 2005; SIGIR, 2007; Al-Taiee and Rasheed, 2009).

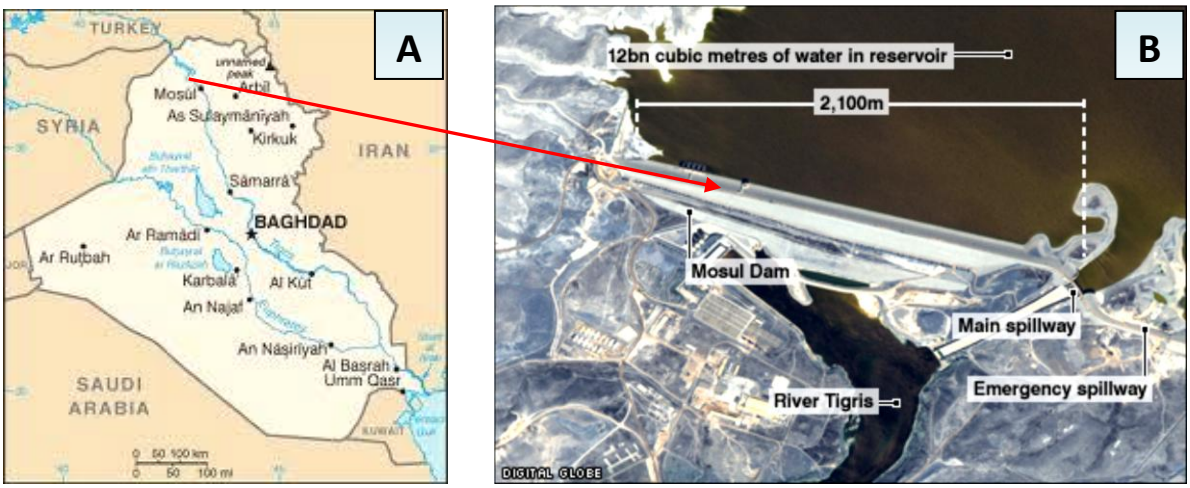

Fig. 2.13: Mosul Dam, Northwest Iraq (plate A, Iraq Maps & Mosul Dam www.google.co.uk downloaded on 20-02-2012; plate B from BBC news, Internet URL: http://news.bbc.co.uk/1/hi/world/middle_east/7070706.stm, downloaded on 30 November 2011.).

2.15.1 Mosul Dam Problems

The Mosul Dam's foundation is very poor from a geological standpoint and, due to the large fresh water reservoir and the associated movement of groundwater, dissolution of gypsum and anhydrite in the foundation and abutments with existing of fresh water has occurred continuously since construction (Kelley et al., 2007) (see Figures 2.14, 2.15 and 2.16 below).

Karstic features, as a key point, have been found in the foundation of the Mosul Dam. From the report of SIGIR (2007), caves in various sizes and shapes exist underneath the Mosul Dam, especially in the mid-line under the centre of the dam and close to the upstream area underneath the reservoir (see Figure 2.14 below). Sinkholes were recognized also in Mosul Dam site (see Figure 2.16 below).

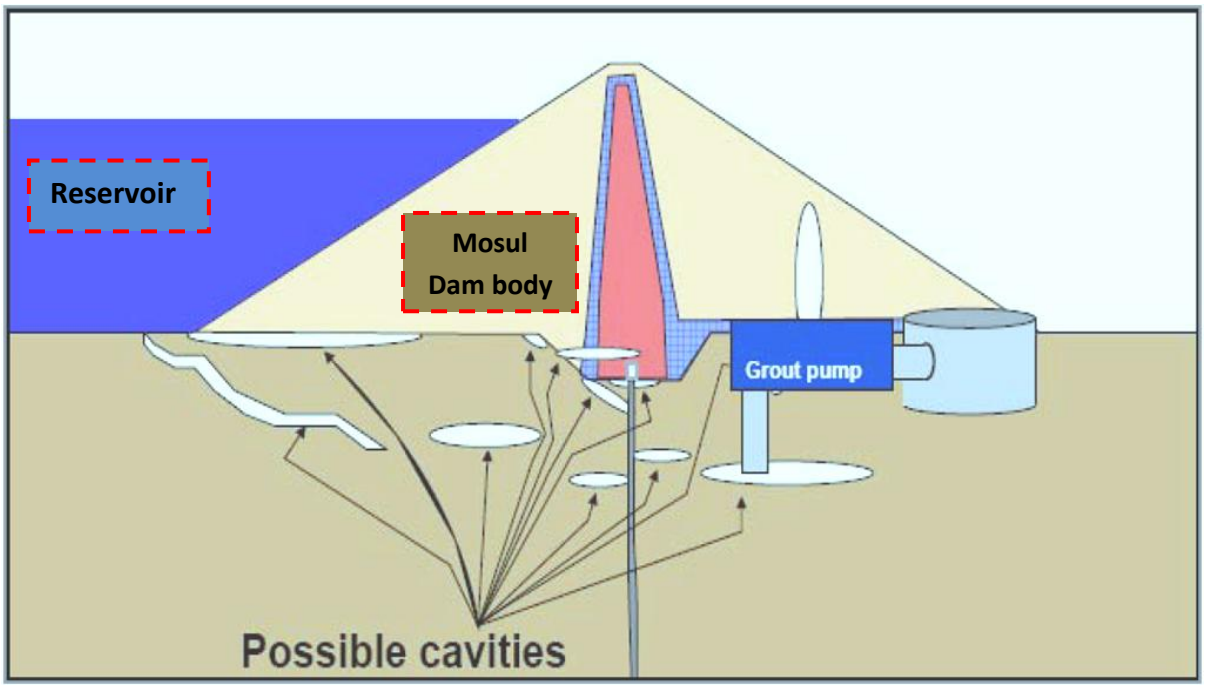

Fig. 2.14: Possible cavities underneath Mosul Dam, mostly close to the reservoir side (from SIGIR, 2007 report).

On the same matter of problems of Mosul Dam, different features and states were recognized. These features are: gypsum and limestone exist in many places in the dam body and reservoir; anhydrite and gypsum bedding is present in the dam's foundation, which are fairly soluble in water and capable of forming varying number and sizes of solution cavities; large earth settlement approximately 100 m upstream from the dam centre line; substantial seepage occurs along both sides of the concrete chute of the spillway; dissolution is happening at quicker rate than it did before construction due to the present of reservoir; the quantity and speed of dissolution in the east abutment increases when lake is at or above 318 m; all low elevated lands showed great deal of wetness during the start of the nineties decade of the last century and the lake was under a close level monitoring; serious problems may be caused by environmental factors in the semi-arid region of the Mosul Dam site, which is facing impacts of existing Tigris River fresh water and semiarid region variable temperature (Abbas et al., 1990; CENWD, 2003; Kelley et al., 2007; MESF, 2007; SIGIR, 2007; Johnson, 2008; Al-Taiee and Rasheed, 2009).

In an attempt to address the dissolution significant volumes of grout have been injected as part of a continuous remediation program since 1985. However, problems still exist and the risk of dissolution-induced collapse may be increasing (Saeedy in MESF, 2007). Saeedy showed that the dam suffered problems since its first construction; even continuous process grouting seems has never solved the problem and may push the situation to further deterioration of the foundation layers and the dam itself. He suggested that further deterioration may be caused by the continued grouting, which is causing the gypsum veins to get larger with time.

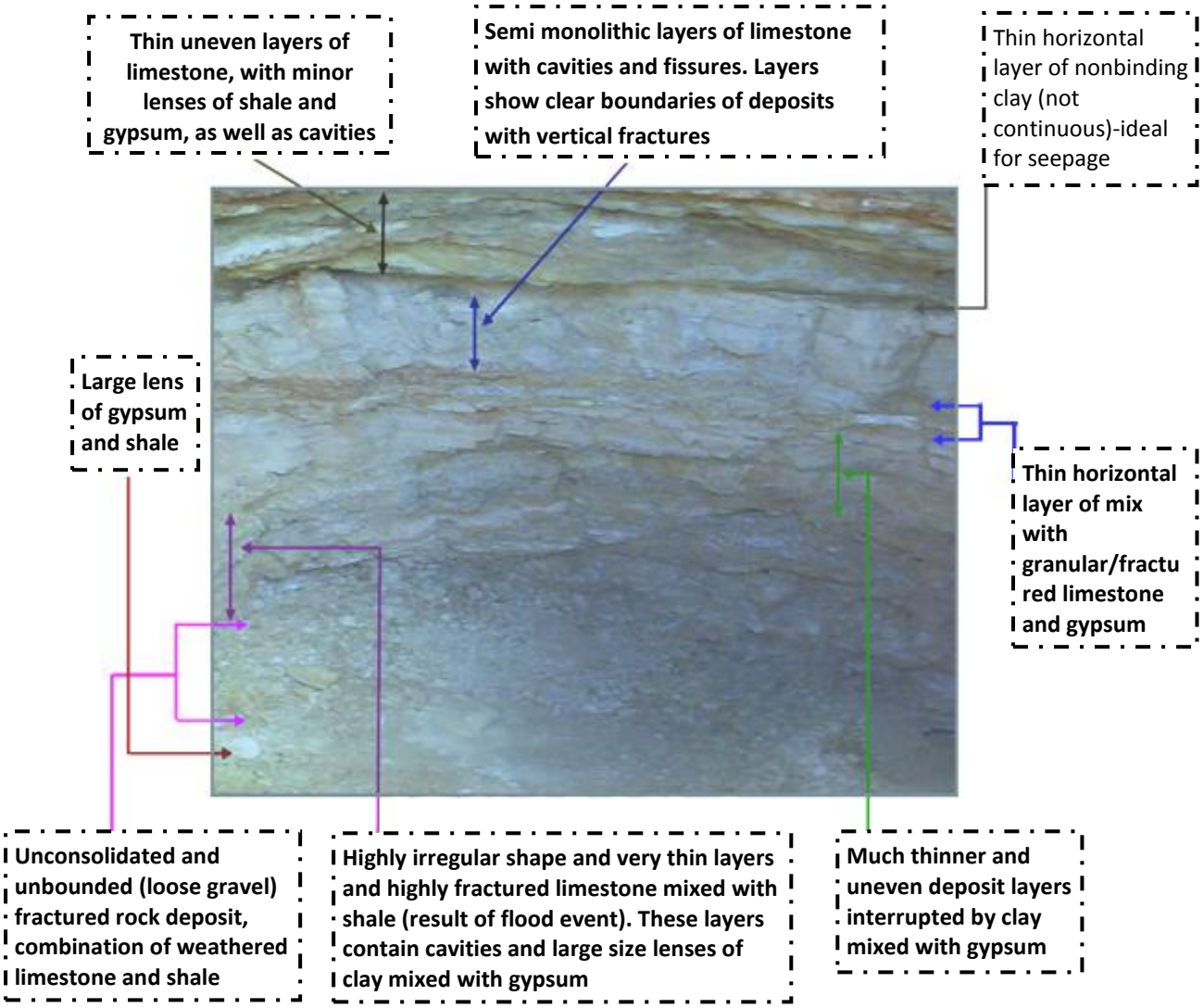

Fig. 2.15: Sample of Mosul Dam Foundation substrates, (from SIGIR, 2007). Note the various gypsum kinds' distribution like lenses, large size lenses of gypsum with clay. Other soluble substrates like limestone also found here.

Fig. 2.16: Sinkhole, 500 m downstream from Mosul Dam (one from other seven sinkholes) (from SIGIR, 2007).

2.15.2 Studies on Mosul Dam

In this section, a brief description of some published works on Mosul Dam issues are presented, which faces dissolution in its foundation. As already mentioned, up to present the dissolution process is still a problem even with continuous grouting. Therefore, it has been studied by experts from Iraq and overseas in order to investigate about the issues to build up useful knowledge and to understand their influences more, which might be then as a tool to produce helpful solutions.

Investigations have been carried out on different parts of the Mosul Dam in order to understand the instability reasons such as geomorphology and instability along the eastern bank of regulating lake, which is on an unstable area located to the north of Mosul and about half kilometre south of the dam. Along the body of the landslip, instability appears to be active, heavy rain and the elevation of water in the regulating lake due to spillway operation may be in charge of the mechanism of reactivated movement of the landslide and causes an increase in leakage water (Thanoon, 1990).

Geological and geophysical study also considered in order to establish the instability issue of the Mosul Dam. Using seismic reflection profiling and deep boreholes, Al-Saigh and Toffeq (1990), showed that pore pressure, water load and lubrication along faults were potentially

responsible for reactivating existing faults within the deeper part of reservoir and obtained that these faults are of particular possible sources of seismicity.

The study of Thanoon et al. (1990) considered the quantitative estimation of the dissolved amount and their rates of dissolution. This study showed that speed of water, hole (fissure like) diameter and solution constitution control dissolution. The rate of dissolution is significantly affected by the increased flow speed and they proposed long-term experiments should be considered regarding dissolution impacts on this dam's foundation.

The geological setting of Mosul Dam and its engineering implications were studied by Kelley et al. (2007). The foundation rocks were found to be mainly of late Miocene age, Fatha Formation, which is up to 352 m thick at the dam and has an upper and lower part. Carbonate dominates the lower part while gypsum dominates its upper element, with a limestone marker bed making the boundaries (Kelley et al, 2007, figure 5). In the upper part, claystone with gypsum and green marl were found. The subsurface rock formations in Mosul Dam area are frequent sequences, which result from depositional processes similar to those observed in modern sabkha settings.

The continuous grouting is considered in some studies on the Mosul Dam such as Kelley et al. (2007). Their study revealed that the dissolution front is moving to the east and downstream. Continuous grouting at one location causes the flow path/seepage of subsurface water to move to another location, rather than stop the seepage.

2.16 Summary

This chapter provides an overview of gypsum, the impacts of its dissolution, and examples of research into gypseous soils using laboratory models. Details on gypsum rocks and gypseous soils problems were introduced. Many studies report these problems in relation to dam stability, but questions remain over exactly how the dissolution affects strength over different time scales. This is a central issue in this thesis and the method used to address it, particularly in the context of the Mosul Dam in Iraq, is explained in the following chapter.

CHAPTER THREE: Methods and Materials

3.1 Introduction

This chapter details the field and laboratory methods and materials applied in this research.

3.2 Sample selection

As the context for research is dam stability, Iraqi samples from representative locations in Iraq were collected. Logistical and security limitations meant that this sampling could not be as extensive as wished. To allow for a comprehensive study, sites with similar gypsum rocks were identified in the UK and an artificial gypseous soil, based on Iraqi soil, was generated. Full geotechnical description is recorded for each sample and digital images are taken for all of them as well.

3.2.1 North Iraq samples

Two different places were selected from the north part of Iraq in order to collect gypsum-rich substrate samples. The first selected area in the Sulaimani governorate is rich with massive layers of gypsum rock. The location (see Figures 1.1 and 1.2) is small local gypsum mining group (Bazyan; elevation = 966m, 0495932 38S and 3945243 *UTM*). Fresh natural samples were collected from the mined layer of gypsum. The second location, Badosh (see Section 3.8.2 and Figures 1.1 and 1.2) has shallow layers of gypseous soils near Mosul Dam area. All the collected samples were labelled and their top surfaces were marked to record the samples' real attitude in the field, for use when applying loads on them. After that, each sample was put in a sealed field bag to preserve its water content and then transported to Brunel University, UK, to be used for this research. Collected samples are shown in Figures 3.1 and 3.2.

3.2.2 Central Iraq samples

Two sites in central Iraq were selected. The first one is in Doz City (see Figures 1.1 and 1.2) where both gypsum rock and gypseous soil were collected and the second one is in Al-Dour used to collect gypseous soil only. As for the samples from north of Iraq, these samples were labelled and placed in the sealed field bags in order to preserve their field properties. The central Iraq samples pictures are shown in Figures 3.3 and 3.4.

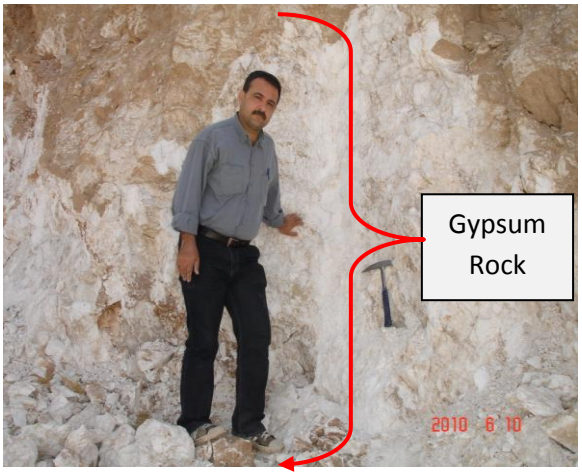

Fig. 3.1: Bazyan, Northern Iraq. Note the massive gypsum rock Unit. Block samples were collected from this area in June 2010.

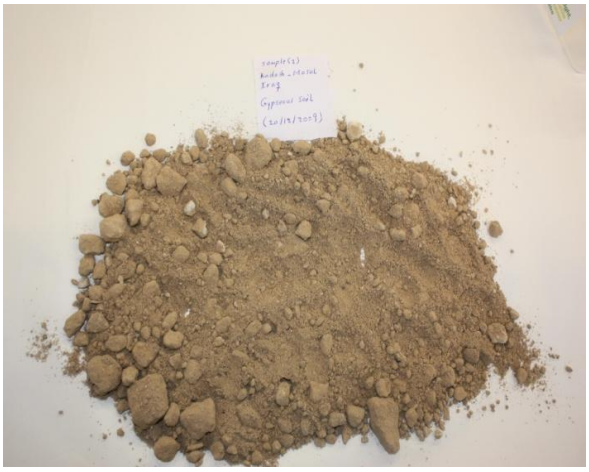

Fig. 3.2: Badosh, North West Iraq sample. Gypseous soil with low gypsum content (sample collected in January 2010). No visible gypsum lumps, small gypsum particles up to 0.125 mm diameter were present.

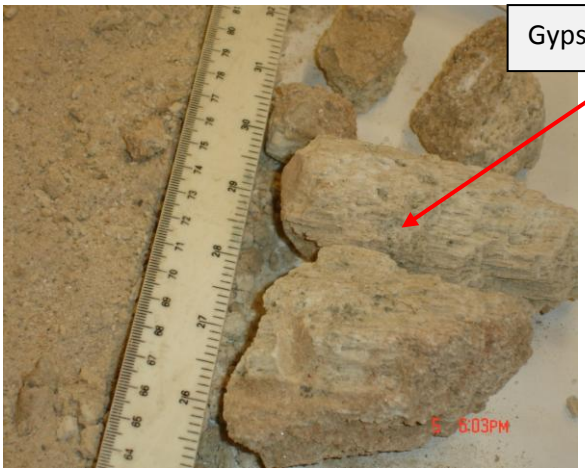

Fig. 3.3: Al-Doz, central Iraq sample, gypseous soil (collected in January 2010). Note the gypsum lumps covered by soil minerals.

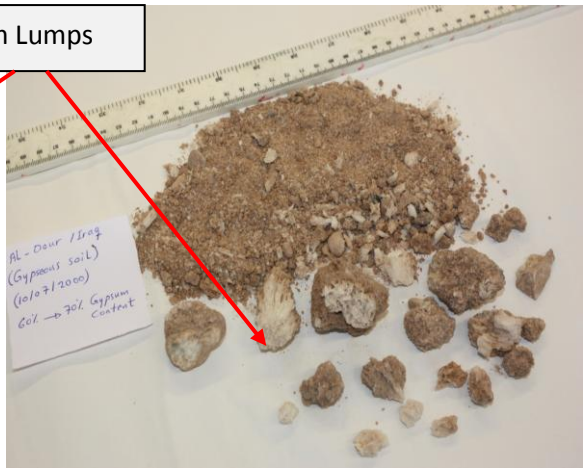

Fig. 3.4: Al-Dour, central Iraq sample, gypseous soils (collected in January 2010). Note the gypsum lumps covered by soil minerals.

3.2.3 South West Iraq samples

Samples were collected from the Tar Al-Najaf area in the Najaf governorate. Gypseous soil problems in this area have been reported by Al-Zubaidy (1998). Three samples were collected from three places in the Tar Al-Najaf area with a distance of about 100 metre between two places of them. All the samples were collected from a depth of 70-150 cm beneath the natural ground level (see Figures 1.1, 1.2 and 3.5).

With regard to geotechnical properties, which may be affected by the extraction process, all the collected Iraqi gypseous soils samples were tested in Iraq to find out their natural water content and field density before transporting them to Brunel University. These tests were done in the soil mechanics laboratory of University of Sulaimani Northern of Iraq. In addition, the same tests to other geotechnical tests were done on the same sealed samples in Brunel University.

Fig. 3.5: Tar Al-Najaf area, south West Iraq, this area is rich with gypseous soil with high gypsum content. Three samples were collected on January 2010 from this area, for depths of 70-150 cm beneath natural ground level.

3.3 UK Field Work

No modern gypseous soils occur in the UK because of the temperate climate. However, many places are rich in gypsum-bearing rocks (Cooper and Waltham, 1999; Cooper and Saunders, 2002; Jones and Cooper, 2005). Sampling these helped address the limited availability of Iraqi gypsum noted above and to supplement those collected in Iraq. From the

UK, two different places were chosen; Aust Cliff and Bantycock Gypsum Mine, to collect the proper gypsum rock samples (see Figures 1.6 to 1.10).

As there are no gypseous soils in the UK, and because of the difficulty in transporting samples from Iraq, it was decided to prepare artificial soil based on the characteristics of the collected Iraqi gypseous soils samples.

3.3.1 Aust Cliff samples

Aust Cliff (see Figures 1.6, 1.8 and 1.10) features gypsum rock lenses and thin layers similar to some sites in Iraq. A variety of gypsum rock samples were collected in November 2009. The distribution of this cliff's gypsum layers are shown in Figures 3.6 and 3.7 below:

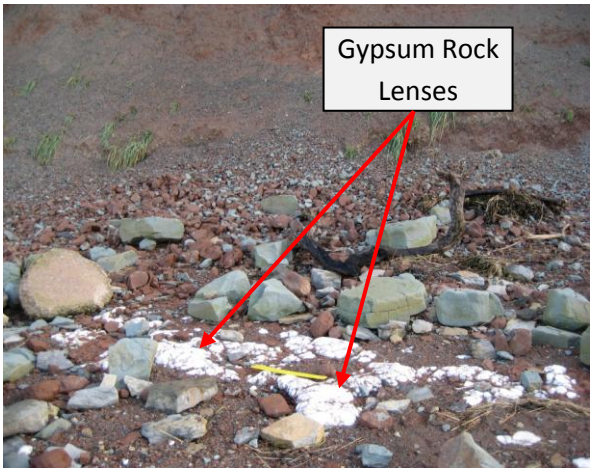

Fig. 3.6: Aust Cliff, UK area. Note the distribution of gypsum lenses exposed on the foreshore. Photograph was taken in November 2009.

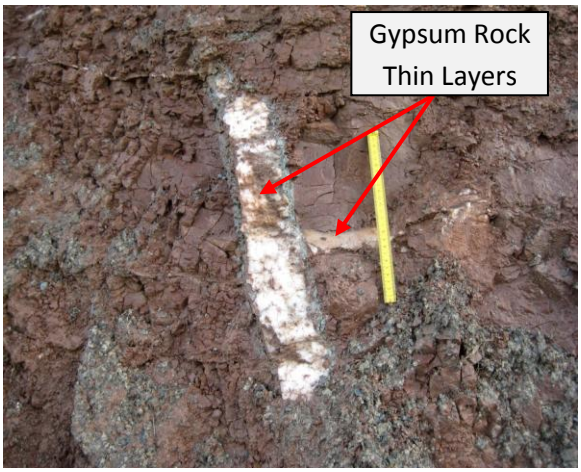

Fig. 3.7: Aust Cliff area, UK. Note the vertically oriented gypsum layer among other soil minerals, mostly clay. Photograph was taken in November 2009.

3.3.2 Bantycock Mine samples

Bantycock gypsum mine is an important source of gypsum (see Figures 1.6, 1.7, 1.9 and 3.10) for the UK community to prepare many building materials. The high quality gypsum in this mine occurs in the highest strata of the Triassic Period (Norian) Mercia Mudstone (see Figure 3.10) in the Cropwell Bishop Formation (Worley and Reeves, 2007). It opened in 1982, closed in 1993 and reopened in October 2007 (Bantycock Mine Group, April 2010;

Worley and Reeves, 2007; OUGS Field Visit, 2008). Sufficient block samples for all the laboratory experiments were collected on two separate visits in 2009 and 2010.

The site features a massive gypsum rock layer overlain by a green marl, which is itself overlain by a clay substrate. The gypsum rock locally contains marl or clay impurities within cracks. The site also features a pink coloured gypsum with marl in filling cracks.

Examples of the blocks that were sampled at Bantycock Gypsum Mine are shown in Figures 3.8 and 3.9:

Fig. 3.8: Bantycock Mine gypsum blocks. Various colours were found here with samples from each kind collected (photograph 2010).

Fig. 3.9: White gypsum rock with clay infilling existing cracks, Bantycock Mine, UK (photograph 2010).

3.4 Laboratory Work Program

Most of the sample preparation and laboratory tests were completed at Brunel University. Although conditions within the general laboratories are kept sufficiently stable to meet environmental requirements for testing, long-term tests were completed in a separate room where temperature and humidity were particularly stable.

Gypsum rock samples prepared from freshly cut material according to dimensions given in ASTM (2010) and ISRM (Bieniawski et al., 1978).

Gypseous soils samples were artificially prepared based on the properties of real gypseous soil samples collected from Iraq. The laboratory works program is shown diagrammatically in Figures 3.11, 3.12, 3.13, 3.14 and 3.15 below.

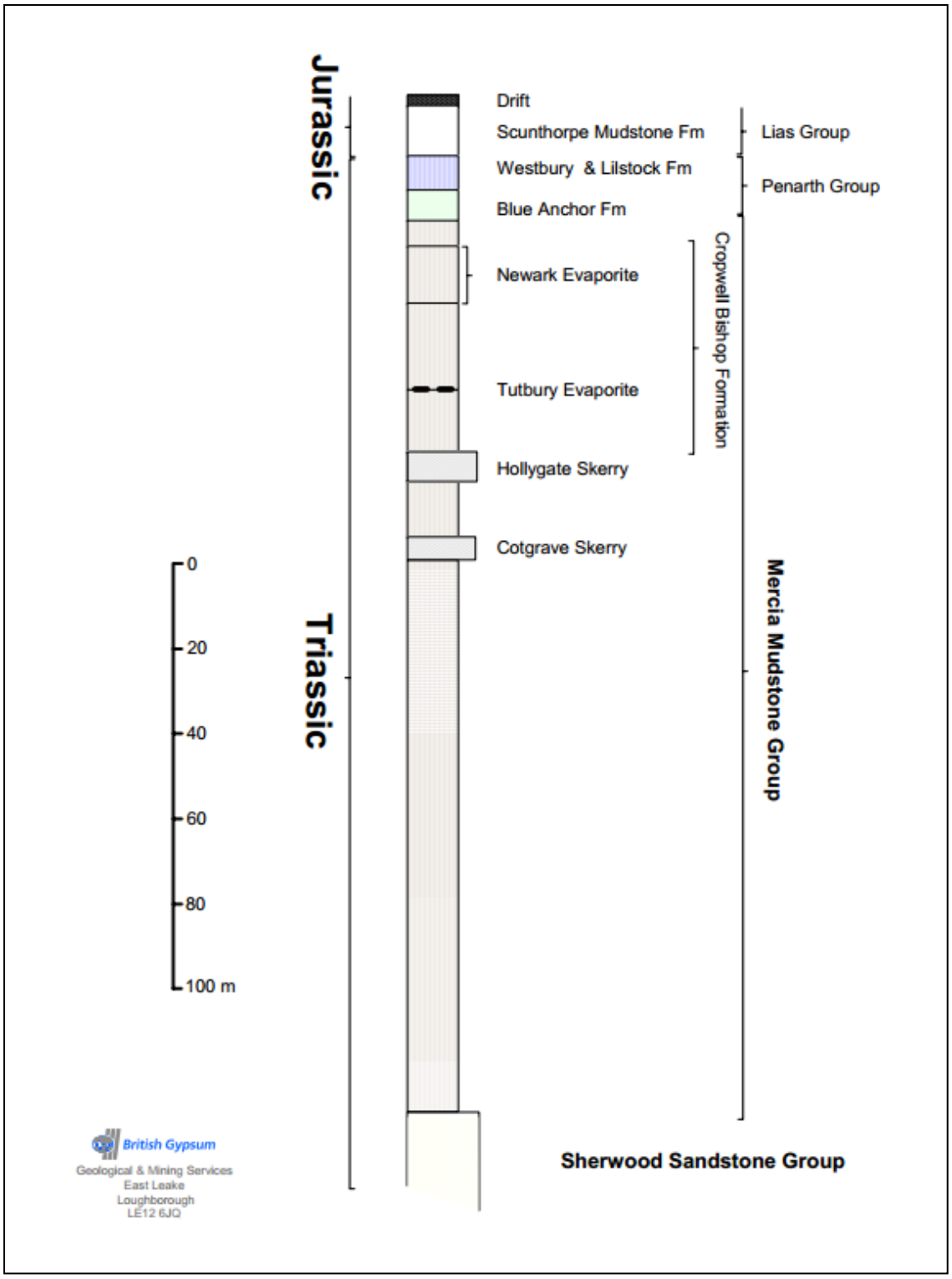

Fig. 3.10: Stratigraphic diagram (from British Gypsum Newark Mines Visit 2007, Field Guide). Gypsum rocks of Bantycock Mine appear in Newark Evaporite layer.

Fig. 3.11: Experimental works chart

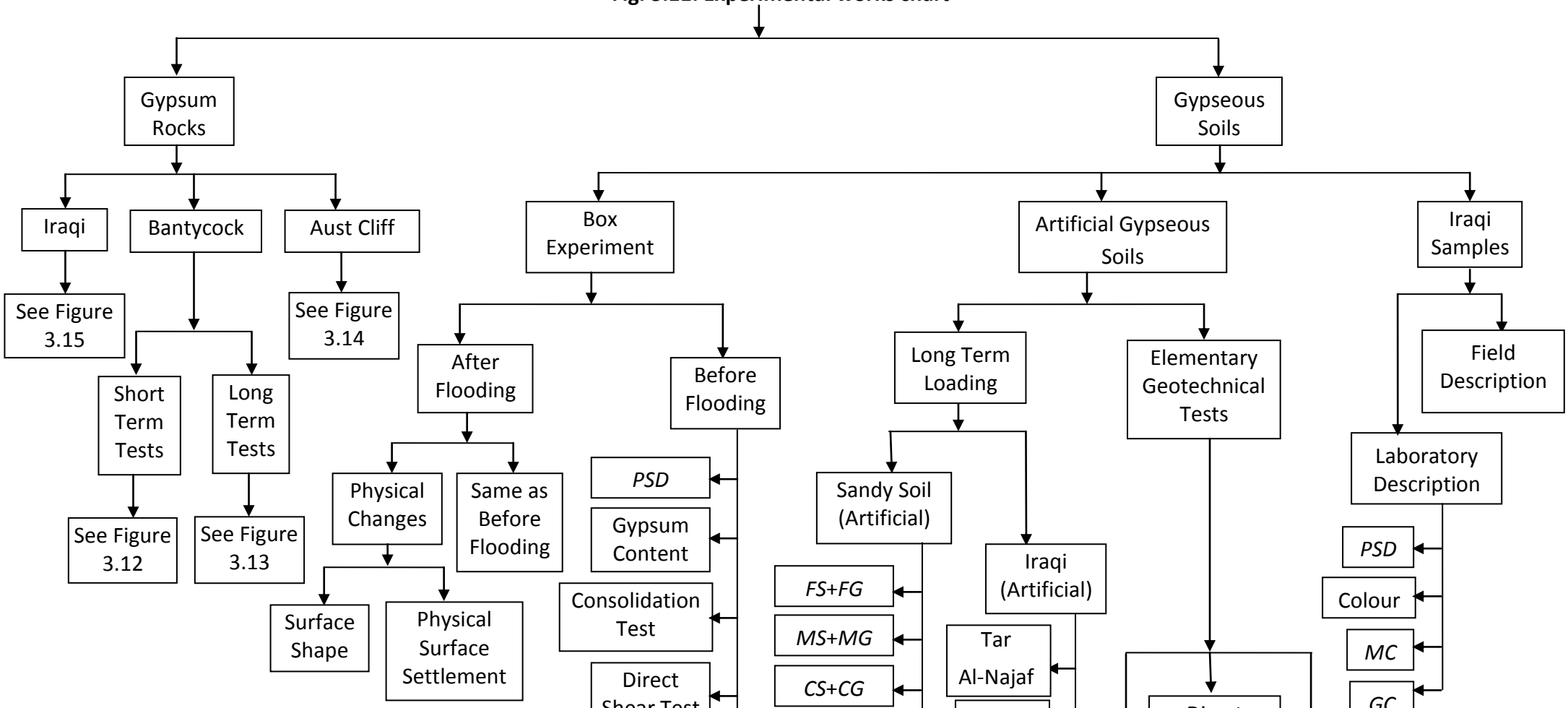

PSD = Particle Size Distribution, ***MC*** = Moisture Content, ***GC*** = Gypsum Content, ***FG*** = Fine Gypsum, ***CS*** = Coarse Sand, ***FS*** = Fine Sand, ***MS*** = Medium Sand, ***MG*** = Medium Gypsum, ***CG*** = Coarse Gypsum, ***CMFG*** = (Coarse + Medium + Fine) Gypsum

Fig. 3.12: Bantycock gypsum rock (short-term tests)

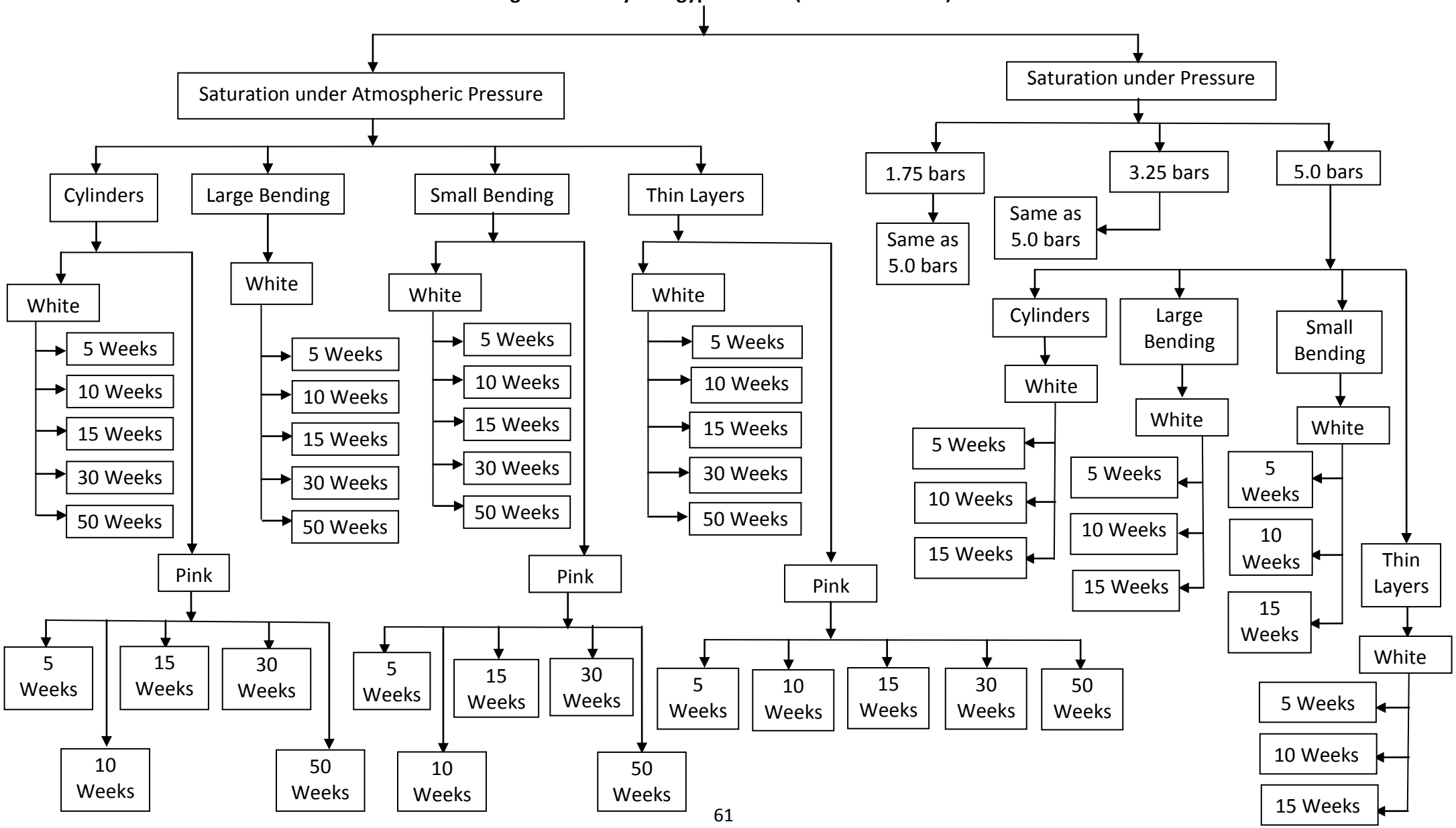

Fig. 3.13: Bantycock gypsum rock (long-term tests)

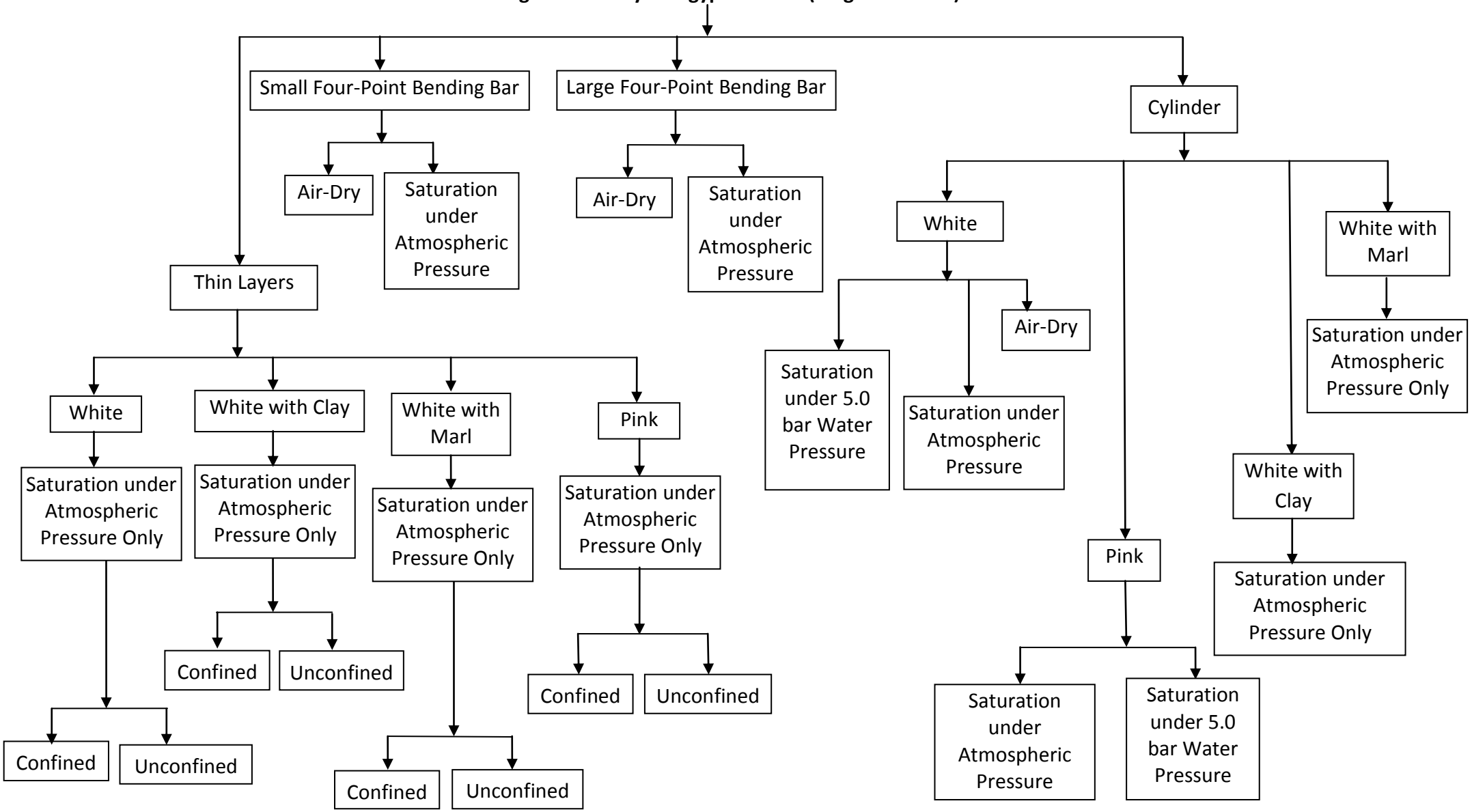

Fig. 3.14: Aust Cliff gypsum rock

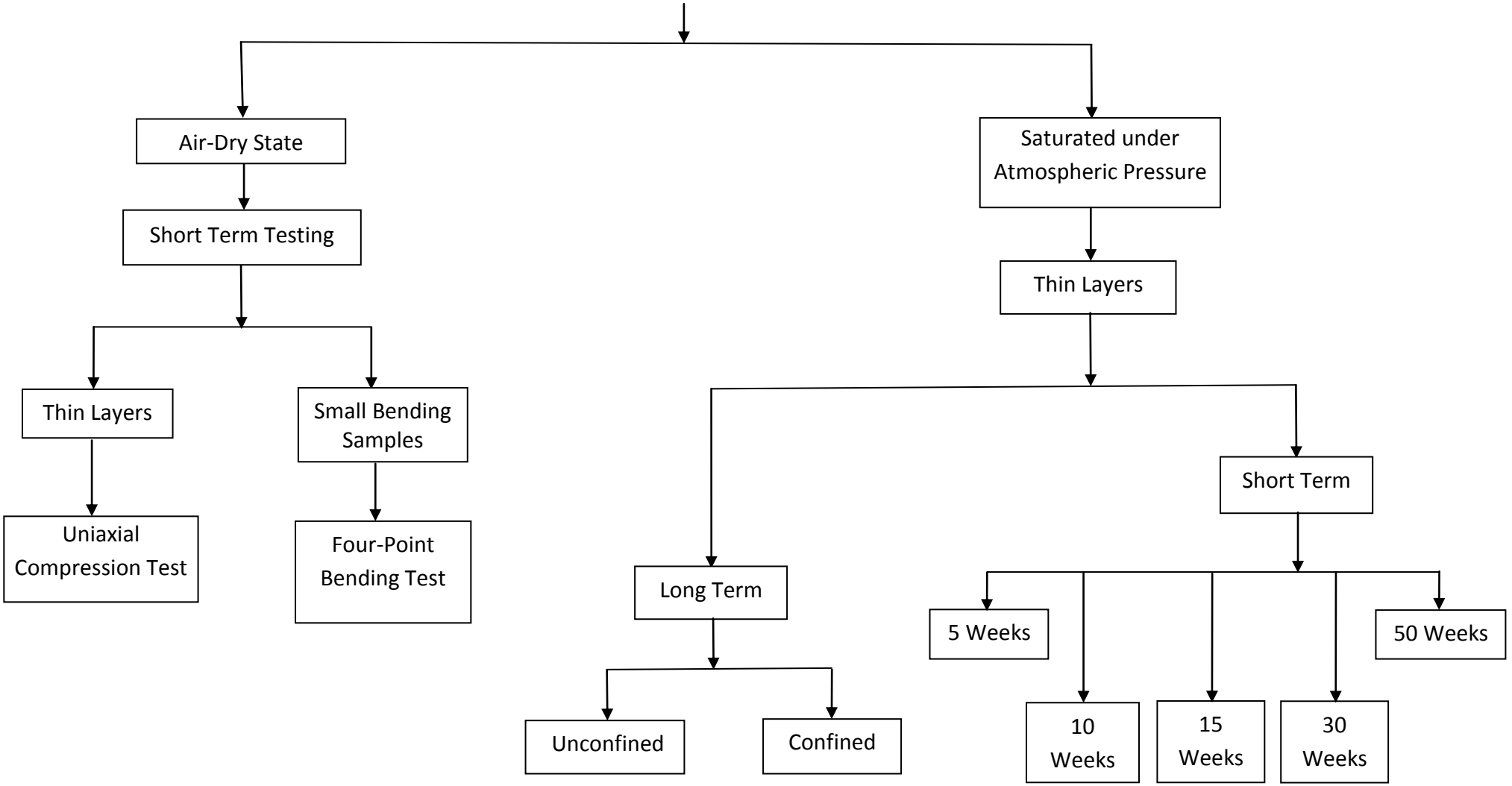

Fig. 3.15: Iraqi gypsum rock

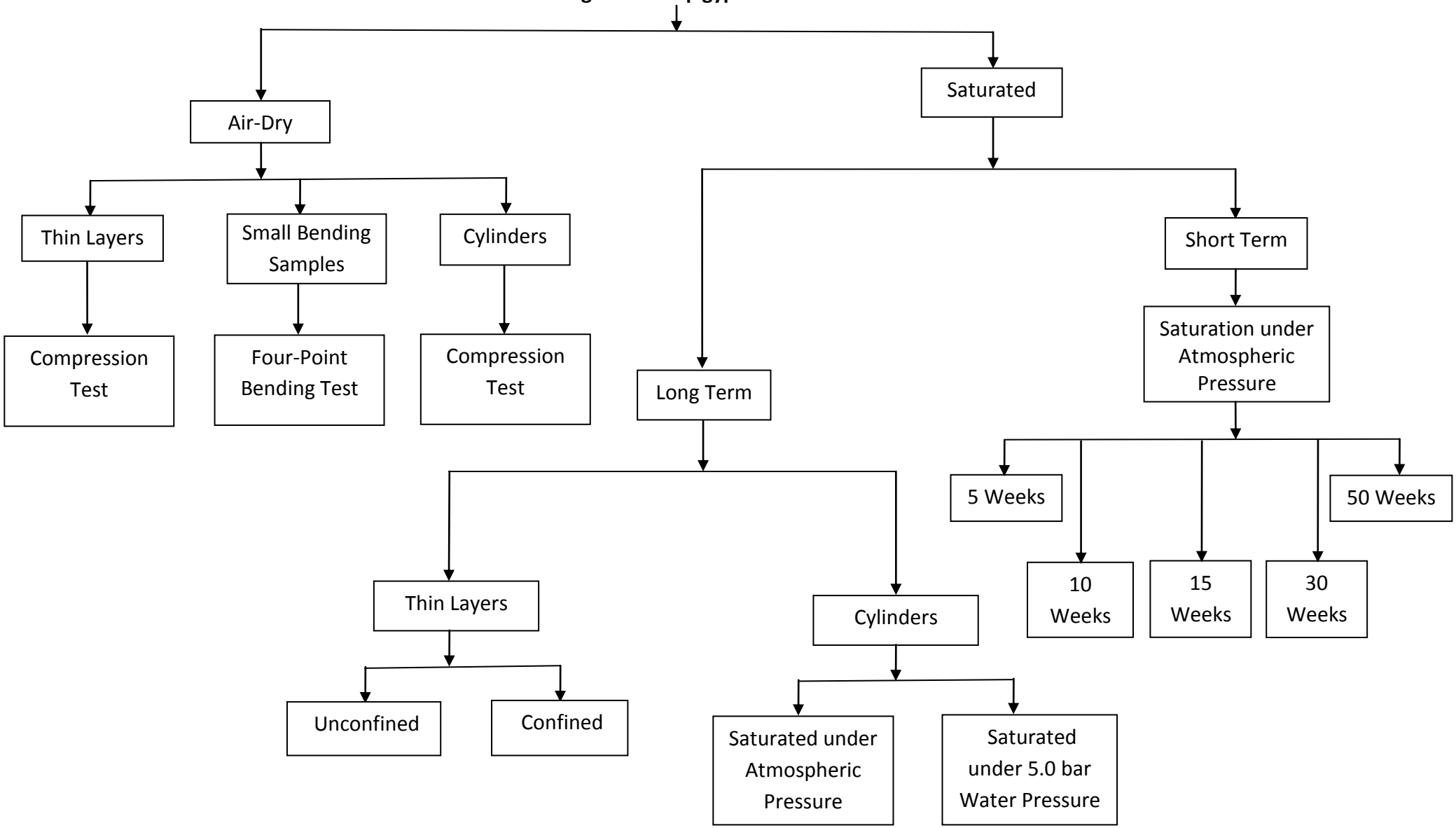

3.5 Influence of Water Type on gypsum dissolution

As dissolution is fundamentally a chemical process, it will be influenced by the characteristics of the water. This was examined in the laboratory before the more detailed tests were begun. Three different kinds of water used; distilled, tap and canal water. Tap and Distilled water collected from Civil Engineering Laboratories at Brunel University. Two samples of canal water were taken from two different locations on the Grande Union Canal at Cowley (canal-1), Uxbridge and at Maple Cross (canal-2) in-Hertfordshire. Both of the canal locations were visited twice, with more than one month between visits to get potentially different properties of canal water.

Gypsum rock was cut into three shapes assess whether sample shape affected sensitivity to dissolution. The shapes were: triangular (20 mm equal sides), cubic (20 x 20 x 20 mm) and rectangular (40 x 20 x 20 mm). These samples were prepared from Iraqi, Bantycock, and Aust Cliff gypsum rock samples. All the three sample kinds were submerged in the same container and the container was duplicated for each water type. The saturation water in each container was changed weekly, with conductivity and pH readings recorded before and after each water change. Samples weights were also recorded each week. The whole experiment lasted for two months.

A similar experiment was completed on four samples from Aust Cliff. Two of these were rectangular (regular shape, 5.0 x 3.5 x 1.5 cm) and the other two are irregular shapes approximately same size as the rectangular. These samples all had the same weights. Two containers were used for this experiment, each container contained one regular and one irregular sample. One of the containers was filled with tap water and the other with distilled water. The whole experiment lasted for one month, with the water changed each week. Sample weights were recorded via a sensitive balance (0.01 g) each week. The temperatures inside the containers were recorded each day in order to assess the temperature influences as well on the experiment.

3.6 Short-Term tests on gypsum rocks

Although the expected problems and failures with dissolvable salt like gypsum in foundation substrates might be more notable with long-term durations, short-term experiments can be

quite useful as well. They help in the assessment of material response to rapid loading as well as reveal some missed information on rock and soil behaviours. These can inform the execution of long-term tests. Rocks and soils can respond quickly to some changes and external factors affect their stability e.g. salt dissolution, saturation, compressibility and collapsibility. Therefore, it was decided to do some short-term experiments for different prepared samples in air dry conditions, and for samples which had been exposed to prolonged of dissolution, which are explained below.

So that the potential impact of water pressure on dissolution-induced weakening could be assessed, two scenarios were examined. The first case involved saturating the prepared gypsum rock samples under atmospheric pressure in containers with known volumes of water. The samples were left inside the containers for durations of 5, 10, 15, 30 and 50 weeks with the water changed every week. Three samples with the same size, colour and origin were considered for each time interval.

The second scenario was conducted through using pressure vessels to saturate rock samples and apply three different levels of water pressures on the submerged samples. The amount of water was kept constant throughout the experiments.

Due to the limited pressure vessels in the Civil Engineering Laboratories, and the limited period of this research, three durations (5, 10 and 15 weeks) were used for the second scenario. These three durations are same as the first three durations used in the first scenario. This allows for a direct comparison and hence an assessment of the role of water pressure.

3.6.1 Samples preparation

Rocks sample dimensions for compression tests have been widely studied, with a range of diverging views on the best sample size. For example cylinders of *NX* (standard diamond drill core size) diameter, uniaxial compression test were used by Karacan and Yilmaz (2000), Yilmaz and Sender (2002), Singh and Singh (1993), Brady and Brown (2004), Agustawijaya (2007), ASTM (2010) and ISRM/Bieniawski et al. (1979). Other compression samples dimensions in Table 3.1 below.

Table 3.1: Dimensions and types of tested cylindrical rock samples (compression test) reported in the literature.

Diameter (mm)	Length/Diameter	Length (mm)	Rock Type	Reference
101.6	3	304.8	Marble	Hudson (1971)
50.8	2.5	127	Sandstone	Sangha et al. (1974)
25.4 – 146.588	1.25	Not given	Cedar quartz diorite	Abou-Sayed et al. (1976)
25	3	75	Gypsum rock	Elizzi (1976)
25.4	3	76.2	Gypsum rock	Ali (1979)
31.75	3	95.25		
38.1	3	114.3		
50.8	3	152.4		
38.1	2	Not given	Gypsum and anhydrite	Bell (1994)
suggested D not less than 50 mm	2	Not given	Rocks	BS ENV 1997-2 (1999)
NX size	2	108		Karacan and Yilmaz (2000)
50	≥ 2	Not given	Rocks	Thuro et al. (2001)
NX size	2	108		Brady and Brown (2004)
50	2	100	Sandstone, granite, sandy-mudstone and granite-gneiss	Yu et al. (2005)
50		100	Salt rocks	Liang et al. (2006)
25.5	Not given	50	Sandstone	Whittles et al. (2006)
NX size	1.6 - 2.5	Not given	Sandstone and siltstone	Agustawijaya (2007)
51 mm and not less than 47 mm	2 - 2.5	Not given	Rocks	MP (2007)
50	2	100	Euville Oolitic Limestone	Eslami et al. (2010)
42, 54 and 93	1.5	Not given	Rock salt	Ozkan et al. (2009)
56.7	2.5	Not given	Gypsum rock	Heidari et al. (2011)

As aforementioned and checking the existing facilities in Brunel University's laboratories, NX = 54 mm and L/D = 2.5, which matches the minimum required range of the ISRM (1978) and ASTM (2010) standards.

Two main types of flexural tests are used: four-point and three-point bending. Published work on flexure shows that there is no recommended dimension for test samples and standards. Concerning four-point test, many studies have been done as shown in Table 3.2 below.

Table 3.2: Dimensions and types of tested rock samples (four-point bending test) reported in the literature.

Length (mm)	Width (mm)	Depth (mm)	Rock Type	Reference
4in	0.5in	0.1in	Coal Measure Rock	Price (1964)
160	20	24	Natural building stone and marble	Cardani and Meda (1999)
320	40	24		
640	80	24		
1240	160	24		
220	50	50	Calcarenite	Coviello et al. (2005)
220	60	50		
160	50	40	Gasbeton	
6 x Depth	50 mm to 3 x Depth	25 - 100	Natural stone	BS EN 13161 (2008)
300	30	15	Sandstone	Fu et al. (2008)
500	50	25	Oil Shale	
220	40	19	Granite	Aliha et al. (2009)
120	20	20	Granite	Efimov (2009)
240	48	24	Sandstone	Moonen (2009)
406.4	114.3	88.9	Synthetic Weak Rock (Sulfaset)	Cho et al. (2010)

So, concerning three-point bending, many studies have been done as shown in Table 3.3 below.

Table 3.3: Dimensions and types of tested rock samples (three-point bending test) reported in the literature.

Length (mm)	Width (mm)	Depth (mm)	Rock Type	Reference
279.4	25.4	50.8 or 76.2	Granite	Hudson et al. (1973)
180	40	20	Marble, Calcite and Dolomatic	Xeidakis et al. (1996)
42	10	10	marble	Kourkoulis et al. (1999)
150	60	20	Granite	Biolzi et al. (2001)
240	40	30		
480	80	60		
1200	200	60		
2400	400	60		
190	60	50	Calcarenite	Coviello et al. (2005)
130	50	40		
100	50	40		
70	50	25		
40	30	20		
250	50	50	Sandstone	Chen and Azzam (2007)
200+/-0.3	50+/-0.3	-	Agglomerated Stone	BS EN 14617-2 (2008)
120	20	20	Granite	Efimov (2009)
Not given	Not given	60 & 45	Sandstone, spanned 146.8 &110	Lin et al. (2009)
70	10	10	Granite and Phyllite Temper	Muller et al. (2010)
180	40	40	Sandstone	Biolzi et al. (2011)
900	200	40		

For flexural tests in this research, two sample size dimensions; 240 x 40 x 20 mm and 140 x 40 x 20 mm were decided on. The first one was easy to prepare from various block samples with or without impurities in their cracks due to its short length. Some difficulties were faced in getting the longer size from pink gypsum with impurities from Bantycock, Aust cliff and Iraqi gypsum rocks. Therefore it was decided to decrease the length to 140 mm to prevent the possible weaknesses due to existing cracks. Both kinds of bending samples have to be tested via four points bending test with different loading position for each one, which is more likely to be representative for natural rock layers situation in real world (Elizzi, 1976; Ali, 1979). Above sizes of small and large four-point bending tests are used to prepare all bending tests bars of short and long term tests.

3.6.2 Drying of samples: Air-Dry situation

After finishing the final stage of samples preparation, all samples were washed to be clean from fine materials and put in oven at 25^{o}C for between 6 and 48 hours. The samples weights were recorded every six hours in order to discover the real time for samples to get constant weights and no temperature influences happen. After 12 hours samples weights remained constant and all samples were left inside the oven for 48 hours to be absolutely sure that samples were completely dry.

Some of the prepared samples were used for air-dry testing as shown in Table 3.4 below. All these kinds of samples were tested using an Instron Universal Device with specific loading rates for each of them as detailed in Section 3.6.7.

Table 3.4: Prepared sample shapes for each gypsum rock type. Y indicates this shape was prepared. N indicates that it was not possible to produce this shape due to cracks and impurities.

Material	Cylinders	Thin layers	Small 4-point	Large 4-point
Bantycock - white	Y	Y	Y	Y
Bantycock – pink & white with clay	Y	Y	Y	N
Aust Cliff	N	Y	Y	N
Iraq	Y	Y	Y	N

3.6.3 Saturation of samples

A specific procedure for rock saturation, recommended by Hawks and Mellor (1970) was followed. Oven dry (25^{o}C) were put they put inside a vacuum desiccator to be evacuated for three hours in their air-dry condition. After that, distilled water was introduced into the desiccator while the evacuation process was still in progress, and then the submerged samples were evacuated for 24 hours. By this process, the submerged samples would be fully saturated. This same process was used by Ali (1979) to fully saturate gypsum rock samples. The system accessories are shown in Figure 3.16 below:

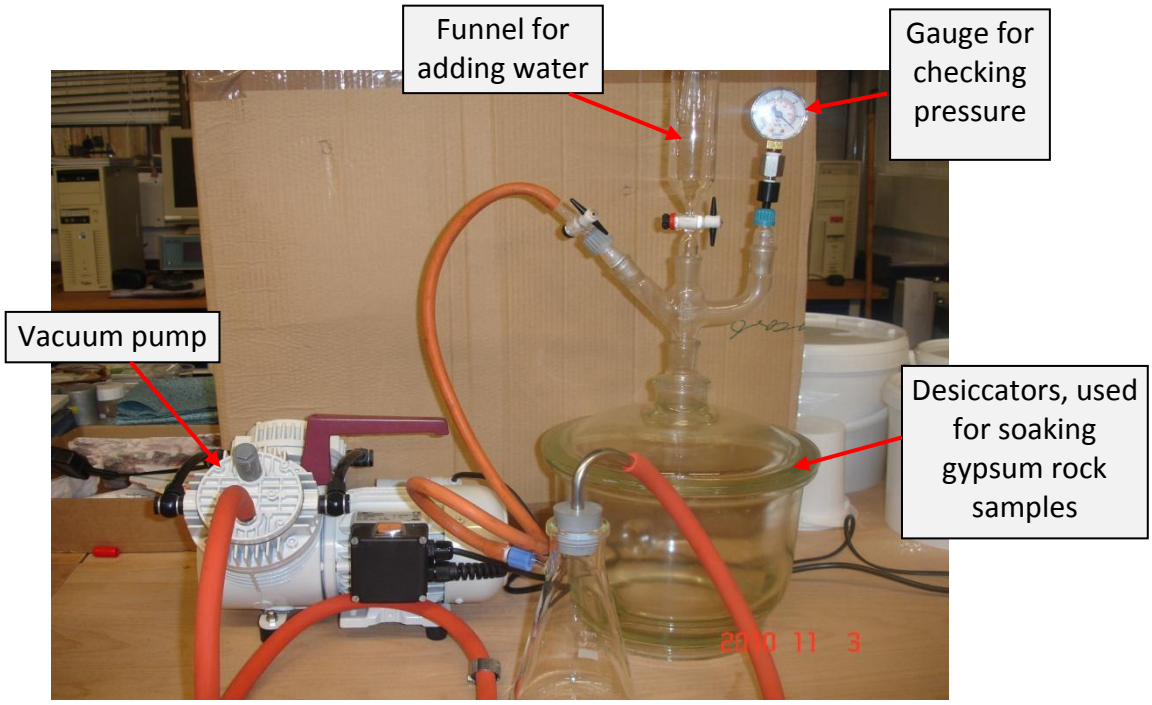

Fig. 3.16: Vacuum saturation equipment, following the method of Hawks and Mellor (1970).

3.6.4 Saturation without Water Pressure scenario

Cylinders, small four-point bending, large four-point bending and thin layers samples were placed in basins and saturated with distilled water for either 5, 10, 15, 30 or 50 weeks, with three samples used for each time interval. The water of saturation was changed each seven days, and samples weights, conductivity and pH were recorded for changed water each week.

3.6.5 Saturation under Water Pressure scenario

A limited number of the prepared samples were placed under a variety of water pressures in order to evaluate whether these samples are sensitive for water pressures. Limits in terms of project duration and the availability of suitable pressure vessels meant that only cylinders, thin layers, and the small and large four-point bending bars could be prepared from the white gypsum rock from Bantycock mine.

Three pressure levels were applied on samples and three different durations were applied for each pressure level. Three durations of 5, 10 and 15 weeks and three water pressure levels of 1.75, 3.25 and 5.0 bars were chosen for each case of applied water pressure. The

saturation water was changed each seven days, and sample weights, conductivity and pH were recorded after each water changing process.

3.6.6 Pressure Vessels

Steel pressure vessels were chosen to allow the simulation of water pressures similar to those found beneath large dams. The pressure vessels are tall cylindrical containers, the base and sides walls of which are made from stainless steel while the top is made from specific plastic material suitable for vessel conditions (Figures 3.17 and 3.18), (Manufacturer A.E.B. srl, Italy. Supplier: www.hopshopuk.com). The dimensions of the vessels are: diameter = 220 mm, height = 560 mm and internal volume for water is 15585.44 cm^3. One inlet valve located on the top surface was used to introduce air and pressurise the vessel up to 6.0 bars. An outlet valve was used to extract the water from the vessel. Samples could be placed into, and removed from the vessel through a removable gate located in the top centre of the vessel. This gate is big enough to enter the prepared gypsum rock samples by one hand.

Each vessel was partially filled with stones to provide a platform on which the introduced sample could be placed. Plastic pipes, special connections and a pressure meter were prepared to be used with the vessels in order to smoothly extract the saturation water, apply pressure on the samples and check the pressure regularly using a pressure meter. Regular checking of the gauge showed that the induced pressure was stable over time. Pressure was temporarily released to allow the water to be changed.

Three UK-made vessels were used in this research, one of them for 1.75 bars applied pressure, the second one for 3.25 bars and the third one for 5.0 bars applied pressure. All the three vessels during the experiments were placed in the same room close together and the room environment kept quite stable around 20^{o}C. Figures 3.17 and 3.18 below show one of the pressure vessels and their parts.

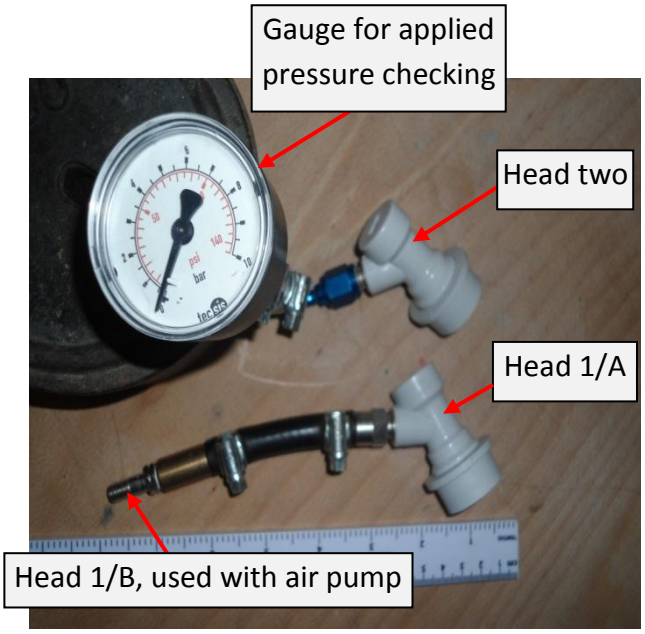

Fig. 3.17: Pressure vessel accessories, the head 1 (A and B without gauge) used for applying air pressure into the vessel, the other head (head 2 with gauge) used for applied pressure to fit the required pressure.

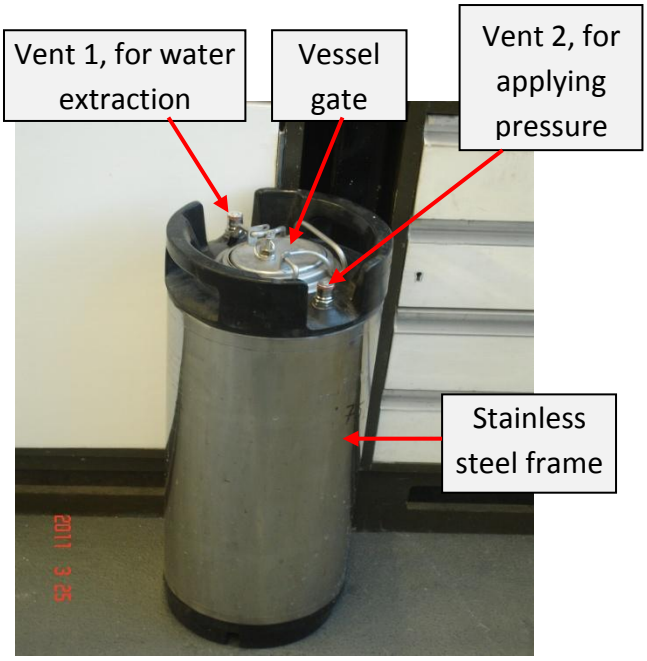

Fig. 3.18: Pressure vessel, diameter = 220 mm x height = 560 mm and internal volume for water is 15585.44 cm^3. Its opening gate allowed one hand to inter inside the vessel.

3.6.7 Loading Rates of Uniaxial and Flexural compression tests/Short-Term

In order to simulate construction of dams as a loading on laboratory samples, distance and load application trial tests were adopted. It was hoped to be in short term concern, therefore the global engineering standards were followed to find out the suitable loading rates for compression tests on cylinders and thin layers and on four-point bending bars.

ASTM (2010) and ISRM (1978) standards were used to determine exactly how to apply load on cylinders. The loading rate was adjusted using test specimens to give a time of failure for air-dry and saturated cylinders which was exactly within the given range of failure listed in both standards. This was 0.025 MPa/sec.

When thin layer samples were tested, it was discovered that the 0.025 MPa/sec is not suitable because of the obtained time of failure is close to creep. Therefore, this loading rate was reduced through doing some trial tests on thin layers. The most suitable rate for the thin layer samples was found to be 0.075 MPa/sec as this recorded the time of failure in the range required by ASTM (2010) and ISRM (1978).

A circumferential extensometer placed at the middle height of the cylinder samples was used to compute the radial strain. This tool used only with cylinders and thin layers as shown in Figures 3.19 and 3.20 below.

Finally, it was decided to keep the loading rate for the four-point bending tests similar to that used for the cylinders and thin layer discs to allow comparison. Pilot tests using 0.025 MPa/sec produced broadly acceptable results but the time of failure was very close to the allowed minimum time of failure, ASTM (2010) is from 2 to 15 min and ISRM (1978) is from 5 to 10 min. Therefore, 0.020 MPa/sec was tested on trial air-dry and fully saturated bending bars with acceptable failure times produced.

All the results from the trial tests on cylinders, thin layers and four-point bending bars will be presented in the next chapter.

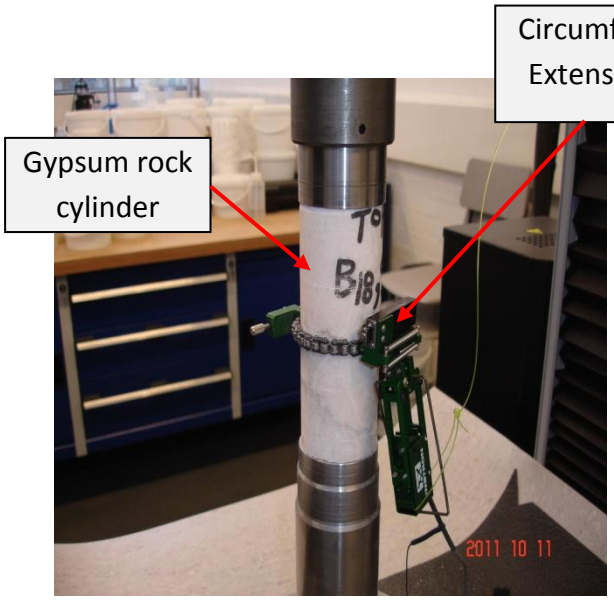

Fig. 3.19: Circumferential extensometer, used here to calculate gypsum cylinder's radial strain at the mid-height of sample during short-term uniaxial testing (diameter = 54 mm x height = 135 mm). Sample no. is B18-S1.

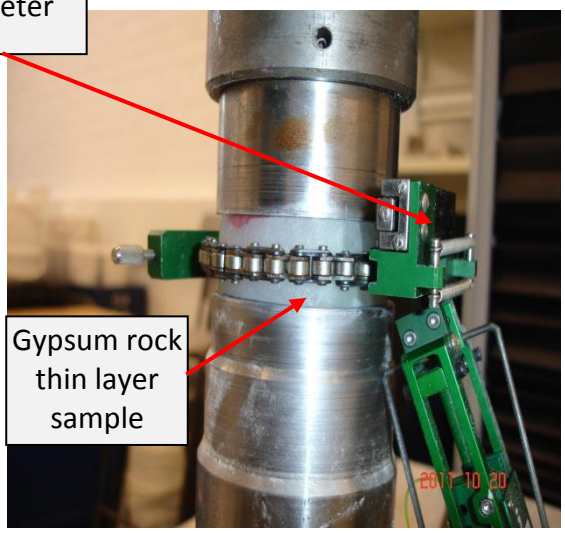

Fig. 3.20: Circumferential extensometer, used here to calculate gypsum thin layers (diameter = 54 mm x height = 20 mm) radial strain at the mid-height of the sample. Sample no. is N1.

3.6.8 Ultrasonic Observations

Ultrasonic waves used to calculate the possible changes through gypsum rocks cylinders, which can be recognized through four properties readable via the ultrasonic device (Pundit

Plus) directly, these properties are: transit time, wave velocity, path length and elastic modulus. The cylinders of short and long term experiments were tested via ultrasonic device in their air-dry and fully saturated state before and after submersion under various durations for short-term tests and after done long term experiments. So, by these ultrasonic observations it might be possible to get some changes on readings and discover the possible development of weaknesses within the cylinders due to applied pressures and dissolution with or without applied water pressure.

3.6.9 *SEM* studies and Chemical Analysis of gypsum rock samples

SEM (Scanning Electronic Microscope) and chemical analysis were conducted on the tested gypsum rock samples (see Section 4.2.6 for details). They carried out in order to find out some micro-properties of tested samples. These properties were found such as particle size distribution and particle shapes were used to correlate with other calculated mechanical properties. Therefore, by these micro-properties, chemical analysis and the mechanical properties, the big picture of behaviour of tested gypsum rock samples will be visible and the real understanding will obtain.

3.6.10 Parameters derived from Four-Point Bending test

The calculated parameters for small and large four-point bending tests for this research are derived using the test equipment shown in Figure 3.22 below, which is modified from the British Standard, BS EN 12390-5:2009, for the testing of hardened concrete. As there are no recommended standards for rock bending tests, BS EN 12390-5:2009 uses the test arrangement shown in Figure 3.21 below with the sample dimensions modified as the hardened concrete sample dimensions are unsuitable for gypsum rock bending samples. An Instron 5584 universal testing machine has been used; the flexural test format and parameters are included in a pre-installed test in this device's software. The calculated parameters for small and large four-point bending tests are shown in Figures 3.21 and 3.22 and explained further below.

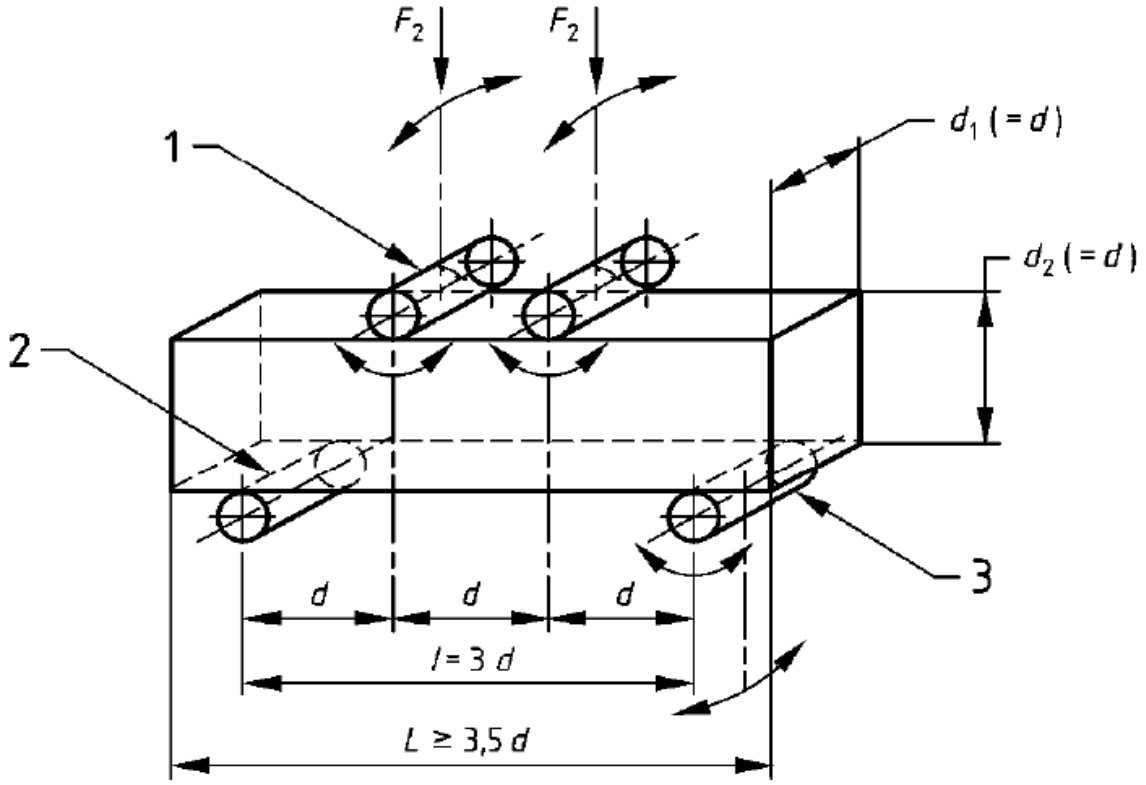

Fig. 3.21: Four-point bending test diagram for testing hardened concrete (from BS EN 12390-5:2009).

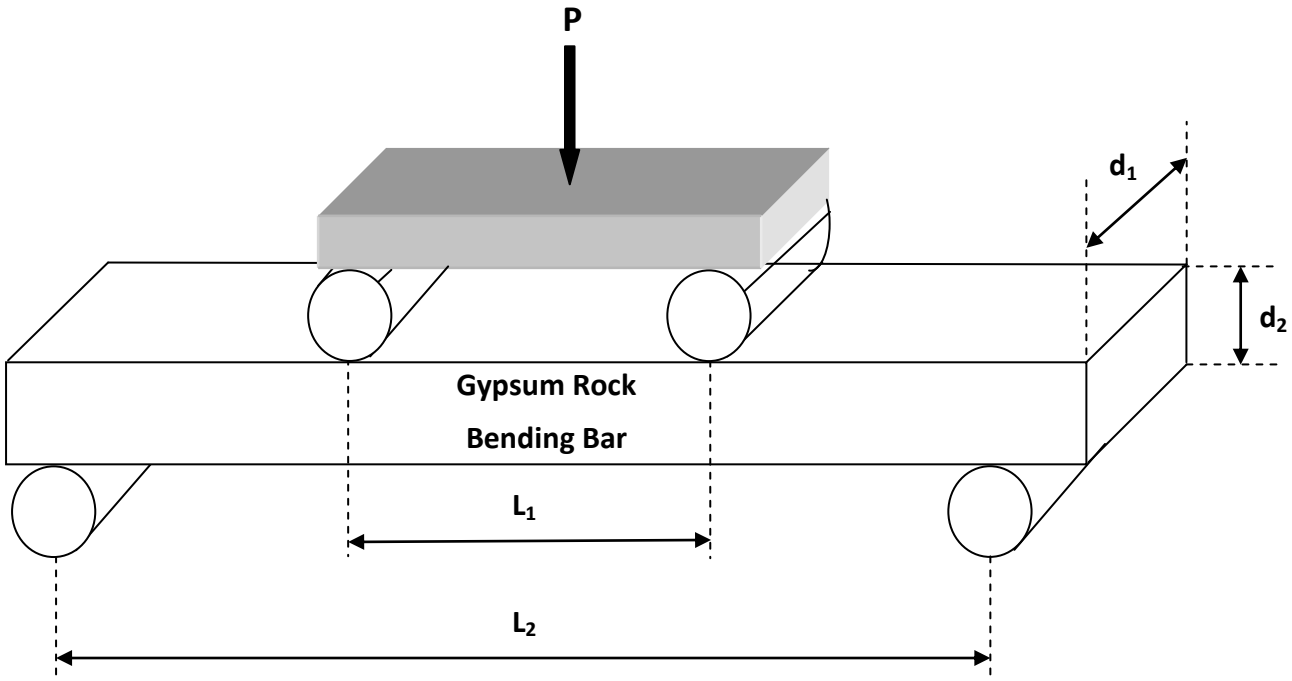

Fig. 3.22: Four-point bending test diagram for testing gypsum rock bars for this research.

As mentioned in Section 3.6.1, two sizes of bending bars were used in this research, small and large bars. Flexural stress was calculated using equation 1 below:

Flexural Stress = $(P \times L_2) / (d_1 \times (d_2)^2)$ ……..1

The calculated axial deflection parameter is the axial extension (in millimetres) recorded by the device for the vertical downward movement. For the large bending bar, L2 is equal to 200 mm, while for small bending bar L2 is equal to 100 mm and L1 is equal to 1/3 of L2 in both sizes.

3.7 Laboratory gypsum rocks work: Long-Term loading

Alteration of the mechanical properties of gypsum substrates beneath dams could occur over long periods. As a result it was decided to do long term experiment on gypsum rocks.

The prepared samples of gypsum rock in two sizes and artificial gypseous soils in one size (details of samples preparation is explained in Section 3.6.1) were tested in the same conditions of long term regards. The applied force and the whole duration of long term experiment were duplicated for each sample. So, the process of changing water of saturation and its comparable quantity also used to be repeated with each sample.

For gypsum rock cylinders, ultrasonic observations were recorded for each sample (samples in an air-dry state before the long term test and after the duration of long term duration test finished). Distilled water was used to fill the cell of each sample with one litre with known conductivity and pH. After seven days, conductivity and pH were recorded and the water was replaced with fresh distilled water. This process was repeated each week for two months for the majority of the tested samples and for one year in three samples.

For the gypsum rock thin layer, confined and unconfined, 200 millilitre of distilled water with known conductivity and pH was used. Again the water of saturation changed each week by another 200 millilitre of distilled water. Conductivity and pH reading were recorded for changed water each time. All the methods, tools and equipments are explained below.

3.7.1 Oedometer testing of thin substrate layers

Oedometers were used to examine the long term response of gypsum rocks and gypseous soils under constant load. Samples are confined within steel rings, and between porous stones on the top and bottom.

Manually-loaded oedometers were used to apply constant load on thin layers of gypsum rocks from Iraq and the UK. These oedometers amplify the stress exerted by manually-loaded weights via a lever system. This system has the advantage of being easy to use and high stresses similar to real world conditions can be achieved without risk to the operator.

Pneumatic oedometers developed by VJ-Tech Ltd were used to do long-term experiments on prepared gypseous soils.

These applied the required forces using a continuously maintained pneumatic pressure. Samples sizes and conditions were identical to those established for the manual oedometers and is the equipment was found to be totally stable in applying constant force on the sample in order to get the same stresses as present in shallow substrates within dam foundations and sites. To provide a range of results for comparison, it was decided to apply confined and unconfined conditions on prepared thin gypsum rock layers for all collected kinds. Porous stones were used in both of two conditions in top and underneath samples, therefore more dissolution action should take place within unconfined (thin layers tested without steel rings) samples and hopefully get more visible pictures in dissolution and dam stress regards.

For artificial gypseous soil samples, only the confined condition was applied, using the same applied forces, type of water used to maintain saturation and duration of experiment. Figures 3.23 and 3.24 below show the two types of device:

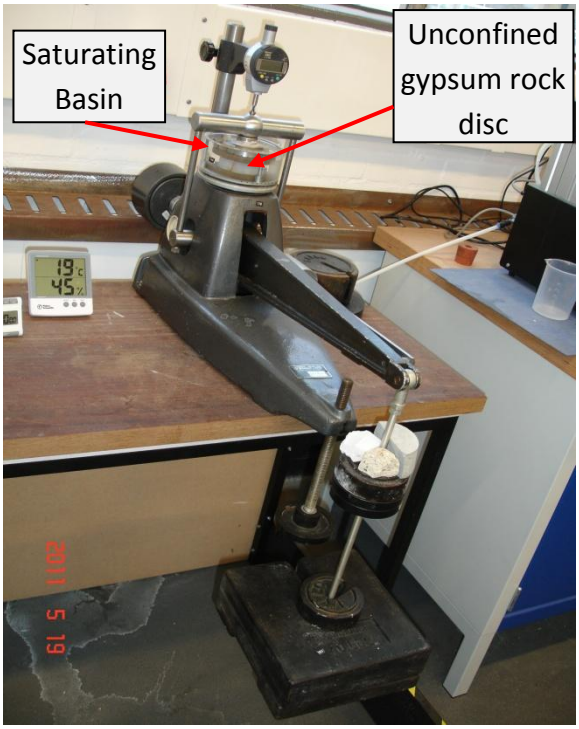

Fig. 3.23: Manual oedometer device, this was used to test thin layers-discs of gypsum rocks in size of diameter = 54 mm x height = 20 mm, unconfined test.

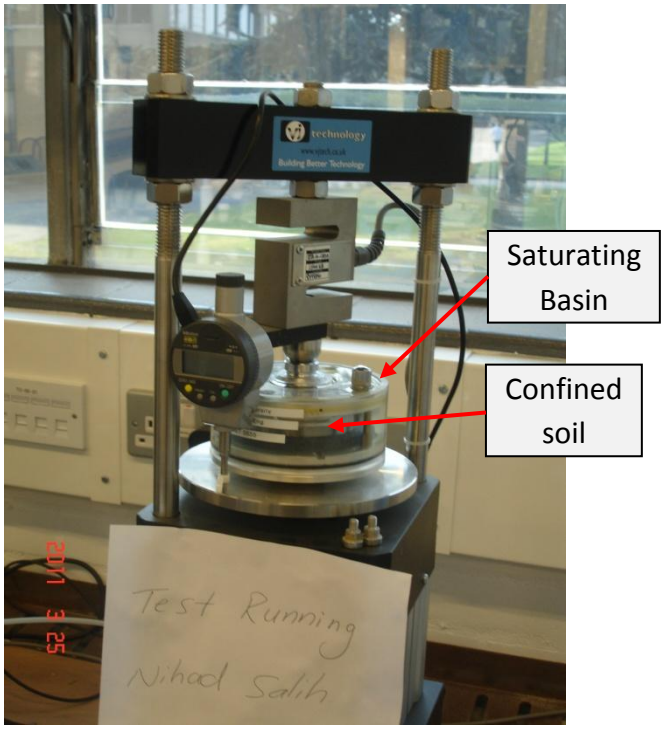

Fig. 3.24: Pneumatic oedometer device, this was used to test the artificial gypseous soils in size of diameter = 50 mm x height = 20 mm. the soil sample confined by a steel ring, the load here applied by air pressure.

3.7.2 A Modified Oedometer developed for Cylinders

The traditional oedometer is only suitable for testing small samples up to 20 mm height. So, that the behaviour of thicker gypsum layers could be assessed, modifications were made to a standard lever arm oedometer to be usable for testing cylinders with 135 mm height. To examine the possible role of water pressure, tests were completed using gypsum cylinder samples that were saturated, and saturated samples subject to surrounding pressure. These samples were placed under a high normal load so that the stress and water context were similar to that found beneath large dams. A triaxial cell was used, with some necessary changes made to the oedometer to be suitable with this cell. The two sides' pillars were made long with sufficient thickness in order to resist the applied stresses on the cylinders without any problems like buckling, even over the prolonged duration of the experiments.

In the same manner, the supporting pillar for the dial gauge holding also made in quite thick diameter in addition to the main beam as well. This beam, which is connecting to the two sides' pillars, was made in sufficient dimension to prevent any unexpected problems. The top metal bar, which holds the dial gauge, was the same origin one without any improvement because of its dimensions are quite suitable to be used with cylinders. Digital dial gauges from Mitatoyo Company were used; their potential sensitivity to temperature change is not significant if the temperature of the surrounding environment is kept stable. Therefore, the laboratory selected for these experiments was an internal room with no windows, where the temperature was stable.

The triaxial cells used for these experiments were prepared in two ways. The first one is with one inlet in the top of the cell and one outlet in the bottom of the same cell. This allowed easy replacement of the water at regular intervals. The second kind of cell was developed to be used for applying all around water pressure on cylinder samples. A small metallic cylindrical part was connected to the top surface of the triaxial cell through the air-releasing valve. The added part has three connection sides. The bottom one is used to connect with the cell through the air-releasing valve. The second one is located on the left side, which was used to supply the cell with compressed air. The third is located on the top surface of the new cylindrical part and was used to locate a pressure meter for using in the control of the applied pressure over the water inside the triaxial cell. Details of the added part are shown in Figure 3.27 below.

To be sure of the accuracy of readings from the digital dial gauges used in these experiments, one analogue dial was used with the digital one in the same device in order to check the digital dial gage reading. All the explained parts above related to the modified oedometer are shown in Figures 3.25, 3.26, 3.27 and 3.28 below:

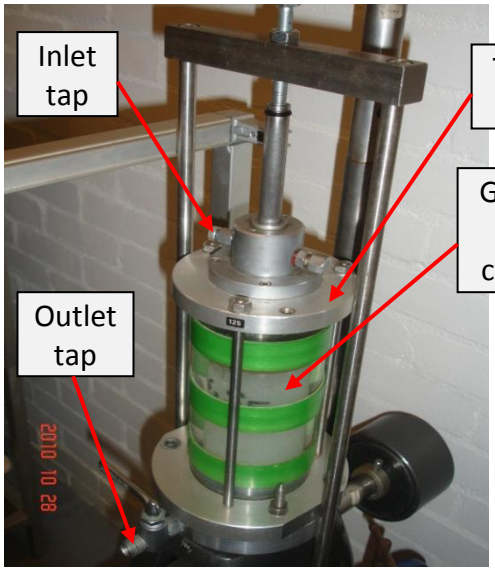

Fig. 3.25: New cell-triaxial cell used for modified oedometer device, tested rock cylinders in size of diameter = 54 mm x height = 135 mm). This cell can be used for saturation with various applied water pressures.

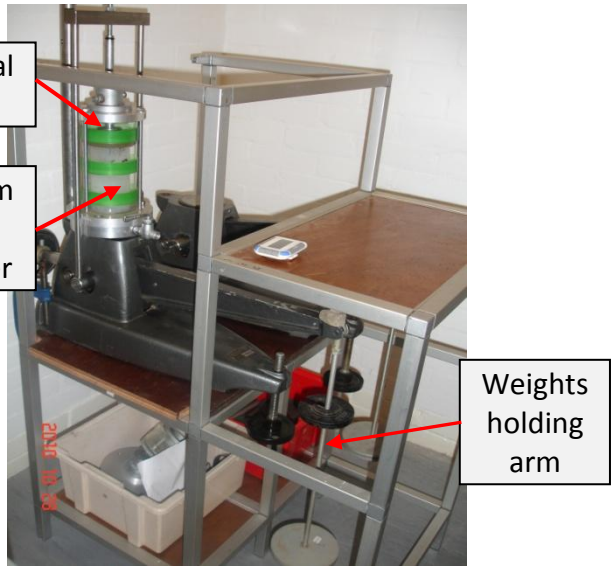

Fig. 3.26: Modified oedometer device (during experiment on soaked gypsum rock cylinder). Lever system loading was used here with manually applying loads.

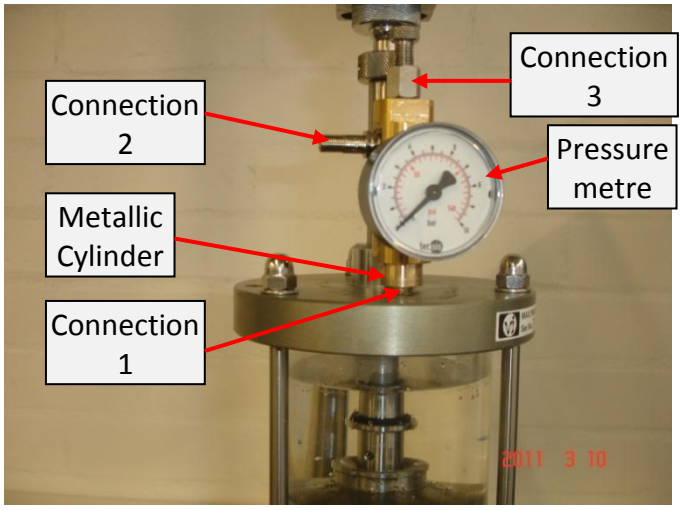

Fig. 3.27: Metallic cylinder part for applying water pressure on gypsum cylinder. Connection 1 is for connection with the cell. Connection 2 is for apply pressurized air, which controlled by the pressure metre. Connection 3 is for air releasing.

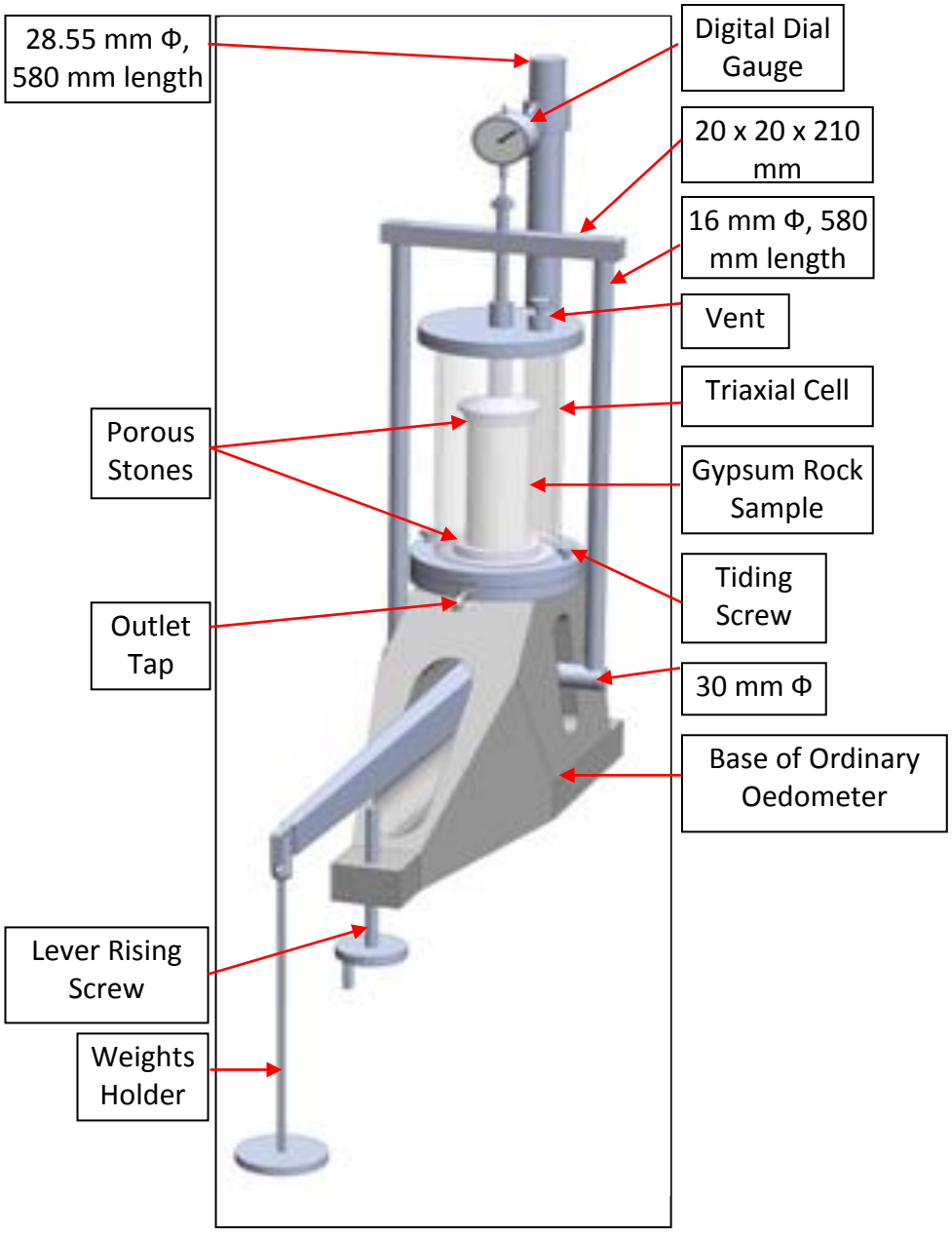

Fig. 3.28: Plan of modified oedometer for gypsum rock cylinder testing. This can be used for testing dry and saturated rock cylinders with various applied water pressures. The cylinders tested here had a diameter = 54 mm x height = 135 mm). This sketch was produced in *Solid works*.

3.7.3 Calibration of the Modified Oedometer device

The modified device was originally an ordinary soil oedometer device, which uses a lever system to apply constant loads on soil samples. The original devices have their own calibration requirements, which are provided by the manufacturing company. The new device had to be calibrated to be absolutely sure of the applied loads used in testing

samples. For this, a pre-calibrated proving ring used in triaxial tests was used to find out the applied stresses with this device. The proving ring for calibration is manufactured to use with high stress levels, much more than this required stresses. The calibrated proving ring with its held digital dial gauge was placed on the modified device base in place of the cell and the process of this experiment was applied in this stage absolutely similar to the real experiments. This action was done through levelling the horizontal metal beam, which connected to the two sides' pillars exactly on top of the used prooving ring and then from the other end of the device, which is the leaver end, loading process (see the next Section 3.7.5) was applied. Figures 3.29, 3.30 and curve in Figure 3.31 below show the calibration process and results.

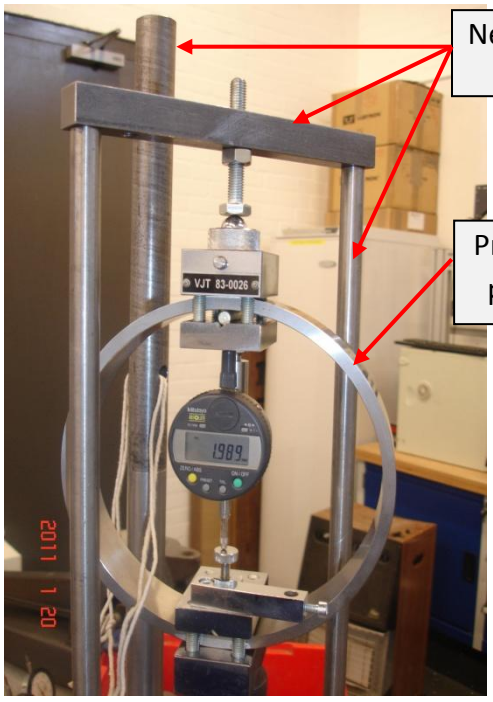

Fig. 3.29: Pre-calibrated proving ring used for calibration process of modified oedometer device.

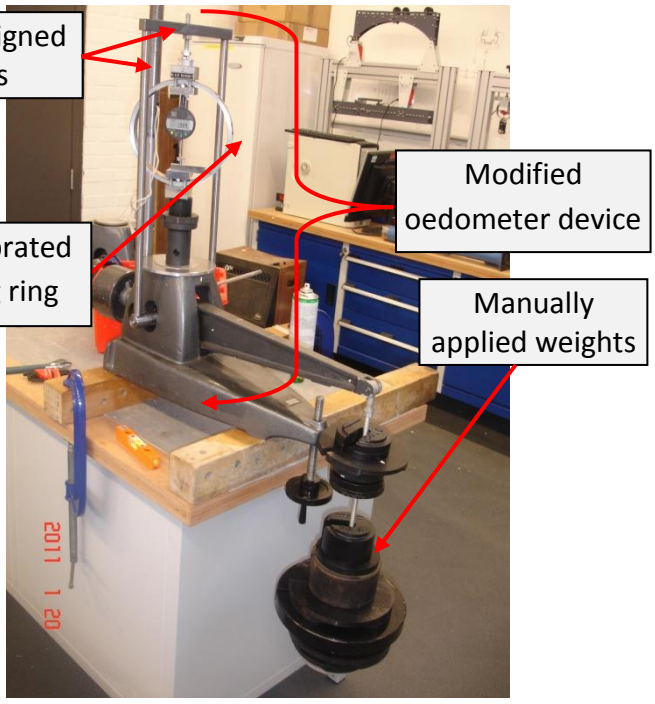

Fig. 3.30: Calibration process of modified oedometer device, shows the applied weights in to calculate the weights on the samples.

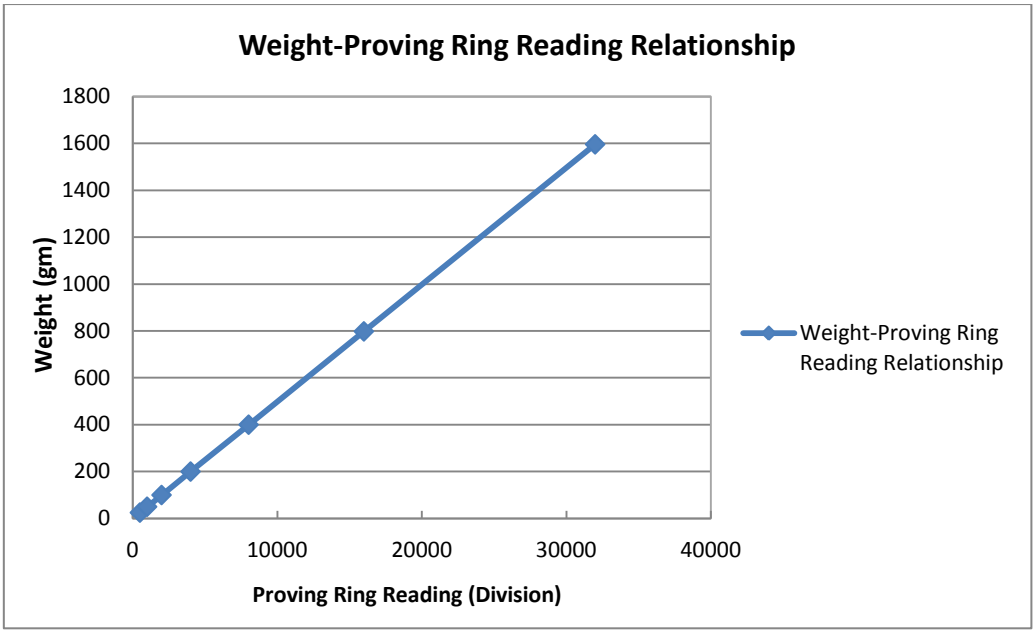

Fig. 3.31: Modified oedometer calibration curve, relationship between applied constant weights and pre-calibrated proving ring reading (the real loads on testing cylinders can be obtained from this relationship).

3.7.4 Long-Term Four Point Bending Methodology using an oedometer

A standard manually-loaded oedometer was modified to be suitable for long term four point bending experiments (as shown in Figures 3.32 and 3.33 below). The same device structure is used with the consolidation cell changed to an open stainless steel box (280 x 80 x 80 mm). This device can be used for testing dry and saturated conditions.

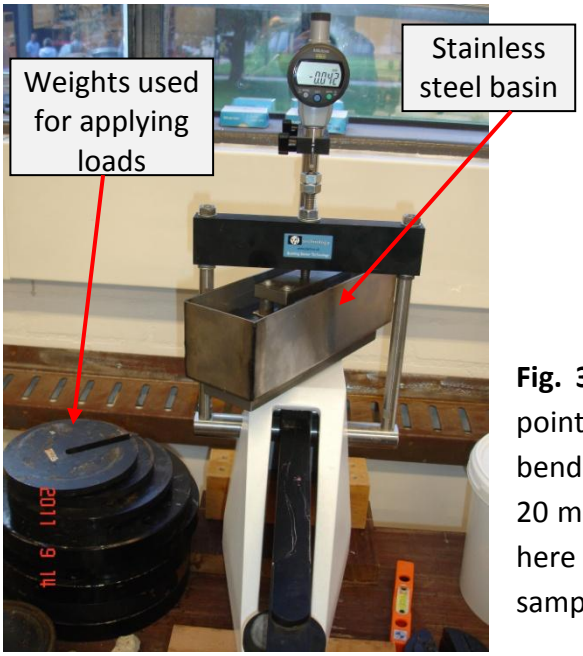

Fig. 3.32: Modified oedometer for testing four-point bending bars in various size (two sizes of bending bars, 240 x 40 x 20 mm and 140 x 40 x 20 mm were tested in this research). This system here can be used for testing dry and saturated samples under atmospheric pressure.

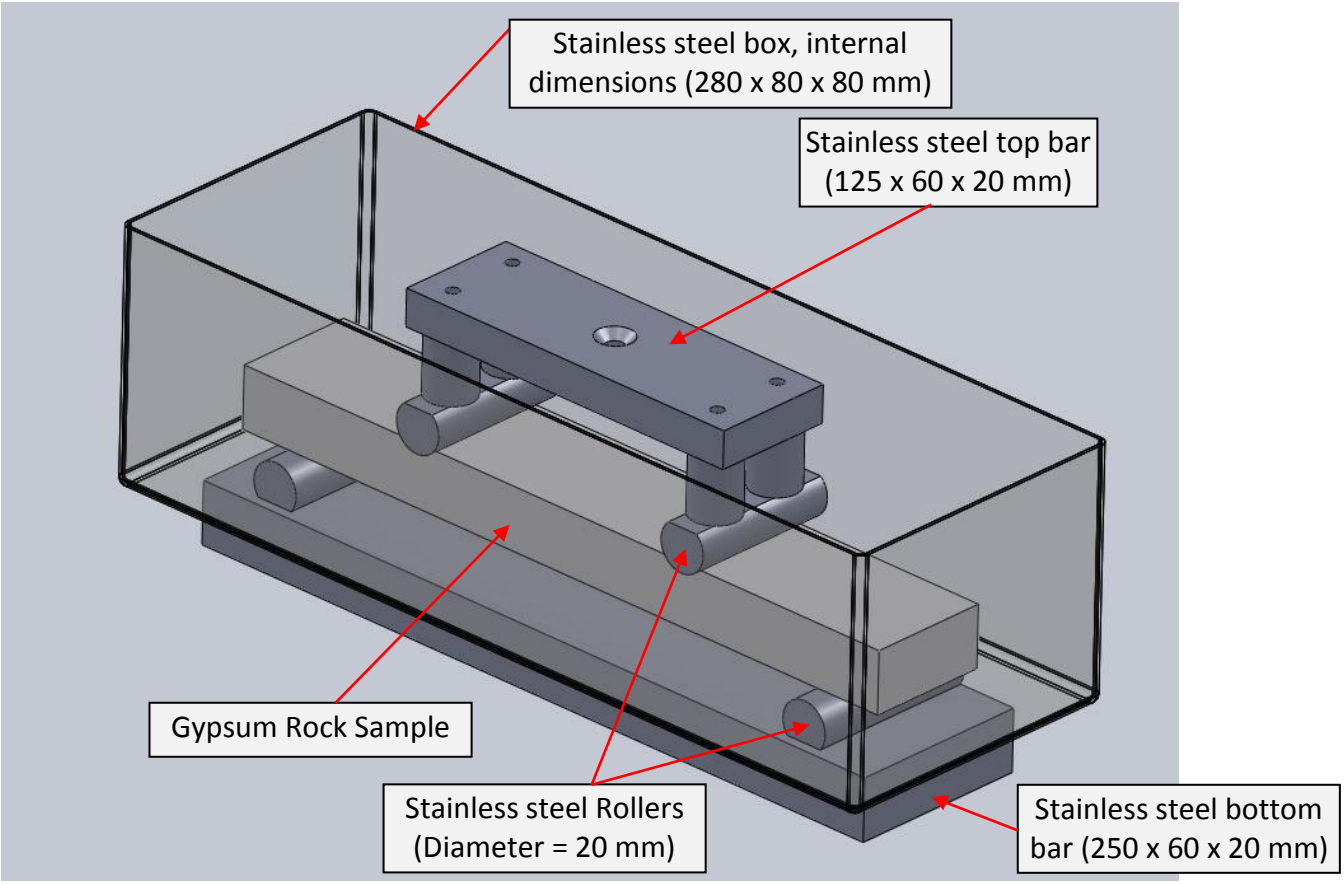

Fig. 3.33: Plan of the four-point bending bar equipment as shown in Figure 3.32. This sketch was produced in *Solid works*.

3.7.5 Stresses applied in Uniaxial and Flexural tests

The applied stresses on all gypsum rock cylinders and on the artificial gypseous soils were completed in eight stages. The increasing stresses in each stage ranged from 28 kPa and end by 2688.35 kPa as: 28, 56, 112, 224, 448, 896, 1792 and 2688.35 kPa. Each one of the first six stresses was applied and left for seven days, the first readings during the first hour of applying each stress were recorded, which depended on the increased reading in the dial gauge. Recording readings were continued through the first 24 hours of the loading in order to discover the immediate and early stage changes or deflections within the loaded sample. For the remaining period of the seven days, two readings were recorded daily. This process was duplicated for each one from the first six loading stages, while the final two stages lasted for 1440 hours (60 days).

This process of applied stresses was used for all rock samples tested in long-term loading through using constant metal weights put on the end of the lever. The prepared artificial gypseous soils were tested through the same way of applied stresses on gypsum rocks, using the pneumatic system. For the artificial gypseous soils, each of the first six loadings was left for 24 hours, while the final seventh loading lasted 1440 hours. The same process of recording data from the dial gages was encouraged for these tests, previous Figure 3.30 show the constant weights applied through lever system.

3.7.6 Iraqi samples

In this section all prepared Iraqi gypsum rocks samples are explained. It was observed that cracks were naturally present within the Iraqi gypsum rocks' structure, and that these cracks were filled with non-gypsum minerals. The thickest layers of gypsum rocks were collected, only limited samples were collected and transported to Brunel University due to both the regulations of transporting from Iraq and the high cost of transportation. Cylinders were prepared from these samples with 54 mm diameters and a length/diameter ratio of 2.5. In addition, thin layers samples were also prepared with dimensions of diameter = 54 mm and thickness = 20 mm for unconfined experiments, 50 mm diameter with 20 mm thickness for confined experiments. Some prepared samples are shown in Figures 3.34 and 3.35 below:

Fig. 3.34: Iraqi gypsum rock bars, used for four-point bending experiment, small size of 140 x 40 x 20 mm. These samples were used for short-term bending test.

Fig. 3.35: Iraqi gypsum rock cylindrical samples: diameter is 54 mm and L/D is 2.5. These samples were used for short and long-term compression tests.

3.7.7 Aust Cliff, UK samples

As mentioned earlier, no locality in the UK has gypseous soil. Two places were chosen to collect gypsum rock samples, Aust Cliff and Bantycock Gypsum Mine.

Gypsum rocks can be seen clearly through the outcrops profile of this cliff at Aust Cliff (Figures 1.6, 1.8 and 1.10). These occur as thin layers and lenses (Figures 3.6 and 3.7). Representative samples of these were collected. Many of these samples contain notable amounts of clays in their cracks and fissures. Some useful un-weathered samples were collected, sealed tightly proper samples' bags and then transported to Brunel University to be used in the experimental works.

From this group of samples only thin layer and small bending samples were prepared for long term experiments, diameter = 54 mm and height = 20 mm and 140 x 40 x 20 mm. Some prepared samples are shown in Figures 3.36 and 3.37. The nature of the material at Aust Cliff meant that it was not possible to prepare larger cylinder samples.

Fig. 3.36: Aust Cliff thin layer/discs sample, diameter is 54 mm and height is 20 mm. This sample was used for short-term compression testing.

Fig. 3.37: Aust Cliff four-point bending samples, each bar size is 140 x 40 x 20 mm. These bars were used in short-term bending test.

3.7.8 UK samples tested, from Bantycock Mine

In order to get thick blocks of gypsum rocks, the British Gypsum Ltd quarry at Bantycock Gypsum Mine in Nottingham-shire was chosen. Two field visits were conducted. Different gypsum rock colours and content were observed. Four main kinds of gypsum rock were identified; white, white with clays infilling cracks, white with marl infilling cracks, and pink. The pink type generally holds an amount of green marl in its cracks and so many cracks were recognized within this kind. Twenty freshly excavated, large block samples representing the four types were collected and transported to Brunel University. At Brunel's Civil Engineering Laboratories the block samples were sealed to prevent possible environmental influences on them and keep their original field properties safe until date of using for experiments.

Cylinders (diameter = 54 mm x height = 135 mm), thin layers (diameter = 54 mm x height = 20 mm) and four point bending (in two dimensions mentioned in Section 3.6.1) samples were prepared from white gypsum; cylinders, thin layers and small bending samples from pink gypsum, only thin layers and small bending samples from white with clay in cracks gypsum. Some pictures of prepared samples are shown in Figures 3.38, 3.39, 3.40 and 3.41 below:

Fig. 3.38: Pink four-point bending bars, from Bantycock samples, UK, (each bar size is 140 x 40 x 20 mm). These bars were used for short-term bending test. Samples numbers are P1 and P2.

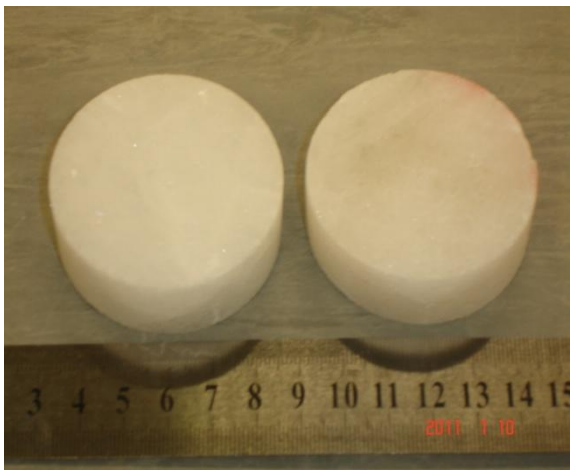

Fig. 3.39: White thin layer/discs samples, from Bantycock samples, UK, (diameter = 54 mm and height = 20 mm). These discs were used for short and long-term compression tests. Samples numbers are W1 and W2.

Fig. 3.40: White four-point bending bars, large size of 240 x 40 x 20 mm, from Bantycock samples, UK. These bars were used for short and long-term bending tests.

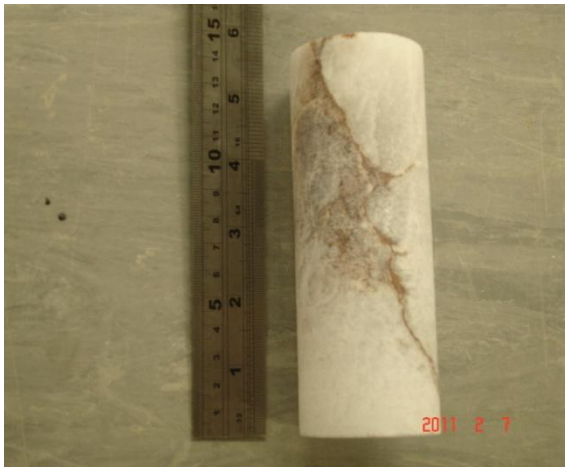

Fig. 3.41: White with clay gypsum rock cylindrical sample, from Bantycock samples, UK, (diameter = 54 mm and height = 135 mm, L/D is 2.5). This sample was used for short and long-term compression tests. Sample number is WC1.

3.8 Laboratory tests of gypseous soils

Gypseous soil particles differ from non-gypsum particles in terms of colours, shapes, particle sizes, particle strengths and many other properties. The exact combination of gypsum and non-gypsum particles in a soil will lead to differing behaviours and responses to environmental conditions. As gypseous soils in Iraq and elsewhere are known to have undergone collapse, probably linked to the presence of the reservoir, it was decided to do some experiments to provide a better insight into how they evolve in a dissolution-affected context. Tests were chosen which were similar to those done on gypsum rocks, though some modifications and alternatives were needed due to the comparatively weak structure of gypseous soils.

Although gypseous soil samples were collected in Iraq, it was not possible to bring sufficient volumes back to the UK for all the possible experimental work. As a result, it was decided to create artificial gypseous soils based on Iraqi soils.

Long-term tests may be much more reliable than the short-term tests to assess the behaviour of gypseous soils under loading and saturation. An oedometer was used to apply the same loads as those applied to gypsum rock (Section 3.7.5), but for confined sample

only due to the weak state of the gypseous soil. The stages of loading were identical, with eight loading stages, with 24 hours duration for each stage, and then each sample had 1440 hours at 1792 kPa, then 1440 hours at 2688 kPa. As with the rock samples, the saturation water was changed each week, and conductivity and pH readings were recorded for the saturation water before and after changing. Digital dial gauges were used in reading the sample settlement, with two readings recorded daily until the final date of the whole experiment. A range of geotechnical possible properties like (dry and saturated densities, void ratio, water content and samples colours in addition to the maximum strain percent) were recorded in the final day after completed experiment.

3.8.1 Tar Al-Najaf sample

Three natural gypseous soils were collected from Tar Al-Najaf in the South West of Iraq and after analysing their gypsum content, the highest gypsum content sample was chosen among them to be used for long-term tests. The chosen sample totally was analysed for gypsum content, particles sizes, particle colours, field density and natural moisture. Gypsum content was computed in four different methods: Acetone method, oven method, *XRD* method and *TDS* (total dissolved solids) method were used to be absolutely sure about the right gypsum percent in the sample. *XRD* analysis was completed in the Experimental Techniques Centre at Brunel University. *TDS* was measured following BS EN 15216:2007 to obtain the real salts content physically through putting the sample in purified water to dissolve the salts and get the free soil minerals without existing salts. The process of putting samples in purified water was repeated until all the salts content dissolved. Tested sample details are presented in Table 3.5 below.

3.8.2 Badosh sample

Two natural gypseous soils samples were collected from northwest Iraq, at Badosh near Mosul, which is close to Mosul Dam (see Figures 1.1 and 1.2). As with Tar Al-Najaf, the same four methods were used to determine gypsum content and other parameters. Both of these samples are quite similar in their content. One of the samples was chosen to be duplicated

as an artificial gypseous soil and use for long-term tests using oedometer. Tested sample details are shown in Table 3.5 below.

3.8.3 Doz sample

One gypseous soil sample was collected from Doz City in the Middle of Iraq (see Figures 1.1 and 1.2). This area is rich in gypsum substrates. Detailed analysis was completed, as for the other soils. After that, an artificial same soil with identical properties was prepared and subjected to long-term oedometer tests. The real sample of Doz city content is shown in Table 3.5 and in Figure 3.42 below.

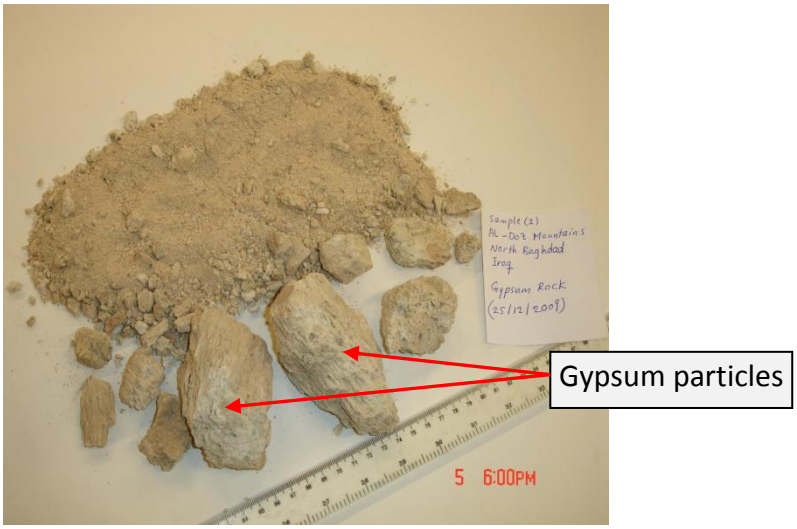

Fig. 3.42: Gypseous soil (sample-1) brought from Al-Doz, Central of Iraq. Note the presence of gypsum particles covered by soil minerals. The fine particles are a mix of gypsum and non-gypsum minerals.

Table 3.5: Real gypseous soil samples properties, these samples collected from North, Central and South of Iraq.

Property	Tar Al-Najaf Sample 1	Badosh Sample 1	Doz, Sample 1
Gypsum Content (%)/Acetone Method (Pansu and Gautheyrou, 2006)	48.1	5.12	40.9
Gypsum Content (%)/*XRD Method*	45	5	40
Gypsum Content (%)/*TDS Method* (BS EN 15216, 2007)	43.38	5.38	38.85
Gypsum Content (%)/*Oven Method* (Al-Mufty and Nashat, 2000)	46.9	4.2	39.15
Field Density (gm/cm^3) (4)	1.5	2	1.59
Natural Water Content (%) (BS ISO 11277, 2009)	5	11	8
Gravel Content (%) (BS ISO 11277, 2009)	28.06	24.60	1.00
Sand Content (%) (BS ISO 11277, 2009)	68.39	24.44	19.11
Silt Content (%) (BS ISO 11277, 2009)	0.75	49.04	79.89
Clay Content (%) (BS ISO 11277, 2009)	2.8	zero	zero
Specific Gravity (Head, 2006)	2.60	2.49	2.27
Colour (Munsell, 2010)	Light Yellowish Brown (6/4), (10YR)	Very Pale Brown (7/4), (10YR)	Light Yellowish Brown (6/4), (10YR)

3.8.4 Sandy Gypseous Soil samples

Examination of the Iraqi gypseous soils showed that they tended to be dominated by coarse grained minerals, in particular sand. It was therefore decided to prepare a range of artificial sandy gypseous soils. The compositions of these sandy soils are shown in Table 3.6. The particle sizes for coarse, medium and fine soil and gypsum follow British Standards (BS ISO 11277:2009).

Table 3.6: Details of artificially-prepared sandy gypseous soils; these soils were prepared after the obtained experience from tested real Iraqi gypseous soil samples. Most of them were coarse-grained materials, soil and gypsum particles.

Sample No.	Particle Size Details
1	Fine Sand (50%) + Fine Gypsum (50%)
2	Medium Sand (50%) + Medium Gypsum (50%)
3	Coarse Sand (50%) + Coarse Gypsum (50%)
4	Fine Sand (50%) + (Fine + Medium + Coarse) Gypsum (50%)
5	Medium Sand (50%) + (Fine + Medium + Coarse) Gypsum (50%)
6	Coarse Sand (50%) + (Fine + Medium + Coarse) Gypsum (50%)

3.8.5 The method of Artificial Gypseous Soil preparation

Artificial soil samples were prepared based on real-world samples from Iraq, paying attention to colour, particle sizes, gypsum content, and natural water content. The prepared materials for each sample were then mixed thoroughly in their dry state. After that, the correct water content was produced using a specific tool (water spray bottle) for uniformly spreading water in very small amounts over the mixed particles. After that, the artificial soil was compacted to the calculated field density. This was done by dividing the mixed soil into three parts for oedometer samples and five parts for box model soil. Lines were drawn on the internal faces of the oedometer mould and box to allow the soil to be laid in thin layers before each layer was compacted. Each compacted sample was left for 24 hours for maturation purpose and then used for the experiments.

3.9 Box Model experiment

To simulate soil modification due to dissolution, a box model experiment was designed. Soil was placed in a large, rigid plastic box (internal dimension: 36.5 x 26.5 x 30.5 cm). The internal face of the box was divided with five equally-spaced lines (see Figure 3.45). These lines provided reference lines for introducing layers of soil into the box, prior to each layer being compacted. In this way, the mixed soil could be compacted perfectly to the required field density and be more similar to its natural state. The base area inside the box was filled firstly with coarse gravel (size = 20 mm with 40 mm thickness) and then over that finer gravel (size = 10 mm with 30 mm thickness, see Figure 3.43 below) was used. These two base layers were used in order to provide freely draining media for salty water movement, so that it could be extracted from an outlet tap at the bottom (see Figure 3.46 below). The internal open side of the outlet tap was covered by a fine mesh (heavy plastic mesh) to reduce loss of fine material.

Distilled water was used for submersion. A stainless steel thin plate filled with holes and fitted with two handles was used each time water was added to the model to prevent surface damage (see Figure 3.44). For more details on the plastic box see Figure 4.92.

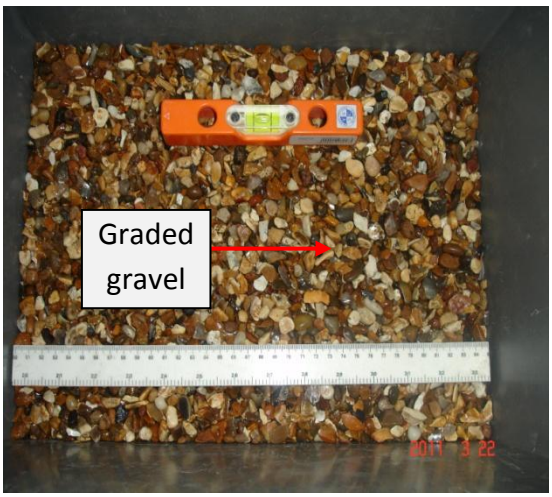

Fig. 3.43: Base materials, graded gravel put as a first layer in the base of box model. This will allow the water of saturation to pass to the outlet tap.

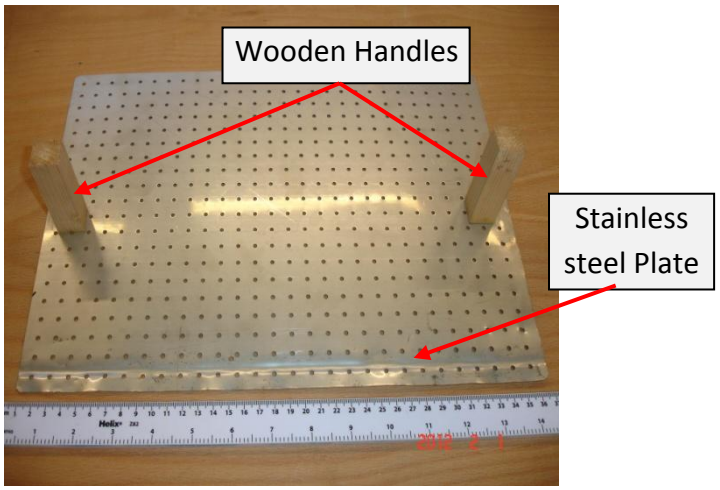

Fig. 3.44: Stainless steel plate with holes. This was used to cover the model's soil surface during the process of filling with water to prevent surface damage.

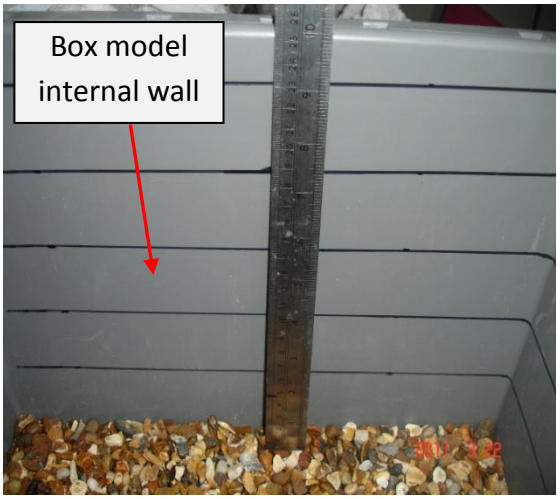

Fig. 3.45: Lines drawn on the internal faces of the box model to mark soil layers levels. These were used as levels for compacting artificial gypseous soil to the required density.

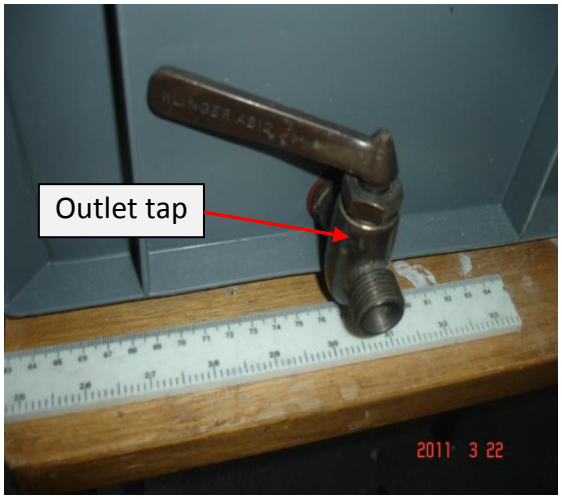

Fig. 3.46: Outlet tap on the external face of box model fitted to the base level. This was used to extract the saturation water once a week for 50 weeks.

3.9.1 The Box Model's soil properties (before 50 weeks)

In addition to the soil properties based on the Tar Al Najaf sample, additional geotechnical properties were computed to provide a baseline of information about the characteristics of the artificial soil. These are shown in Table 3.5 above, and considered further in the results chapter (Chapter 4).

3.9.2 The Box Model's soil properties (after 50 weeks)

After 50 weeks exposure to fresh water seepage, samples were extracted from the top, central depth and bottom of the box soil. These samples were used to determine the same properties calculated on the original soil at the start of the experiment. By examining these three layers, it was easy to see the changes through profile due to flooding of fresh water, and to find out the new pattern of soil content and structure (see Section 4.7).

3.10 Supplementary tests

Some supplementary tests were done separately to find out some extra information help in controlling the other done experiments. Pilot experiments were conducted in order to find out the suitable loading rate to be applied on prepared cylinders, thin layers and bending samples. Activities using different water sources were tested, for dissolving gypsum rock. Methods on the possible way to compute changes on saturated gypsum rocks Include strain gauge and drawn mesh on gypsum rock surface. In the same regards, different calibration curves were also checked to be used in some way with gypsum dissolution process, which are; gypsum-conductivity, gypsum-brine water, loading-unloading and developed oedometer calibration curve. These supplementary tests will be explained below.

3.10.1 Strain Gauge test

Material such as gypsum can deform in different directions. The magnitude of these deflections can frequently be obtained through using strain gauges glued on samples surfaces during load application. The experimental conditions in this research meant a variety of gypsum rock samples had to be submerged for long-term periods. Any tools and devices used to check the changes in the samples should remain stable. As there was concern about the impact of prolonged soaking on the effectiveness on the used strain gage, a test was adopted. Cubic gypsum rock samples with sizes of 50 x 30 x 30 mm were prepared with a smooth surface. A strain gauge was glued onto the surface using an appropriate resin. No solution could be found to this problem and the option of attaching strain gauges to samples was abandoned, Figure 3.47 shows the materials used in this experiment.

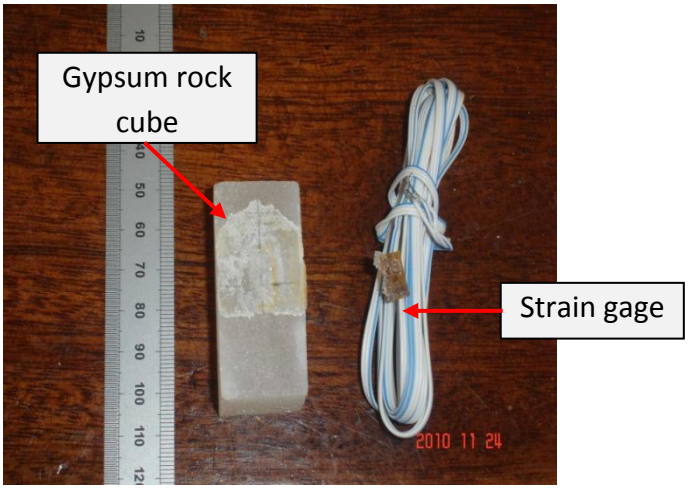

Fig. 3.47: Strain gauge experimental equipment.

3.10.2 Drawn Mesh on samples surface

After the failure of the strain gauge test, it was decided to apply another method to find out the circumferential deflections. A smooth cubic sample was cut to a size of 100 x 50 x 50 mm. A mesh was drawn with black waterproof, permanent ink over the surface of the prepared sample. The marked sample was placed in a container and submerged in distilled water. After one week the mesh lines started to release from the rock surface and did not remain over the sample surface any more, meaning that this approach to assessing was not applicable.

3.10.3 Gypsum-Conductivity Calibration Curve

To assess how much dissolution was taking place, weekly conductivity readings were taken during the main experiments of this research. To clarify the relationship between gypsum weight and conductivity reading, a simple test was completed. Gypsum powder was prepared from Bantycock gypsum samples and used for this experiment. The process of dissolution started from 0.25 g of gypsum powder mixed with one litre of distilled water. This was mixed thoroughly using an electrical mixer with 1000 cycle/min for 15 min and then a conductivity reading was recorded. A further 0.25 g of gypsum powder was added to the solution and same process was repeated. The test was repeated until 3.0 g of gypsum powder had been dissolved in the one litre of distilled water. Figure 3.48 below shows the

relationship between the weight gypsum powder that had been dissolved and the conductivity readings. The increase in conductivity stopped when the solution reached saturation.

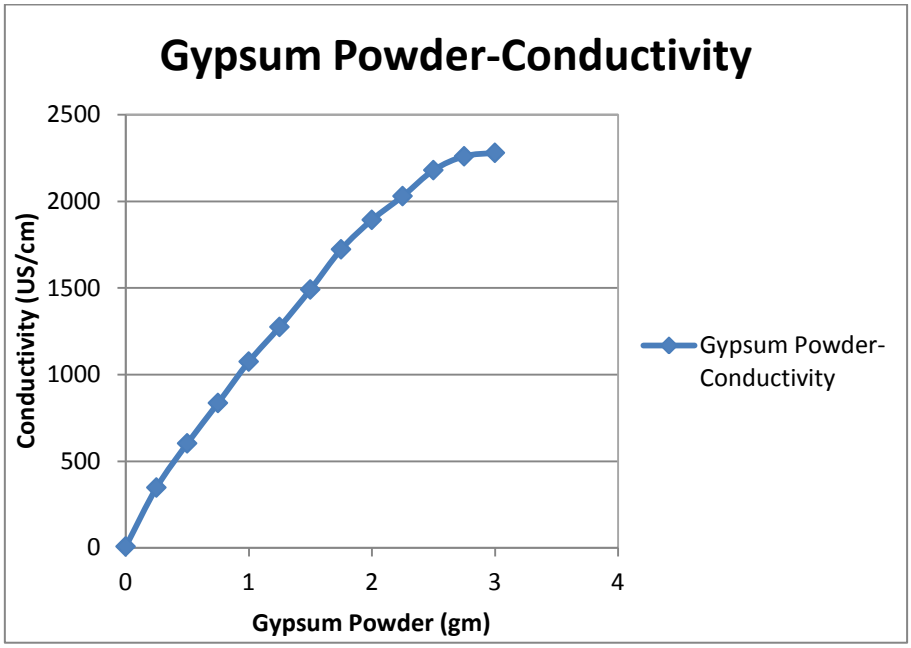

Fig. 3.48: Gypsum powder weight-conductivity relationship, this was used to calculate the dissolved gypsum weights from recorded conductivity of waters of saturation after each week of the experiments, the conductivity tend to be stable after 3.0 g of gypsum powder added.

3.10.4 Gypsum rock dissolution in Brine Water (Calibration Curve)

In order to understand the solubility of gypsum rocks in brine water (focused on brine water, which contains gypsum salt as the major mineral), five gypsum rock samples were prepared from Bantycock blocks. All the prepared samples were 50 mm in diameter and 20 mm in height. The brine water was prepared by mixing 3.0 g of gypsum powder with one litre of distilled water. The rock samples were weighed, fully-saturated and added to the brine water basin following the approach in Section 3.6.3. The samples were left for seven days to assess any changes. Therefore, sample weights were recorded regularly each day until the end of the experiment. It was discovered that no changes on samples weight were obtained.

From this experiment, it is clear that if gypsum rocks contacted water saturated with dissolved gypsum salt, no notable dissolution might be expected.

3.10.5 Loading-Unloading experiment

Three thin layer samples with dimensions of 54 mm diameter x 20 mm height were prepared from white Bantycock gypsum rock. Each sample was used to test loading impacts in seven stages start from 28 kPa and end by 1792 kPa (to allow an assessment of elasticity) and unloading impacts in five stages after loading stages finish. Each stage in loading and unloading stages took three days and the water of saturation remained without changing until the experiments finished. These stages were decided on in order to discover the samples ability to deal with loading and unloading stages in saturation state, which is the worst case compare to air dry state. Weight, density and colour of tested samples were recorded in air dry and fully saturated conditions. After that, the same calculated properties were recorded for the samples after experiments, which then used to find out the changes on tested samples due to loading, unloading and saturation conditions.

3.11 Summary

In this chapter, details have been provided on the sampling locations for gypsum rocks and gypseous soils. All the conducted pilot experiments were presented here. All the adopted experimental tests and observations were explained as well, including the development of some laboratory devices to allow the experiments to simulate conditions similar to real world states such as at Mosul Dam. The simulated conditions were applied on a variety of prepared samples for both gypsum rocks or for artificially-prepared gypseous soils. Short and long term observations were conducted on cylinders, thin layers and four point bending samples from Iraq and the UK (106 samples for pilot studies and 360 samples for long and short term tests). These experiments mean a wide range of mechanical properties could be examined and a significant body of new data could be collected. These results are presented in the results chapter (Chapter 4).

CHAPTER FOUR: RESULTS, PROCESSING & COMPARISONS

4.1 Introduction

This chapter includes all the results derived from the methods described in chapter three.

4.2 Pilot and Supplementary studies

4.2.1 Cylinders Loading Rates

In order to find the proper loading rate to be applied on cylinder rock samples, different loading rates were applied using trial samples. Results for 0.1 MPa/sec and 0.05 MPa/sec showed that the times to failures respectively are: 1 min and 27 sec, 2 min and 47 sec, 2 min and 4 sec; 3 min and 19.7 sec, 4 min and 16 sec, 3 min and 43 sec, 3 min and 10 sec, below and above the minimum values of internationally applied standards (ISRM/Bieniawski et al., 1978; ASTM D7012-10, 2010) (Figure 4.1, 4.2), 5 to 10 min/ISRM and 2 to 15 min/ASTM. A loading rate of 0.025 MPa/sec was applied on air-dry and saturated cylinders and found to be the most suitable one with a time to failure of 9 min and 0.7 sec for air-dry specimen and 3 min and 34.7 sec for saturated specimen (Figure 4.3).

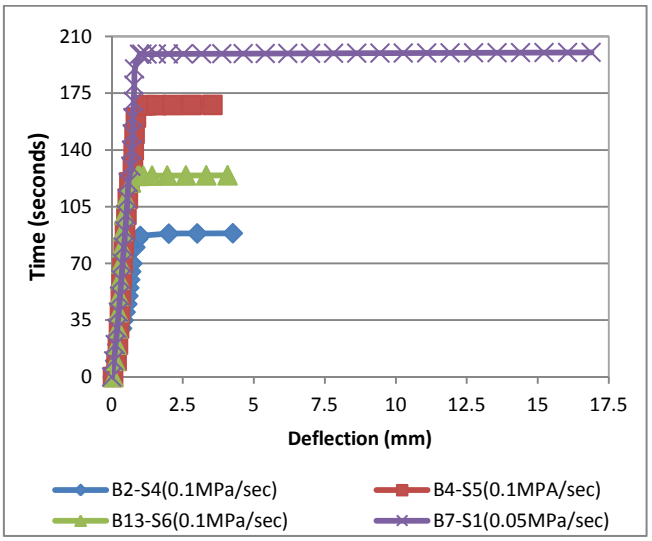

Fig. 4.1: Air-dry cylinders trial experiment-load application (0.01 MPa/sec and 0.05 MPa/sec).

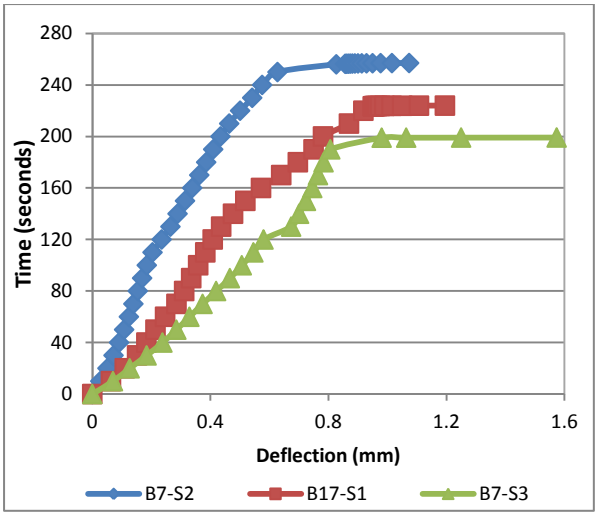

Fig. 4.2: Air-dry cylinders trial-load application experiments (0.05 MPa/sec). Sample B7-S3 weakened at about 120 sec and then recovered at about 128 sec.

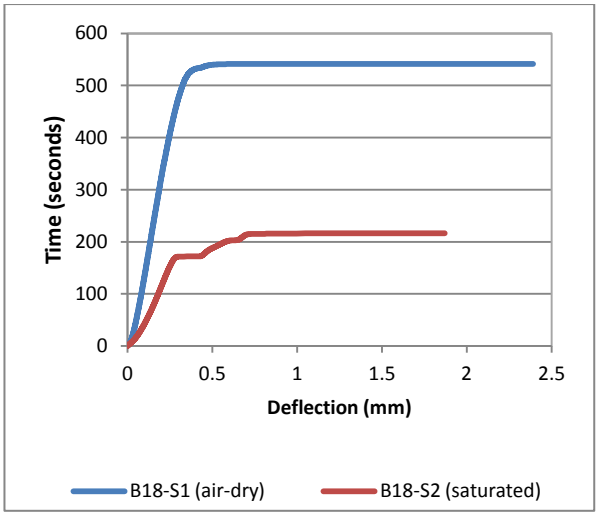

Fig. 4.3: Air-dry and saturated cylinders trial experiment-load application (0.025 MPa/sec), sample B18-S2 weakened at about 75 sec and then recovered until about 215 sec.

4.2.2 Thin Layers Loading Rates

0.5 MPa/sec, 0.25 MPa/sec, 0.1 MPa/sec and 25 N/mm^2/min loading rates (Elizzi, 1976; ISRM/Bieniawski et al., 1978; Ali, 1979; BS EN 1926, 2006; ASTM D7012-10, 2010) were applied to trial thin layer samples as shown in Figure 4.4, but the time to failure was too high for 0.5 MPa/sec rate, with the acceptable ranges (5 to 10 min/ISRM and 2 to 15 min/ASTM) and too low for others rates. When the same loading rate that was used for cylinders (0.025 MPa/sec) was applied to the thin layers, the time to failure was found to be very long (27 min and 58 sec). A loading rate of 0.075 MPa/sec was found to be the best rate for both air-dry and saturated thin layers, which was close to the minimum ones listed in cylinder standards, 5 to 10 min/ISRM and 2 to 15 min/ASTM (Figures 4.5 and 4.6).

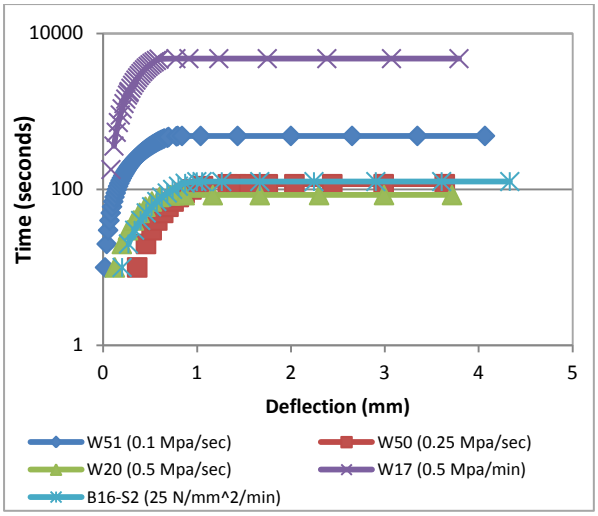

Fig. 4.4: Air-dry thin layers trial experiments-different loading rates. Note the failure in all samples occurred in single events.

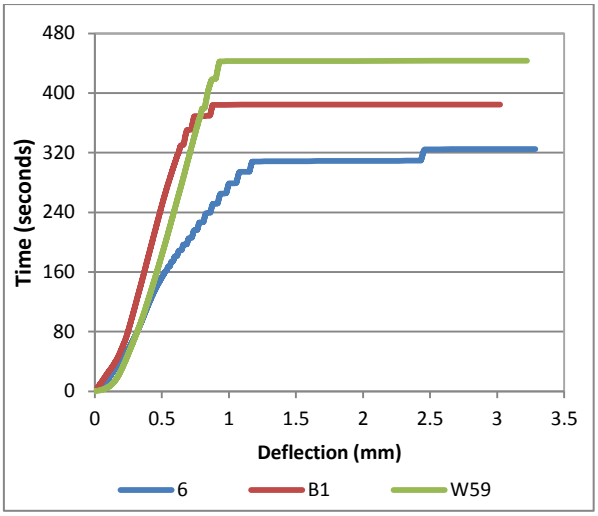

Fig. 4.5: Air-dry thin layers trial experiments (0.075 MPa/sec loading rate), sample 6 weakened at about 310 sec and then recovered until about 325 sec.

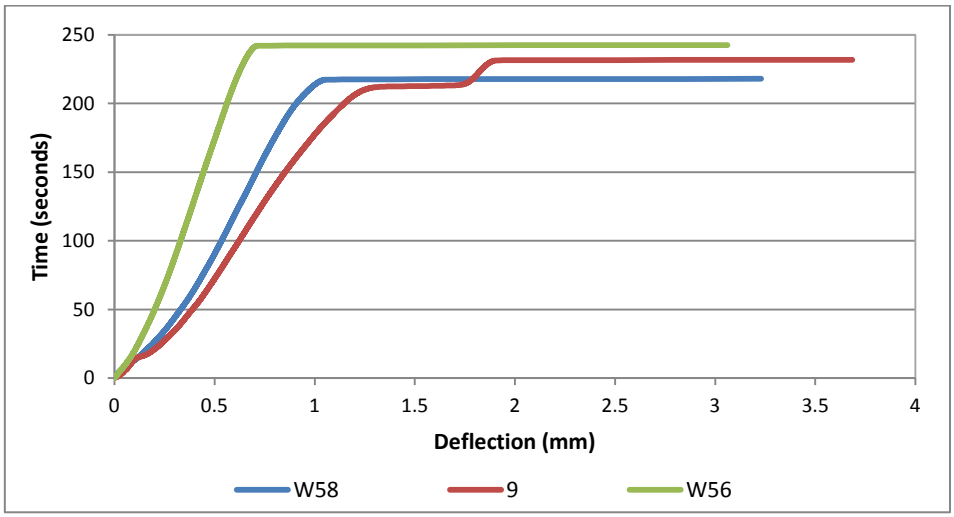

Fig. 4.6: Saturated thin layers trial experiments (0.075 MPa/sec Loading rate), sample 9 weakened at about 210 sec and then recovered until about 230 sec.

4.2.3 Large and Small Bending Loading Rates

For the small bending bar samples, a variety of loading rates of 0.02 mm/sec, 0.01 MPa/sec and 0.04 MPa/sec (selected from ASTM 1635-00, 2006 and BS EN 12390-5, 2009, which are on the flexural tests of concrete and soil-cement simple beam) were applied in order to identify the most suitable. Then, after identifying that the checked loading rates are not suitable due to the short time of failures (shown in Figure 4.7), an extension rate 0.01 mm/min was applied on air-dry bars and also the results are not suitable due to the long time to failure were obtained, as shown in Figure 4.8 below. After that, three loading rates;

0.015, 0.02 and 0.025 MPa/sec were applied to both small and large bending bar samples in the air-dry state. A rate of 0.02 MPa/sec was identified as the best because of it is very close to the selected loading rates for cylinder samples of 0.025 MPa/sec. The selected loading rate for bar samples, 0.02MPa/sec, was then applied on saturated samples to check the time to failure, as most samples of this research are saturated in five durations of 5, 10, 15, 30 and 50 week as shown in Figures 4.9 and 4.10 below.

The same loading rate of 0.02 MPa/sec was applied on air-dry and saturated large bending bar samples and again found to be suitable (Figures 4.11 and 4.12).

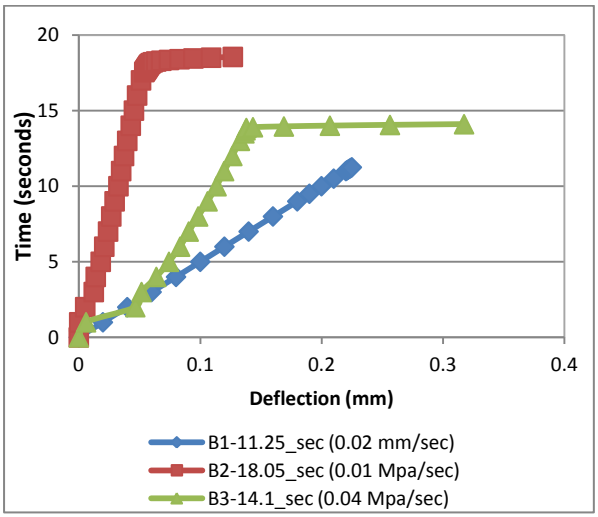

Fig. 4.7: Air-dry small bending trial experiments-different loading Rates.

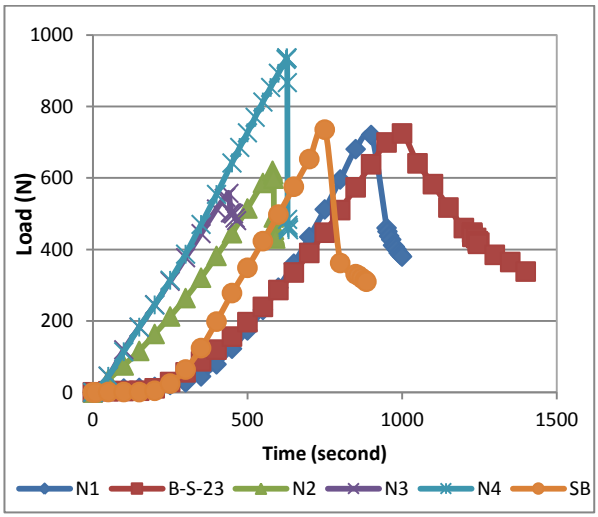

Fig. 4.8: Air-dry small bending trial experiment (0.01 mm/min).

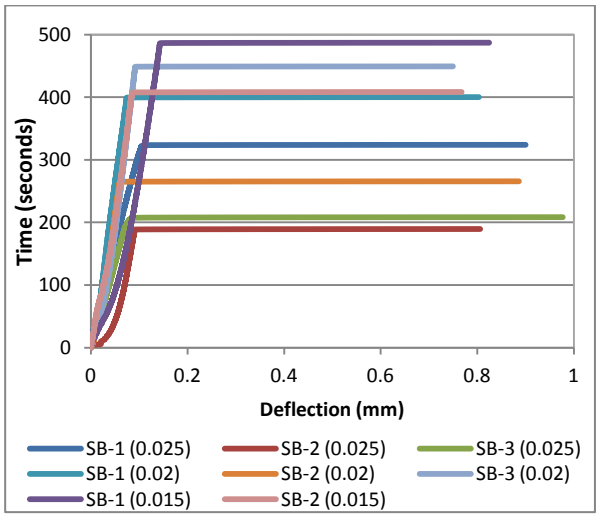

Fig. 4.9: Air-dry small bending- trial experiments-different loading rates (0.015, 0.02 and 0.025 MPa/sec) as shown inside brackets.

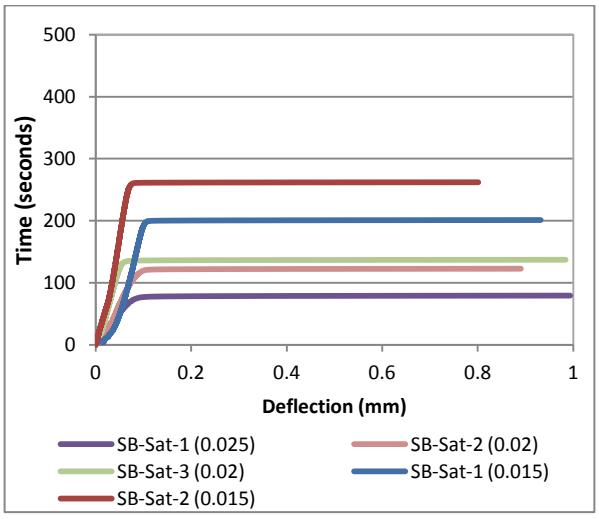

Fig. 4.10: Saturated small bending- trial experiments-different loading rates (0.015, 0.02 and 0.025 MPa/sec) as shown inside brackets.

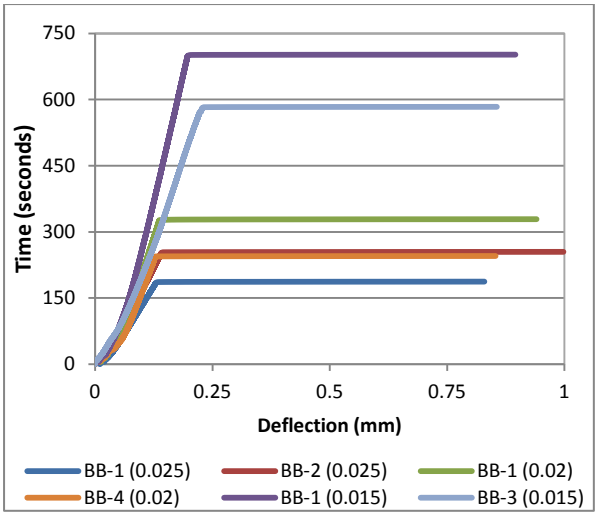

Fig 4.11: Air-dry large bending- trial experiments-different loading rates (0.015, 0.02 and 0.025 MPa/sec).

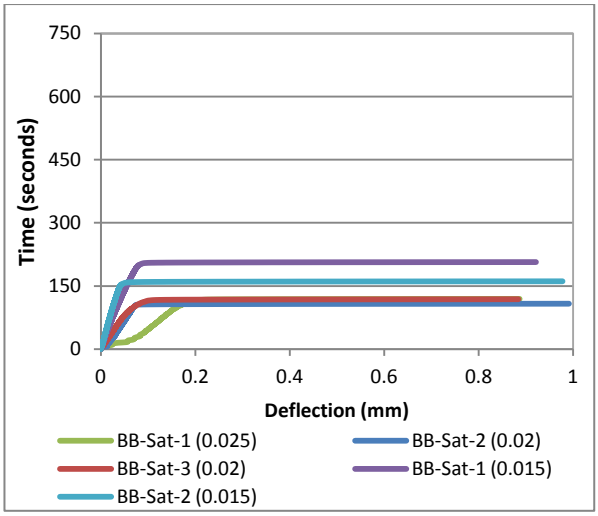

Fig 4.12: Saturated large bending- trial experiments-different loading rates (0.015, 0.02 and 0.025 MPa/sec).

4.2.4 Water Type and Gypsum Dissolution experiment

In order to find the dissolution of gypsum samples of this study (Bantycock and Aust Cliff/UK and Iraqi) with different water types; distilled, tap, Grand Union Canal (at Cowley in Uxbridge, canal-1 and at Maple Cross in Hertfordshire, canal-2) water were used. Three shapes of gypsum samples; rectangular, cubic and triangular (see Section 3.5 of chapter 3) were experimented to assess their influence on the gypsum dissolution process. Comparison in general among gypsum rock types' dissolution and comparison of dissolution of gypsum types with distilled water only are shown below in Figures 4.13, 4.14, 4.15 and 4.16, while Figure 4.17 and 4.18 below show the comparison among rectangular, cubic and triangular mass reductions.

It can be noticed the aggressivity of distilled water to dissolve all types of experimented gypsum samples compare to other types of saturation water, see Figure 4.14-4.15.

It can be seen from the Figures 4.17 and 4.18 that the intact white/Bantycock gypsum in general is more affected by distilled water compared to other gypsum samples. This reveals the role of impurities inside tested samples to influence the dissolution process through interact with gypsum minerals.

There is an impact of shape and size on dissolution of gypsum. Figure 4.17 show that the intact white/Bantycock sample is more dissolvable than other samples; this reveals the influences of impurities on dissolution process. Figure 4.18/A & B show also the impacts of impurities to decrease/increase gypsum dissolution.

In comparison between rectangular and cubic shapes in Figure 4.17/A, B & C, it can be seen that decreases of sample size increases dissolution. As a result, in general the percentage lost in sample mass was least for the triangular sample. The lower dissolution of triangular shape compare to cubic is due to the area of the rectangular and cubic samples that was indirect with the water was greater than for the triangular sample.

The other cases of Figure 4.17/A & B may reveal the influences of impurities on dissolution process.

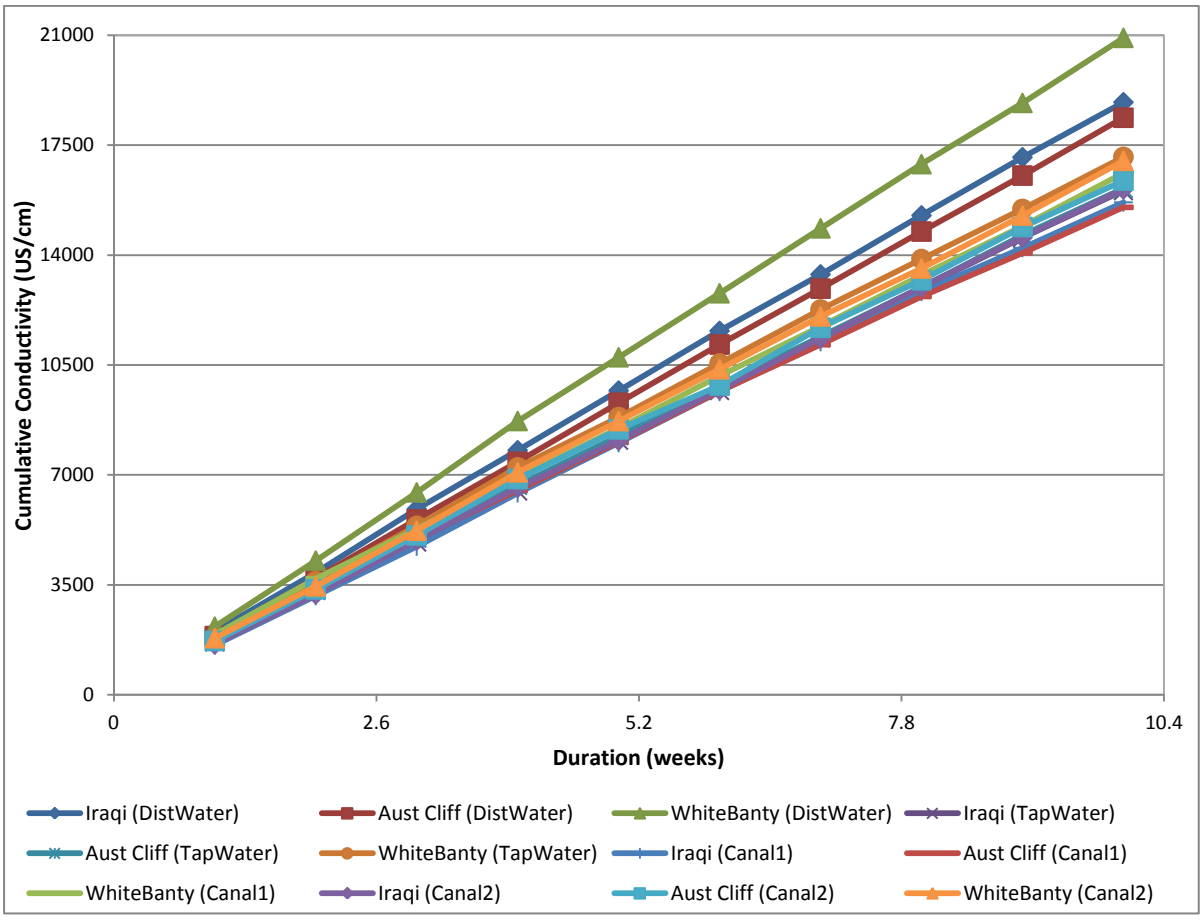

Fig. 4.13: Cumulative conductivity values over ten weeks period; distilled, tap and two different canal waters from the UK have been used. White/Bantycock and Aust Cliff gypsum from the UK and Iraqi gypsum have been tested.

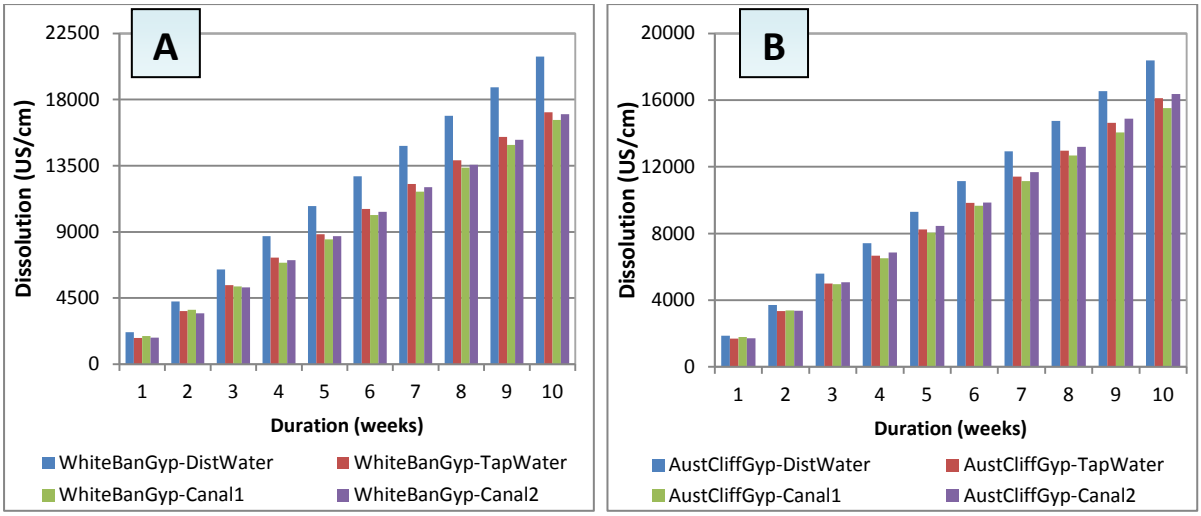

Fig. 4.14: Comparison of dissolution data by distilled, tap, canal1 and canal2. Part A for White/Bantycock gypsum and part B for Aust Cliff Gypsum. (Canals' locations are shown in Section 3.5).

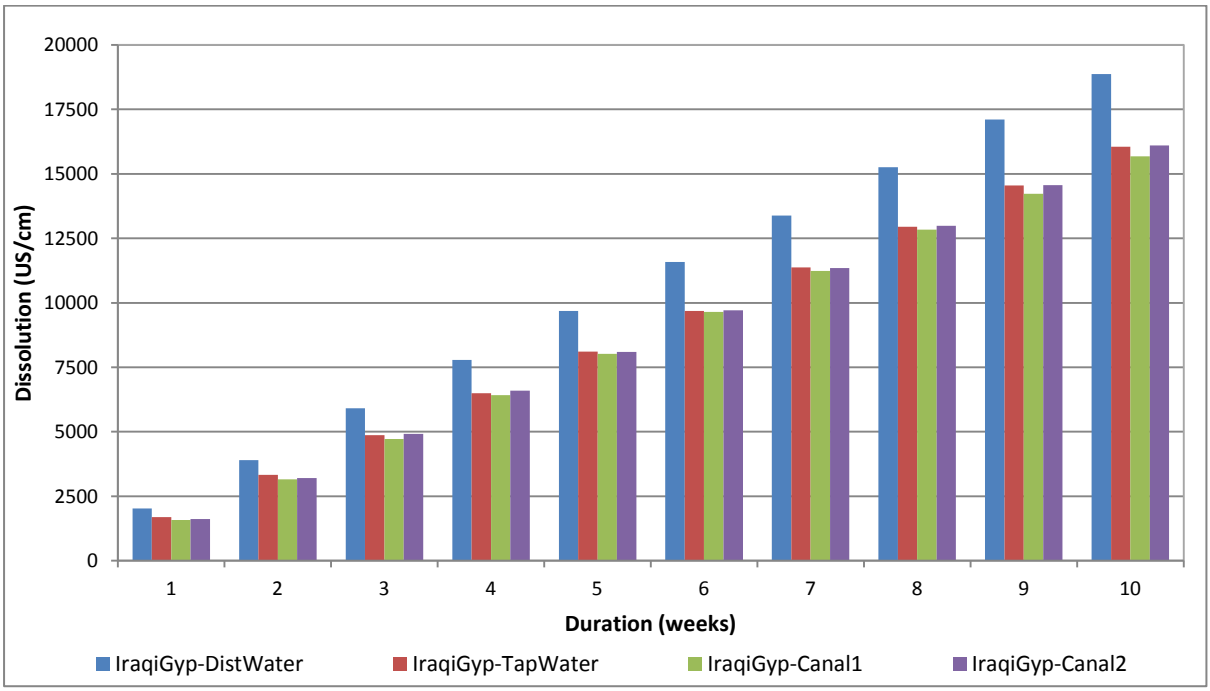

Fig. 4.15: Comparison among dissolution data by distilled, tap, canal1 and canal2 for Iraqi gypsum rock sample.

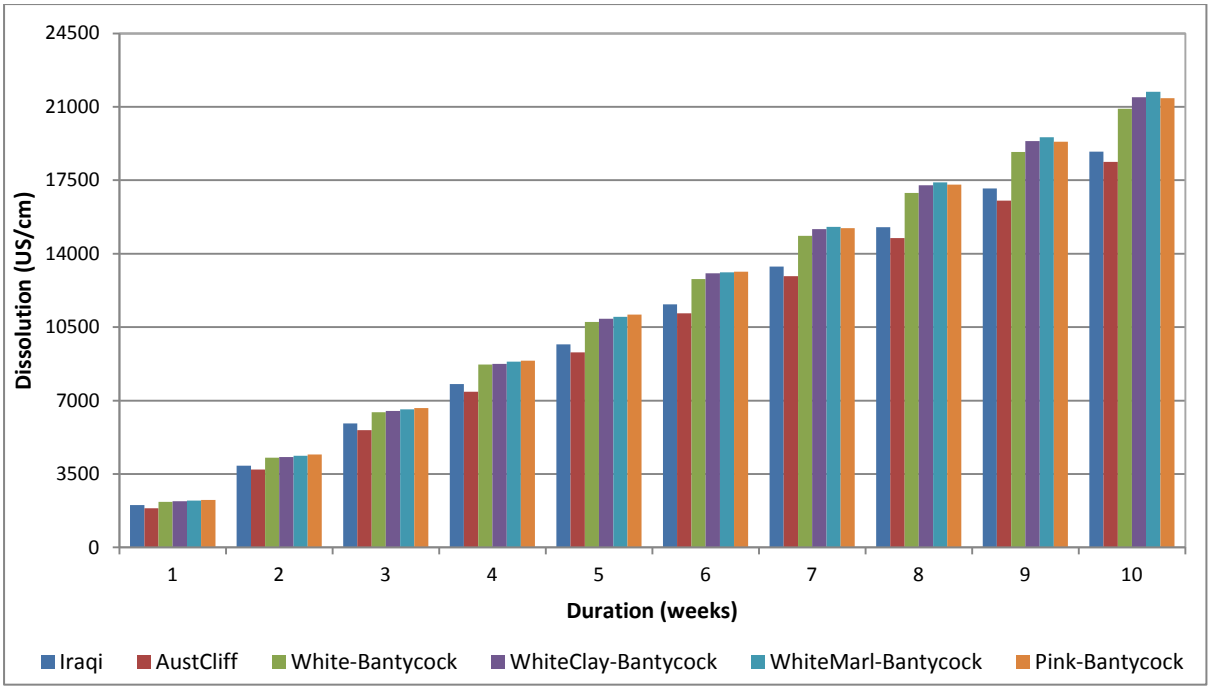

Fig. 4.16: Comparison among dissolution data of white/Bantycock, Aust Cliff, Iraqi, pink/Bantycock, white & clay/Bantycock and white & marl/Bantycock gypsum by distilled water.

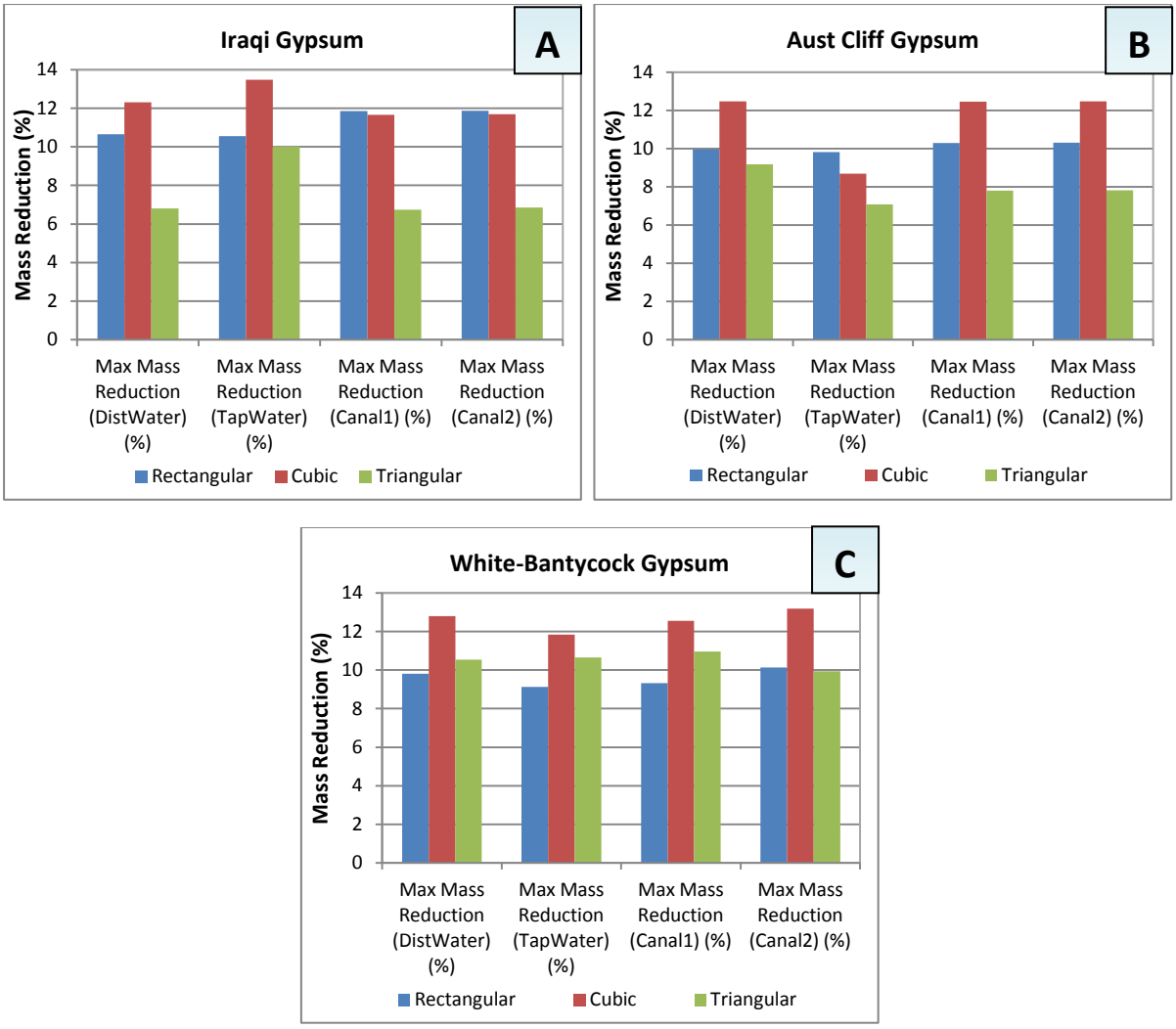

Fig. 4.17: Comparison of three water types used to saturate Iraqi and UK gypsum in three cut sample shapes: rectangular, cubic and triangular. Part A shows the maximum mass reduction of the Iraqi gypsum, part B shows the maximum mass reduction of Aust Cliff/UK gypsum, part C shows the maximum mass reduction of white/Bantycock gypsum.

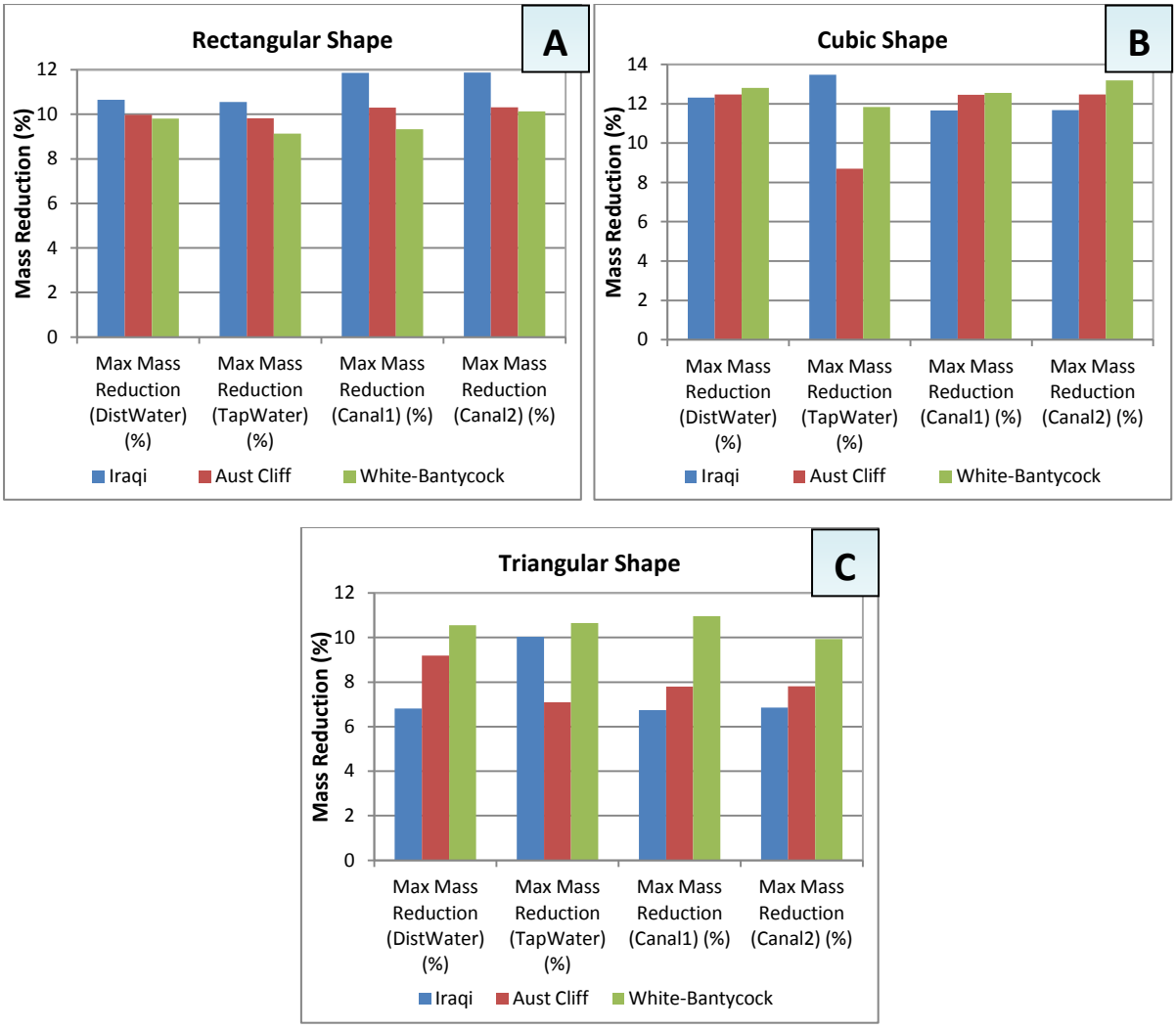

Fig. 4.18: Comparison of three water types used to saturate Iraqi and UK gypsum in three cut sample shapes: rectangular, cubic and triangular. The three parts of A, B and C show the maximum mass reduction values for the Iraqi and UK gypsum samples for different shapes, part A for rectangular shape, part B for cubic shape and part C for triangular shape.

4.2.5 Loading-Unloading experiment

In order to find UK and Iraqi gypsum sensitivity for loading and unloading stages, gradual stress application in theory equal to distributed stress from Mosul Dam was applied. These samples were left for three days inside water for each loading stage as shown in Figure 4.19 below. It can be seen that the intact white/Bantycock sample is more affected by loading-unloading stages and recorded the highest strain percent. Then, the Iraqi sample is less affected, while the lowest affected sample is Aust Cliff sample. In general, although the application of loading-unloading stages on gypsum rock samples is not caused failure, it causes notable changes on samples response for loading and leave different strain percents which stayed along the samples even when loading released and the samples particles compacted before creep stage.

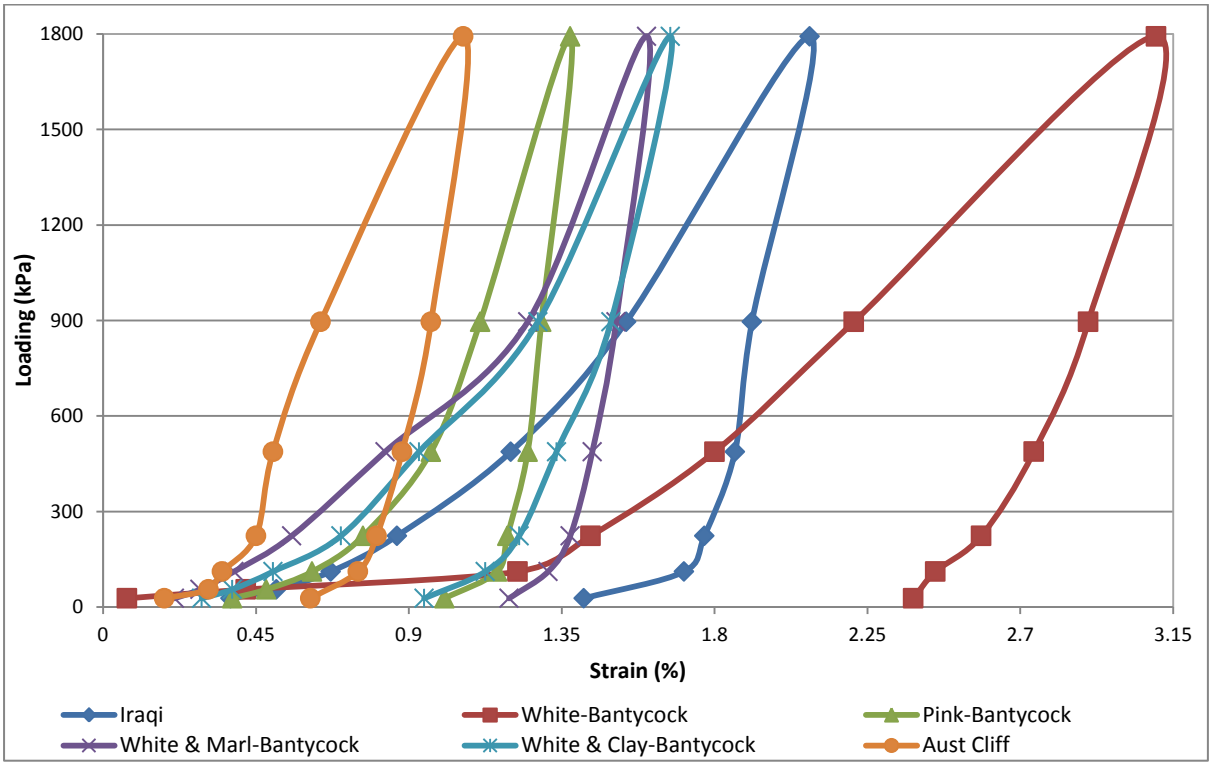

Fig. 4.19: Loading-unloading relationship with strain percent of thin layer samples of gypsum rock from the UK and Iraq. Thin layers are in size of 54 mm diameter X 20 mm height.

4.2.6 *SEM* studies and Chemical Analysis of gypsum rock samples

Table 4.1: Description of the UK and Iraqi gypsum particles, the description based on *SEM* (Scanning Electronic Microscope) photos presents in Figures 4.20 to 4.25 below.

Gypsum Sample Type	Particle Size	Particles Gradation	Particles Shape	Notes
White/Bantycock, UK (see Figure 4.20)	4 to 114 micron	Poorly graded	Have three shapes randomly: longitudinal, semi-square and semi-circular/elliptical	Very sharp edges of particles, mostly medium size, some large and small sizes are found
Pink/Bantycock, UK (see Figure 4.21)	2 to 177 micron	Not very well graded	Mostly semi-elliptical and longitudinal	Middle and large sizes are more than fine size
White with marl/Bantycock, UK (see Figure 4.22)	3 to 114 micron	Not very well graded	Coarse particles are mostly angular and semi-circular, small particles are mostly longitudinal, medium particles have all shapes	Sharp edges of particles
White with clay/Bantycock, UK (see Figure 4.23)	2 to 114 micron	Not very well graded	Coarse and fine particles are mostly semi-circular, while medium particles are mostly semi-elliptical and longitudinal	Different sizes of particles, mostly medium and coarse
Aust Cliff, UK (see Figure 4.24)	2 to 97 micron	Not well graded	Coarse particles are mostly angular and semi-circular, small particles are mostly semi-circular and semi-elliptical, medium particles are mostly semi-elliptical and longitudinal	Existing of some large particles in size of about 97 micron
Iraqi (see Figure 4.25)	1 to 28 micron	Looks well graded	Mostly semi-circular and semi-elliptical	Mostly fine particles, some concentration of fine particles with impurities/other minerals together make dense look for some places

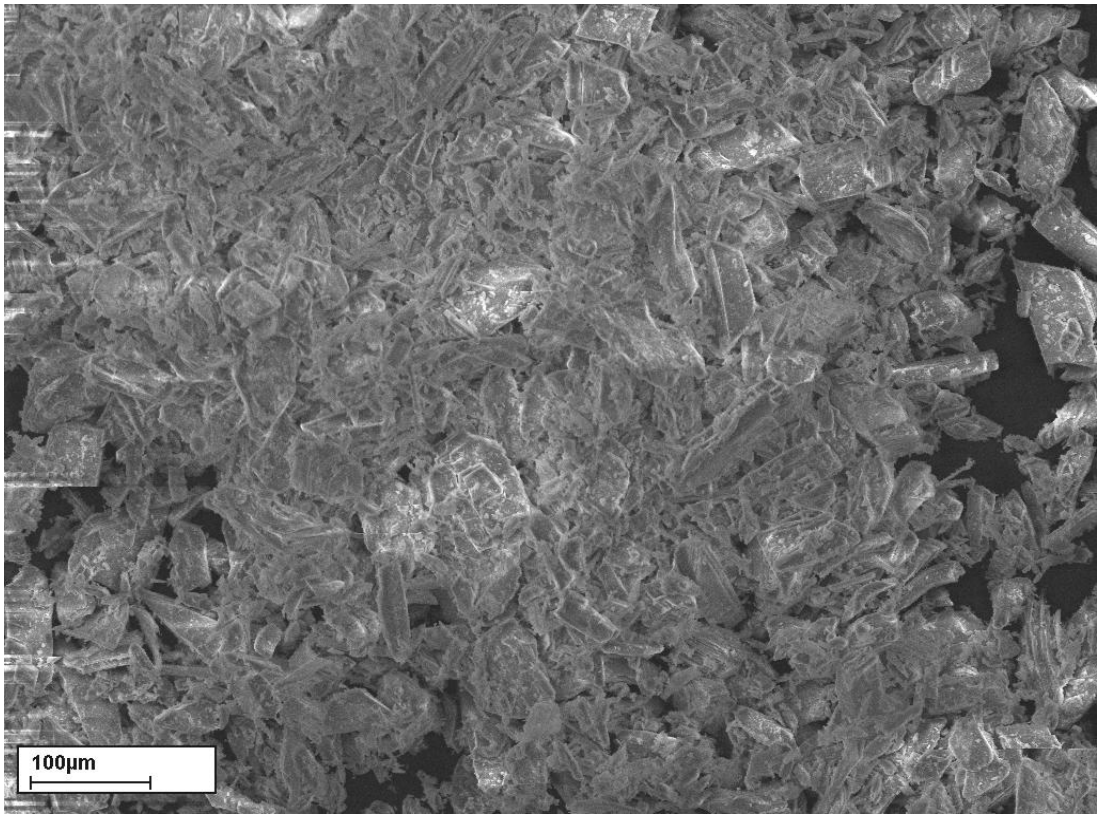

Fig. 4.20: *SEM* photo of white/Bantycock gypsum rock sample (see Table 4.1 for more details).

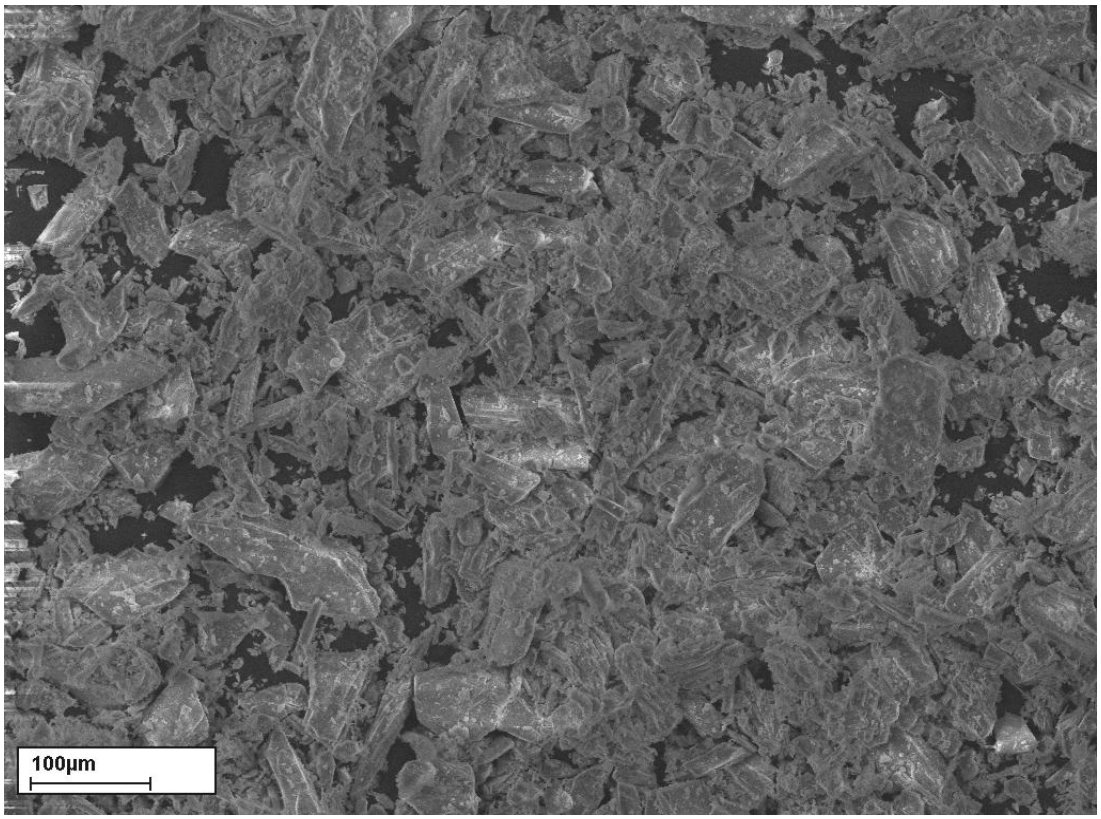

Fig. 4.21: *SEM* photo of pink/Bantycock gypsum rock sample (see Table 4.1 for more details).

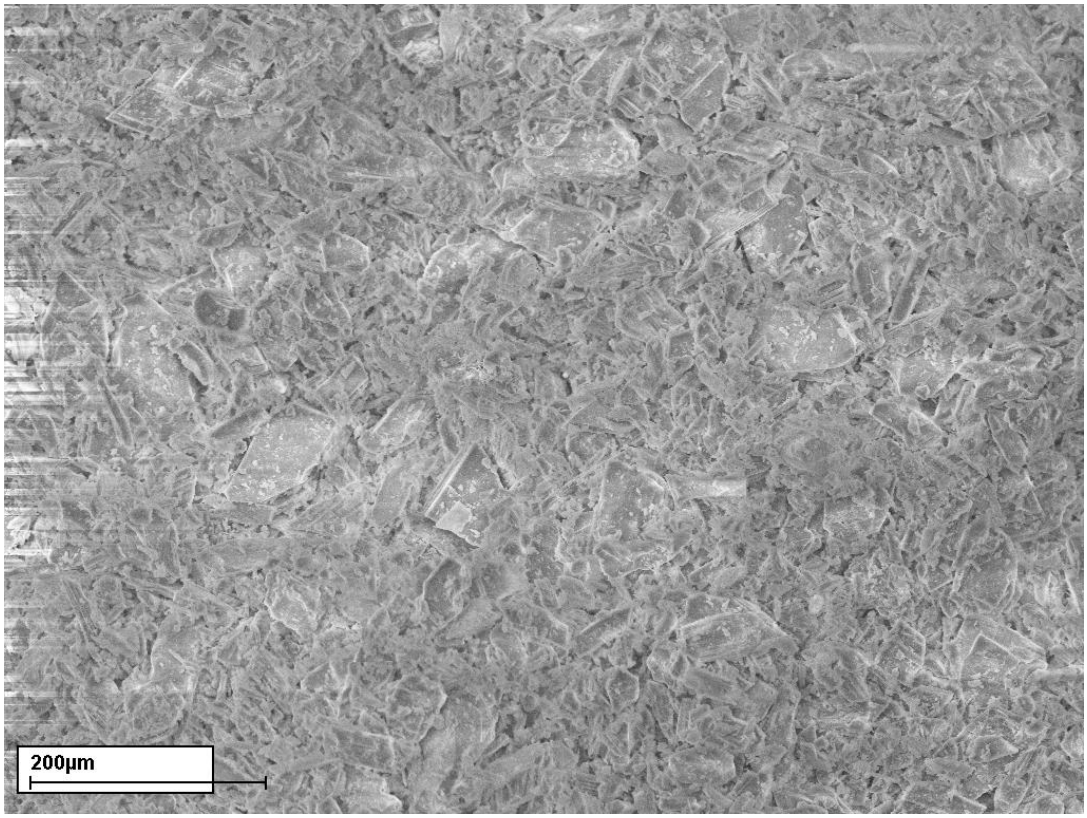

Fig. 4.22: *SEM* photo of white with marl/Bantycock gypsum rock sample (see Table 4.1 for more details).

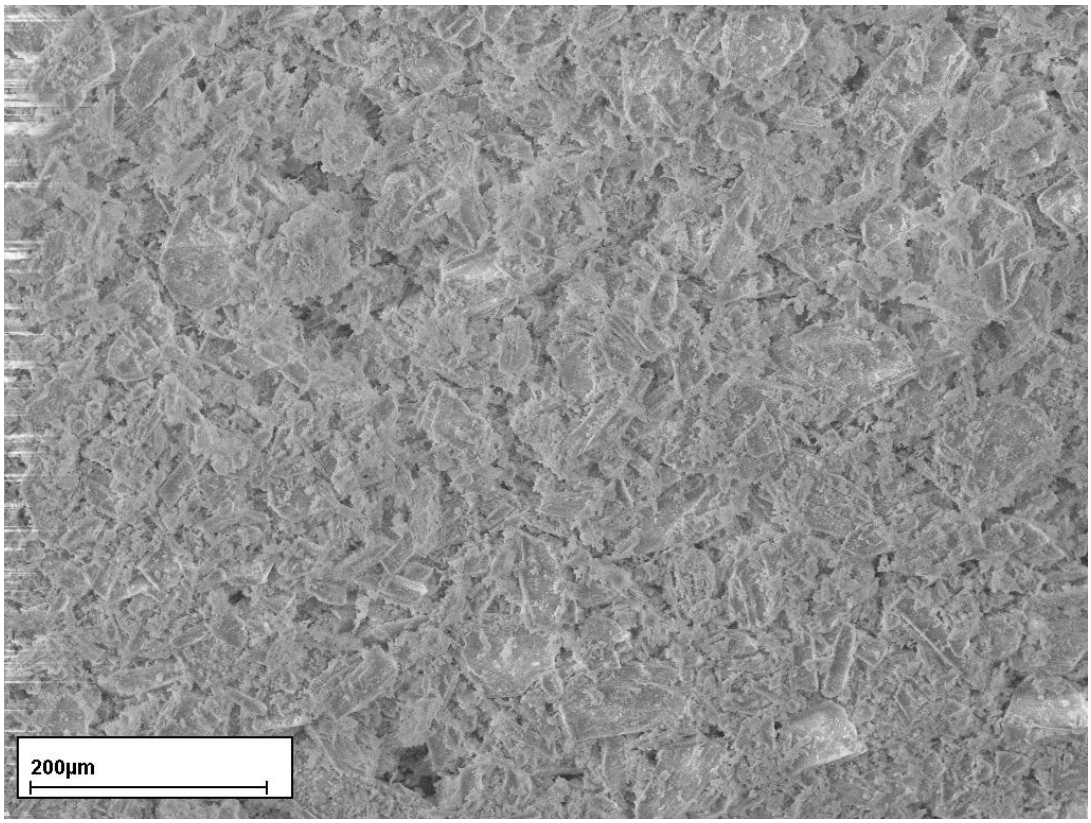

Fig. 4.23: *SEM* photo of white with clay/Bantycock gypsum rock sample (see Table 4.1 for more details).

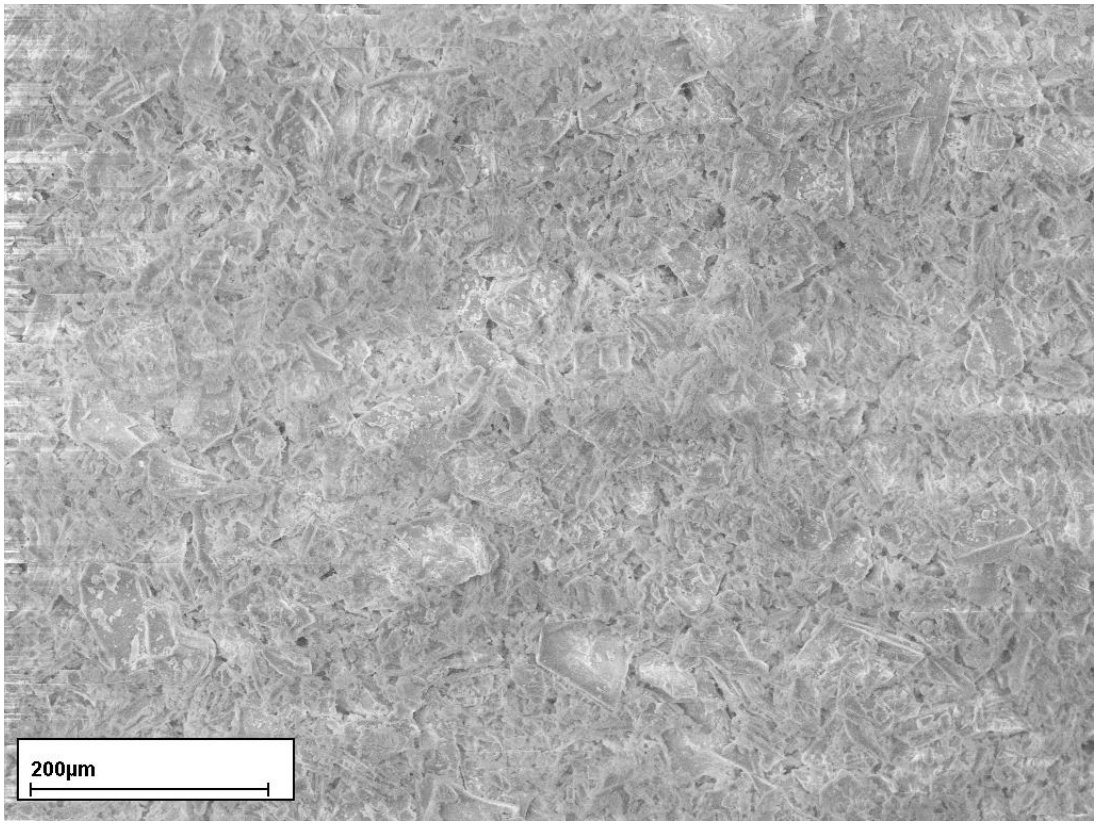

Fig. 4.24: *SEM* photo of Aust Cliff gypsum rock sample (see Table 4.1 for more details).

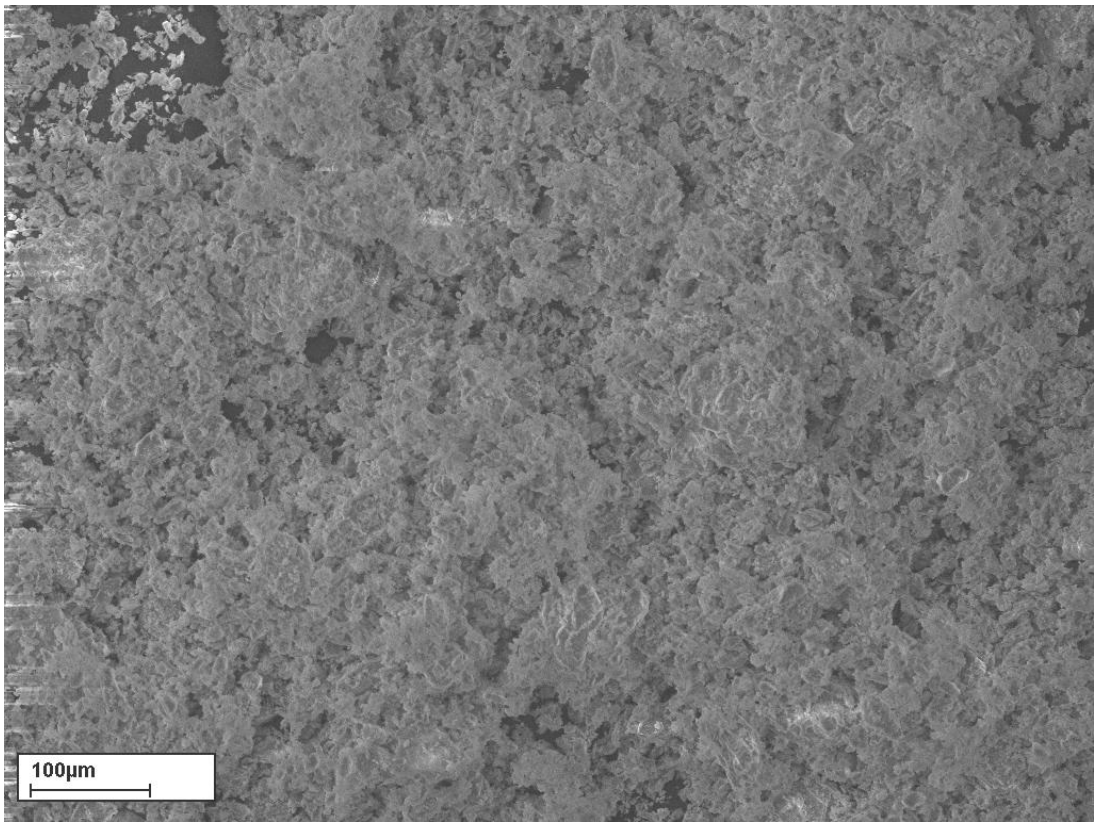

Fig. 4.25: *SEM* photo of Iraqi gypsum rock sample (see Table 4.1 for more details).

Table 4.2: Chemical Analysis (*SEM*) for UK and Iraqi gypsum rocks (Spectrum is one tested area, *Mg* = Magnesium, *Al* = Aluminium, *Si* = Silicon, *S* = Sulfur, *Ca* = Calcium, *pb* = Lead, *O* = Oxygen, *K* = Potassium, *Fe* = Iron, *Na* = Sodium, *Sc* = Scandium).

Sample 1, white/Bantycock gypsum rock (*WBG*)-minerals content (%)									
Spectrum No.	***S***	***Ca***	***O***	***Pb***	**-**	**-**	**-**	**-**	**-**
Spectrum 1	21.53	29.97	44.51	3.99	-	-	-	-	-
Spectrum 2	21.41	29.90	44.32	4.38	-	-	-	-	-
Spectrum 3	21.23	30.31	44.20	4.26	-	-	-	-	-
Sample 2, pink/Bantycock gypsum (*PBG*)-minerals content (%)									
Spectrum No.	***S***	***Ca***	***O***	***Pb***	***Si***	***Al***	***Mg***	**-**	**-**
Spectrum 1	20.70	28.91	44.98	2.98	1.07	0.47	0.91	-	-
Spectrum 2	20.60	29.03	44.86	3.11	1.11	0.37	0.92	-	-
Spectrum 3	21.04	28.53	45.04	3.36	0.95	0.5	0.57	-	-
Sample 3, Bazyan/Iraq gypsum rock (*IG*)-minerals content (%)									
Spectrum No.	***S***	***Ca***	***O***	***Pb***	***Si***	**-**	**-**	**-**	**-**
Spectrum 1	22.02	28.95	45.13	3.61	0.29	-	-	-	-
Spectrum 2	21.67	29.57	44.85	3.62	0.28	-	-	-	-
Spectrum 3	21.95	30.14	45.10	2.81	-	-	-	-	-
Sample 4, white with marl/Bantycock gypsum rock (*WBG-M*)-minerals content (%)									
Spectrum No.	***S***	***Ca***	***O***	***Pb***	***Si***	***Al***	***Mg***	***Fe***	***K***
Spectrum 1	21.46	28.30	45.32	3.24	0.92	0.40	0.36	-	-
Spectrum 2	20.93	28.40	44.71	3.57	1.06	-	0.53	0.51	0.29
Spectrum 3	21.26	28.59	45.06	3.50	1.06	-	0.52	-	-
Sample 5, white with clay/Bantycock gypsum rock (*WBG-C*)-minerals content (%)									
Spectrum No.	***S***	***Ca***	***O***	***Pb***	***Si***	***Al***	**-**	**-**	***Sc***
Spectrum 1	20.81	29.15	44.24	4.35	0.56	-	-	-	0.90
Spectrum 2	20.91	29.55	44.47	4.07	0.69	0.31	-	-	-
Spectrum 3	21.49	29.10	44.89	3.80	0.72	-	-	-	-
Sample 6, Aust Cliff gypsum rock (*ACG*)-minerals content (%)									
Spectrum No.	***S***	***Ca***	***O***	***Pb***	***Si***	**-**	**-**	***Fe***	**-**
Spectrum 1	15.35	40.15	40.48	2.92	1.09	-	-	-	-
Spectrum 2	16.87	36.80	41.47	3.78	1.08	-	-	-	-
Spectrum 3	16.14	36.82	41.00	4.08	1.49	-	-	0.46	-

Table 4.3: Gypsum content for different UK and Iraqi gypsum rock and gypseous soil samples (*SEM* analysis).

Sample No.	Sample Origin	Gypsum Content (%)
1	White/Bantycock gypsum	96
2	Pink/Bantycock	94
3	Bazyan/Iraq	96
4	White with marl/Bantycock	94
5	White with clay/Bantycock	96
6	Aust Cliff	80
7	Koya (Haybat Sultan)/Iraq	94
8	Badosh (Mosul)/Iraq	5
9	Tar Al-Najaf/Iraq	40
10	Doz/Iraq	40

4.3 Gypsum rock: Short-Term work

Uniaxial compression tests were completed on samples from Iraq and the UK, statistical parameters also calculated for tested samples/three samples for saturation conditions and five for air-dry condition. Table 4.4 is presenting Bantycock thin layers tested samples. Table 4.5 shows the results of Aust Cliff thin layers/short-term results and 4.6 shows Iraqi thin layers/short-term results. After that the comparison results will be presented in Section 4.3.4.

4.3.1 Bantycock thin layer samples

From Table 4.4, the calculated compressive strength is in the range of 25 to 43 MPa and from 33 to 50 MPa for white/Bantycock (*WBG*) and pink/Bantycock (*PBG*) samples respectively at air-dry state.

Saturation weakens both types of gypsum thin layers. It can be seen that the mean values of compressive strength ($б_c$), load at failure (*FL*), time to failure (*TL*), shear modulus (*SM*), mass (*wt*) and volume (*vol*) were decreased, while dissolution amount was increased progressively due to saturation over time progress for both types.

Only intact samples of white/Bantycock gypsum were used to examine the impacts of water pressure on dissolution process (explained in Section 3.6.5). Speeding up gypsum dissolution

process is noticed within the application of 1.75, 3.25 and 5.0 bar compare to saturation under atmospheric pressure. It can be seen that the reduction of $б_c$, *TL*, *FL*, *SM*, *wt* and *vol* of *WBG* due to water pressure is greater than the reduction due to saturation under atmospheric pressure. The dissolution rate per week for *WBG* under 1.75 bars is higher than dissolution rate of *WBG* in saturation state under atmospheric pressure. By water pressure increases and time progresses, the dissolution rate per week increases.

Table 4.4: Compressive strength, Poisson's ratio, load at failure, time to failure, shear modulus, maximum axial deflection, maximum horizontal deflection, maximum mass and volume reductions, cumulative and rate of dissolution of thin layer/disc samples calculated from uniaxial compression test. The samples were prepared from Bantycock Mine gypsum rocks; five of these were air-dry and three were saturated. Samples collected April 2010 and April 2011. *Note: The Poisson's ratios for some samples are unrealistic and reflect the disintegration of the samples.

Compressive Strength (MPa)					
Thin Layer Kind	**Min**	**Max**	**SD**	**Mean**	**Median**
White-Air Dry	25.026	43.263	6.8141	34.716	34.607
White-SatOnly-5Week	27.228	30.563	1.668	28.884	28.86
White-SatOnly-10Week	25.41	28.808	1.909	26.607	25.601
White-SatOnly-15Week	24.647	27.019	1.362	26.219	26.99
White-SatOnly-30Week	21.699	28.868	3.694	24.768	23.737
White-SatOnly-50Week	9.288	16.529	3.639	13.122	13.548
White-5Week-1.75bar	22.966	24.544	0.791	23.718	23.644
White-10Week-1.75bar	21.482	25.636	2.09	23.426	23.161
White-15Week-1.75bar	19.89	21.727	1.041	20.526	19.959
White-5Week-3.25bar	20.159	26.582	3.293	23.791	24.631
White-10Week-3.25bar	21.624	23.052	0.817	22.109	21.65
White-15Week-3.25bar	20.047	21.347	0.69	20.563	20.294
White-5Week-5.0bar	21.101	25.623	2.316	23.65	24.227
White-10Week-5.0bar	19.432	23.648	2.253	21.999	22.918
White-15Week-5.0bar	14.68	21.709	3.628	18.714	19.752
Pink-Air Dry	33.498	50.508	6.713	40.919	42.149
Pink-SatOnly-5Week	27.955	42.988	8.597	33.062	28.244
Pink-SatOnly-10Week	28.733	34.445	2.999	31.06	30.0
Pink-SatOnly-15Week	25.678	30.265	2.632	27.226	25.734
Pink-SatOnly-30Week	21.767	26.799	2.905	23.445	21.767
Pink-SatOnly-50Week	20.696	25.831	2.882	22.509	20.998
White & Clay-Air Dry	23.584	59.59	14.206	42.388	38.755
Poisson's Ratio*					
Thin Layer Kind	**Min**	**Max**	**SD**	**Mean**	**Median**
White-Air Dry	0.156	1.064	0.338	0.545	0.5298

White-SatOnly-5Week	0.234	0.886	0.335	0.515	0.425
White-SatOnly-10Week	0.091	0.791	0.35	0.443	0.448
White-SatOnly-15Week	1.112	1.657	0.281	1.344	1.264
White-SatOnly-30Week	0.542	1.095	0.315	0.906	1.08
White-SatOnly-50Week	1.04	1.203	0.082	1.128	1.141
White-5Week-1.75bar	0.876	0.942	0.034	0.906	0.898
White-10Week-1.75bar	0.598	0.747	0.075	0.673	0.676
White-15Week-1.75bar	0.688	0.811	0.064	0.739	0.718
White-5Week-3.25bar	0.228	0.794	0.285	0.532	0.574
White-10Week-3.25bar	0.442	0.547	0.057	0.507	0.533
White-15Week-3.25bar	0.366	0.683	0.163	0.504	0.462
White-5Week-5.0bar	0.584	1.039	0.237	0.774	0.7004
White-10Week-5.0bar	0.639	0.802	0.083	0.714	0.699
White-15Week-5.0bar	0.488	0.914	0.224	0.661	0.5797
Pink-Air Dry	0.432	0.667	0.089	0.557	0.564
Pink-SatOnly-5Week	0.468	0.656	0.094	0.563	0.566
Pink-SatOnly-10Week	0.479	0.603	0.064	0.533	0.517
Pink-SatOnly-15Week	0.704	0.93	0.1196	0.794	0.749
Pink-SatOnly-30Week	0.052	1.112	0.588	0.729	1.024
Pink-SatOnly-50Week	1.087	1.476	0.195	1.284	1.289
White & Clay-Air Dry	0.229	0.798	0.253	0.488	0.518
Load at Failure (N)					
Thin Layer Kind	**Min**	**Max**	**SD**	**Mean**	**Median**
White-Air Dry	57314	99082.3	15605.8	79508.1	79257.9
White-SatOnly-5Week	61635.8	69138.1	3752.4	65332	65222.1
White-SatOnly-10Week	57208.2	64273.3	3945.95	59725.6	57695.3
White-SatOnly-15Week	54920.1	60173.6	2929.2	58295.3	59792.1
White-SatOnly-30Week	46183.7	60842.3	7665.7	52216.23	49622.7
White-SatOnly-50Week	18564.3	33059	7289.6	26263.9	27168.5
White-5Week-1.75bar	46237.5	5268.9	3882.5	50720.6	52955.5
White-10Week-1.75bar	39976.7	55126.3	7769.24	48548.7	50543.2
White-15Week-1.75bar	44366	48267	2239.82	45680.8	44409.4
White-5Week-3.25bar	44229.5	58810.1	7466.2	52449.97	54310.03
White-10Week-3.25bar	46137.5	48934.7	1539.7	47164.4	46421
White-15Week-3.25bar	40962.2	43430.5	1245.72	42098.57	41903
White-5Week-5.0bar	5744.6	53408.2	25758.3	35219.57	46505.9
White-10Week-5.0bar	39976.7	50449.7	5703.6	46518.33	49128.6
White-15Week-5.0bar	29578.6	43769.6	7394.21	37875.23	40277.5
Pink-Air Dry	76716.7	115741	15373.39	93713.26	96531.5
Pink-SatOnly-5Week	63231.8	95982.8	18817.16	74255.4	63551.6
Pink-SatOnly-10Week	64283.8	77267.8	6766.57	69674.23	67471.1
Pink-SatOnly-15Week	56870	67603.2	6168.66	60480.47	56968.2
Pink-SatOnly-30Week	45651.3	56462.1	5568.89	50283.37	48736.7
Pink-SatOnly-50Week	40715	52232.4	6228.83	45103.1	42361.9
White & Clay-Air Dry	54012.8	136474	32535.74	97078.34	88756.6
Time to Failure (seconds)					
Thin Layer Kind	**Min**	**Max**	**SD**	**Mean**	**Median**
White-Air Dry	332.75	574.65	90.54	461.52	459.8
White-SatOnly-5Week	357.5	401.15	21.83	379.05	378.5

White-SatOnly-10Week	331.75	373.1	23.108	346.467	334.55
White-SatOnly-15Week	318.05	348.55	17.061	337.717	346.55
White-SatOnly-30Week	267.35	352.98	47.408	298.409	274.9
White-SatOnly-50Week	106.88	191.03	42.314	151.544	156.73
White-5Week-1.75bar	269.2	292.9	12.502	283.35	287.95
White-10Week-1.75bar	231.27	320.85	45.983	282.075	294.1
White-15Week-1.75bar	257.25	279.5	12.581	264.983	258.2
White-5Week-3.25bar	257.3	342.25	43.521	305.25	316.2
White-10Week-3.25bar	267.65	283.7	9.005	273.317	268.6
White-15Week-3.25bar	238.24	251.6	6.813	244.147	242.6
White-5Week-5.0bar	269.2	331.3	31.506	303.333	309.5
White-10Week-5.0bar	231.274	286.9	30.472	266.675	280.65
White-15Week-5.0bar	169.25	253.2	42.659	206.833	198.05
Pink-Air Dry	445.25	672.35	89.509	544.22	560.7
Pink-SatOnly-5Week	366.3	557.55	109.803	430.767	368.45
Pink-SatOnly-10Week	373.3	448.05	38.948	404.35	391.7
Pink-SatOnly-15Week	329.7	392	35.868	350.583	330.05
Pink-SatOnly-30Week	264.6	327.05	32.173	291.35	282.4
Pink-SatOnly-50Week	238.49	298.51	32.407	261.435	247.304
White & Clay-Air Dry	313.3	793.3	189.37	563.82	515
Shear Modulus (GPa)					
Thin Layer Kind	**Min**	**Max**	**SD**	**Mean**	**Median**
White-Air Dry	9.159	18.713	3.988	11.698	10.571
White-SatOnly-5Week	0.083	0.292	0.106	0.177	0.156
White-SatOnly-10Week	0.137	0.263	0.069	0.217	0.25
White-SatOnly-15Week	0.088	0.143	0.03	0.122	0.136
White-SatOnly-30Week	0.063	0.152	0.045	0.102	0.091
White-SatOnly-50Week	0.024	0.036	0.007	0.031	0.033
White-5Week-1.75bar	0.044	0.05	0.003	0.047	0.047
White-10Week-1.75bar	0.066	0.095	0.014	0.081	0.081
White-15Week-1.75bar	0.081	0.115	0.018	0.101	0.108
White-5Week-3.25bar	0.086	0.118	0.016	0.103	0.104
White-10Week-3.25bar	0.139	0.172	0.018	0.152	0.144
White-15Week-3.25bar	0.058	0.173	0.06	0.126	0.148
White-5Week-5.0bar	0.06	0.145	0.048	0.115	0.14
White-10Week-5.0bar	0.069	0.119	0.025	0.093	0.09
White-15Week-5.0bar	0.042	0.121	0.044	0.093	0.115
Pink-Air Dry	11.044	15.163	1.519	13.086	13.105
Pink-SatOnly-5Week	0.191	0.289	0.049	0.236	0.228
Pink-SatOnly-10Week	0.171	0.198	0.014	0.185	0.188
Pink-SatOnly-15Week	0.119	0.155	0.018	0.139	0.141
Pink-SatOnly-30Week	0.057	1.551	0.859	0.559	0.068
Pink-SatOnly-50Week	0.038	0.05	0.006	0.044	0.06
White &Clay-Air Dry	7.108	24.249	7.33	15.146	12.163
Max Axial Deflection (mm)					
Thin Layer Kind	**Min**	**Max**	**SD**	**Mean**	**Median**
White-Air Dry	0.699	1.083	0.159	0.928	0.999
White-SatOnly-5Week	0.696	3.499	1.493	1.801	1.207
White-SatOnly-10Week	0.84	1.179	0.177	1.039	1.097

White-SatOnly-15Week	1.264	3.406	1.206	2.015	1.375
White-SatOnly-30Week	1.033	3.588	1.384	2.618	3.233
White-SatOnly-50Week	1.5	2.001	0.289	1.668	1.501
White-5Week-1.75bar	1.443	3.314	1.068	2.675	3.27
White-10Week-1.75bar	1.332	2.045	0.399	1.585	1.377
White-15Week-1.75bar	1.201	1.309	0.055	1.261	1.272
White-5Week-3.25bar	0.949	1.566	0.345	1.347	1.525
White-10Week-3.25bar	0.961	1.083	0.066	1.008	0.98
White-15Week-3.25bar	0.763	2.041	0.6997	1.237	1.237
White-5Week-5.0bar	0.978	2.117	0.591	1.457	1.275
White-10Week-5.0bar	1.785	2.045	0.146	1.952	2.027
White-15Week-5.0bar	1.141	4.083	1.553	2.324	1.749
Pink-Air Dry	0.699	1.416	0.291	0.924	0.832
Pink-SatOnly-5Week	0.925	1.075	0.086	1.024	1.072
Pink-SatOnly-10Week	1.009	1.154	0.083	1.104	1.149
Pink-SatOnly-15Week	1.127	1.292	0.0897	1.23	1.271
Pink-SatOnly-30Week	1.393	1.962	0.287	1.701	1.749
Pink-SatOnly-50Week	2.78	3.42	0.355	3.012	2.835
White & Clay-Air Dry	0.847	1.182	0.125	1.014	1.020
Max Horizontal Deflection (mm)					
Thin Layer Kind	**Min**	**Max**	**SD**	**Mean**	**Median**
White-Air Dry	1.096	3.026	0.791	2.481	2.694
White-SatOnly-5Week	1.648	9.347	3.962	4.956	3.873
White-SatOnly-10Week	3.015	5.023	1.009	4.079	4.1996
White-SatOnly-15Week	5.273	9.637	2.301	7.033	6.188
White-SatOnly-30Week	4.004	10.26	3.451	7.974	9.658
White-SatOnly-50Week	5.173	8.835	2.014	6.52	5.553
White-5Week-1.75bar	5.109	10.305	2.774	8.268	9.391
White-10Week-1.75bar	4.381	9.681	2.928	6.313	4.876
White-15Week-1.75bar	4.625	6.254	0.85	5.299	5.018
White-5Week-3.25bar	3.328	5.796	1.256	4.699	4.973
White-10Week-3.25bar	3.515	4.627	0.572	3.994	3.839
White-15Week-3.25bar	2.427	9.551	4.03	4.901	2.724
White-5Week-5.0bar	3.86	9.769	2.979	6.598	6.164
White-10Week-5.0bar	9.116	9.681	0.287	9.371	9.315
White-15Week-5.0bar	4.883	14.139	4.681	9.103	8.288
Pink-Air Dry	0.854	5.799	2.048	2.228	1.717
Pink-SatOnly-5Week	1.024	3.812	1.433	2.609	2.99
Pink-SatOnly-10Week	3.333	4.36	0.516	3.873	3.926
Pink-SatOnly-15Week	4.508	5.982	0.758	5.143	4.938
Pink-SatOnly-30Week	6.508	8.523	1.065	7.714	8.112
Pink-SatOnly-50Week	10.582	11.976	0.758	11.106	10.76
White & Clay-Air Dry	1.049	4.516	1.416	2.444	2.169
Max Mass Reduction (%)					
Thin Layer Kind	**Min**	**Max**	**SD**	**Mean**	**Median**
White-SatOnly-5Week	2.2014	2.3941	0.097	2.302	2.31
White-SatOnly-10Week	4.359	4.635	0.139	4.508	4.531
White-SatOnly-15Week	6.5631	6.92	0.1795	6.7304	6.708
White-SatOnly-30Week	12.44	13.6	0.584	13.057	13.13

White-SatOnly-50Week	21.57	23.13	0.794	22.437	22.61
White-5Week-1.75bar	7.053	7.181	0.067	7.128	7.15
White-10Week-1.75bar	8.88	13.88	2.602	11.797	12.63
White-15Week-1.75bar	18.58	18.72	0.071	18.657	18.67
White-5Week-3.25bar	6.997	7.03	0.018	7.017	7.024
White-10Week-3.25bar	14.632	15.099	0.24	14.834	14.77
White-15Week-3.25bar	21.447	21.669	0.114	21.574	21.605
White-5Week-5.0bar	7.3665	7.887	0.281	7.687	7.808
White-10Week-5.0bar	15.865	16.291	0.218	16.104	16.156
White-15Week-5.0bar	23.822	24.938	0.645	24.563	24.93
Pink-SatOnly-5Week	2.163	2.2933	0.067	2.236	2.252
Pink-SatOnly-10Week	3.78	4.54	0.396	4.223	4.35
Pink-SatOnly-15Week	6.285	7.347	0.542	6.755	6.632
Pink-SatOnly-30Week	12.78	14.204	0.784	13.302	12.923
Pink-SatOnly-50Week	20.77	26.862	3.167	23.315	22.312

Max Volume Reduction (%)						Cumulative Dissolution (US/cm)	Dissolution Rate per Week
Thin Layer Kind	Min	Max	SD	Mean	Median		
White-SatOnly-5Week	1.38	2.862	0.791	1.961	1.641	6693.1	1338.6
White-SatOnly-10Week	2.784	3.94	0.605	3.258	3.05	13293.9	1320.2
White-SatOnly-15Week	4.47	5.52	0.525	4.997	5	20159.4	1373.1
White-SatOnly-30Week	11.12	26.56	8.265	17.137	13.73	40657.2	1366.5
White-SatOnly-50Week	19.88	22.01	1.065	20.93	20.9	67030	1318.6
White-5Week-1.75bar	6.967	7.21	0.1297	7.062	7.01	9611	1922.2
White-10Week-1.75bar	7.58	14.174	3.704	11.851	13.8	19842	2046.2
White-15Week-1.75bar	16.066	22.253	3.0997	19.045	18.814	29339	1899.4
White-5Week-3.25bar	6.574	8.251	0.881	7.256	6.942	10043.7	2008.7
White-10Week-3.25bar	11.963	13.816	1.054	13.18	13.759	19849.8	1961.22
White-15Week-3.25bar	19.671	21.825	1.111	20.906	21.223	29852.5	2000.5
White-5Week-5.0bar	8.14	8.632	0.2597	8.338	8.242	10114.7	2022.9
White-10Week-5.0bar	14.242	15.575	0.676	14.843	14.71	20350.3	2047.12
White-15Week-5.0bar	22.262	24.664	1.325	23.139	22.492	30855.4	2101.02
Pink-SatOnly-5Week	1.93	2.04	0.055	1.983	1.98	7081.3	1416.3
Pink-SatOnly-10Week	3.452	3.631	0.091	3.531	3.51	14516	1486.94
Pink-SatOnly-15Week	3.87	6.2	1.173	5.114	5.273	20236.8	1144.16
Pink-SatOnly-30Week	12.803	13.795	0.538	13.179	12.94	40686.4	1363.31
Pink-SatOnly-50Week	19.502	25.636	3.323	21.831	20.354	66517.4	1291.55

4.3.2 Aust Cliff thin layer samples

From Table 4.5, the obtained compressive strength is in the range of 33 to 43 MPa for Aust Cliff/UK (*ACG*) samples respectively at air-dry state.

Saturation weakens those gypsum thin layers. As with the Bantycock samples, it can be seen that the mean values of $б_c$, *FL*, *TL*, *wt* and *vol* were decreased, while dissolution amount was increased progressively due to saturation over time progress.

Table 4.5: Compressive strength, Poisson's ratio, load at failure, time to failure, shear modulus, maximum axial deflection, maximum horizontal deflection, maximum mass reduction, maximum volume reductions, cumulative dissolution and dissolution rate per week after 50 week of uniaxial compression testing of air-dry and saturated thin layers samples (collected from Aust Cliff, November 2009). *Note: The Poisson's ratios for some samples are unrealistic and reflect the disintegration of the samples.

Compressive Strength (MPa)						Cumulative Dissolution (US/cm)	Dissolution Rate per Week
Aust Cliff Thin Layers	**Min**	**Max**	**SD**	**Mean**	**Median**		
Air Dry	33.268	43.163	4.024	38.666	40.514	0	0
SatOnly-5Week	25.514	30.933	3.104	29.098	30.846	6928.7	1385.74
SatOnly-10Week	14.081	30.391	8.662	23.922	27.294	12928.7	1200
SatOnly-15Week	11.75	23.151	5.708	17.616	17.947	21453	1704.86
SatOnly-30Week	4.948	33.896	15.127	16.883	11.805	41695.2	1349.48
SatOnly-50Week	11.871	16.199	2.175	13.91	13.659	68298.1	1330.145
Poisson's Ratio*							
Aust Cliff Thin Layers	**Min**	**Max**	**SD**	**Mean**	**Median**		
Air Dry	0.271	0.923	0.244	0.638	0.647		
SatOnly-5Week	0.464	0.635	0.099	0.521	0.464		
SatOnly-10Week	0.223	1.699	0.768	0.838	0.592		
SatOnly-15Week	0.601	1.027	0.232	0.867	0.973		
SatOnly-30Week	0.452	1.2097	0.382	0.801	0.741		
SatOnly-50Week	0.906	1.051	0.072	0.979	0.982		
Load at Failure (N)							
Aust Cliff Thin Layers	**Min**	**Max**	**SD**	**Mean**	**Median**		
Air Dry	76190.6	98853.3	9216.11	88554.6	92786.5		
SatOnly-5Week	57695.3	69138.12	6606.51	65323.8	69138.1		
SatOnly-10Week	31960.1	69369.7	19748.16	54321.9	61635.8		
SatOnly-15Week	39904.8	49602.34	5598.87	46369.8	49602.3		
SatOnly-30Week	10000	69138.22	30912.06	34365.8	23959.2		
SatOnly-50Week	23935.3	30948.8	3636.22	268886.8	25776.4		
Time to Failure (seconds)							
Aust Cliff Thin Layers	**Min**	**Max**	**SD**	**Mean**	**Median**		
Air Dry	442.15	574.10	53.682	514.13	538.75		
SatOnly-5Week	334.55	401.15	35.609	375.133	389.698		
SatOnly-10Week	184.7	403.7	115.438	315.3	357.5		
SatOnly-15Week	231.2	287.75	31.151	267.023	282.12		
SatOnly-30Week	57.952	387.698	172.075	194.383	137.5		
SatOnly-50Week	137.8	178.3	20.987	154.867	148.5		
Shear Modulus (GPa)							
Aust Cliff Thin Layers	**Min**	**Max**	**SD**	**Mean**	**Median**		
Air Dry	8.651	15.966	2.895	12.141	12.296		
SatOnly-5Week	0.161	0.257	0.049	0.204	0.195		
SatOnly-10Week	0.031	0.3114	0.148	0.145	0.092		
SatOnly-15Week	0.0395	0.069	0.015	0.054	0.052		
SatOnly-30Week	0.038	0.164	0.072	0.08	0.039		
SatOnly-50Week	0.023	0.046	0.012	0.037	0.043		
Max Axial Deflection (mm)							
Aust Cliff Thin Layers	**Min**	**Max**	**SD**	**Mean**	**Median**		

Air Dry	0.841	1.399	0.201	1.106	1.098
SatOnly-5Week	0.84	1.207	0.2044	1.076	1.18
SatOnly-10Week	0.696	4.081	1.715	2.228	1.907
SatOnly-15Week	2.168	2.498	0.168	2.351	2.389
SatOnly-30Week	0.431	2.641	1.123	1.421	1.19
SatOnly-50Week	2.129	2.756	0.335	2.374	2.237
Max Horizontal Deflection (mm)					
Aust Cliff Thin Layers	**Min**	**Max**	**SD**	**Mean**	**Median**
Air Dry	1.378	4.42	1.214	3.096	3.091
SatOnly-5Week	3.015	3.873	0.43	3.459	3.487
SatOnly-10Week	1.648	9.39	4.37	6.69	9.032
SatOnly-15Week	9.222	10.30	0.581	9.636	9.386
SatOnly-30Week	1.107	10.276	4.702	5.0898	3.887
SatOnly-50Week	8.264	12.641	2.246	10.161	9.576
Max Mass Reduction (%)					
Aust Cliff Thin Layers	**Min**	**Max**	**SD**	**Mean**	**Median**
SatOnly-5Week	3.715	3.962	0.124	3.841	3.845
SatOnly-10Week	4.35	5.92	0.892	4.89	4.4
SatOnly-15Week	9.63	12.66	1.533	11.01	10.74
SatOnly-30Week	18.9	20.55	0.948	19.455	18.915
SatOnly-50Week	19.84	29.84	5.167	25.593	27.099
Max Volume Reduction (%)					
Aust Cliff Thin Layers	**Min**	**Max**	**SD**	**Mean**	**Median**
SatOnly-5Week	4.063	4.9443	0.495	4.373	4.113
SatOnly-10Week	2.151	11.36	5.119	5.464	2.88
SatOnly-15Week	6.033	9.568	1.768	7.784	7.75
SatOnly-30Week	20.12	21.05	0.487	20.501	20.332
SatOnly-50Week	22.561	27.7	2.964	25.984	27.69

4.3.3 Iraqi thin layer samples

From Table 4.6, the obtained compressive strength is in the range of 82 to 88 MPa for air dry Iraqi (*IG*) samples.

Saturation weakens those gypsum thin layers. It can be seen that the mean values of σ_c, *FL*, *TL*, *SM*, *wt* and *vol* were decreased, while the dissolution amount was increased progressively due to saturation over time.

Table 4.6: Compressive strength, Poisson's ratio, load at failure, time to failure, shear modulus, maximum axial deflection, maximum horizontal deflection, maximum weight reduction, maximum volume reduction and maximum recorded dissolution after 50 weeks of saturation and uniaxial compression testing of thin layers/discs samples. The samples were prepared from specimens collected from Iraq in June 2010). *Note: The Poisson's ratios for some samples are unrealistic and reflect the disintegration of the samples.

Compressive Strength (MPa)						Max Dissolution (US/cm)	Dissolution Rate per Week
Iraqi Thin Layer	**Min**	**Max**	**SD**	**Mean**	**Median**		
Air Dry	82.451	88.681	2.656	85.866	86.15	0	0
SatOnly-5Week	37.309	65.642	16.088	47.074	38.271	7070.7	1414.14
SatOnly-10Week	28.712	38.578	5.361	34.856	37.279	14047.7	1395.4
SatOnly-15Week	24.365	43.214	9.536	32.948	31.267	21227	1435.86
SatOnly-30Week	23.198	35.09	6.405	27.77	25.021	41994.2	1384.48
SatOnly-50Week	13.205	32.224	9.98	20.967	17.472	69607.9	1380.685
Poisson's Ratio*							
Iraqi Thin Layer	**Min**	**Max**	**SD**	**Mean**	**Median**		
Air Dry	0.171682	0.43903	0.109	0.258	0.203		
SatOnly-5Week	0.605542	0.790603	0.097	0.681	0.648		
SatOnly-10Week	0.562996	0.727279	0.083	0.651	0.661		
SatOnly-15Week	0.530201	1.035455	0.253	0.783	0.783		
SatOnly-30Week	0.790572	1.162752	0.187	0.969	0.953		
SatOnly-50Week	0.571808	0.886216	0.159	0.741	0.764		
Load at Failure (N)							
Iraqi Thin Layer	**Min**	**Max**	**SD**	**Mean**	**Median**		
Air Dry	188832.3	203099.3	6752.85	197812.1	201737.7		
SatOnly-5Week	85255.4	147059	35220.86	106400.4	86886.7		
SatOnly-10Week	63914.3	86629.1	12516.73	78309.13	84384		
SatOnly-15Week	53510.9	96119.2	21539.99	72979.8	69309.3		
SatOnly-30Week	47423.6	72161.2	13023.36	57438.63	52731.1		
SatOnly-50Week	25534.4	59240.72	17672.14	39317.51	33177.4		
Time to Failure (seconds)							
Iraqi Thin Layer	**Min**	**Max**	**SD**	**Mean**	**Median**		
Air Dry	1100.05	1182.5	38.718	1152.02	1174.3		
SatOnly-5Week	496.3	856.1	205.085	619.35	505.65		
SatOnly-10Week	371.9	504.3	72.93	455.77	491.1		
SatOnly-15Week	311.4	559.45	125.4	424.73	403.35		
SatOnly-30Week	275.85	408.65	69.508	330.38	306.65		
SatOnly-50Week	143.75	338.3	103.568	220.5	179.45		
Shear Modulus (GPa)							
Iraqi Thin Layer	**Min**	**Max**	**SD**	**Mean**	**Median**		
Air Dry	28.648	36.865	3.308	34.351	35.83		
SatOnly-5Week	0.169	0.232	0.034	0.193	0.178		
SatOnly-10Week	0.137	0.189	0.028	0.168	0.179		
SatOnly-15Week	0.13	0.186	0.03	0.152	0.14		
SatOnly-30Week	0.064	0.158	0.047	0.114	0.119		
SatOnly-50Week	0.055	0.083	0.015	0.072	0.078		
Max Axial Deflection (mm)							
Iraqi Thin Layer	**Min**	**Max**	**SD**	**Mean**	**Median**		

Air Dry	1.2	1.664	0.18	1.457	1.457
SatOnly-5Week	1.266	1.909	0.341	1.521	1.389
SatOnly-10Week	1.05	1.457	0.219	1.30	1.394
SatOnly-15Week	0.892	1.58	0.388	1.339	1.546
SatOnly-30Week	1.092	3.268	1.238	1.839	1.156
SatOnly-50Week	1.518	3.481	1.013	2.355	2.068
Max Horizontal Deflection (mm)					
Iraqi Thin Layer	**Min**	**Max**	**SD**	**Mean**	**Median**
Air Dry	2.733	9.692	2.549	6.462	7.004
SatOnly-5Week	4.444	6.11	0.845	5.357	5.518
SatOnly-10Week	3.347	4.887	0.859	4.337	4.776
SatOnly-15Week	3.619	6.324	1.43	5.241	5.779
SatOnly-30Week	5.31	9.476	2.369	6.743	5.441
SatOnly-50Week	6.421	9.582	1.664	8.302	8.904
Max Mass Reduction (%)					
Iraqi Thin Layer	**Min**	**Max**	**SD**	**Mean**	**Median**
SatOnly-5Week	1.58	1.998	0.211	1.807	1.842
SatOnly-10Week	2.713	4.67	0.992	3.598	3.41
SatOnly-15Week	6.399	7.08	0.376	6.648	6.465
SatOnly-30Week	12.85	17.399	2.364	15.497	16.242
SatOnly-50Week	22.87	28.69	3.129	25.117	23.79
Max Volume Reduction (%)					
Iraqi Thin Layer	**Min**	**Max**	**SD**	**Mean**	**Median**
SatOnly-5Week	1.09	3.141	1.04	2.017	1.82
SatOnly-10Week	2.591	5.99	1.719	4.44	4.74
SatOnly-15Week	4.634	6.903	1.138	5.717	5.613
SatOnly-30Week	13.59	17.797	2.407	16.369	17.721
SatOnly-50Week	25.44	30.858	2.918	28.775	30.026

4.3.4 Compared thin layers results

Compressive strength test parameters (mean) such as Poisson's ratio, load at failure, time to failure and shear modulus, mass and volume reductions, and dissolution amount were used to construct comparison relationships among tested gypsum rock thin layer samples. Air-dry and saturated samples under different levels of water pressure were compared in this section. XY scatter and columns chart were used in the construction of those comparisons as shown in Figure 4.26-4.30.

From the comparisons of air-dry state, it can be seen that the Iraqi sample is the strongest one as shown in Figure 4.30, while the intact white/Bantycock sample is the weakest one. Close results were revealed for UK samples. The impurities seam to make the gypsum rock stronger.

From the comparisons of saturation state under atmospheric pressure, it can be seen that there is a role of saturation to weaken gypsum rock thin layer and this role will continue to weaken samples over time progress. Close results were obtained in general among UK samples. Aust cliff sample is the highest weakened over time, while Iraqi one is the lowest weakened (see Figure 4.30/F).

From the comparisons among tested white/Bantycock thin layer in saturation under 1.75, 3.25 and 5.0 bar pressure, it can be seen that there is a notable role of water pressure on dissolution amount compare to dissolution under atmospheric pressure. The dissolution increased progressively when water pressure increased. So, water pressure continues to weaken samples over time progress. Notable divergence among saturation under atmospheric pressure and under water pressure for tested samples in terms of mass, volume reductions and dissolution curves was recognized over time progress.

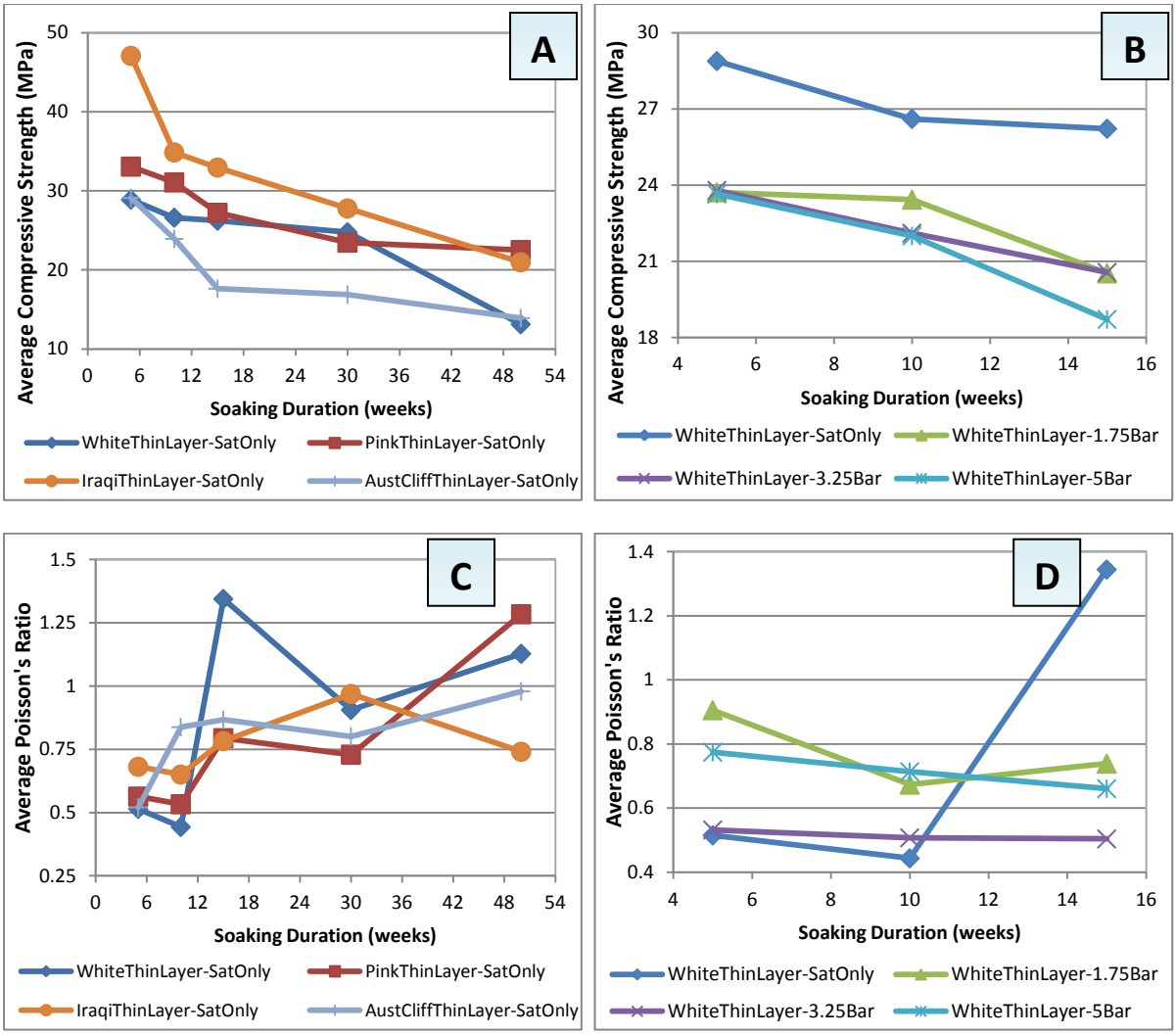

Fig. 4.26: Average compressive strength results of gypsum rock thin layers shown in parts A and B. Average Poisson's ratio results of gypsum rock thin layers shown in parts C and D. In these parts the relationship of compressive strength and Poisson's ratio with soaking period lasted for 50 week is shown. Tested gypsum rock thin layers are 54 mm diameter X 20 mm height and from different origins (UK and Iraq). Parts A and C are on the comparison among tested samples after saturation under atmospheric pressure. Parts B and D are on the comparison among white/Bantycock thin layers after saturation under water pressure of 1.75, 3.25 and 5.0 bar.

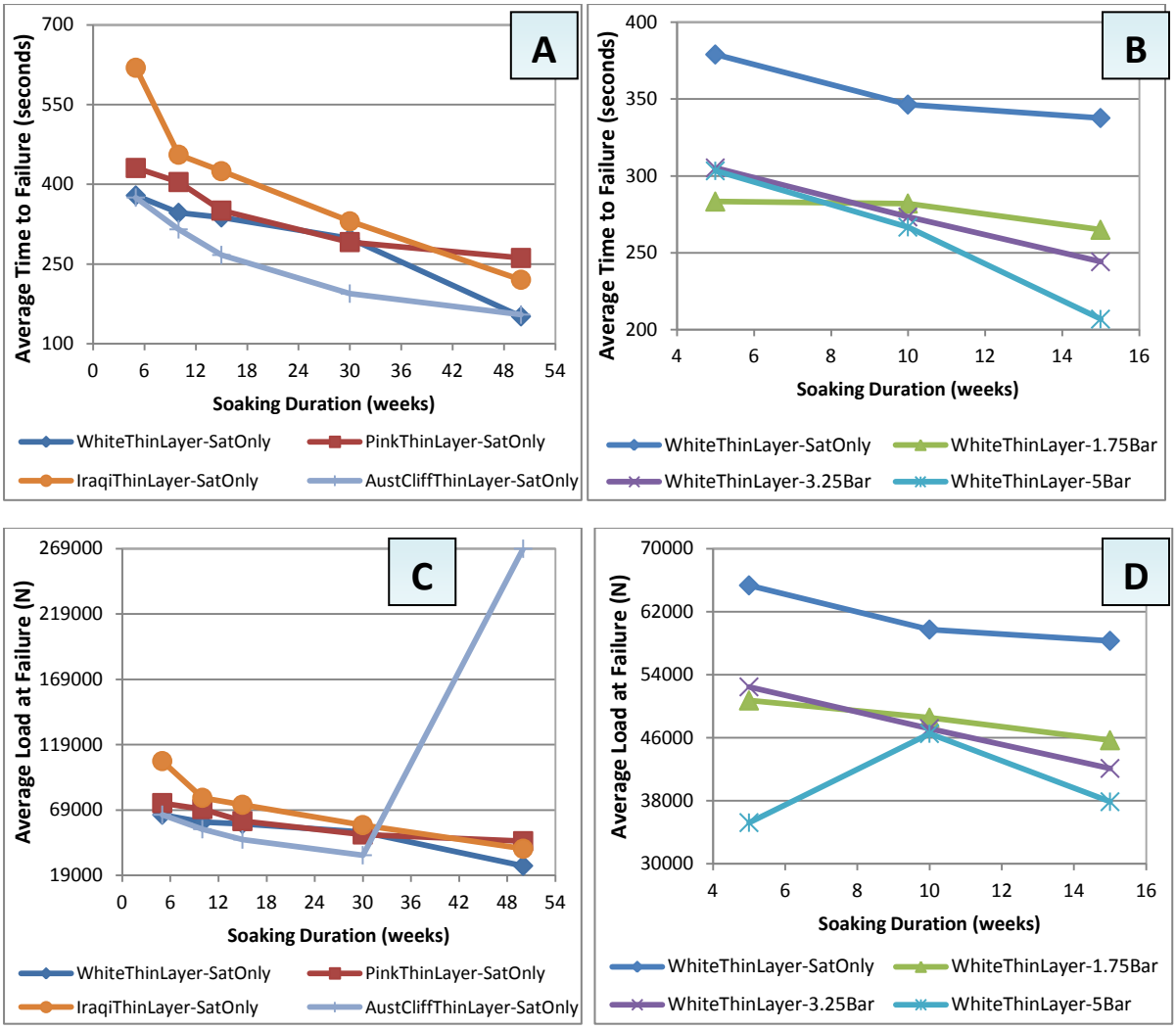

Fig. 4.27: Average time to failure results of gypsum rock thin layers shown in parts A and B. Average load at failure of gypsum rock thin layers shown in parts C and D. In these parts, the relationship of average time to failure and load at failure with soaking period lasted for 50 week is shown. Tested gypsum rock thin layers are in size of 54 mm diameter X 20 mm height and from different origins (UK and Iraq). Parts A and C are on the comparison among tested samples after saturation under atmospheric pressure. Parts B and D are on the comparison among tested white/Bantycock gypsum thin layers after saturation under water pressure of 1.75, 3.25 and 5.0 bar. Note in part C, the unexpectedly high load at failure for the Aust Cliff sample.

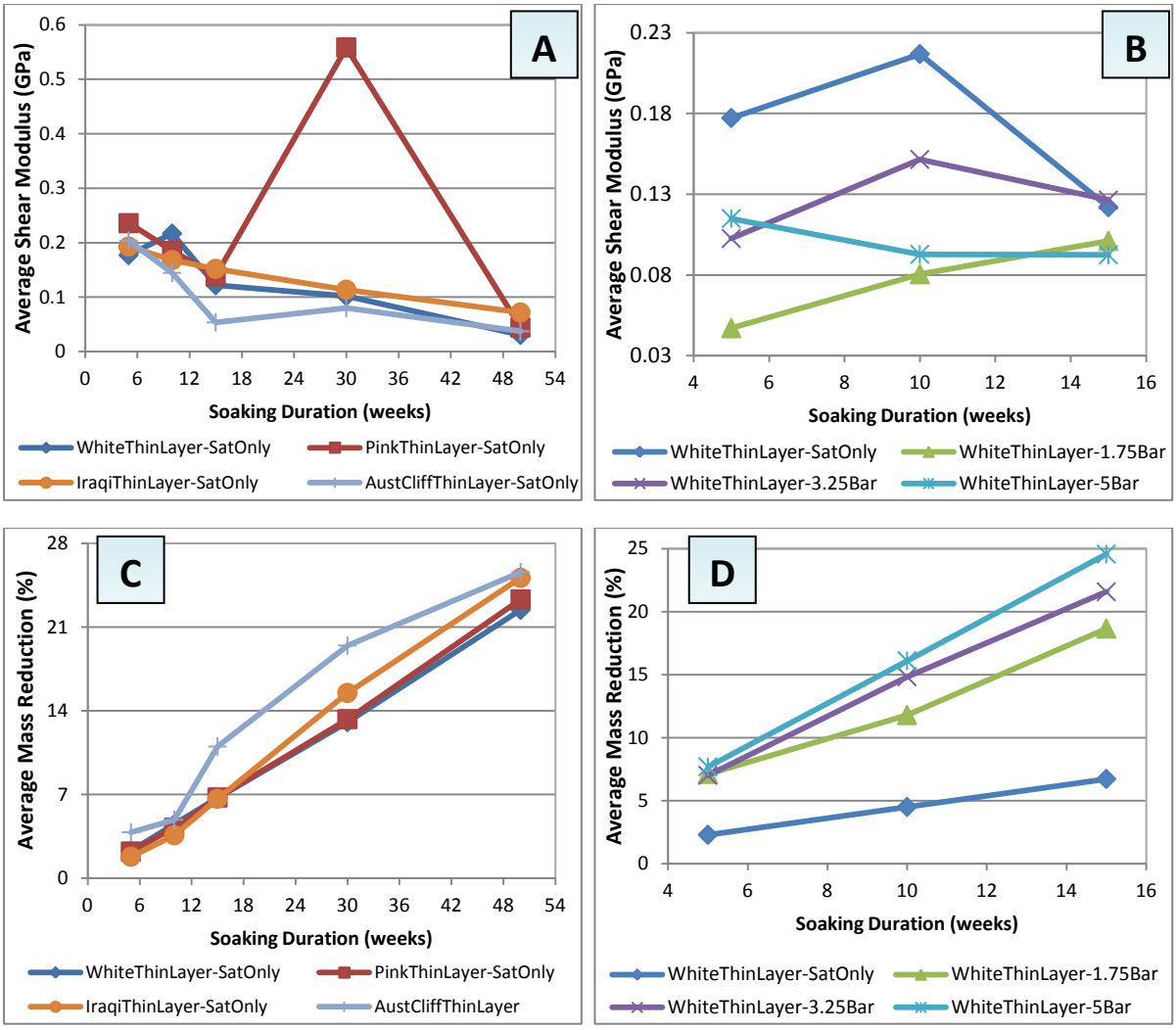

Fig. 4.28: Average shear modulus results of gypsum rock thin layers shown in parts A and B. Average mass reduction of gypsum rock thin layers shown in parts C and D. In these parts, the relationship of average shear modulus and average mass reduction with soaking period lasted for 50 week is shown. Tested gypsum rock thin layers are 54 mm diameter X 20 mm height and from different origins (UK and Iraq). Parts A and C are on the comparison between tested samples after saturation under atmospheric pressure. Parts B and D are on the comparison among tested white/Bantycock gypsum thin layers after saturation under water pressure of 1.75, 3.25 and 5.0 bar.

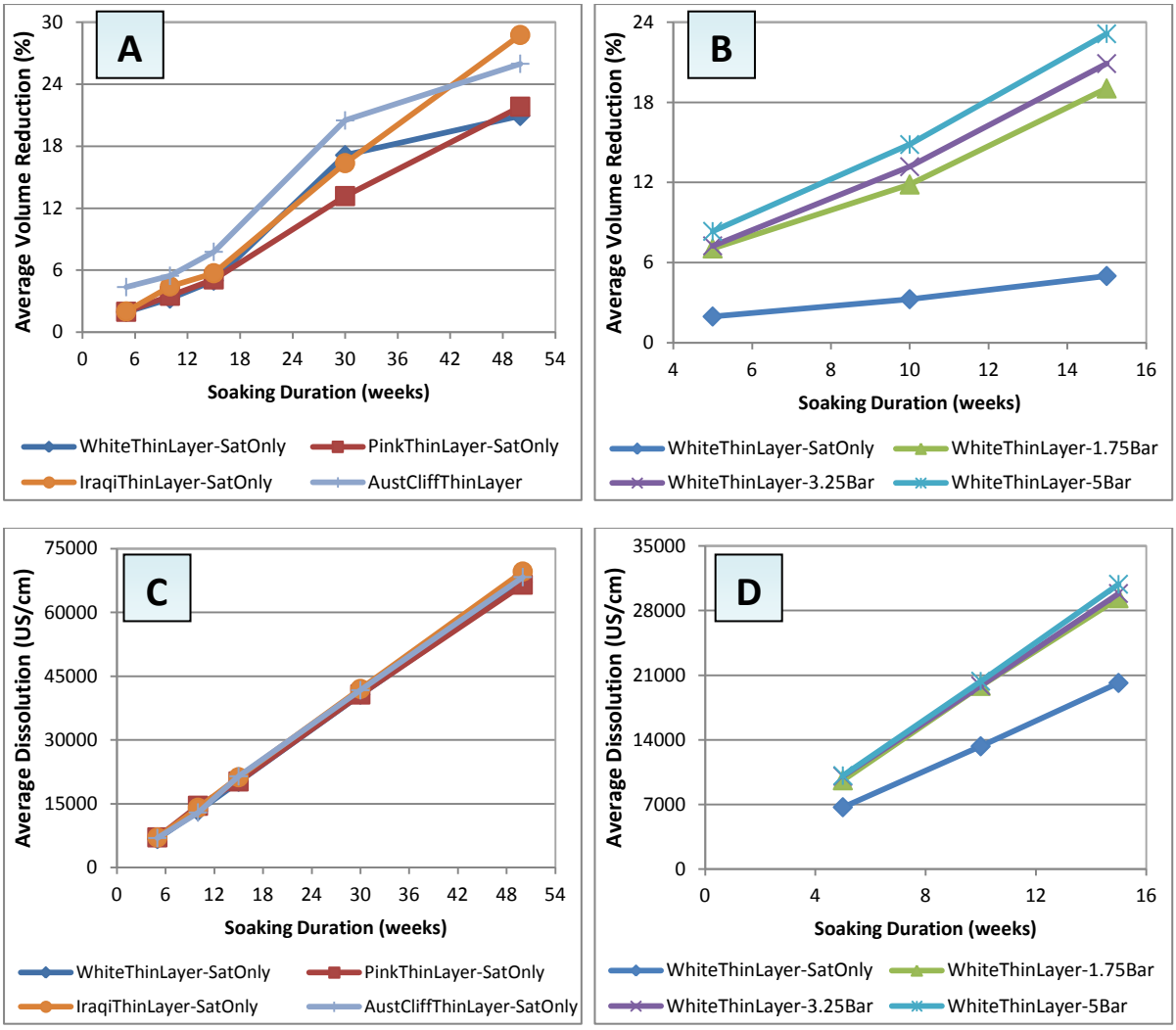

Fig. 4.29: Average volume reduction results of gypsum rock thin layers shown in parts A and B. Average dissolution results of gypsum rock thin layers shown in parts C and D. In these parts, the relationship of average volume reduction and average dissolution with soaking period lasted for 50 week is shown. Tested gypsum rock thin layers are in size of 54 mm diameter X 20 mm height and from different origins (UK and Iraq). Parts A and C are on the comparison among tested samples after saturation under atmospheric pressure. Parts B and D are on the comparison among tested white/Bantycock gypsum thin layers after saturation under water pressure of 1.75, 3.25 and 5.0 bar.

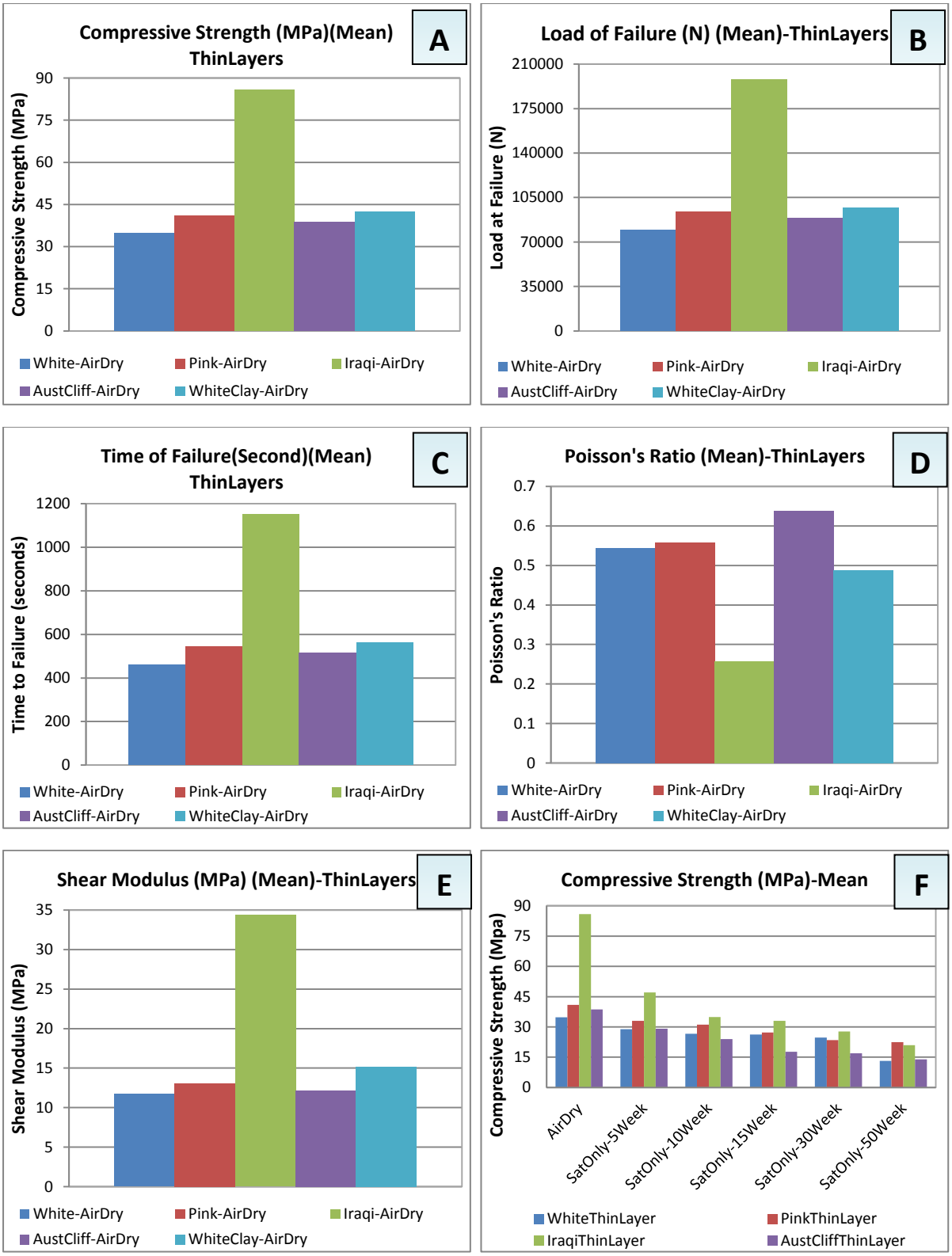

Fig. 4.30: Comparison of the results of air-dry thin layers from UK and Iraq in parts A to E and part F for the results comparison of saturated thin layers. Part A is for the compressive strength, part B is for the load at failure, part C is for the time to failure, part D is for the Poisson's ratio, part E is for the shear modulus and part F is for the compressive strength of saturated thin layers from UK and Iraq. The tested samples' size is 54 mm Diameter X 20 mm Height.

4.3.5 Bantycock bending samples

Two kinds of four-point bending bars were tested in short-term mode. Table 4.7 below shows the statistical results of large four-point bending results; the tested samples were only white gypsum from Bantycock Mine because the other types of gypsum were unsuitable due to cracks and impurities. Table 4.8 show the results of small four-point bending bars.

From Table 4.7, the calculated flexural stress at failure ($Fб_c$) is in the range of 5.8 to 8.13 MPa for white/Bantycock large four-point bending (*LFB*) samples at air-dry state.

Saturation state notably weakens *LFB* samples and it was continued to cause more weakening samples over time progress. It can be seen that those bars exhibited to a considerable drop in $Fб_c$, *TF* and *LF*, *vol* and *wt* and increase in dissolution amounts due to saturation under atmospheric pressure compare to the air-dry state.

Speeding up gypsum dissolution process is noticed within the application of 1.75, 3.25 and 5.0 bar compare to saturation under atmospheric pressure, more progressive increase of dissolution over time progresses. It can be seen that the $Fб_c$, *TF*, *LF*, *wt* and *vol* of *LFB* decreases and dissolution amount and rate increase due to water pressure application more than their decreased values due to saturation under atmospheric pressure.

Table 4.7: Flexural stress at failure, load at failure, maximum volume reduction, time to failure, flexural modulus, vertical deflection, maximum mass reduction and cumulative dissolution are for large four-point bending bars tested after 50 weeks of saturation. These data calculated were from four-point bending test of large bars in size of 240 x 40 x 20 mm, which prepared from collected samples from Bantycock Mine/UK on field trip April 2010 and April 2011.

Flexural stress at Failure (MPa)						Max Dissolution (US/cm)	Dissolution Rate per Week
Large Bar State	Min	Max	SD	Mean	Median		
Air-Dry	5.835	8.132	0.935	6.533	6.135	0	0
Sat-5Week	2.184	3.567	0.778	2.669	2.257	7533.6	1506.72
Sat-10Week	2.207	2.371	0.083	2.297	2.312	14997.9	1492.86
Sat-15Week	1.448	2.519	0.552	2.061	2.215	23328.6	1666.14
Sat-30Week	1.172	1.857	0.348	1.477	1.403	43316.4	1333.33
Sat-50Week	1.31	1.607	0.152	1.441	1.405	70372.4	1352.8
1.75bar-5Week	1.89	3.045	0.662	2.655	3.026	10724.7	2144.94

1.75bar-10Week	1.938	2.438	0.253	2.168	2.126	21582.2	2171.5
1.75bar-15Week	1.566	2.178	0.31	1.842	1.783	32056.1	2094.78
3.25bar-5Week	2.315	2.811	0.252	2.589	2.639	10974.7	2194.94
3.25bar-10Week	1.809	1.942	0.0704	1.888	1.914	21825.1	2170.08
3.25bar-15Week	1.616	1.888	0.136	1.755	1.762	32944.8	2223.94
5.0bar-5Week	2.332	2.648	0.162	2.509	2.546	11316.1	2263.22
5.0bar-10Week	1.624	1.88	0.142	1.788	1.859	22578	2252.38
5.0bar-15Week	1.448	1.829	0.191	1.629	1.611	33911	2266.6

Load at Failure (N)

Large Bar State	Min	Max	SD	Mean	Median
Air-Dry	466.833	650.52	73.513	525.483	505.173
Sat-5Week	174.682	285.365	62.274	213.537	180.564
Sat-10Week	176.571	189.65	6.629	183.738	184.993
Sat-15Week	115.837	201.554	44.168	164.857	177.181
Sat-30Week	93.789	148.527	27.847	118.193	112.262
Sat-50Week	104.772	128.577	12.153	115.256	112.42
1.75bar-5Week	151.166	243.623	52.929	212.276	242.04
1.75bar-10Week	155.033	195.065	20.218	173.403	170.111
1.75bar-15Week	125.313	174.23	24.806	147.382	142.604
3.25bar-5Week	185.228	224.877	20.134	207.084	211.147
3.25bar-10Week	144.679	155.349	5.634	151.06	153.151
3.25bar-15Week	129.301	151.042	10.879	140.424	140.929
5.0bar-5Week	186.527	211.833	12.921	200.69	203.711
5.0bar-10Week	129.918	150.367	11.362	143.004	148.726
5.0bar-15Week	115.837	146.277	15.273	146.277	128.863

Max Volume Reduction (%)

Large Bar State	Min	Max	SD	Mean	Median
Sat-5Week	0.455	2.669	1.173	1.786	2.234
Sat-10Week	4.827	5.34	0.261	5.112	5.17
Sat-15Week	3.44	6.632	1.652	5.282	5.774
Sat-30Week	23.22	24.541	0.722	23.712	23.376
Sat-50Week	21.24	41.158	10.115	32.22	34.263
1.75bar-5Week	6.911	8.01	0.5502	7.444	7.41
1.75bar-10Week	10.883	11.28	0.211	11.122	11.203
1.75bar-15Week	11.04	12.152	0.556	11.584	11.56
3.25bar-5Week	7.3704	8.41	0.543	7.98	8.16
3.25bar-10Week	10.115	15.824	3.14	13.724	15.233
3.25bar-15Week	13.34	14.636	0.658	14.052	14.1804
5.0bar-5Week	7.968	8.633	0.352	8.234	8.1
5.0bar-10Week	14.17	17.01	1.438	15.46	15.2
5.0bar-15Week	14.644	17.414	1.551	15.626	14.82

Time to Failure (seconds)

Large Bar State	Min	Max	SD	Mean	Median
Air-Dry	280.9	400.1	46.957	320.16	304.2
Sat-5Week	105.8	163.1	32.882	125.133	106.5
Sat-10Week	102.2	112.4	5.86	105.633	102.3
Sat-15Week	63.2	116.6	27.432	93.533	100.8
Sat-30Week	52.1	80.4	14.15	66.3	66.4
Sat-50Week	54.4	71.6	8.685	63.7	65.1
1.75bar-5Week	85.3	144	33.112	123.5	141.2
1.75bar-10Week	91.1	113.7	11.663	100.733	97.4
1.75bar-15Week	57.9	88.0	15.912	69.967	64

3.25bar-5Week	107.9	131.2	11.694	120.133	121.3
3.25bar-10Week	77.6	86.9	4.661	82.433	82.8
3.25bar-15Week	61.3	83.2	11.185	73.567	76.2
5.0bar-5Week	112	124.9	6.616	117.6	115.9
5.0bar-10Week	76.7	88.8	6.507	84.133	86.9
5.0bar-15Week	63.2	84.1	10.545	72.833	71.2
Flexural Modulus (GPa)					
Large Bar State	**Min**	**Max**	**SD**	**Mean**	**Median**
Air-Dry	17.051	22.288	1.912	19.345	19.234
Sat-5Week	0.349	8.074	3.9203	3.825	3.0511
Sat-10Week	10.364	15.948	3.147	12.317	10.64
Sat-15Week	6.125	8.512	1.363	7.698	8.457
Sat-30Week	1.769	8.133	3.189	4.831	4.59
Sat-50Week	3.54	9.355	2.908	6.444	6.437
1.75bar-5Week	4.543	12.592	4.513	7.388	5.03
1.75bar-10Week	6.968	17.469	5.909	10.654	7.525
1.75bar-15Week	0.67	0.904	0.128	0.752	0.698
3.25bar-5Week	6.511	26.951	10.267	17.301	18.442
3.25bar-10Week	0.439	20.067	9.915	9.44	7.813
3.25bar-15Week	0.6402	20.365	10.248	8.897	5.684
5.0bar-5Week	2.612	19.081	8.714	9.202	5.911
5.0bar-10Week	0.896	4.416	1.793	2.459	2.066
5.0bar-15Week	4.698	7.052	1.186	5.958	6.125
Vertical Deflection (mm)					
Large Bar State	**Min**	**Max**	**SD**	**Mean**	**Median**
Air-Dry	0.115	0.214	0.041	0.148	0.127
Sat-5Week	0.131	0.233	0.054	0.192	0.212
Sat-10Week	0.095	0.131	0.019	0.116	0.121
Sat-15Week	0.079	0.13	0.027	0.109	0.119
Sat-30Week	0.124	0.222	0.054	0.161	0.137
Sat-50Week	0.082	0.191	0.056	0.131	0.121
1.75bar-5Week	0.129	0.328	0.112	0.199	0.141
1.75bar-10Week	0.095	0.136	0.022	0.119	0.125
1.75bar-15Week	0.051	0.079	0.014	0.063	0.061
3.25bar-5Week	0.0997	0.161	0.035	0.1204	0.101
3.25bar-10Week	0.069	0.126	0.029	0.098	0.0997
3.25bar-15Week	0.061	0.126	0.035	0.086	0.073
5.0bar-5Week	0.079	0.234	0.078	0.156	0.155
5.0bar-10Week	0.134	0.553	0.213	0.32	0.273
5.0bar-15Week	0.079	0.247	0.092	0.142	0.1005
Max Mass Reduction (%)					
Large Bar State	**Min**	**Max**	**SD**	**Mean**	**Median**
Sat-5Week	2.691	2.77	0.0395	2.728	2.724
Sat-10Week	5.65	5.96	0.166	5.771	5.704
Sat-15Week	7.412	8.451	0.522	7.9024	7.844
Sat-30Week	15.5	16.73	0.66	15.977	15.7
Sat-50Week	24.38	27.389	1.533	26.053	26.39
1.75bar-5Week	3.75	4.112	0.186	3.954	4.001
1.75bar-10Week	7.89	8.04	0.076	7.97	7.98
1.75bar-15Week	11.58	11.763	0.094	11.684	11.71
3.25bar-5Week	4.094	4.3899	0.149	4.249	4.263
3.25bar-10Week	6.81	8.833	1.119	8.098	8.65
3.25bar-15Week	12.54	13.222	0.394	12.995	13.222

5.0bar-5Week	4.54	4.68	0.079	4.631	4.672
5.0bar-10Week	9.003	9.63	0.335	9.248	9.11
5.0bar-15Week	13.574	14.464	0.469	13.933	13.762

From Table 4.8, the calculated flexural stress to failure is in the range of 6.5 to 10.1, 4.91 to 8.22, 4.4 to 6.6, 1.5 to 7.73 and 3 to 7.7 MPa for white/Bantycock (*SFB-WBG*), Pink/Bantycock (*SFB-PBG*), white & clay/Bantycock (*SFB-WCBG)* and white & marl/Bantycock (*SFB-WMBG*) small four-point bending samples respectively at air-dry state.

Saturation state weakens the *SFB-WBG* and *SFB-PBG* samples and it was continued to cause more weakening of those samples over time progress. It can be seen that the Mean data of $Fб_c$, *TF*, *LF*, *wt* and *vol* of white and pink *SFB* bars decreased due to saturation under atmospheric pressure compare to the air-dry state.

Speeding up gypsum dissolution process is noticed within the application of 1.75, 3.25 and 5.0 bar compare to saturation under atmospheric pressure, more progressive increase of dissolution over time progresses. It can be seen that the values of *Fбc*, *TF*, *LF*, *wt* and *vol* of *SFB-WBG* samples decreases and dissolution amount and rate increased due to water pressure application more than dissolution due to saturation under atmospheric pressure case.

Table 4.8: Flexural stress at failure, load at failure, maximum volume reduction, time to failure, flexural modulus, vertical deflection, maximum mass reduction and cumulative dissolution are for small four-point bending bars tested after 50 weeks of saturation. Samples are in size of 140 x 40 x 20 mm, which were prepared from collected samples from Bantycock Mine/UK on field trip April 2010 and April 2011.

Flexural Stress at Failure (MPa)					
Small Bar State	**Min**	**Max**	**SD**	**Mean**	**Median**
White-Air Dry	6.454	10.078	1.444	7.763	7.418
White-SatOnly-5Week	2.206	3.234	0.548	2.83	3.05
White-SatOnly-10Week	2.039	2.602	0.285	2.345	2.393
White-SatOnly-15Week	1.987	2.355	0.211	2.231	2.35
White-SatOnly-30Week	1.421	2.29	0.445	1.911	2.021
White-SatOnly-50Week	0.803	2.012	0.604	1.408	1.409
White-1.75bar-5Week	2.007	3.13	0.569	2.623	2.733
White-1.75bar-10Week	1.577	2.626	0.551	2.197	2.389

White-1.75bar-15Week	1.676	2.22	0.275	1.974	2.059
White-3.25bar-5Week	1.73	3.119	0.708	2.504	2.662
White-3.25bar-10Week	1.421	2.557	0.639	2.157	2.493
White-3.25bar-15Week	1.48	2.33	0.441	1.973	2.112
White-5.0bar-5Week	1.779	2.627	0.452	2.113	1.932
White-5.0bar-10Week	0.909	2.781	1.019	2.078	2.544
White-5.0bar-15Week	1.633	2.352	0.395	1.898	1.71
Pink-Air Dry	4.909	8.22	1.492	6.213	5.362
Pink-SatOnly-5Week	0.615	4.016	1.80	2.657	3.339
Pink-SatOnly-10Week	1.392	1.95	0.279	1.673	1.678
Pink-SatOnly-15Week	1.267	2.282	0.541	1.665	1.448
Pink-SatOnly-30Week	1.236	1.578	0.184	1.368	1.289
Pink-SatOnly-50Week	0.8097	1.368	0.299	1.027	0.904
White & Clay-Air Dry	4.347	6.614	0.926	5.59	5.351
White & Marl-Air Dry	1.56	7.732	2.421	5.78	6.599
White & Cracks-Air Dry	3.082	7.751	1.985	4.614	3.466
Load at Failure (N)					
Small Bar State	**Min**	**Max**	**SD**	**Mean**	**Median**
White-Air Dry	1032.7	1612.485	231.072	1242.092	1186.817
White-SatOnly-5Week	352.977	517.449	87.686	452.783	487.923
White-SatOnly-10Week	326.274	416.374	45.543	375.182	382.898
White-SatOnly-15Week	317.97	376.73	33.697	356.877	375.932
White-SatOnly-30Week	227.317	366.342	71.182	305.677	323.37
White-SatOnly-50Week	128.545	321.959	96.707	225.289	225.361
White-1.75bar-5Week	321.099	500.718	91.085	419.677	437.214
White-1.75bar-10Week	252.272	420.196	88.074	351.589	382.299
White-1.75bar-15Week	268.228	355.136	44.045	315.833	324.137
White-3.25bar-5Week	276.754	499.048	113.301	400.594	425.98
White-3.25bar-10Week	227.299	409.15	102.17	345.128	398.935
White-3.25bar-15Week	236.797	372.789	70.625	315.815	337.859
White-5.0bar-5Week	284.665	420.385	72.349	338.04	309.071
White-5.0bar-10Week	145.473	444.956	163.078	332.506	407.09
White-5.0bar-15Week	261.228	376.387	63.203	303.76	273.666
Pink-Air Dry	785.489	1315.174	238.778	994.08	857.9
Pink-SatOnly-5Week	98.443	642.576	288.024	425.091	534.256
Pink-SatOnly-10Week	222.703	311.926	44.617	267.702	268.478
Pink-SatOnly-15Week	202.712	365.068	86.607	266.465	231.615
Pink-SatOnly-30Week	197.798	252.43	29.426	218.797	206.162
Pink-SatOnly-50Week	129.547	218.89	47.834	164.343	144.592
White & Clay-Air Dry	695.469	1058.294	148.102	695.469	856.097
White & Marl-Air Dry	249.535	1237.054	387.393	924.837	1055.763
White & Cracks-Air Dry	493.167	1240.071	317.611	738.268	554.53
Time to Failure (seconds)					
Small Bar State	**Min**	**Max**	**SD**	**Mean**	**Median**
White-Air Dry	319.6	497.4	72.775	381.82	359.9
White-SatOnly-5Week	105	156.7	28.207	137.367	150.4
White-SatOnly-10Week	94.8	120.9	13.384	109.567	113
White-SatOnly-15Week	83.7	107.6	12.929	98.5	104.2
White-SatOnly-30Week	69.1	109	20.608	92.033	98
White-SatOnly-50Week	38.7	92.4	26.947	66.867	69.5
White-1.75bar-5Week	83.6	140.5	28.773	114.533	119.5
White-1.75bar-10Week	63	117.9	27.901	93.333	99.1
White-1.75bar-15Week	82.6	104.3	11.364	95.4	99.3

White-3.25bar-5Week	79.1	150.2	36.569	119.6	129.5
White-3.25bar-10Week	69.1	120.9	29.907	103.633	120.9
White-3.25bar-15Week	73.3	115.7	21.491	96.533	100.6
White-5.0bar-5Week	85.7	123.5	19.884	101.033	93.9
White-5.0bar-10Week	42.8	136.3	50.783	101	123.9
White-5.0bar-15Week	69.6	106	19.474	83.8	75.8
Pink-Air Dry	233.6	353.9	51.868	282.86	255.1
Pink-SatOnly-5Week	19.3	198.4	94.908	127	163.3
Pink-SatOnly-10Week	62.6	93.8	15.886	79.933	83.4
Pink-SatOnly-15Week	70.5	111.9	23.591	84.667	71.6
Pink-SatOnly-30Week	60.6	76.3	8.616	66.4	62.3
Pink-SatOnly-50Week	29.1	56.7	14.748	39.9	33.9
White & Clay-Air Dry	215.9	325	45.449	274.7	261.4
White & Marl-Air Dry	67.7	383.1	123.091	281.8	317.8
White & Cracks-Air Dry	154.2	383.4	99.051	227.14	171.5
Flexural Modulus (GPa)					
Small Bar State	**Min**	**Max**	**SD**	**Mean**	**Median**
White-Air Dry	7.637	13.567	2.302	10.054	9.66
White-SatOnly-5Week	2.981	5.695	1.458	4.031	3.418
White-SatOnly-10Week	2.006	2.625	0.327	2.377	2.50
White-SatOnly-15Week	1.556	5.665	2.188	3.177	2.312
White-SatOnly-30Week	1.435	1.763	0.169	1.576	1.53
White-SatOnly-50Week	1.78	6.386	2.54	3.465	2.229
White-1.75bar-5Week	2.658	4.746	1.113	3.48	3.035
White-1.75bar-10Week	2.996	6.408	1.957	5.256	6.363
White-1.75bar-15Week	1.684	2.969	0.674	2.445	2.682
White-3.25bar-5Week	3.954	7.953	2.021	5.782	5.44
White-3.25bar-10Week	1.313	2.967	0.858	2.008	1.745
White-3.25bar-15Week	2.388	7.111	2.514	4.251	3.255
White-5.0bar-5Week	2.524	4.119	0.841	3.168	2.861
White-5.0bar-10Week	2.216	8.461	3.228	4.867	3.924
White-5.0bar-15Week	1.336	2.319	0.535	1.95	2.194
Pink-Air Dry	9.053	14.27	2.2	11.071	10.609
Pink-SatOnly-5Week	4.76	8.065	1.689	6.615	7.02
Pink-SatOnly-10Week	1.239	5.114	1.971	2.969	2.553
Pink-SatOnly-15Week	1.613	3.228	0.812	2.372	2.276
Pink-SatOnly-30Week	1.863	3.704	1.028	2.519	1.991
Pink-SatOnly-50Week	1.166	3.827	1.345	2.382	2.155
White & Clay-Air Dry	3.327	10.729	2.968	7.624	7.624
White & Marl-Air Dry	7.424	14.367	3.007	10.005	8.204
White & Cracks-Air Dry	3.652	9.626	2.343	6.414	6.414
Vertical Deflection (mm)					
Small Bar State	**Min**	**Max**	**SD**	**Mean**	**Median**
White-Air Dry	0.049	0.102	0.023	0.08	0.09
White-SatOnly-5Week	0.065	0.131	0.037	0.108	0.129
White-SatOnly-10Week	0.143	0.18	0.020	0.166	0.175
White-SatOnly-15Week	0.051	0.233	0.091	0.138	0.131
White-SatOnly-30Week	0.145	0.232	0.049	0.175	0.149
White-SatOnly-50Week	0.023	0.103	0.044	0.073	0.093
White-1.75bar-5Week	0.072	0.16	0.044	0.118	0.12
White-1.75bar-10Week	0.065	0.117	0.029	0.083	0.067
White-1.75bar-15Week	0.078	0.175	0.052	0.117	0.096
White-3.25bar-5Week	0.0597	0.168	0.056	0.105	0.088

White-3.25bar-10Week	0.099	0.138	0.021	0.115	0.108
White-3.25bar-15Week	0.071	0.083	0.007	0.079	0.083
White-5.0bar-5Week	0.075	0.081	0.003	0.078	0.077
White-5.0bar-10Week	0.043	0.116	0.038	0.073	0.06
White-5.0bar-15Week	0.136	0.2099	0.037	0.176	0.183
Pink-Air Dry	0.053	0.082	0.012	0.061	0.055
Pink-SatOnly-5Week	0.0198	0.143	0.062	0.081	0.082
Pink-SatOnly-10Week	0.054	0.234	0.092	0.134	0.114
Pink-SatOnly-15Week	0.124	0.552	0.237	0.28	0.162
Pink-SatOnly-30Week	0.119	0.137	0.0095	0.126	0.123
Pink-SatOnly-50Week	0.034	0.213	0.093	0.109	0.081
White & Clay-Air Dry	0.055	0.157	0.039	0.09	0.078
White & Marl-Air Dry	0.038	0.099	0.027	0.073	0.078
White & Cracks-Air Dry	0.051	0.1004	0.018	0.076	0.0753

Max Mass Reduction (%)

Small Bar State	Min	Max	SD	Mean	Median
White-SatOnly-5Week	2.135	2.329	0.097	2.232	2.232
White-SatOnly-10Week	4.062	5.21	0.587	4.707	4.85
White-SatOnly-15Week	6.78	7.601	0.422	7.247	7.36
White-SatOnly-30Week	14.96	15.423	0.267	15.114	14.96
White-SatOnly-50Week	23.103	25.51	1.301	24.591	25.16
White-1.75bar-5Week	5.26	5.795	0.271	5.552	5.6
White-1.75bar-10Week	10.35	10.662	0.18	10.557	10.66
White-1.75bar-15Week	14.665	15.181	0.263	14.953	15.013
White-3.25bar-5Week	5.55	5.95	0.218	5.8	5.898
White-3.25bar-10Week	11.411	11.971	0.291	11.646	11.557
White-3.25bar-15Week	17.851	23.897	3.468	19.893	17.93
White-5.0bar-5Week	6.345	7.001	0.346	6.61	6.483
White-5.0bar-10Week	12.95	13.063	0.057	13.005	13.003
White-5.0bar-15Week	18.058	19.409	0.725	18.886	19.19
Pink-SatOnly-5Week	1.8	2.64	0.423	2.248	2.303
Pink-SatOnly-10Week	5.27	5.48	0.121	5.34	5.27
Pink-SatOnly-15Week	6.93	8.63	0.851	7.763	7.73
Pink-SatOnly-30Week	13.31	15.6	1.17	14.593	14.87
Pink-SatOnly-50Week	23.57	25.21	0.93	24.644	25.151

Max Volume Reduction (%)

Small Bar State	Min	Max	SD	Mean	Median	Max Dissolution (US/cm)	Dissolution Rate per week
White-SatOnly-5Week	1.574	2.552	0.562	1.904	1.584	6214.1	1242.82
White-SatOnly-10Week	2.26	3.813	0.859	3.248	3.671	12194	1195.98
White-SatOnly-15Week	5	6.467	0.779	5.582	5.28	19089.4	1379.08
White-SatOnly-30Week	18.503	19.882	0.69	19.202	19.221	37357.8	1217.89
White-SatOnly-50Week	29.184	33.67	2.392	31.906	32.864	62105	1237.36
White-1.75bar-5Week	7.722	8.6702	0.476	8.173	8.126	10844.7	2168.94
White-1.75bar-10Week	10.494	11.03	0.269	10.778	10.81	21632.5	2157.56
White-1.75bar-15Week	19.614	22.626	1.585	20.835	20.266	32967.6	2267.02
White-3.25bar-5Week	7.724	9.338	0.864	8.709	9.065	11054.7	2210.94
White-3.25bar-10Week	16.572	16.945	0.192	16.734	16.684	21846.7	2158.4
White-3.25bar-15Week	20.121	23.343	1.637	21.898	22.229	33036.9	2238.04
White-5.0bar-5Week	9.66	10.003	0.172	9.836	9.844	11204.7	2240.94
White-5.0bar-10Week	17.409	18.506	0.569	18.045	18.219	22571	2273.26
White-5.0bar-15Week	25.887	26.088	0.104	26.003	26.035	33732.2	2232.24

Pink-SatOnly-5Week	1.567	3.004	0.721	2.317	2.378	6537.3	1307.46
Pink-SatOnly-10Week	7.599	8.797	0.599	8.202	8.211	11646.07	1021.75
Pink-SatOnly-15Week	9.527	12.407	1.592	11.358	12.141	19443.4	1559.47
Pink-SatOnly-30Week	17.127	23.353	3.241	20.761	21.804	37137.6	1179.61
Pink-SatOnly-50Week	31.5	33.01	0.846	32.475	32.914	61857.8	1236.01

4.3.6 Aust Cliff bending samples

Table 4.9: Presents statistical analysis for Aust Cliff small four-point bending bars in size of 140 x 40 x 20 mm. These bars were prepared from collected samples from Aust Cliff, UK in November 2009.

Aust Cliff/UK Small Four-Point Bending Test (Air-Dry)					
Property	**Min**	**Max**	**SD**	**Mean**	**Median**
Compressive Stress at Failure (MPa)	1.609	3.1544	0.592	2.383	2.481
Load at Failure (N)	257.489	504.7036	94.669	381.309	396.918
Time to Failure (seconds)	73.3	153.5	31.717	111	114.8
Flexural Modulus (GPa)	1.803	6.70982	2.098	4.202	3.52
Vertical Deflection (mm)	0.044	0.0996	0.024	0.071	0.076

4.3.7 Iraqi bending samples

Table 4.10: Presents statistical analysis for Iraqi small four-point bending bars in size of 140 x 40 x 20 mm. These bars were prepared from collected samples from Bazyan, Iraq in June 2010.

Iraqi Small Four-Point Bending Test (Air-Dry)					
Property	**Min**	**Max**	**SD**	**Mean**	**Median**
Compressive Stress at Failure (MPa)	4.872	8.007	1.181	6.202	6.071
Load at Failure (N)	779.572	1281.039	188.961	992.344	971.289
Time to Failure (seconds)	230.3	395.2	61.966	301.34	295.1
Flexural Modulus (GPa)	4.622	9.624	2.132	7.617	7.617
Vertical Deflection (mm)	0.05	0.113	0.023	0.078	0.077

4.3.8 Compared bending results

Two kinds of comparison have been demonstrated; the first is on the comparison between *SFB-WBG* and *SFB-PBG* in saturation state only, while the second is on the comparison among saturation state and applied water pressure on *LFB-WBG* only.

Flexure test parameters (mean) such as flexural stress at failure ($Fб_c$), load at failure, time to failure and mass and volume reductions, flexural modulus, vertical deflection and dissolution amount were used to construct comparison relationships among *LFB-WBG* tested samples. XY scatter was used in the construction of those comparisons as shown in Figure 4.31-4.32.

Similarly, those parameters were used to construct comparison relationships among *SFB-WBG*, *SFB-PBG*, *SFB-ACG*, *SFB-WCBG*, *SFB-WMBG* and *SFB-WCrBG* tested samples. XY scatter and column charts were used in the construction of those comparisons as shown in Figure 4.33-4.37.

From the comparisons of air-dry state, it can be seen that the intact *SFB-WBG* sample is the strongest one as shown in Figure 4.37, while the *SFB-ACG* sample is the weakest one. The impurities and existing cracks seem to make the gypsum rock weaker. Existing impurities inside macro-cracks of *SFB-ACG*, *SFB-WCBG*, *SFB-WMBG*, *SFB-PBG and SFB-IG* samples reduced the bars strength compared with the intact *SFB-WBG* sample. However, the *SFB-PBG and SFB-IG* samples are still strong (see Figure 4.37), which might be resulted from their high density or older geological age. *SFB-ACG* is the weakest one, which are originally thin layers or lenses (see Figure 1.8 of Chapter 1) and naturally not well compacted compare to Bantycock and Iraqi gypsum. Macro-cracks, which are distributed randomly, have notably decreased small bars' ability due to the weak existing positions make these bars less able to resist axial stress.

From the comparisons among the tested *LFB-WBG* samples in saturation under 1.75, 3.25 and 5.0 bar pressure, it can be seen that there is a notable role of water pressure on dissolution amount compare to dissolution under atmospheric pressure. The dissolution increased progressively when water pressure increased. So, water pressure continues to weaken samples over time progress. A divergence among saturation under atmospheric pressure and under water pressure for tested samples in terms of mass, volume reductions and dissolution curves was recognized over time.

From the comparison of saturation under atmospheric pressure state, it can be seen that there saturation weakens gypsum rock small four-point bending bars and this role will continue to weaken samples over time progress. The *SFB-WBG* experienced greater

reductions in $F\delta_c$, *TF* and *LF* than *PBG*. While, the *wt* and *vol* reductions of *PBG* is more than *WBG*. This contradicting results is due to the dissolution of *PBG* is more than the *WBG* and the impurities/other minerals rather than gypsum keep the *PBG* stronger even dissolved more.

SFB-WBG sample is stronger than *SFB-PBG* as shown in Figure 4.33-4.35. Similar behaviour for *SFB-WBG* and *SFB-PBG* is noticed. The reduced values of $F\delta_c$, *TF* and *LF* of *SFB-PBG* are more than *SFB-WBG*. Very little differences in *wt* reductions for *SFB-PBG* and *SFB-WBG* and convergence started from 30 week to 50 week, Figure 4.35/C. Moreover, in Figure 4.36/A, both of *SFB-PBG* and *SFB-WBG* behave in a similar way, with a divergence start from 5 weeks until 15 weeks then convergence started which lasted until 50 weeks.

The increase in length between small and large bending bars, is associated with a reduction in strength from 7.763 MPa to 6.533 MPa, which is about 15.8 percent reduction.

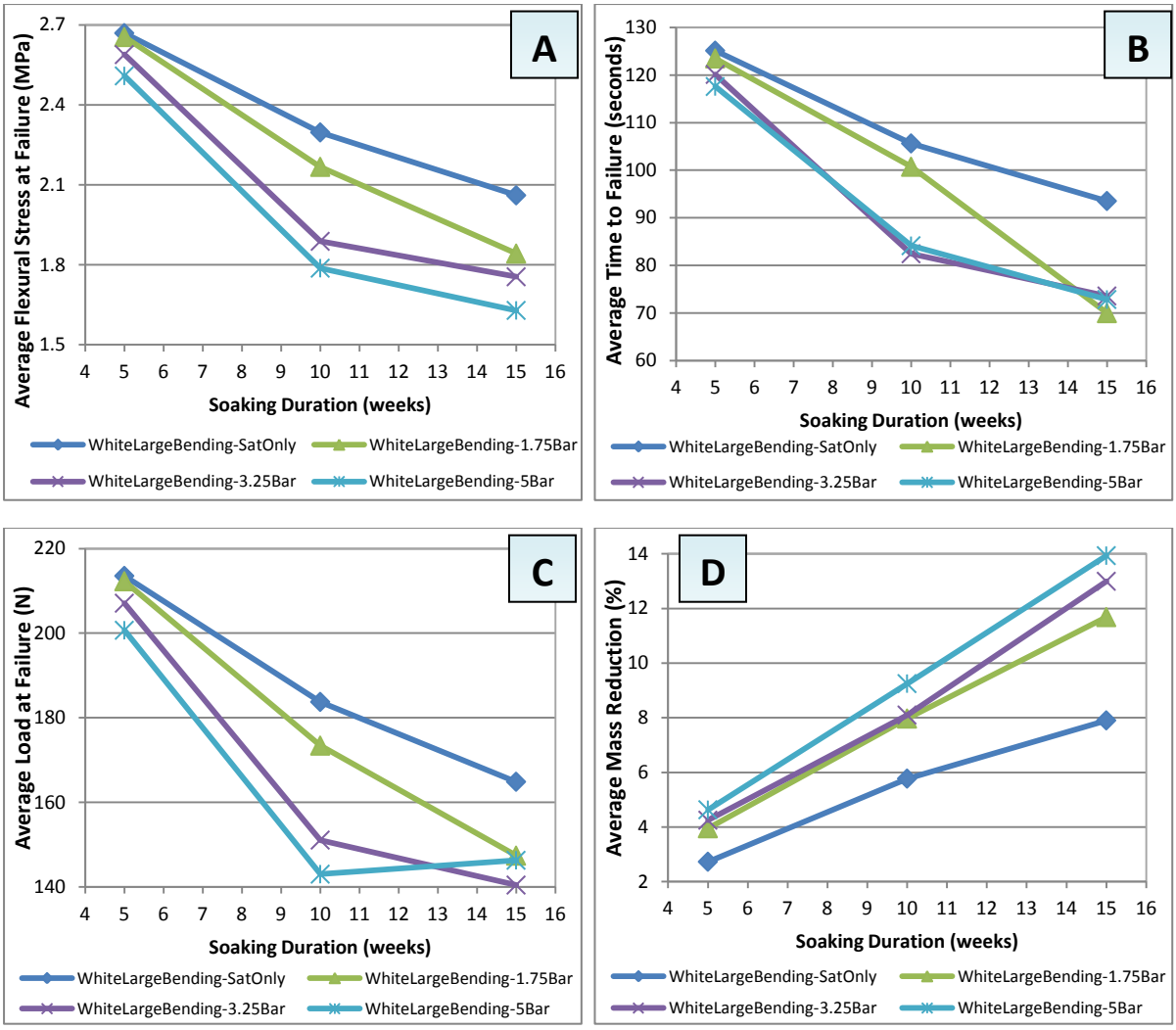

Fig. 4.31: A comparison of flexural tests parameters of large four-point bending bars tested after saturation under different levels of water pressure. The tested samples size is 240 x 40 x 20 mm, prepared from white gypsum from Bantycock Mine/UK. Part A is for the comparison of average flexural stress at failure values, part B is for the comparison of time to failure, part C for the comparison of average load at failure and part D is for the comparison of average mass reduction.

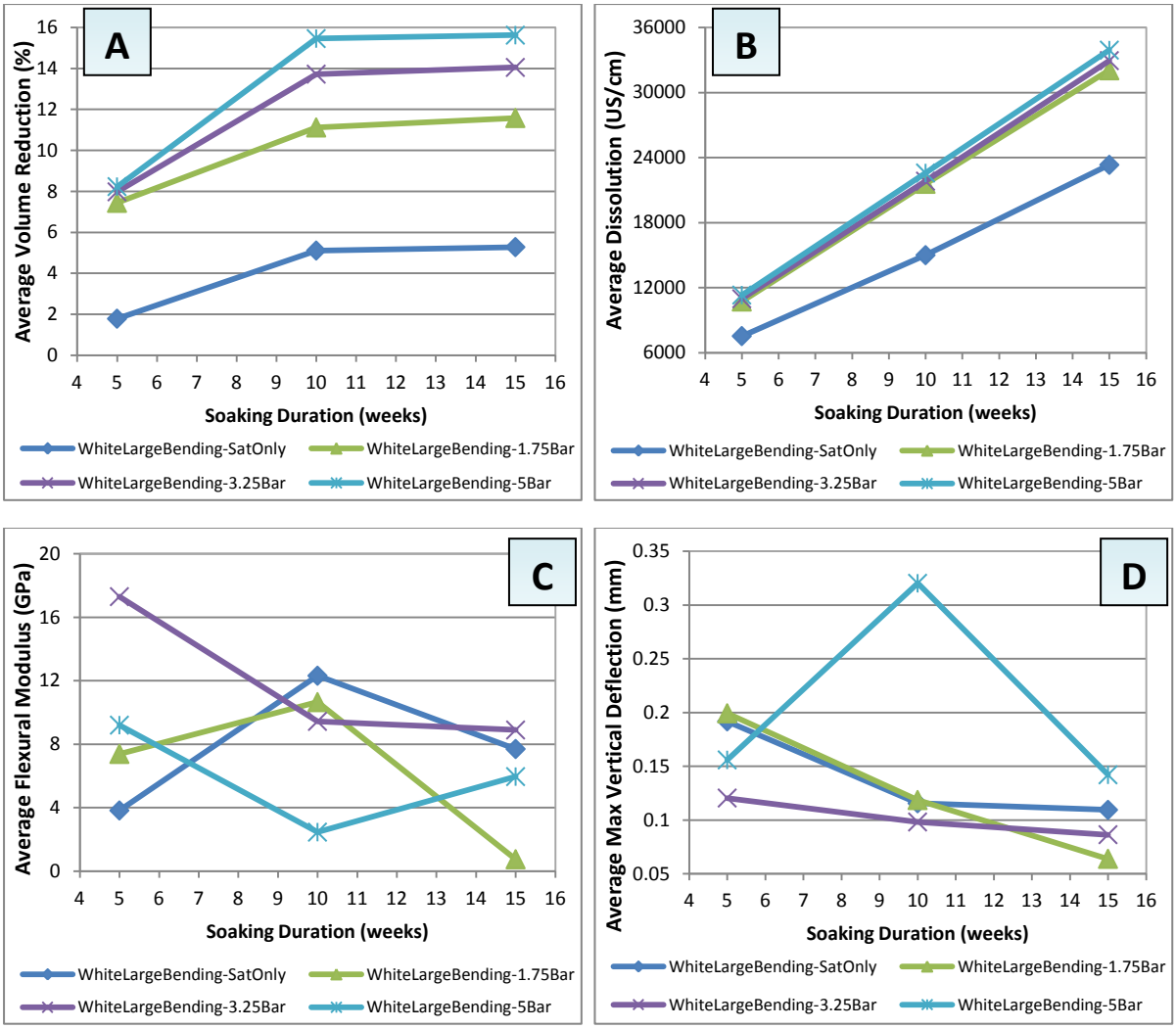

Fig. 4.32: Comparison of flexural tests parameters of large four-point bending bars tested after saturation under different levels of water pressure. The tested samples size is 240 x 40 x 20 mm, prepared from white gypsum from Bantycock Mine/UK. Part A is for the comparison of average volume reduction, part B is for the comparison of average dissolution, part C for the comparison of average flexural modulus and part D is for the comparison of average maximum vertical deflection.

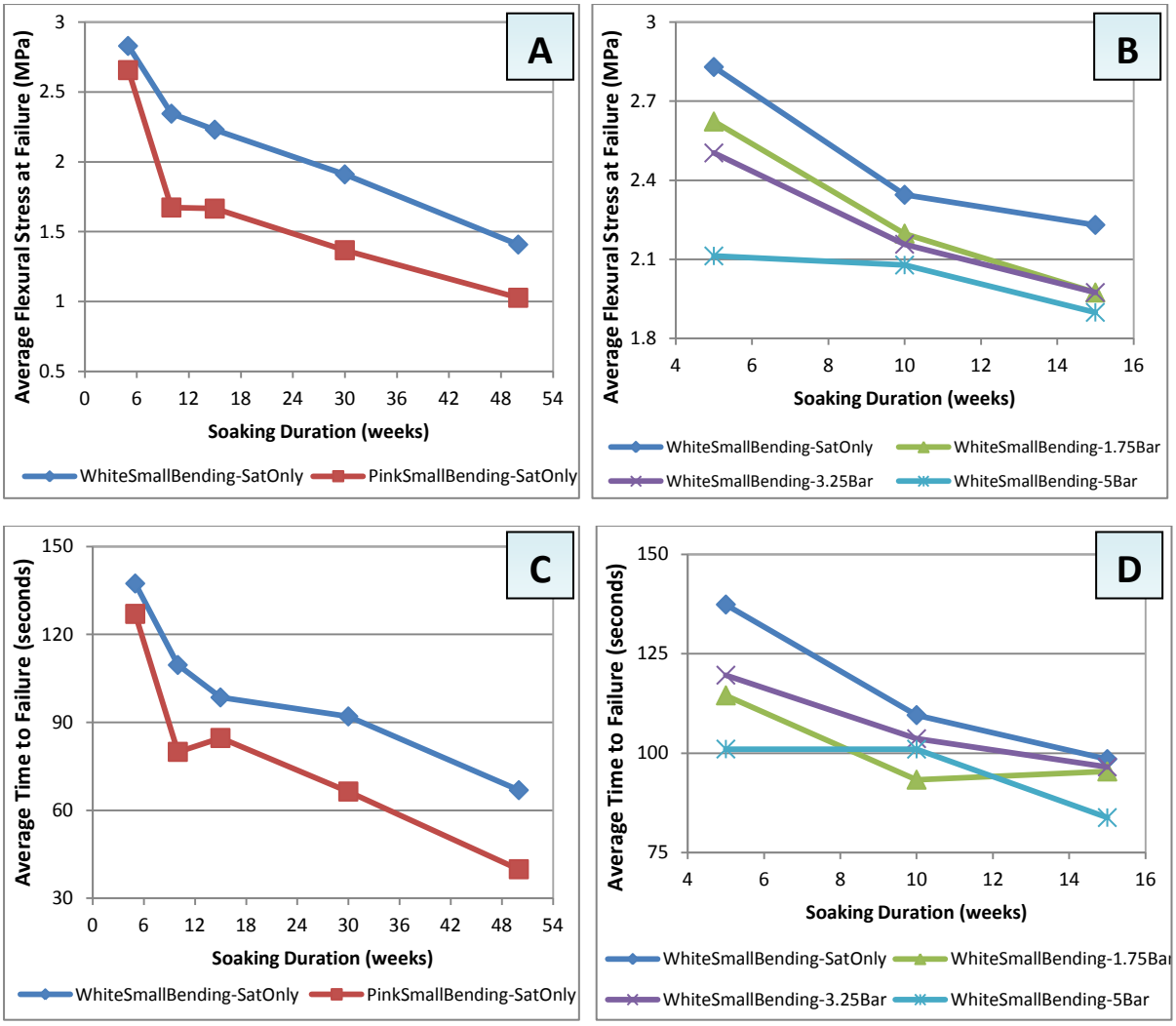

Fig. 4.33: Comparison of flexural tests parameters of small four-point bending bars tested after saturation under different levels of water pressure. The tested samples size is 140 x 40 x 20 mm. Part A is for the comparison of average flexural stress at failure of white/Bantycock and pink/Bantycock small bars tested after saturation under atmospheric pressure. Part B is for the comparison of average flexural stress at failure of white/Bantycock small bars tested under different levels of water pressure. Part C is for the comparison of average time to failure of white/Bantycock and pink/Bantycock small bars tested after saturation under atmospheric pressure. Part D is for the comparison of average time to failure of white/Bantycock small bars tested under different levels of water pressure.

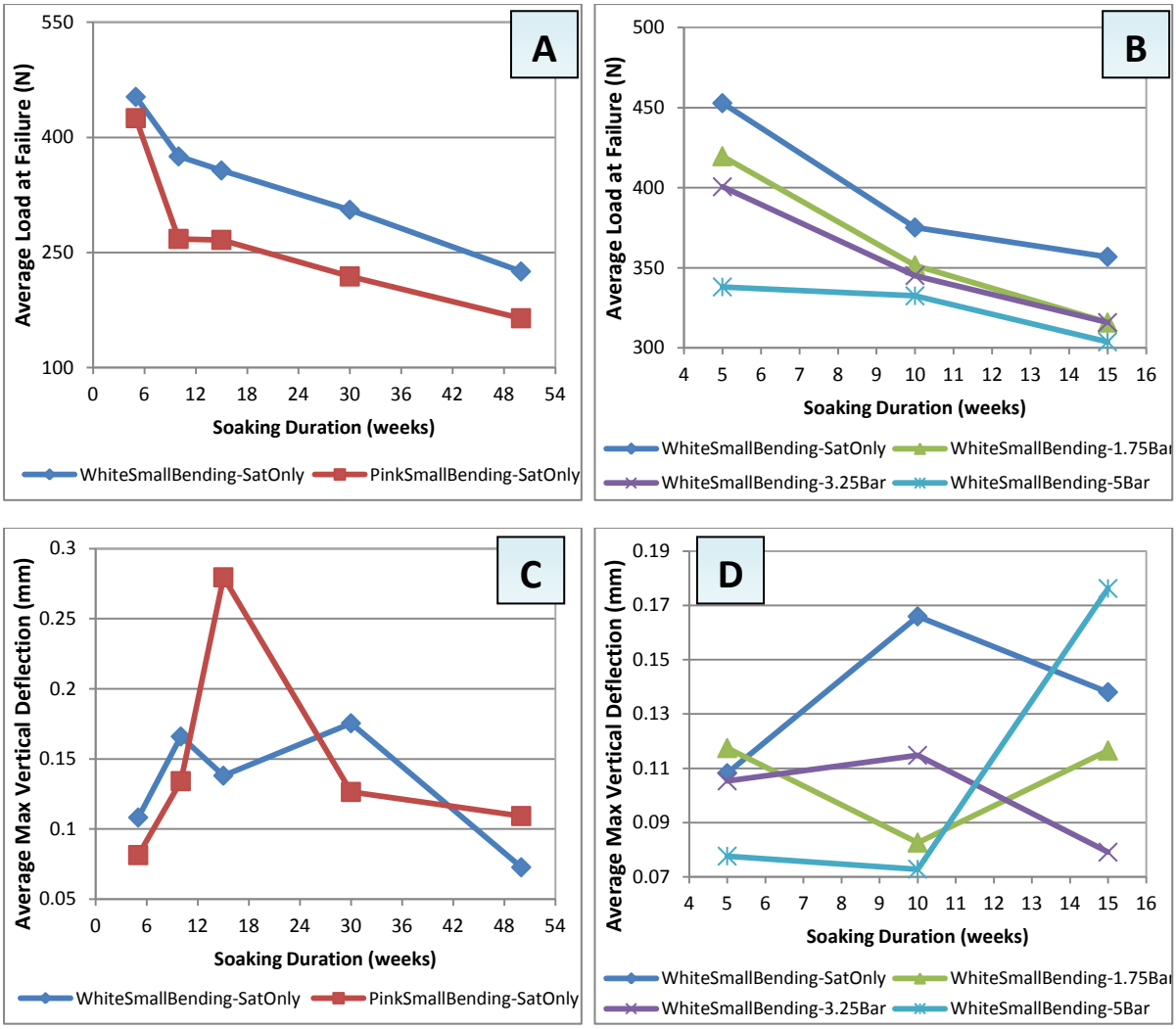

Fig. 4.34: Comparison of flexural tests parameters of small four-point bending bars tested after saturation under different levels of water pressure. The tested samples size is 140 x 40 x 20 mm. Part A is for the comparison of average load at failure of white/Bantycock and pink/Bantycock small bars tested after saturation under atmospheric pressure. Part B is for the comparison of average load at failure of white/Bantycock small bars tested under different levels of water pressure. Part C is for the comparison of average maximum vertical deflection of white/Bantycock and pink/Bantycock small bars tested after saturation under atmospheric pressure. Part D is for the comparison of maximum vertical deflection of white/Bantycock small bars tested under different levels of water pressure.

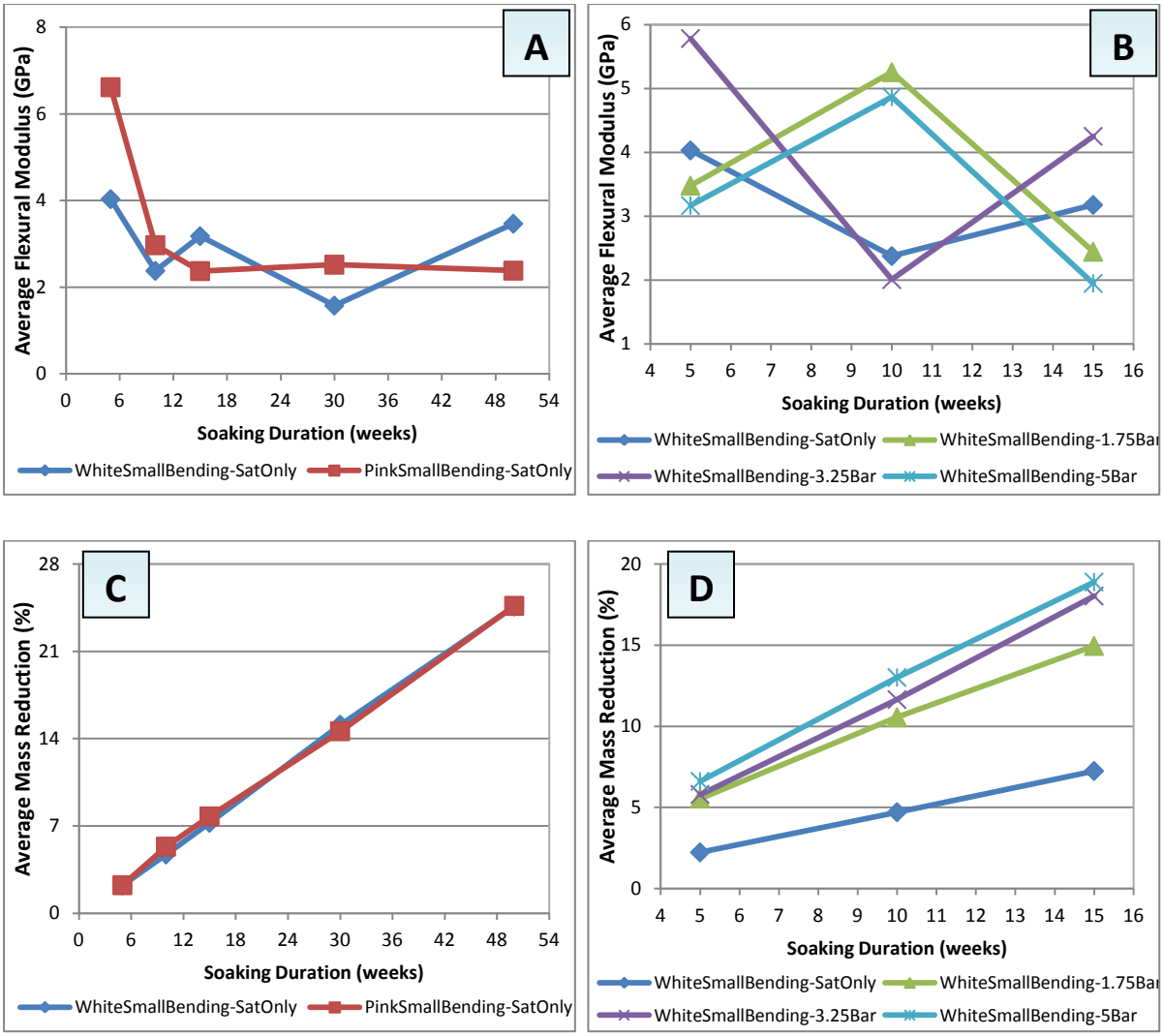

Fig. 4.35: Comparison among flexural tests parameters of small four-point bending bars tested after saturation under different levels of water pressure. The tested samples size is 140 x 40 x 20 mm. Part A is for the comparison of average flexural modulus values of white/Bantycock and pink/Bantycock small bars tested after saturation under atmospheric pressure. Part B is for the comparison of average flexural modulus values of white/Bantycock small bars tested under different levels of water pressure. Part C is for the comparison of average mass reduction values of white/Bantycock and pink/Bantycock small bars tested after saturation under atmospheric pressure. Part D is for the comparison of average mass reduction values of white/Bantycock small bars tested under different levels of water pressure.

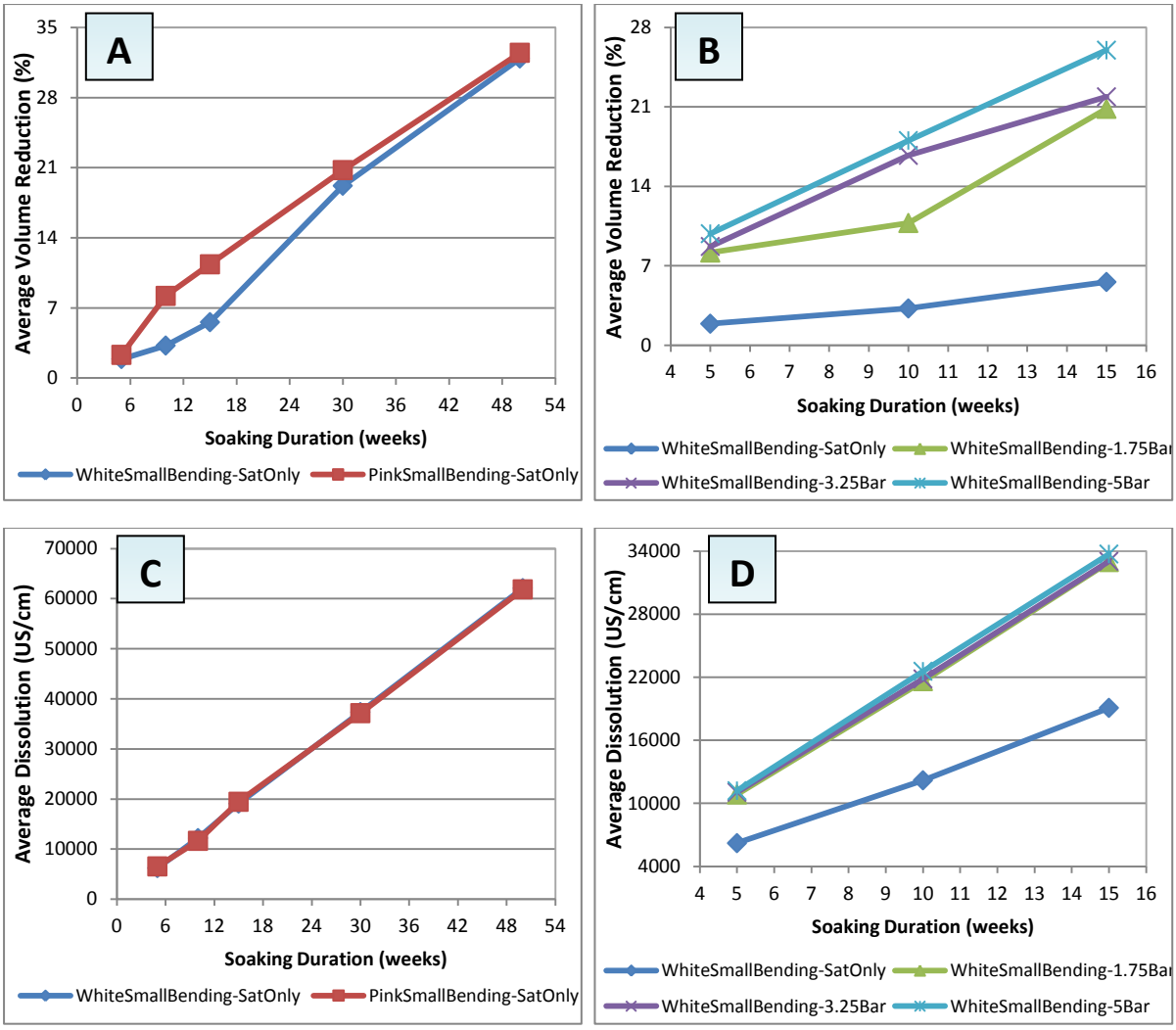

Fig. 4.36: Comparison among flexural tests parameters of small four-point bending bars tested after saturation under different levels of water pressure. The tested samples size is 140 x 40 x 20 mm. Part A is for the comparison of average volume reduction values of white/Bantycock and pink/Bantycock small bars tested after saturation under atmospheric pressure. Part B is for the comparison of average volume reduction values of white/Bantycock small bars tested under different levels of water pressure. Part C is for the comparison of average dissolution values of white/Bantycock and pink/Bantycock small bars tested after saturation under atmospheric pressure. Part D is for the comparison of average dissolution values of white/Bantycock small bars tested under different levels of water pressure.

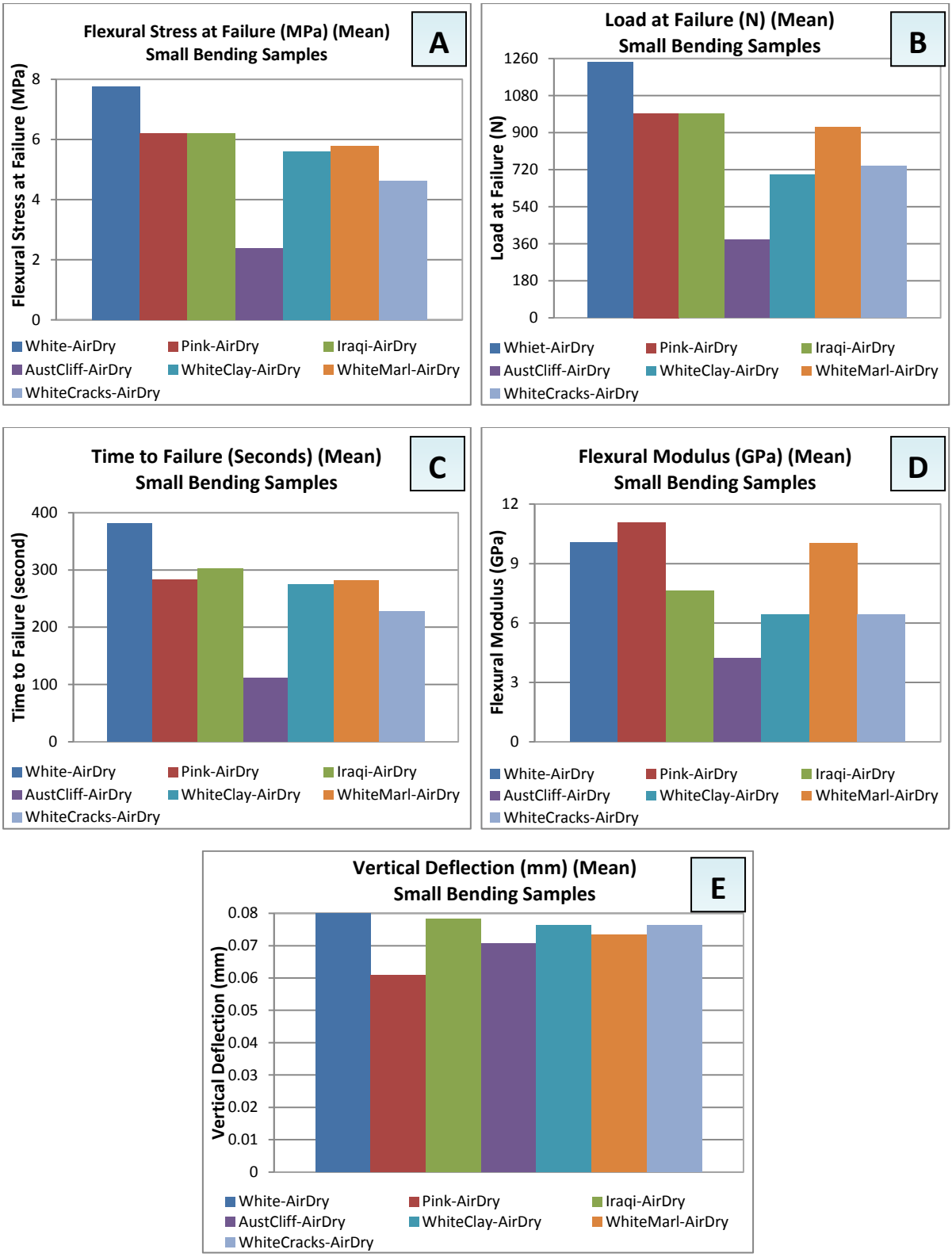

Fig. 4.37: Comparisons of flexural tests parameters of air dry small four-point bending bars. Tested samples' size are of 140 x 40 x 20 mm. Part A is for the flexural stress at failure values, Part B is for the load at failure values, Part C is for the time to failure values, Parts D and E are for the flexural modulus and vertical deflection values respectively.

4.3.9 Bantycock cylinders

From Table 4.11, the calculated compressive strength is in the range of 9.5 to 13.92 MPa, 11.88 to 15.1 MPa, 11.1 to 13.51 MPa and 7.9 to 13.26 MPa for white/Bantycock cylinders (*Cyl-WBG*), pink/Bantycock cylinders (*Cyl-PBG*), white & Clay/Bantycock cylinders and Iraqi gypsum cylinders (*Cyl-IG*) samples respectively at air-dry state.

Saturation state weakens both of *Cyl-WBG* and *Cyl-PBG*. It can be seen that the $б_c$, *TF*, *LF*, *BM*, *AD*, *HD*, *wt*, *vol*, *EMU* and *VU* from ultrasonic observations of *WBG* and *PBG* decreases, while dissolution amount was increased progressively due to saturation (under atmospheric pressure) over time progress for both types.

Only intact samples of white/Bantycock gypsum were used to examine the impacts of water pressure on dissolution process. An increase in gypsum dissolution was noticed within the application of 1.75, 3.25 and 5.0 bar compared to saturation under atmospheric pressure. It can be seen that the values of $б_c$, *TF*, *LF*, *AD*, *HD*, *wt*, *vol*, *EMU* and *VU* were decreased more in tests at higher water pressure more than in tests completed at atmospheric pressure. Dissolution rate increases with water pressure, while the amount dissolved per week remained semi-stable.

Table 4.11: Summary statistics for uniaxial compression tests parameters of Bantycock gypsum rock cylinders. These cylindrical samples are 54 mm diameter x 135 mm height. These samples were prepared from collected gypsum block samples from Bantycock Mine/UK in April 2010 and April 2011. *SD* is standard deviation.

Compressive Strength (MPa)					
Cylinder State	**Min**	**Max**	**SD**	**Mean**	**Median**
White-Air Dry	9.547	13.922	1.932	11.551	10.752
White-SatOnly-5Week	7.568	9.745	1.154	8.878	1.154
White-SatOnly-10Week	6.855	8.106	0.635	7.416	7.288
White-SatOnly-15Week	6.377	8.253	0.939	7.339	7.385
White-SatOnly-30Week	3.194	10.261	3.701	6.093	4.823
White-SatOnly-50Week	2.313	5.345	1.552	4.019	4.399
White-5Week-1.75bar	7.785	9.87	1.043	8.838	8.858
White-10Week-1.75bar	6.675	8.238	0.784	7.42	7.348
White-15Week-1.75bar	5.517	8.025	1.272	6.893	7.137
White-5Week-3.25bar	6.061	10.582	2.29	8.532	8.953
White-10Week-3.25bar	6.594	7.354	0.39	7.025	7.128
White-15Week-3.25bar	5.666	8.392	1.428	6.275	7.767
White-5Week-5.0bar	5.82	8.897	1.74	7.829	8.796
White-10Week-5.0bar	5.869	8.491	1.479	6.785	5.995
White-15Week-5.0bar	5.058	7.935	1.529	6.196	5.596

Pink-Air Dry	11.888	15.045	1.243	13.409	13.476
Pink-SatOnly-5Week	5.459	8.471	1.547	6.762	6.355
Pink-SatOnly-10Week	4.672	6.319	0.889	5.688	6.073
Pink-SatOnly-15Week	4.313	6.354	1.05	5.475	5.757
Pink-SatOnly-30Week	5.21	5.692	0.243	5.466	5.498
Pink-SatOnly-50Week	5.142	5.318	0.101	5.258	5.314
White & Clay-Air Dry	11.124	13.508	0.983	12.518	13.011
Time to Failure (seconds)					
Cylinder State	**Min**	**Max**	**SD**	**Mean**	**Median**
White-Air Dry	378.15	556.4	79.134	458.97	422.7
White-SatOnly-5Week	282.6	369.7	46.514	335.583	354.45
White-SatOnly-10Week	254.5	305.4	25.924	277.1	271.4
White-SatOnly-15Week	230.75	304.85	37.012	269.15	271.85
White-SatOnly-30Week	100.5	335.1	122.861	196.7	154.5
White-SatOnly-50Week	55.75	148.25	47.712	108.767	122.3
White-5Week-1.75bar	290.75	371.25	40.257	331.433	332.3
White-10Week-1.75bar	242.65	289.9	23.627	266.45	266.8
White-15Week-1.75bar	172.25	256	42.305	217.6	224.55
White-5Week-3.25bar	223.05	396.25	88.033	318.783	337.05
White-10Week-3.25bar	228.85	251.85	11.962	242.25	246.05
White-15Week-3.25bar	181.45	266.55	43.877	230.183	242.55
White-5Week-5.0bar	213.35	335.95	69.671	293.767	332
White-10Week-5.0bar	208.05	301.2	53.78	239.1	208.05
White-15Week-5.0bar	154.65	188.45	17.664	168.583	162.65
Pink-Air Dry	469.8	596.9	50.328	530.83	534.05
Pink-SatOnly-5Week	206.1	318	57.682	256.75	237.75
Pink-SatOnly-10Week	159.85	229.85	38.724	185.283	166.15
Pink-SatOnly-15Week	141.9	208.4	33.994	179.233	187.4
Pink-SatOnly-30Week	183.8	201.05	8.882	193.65	196.1
Pink-SatOnly-50Week	151.95	157.5	2.902	155.217	156.2
White & Clay-Air Dry	440.7	535.75	39.356	496.36	515.25
Poisson's Ratio					
Cylinder State	**Min**	**Max**	**SD**	**Mean**	**Median**
White-Air Dry	0.045	0.09	0.017	0.059	0.053
White-SatOnly-5Week	0.045	0.064	0.0104	0.057	0.061
White-SatOnly-10Week	0.055	0.076	0.012	0.062	0.056
White-SatOnly-15Week	0.061	0.105	0.024	0.088	0.097
White-SatOnly-30Week	0.057	0.159	0.053	0.099	0.08
White-SatOnly-50Week	0.026	0.045	0.009	0.035	0.033
White-5Week-1.75bar	0.025	0.055	0.016	0.042	0.047
White-10Week-1.75bar	0.021	0.073	0.028	0.0403	0.027
White-15Week-1.75bar	0.043	0.113	0.037	0.071	0.058
White-5Week-3.25bar	0.053	0.086	0.017	0.073	0.079
White-10Week-3.25bar	0.019	0.026	0.0034	0.023	0.023
White-15Week-3.25bar	0.008	0.089	0.045	0.05	0.053
White-5Week-5.0bar	0.018	0.104	0.044	0.057	0.05
White-10Week-5.0bar	0.015	0.051	0.0202	0.028	0.017
White-15Week-5.0bar	0.041	0.083	0.021	0.061	0.061
Pink-Air Dry	0.046	0.314	0.111	0.116	0.075
Pink-SatOnly-5Week	0.046	0.095	0.025	0.068	0.064
Pink-SatOnly-10Week	0.046	0.233	0.099	0.121	0.083
Pink-SatOnly-15Week	0.067	0.127	0.031	0.103	0.113
Pink-SatOnly-30Week	0.099	0.163	0.033	0.136	0.145

Pink-SatOnly-50Week	0.026	0.044	0.009	0.033	0.03
White & Clay-Air Dry	0.045	0.212	0.063	0.119	0.1102
Load at Failure (N)					
Cylinder State	**Min**	**Max**	**SD**	**Mean**	**Median**
White-Air Dry	21865.5	31884.6	4423.57	26453.98	24623.5
White-SatOnly-5Week	16446.7	21387.1	2646.05	19464.53	20559.8
White-SatOnly-10Week	14796.3	17660.3	1449.97	16096.9	15834.1
White-SatOnly-15Week	13472.7	17703.1	2118.9	15660.17	15804.7
White-SatOnly-30Week	6099.79	19525.6	7053.36	44562.8	9063
White-SatOnly-50Week	3801.49	8688.81	2504.3	6561.4	7193.89
White-5Week-1.75bar	16956.4	21500.2	2272.23	19250.5	19294.9
White-10Week-1.75bar	14153.3	16814	1330.37	15488.23	15497.4
White-15Week-1.75bar	10202.9	14904.5	2372.01	12736.43	13101.9
White-5Week-3.25bar	13072.8	22935	5017.35	18538.7	19608.3
White-10Week-3.25bar	13285.2	14669.2	715.59	14082.4	14292.8
White-15Week-3.25bar	10598.9	15504.8	2530.7	13411.23	14130
White-5Week-5.0bar	12455.4	19440.1	3966.22	17033.17	19204
White-10Week-5.0bar	12126.5	17556.4	3091.38	13987.9	12280.8
White-15Week-5.0bar	9072.88	11085.8	1056.87	9893.14	9520.73
Pink-Air Dry	27225.5	34456	2846.28	30710.2	30862.9
Pink-SatOnly-5Week	12075.4	18444.6	3268.83	14834.33	13983
Pink-SatOnly-10Week	9827.53	13474.8	1888.46	11934.38	12500.8
Pink-SatOnly-15Week	8112.3	11951.83	1965.13	10274.44	10759.2
Pink-SatOnly-30Week	10736.1	11716.4	509.32	11306.17	11466
Pink-SatOnly-50Week	8717.23	9039.95	182.45	8927.75	9026.08
White & Clay-Air Dry	25476	30936.1	2252.17	28668	29797.3

Shear Modulus (GPa)						**Max Dissolution (US/cm)**	**Dissolution Rate per Week**
Cylinder State	**Min**	**Max**	**SD**	**Mean**	**Median**		
White-Air Dry	0.779	1.817	0.413	1.107	0.97	0	0
White-SatOnly-5Week	0.714	1.556	0.423	1.11	1.061	10277	2055.4
White-SatOnly-10Week	1.151	1.899	0.374	1.529	1.536	19643.6	1873.32
White-SatOnly-15Week	0.773	1.197	0.213	0.997	1.022	29139	1899.08
White-SatOnly-30Week	1.022	1.537	0.272	1.23	1.131	57648.9	1900.66
White-SatOnly-50Week	0.854	1.289	0.243	1.134	1.261	96445.4	1939.83
White-5Week-1.75bar	0.572	1.429	0.468	1.109	1.328	10851.2	2170.24
White-10Week-1.75bar	0.552	0.794	0.121	0.673	0.674	21843.4	2198.44
White-15Week-1.75bar	0.711	1.615	0.458	1.12	1.035	32971.9	2225.7
White-5Week-3.25bar	1.438	1.872	0.231	1.702	1.795	11151.2	2230.24
White-10Week-3.25bar	0.541	0.898	0.197	0.672	0.578	22433.4	2256.44
White-15Week-3.25bar	0.541	1.185	0.324	0.885	0.929	33871.8	2287.68
White-5Week-5.0bar	1.071	1.551	0.25	1.278	1.206	11449.1	2289.2
White-10Week-5.0bar	0.688	1.358	0.378	1.124	1.325	23018	2313.78
White-15Week-5.0bar	0.943	1.291	0.174	1.12	1.127	34578.9	2312.18
Pink-Air Dry	0.755	1.069	0.146	0.91	0.841	0	0
Pink-SatOnly-5Week	0.805	1.078	0.143	0.967	1.017	10126.3	2025.26
Pink-SatOnly-10Week	0.723	1.317	0.298	1.033	1.06	19907.6	1956.26
Pink-SatOnly-15Week	1.151	1.77	0.31	1.451	1.431	30076.3	2033.74
Pink-SatOnly-30Week	0.703	0.973	0.136	0.827	0.803	59429.1	1956.85
Pink-SatOnly-50Week	0.982	1.322	0.174	1.174	1.218	97273.3	1892.21
White & Clay-Air Dry	0.648	1.892	0.446	1.32	1.356	0	0
Bulk Modulus (GPa)							
Cylinder State	**Min**	**Max**	**SD**	**Mean**	**Median**		

White-Air Dry	0.596	1.607	0.405	0.904	0.761
White-SatOnly-5Week	0.546	1.264	0.36	0.889	0.856
White-SatOnly-10Week	0.912	1.607	0.348	1.244	1.213
White-SatOnly-15Week	0.622	1.115	0.249	0.888	0.928
White-SatOnly-30Week	0.969	1.222	0.131	1.116	1.156
White-SatOnly-50Week	0.629	0.965	0.185	0.841	0.93
White-5Week-1.75bar	0.411	1.101	0.385	0.854	1.049
White-10Week-1.75bar	0.392	0.575	0.103	0.51	0.564
White-15Week-1.75bar	0.54	1.289	0.377	0.941	0.993
White-5Week-3.25bar	1.131	1.598	0.262	1.433	1.571
White-10Week-3.25bar	0.387	0.648	0.145	0.481	0.408
White-15Week-3.25bar	0.369	0.931	0.298	0.707	0.821
White-5Week-5.0bar	0.833	1.445	0.349	1.042	0.848
White-10Week-5.0bar	0.483	1.06	0.301	0.822	0.923
White-15Week-5.0bar	0.815	1.04	0.121	0.902	0.851
Pink-Air Dry	0.638	1.974	0.551	1.974	0.815
Pink-SatOnly-5Week	0.654	0.971	0.16	0.802	0.781
Pink-SatOnly-10Week	0.555	2.022	0.764	1.165	0.919
Pink-SatOnly-15Week	0.946	1.782	0.418	1.367	1.374
Pink-SatOnly-30Week	0.643	1.118	0.238	0.875	0.863
Pink-SatOnly-50Week	0.717	1.009	0.146	0.868	0.88
White & Clay-Air Dry	0.496	2.658	0.79	1.412	1.201
Max Axial Deflection (mm)					
Cylinder State	**Min**	**Max**	**SD**	**Mean**	**Median**
White-Air Dry	0.534	1.33	0.29	0.994	1.015
White-SatOnly-5Week	0.477	1.036	0.283	0.477	0.684
White-SatOnly-10Week	0.2998	0.756	0.228	0.523	0.512
White-SatOnly-15Week	0.564	1.061	0.274	0.746	0.614
White-SatOnly-30Week	0.248	0.711	0.243	0.521	0.605
White-SatOnly-50Week	0.605	3.043	1.368	1.466	0.749
White-5Week-1.75bar	0.37	0.623	0.144	0.536	0.616
White-10Week-1.75bar	0.775	1.016	0.123	0.88	0.85
White-15Week-1.75bar	0.727	1.123	0.218	0.872	0.766
White-5Week-3.25bar	0.327	0.568	0.132	0.478	0.539
White-10Week-3.25bar	0.917	1.055	0.075	0.969	0.934
White-15Week-3.25bar	0.577	1.203	0.317	0.861	0.803
White-5Week-5.0bar	0.554	0.808	0.128	0.686	0.697
White-10Week-5.0bar	0.633	1.024	0.197	0.813	0.783
White-15Week-5.0bar	0.399	0.849	0.25	0.687	0.812
Pink-Air Dry	0.576	1.487	0.326	0.976	0.941
Pink-SatOnly-5Week	0.437	1.58	0.617	0.874	0.605
Pink-SatOnly-10Week	0.506	1.193	0.382	0.753	0.559
Pink-SatOnly-15Week	0.356	0.653	0.15	0.513	0.532
Pink-SatOnly-30Week	0.573	0.889	0.177	0.777	0.869
Pink-SatOnly-50Week	0.431	1.551	0.642	0.809	0.446
White & Clay-Air Dry	0.459	1.112	0.243	0.819	0.825
Max Horizontal Deflection (mm)					
Cylinder State	**Min**	**Max**	**SD**	**Mean**	**Median**
White-Air Dry	0.004	2.178	1.014	0.966	0.747
White-SatOnly-5Week	0.107	0.248	0.07	0.181	0.187
White-SatOnly-10Week	0.027	0.068	0.021	0.045	0.041
White-SatOnly-15Week	0.017	0.228	0.112	0.101	0.059
White-SatOnly-30Week	0.023	1.538	0.861	0.544	0.07

White-SatOnly-50Week	0.005	3.779	2.164	1.281	0.06
White-5Week-1.75bar	0.022	0.028	0.003	0.025	0.025
White-10Week-1.75bar	0.022	0.033	0.006	0.027	0.025
White-15Week-1.75bar	0.029	1.529	0.842	0.557	0.114
White-5Week-3.25bar	0.327	0.568	0.132	0.478	0.539
White-10Week-3.25bar	0.019	0.093	0.038	0.053	0.047
White-15Week-3.25bar	0.003	0.066	0.035	0.026	0.008
White-5Week-5.0bar	0.127	0.775	0.332	0.494	0.579
White-10Week-5.0bar	0.005	0.094	0.045	0.044	0.032
White-15Week-5.0bar	0.006	0.046	0.022	0.021	0.01
Pink-Air Dry	0.045	2.161	0.91	0.567	0.089
Pink-SatOnly-5Week	0.021	0.165	0.074	0.083	0.063
Pink-SatOnly-10Week	0.007	1.099	0.628	0.374	0.015
Pink-SatOnly-15Week	0.098	0.807	0.408	0.336	0.103
Pink-SatOnly-30Week	0.116	0.421	0.165	0.231	0.158
Pink-SatOnly-50Week	0.005	0.068	0.035	0.046	0.065
White & Clay-Air Dry	0.033	1.282	0.533	0.414	0.098
Max Mass Reduction (%)					
Cylinder State	**Min**	**Max**	**SD**	**Mean**	**Median**
White-SatOnly-5Week	2.39	2.674	0.164	2.485	2.39
White-SatOnly-10Week	4.204	4.602	0.1996	4.395	4.38
White-SatOnly-15Week	6.77	7.122	0.177	6.955	6.972
White-SatOnly-30Week	13.59	15.35	0.9	14.58	14.8
White-SatOnly-50Week	22.94	23.997	0.533	23.507	23.583
White-5Week-1.75bar	3.09	3.19	0.051	3.135	3.124
White-10Week-1.75bar	6.14	6.213	0.037	6.172	6.164
White-15Week-1.75bar	9.239	9.26	0.012	9.246	0.012
White-5Week-3.25bar	3.28	3.422	0.074	3.34	3.318
White-10Week-3.25bar	0.29	6.405	0.29	6.575	6.41
White-15Week-3.25bar	9.655	9.731	0.038	9.695	9.7
White-5Week-5.0bar	3.53	3.563	0.019	3.541	3.53
White-10Week-5.0bar	7.14	7.256	0.061	7.208	7.227
White-15Week-5.0bar	8.71	10.86	1.214	10.11	10.76
Pink-SatOnly-5Week	1.96	2.16	0.1	2.064	2.072
Pink-SatOnly-10Week	4.393	4.82	0.23	4.655	4.753
Pink-SatOnly-15Week	6.46	7.007	0.276	6.714	6.674
Pink-SatOnly-30Week	13.47	13.96	0.249	13.74	13.79
Pink-SatOnly-50Week	22.391	22.85	0.25	22.677	22.79
Max Volume Reduction (%)					
Cylinder State	**Min**	**Max**	**SD**	**Mean**	**Median**
White-SatOnly-5Week	3.91	5.53	0.822	4.638	4.474
White-SatOnly-10Week	5.59	6.02	0.216	5.813	5.83
White-SatOnly-15Week	8.044	9.51	0.832	8.55	8.096
White-SatOnly-30Week	18.752	20.042	0.732	19.597	19.998
White-SatOnly-50Week	31.56	32.22	0.332	31.871	31.832
White-5Week-1.75bar	4.86	5.09	0.115	4.98	4.99
White-10Week-1.75bar	7.312	7.916	0.344	7.519	7.329
White-15Week-1.75bar	10.805	11.02	0.123	10.947	11.075
White-5Week-3.25bar	4.26	6.77	1.307	5.305	4.884
White-10Week-3.25bar	8.17	8.811	0.33	8.445	8.355
White-15Week-3.25bar	11.23	13.04	0.922	12.035	11.834
White-5Week-5.0bar	5.313	6.282	0.486	5.778	5.74
White-10Week-5.0bar	10.293	10.566	0.15	10.393	10.32

White-15Week-5.0bar	10.693	13.742	1.526	12.262	12.353
Pink-SatOnly-5Week	3.296	4.37	0.539	3.805	3.75
Pink-SatOnly-10Week	6.57	7.86	0.646	7.23	7.259
Pink-SatOnly-15Week	10.26	10.353	5971.318	10.367	10.489
Pink-SatOnly-30Week	20.194	20.7	0.288	20.368	20.21
Pink-SatOnly-50Week	29.321	29.844	0.262	29.583	29.584
Max Modulus Reduction (%) (Ultrasonic Observation)					
Cylinder State	**Min**	**Max**	**SD**	**Mean**	**Median**
White-SatOnly-5Week	17.42	81.38	34.588	57.007	72.22
White-SatOnly-10Week	26.37	57.455	17.408	46.439	55.492
White-SatOnly-15Week	23.844	31.871	4.014	27.905	28
White-SatOnly-30Week	23.51	75.98	27.255	45.48	36.95
White-SatOnly-50Week	54.701	83.27	16.156	73.34367	82.06
White-5Week-1.75bar	49.633	54.274	2.447	51.506	50.611
White-10Week-1.75bar	59.962	76.07	8.138	67.34167	65.993
White-15Week-1.75bar	25.024	37.134	6.992	29.0607	25.024
White-5Week-3.25bar	29.452	66.513	21.223	53.9557	65.902
White-10Week-3.25bar	60.234	69.33	4.796	65.66133	67.42
White-15Week-3.25bar	58.99	76.996	9.017	67.70867	67.14
White-5Week-5.0bar	62.76	71.89	4.703	66.67167	65.365
White-10Week-5.0bar	13.584	28.014	8.162	18.596	14.19
White-15Week-5.0bar	6.455	40.51	17.54	21.05333	16.195
Pink-SatOnly-5Week	46.281	48.15	1.022	47.45367	47.93
Pink-SatOnly-10Week	37.34	101.3	32.123	71.06667	74.56
Pink-SatOnly-15Week	9.694	49.14	20.095	31.63867	36.082
Pink-SatOnly-30Week	18.27	91.41	36.593	55.58067	57.062
Pink-SatOnly-50Week	2.603	88.93	47.086	34.90433	13.18
Max Velocity Reduction (%) (Ultrasonic Observation)					
Cylinder State	**Min**	**Max**	**SD**	**Mean**	**Median**
White-SatOnly-5Week	0.76	1.82	0.542	1.225	1.094
White-SatOnly-10Week	1.51	3.731	1.199	2.36	1.84
White-SatOnly-15Week	1.12	6.85	3.204	3.156	1.499
White-SatOnly-30Week	1.87	32.63	16.225	14.267	8.3
White-SatOnly-50Week	80.129	84.604	2.366	82.811	83.7
White-5Week-1.75bar	83.571	83.82	0.14	83.658	83.584
White-10Week-1.75bar	55.135	84.183	16.65	74.36	83.761
White-15Week-1.75bar	1.49	1.523	0.019	1.512	1.523
White-5Week-3.25bar	83.34	83.702	0.191	83.556	83.627
White-10Week-3.25bar	83.522	83.73	0.111	83.649	83.695
White-15Week-3.25bar	2.553	2.941	0.216	2.692	2.582
White-5Week-5.0bar	83.64	84.002	0.181	83.821	83.82
White-10Week-5.0bar	0.762	40.75	21.948	25.982	36.434
White-15Week-5.0bar	0.39	1.48	0.554	0.877	0.76
Pink-SatOnly-5Week	0.37	6.129	3.017	3.769	4.809
Pink-SatOnly-10Week	4.244	61.396	32.353	41.578	59.095
Pink-SatOnly-15Week	83.82	84.004	0.106	83.942	84.002
Pink-SatOnly-30Week	36.697	60.64	12.906	51.452	57.02
Pink-SatOnly-50Week	28.26	93.8	32.782	60.517	59.49

4.3.10 Iraqi cylinders

Table 4.12: Summary statistics for uniaxial compression test parameters of tested Iraqi cylinders. These cylindrical samples are 54 mm diameter x 135 mm height and tested in air-dry state. These samples were prepared from gypsum block samples collected from Northern Iraq in June 2010. SD is standard deviation.

Iraqi Cylinders-Air Dry				
Compressive Strength (MPa)				
Min	**Max**	**SD**	**Mean**	**Median**
7.904	13.255	1.92	10.522	10.268
Poisson's Ratio				
0.049	1.825	0.771	0.45	0.129
Load at Failure (N)				
18102.4	30357.4	4395.67	24095.92	23517
Time to Failure (seconds)				
309.3	525.15	77.686	415.75	405.7
Shear Modulus (GPa)				
0.241	1.363	0.492	0.966	1.197
Bulk Modulus (GPa)				
0.171	1.743	0.729	0.877	1.077
Max Axial Deflection (mm)				
0.053	1.263	0.473	0.611	0.453
Max Horizontal Deflection (mm)				
0.031	1.529	0.573	0.67	0.576

4.3.11 Compared cylinders results

Uniaxial compressive stress test parameters (mean) such as compressive strength, Poisson's ratio, load at failure, time to failure, shear modulus, bulk modulus, maximum axial deflection, maximum horizontal deflection, mass and volume reductions, and dissolution amount were used to construct comparison relationships among tested gypsum rock cylindrical samples. XY scatter and columns chart were used in the construction of those comparisons as shown in Figures 4.38-4.45.

From the comparisons of air-dry state, it can be seen that the *Cyl-PBG* sample is the strongest one as shown in Figure 4.44/A, while the *Cyl-IG* sample is the weakest one.

From the comparisons of saturation state under atmospheric pressure, it can be seen that there is a role of saturation to weaken gypsum rock cylinders and this role will continue to weaken samples over time progress. *Cyl-WBG* is stronger than *Cyl-PBG*. The dissolution rate per week for *Cyl-PBG* is slightly higher in most weeks than *Cyl-WBG* dissolution rate in saturation state under atmospheric pressure. The *Cyl-WBG* samples exhibited to a considerable drop in $б_c$, *wt*, *AD*, *vol* and *EMU*. Consequently, the *Cyl-PBG* samples exhibited to higher *TF*, *LF*, *BM*, *HD* and *VU* reductions. Little differences in *wt* reduction between *Cyl-PBG* and *Cyl-WBG* with parallel behaviours are recognized as shown in Figure 4.42/A. It seems that the reductions in mentioned cylinders' parameters due to saturation are influenced by properties of each cylinder such as cracks distribution, impurities appearance and rock fabric.

From the comparisons among tested white/Bantycock cylinders in saturation under 1.75, 3.25 and 5.0 bar pressure, it can be seen that there is a notable role of water pressure on dissolution amount compare to dissolution under atmospheric pressure. The dissolution increased progressively when water pressure increased. So, water pressure continues to weaken samples over time progress.

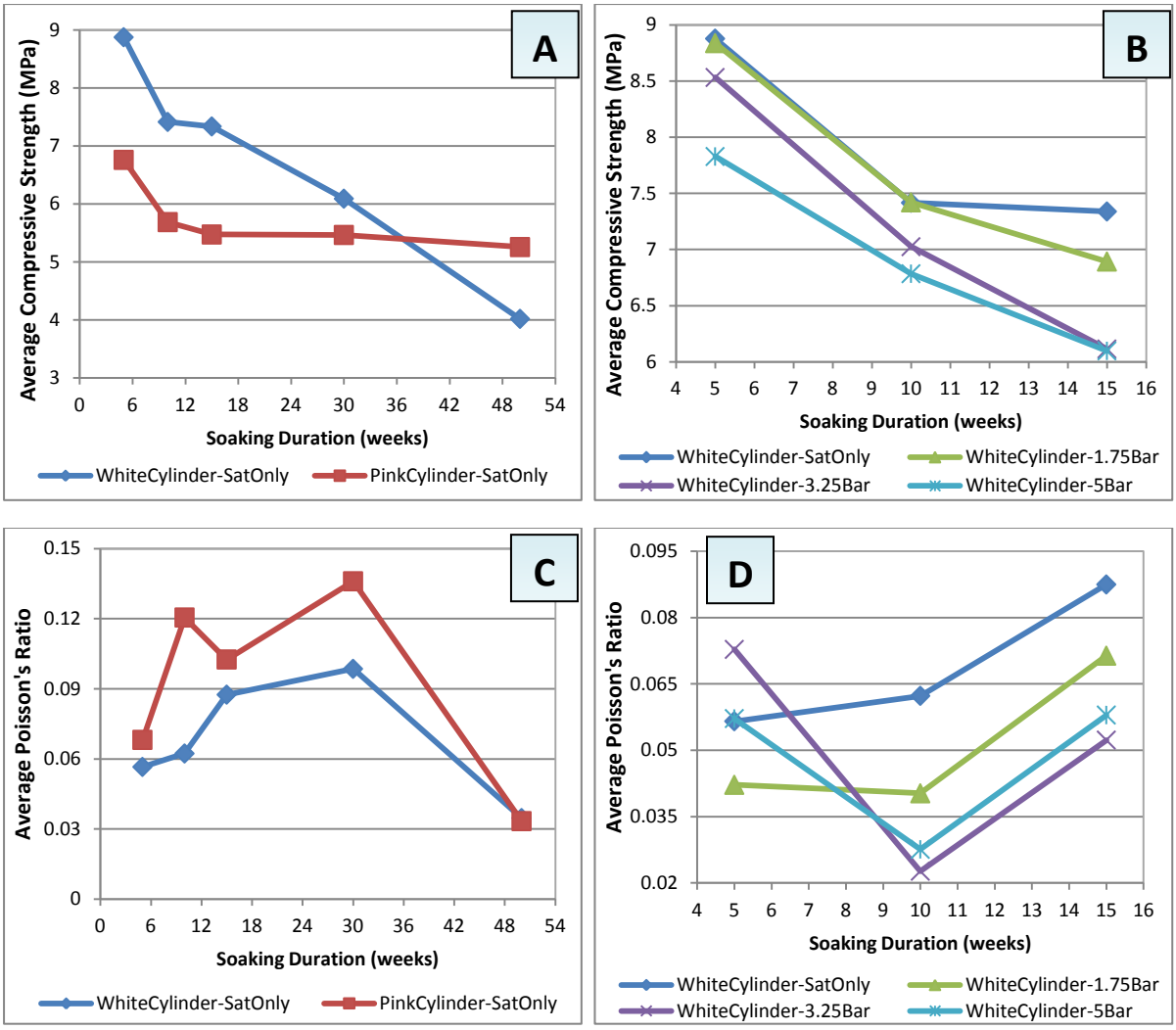

Fig. 4.38: Comparison of uniaxial compression tests parameters of white/Bantycock and pink/Bantycock gypsum cylinders. The tested cylinders size is 54 mm in diameter x 135 mm in height. These cylindrical samples were tested after saturation under different levels of water pressure. Part A is for the comparison of average compressive strength values of white/Bantycock and pink/Bantycock cylinders tested after saturation under atmospheric pressure. Part B is for the comparison of average compressive strength values of white/Bantycock cylinders tested under different levels of water pressure. Part C is for the comparison of average Poisson's ratio values of white/Bantycock and pink/Bantycock cylinders tested after saturation under atmospheric pressure. Part D is for the comparison of average Poisson's ratio values of white/Bantycock cylinders tested under different levels of water pressure.

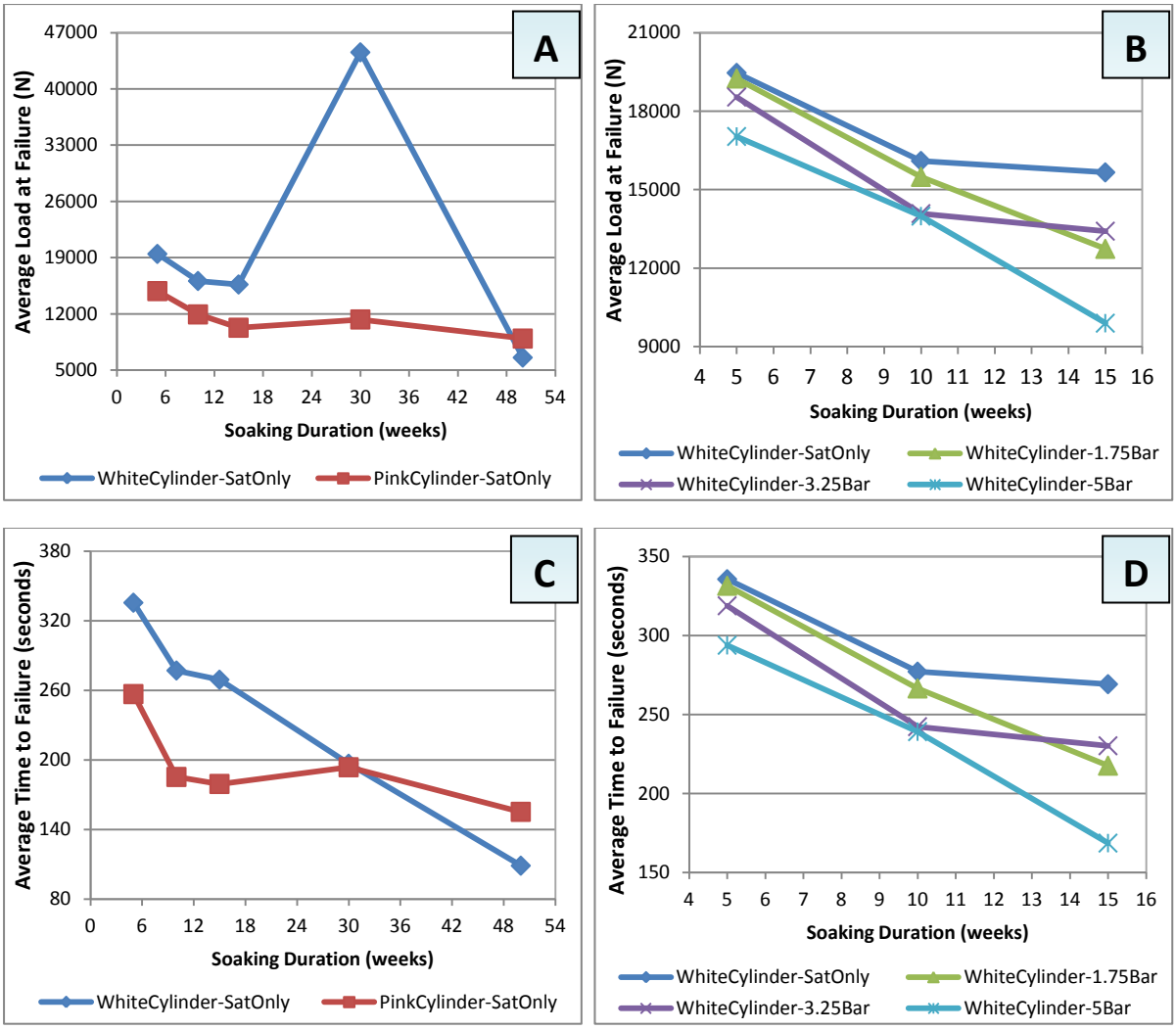

Fig. 4.39: Comparisons among uniaxial compression test parameters of white/Bantycock and pink/Bantycock gypsum cylinders. The tested cylinders size is 54 mm in diameter x 135 mm in height. These cylindrical samples were tested after saturation under different levels of water pressure. Part A is for the comparison of average load at failure values of white/Bantycock and pink/Bantycock cylinders tested after saturation under atmospheric pressure. Part B is for the comparison of average load at failure values of white/Bantycock cylinders tested under different levels of water pressure. Part C is for the comparison of average time to failure values of white/Bantycock and pink/Bantycock cylinders tested after saturation under atmospheric pressure. Part D is for the comparison of average time to failure values of white/Bantycock cylinders tested under different levels of water pressure.

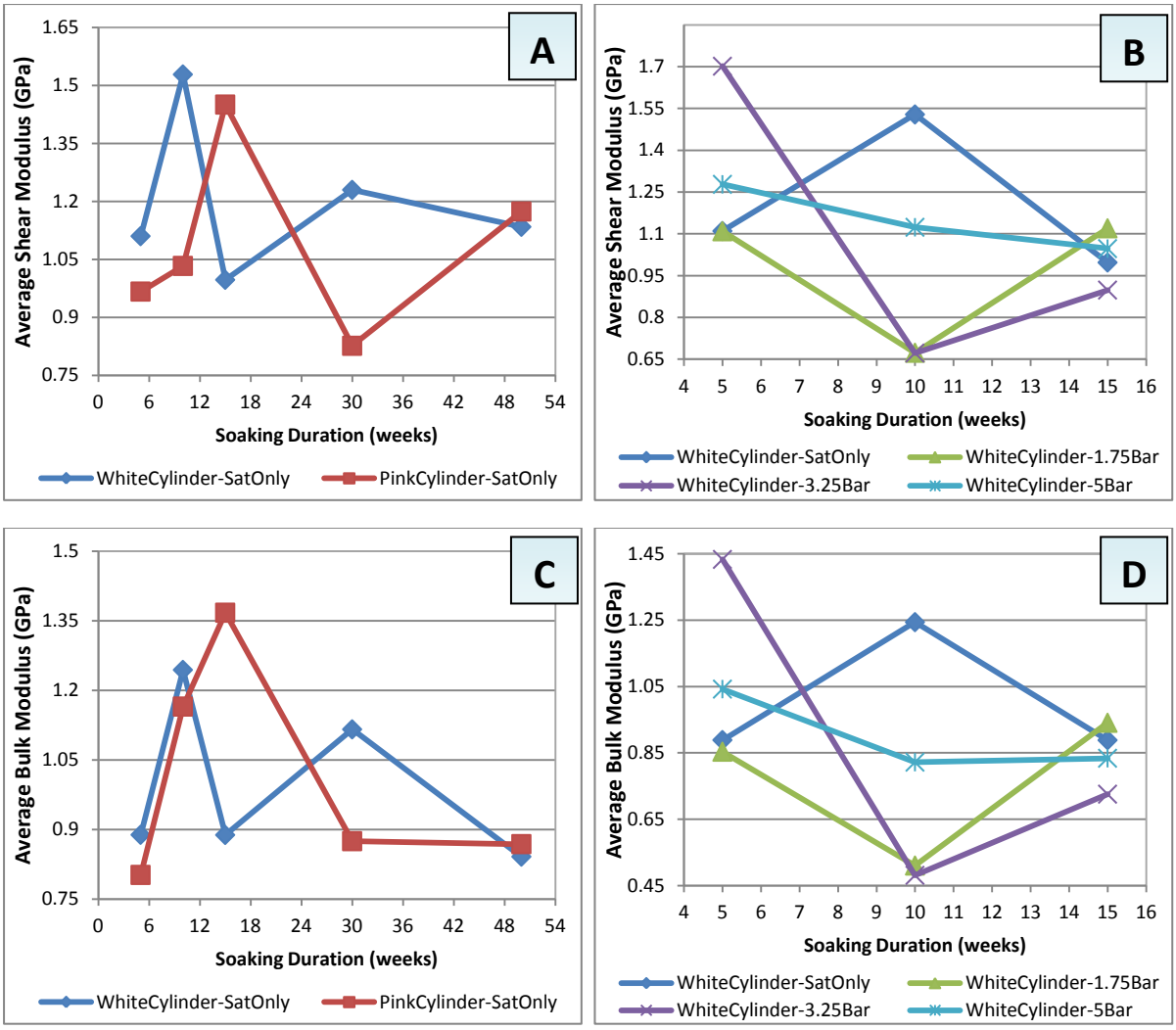

Fig. 4.40: Comparisons of uniaxial compression test parameters of white/Bantycock and pink/Bantycock gypsum cylinders. The tested cylinders size is 54 mm in diameter x 135 mm in height. These cylindrical samples were tested after saturation under different levels of water pressure. Part A is for the comparison of average shear modulus values of white/Bantycock and pink/Bantycock cylinders tested after saturation under atmospheric pressure. Part B is for the comparison of average shear modulus values of white/Bantycock cylinders tested under different levels of water pressure. Part C is for the comparison of average bulk modulus values of white/Bantycock and pink/Bantycock cylinders tested after saturation under atmospheric pressure. Part D is for the comparison of average bulk modulus values of white/Bantycock cylinders tested under different levels of water pressure.

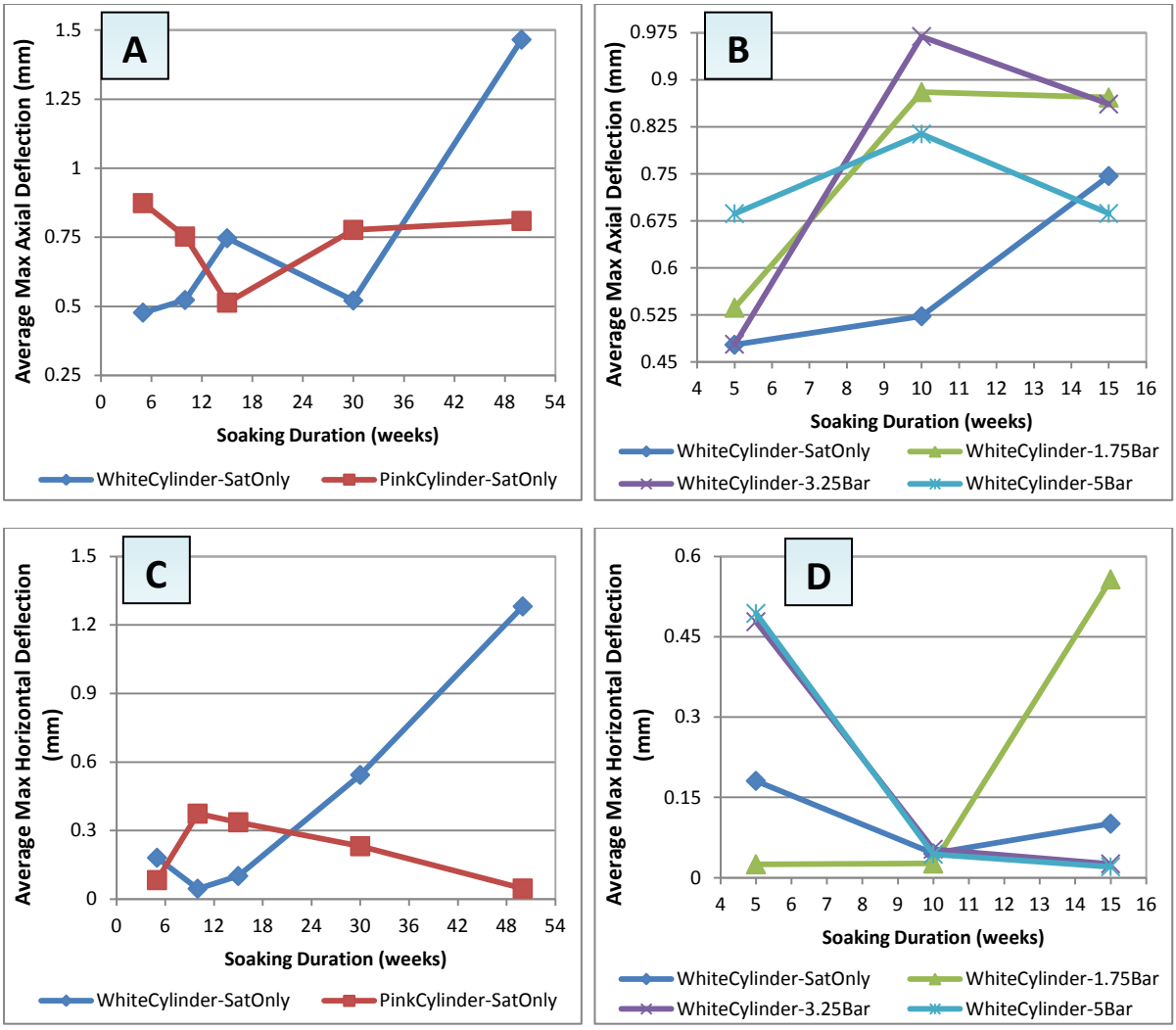

Fig. 4.41: Comparisons of uniaxial compression test parameters of white/Bantycock and pink/Bantycock gypsum cylinders. The tested cylinders' size is 54 mm in diameter x 135 mm in height. These cylindrical samples were tested after saturation under different levels of water pressure. Part A is for the comparison of average values of maximum axial deflection of white/Bantycock and pink/Bantycock cylinders tested after saturation under atmospheric pressure. Part B is for the comparison of average values of maximum axial deflection of white/Bantycock cylinders tested under different levels of water pressure. Part C is for the comparison of average values of maximum horizontal deflection of white/Bantycock and pink/Bantycock cylinders tested after saturation under atmospheric pressure. Part D is for the comparison maximum horizontal deflection of white/Bantycock cylinders tested under different levels of water pressure.

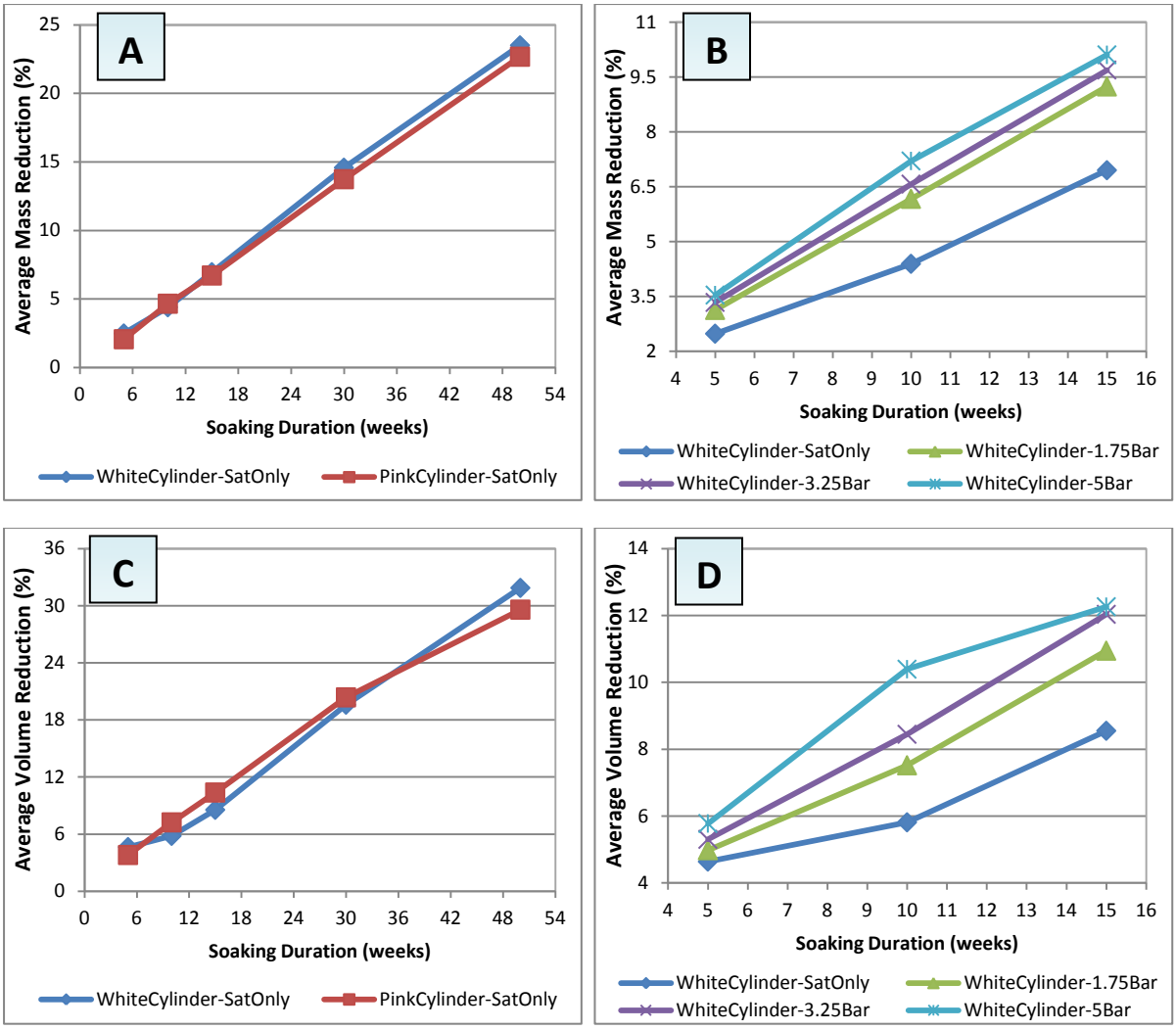

Fig. 4.42: Comparisons of uniaxial compression test parameters of white/Bantycock and pink/Bantycock gypsum cylinders. The tested cylinders' size is 54 mm in diameter x 135 mm in height. These cylindrical samples were tested after saturation under different levels of water pressure. Part A is for the comparison of average mass reduction values of white/Bantycock and pink/Bantycock cylinders tested after saturation under atmospheric pressure. Part B is for the comparison of average mass reduction values of white/Bantycock cylinders tested under different levels of water pressure. Part C is for the comparison of average volume reduction values of white/Bantycock and pink/Bantycock cylinders tested after saturation under atmospheric pressure. Part D is for the comparison of average volume reduction values of white/Bantycock cylinders tested under different levels of water pressure.

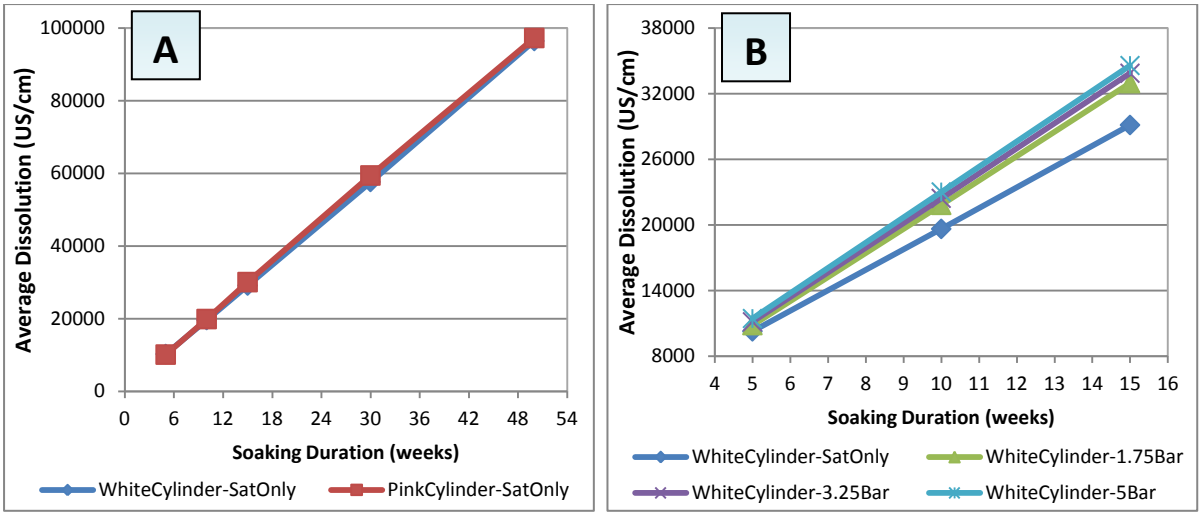

Fig. 4.43: Comparisons of uniaxial compression test parameters of white/Bantycock and pink/Bantycock gypsum cylinders. The tested cylinders' size is 54 mm in diameter x 135 mm in height. These cylindrical samples were tested after saturation under different levels of water pressure. Part A is for the comparison of average dissolution values of white/Bantycock and pink/Bantycock cylinders tested after saturation under atmospheric pressure. Part B is for the comparison of average dissolution values of white/Bantycock cylinders tested under different levels of water pressure.

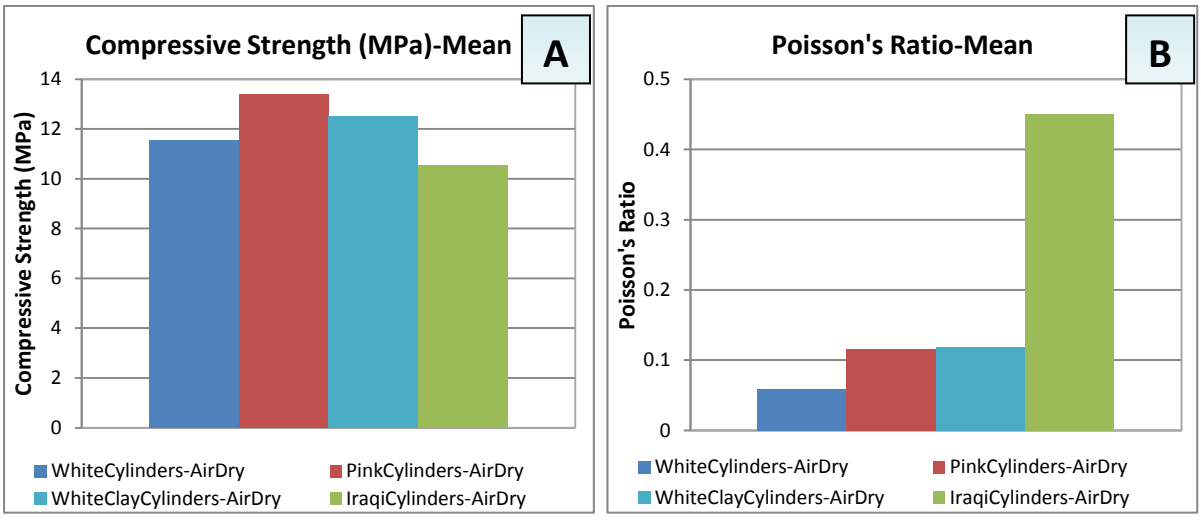

Fig. 4.44: Comparisons of uniaxial compression test parameters of different gypsum cylindrical samples from the UK and Iraq. The tested cylinders' size is 54 mm in diameter x 135 mm in height. These cylindrical samples were tested at air-dry state. Part A is for the comparison of compressive strength values. Part B is for the comparison of Poisson's ratio values.

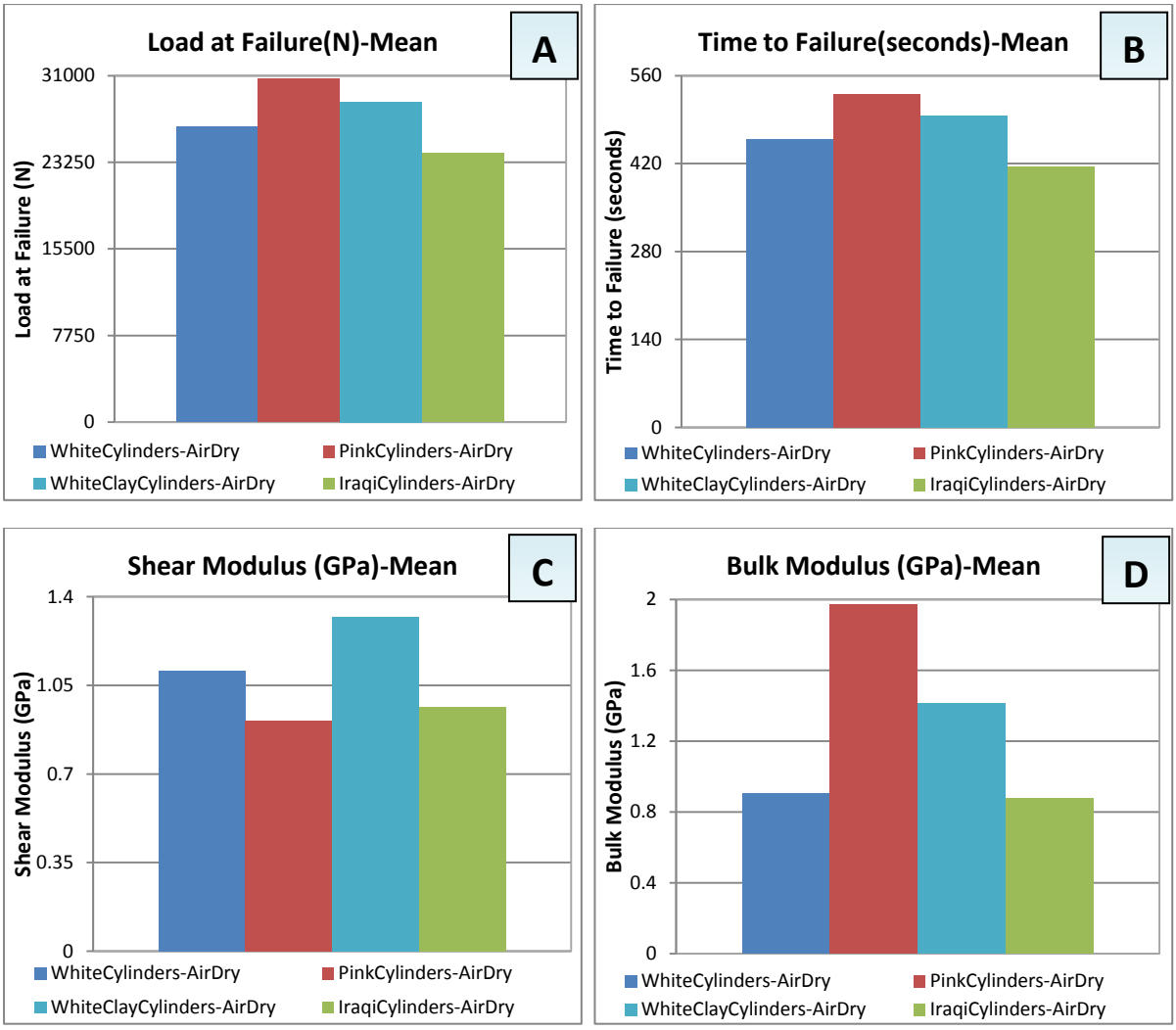

Fig. 4.45: Comparisons of uniaxial compression test parameters of different gypsum cylindrical samples from the UK and Iraq. The tested cylinders' size is 54 mm in diameter x 135 mm in height. These cylindrical samples were tested at air-dry state. Part A is for the comparison of load at failure values. Part B is for the comparison of time to failure values. Part C is for the comparison of shear modulus values. Part D is for the comparison of bulk modulus values.

Table 4.13: Presents ultrasonic observation data for white/Bantycock gypsum rock cylinders.

White Cylinder State	Transit Time (Useos)	Velocity (m/sec)	Path Length (mm)	Elastic Modulus (GN/m^2)
Air-Dry	27.77	18870.67	108.67	159.7
Saturated under atmospheric pressure				
5 week	27.03	18821.7	108	100.2
10 week	26.3	18821.67	104.66	82.97
15 week	26.17	18498.33	104.33	68.27
10 week	19.833	15974.33	79.33	63.47
15 week	10.633	14588.67	42	61.2
Saturated under 1.75 bar water pressure				
5 week	27.27	18451	108	60.97
10 week	27	4753.7	105.33	30.8
15 week	26.33	3015	105	21.33
Saturated under 3.25 bar water pressure				
5 week	26.53	17847	105.67	42.87
10 week	26.1	3037.67	104	21.07
15 week	20.87	2940.67	83	19.87
Saturated under 5.0 bar water pressure				
5 week	26.2	13748	104.67	21.533
10 week	25.5	3053	103.1	20.73
15 week	14.7	2810	58.33	15.58

4.3.12 Compared Short-Term results

Figure 4.46 below is on the impacts of used water of saturation volume on dissolution amount of different gypsum rock shapes.

It can be seen that similar behaviours are obtained for all gypsum specimen types. Increases of volume of water used to saturate gypsum decreases the amount of gypsum dissolution. This phenomenon can be recognized within *SFB* and *LFB* specimens. So, significant impacts of sample size on dissolution of bending bars and *ThL*. Increases of gypsum volume cause an increase in salt dissolution amount, which can be found within cylinders. The larger surface area facing water causes larger dissolution amount of samples such as cylinder and large bending bar. However, the thin layers exhibited larger amounts of dissolution compared to

small bending bars, which might relate to the impact of the circular shape of thin layer samples causing higher dissolution (see also Figure 4.47).

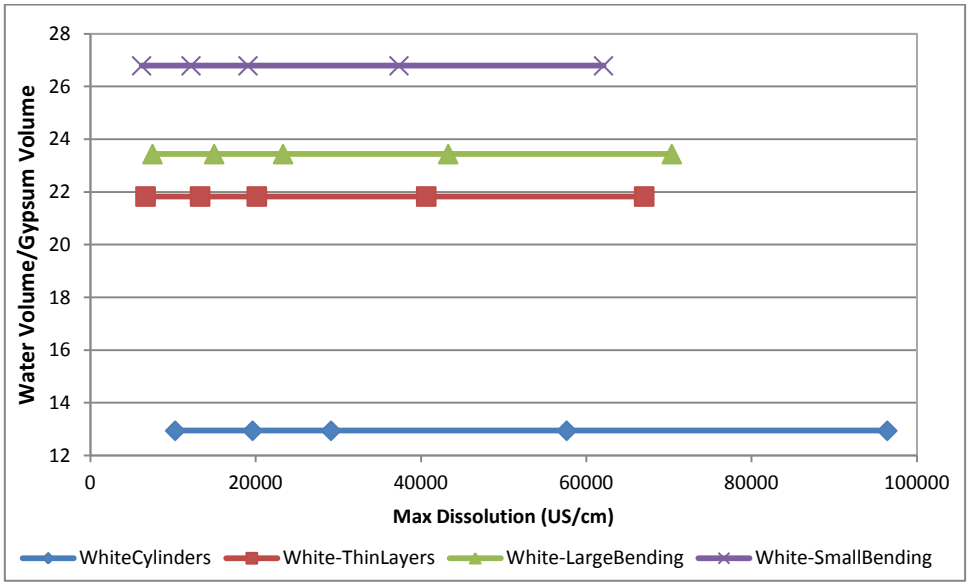

Fig. 4.46: The relationship of water volume/gypsum volume with maximum dissolution values of white/Bantycock gypsum from the UK. The saturation condition of these samples was carried out under atmospheric pressure. More details on dissolution of gypsum samples shown in next Figure 4.47. Each data point represents a reading at 5, 10, 15, 30 and 50 weeks.

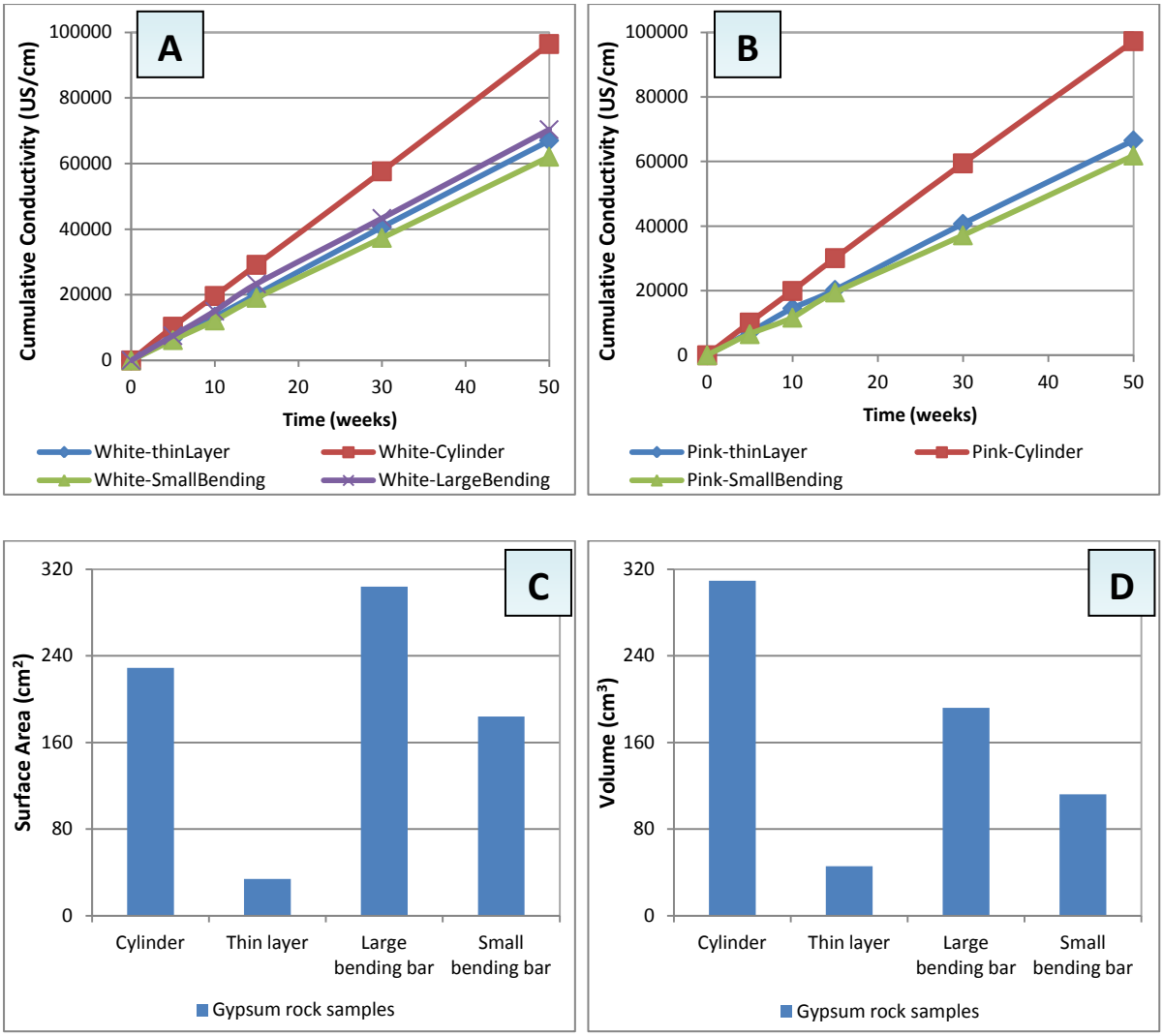

Fig. 4.47: Comparisons of gypsum rock samples of short term tests. Part A is for the comparison of cumulative conductivity values of white/Bantycock gypsum rock samples. Part B is for the comparison of cumulative conductivity values of pink/Bantycock gypsum rock samples. Part C is for the comparison of surface areas of gypsum rock samples. Part D is for the comparison of volume values of different gypsum rock samples.

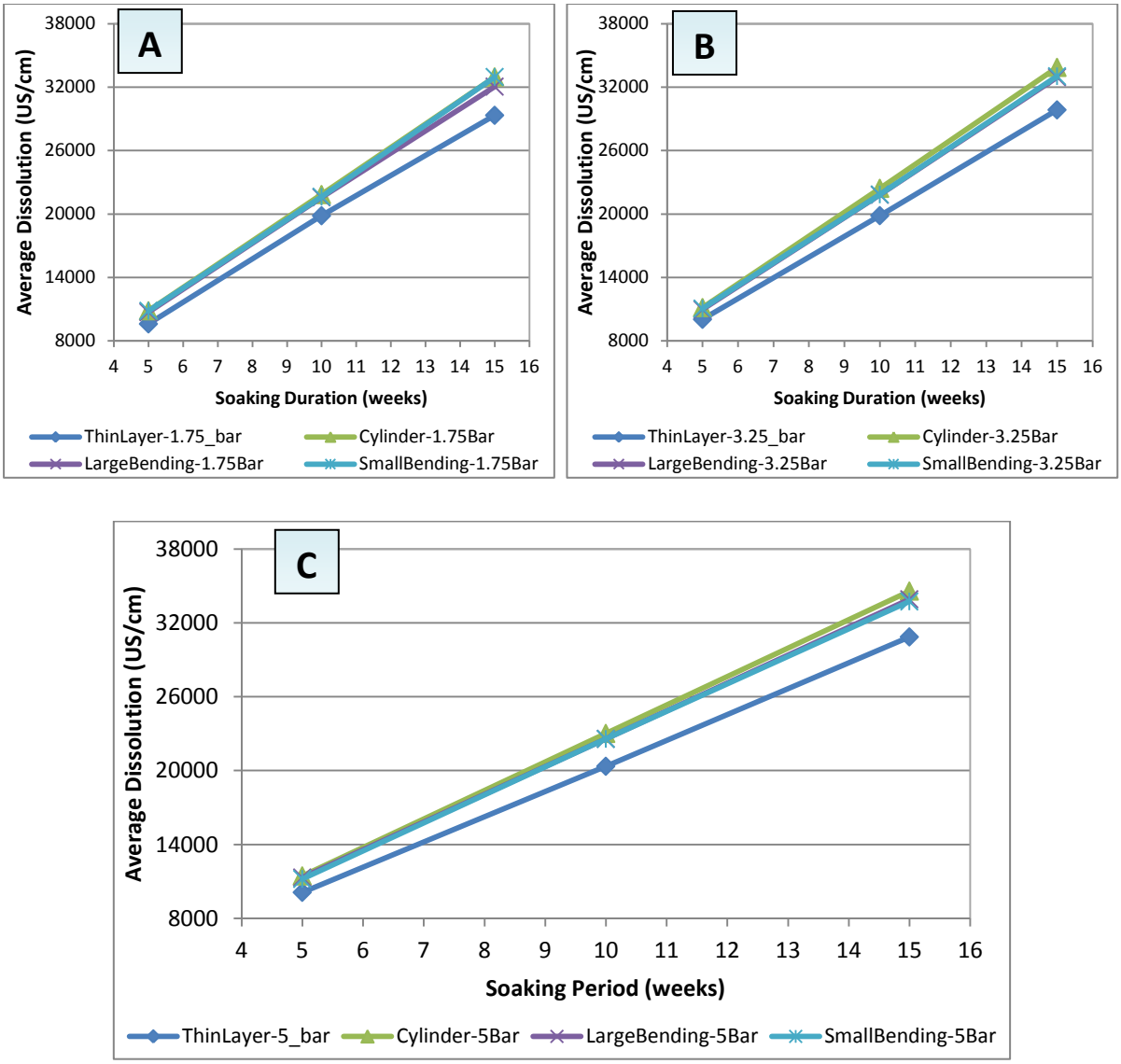

Fig. 4.48: Average dissolution values relationship with soaking period of different gypsum rock samples. These samples have different sizes and shapes as shown on each part. These samples were examined after saturation under various levels of water pressure. Part A is for the saturated samples under 1.75 bar water pressure. Part B is for the saturated samples under 3.25 bar water pressure. Part C is for the saturated samples under 5.0 bar water pressure.

4.4 Gypsum rock: Long-Term work

4.4.1 Thin layers results

It can be seen from Figures 4.49-4.52 and Tables 4.14-4.16 that the confinement process influences the behaviour of gypsum within time progress. The confined *IG* specimen showed the higher dissolution values, while the *WBG* specimen indicates the lower dissolution which rapidly increases until 15 days and then increases less rapidly. The confined *PBG*, *ACG* and *WBG* samples dissolution are less by 15.97, 30.4 and 62.52 percent than the confined *IG* dissolution respectively. It seems that the impurities or other minerals in sample cracks increase the dissolution upon confinement, but have no effect in the unconfined state.

There were no significant impacts on the materials' response to loading stages due to confinement (see Figure 4.49).

From Figure 4.50-4.51, it can be seen that all creep curves for the unconfined state increase initially with time before a linear increase is established; however the *PBG* specimen creep is behaved in slightly logarithmic way. Continuous small step-rest periods are obtained within unconfined and confined creep curves. This behaviour indicates that the strain failure is occurs gradually and slowly due to the low stress/1792 kPa. The remaining period of *PBG* specimen is longer than others.

From Table 4.14-4.15, in focus on constants *A* and *B* relation with confinement process for 1792 kPa creep curves, constant *A* decreases on confinement for *WBG* and *PBG*, while for *ACG* and *IG* it increases. This means that the instantaneous response of *WBG* and *PBG* are more than the other two when a confinement process applied. Constant *B* decreases on confinement for *WBG* and *ACG*, while for *PBG* it increases and for *IG* it remains constant. This means that confinement process decreases the response of *WBG* and *ACG* for creep with time, while increases the creep recorded for *PBG* and no changes for *IG*.

Constant *A* (of creep curves for 2688.35 kPa) increases on confinement for *WBG* and *ACG* and *IG*, while for *PBG* it increases. This means that the instantaneous response of *WBG* and *ACG* and *IG* are more than *PBG* when confinement process applied. Constant B decreases on confinement for *WBG* and *ACG*, while for *PBG* and *IG* it remains constant. This means that

confinement process decreases the response of *WBG* and *ACG* for creep with time, while continue the creep recorded in constant increment on time progress for *PBG* and *IG*.

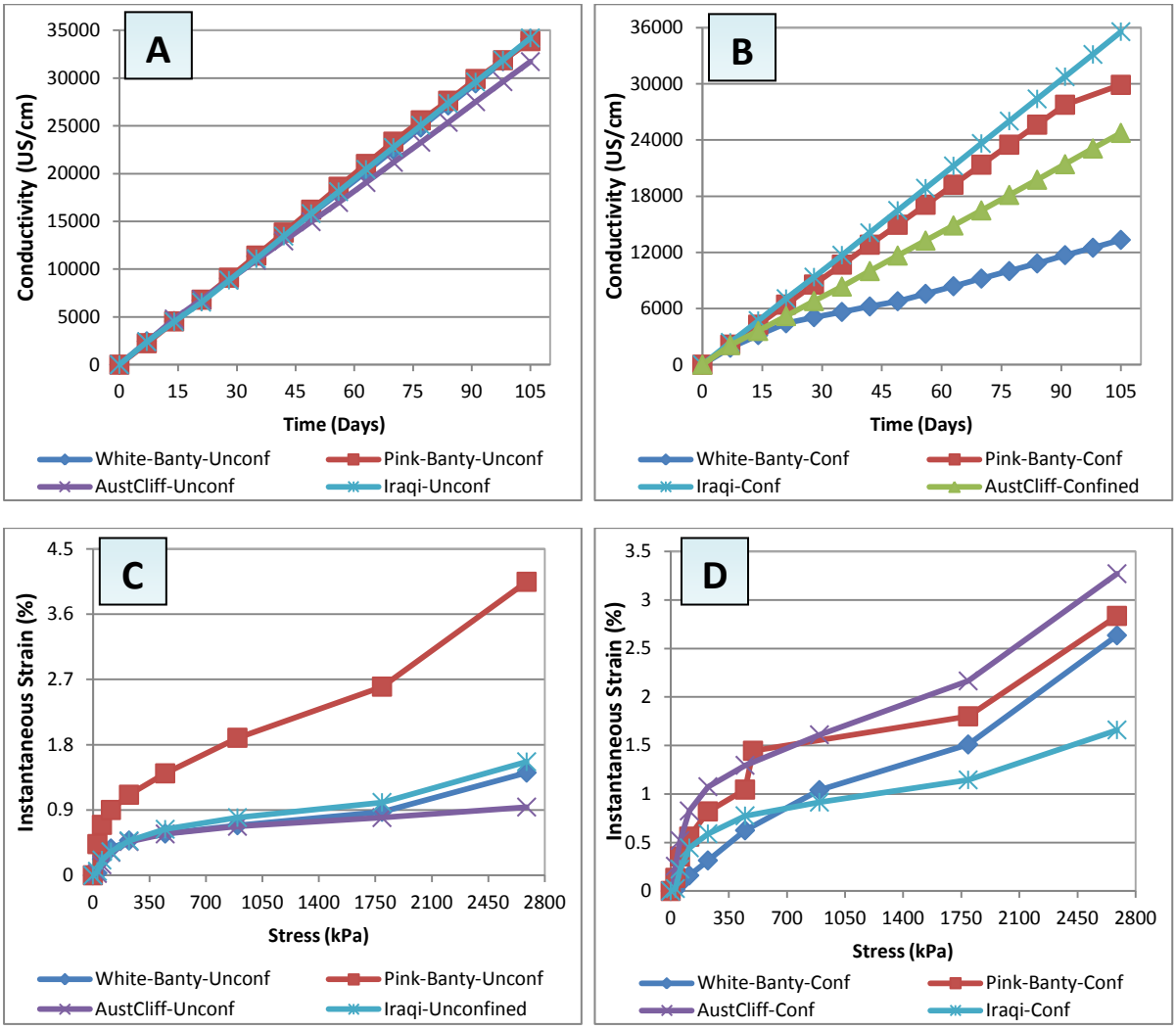

Fig. 4.49: Comparisons of UK and Iraqi gypsum rock thin layers tested in two cases of confinement. The tested samples size is 54 mm diameter x 20 mm height. Thin layers prepared from collected specimens on UK field trips: November 2009, April 2010 and April 2011; on Iraqi field trip on June 2010. Part A shows the cumulative conductivity of unconfined samples. Part B shows the cumulative conductivity of confined samples. Part C shows the instantaneous strain relationship with applied axial stresses of unconfined samples. Part D shows the instantaneous strain relationship with applied axial stresses of confined samples.

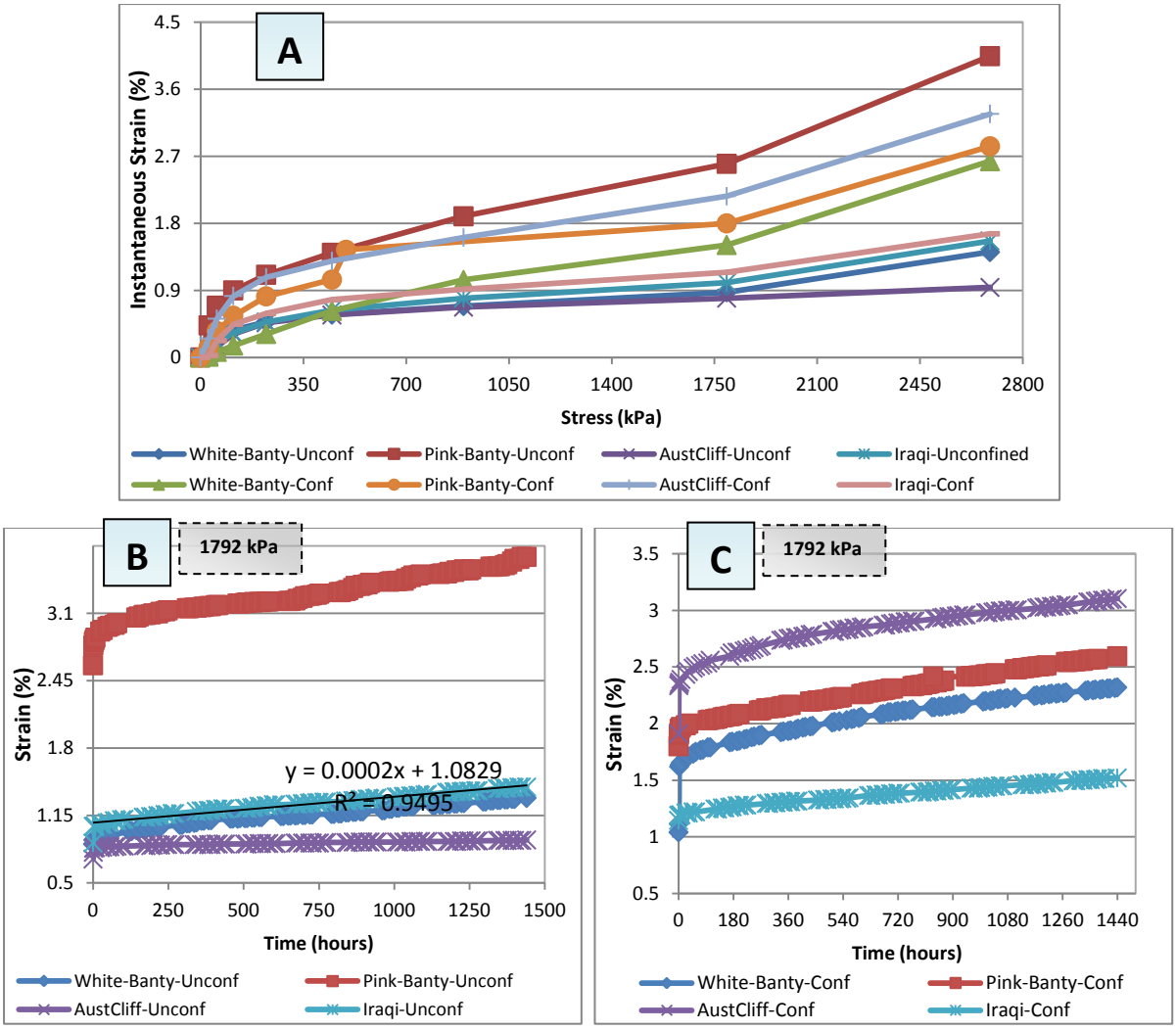

Fig. 4.50: Comparisons of UK and Iraqi gypsum rock thin layers tested in two cases of confinement. The tested samples size is 54 mm diameter x 20 mm height. Thin layers prepared from collected specimens on UK field trips: November 2009, April 2010 and April 2011; on Iraqi field trip on June 2010. Part A shows the instantaneous strain percent relationship with applied axial stresses of unconfined and confined samples. Part B shows the creep strain percent of unconfined samples under 1792 kPa applied axial stress. Part C shows the creep strain percent relationship with applied axial stresses of confined samples under 1792 kPa applied axial stress.

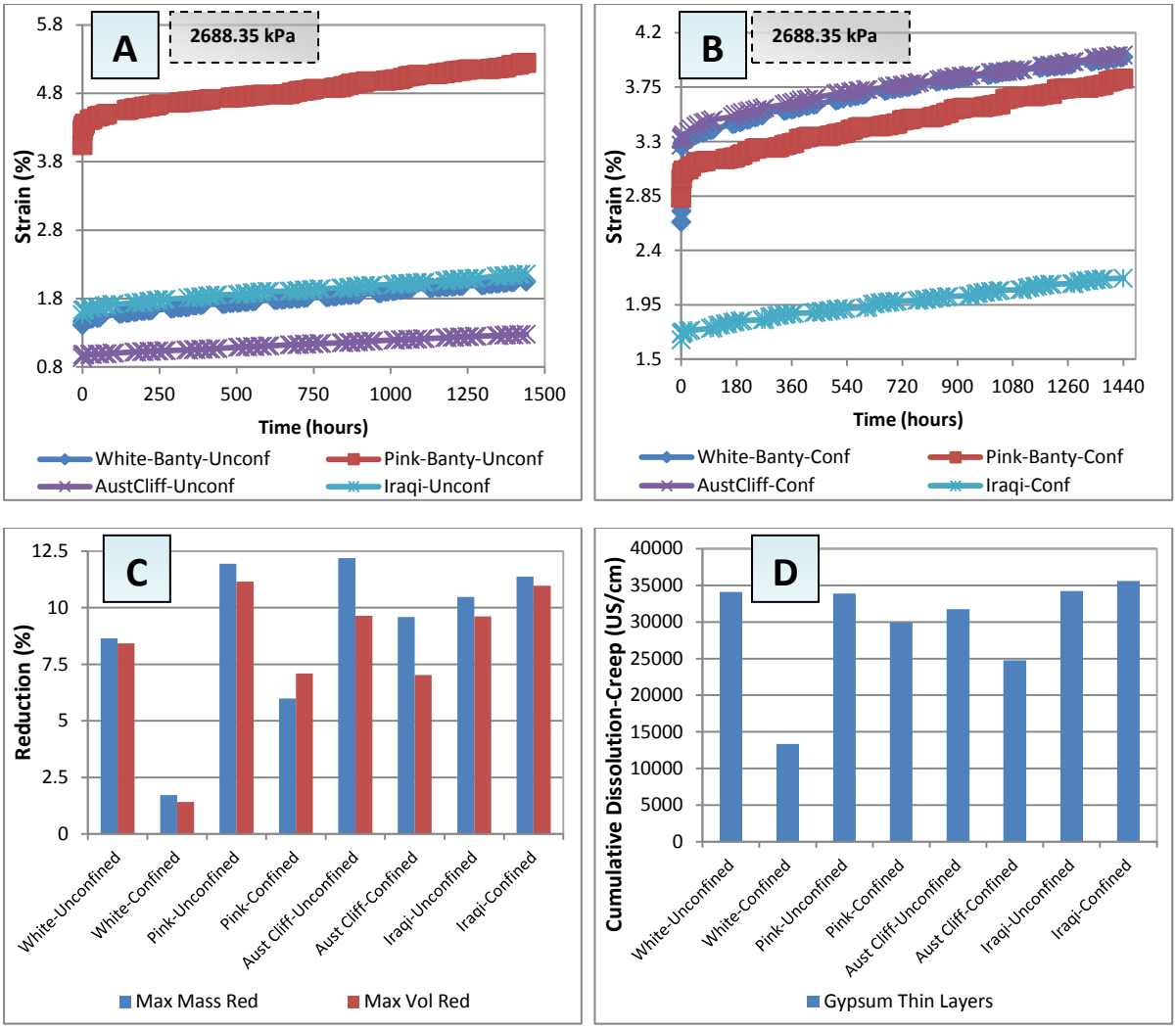

Fig. 4.51: Comparisons of UK and Iraqi gypsum rock thin layers tested in two cases of confinement. The tested samples size is 54 mm diameter x 20 mm height. Thin layers prepared from collected specimens on UK field trips: November 2009, April 2010 and April 2011; on Iraqi field trip on June 2010. Part A shows the creep strain percent of unconfined samples under 2688.35 kPa applied axial stress. Part B shows the creep strain percent of confined samples under 2688.35 kPa applied axial stress. Part C shows the comparisons among confined and unconfined samples in terms of mass and volume reduction percents. Part D shows the comparison between confined and unconfined samples in terms of creep cumulative conductivity (dissolution) value.

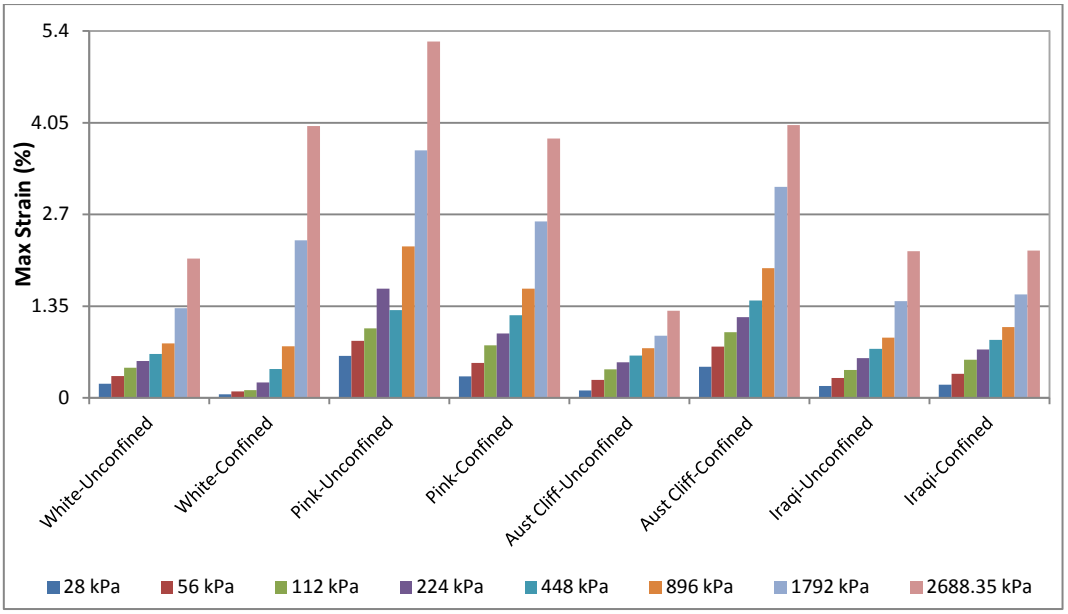

Fig. 4.52: Comparison of UK and Iraqi gypsum rock thin layers tested in two cases of confinement. It shows the maximum strain percent due to each loading stages. The tested samples size is 54 mm diameter x 20 mm height. Thin layers prepared from collected specimens on UK field trips: November 2009, April 2010 and April 2011; on Iraqi field trip on June 2010.

Table 4.14: Creep equations of confined and unconfined thin layers (gypsum rock) samples tested in long-term mode. These samples were tested under 1792 kPa applied axial stress in saturation state under atmospheric pressure. Equations of primary and secondary creep stages are presented. Y is strain percent and X is time in hours. Note: exponential equation is: $Y=Ae^{BX}$ and linear equation is: Y=AX + B. A and B are constants.

Thin Layers Origin	State of Testing/Creep	Formula of Creep	R^2 Value
White/Bantycock	Saturated (Unconfined)	$Y = 2.7315\ e^{0.0487X}$ *(Primary & Secondary)* $Y = 0.9753\ e^{0.0002X}$ (Secondary)	0.9082 0.9355
White/Bantycock	Saturated (Confined)	$Y = 1.2983\ e^{0.0739X}$ *(Primary & Secondary)* Y = 0.0004 X + 1.7825 (Secondary)	0.8951 0.9719
Pink/Bantycock	Saturated (Unconfined)	$Y = 2.9431\ e^{0.0001X}$ *(Primary & Secondary)* $Y = 3.0045\ e^{0.0001X}$ (Secondary)	0.9235 0.9867
Pink/Bantycock	Saturated (Confined)	$Y = 1.986\ e^{0.0002X}$ *(Primary & Secondary)* Y = 0.0004 X + 2.0045 (Secondary)	0.9682 0.9968
Aust Cliff	Saturated (Unconfined)	Y = 0.0177 ln X + 0.7727 *(Primary & Secondary)* Y = 0.00004 X + 0.852 (Secondary)	0.895 0.9492
Aust Cliff	Saturated (Confined)	$Y = 2.005\ e^{0.0559X}$ *(Primary & Secondary)* $y = 1.803\ e^{0.0726X}$ (Secondary)	0.9222 0.9772
Iraqi	Saturated (Unconfined)	$Y = 1.0832\ e^{0.0002X}$ *(Primary & Secondary)* Y = 0.0002 X + 1.091 (Secondary)	0.9198 0.9835
Iraqi	Saturated (Confined)	$Y = 1.2194\ e^{0.0002X}$ *(Primary & Secondary)* Y = 0.0002 X + 1.2283 (Secondary)	0.9723 0.9943

Table 4.15: Creep equations of confined and unconfined thin layers (gypsum rock) samples tested in long-term mode. These samples were tested under 2688.35 kPa applied axial stress in saturation state under atmospheric pressure. Equations of primary and secondary creep stages are presented. Y is strain percent and X is time in hours. Note: exponential equation is $Y=Ae^{BX}$ and linear equation is Y=AX + B. A and B are constants.

Thin Layers Origin	State of Testing/Creep	Formula of Creep	R^2 Value
White/Bantycock	Saturated (Unconfined)	$Y = 0.0004 X + 1.527$ *(Primary & Secondary)* $Y = 0.0004 X + 1.5472$ *(Secondary)*	0.9809 0.9911
White/Bantycock	Saturated (Confined)	$Y = 3.0811 e^{0.0002X}$ *(Primary & Secondary)* $Y = 0.0005 X + 3.3789$ *(Secondary)*	0.9692 0.9719
Pink/Bantycock	Saturated (Unconfined)	$Y = 4.4306 e^{0.0001X}$ *(Primary & Secondary)* $Y = 0.0005 X + 4.4809$ *(Secondary)*	0.9407 0.9935
Pink/Bantycock	Saturated (Confined)	$Y = 3.4288 e^{0.0001X}$ *(Primary & Secondary)* $Y = 0.0005 X + 3.0988$ *(Secondary)*	0.9508 0.9942
Aust Cliff	Saturated (Unconfined)	$Y = 0.9823 e^{0.0002X}$ *(Primary & Secondary)* $Y = 0.0002 X + 0.9815$ *(Secondary)*	0.9934 0.9993
Aust Cliff	Saturated (Confined)	$Y = 3.4288 e^{0.0001X}$ *(Primary & Secondary)* $Y = 0.0004 X + 3.4569$ *(Secondary)*	0.9508 0.9792
Iraqi	Saturated (Unconfined)	$Y = 1.6902 e^{0.0002X}$ *(Primary & Secondary)* $Y = 0.0003 X + 1.6876$ *(Secondary)*	0.9817 0.9912
Iraqi	Saturated (Confined)	$Y = 1.746 e^{0.0002X}$ *(Primary & Secondary)* $Y = 0.0003 X + 1.7567$ *(Secondary)*	0.9793 0.9937

Table 4.16: Dissolution dataset of UK and Iraqi thin layer samples (gypsum rock) for long term testing. Note that the volume of saturation water is constant for confined and unconfined samples.

Time (days)	Cumulative Conductivity (US/cm)							
	Thin layers Samples-Unconfined				Thin layers Samples-Confined			
	White Bantycock	Pink Bantycock	Iraqi	Aust Cliff	White Bantycock	Pink Bantycock	Iraqi	Aust Cliff
0	0	0	0	0	0	0	0	0
7	2446	2246	2403.6	2392.3	1808.4	2138	2378	2092.3
14	4559	4529	4507.9	4780.5	3160.4	4268	4706	3605
21	6722	6801.9	6542.2	6819.2	4422.5	6416	7054	5197.6
28	9034.9	9104.8	8836.5	8865.2	5075.1	8561	9352	6795.6
35	11347.8	11417.7	11089.7	10921.2	5632.1	10686	11700	8344.4
42	13660.8	13830.7	13452.9	12952.2	6219.9	12815	14090	9999.6
49	15763.8	16220.7	15815.2	14964.2	6778.9	14949	16475	11658.9
56	17959.8	18621.7	18113.2	16976.4	7568	17084	18845	13258.7
63	20172.8	21007.7	20438.5	19065.4	8379.7	19225	21234	14870.7
70	22487	23341.9	22748.5	21175.4	9196.7	21365	23629	16480.7
77	24831.2	25575.5	25050.5	23277.4	9999.9	23500	26025	18134.9
84	27134.8	27629.1	27350.1	25366.4	10812.7	25642	28390	19758.9
91	29448.4	29902.7	29595.1	27523	11702.7	27770	30765	21416.9
98	31758.4	31868.3	31895.1	29622.2	12492.7	29895	33145	23091.9
105	34098.4	33869.5	34199.3	31720.4	13332.7	32022	35575	24761.9

4.4.2 Bantycock bending results

Figures from 4.53 to 4.57 show the outcomes of small and large four-point banding long-term testing. Small bars are in size of 140 x 40 x 20 mm, while large bars are in size of 240 x 40 x 20 mm

From Figure 4.53-4.54, it can be seen that the lower loading stages, 28 and 56 kPa, do not change the creep curves shape or make differences in behaviour between the air-dry and saturated states. Increasing axial stresses causes changes in the curves with an increase in vertical deflection. Saturation affects in *SFB* bars weaknesses. Time also has an impact to increase both the air-dry and saturated bars' deflection under constant axial stress. In general, the creep behaviour is a gradual marginal strain increment indicating that the failure/collapse results from a gradual process and then a sudden collapse.

From Figure 4.55-4.57, it can be seen that the lower loading stage, 28 kPa, does not change the creep curve shape in the first hour loading, while divergences between saturated and air-dry specimens are obtained after about 70 hours. Increasing loads do not cause changes in the curves form in the first hour of loading at 56 kPa, while creep duration within this stage caused failure of saturated specimens. Time duration increases under constant stress increases the bars' deflection in air-dry state.

In comparison between small and large bending bars, the *LFB* specimens are more sensitive to saturation compare to the *SFB* bars. Step-wise behaviours are indicated due to longer duration of loading despite the amount of water being constant each week. The collapse of *LFB* and *SFB* collapse is sudden; however a long time is needed to achieve this failure. Increased bending span indicated weaker behaviour upon saturation and saturated specimens failed at low stress/56 kPa.

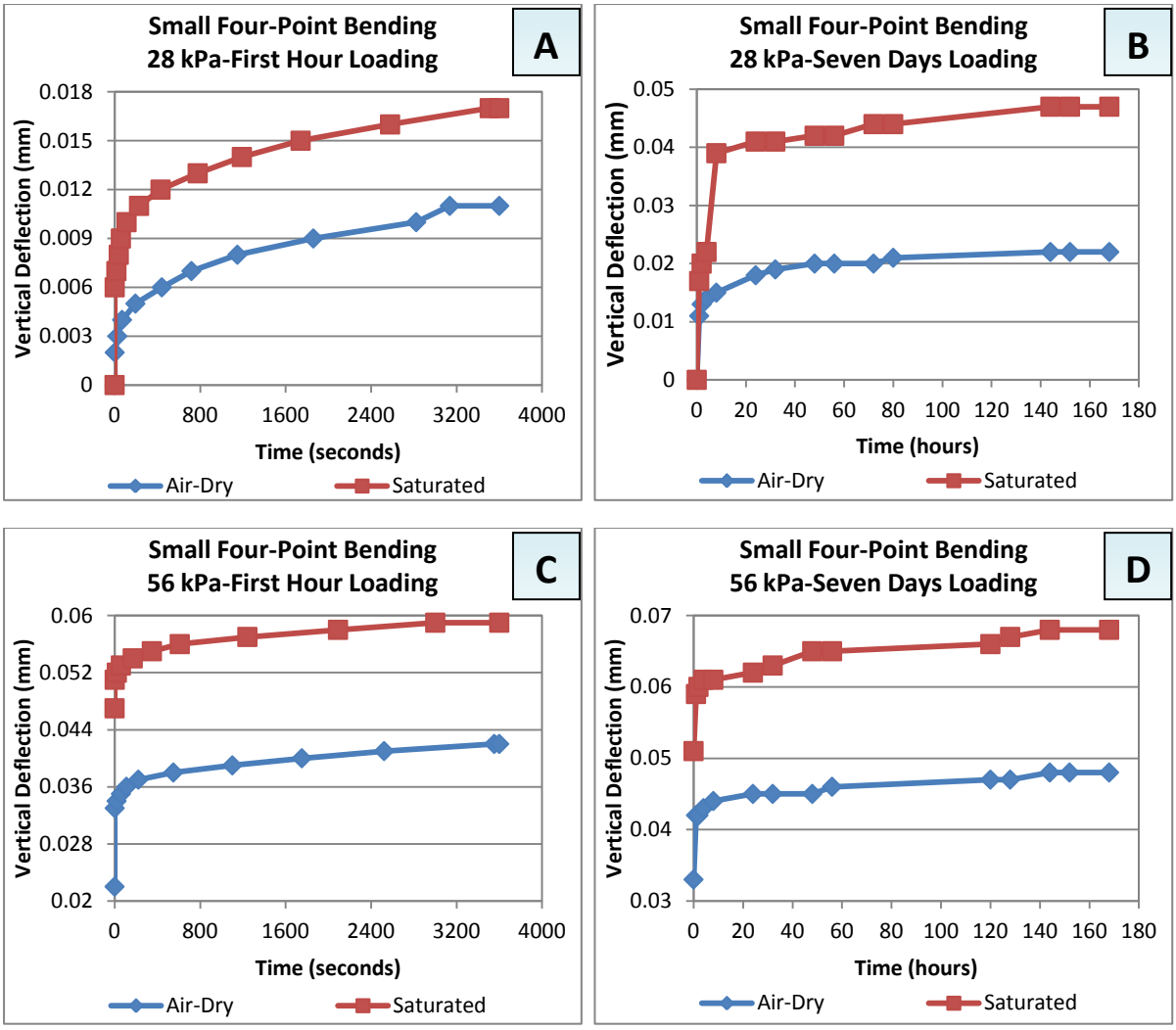

Fig. 4.53: Results of creep test of small four-point bending bars. It shows comparisons between air-dry and saturated bars (saturation under atmospheric pressure). Parts A and B show the creep vertical deflection under 28 kPa axial stress. Parts C and D show the creep vertical deflection due to applied 56 kPa axial stress. Each of these two loading stages lasted for seven days. Used samples are white Bantycock Mine/UK gypsum prepared from collected specimens on field trip on April 2010.

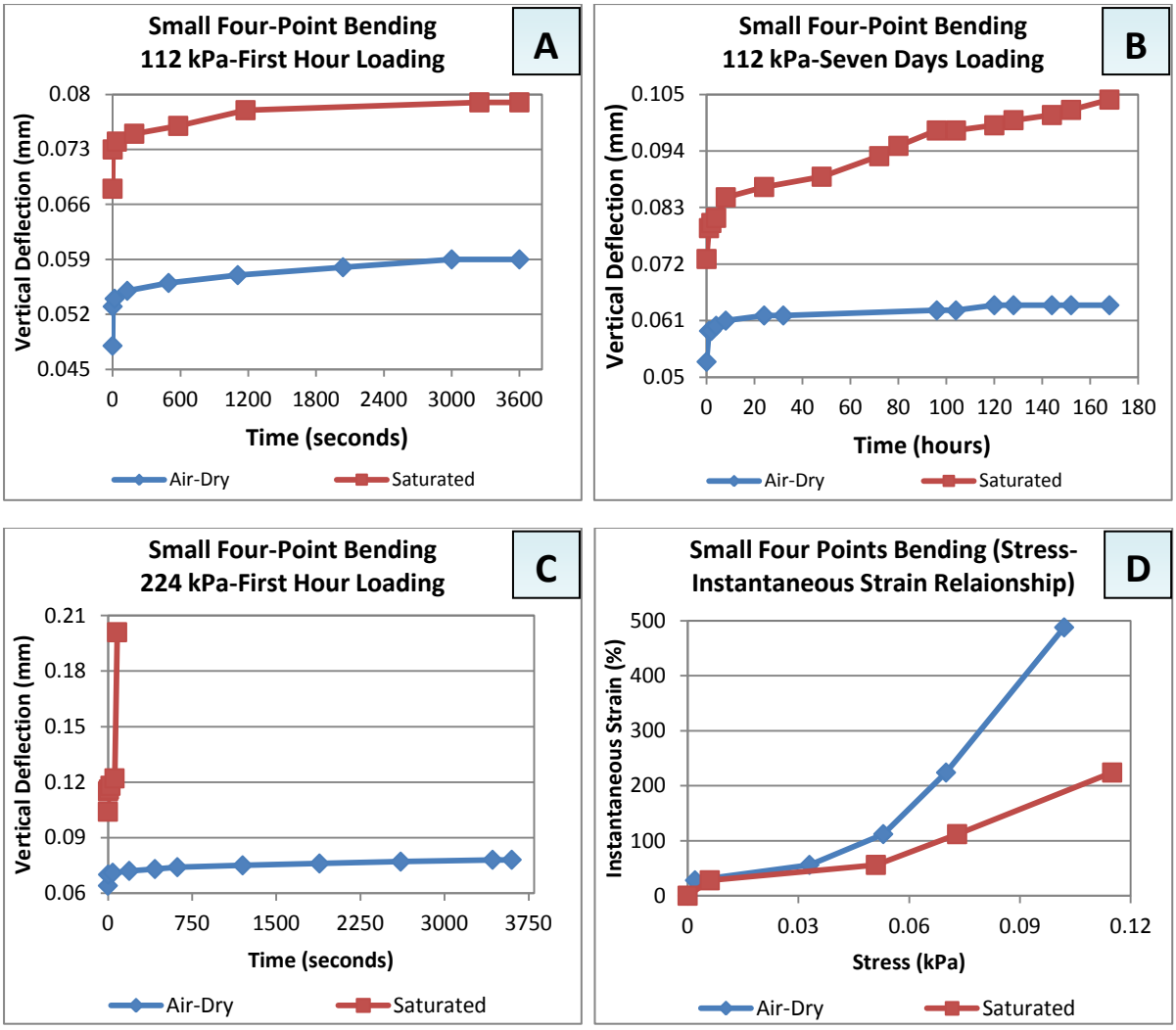

Fig. 4.54: Results of creep test of small four-point bending bars. It shows comparisons between air-dry and saturated bars (saturation under atmospheric pressure). Parts A and B show the creep vertical deflection under 112 kPa applied axial stress. Part C shows the creep vertical deflection under 224 kPa applied axial stress (saturated sample was failed in this stage). Each of these loading stages was lasted for seven days. Part D shows instantaneous strain relationship with applied axial stresses of air-dry and saturated samples. Used samples are white Bantycock Mine/UK gypsum prepared from collected specimens on field trip on April 2010.

Table 4.17: Represents different calculated properties of tested small four-point bending samples in long-term mode. Three samples for each air-dry and saturated condition are tested. Tested samples were prepared from collected gypsum rock from Bantycock Mine/UK in April 2010.

Sample State-Small Bending	AirDry-1	AirDry-1	AirDry-1	Saturated-1	Saturated-2	Saturated-3
Time to failure (hours)	776	777	775.5	504.02	504.14	504.38
Max Vertical Deflection (mm)	0.12	0.2	0.21	0.12	0.13	0.12
Load at Failure (gm)	9328	9328	9328	4664	4664	4664
Length Reduction (%)	-	-	-	0.03	0.05	0.04
Width Reduction (%)	-	-	-	0.49	0.48	0.5
Depth Reduction (%)	-	-	-	0.66	0.65	0.69
Mass Reduction (%)	-	-	-	1.42	1.35	1.32
Volume Reduction (%)	-	-	-	1.17	1.68	1.67

Table 4.18: Creep equations of tested small four-point bending gypsum bars. Each gradual loading stage lasted for seven days. Equations of primary and secondary creep stages are presented. Y is strain percent and X is time in hours. Note: exponential equation is $Y=Ae^{BX}$, logarithmic equation is Y=A ln X + B and linear equation is Y=AX + B. A and B are constants.

28 kPa Applied Stress			
Small-Bending Origin	**State of Testing/Creep**	**Formula of Creep**	**R^2 Value**
White/Bantycock	Air-Dry	Y = 0.0022 ln X + 0.0111 *(Primary & Secondary)* Y = 0.0023 ln X + 0.0107 *(Secondary)*	0.9923 0.9752
White/Bantycock	Saturated	Y = 0.006 ln X + 0.0183 *(Primary & Secondary)* Y = 0.00005 X + 0.0395 *(Secondary)*	0.9122 0.9601
56 kPa Applied Stress			
White/Bantycock	Air-Dry	Y = 0.002 ln X + 0.0376 *(Primary & Secondary)* Y = 0.00003 X + 0.0438 *(Secondary)*	0.8011 0.9333
White/Bantycock	Saturated	Y = 0.0024 ln X + 0.0547 *(Primary & Secondary)* Y = 0.0005 X + 0.0615 *(Secondary)*	0.8566 0.9135
112 kPa Applied Stress			
White/Bantycock	Air-Dry	$Y = 0.0587\ e^{0.0169X}$ *(Primary & Secondary)* $Y = 0.0587\ e^{0.0167X}$ *(Secondary)*	0.9778 0.9323
White/Bantycock	Saturated	$Y = 0.079\ e^{0.0017X}$ *(Primary & Secondary)* Y = 0.0001 X + 0.0845 *(Secondary)*	0.9246 0.9777
224 kPa Applied Stress			
White/Bantycock	Air-Dry	Y = 0.0017 ln X + 0.0763 *(Primary & Secondary)* Y = 0.00003 X + 0.0802 *(Secondary)*	0.9207 0.9404

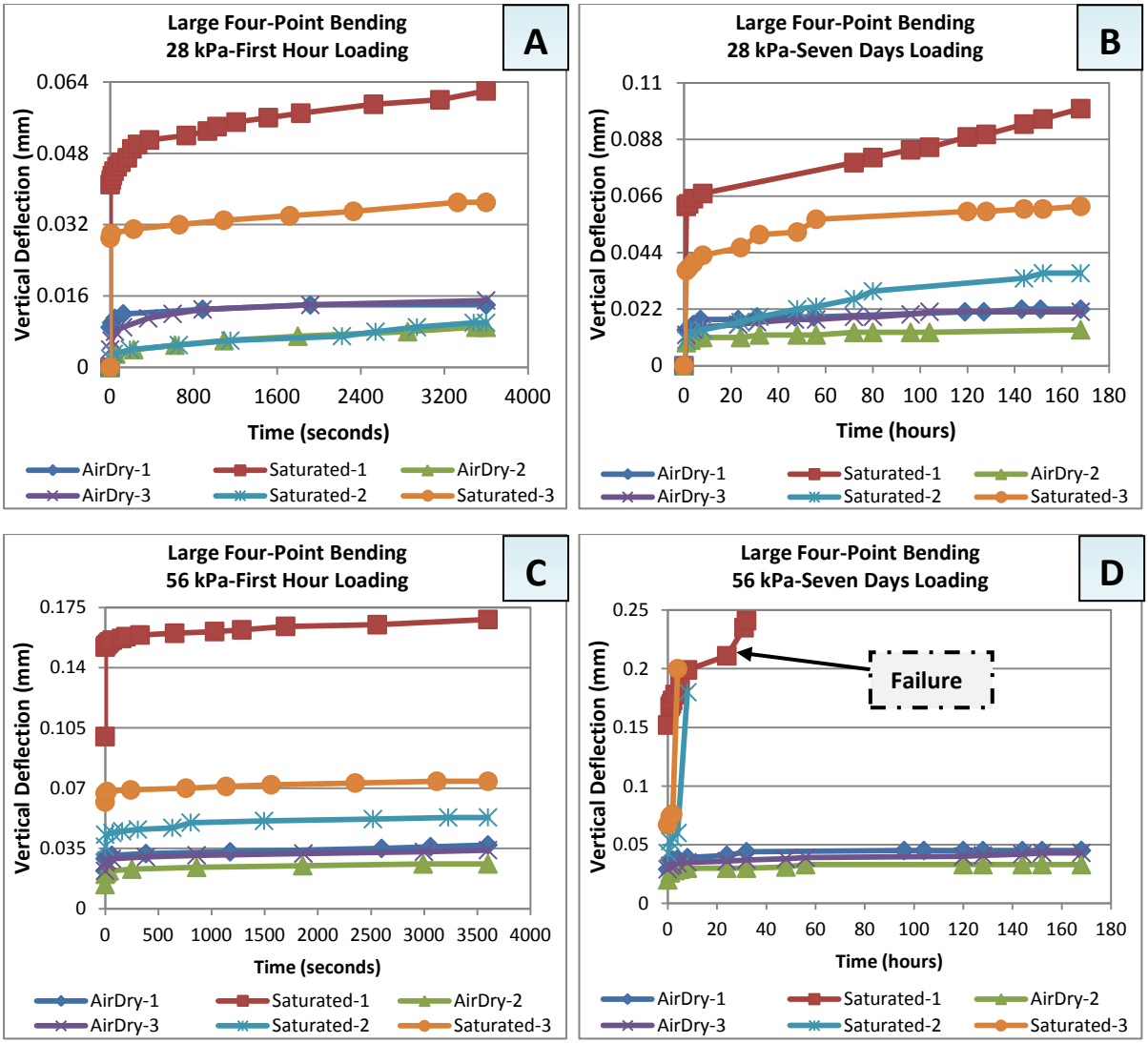

Fig. 4.55: Creep test results of large four-point bending bars. It shows comparisons between air-dry and saturated bars (saturation under atmospheric pressure). Parts A and B show the creep vertical deflections of samples under axial stress of 28 kPa. Parts C and D show the creep vertical deflections of samples under axial stress of 56 kPa. Each of these two loading stages was lasted for seven days. Used samples are white Bantycock Mine/UK gypsum prepared from specimens collected in April 2010. All saturated samples failed in the stage of 56 kPa applied axial stress.

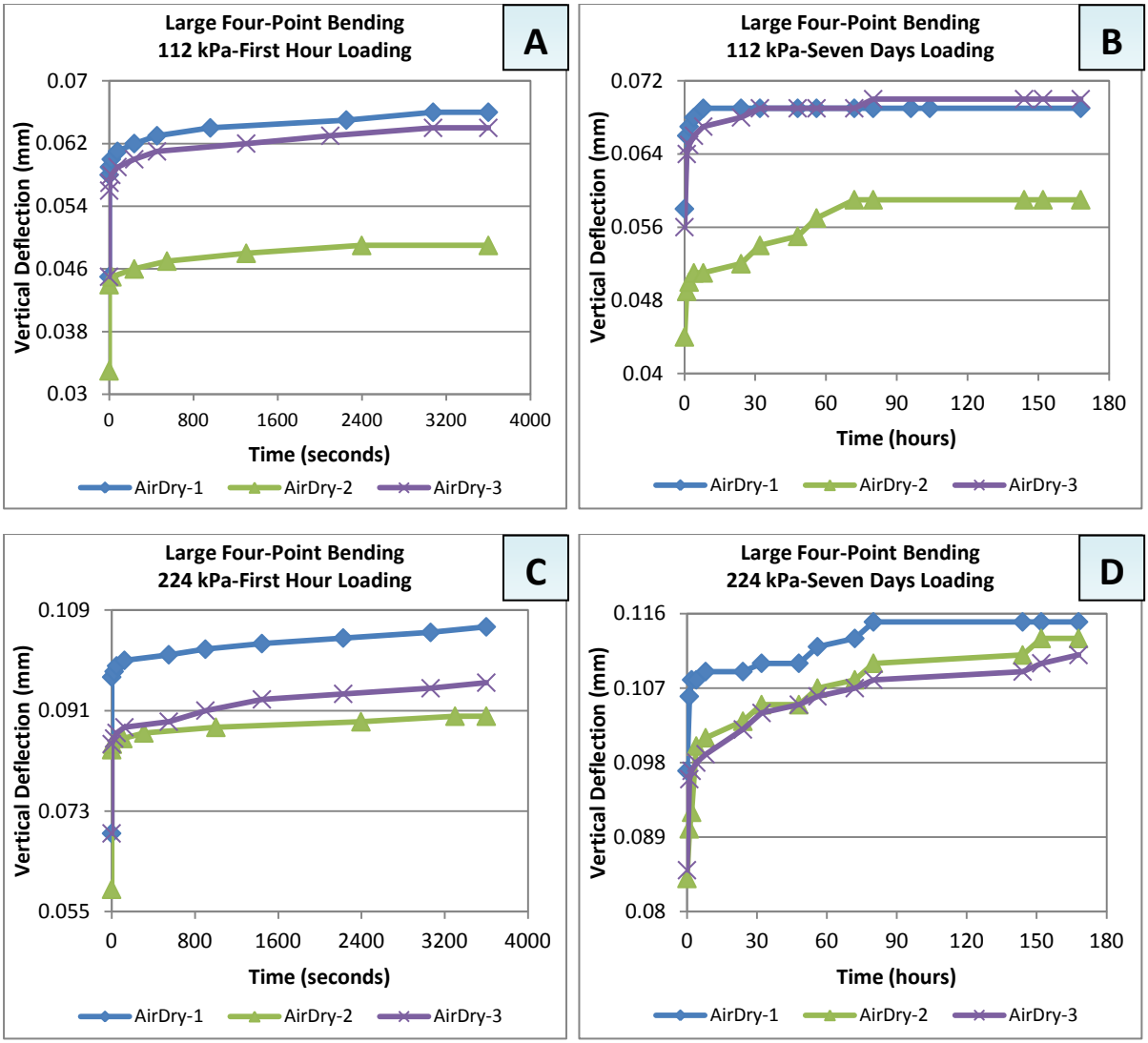

Fig. 4.56: Results of creep test of air-dry large four-point bending bars. Parts A and B show the creep vertical deflections of samples under axial stress of 112 kPa. Parts C and D show the creep vertical deflections of samples under axial stress of 224 kPa. Each of these two loading stages was lasted for seven days. Used samples are white gypsum from Bantycock Mine/UK, prepared from specimens collected in April 2010.

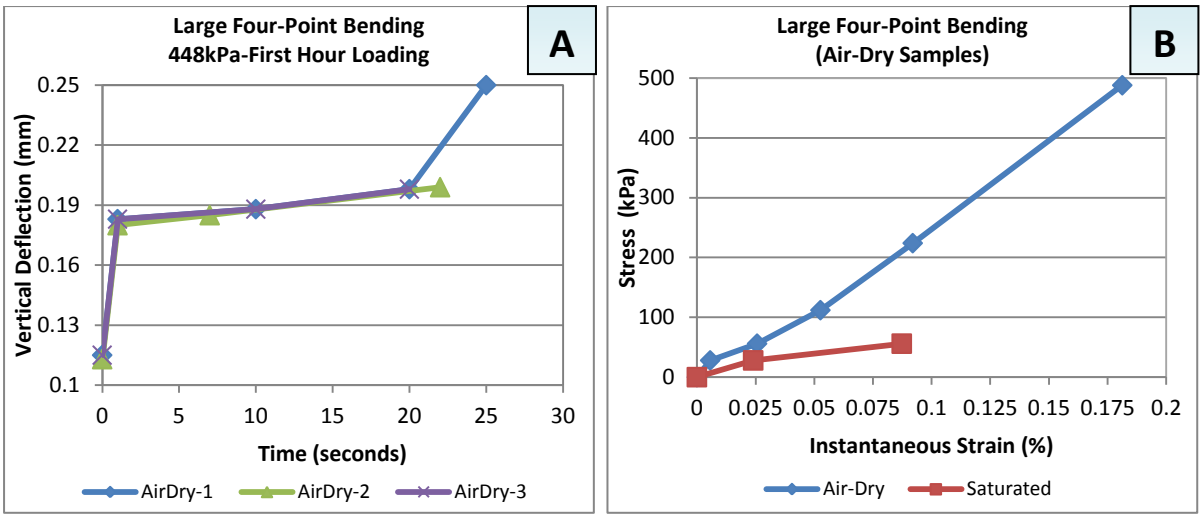

Fig. 4.57: Results of creep test of air-dry large four-point bending bars. Part A shows the creep vertical deflections of samples under axial stress of 448 kPa. All air-dry samples were failed in this stage of loading. Part B shows a comparison between air-dry and saturated samples through axial stresses-instantaneous strain relationship. Used samples are white gypsum from Bantycock Mine/UK, prepared from specimens collected in April 2010.

Table 4.19: Represents different calculated properties of large four-point bending samples tested in long-term mode. Three samples for each air-dry and saturated condition were used. Tested samples were prepared from collected gypsum rock from Bantycock Mine/UK in April 2010.

Sample State-Large Bending	Air Dry (1)	Air Dry (2)	Air Dry (3)	Saturated (1)	Saturated (2)	Saturated (3)
Time to Failure (hours)	672.01	672.01	672.01	200	176	172
Max Vertical Deflection (mm)	0.25	0.2	0.2	0.24	0.18	0.2
Load at Failure (gm)	9328	9328	9328	1166	1166	1166
Length Reduction (%)	-	-	-	0.08	0.86	0.82
Width Reduction (%)	-	-	-	0.59	0.5	0.57
Depth Reduction (%)	-	-	-	3.44	2.94	3.12
Mass Reduction (%)	-	-	-	1.33	0.98	1.25
Volume Reduction (%)	-	-	-	4.09	3.67	3.81

Table 4.20: Creep equations of large four-point bending gypsum bars tested in long-term mode. It shows the creep equations of each stage of loading until failure. Equations of primary and secondary creep stages are presented. Y is strain percent and X is time in hours. Note: exponential equation is $Y=Ae^{BX}$, logarithmic equation is Y=A ln X + B and linear equation is Y=AX + B. A and B are constants.

Large Sample Origin (Four-Point Bending Test)	State of Testing/Creep	Creep Equation	R^2 Value
28 kPa Applied Stress			
White/Bantycock	Air-Dry 1	$Y = 0.0143\ e^{0.082X}$ *(Primary & Secondary)* $Y = 0.00003\ X + 0.0177$ *(Secondary)*	0.9512 0.9734
White/Bantycock	Air-Dry 2	$Y = 0.0092\ e^{0.0757X}$ *(Primary & Secondary)* $Y = 0.00002\ X + 0.011$ *(Secondary)*	0.9344 0.8993
White/Bantycock	Air-Dry 3	$Y = 0.0119\ e^{0.1099X}$ *(Primary & Secondary)* $Y = 0.0115\ e^{0.1183X}$ *(Secondary)*	0.9752 0.9354
White/Bantycock	Saturated 1	$Y = 0.0639\ e^{0.0027X}$ *(Primary & Secondary)* $Y = 0.0002\ X + 0.0644$ *(Secondary)*	0.9906 0.9973
White/Bantycock	Saturated 2	$Y = 0.009\ e^{0.2524X}$ *(Primary & Secondary)* $Y = 0.0001\ X + 0.0143$ *(Secondary)*	0.9411 0.9644
White/Bantycock	Saturated 3	$Y = 0.0351\ e^{0.1087X}$ *(Primary & Secondary)* $Y = 0.0324\ e^{0.1272X}$ *(Secondary)*	0.9714 0.9566
56 kPa Applied Stress			
White/Bantycock	Air-Dry 1	$Y = 0.0026 \ln X + 0.0322$ *(Primary & Secondary)* $Y = 0.0362\ e^{0.0448X}$ *(Secondary)*	0.9181 0.958
White/Bantycock	Air-Dry 2	$Y = 0.0021 \ln X + 0.0229$ *(Primary & Secondary)* $Y = 0.0269\ e^{0.0406X}$ *(Secondary)*	0.898 0.786
White/Bantycock	Air-Dry 3	$Y = 0.0296\ e^{0.064X}$ *(Primary & Secondary)* $Y = 0.00005\ X + 0.0353$ *(Secondary)*	0.9472 0.9551
White/Bantycock	Saturated 1	$Y = 0.1561\ e^{0.0943X}$ *(Secondary & Tertiary)*	0.9052
White/Bantycock	Saturated 2	$Y = 0.0385\ e^{0.1785X}$ *(Secondary & Tertiary)*	0.8959
112 kPa Applied Stress			
White/Bantycock	Air-Dry 1	$Y = 0.0015 \ln X + 0.063$ *(Primary & Secondary)*	0.6183
White/Bantycock	Air-Dry 2	$Y = 0.0454\ e^{0.0506X}$ *(Primary & Secondary)* $Y = 4.4306\ e^{0.048X}$ *(Secondary)*	0.9029 0.8696
White/Bantycock	Air-Dry 3	$Y = 0.002 \ln X + 0.0604$ *(Primary & Secondary)* $Y = 0.001 \ln X + 0.0651$ *(Secondary)*	0.8233 0.9124
224 kPa Applied Stress			
White/Bantycock	Air-Dry 1	$Y = 0.0026 \ln X + 0.1013$ *(Primary & Secondary)* $Y = 0.1026\ e^{0.0222X}$ *(Secondary)*	0.835 0.8111
White/Bantycock	Air-Dry 2	$Y = 0.0051 \ln X + 0.0857$ *(Primary & Secondary)* $Y = 0.0918\ e^{0.0392X}$ *(Secondary)*	0.975 0.9322
White/Bantycock	Air-Dry 3	$Y = 0.0039 \ln X + 0.0893$ *(Primary & Secondary)* $Y = 0.0913\ e^{0.037X}$ *(Secondary)*	0.9144 0.9832
448 kPa Applied Stress			
White/Bantycock	Air-Dry 1	$Y = 0.1739\ e^{0.0111X}$ *(Primary & Secondary)*	0.695

4.4.3 Cylinders results

From Figure 4.58-4.61, it can be seen that all of tested gypsum types are in good agreement and slight differences in strain records among them except for *IG*. Saturated *IG*'s specimens under atmospheric pressure are more sensitive to instantaneous and creep due to constant stresses. Step-wise periods are noticed also here, especially in the *IG* specimen. The largest strain recorded for saturated samples is established by *IG* specimen under atmospheric pressure, while the smallest is caused by *WBG* saturated sample under 5.0 bars. It seems that there are no clear impacts of the application of 5.0 bar water pressure on creep curves. The application of 5.0 bars decreased the recorded strain percent, in the *WBG*, *PBG* and *IG* specimens.

It can be understood that the creep increases due to saturation. The mechanism of it is complicated and might be due to the combined impacts of axial loading and solution. By this state, re-crystallization may take place and thus creep strain increases on saturation.

From Table 4.21-4.22, it can be seen that all creep curves follow an exponential form. Constant *A* decreased with the application of 5.0 bar water pressure for *WBG*, *PBG* and *IG*. While, constant *B* increased noticeably for *IG* and very slightly for *WBG* and *PBG*.

From Figure 4.62 (one year experiment on gypsum rock cylinders), it can be noticed that the application of constant stress of 2688.35 kPa caused gypsum rock cylinders to collapse after a long period of time. The faster collapse is at about 4000 hour for *WBG* cylinder in saturation state under 5.0 bar water pressure. The slower collapse is at about 6800 hour for *IG* cylinder in saturation state under atmospheric pressure. The application of 5.0 bar water pressure is more aggressive over time and leads to faster specimen collapse compared with saturated samples under atmospheric pressure. The *WBG* cylinder is stronger than *IG* cylinder within the same condition of saturation, which might reflect the existing cracks in the *IG* cylinder.

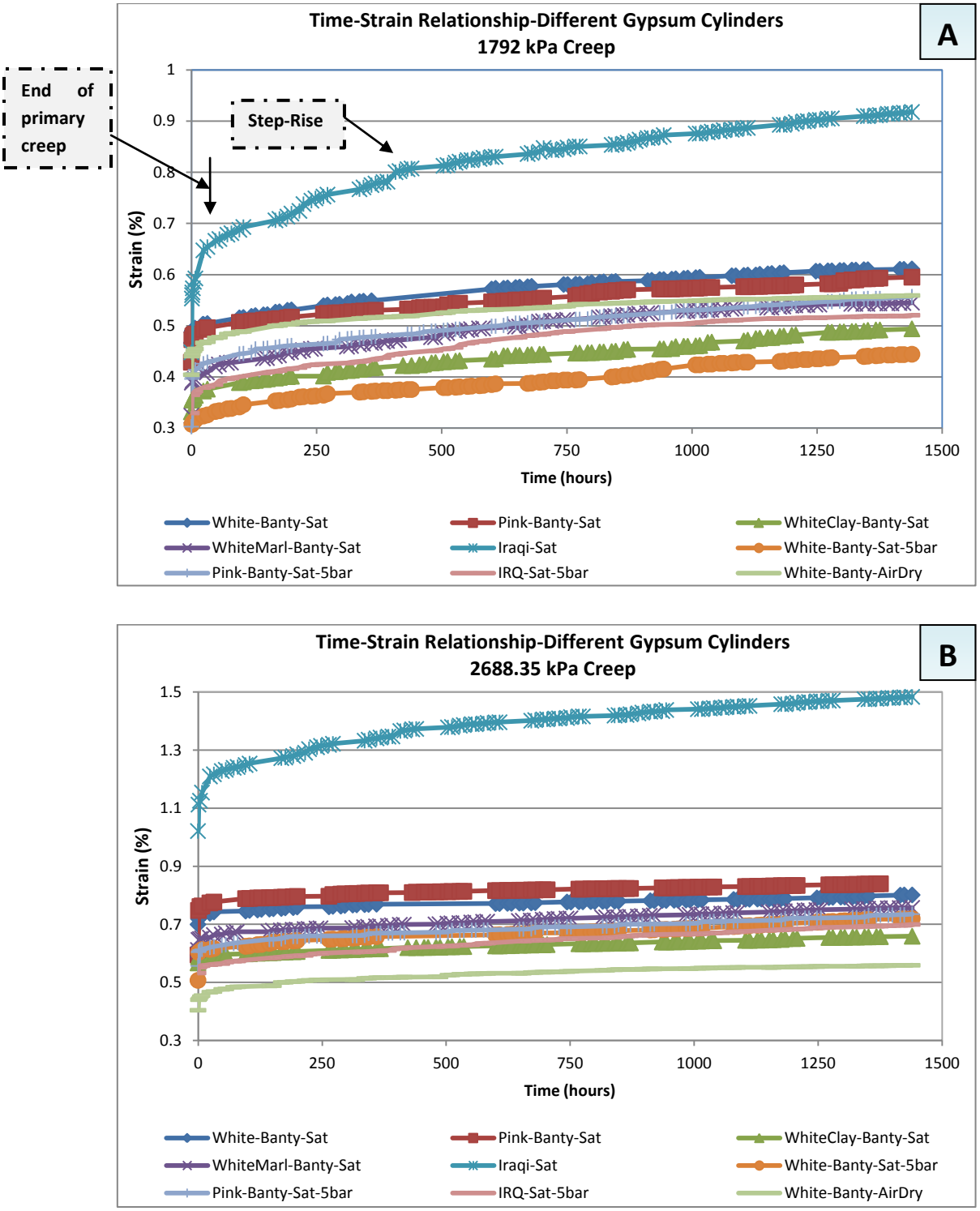

Fig. 4.58: Present time-settlement relationship for different gypsum rock cylinders from the UK and Iraq saturated under different levels of water pressure. Used gypsum cylinders are 54 mm diameter x 135 mm height. Part A is for the 1792 kPa applied axial stress. Part B is for the 2688.35 kPa applied axial stress. Each of those two loading stages lasted for 1440 hour. Saturated Iraqi cylinders under atmospheric pressure recorded the highest creep strain.

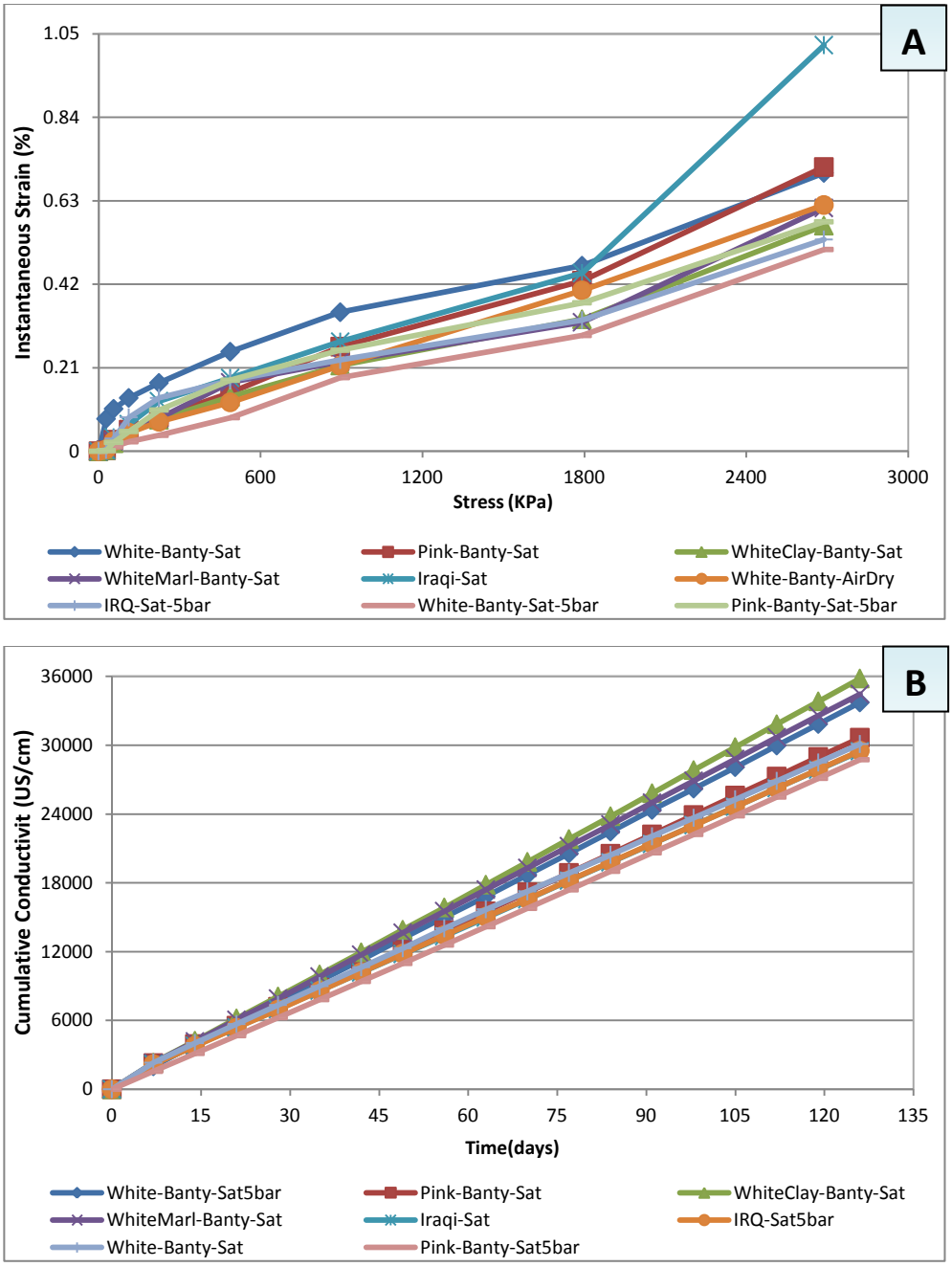

Fig. 4.59: Comparison between different gypsum rock cylinders from the UK and Iraq tested in saturation state under different levels of water pressure. Tested gypsum rock cylinders are in size of 54 mm diameter x 135 mm height. Part A shows stress-instantaneous strain relationship for these cylinders. Part B shows the comparison among cumulative conductivities (dissolution) of tested cylinders.

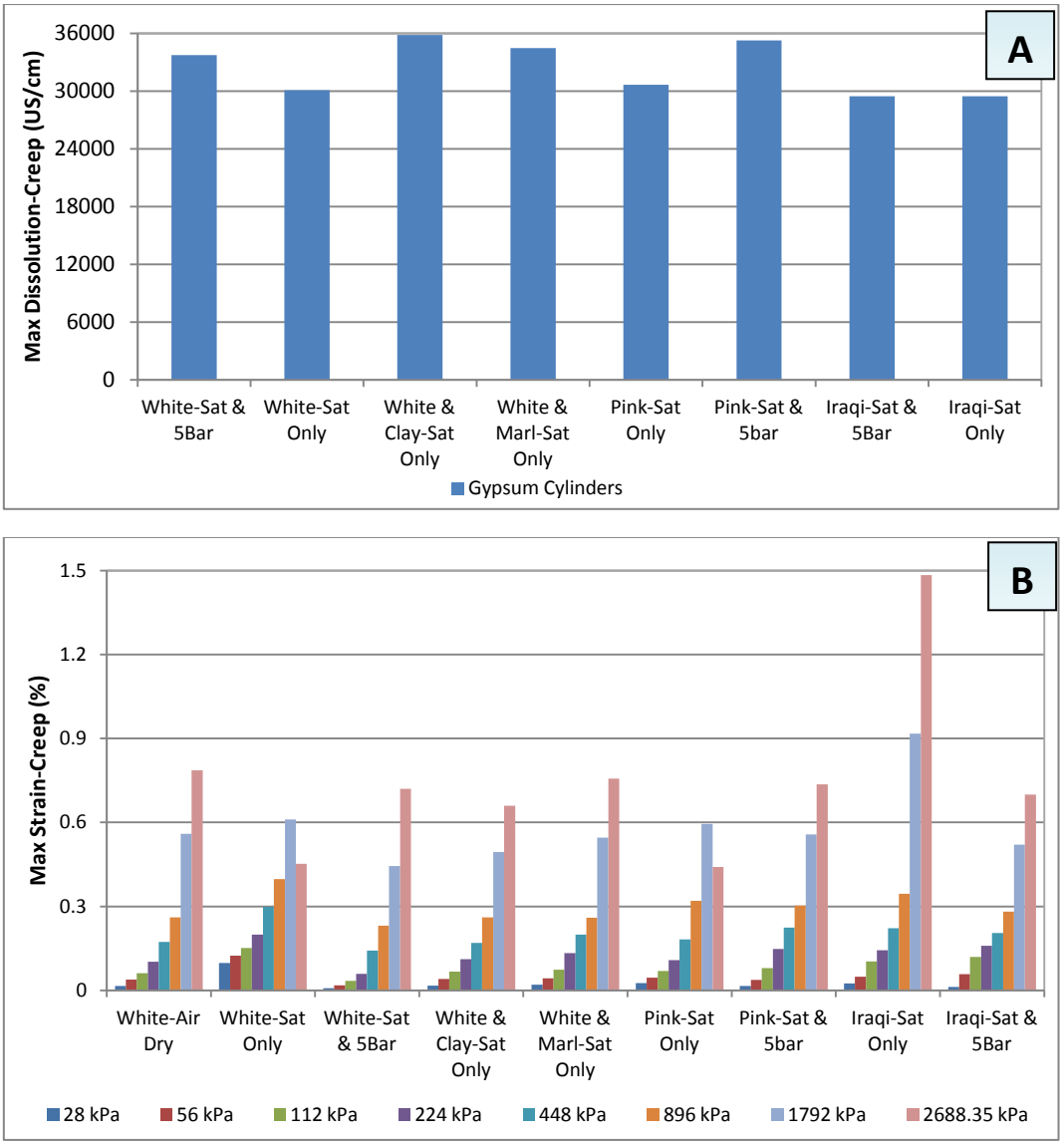

Fig. 4.60: Comparison between different gypsum rock cylinders from the UK and Iraq tested in saturated state under different levels of water pressure. Tested gypsum rock cylinders are in size of 54 mm diameter x 135 mm height from Bantycock Mine/UK gypsum collected in April 2010 and from northern of Iraq collected in June 2010. Part A shows the comparison of maximum creep dissolution among tested gypsum cylinders. Part B presents the comparison of maximum creep strain percent among tested gypsum cylinders.

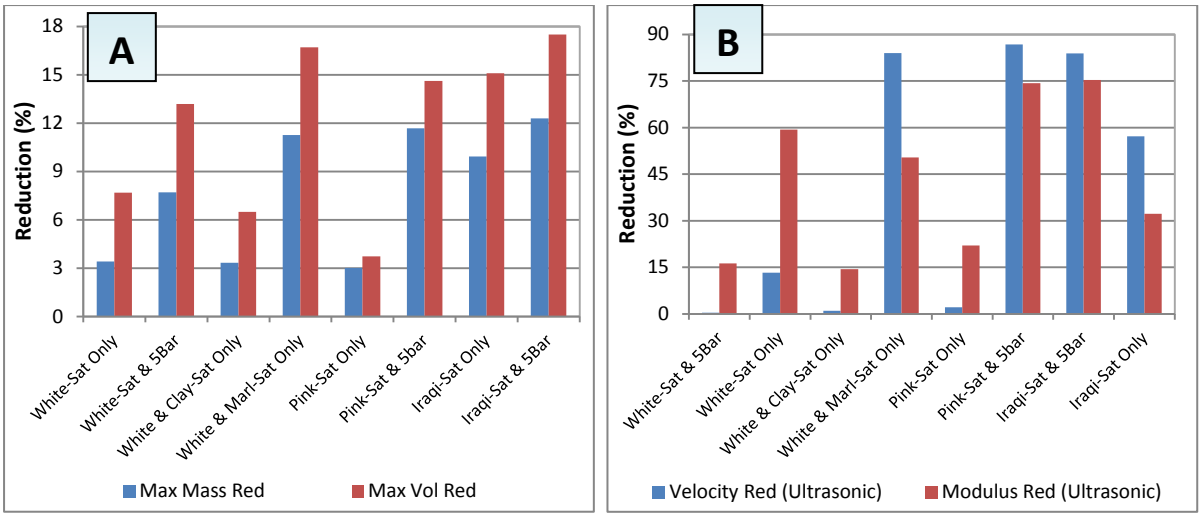

Fig. 4.61: Comparisons between different gypsum rock cylinders from the UK and Iraq tested in saturation state under different levels of water pressure. Part A shows the comparisons of mass and volume reductions. Part B presents the comparisons of velocity and elastic modulus reductions (these parameters are recorded from ultrasound observations). Used samples are 54 mm diameter x 135 mm height.

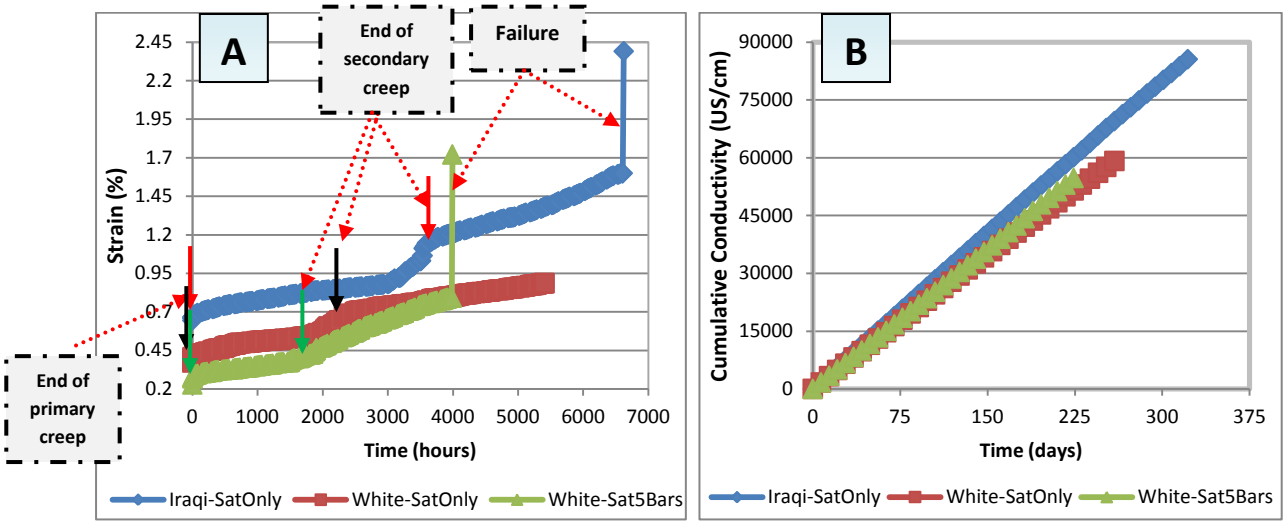

Fig. 4.62: Results of one-year loaded gypsum cylinders. Part A shows creep strain percent versus time. It can be seen that the Iraqi cylinder saturated under atmospheric pressure and white/Bantycock cylinder saturated under 5.0 bars water pressure failed at about 4000 and 6800 hour respectively. Part B presents cumulative conductivity (dissolution) versus time. The samples are 54 mm diameter x 135 mm height. Note that the Iraqi cylinder behaves differently at 2688.35 kPa stress in the case of saturation without water pressure.

Table 4.21: Creep equations of tested gypsum cylindrical samples in long-term mode for 1792 kPa loading stage; equations of primary and secondary creep stages are presented. Y is strain percent and X is time in hours. Note: exponential equation is $Y=Ae^{BX}$, logarithmic equation is Y=A ln X + B and linear equation is Y=AX + B. A and B are constants.

Cylinder Origin	State of Testing/Creep	Creep Equation	R^2 Value
White/Bantycock	Air-Dry	$Y = 0.4155\ e^{0.0392X}$ *(Primary & Secondary)* $Y = 0.3738\ e^{0.0553X}$ *(Secondary)*	0.9466 0.9906
White/Bantycock	Saturation-Only	$Y = 0.5093\ e^{0.0001X}$ *(Primary & Secondary)* $Y = 0.00007\ X + 0.5179$ *(Secondary)*	0.9279 0.9548
White/Bantycock	Saturation 5.0 bar	$Y = 0.337\ e^{0.0002X}$ *(Primary & Secondary)* $Y = 0.00007\ X + 0.3422$ *(Secondary)*	0.9499 0.9872
Pink/Bantycock	Saturation-Only	$Y = 0.5013e^{0.0001X}$ *(Primary & Secondary)* $Y = 0.00006\ X + 0.5062$ *(Secondary)*	0.9435 0.9801
Pink/Bantycock	Saturation 5.0 bar	$Y = 0.4397\ e^{0.0002X}$ *(Primary & Secondary)* $Y = 0.00008\ X + 0.4495$ *(Secondary)*	0.9182 0.9913
White & Clay/Bantycock	Saturation-Only	$Y = 0.3809\ e^{0.0002X}$ *(Primary & Secondary)* $Y = 0.00008\ X + 0.3875$ *(Secondary)*	0.9444 0.9913
White & Marl/Bantycock	Saturation-Only	$Y = 0.2647\ e^{0.0993X}$ *(Primary & Secondary)* $Y = 0.4278\ e^{0.0002X}$ *(Secondary)*	0.9713 0.9009
Iraqi	Saturation-Only	$Y = 0.5057\ e^{0.0777X}$ *(Primary & Secondary)* $Y = 0.0889\ \ln X + 0.2621$ *(Secondary)*	0.9496 0.9832
Iraqi	Saturation 5.0 bar	$Y = 0.4\ e^{0.1213X}$ *(Primary & Secondary)* $Y = 0.2173\ e^{0.0002X}$ *(Secondary)*	0.9799 0.9832

Table 4.22: Creep equations of tested gypsum cylindrical samples in long-term mode for the 2688.35 kPa loading stage; equations of primary and secondary creep stages are presented. Y is strain percent and X is time in hours. Note: exponential equation is $Y=Ae^{BX}$, logarithmic equation is Y=A ln X + B and linear equation is Y=AX + B. A and B are constants.

Cylinder Origin	State of Testing/Creep	Creep Equation	R^2 Value
White/Bantycock	Air-Dry	$Y = 0.5966\ e^{0.037X}$ *(Primary & Secondary)* $Y = 0.0333\ \ln X + 0.5438$ *(Secondary)*	0.9651 0.9959
White/Bantycock	Saturation-Only	$Y = 0.7037\ e^{0.0156X}$ *(Primary & Secondary)* $Y = 0.00003\ X + 0.7529$ *(Secondary)*	0.9053 0.9754
White/Bantycock	Saturation 5.0 bar	$Y = 0.5311\ e^{0.0374X}$ *(Primary & Secondary)* $Y = 0.00007\ X + 0.6232$ *(Secondary)*	0.8764 0.9679
Pink/Bantycock	Saturation-Only	$Y = 0.731\ e^{0.0178X}$ *(Primary & Secondary)* $Y = 0.701\ e^{0.0242X}$ *(Secondary)*	0.9318 0.9733
Pink/Bantycock	Saturation 5.0 bar	$Y = 0.00008\ X + 0.6304$ *(Primary & Secondary)* $Y = 0.00007\ X + 0.6347$ *(Secondary)*	0.9034 0.9467
White & Clay/Bantycock	Saturation-Only	$Y = 0.5956\ e^{0.00007X}$ *(Primary & Secondary)* $Y = 0.00004\ X + 0.5995$ *(Secondary)*	0.9578 0.9935
White & Marl/Bantycock	Saturation-Only	$Y = 0.6639\ e^{0.0001X}$ *(Primary & Secondary)* $Y = 0.00006\ X + 0.671$ *(Secondary)*	0.9365 0.9954
Iraqi	Saturation-Only	$Y = 0.9847\ e^{0.0543X}$ *(Primary & Secondary)* $Y = 0.9622\ e^{0.0583X}$ *(Secondary)*	0.9684 0.9695
Iraqi	Saturation 5.0 bar	$Y = 0.5708\ e^{0.0002X}$ *(Primary & Secondary)*$Y =$ $0.00009\ X + 0.5726$ *(Secondary)*	0.9557 0.9746

4.4.4 Compared Short and Long Term results

From Section 4.3-4.4 on gypsum rock work, it can be seen that gypsum rocks are brittle in their failure in both short and long-term. Gypsum rocks in both short and long term loading conditions are affected by the presence of saturation and more effects are recorded with the application of different water pressures. The application of 1.75, 3.25 and 5.0 bar water pressure in both short and long term tests increased dissolution and decreased *wt*, *vol*, and *TF* which resulted in lower resistance ability in both short and long-term loading. Short-term *MaxS* is higher than long-term for thin layer samples, while short-term *MaxS* is smaller than long-term for small and large four-point bending and cylinders.

The differences can be summarized as: gypsum rocks cylinders failed in creep test in saturated conditions with and without additional water pressure due to applied stress equal to about a quarter of uniaxial compressive strength. While, they failed in short term loading at higher stresses as shown in Table 4.11.

From Figure 4.63-4.65, it can be seen that the thin layers are stronger than cylinders in all types of gypsum rock. Creep strain percent is higher in the case of tested cylinders than thin layers' creep strain.

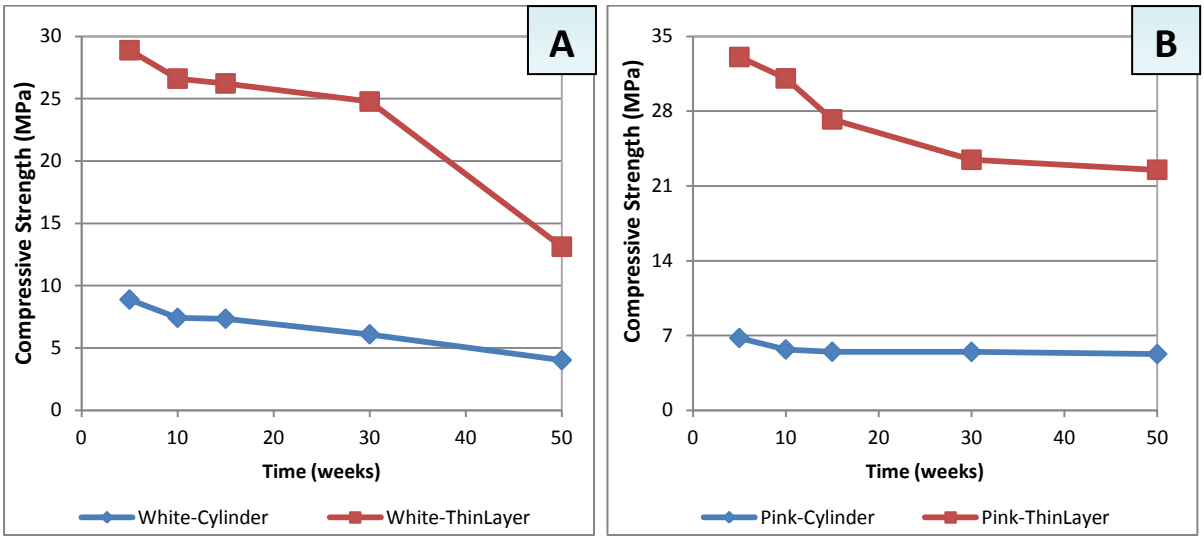

Fig. 4.63: Comparison between the compressive strength results of thin layers and cylinders of short-term tests. Part A is for the white/Bantycock gypsum rock samples (cylinders and thin layers). Part B shows the pink/Bantycock gypsum rock samples (cylinders and thin layers).

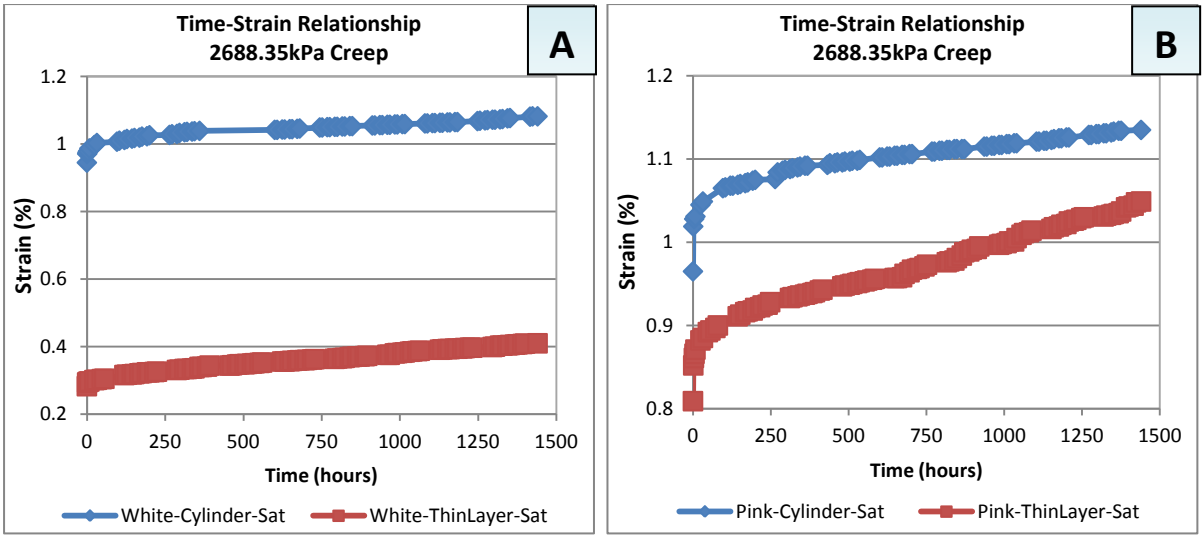

Fig. 4.64: Comparison between the results of gypsum rock thin layers and cylinders in terms of time-strain relationship. Part A shows the white/Bantycock gypsum rock samples (cylinders and thin layers). Part B shows the pink/Bantycock gypsum rock samples (cylinders and thin layers).

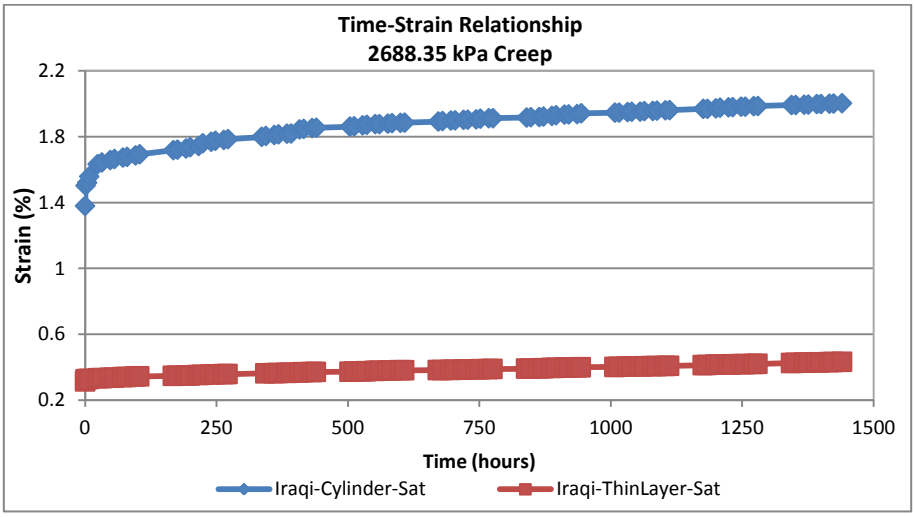

Fig. 4.65: Comparison between the results of Iraqi gypsum rock thin layers and cylinders in terms of time-strain relationship. It shows the creep strain of samples tested for 1440 hour under 2688.35 kPa.

4.5 Gypseous soil: Short-Term work

The calculated properties shown in Table 4.23 illustrate that a variety of geotechnical properties can be found within real world gypseous soils in Iraq. It can be seen also that these samples are not very wet in natural and not very dense.

From Figure 4.66-4.69, it can be noticed that the geotechnical properties of gypseous soils are related to each other. Increase of gypsum content influences on some geotechnical properties such as compression index, expansion index, initial void ratio, natural water content and specific gravity.

The responses of gypseous soil various with axial loading. This may be influenced by gypsum content, soil mineral particle size distribution, soil density and initial void ratio. Saturation process weakens gypseous soil.

Table 4.23: Presents different geotechnical properties (calculated) of real Iraqi gypseous soil samples tested in short-term mode. Tested samples were prepared from collected gypseous soils from North, Central and South of Iraq in December 2009. Tests were conducted according to Head (2006), Fratta et al. (2007), and Head and Epps (2011)

Iraqi Real Gypseous Soils-Different Geotechnical Tests Results			
Soil Parameter	**Tar Al-Najaf**	**Badosh**	**Doz**
Gravel (%)	28.06	24.601	1.003
Sand (%)	68.39	24.44	19.111
Silt (%)	0.75	49.041	79.886
Clay (%)	2.8	0	0
D_{10} (mm)	0.18	0	0
D_{30} (mm)	0.36	0	0
D_{60} (mm)	1.54	0.188	0.0214
Coefficient of Uniformity	8.79	0	0
Coefficient of Gradation	0.49	0	0
Cohesion (*CU*-Direct Shear)(kN/m^2)	14.5	11.694	0
Angle of Internal Friction (*CU*-Direct Shear)(degree)	35.25	33.11	37.999
Cohesion (*UU*)(kN/m^2)	15.83	0	10
Angle of Internal Friction (*UU*-Direct Shear)(degree)	11.88	10.074	11.31
Wet Density (gm/cm^3)	1.5	2	1.591
Dry Density (gm/cm^3)	1.429	1.802	1.473
Natural Moisture Content (%)	5	11	8
Initial Void Ratio	0.13	0.273	0.181
Collapse Potential (%) (ASTM, 1996)	1.59	2.035	2.88
Compression Index, *Cc*	0.05	0.362	0.138
Expansion Index, *Cr*	0.002	0.004	0.013
Specific Gravity, *Gs*	2.599	2.485	2.268
Gypsum Content (%)	45	5	40

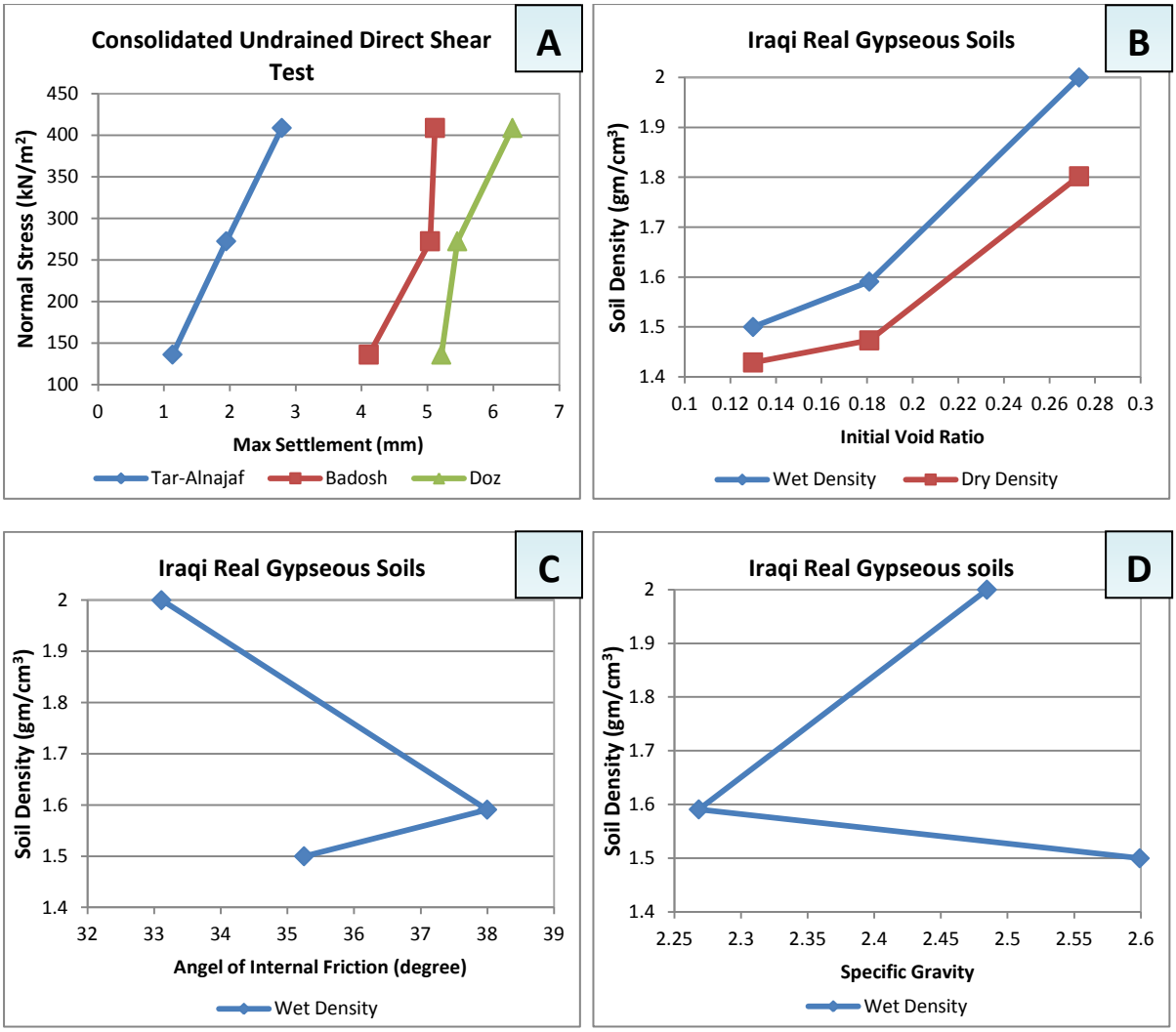

Fig. 4.66: Relationships between some geotechnical properties of Iraqi real gypseous soils (Tar Al-Najaf, Badosh and Doz samples). Iraqi gypseous soils samples collected on field trip to North, Central and South of Iraq on December 2009. Part A shows maximum settlement due to normal loads applied in consolidated un-drained direct shear test. Part B shows real gypseous soils wet and dry densities versus initial void ratio. Part C shows angle of internal friction relation with wet density. Part D shows specific gravity relation with wet density.

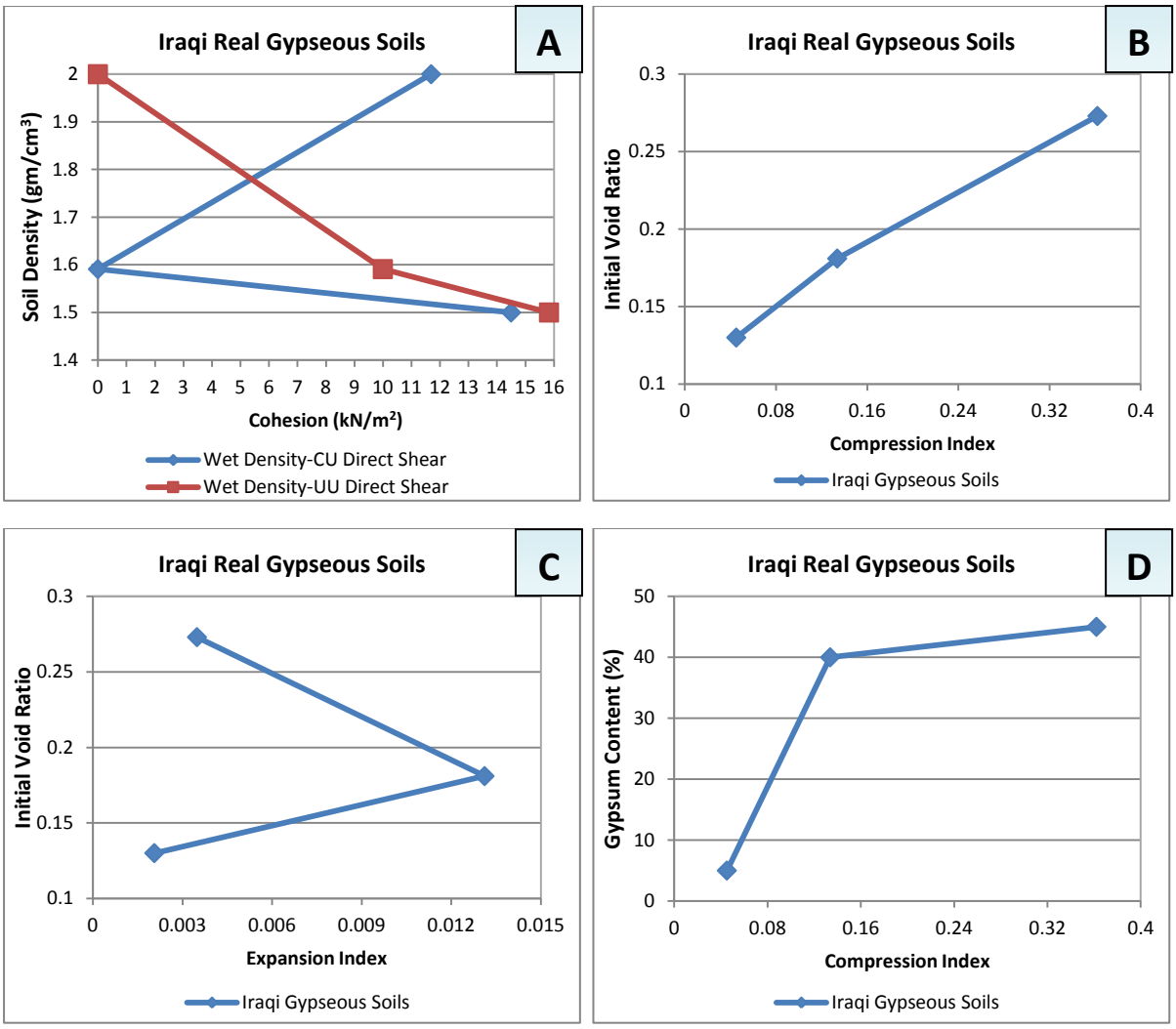

Fig. 4.67: Relationships between some geotechnical properties of Iraqi real gypseous soils (Tar Al-Najaf, Badosh and Doz samples). Iraqi gypseous soils samples collected on field trip to North, Central and South of Iraq on December 2009. Part A shows cohesion relation with wet density from consolidated un-drained and consolidated drained direct shear tests. Part B shows linear relationship of compression index with initial void ratio from consolidation test. Part C shows expansion index relationship with initial void ratio from consolidation test. Part D shows compression index (from consolidation test) relationship with initial void ratio.

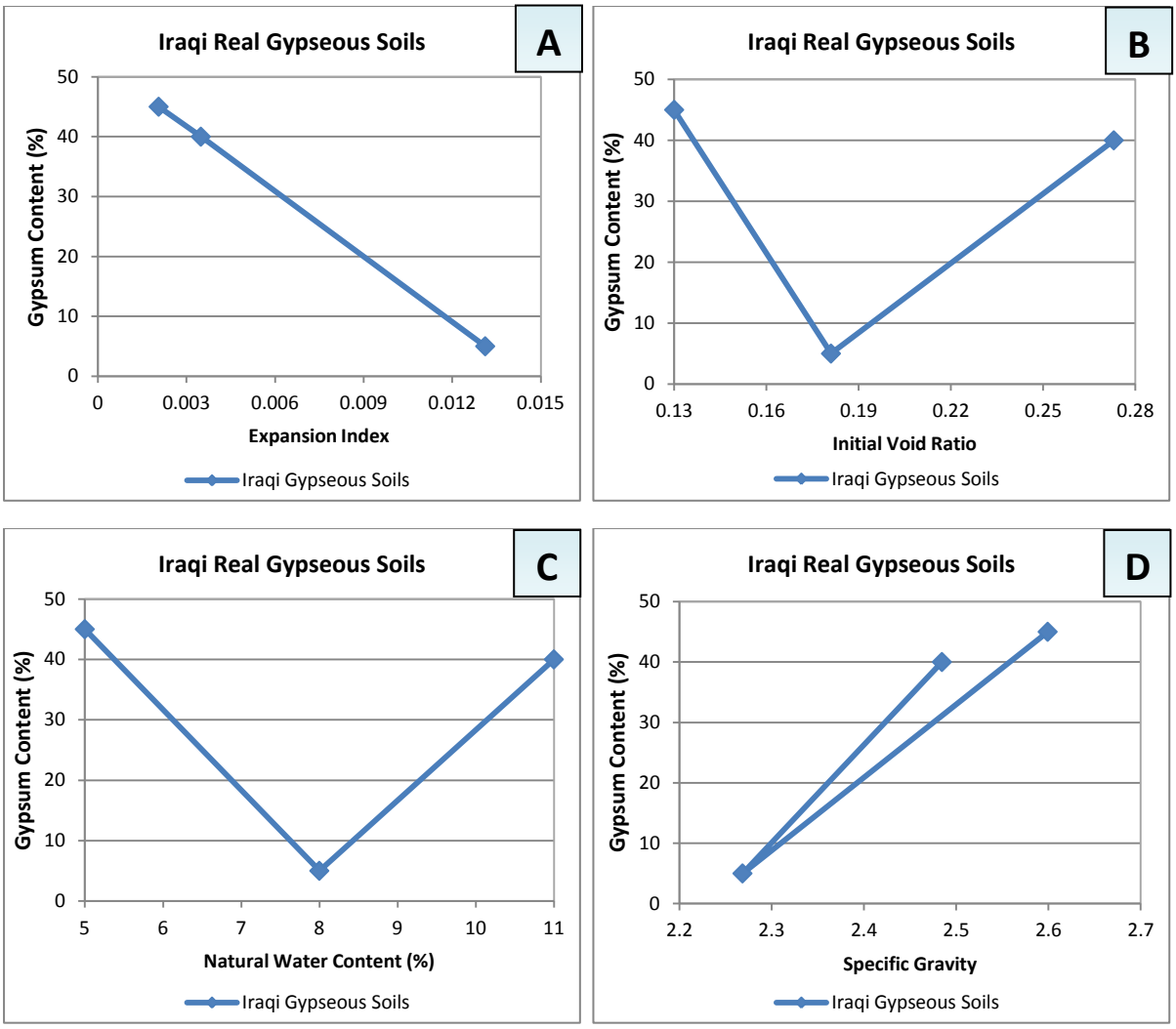

Fig. 4.68: Relationship of gypsum content with some geotechnical properties of Iraqi real gypseous soils (Tar Al-Najaf, Badosh and Doz samples). Iraqi gypseous soils samples collected on field trip to North, Central and South of Iraq on December 2009. Part A shows linear relationship of expansion index (from consolidation test) with gypsum content. Part B shows initial void ratio relationship with gypsum content. Part C shows natural water content relationship with gypsum content. Part D presents specific gravity relationship with gypsum content.

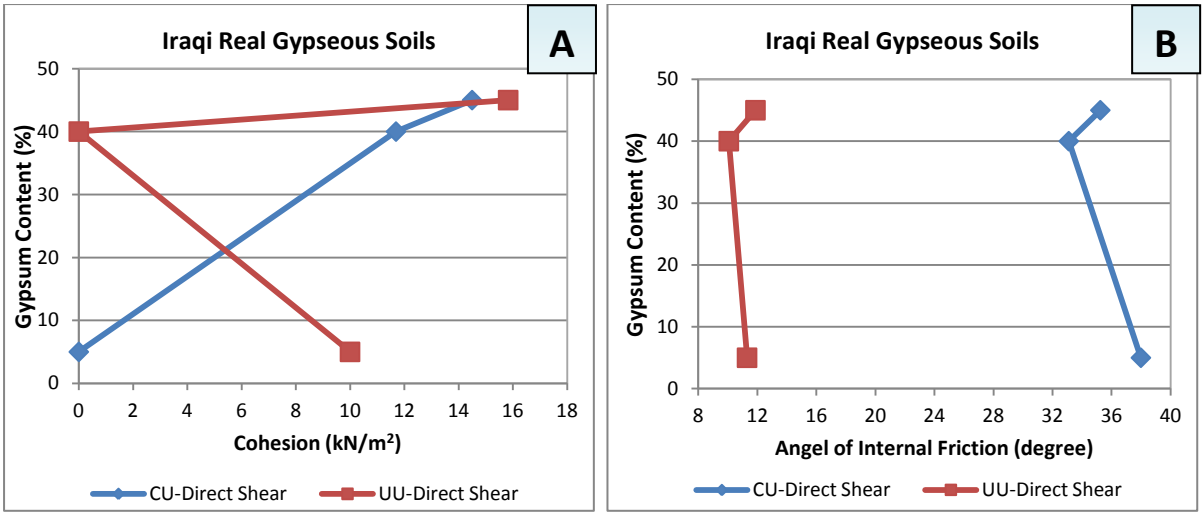

Fig. 4.69: Relationship of gypsum content with some geotechnical properties of Iraqi real gypseous soils (Tar Al-Najaf, Badosh and Doz samples). Iraqi gypseous soils samples collected on field trip to North, Central and South of Iraq on December 2009. Part A shows cohesion (from un-consolidated un-drained and consolidated un-drained direct shear tests) relationship with gypsum content. Part B shows angle of internal friction (from un-consolidated un-drained and consolidated un-drained direct shear test) relationship with gypsum content.

4.6 Gypseous soil: Long-Term work

The results for artificially-prepared gypseous soils based on the real world samples from North, Central and South Iraq are present here. The outcomes involve: time-conductivity, time-strain for loading stages (28, 56, 112, 224, 448, 896, 1792 and 2688.35 kPa), creep readings for 1440 hours for both 1792 and 2688.35 kPa and time-instantaneous strain.

4.6.1 Loading stages results

Figures 4.70-4.72 show the loading stages of real Iraqi and artificially-prepared gypseous soils. The loading stages are: 28, 56, 112, 224, 448, 896, 1792 and 2688.35 kPa. Each loading stage lasted for 24 hour except the final two loadings, 1792 and 2688.35 kPa, were lasted for 1440 hour. A continuous process of strain recording was carried out.

In general, increases of applied stress increases the instantaneous and creep strain. The tested samples recorded sharp initial increases in strain within the application of stresses and then tended to be flat.

As shown in Figure 4.72/C, the increase of applied stress changed the rate of instantaneous strain over time, from being initially rapid, then slowing, before increasing again. The tested samples seem to be notably affected by stress increase when saturated.

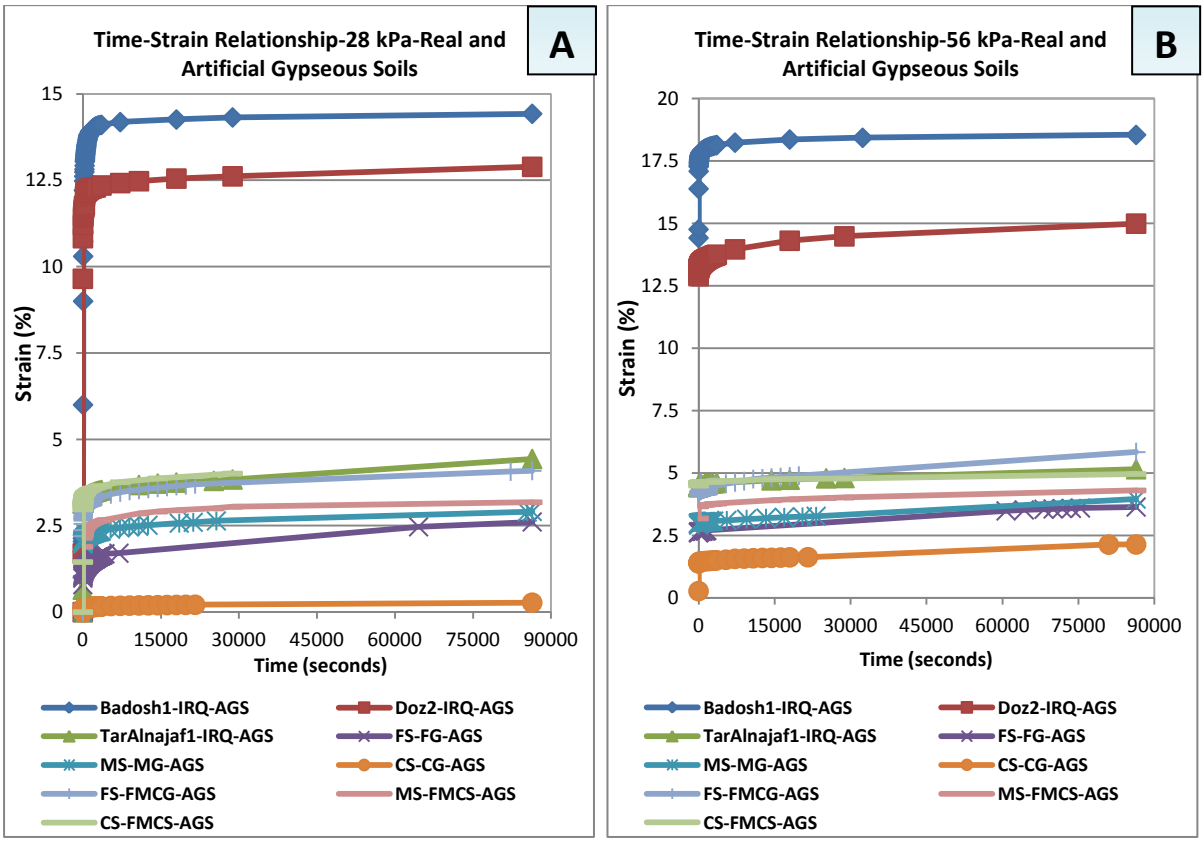

Fig. 4.70: Time-strain percent relationship for one-day creep for real and artificially-prepared gypseous soils. Part A is for the strain data due to 28 kPa applied stress. Part B is for the strain data due to 56 kPa applied stress. Real Iraqi gypseous soils samples collected on field trip to North, Central and South of Iraq on December 2009. Artificially-prepared gypseous soils (*FS-FG-AGS*, *CS-CG-AGS*, *MS-FMCS-AGS*, *MS-MG-AGS*, *FS-FMCG-AGS* and *CS-FMCG-AGS*) were prepared with properties similar to the worst one from Iraqi real gypseous soils, with the highest gypsum content (Tar Al-Najaf sample). Note that Tar Al-Najaf sample behaved slightly differently.

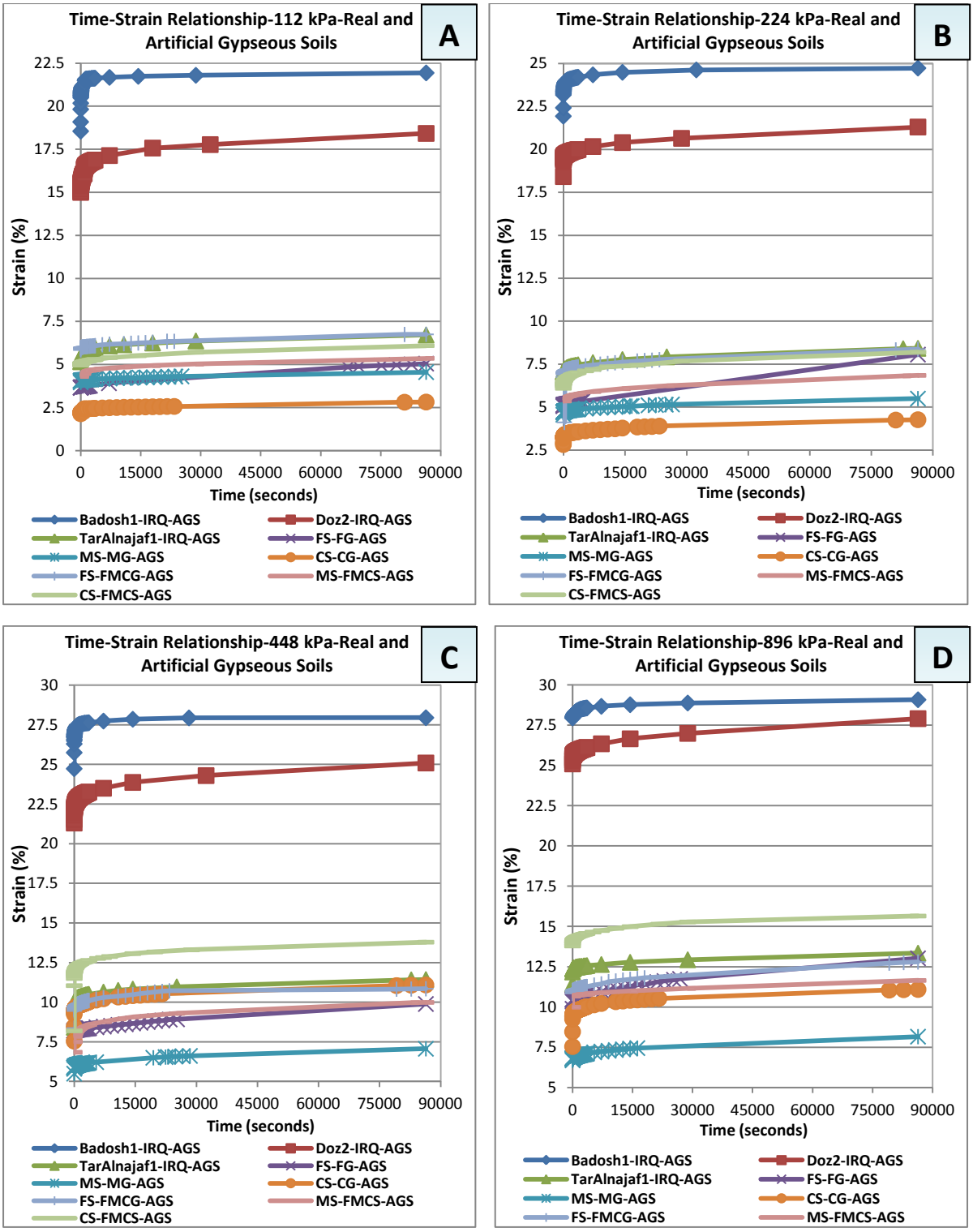

Fig. 4.71: Time-strain relationship for one-day creep for real and artificially-prepared gypseous soils. Part A is for the strain data due to 112 kPa applied stress, part B is for the strain data due to 224 kPa applied stress, part C is for the strain data due to 448 kPa applied stress and part D is for the strain data due to 896 kPa applied stress. Real Iraqi gypseous soils samples collected on field trip to North, Central and South of Iraq on December 2009. Artificially-prepared gypseous soils (*FS-FG-AGS*, *CS-CG-AGS*, *MS-FMCS-AGS*, *MS-MG-AGS*, *FS-FMCG-AGS* and *CS-FMCG-AGS*) were prepared in properties close to the maximum gypsum content sample found in the Iraqi real gypseous soils with highest gypsum content. Note that *FS-FMCG-AGS* behave differently in B & D.

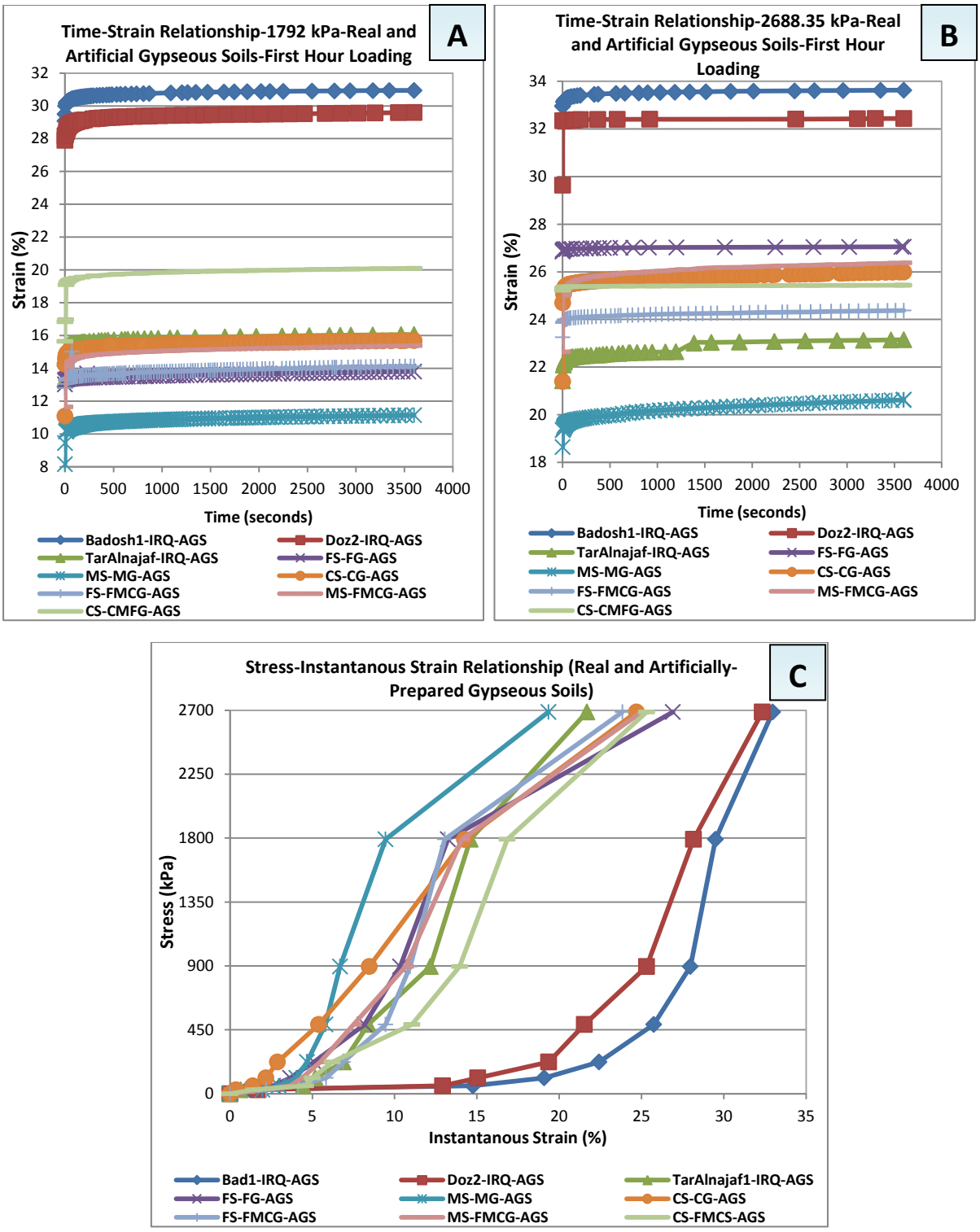

Fig. 4.72: Parts A and B present time-strain relationship for creep stages of 1792 and 2688.35 kPa for different real and artificially-prepared gypseous soils (soil types and methods of collection and preparation are explained in Figure 4.70-4.71). The Tar Al-Najaf sample showed one step-rest segment after about 1400 second in part B. Part C presents stress-instantaneous strain relationship for long term tests loading stages for same samples of parts A and B.

4.6.2 Creep results for Artificially-Prepared Gypseous Soils

It can be seen from Figure 4.73/A that all samples are shown a sharp strain increase at the beginning of stress application. All samples except *FS-FG-AGS* sample are in good agreement and behave in similar flat modes under the stress of 1792 kPa as shown in Figure 4.73/A. All samples except *FS-FG-AGS* and *CS-CG-AGS* are in good agreement and behave in similar flat mode under the stress of 2688.35 kPa as shown in Figure 4.73/B. Many short stepwise segments are found, especially in time-strain percent curves of 2688.35 kPa.

The applied stress causes the artificially-prepared gypseous soil samples to change their behaviour over time to show much more increase in strain percent compared to real gypseous soil samples. So, over time, the artificially-prepared gypseous soil samples changed the flat behaviour to slightly steep strain percent increase due to constant applied stresses. Note that the *FS-FG-AGS* and *CS-CG-AGS* samples showed divergence after about 1000 hour compare to other samples in Figure 4.73/B.

The creep curves equations shown in Table 4.24-4.25 follow in general a power law, with a few following exponential laws and one a logarithmic law. Increases of applied stress from 1792 to 2688.35 kPa decrease the constant *A*. Increases of applied stress from 1792 to 2688.35 kPa increase the constant *B*. This shows that the elastic response of these soil samples decreased due to the compressibility of soil materials, which took place with the progressively applied stresses before the final application of 2688.35 kPa. The increase in constant *B* means that the samples tend to increase creep strain rate, which may increase the opportunity of collapse. The fitting curves here are in good agreements, as showing by the R^2 values presented in each table.

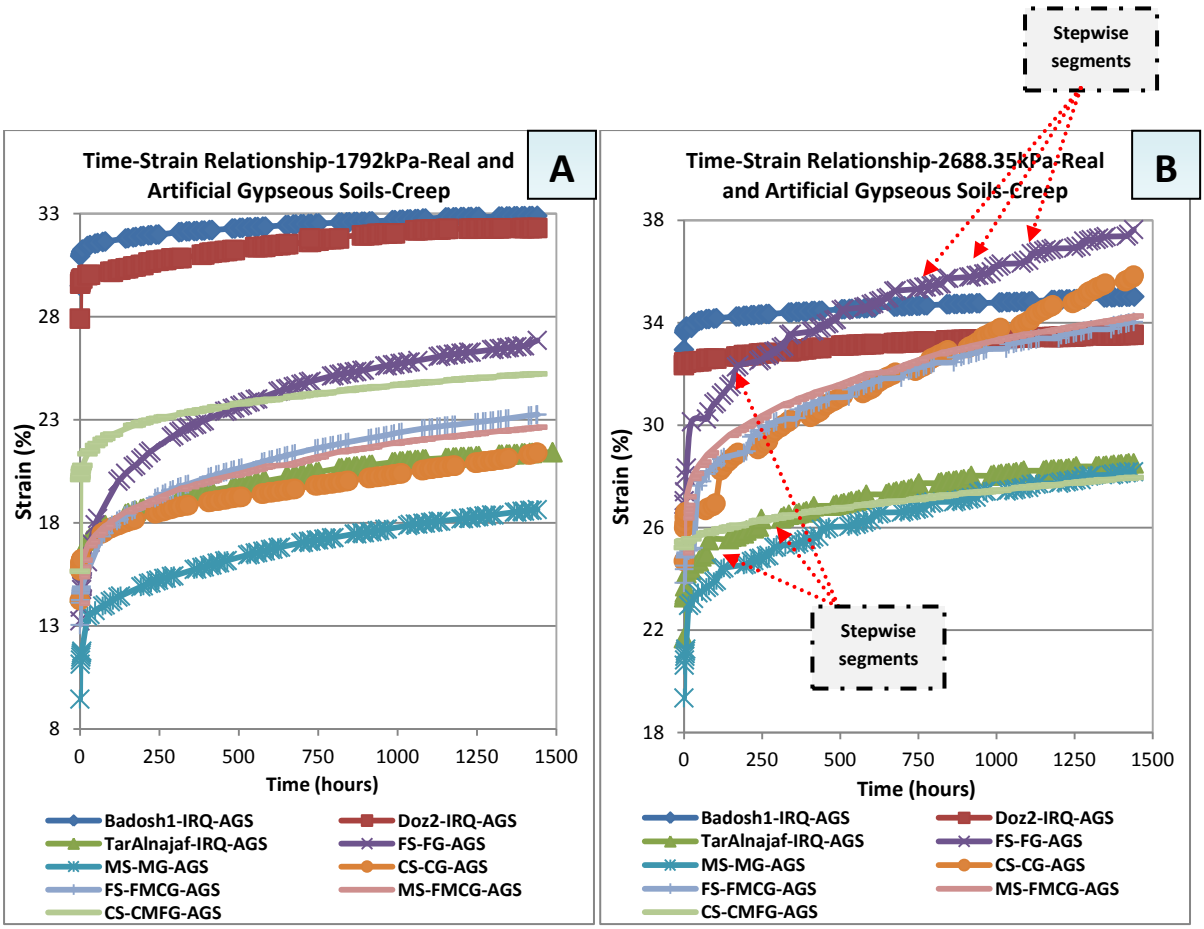

Fig. 4.73: Parts A and B present time-strain percent relationship for creep tests under axial stresses of 1792 kPa and 2688.35 kPa respectively. Each creep stage lasted for 1440 hours. The creep tests were carried out on saturated samples under atmospheric pressure. Real Iraqi gypseous soils samples were collected from North, Central and South of Iraq in December 2009. Artificial gypseous soils were prepared to match the properties of the Iraqi real gypseous soil with the highest gypsum content (Tar Al-Najaf gypseous soil sample).

4.6.3 Dissolution results

It can be seen from the relation of cumulative conductivity with time in Figure 4.74 and Table 4.26 that the *CS-CG-AGS* sample has the largest dissolution amount over time. This might be related to the larger area of gypsum salt here exposed to the saturation water and more additional areas of gypsum salt resulted from crushing gypsum particles by loading, which caused the gypsum salt to be dissolved more than others.

It can be seen in Table 4.26 that there is no notable relation between maximum recorded strain/height reductions. This may result from the range of gypsum particle size used in each samples. Gypsum content is significantly reduced in its percent by long term soaking under atmospheric pressure and notable maximum strain/height reduction is recognized.

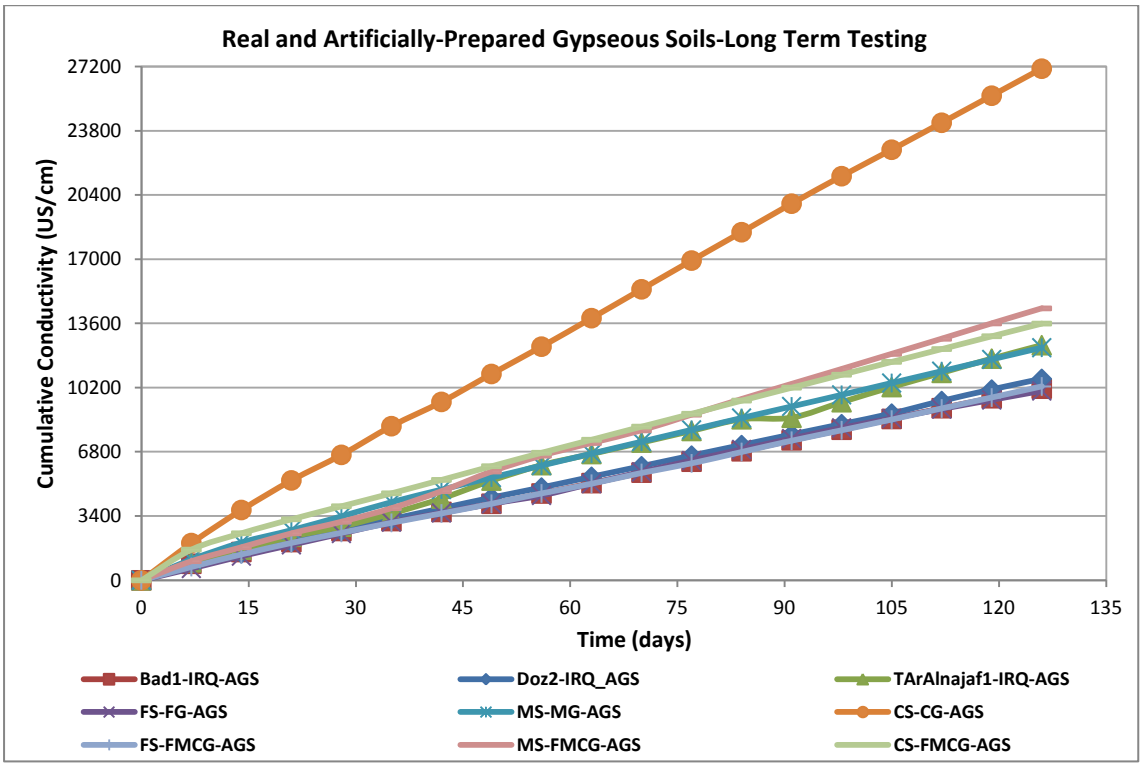

Fig. 4.74: Cumulative conductivity (dissolution) relationship with time during loading and creep stages of long term testing. These tests were carried out on Iraqi real and artificially-prepared gypseous soils. The *CS-CG-AGS* sample showed the highest dissolution amount. Real Iraqi gypseous soils samples were collected from the North, Central and South of Iraq on December 2009. Artificially-prepared gypseous soils (*FS-FG-AGS*, *CS-CG-AGS*, *MS-FMCS-AGS*, *MS-MG-AGS*, *FS-FMCG-AGS* and *CS-FMCG-AGS*) were prepared to match the properties of the Iraqi real gypseous soil with the highest gypsum content (Tar Al-Najaf gypseous soil sample).

Table 4.24: Creep equations of tested real and artificially-prepared gypseous soils samples. These tests were carried out in long-term mode under 1792 kPa applied stress. Equations of primary and secondary creep stages are presented (see Figure 4.50/A). Y is strain percent and X is time in hours. Note: power equation is $Y=A\ X^B$, exponential equation is $Y=Ae^{BX}$ and linear equation is Y=AX + B. A and B are constants.

Soil Type	State of Creep Testing	Creep Equation	R^2 Value
Iraqi/Badosh-*RGS*	Saturation under atmospheric pressure	$Y = 33.129\ X^{0.0069}$	0.9205
Iraqi/Doz- *RGS*	Saturation under atmospheric pressure	$Y = 32.585\ e^{0.00002X}$	0.9264
Iraqi/Tar Al-Najaf-*RGS*	Saturation under atmospheric pressure	$Y = 21.7\ X^{0.036}$	0.9529
FS-FG-AGS	Saturation under atmospheric pressure	$Y = 24.64\ X^{0.0542}$	0.9306
MS-MG-AGS	Saturation under atmospheric pressure	$Y = 19.138\ X^{0.0507}$	0.9704
CS-CG-AGS	Saturation under atmospheric pressure	$Y = 27.375\ e^{0.0002X}$	0.939
FS-FMCG-AGS	Saturation under atmospheric pressure	$Y = 22.138\ X^{0.0563}$	0.9468
MS- FMCG -AGS	Saturation under atmospheric pressure	$Y = 24.157\ X^{0.045}$	0.9317
CS- FMCG -AGS	Saturation under atmospheric pressure	$Y = 25.785\ e^{0.00006X}$	0.9553

Table 4.25: Creep equations of tested real and artificially-prepared gypseous soils samples. These tests were carried out in long-term mode under 2688.35 kPa applied stress. Equations of primary and secondary creep stages are presented (see Figure 4.50/B). Y is strain percent and X is time in hours. Note: logarithmic equation is Y=A ln X + B and linear equation is Y=AX + B. A and B are constants.

Soil Type	State of Creep Testing	Creep Equation	R^2 Value
Iraqi/Badosh-*RGS*	Saturation under atmospheric pressure	$Y = 30.126\ X^{0.0116}$	0.9284
Iraqi/Doz-*RGS*	Saturation under atmospheric pressure	$Y = 28.021\ X^{0.0185}$	0.856
Iraqi/Tar Al-Najaf-*RGS*	Saturation under atmospheric pressure	$Y = 14.519\ X^{0.0514}$	0.952
FS-FG-AGS	Saturation under atmospheric pressure	$Y = 11.598\ X^{0.1141}$	0.9842
MS-MG-AGS	Saturation under atmospheric pressure	$Y = 9.7109\ X^{0.0857}$	0.968
CS-CG-AGS	Saturation under atmospheric pressure	$Y = 14.709\ X^{0.0457}$	0.9166
FS-FMCG-AGS	Saturation under atmospheric pressure	$Y = 12.916\ X^{0.077}$	0.9539
MS- FMCG-AGS	Saturation under atmospheric pressure	$Y = 13.616\ X^{0.0667}$	0.9521
CS- FMCG-AGS	Saturation under atmospheric pressure	$Y = 0.9054\ \ln X + 18.299$	0.9216

4.6.4 Compared results

On the influences of gypsum content, it can be seen that it increases with increases of the dissolution amount in non linear relationship as shown in Figure 4.75/B. So, gypsum content decreases the maximum strain percent in a non-linear relationship, as shown in Figure 4.76/A & B. This may depend on initial void ratio, dissolved gypsum content and soil particle size.

Increase of dissolution amount increases the strain percent as shown in Figure 4.76/C. The response is stepwise, with periods of slow adjustment punctuated by abrupt, minor failures. Such behaviour is found in general for all tested real and artificially-prepared gypseous soils.

Sample responses for stresses are various and it seems that they more affected by higher applied stress of 2688.35 kPa. In fact, *FS-FG-AGS*, *FS-FMCG-AGS*, *MS-MG-AGS*, *MS-FMCG-AGS* and *CS-CG-AGS* are more affected by higher applied stress and they changed their behaviour as shown in the changes slopes of these samples in Figure 4.76/C. The *CS-CG-AGS* sample response is more than other samples, which shows the highest dissolution amount, while *FS-FG-AGS* sample shows the highest strain percent.

Gypseous soil is influenced by loading as reflected by instantaneous and creep strain. These strains values depend on properties such as soil particle size distribution, gypsum particle size distribution, initial void ratio, gypsum content, field density, volume of applied stresses, saturation water purity and soil structure (see Figure 4.70-4.76).

In general, the dissolution of gypsum and recorded strain percents are not in a linear relationship with gypsum content (Figure 4.75).

Table 4.26: Comparisons among different properties of real and artificially-prepared gypseous soil samples. These properties were calculated for mentioned samples before and after long-term loading experiments. Tested samples were prepared from gypseous soils collected from North, Central and South of Iraq in December 2009. Artificially-prepared gypseous soils (*FS-FG-AGS*, *CS-CG-AGS*, *MS-FMCS-AGS*, *MS-MG-AGS*, *FS-FMCG-AGS* and *CS-FMCG-AGS*) were prepared to match the properties of the Iraqi real gypseous soil with the highest gypsum content (Tar Al-Najaf gypseous soil sample).

Soil Type	Gypsum Content (%)	New Gypsum Content (%)	Gypsum Content Reduction (%)	Maximum Dissolution (US/cm)	Maximum Strain/Height Reduction (%)
Badosh-1	5	3.242	35.17	10149	35.02
Doz-2	40	17.415	56.462	10667.4	33.53
TarAlnajaf-1	45	22.68	49.6	12452.4	28.51
FS-FG-AGS	50	32.076	35.849	10029.7	37.635
MS-MG-AGS	50	27.98	44.04	12321.2	28.185
CS-CG-AGS	50	1.575	96.85	27095.4	35.838
FS-FMCG-AGS	50	31.654	36.693	10265.7	34.035
MS-FMCG-AGS	50	24.266	51.469	14399.8	34.261
CS-FMCG-AGS	50	25.705	48.59	13596.4	27.96

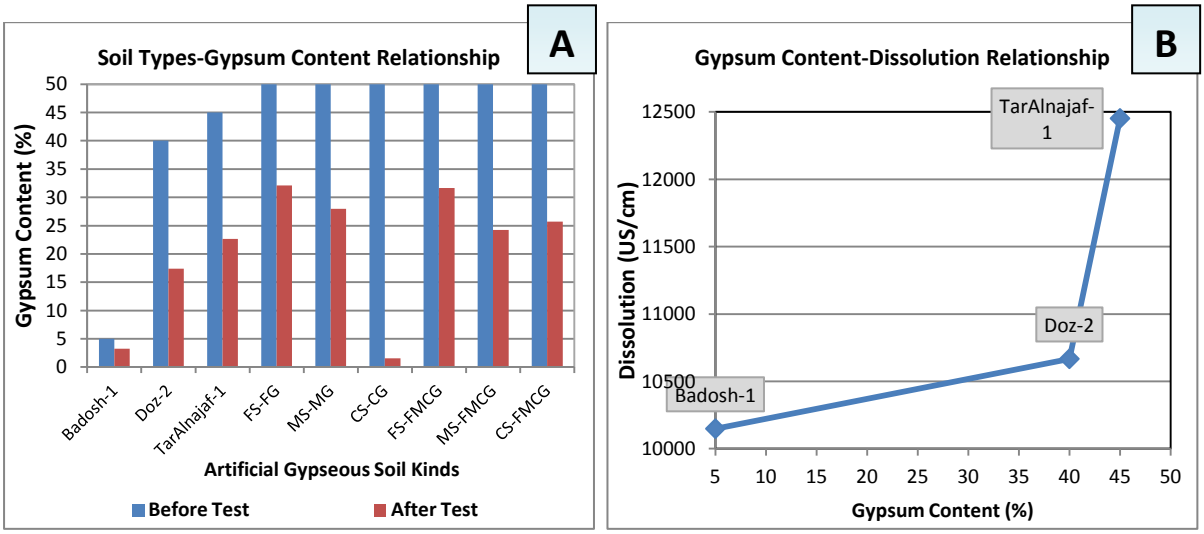

Fig. 4.75: Part A shows gypsum content reductions due to long-term testing of real and artificially-prepared gypseous soils (details explained in above Table 4.26). Part B presents dissolution versus gypsum content for three Iraqi real gypseous soils (Tar Al-Najaf, Badosh and Doz samples). Real Iraqi gypseous soils samples collected in North, Central and South of Iraq in December 2009.

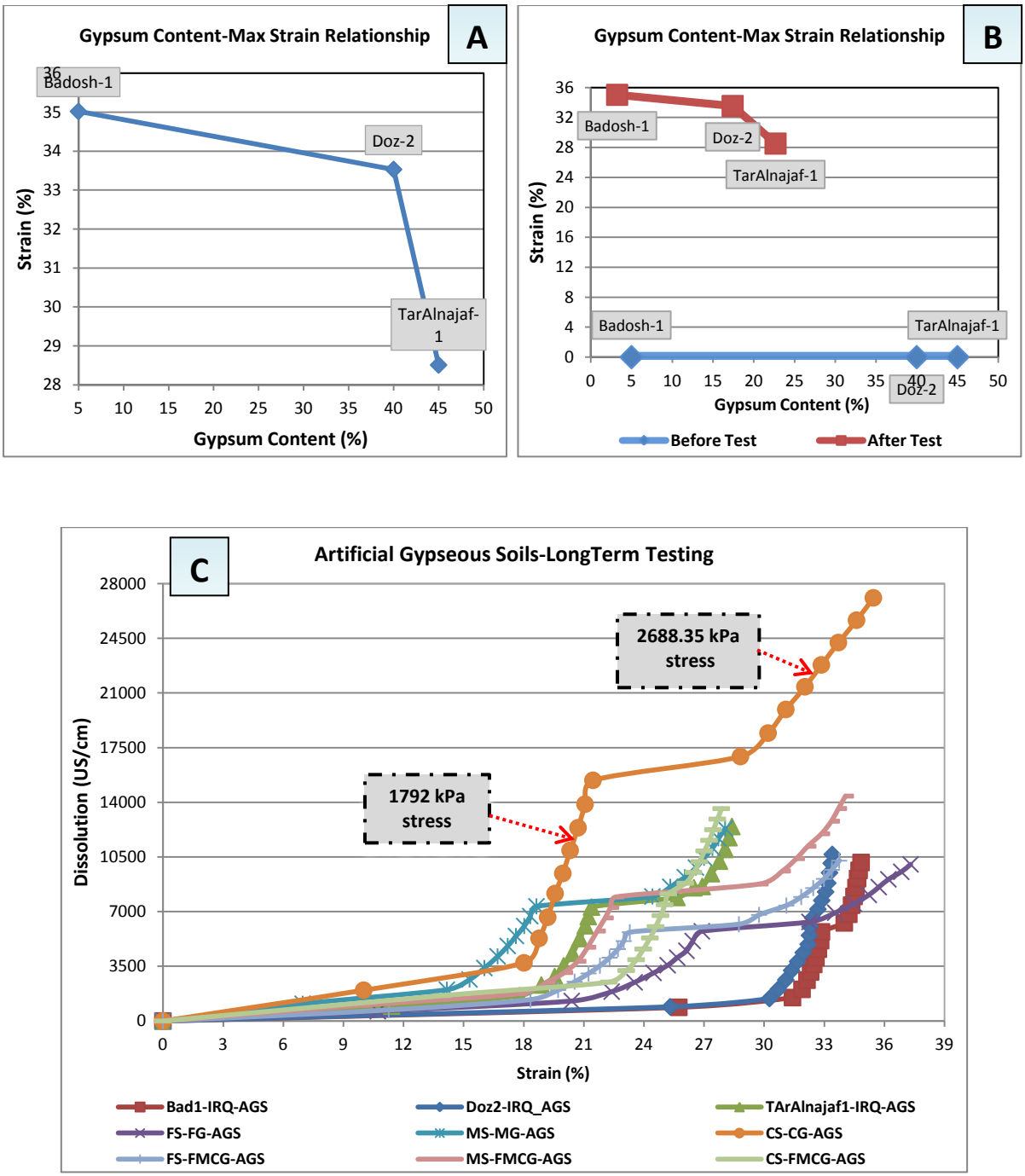

Fig. 4.76: Part A presents maximum strain percent versus gypsum content of Iraqi real gypseous soils (Tar Al-Najaf, Badosh and Doz samples). Part B shows the impact of long term testing on the relationship between maximum strain percent and gypsum content. Part C presents dissolution versus strain percent for all tested real and artificially-prepared gypseous soil samples (details explained in above Table 4.26). Iraqi gypseous soils samples collected from North, Central and South of Iraq in December 2009.

4.7 Box Model results

From Figures 4.77-4.84 and Tables 4.27-4.30, box model soil layers were weakened due to 50 week flooding and a notable amount of gypsum content was dissolved, which various for each layer. The fine soil particles were washed out after 50 weeks of water flooding as shown in Figure 4.83/D.

With weekly changing water of saturation, each layer structure changed. The box model soil as a whole compacted, with density varying between layers (see Figure 4.92/B). The top surface showed higher densities than other layers.

As can be seen from the creep equations in Tables 4.27 and 4.28, the creep curves equations follow a power law for 1792 kPa, while, for the 2688.35 kPa creep curves, they follow exponential law. Increases of applied stress from 1792 to 2688.35 kPa increase constant *A* and decrease constant *B*.

In general, the *Cp* decreased compared to the original soil depending on amount of gypsum dissolved from each layer, more gypsum remain may cause more collapse.

It can be seen from the results of *UU-D* and *CU-D* test that increased stress directly led to increased settlement.

The first/top layer demonstrated the lowest instantaneous strain and maximum strain compare to other layers after 50 week. In addition, the dissolution of gypsum is aggressive in the top of model due to the continuous contact with flooding water. The increase in strain with increased stress is not quite linear.

Moreover, it can be seen that the soil before 50 weeks flooding showed the highest strain percent in all stages of loading, while the top layer showed the lowest percent. Overall, box model gypseous soil become more compressible after 50 week.

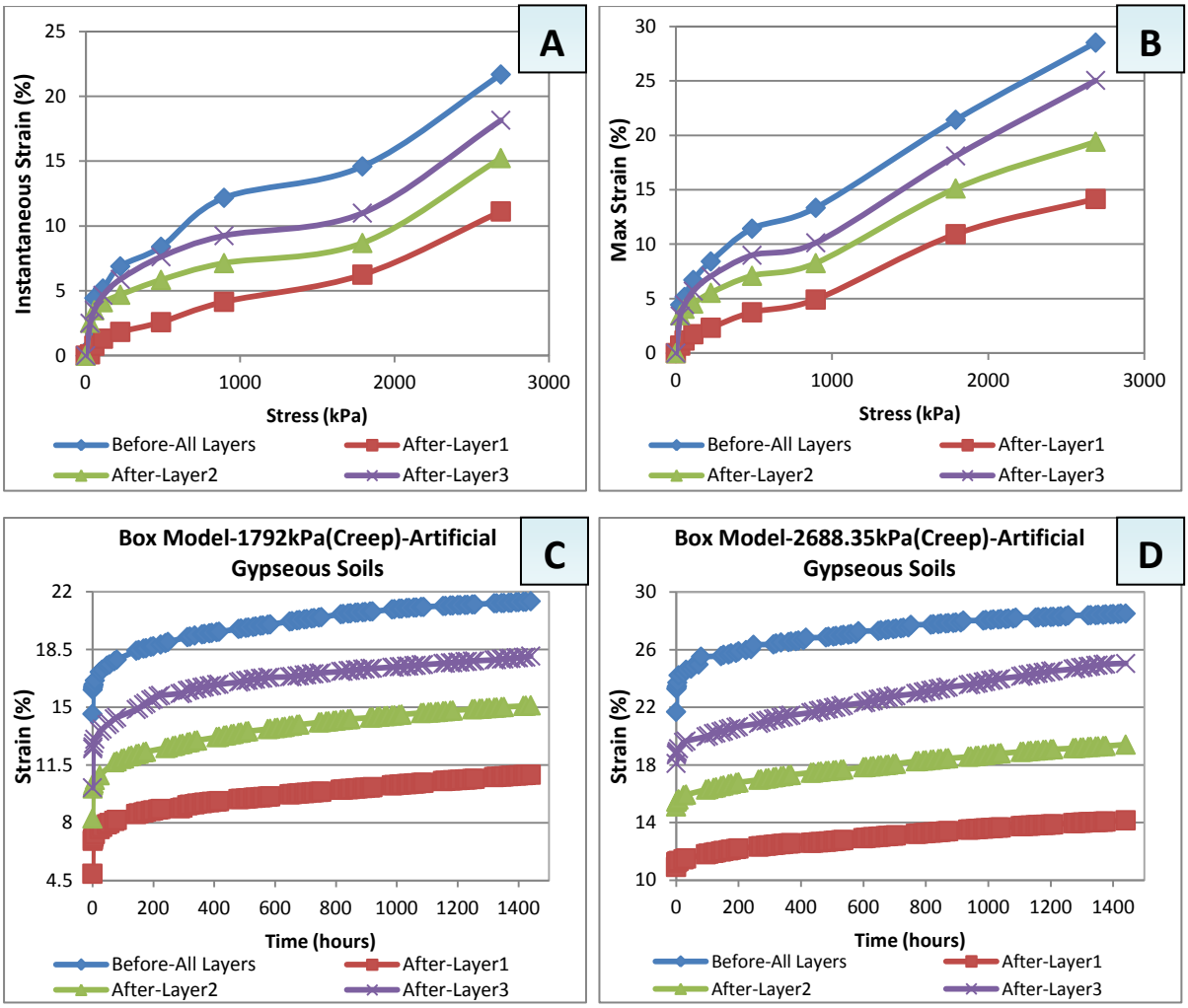

Fig. 4.77: Box model outcomes on artificially-prepared gypseous soil with 50% gypsum content. Part A presents stress versus instantaneous strain. Part B presents stress versus maximum strain of each loading stage. Parts C and D show time-strain relationship for 1792 kPa and 2688.35 kPa applied creep stresses respectively.

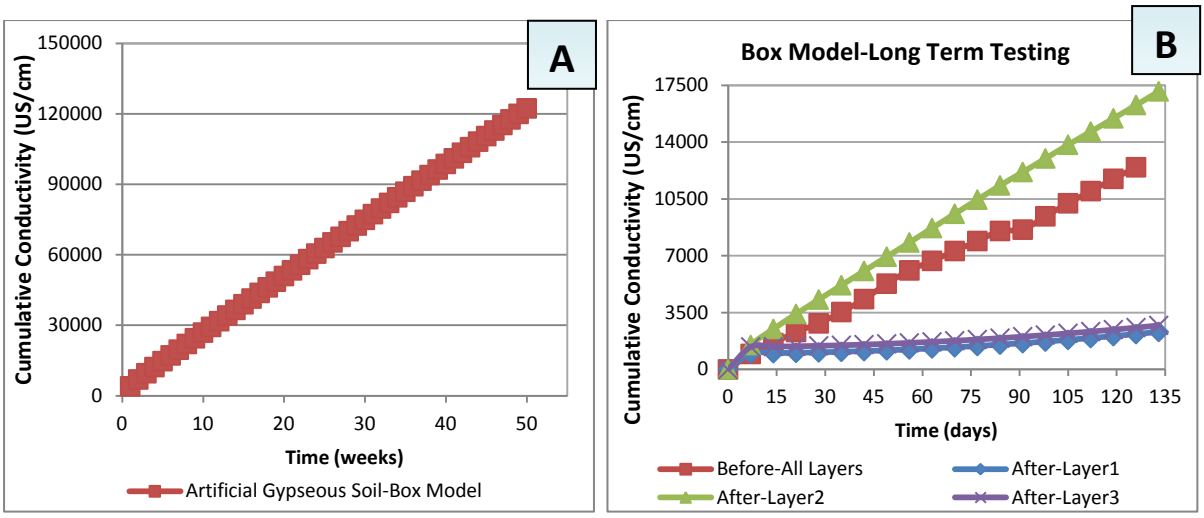

Fig 4.78: Box model outcomes on artificially-prepared gypseous soils with 50% gypsum content, which is like Tar Al-Najaf gypseous soil-southern of Iraq sample. Part A shows time versus cumulative conductivity (dissolution) readings of box model water of saturation. Part B is for the samples taken from the box model soil before and after 50 weeks flooding and tested in a conventional oedometer.

Table 4.27: Creep equations of tested box model soil layers (artificially-prepared gypseous soil) before and after 50 weeks of model flooding. Each layer tested in long-term mode for 1792 kPa loading stage; equations of primary and secondary creep stages are presented (see Figure 4.77/C). Y is strain percent and X is time in hours. Note: power equation is $Y=A\ X^B$. A and B are constants.

Soil Type	State of Testing/creep	Creep Equation	R^2 Value
All Layers-Before	Saturation under atmospheric pressure	$Y = 14.519\ X^{0.0514}$	0.9519
Layer1-After	Saturation under atmospheric pressure	$Y = 5.5816\ X^{0.0875}$	0.9409
Layer2-After	Saturation under atmospheric pressure	$Y = 8.4818\ X^{0.0761}$	0.9465
Layer3-After	Saturation under atmospheric pressure	$Y = 10.727\ X^{0.07}$	0.9684

Table 4.28: Equations of time-strain curves of box model soil layers (artificially-prepared gypseous soil) before and after 50 week model flooding. Each layer tested in long-term loading under 2688.35 kPa applied stress. Equations of primary and secondary creep stages are presented (see Figure 4.77/D). Y is strain percent and X is time in hours. Note: power equation is $Y=A\ X^{B}$ and exponential equation is $Y=A\ e^{BX}$. A and B are constants.

Soil Type	State of Testing/creep	Creep Equation	R^2 Value
All Layers-Before	Saturation under atmospheric pressure	$Y = 21.7\ X^{0.036}$	0.9529
Layer1-After	Saturation under atmospheric pressure	$Y = 11.69\ e^{0.0001X}$	0.9445
Layer2-After	Saturation under atmospheric pressure	$Y = 16.15\ e^{0.0001X}$	0.9368
Layer3-After	Saturation under atmospheric pressure	$Y = 19.685\ e^{0.0002X}$	0.9565

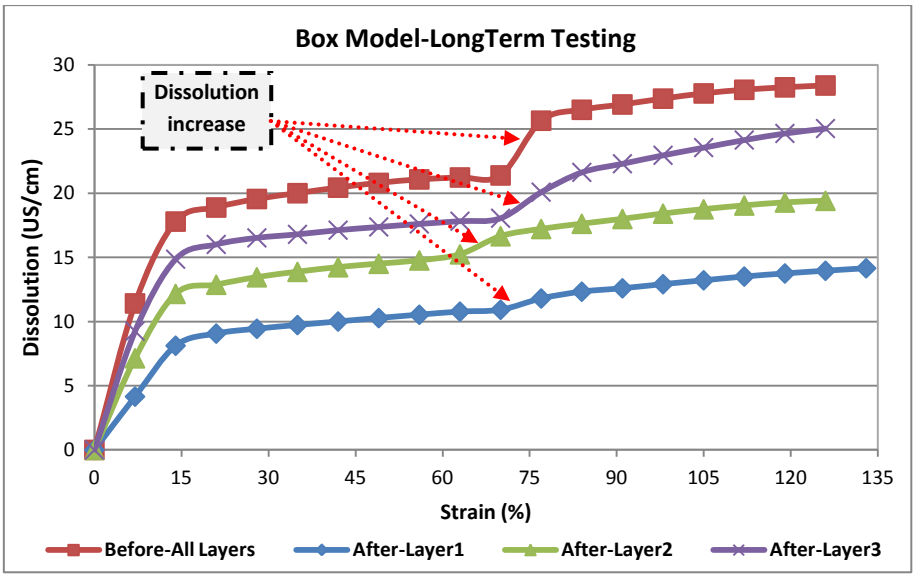

Fig. 4.79: Dissolution relationship with strain percent of box model soil layers before and after 50 week model flooding. Note the dissolution amount increases at about 72% with the soil before 50 week flooding showing the highest increase. These dissolution amount increases may be due to the application of 2688.35 kPa axial stress.

Table 4.29: Comparison between maximum strain percent due to loading stages of long-term tests of box model soil layers before and after 50 week flooding.

Layers	Max Strain 28 kPa (%)	Max Strain 56 kPa (%)	Max Strain 112 kPa (%)	Max Strain 224 kPa (%)	Max Strain 448 kPa (%)	Max Strain 896 kPa (%)	Max Strain 1792 kPa (%)	Max Strain 2688.35 kPa (%)
All Layers Before	4.435	5.155	6.715	8.42	11.431	13.345	21.425	28.51
Layer1 After	0.69	1.16	1.735	2.33	3.75	4.92	10.92	14.155
Layer2 After	3.485	4.075	4.55	5.54	7.1	8.265	15.12	19.41
Layer3 After	3.41	4.46	5.7	7.055	8.99	10.13	18.105	25.045

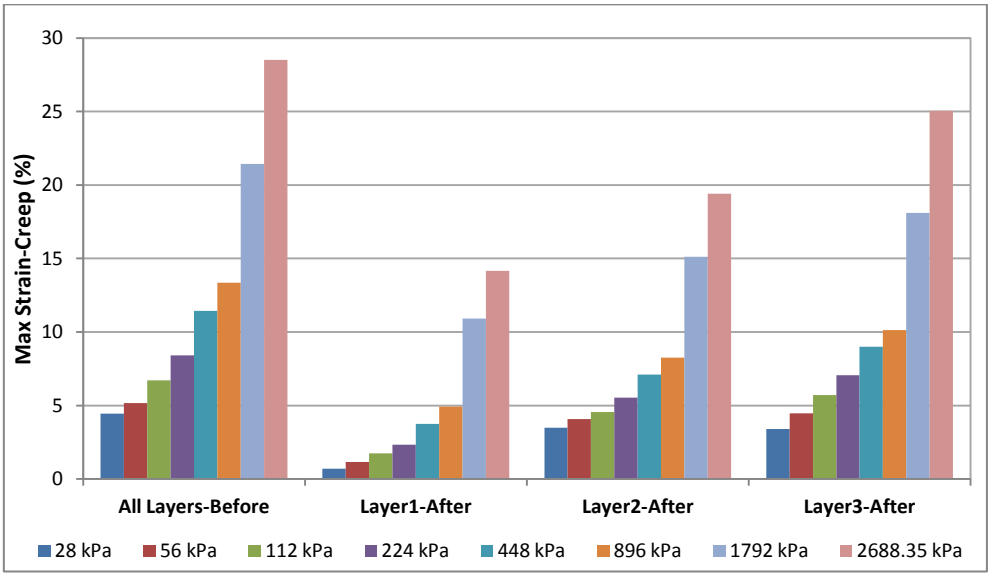

Fig. 4.80: Maximum strain percent relationship with loading stages of long-term tests. This relationship is for the box model soil layers before and after 50 week of model flooding.

Table 4.30: Outcomes of box model soil layers tested in long-term mode before and after 50 week model flooding. G_s is specific gravity, C_c is compression index-consolidation test, C_r is expansion index-consolidation test, *C-UU* and *φ-UU* are cohesion and angel of internal friction-unconsolidated un-drained direct shear, *C-CU* and *φ-CU* are cohesion and angel of internal friction-consolidated un-drained direct shear, *GC* is gypsum content, C_p is collapse potential, *WD* is wet density, *DD* is dry density, e_o is initial void ratio, C_g is coefficient of gradation, C_u is the coefficient of uniformity and *D10*, *D30*, *D60* are particles sizes for which 10, 30 and 60 percent of the soil sample by weight is finer respectively.

Layers	G_s	Gravel (%)	Sand (%)	Silt (%)	Clay (%)	C_c	Cr	C-CU (kN/m²)	φ-UU (kN/m²)	C-CU (kN/m²)	φ-UU (kN/m²)	GC (%)	C_p (%)	WD (gm/cm³)	DD (gm/cm³)	e_o	D_{10}	D_{30}	D_{60}	C_g	C_u
All Before	2.599	28.06	68.389	0.75	2.8	0.045	0.0021	14.5	35.25	15.83	11.88	45	1.593	1.5	1.429	0.13	0.175	0.364	1.539	0.493	8.79
1 After	2.536	23.548	75.802	0.65	0	0.118	0.0133	0	40.601	0	17.098	24.27	1.47	1.892	1.604	0.44	0.146	0.223	1.082	0.317	7.436
2 After	2.625	22.96	75.86	1.183	0	0.105	0.0037	8.696	38.81	6.281	16.43	32.95	1.163	2.009	1.673	0.513	0.15	0.231	1.189	0.2999	7.928
3 After	2.361	21.03	77.68	1.29	0	0.067	0.0053	50	38.66	11	16.86	21.88	1.393	2.017	1.702	0.335	0.147	0.22	0.97	0.339	6.599

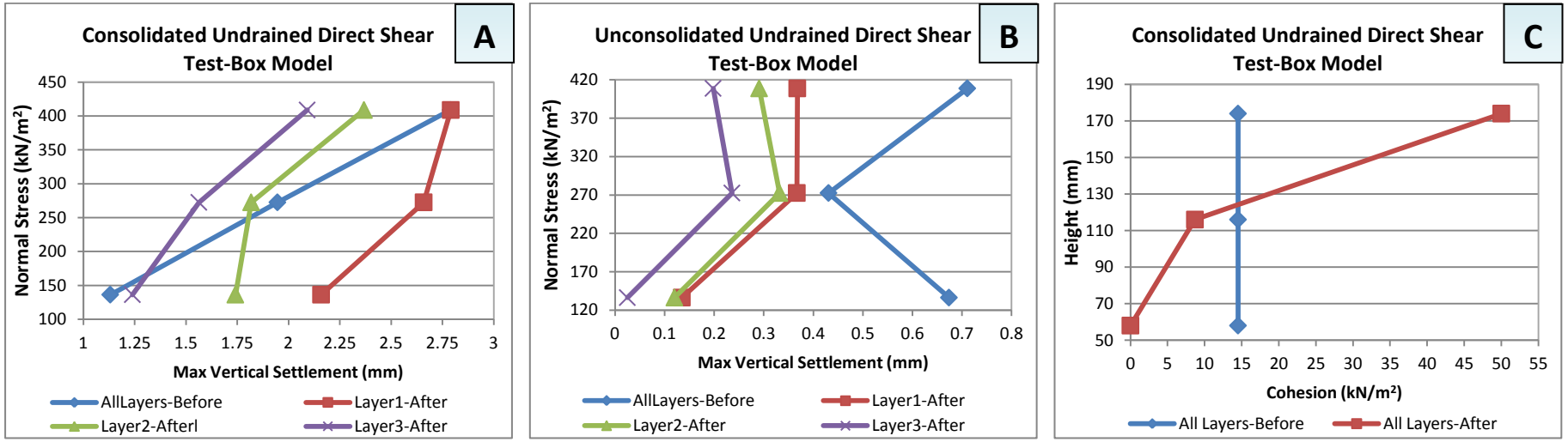

Fig. 4.81: Shows in part A, the maximum vertical settlement versus normal stress from consolidated un-drained direct shear test. Part B shows the maximum vertical settlement versus normal stress from unconsolidated un-drained direct shear test. Part C presents the cohesion changes due to 50 week box model flooding.

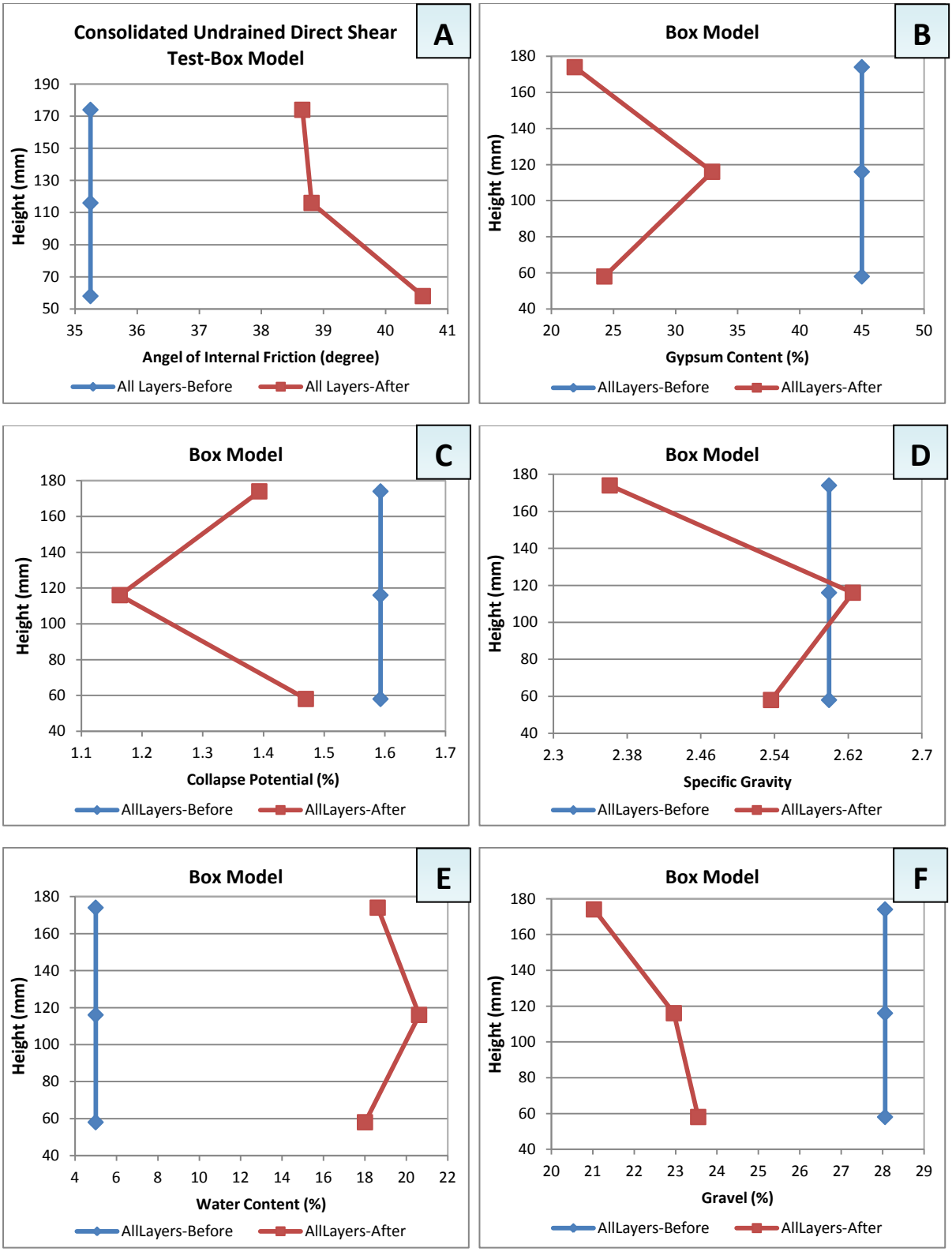

Fig. 4.82: Box model outcomes before and after 50 weeks of model flooding. Part A is for the angle of internal friction, part B is for the gypsum content, part C is for the collapse potential, part D is for the specific gravity, part E is for the water content and part F is for the gravel percent.

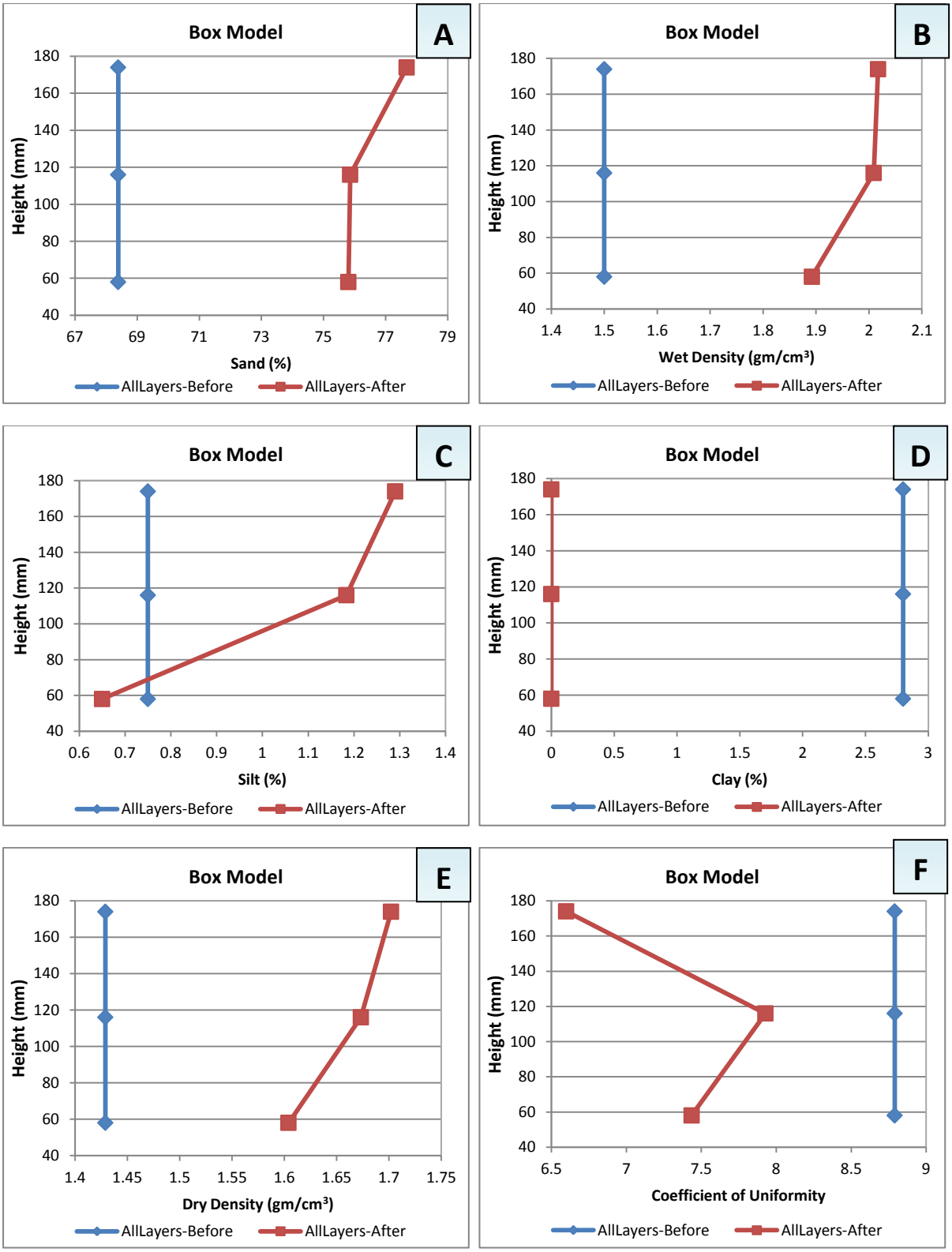

Fig. 4.83: Box model outcomes before and after 50 weeks of model flooding. Part A is for the sand percent, part B is for the wet density, part C is for the silt percent, part D is for the clay percent, part E is for the dry density and part F is for the coefficient of uniformity.

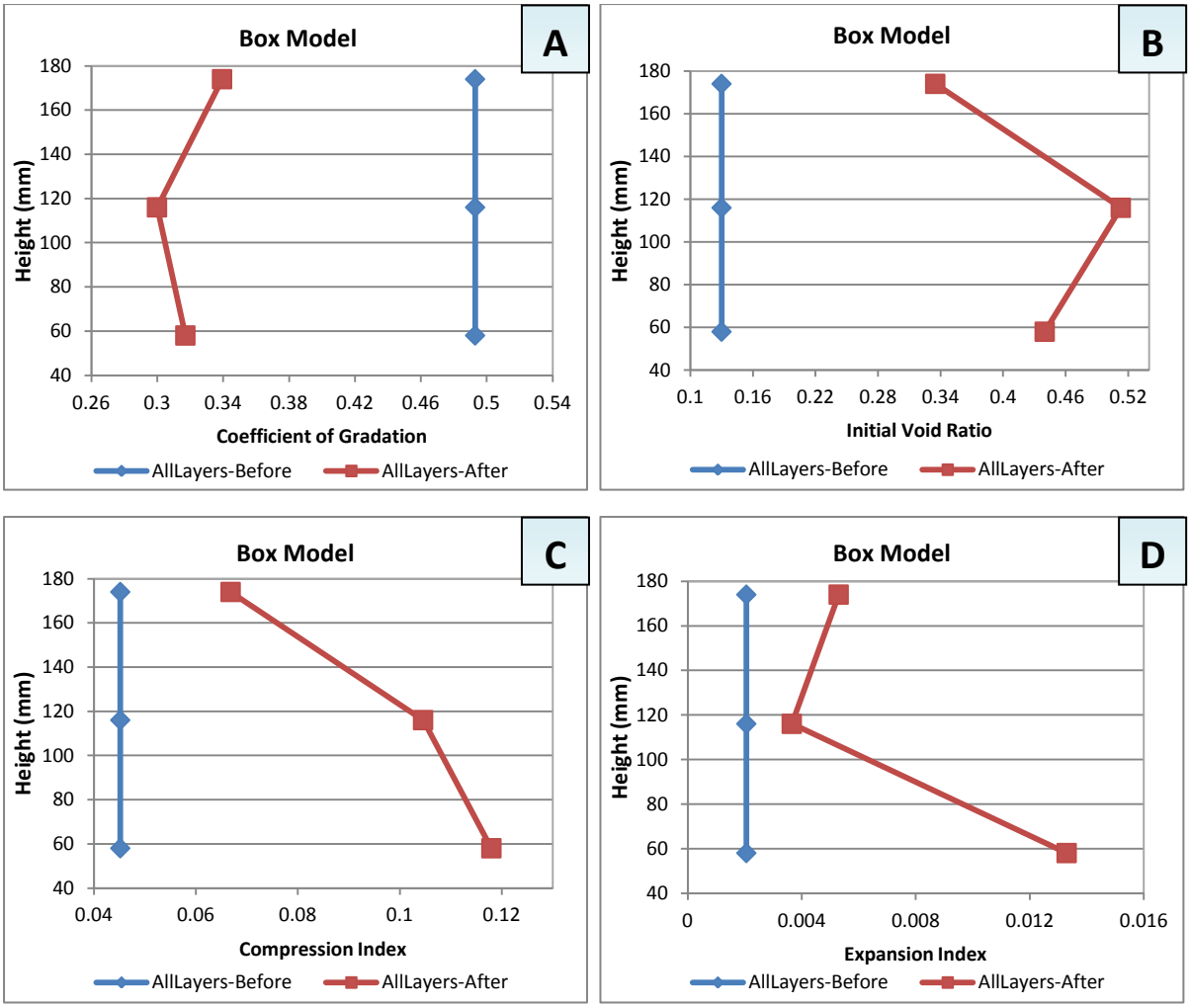

Fig. 4.84: Box model outcomes before and after 50 weeks of model flooding. Part A is for the coefficient of gradation, part B is for the initial void ratio, part C is for the compression index and part D is for the expansion index.

4.8 Tested samples Photos

Photographs of typical samples used in this research are presented below. These include rock samples before and after the dissolution process, samples after short-term loading and samples after long-term loading.

4.8.1 Air-Dry samples

PBG specimens are presented in Figures 4.85/B and 4.86/B & D. Note the macro cracks filled with dark green material, which is almost Marl.

In Figure 4.86/F, G & H, it can be seen that the *IG* has abundant micro-cracks distributed in different directions and filled with dark fine grained material inter-bedded between gypsum layers.

The similarities between *ThL-PBG* and *ThL-WCBG* specimens, with the existing cracks filled with almost clayey materials, which can be noticed from Figure 4.86.

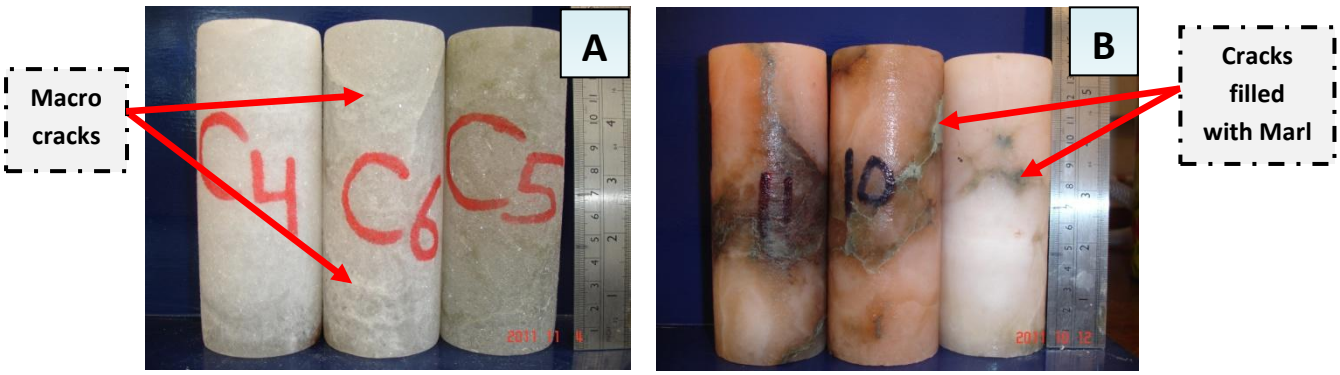

Fig. 4.85: A is the white cylinders and B is the pink cylinders from Bantycock Mine/UK gypsum block samples.

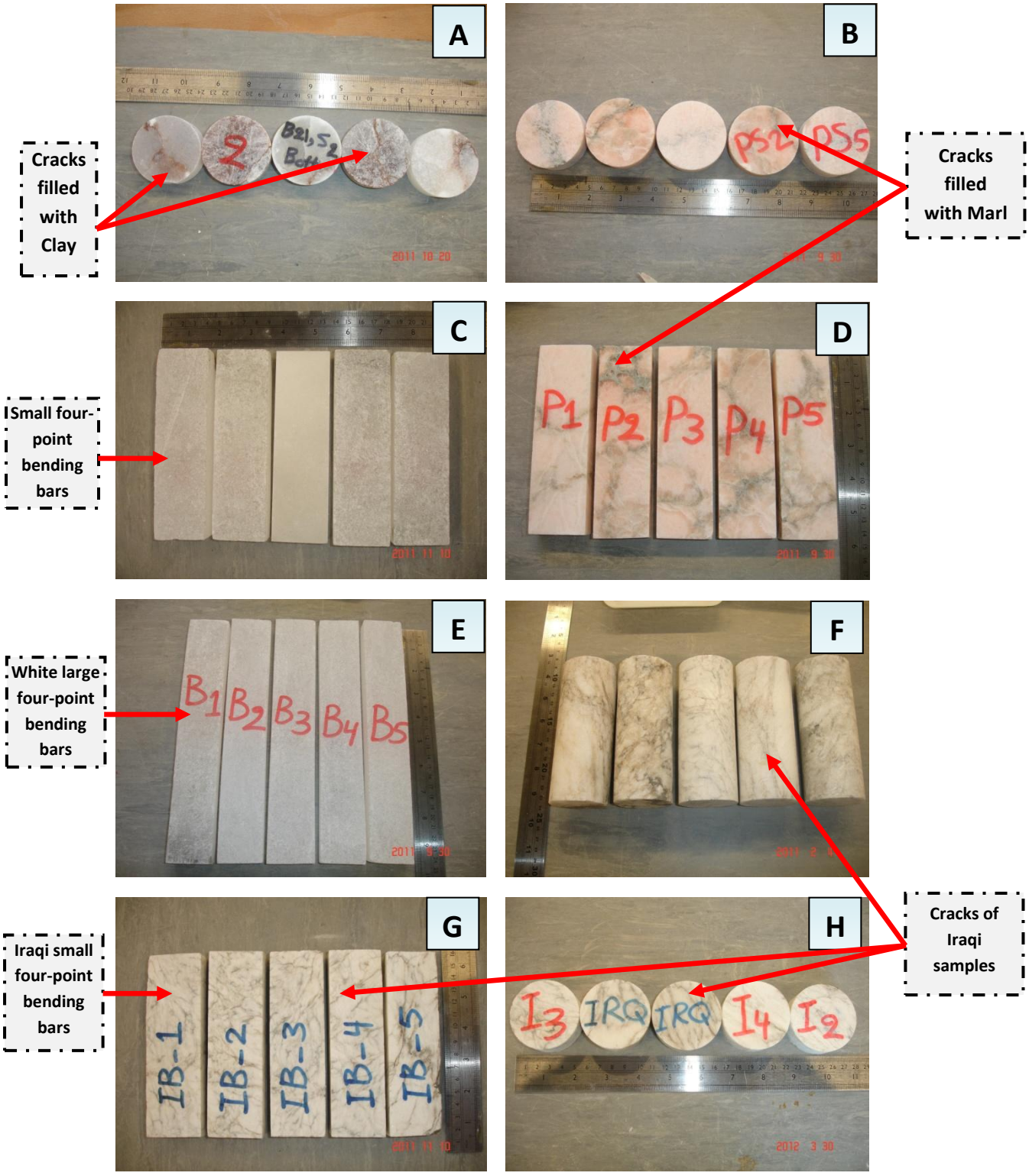

Fig. 4.86: Various air-dry gypsum rock samples. Part A is for the white & clay/Bantycock thin layers. Part B is for the pink/Bantycock thin layers. Part C is for the intact white/Bantycock small four-point bending bars. Part D is for the pink/Bantycock small four-point bending bars. Part E is for the intact white/Bantycock large four-point bending bars. Part F is for the Iraqi cylinders. Part G is for the Iraqi small four-point bending bars. Part H is for the Iraqi thin layers.

4.8.2 Samples after Dissolution

It can be seen in Figure 4.87/A & B that the top sides of cylindrical samples are dissolved more than bottom sides, which can be noticed with WBG and PBG. This difference may reflect the progressive accumulation of denser, salt-saturated water at the bottom of the test container during the test.

In contrast, the thin layer samples either the UK ones in Figure 4.88/A, B & G or the Iraqi one in Figure 4.88/F are dissolved on all sides, though the amount dissolved varies between samples.

In regards of *SFB* and *LFB*, as shown in Figure 4.88/D & E, the dissolution took place more at both two ends then at the long sides, while the lowest dissolution zones are the top and bottom surfaces.

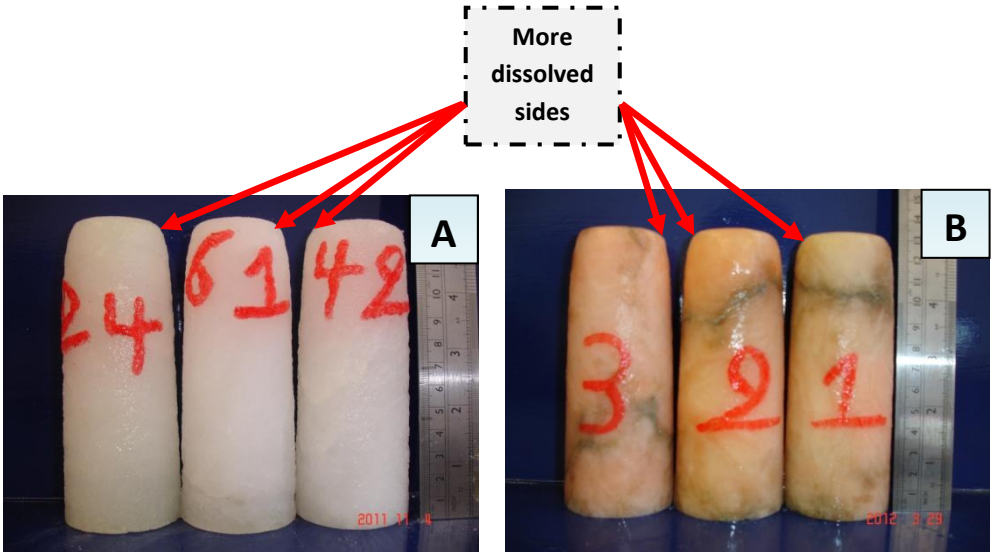

Fig. 4.87: Various cylindrical samples after 50 weeks saturation under atmospheric pressure. Part A is for the white cylinders. Part B is for the pink cylinders. All these samples are from Bantycock Mine/UK gypsum block samples.

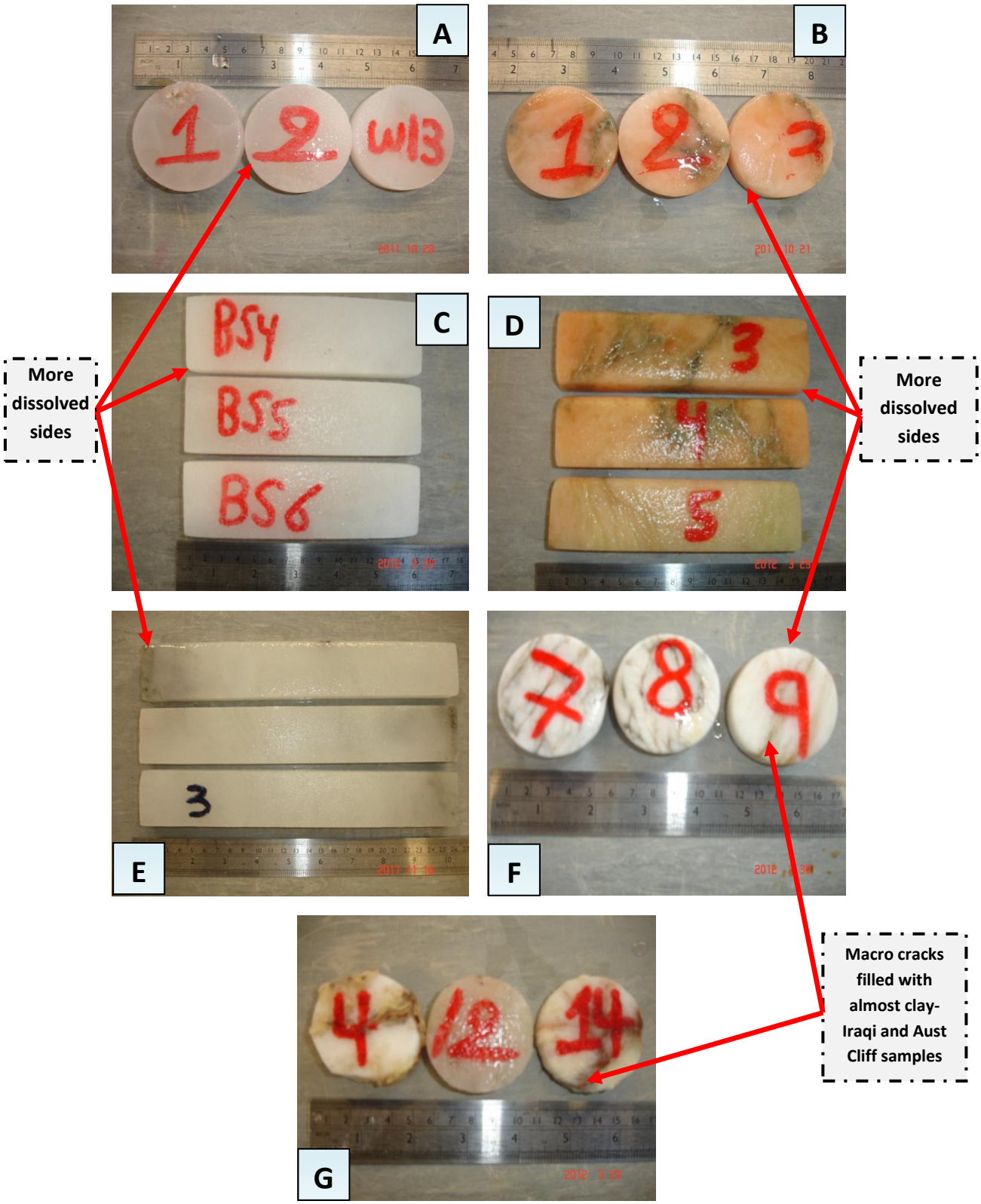

Fig. 4.88: Various gypsum rock samples after 50 week saturation under atmospheric pressure. Part A is for the white/Bantycock thin layers. Part B is for the pink/Bantycock thin layers. Part C is for the white/Bantycock small four-point bending bars. Part D is for the pink/Bantycock small four-point bending bars. Part E is for the white/Bantycock large four-point bending bars. Part F is for the Iraqi thin layers. Part G is for the Aust Cliff thin layers.

4.8.3 Samples after Short-Term testing

As can be seen in Figures 4.89 and 4.90, the *Cyl* samples are failed with shear failure mode in general. The *Cyl-WBG* experienced shorter shear failure, which started from the top surface then extended to end near the mid-point of the tested specimens as shown in Figure 4.89/A.

In contrast, the shear mode was longer in *Cyl-PBG* and extended from top to bottom surface as shown in Figure 4.89/B. A similar mode of shear failure also was experienced by *Cyl-IG* as shown in Figure 4.89/H, which may result from the similarity of distributed macro-cracks and the existing mineral inside these cracks. As noticed during the testing of these specimens, few seconds before failure, the specimens started to propagate cracks from top to mid-point or bottom surface and then was observed to suddenly fail as shown on the figures.

In Figure 4.89/E, F & G, there were no significant differences in the system of failure mode of *SFB-PBG* and *SFB-WBG* although the pink ones indicated micro-cracks in their skeleton. In fact, the failure zone is located in the remaining length of the span between the bottom supporting points for both *SFB* and *LFB*. This shows that the selection of two sizes of four-point bending is successful and no random failure zones are established within *SFB* and *LFB* specimens. This also applies to the tested *SFB-IG* samples shown in Figure 4.90/A.

All the *ThL* samples experienced similar failure modes as shown in Figure 4.89/C & D and Figure 4.90/B. As noticed during the testing of these samples, a few seconds before failure, the specimens started to propagate cracks from the top to the bottom surface and then failed and suddenly crumbled.

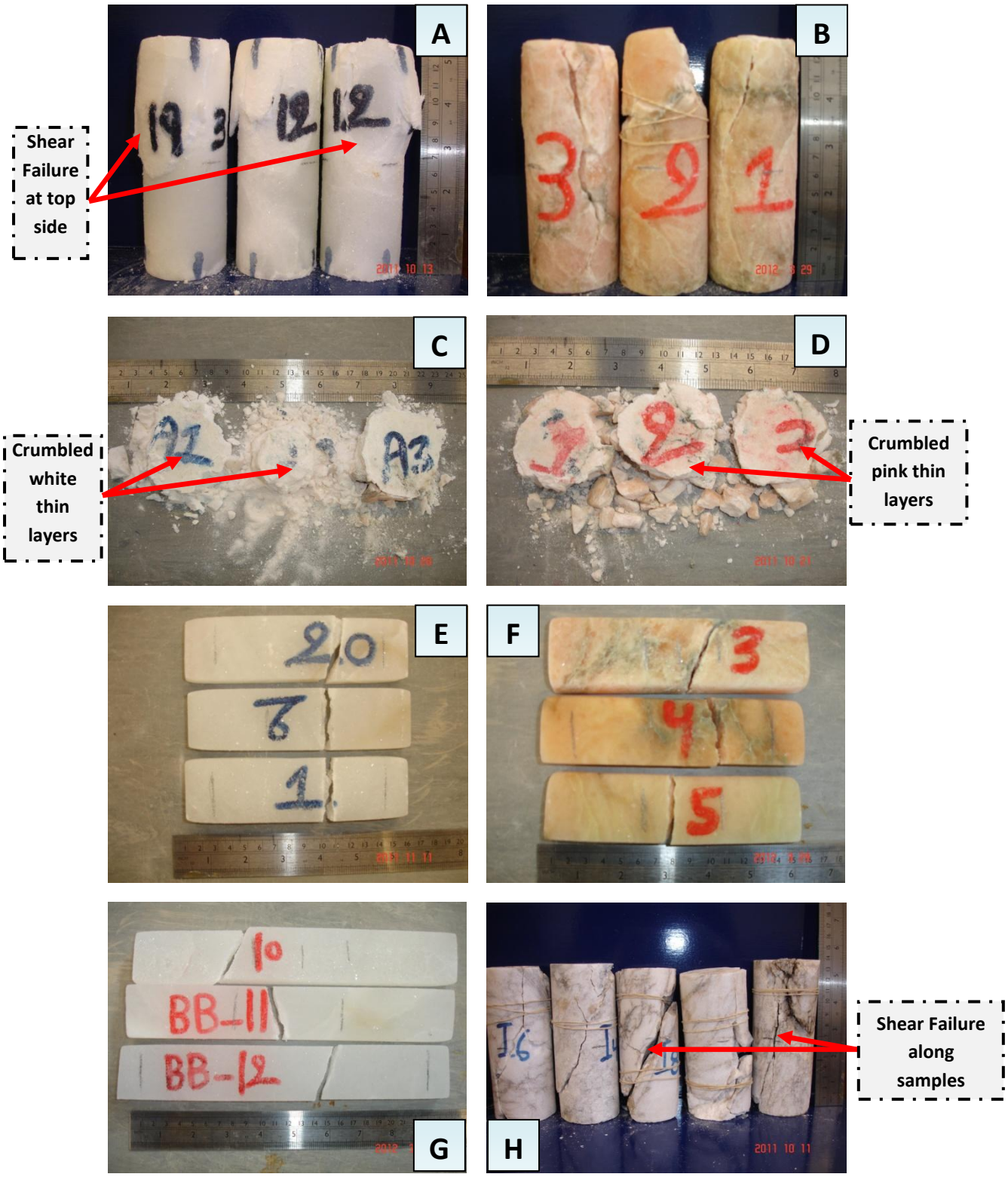

Fig. 4.89: Various gypsum rock samples after short-term testing. Part A is for the white/Bantycock cylinders. Part B is for the pink/Bantycock cylinders. Part C is for the white/Bantycock thin layers. Part D is for the pink/Bantycock thin layers. Part E is for the white/Bantycock small four-point bending bars. Part F is for the pink/Bantycock small four-point bending bars. Part G is for the white/Bantycock large four-point bending bars. Part H is for the Iraqi cylinders.

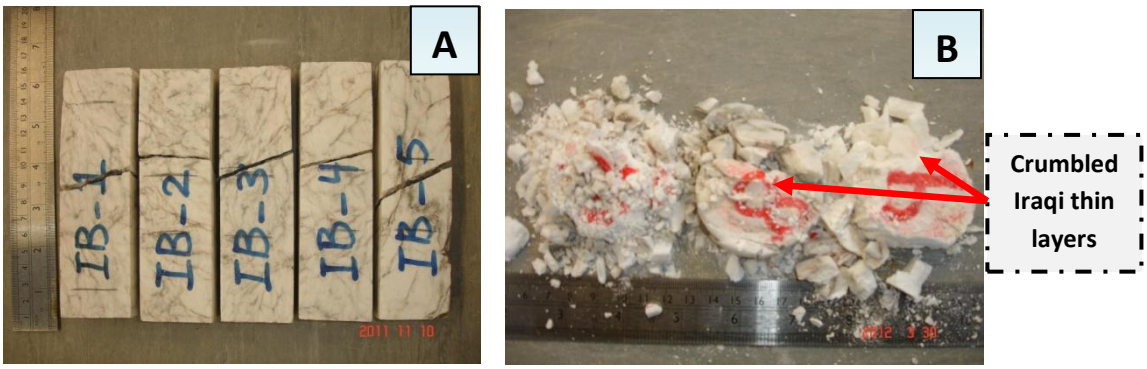

Fig. 4.90: Various Iraqi gypsum rock samples after short-term tests. Part A is for the small four-point bending bars and part B is for the failed thin layers.

4.8.4 Samples after Long-Term testing

It can be seen that the tested *Cyl* samples shown in Figure 4.91/A did not fail after the two months of creep tests duration under stresses of 1792 and 2688.35 kPa. The *WBG* and *IG* samples established higher dissolution susceptibility compared to the other cylindrical specimens. Linear features and micro-cracks were present within un-failed long-term cylinders shown in Figure 4.91/A.

Consequently, the *Cyl* samples loaded for one year exhibited shear failure mode, which is very similar to those happened due to short term tests (see Figures 4.89/A, B & H).

The *ThL* samples like *Cyl* samples did not show failure after the two months of creep tests under stresses of 1792 and 2688.35 kPa (Figure 4.91/B & D) and the same dissolution implications are established.

The failures of *SFB* and *LFB* samples shown in Figure 4.91/C & E are similar to those obtained after short term tests. Hence, the *SFB* and *LFB* short term tests are helpful in determining the specimens' failure mode, which might be useful to understand the failure mode of long term tests.

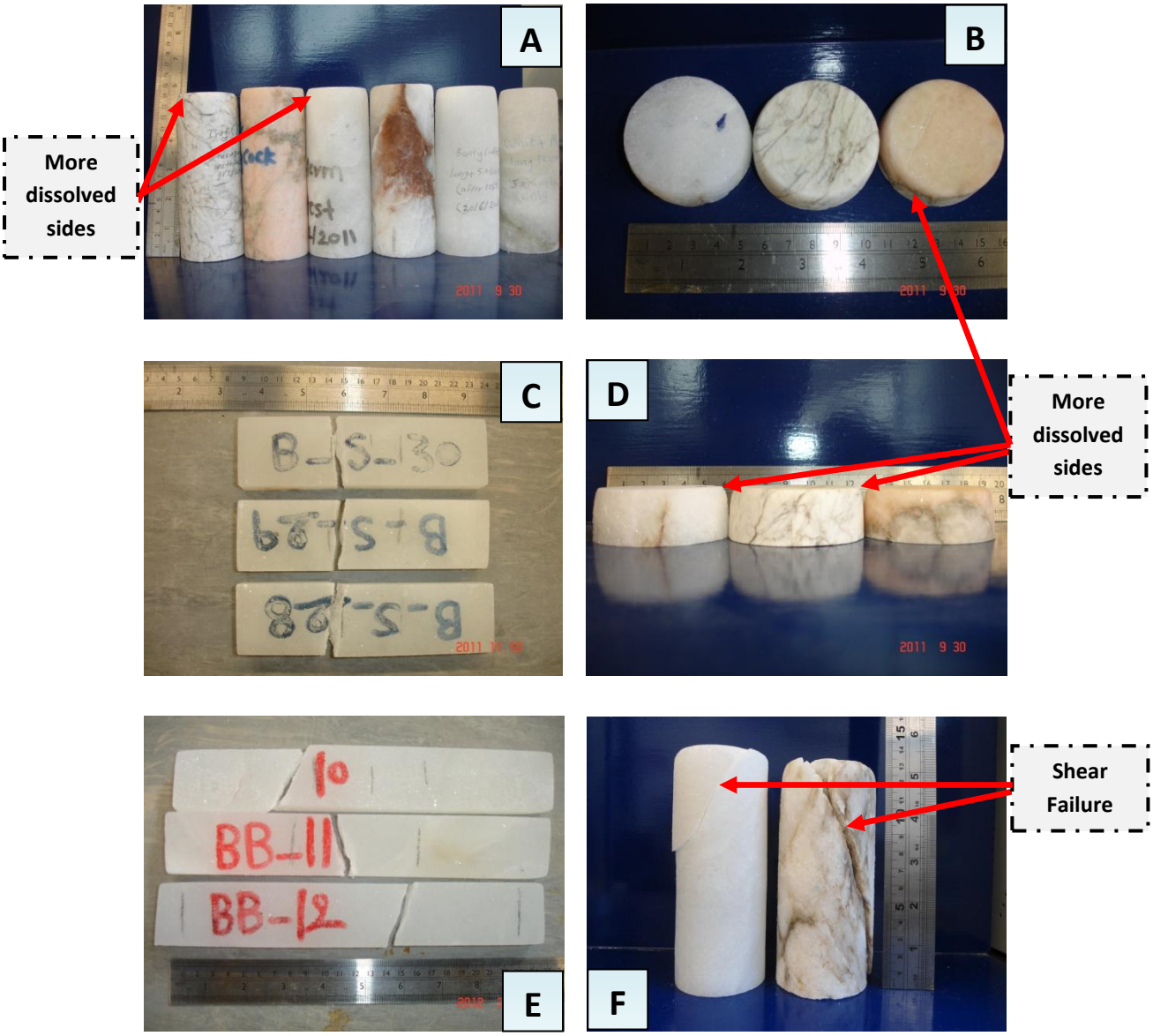

Fig. 4.91: Various gypsum rock samples after long term testing. Part A is for different UK and Iraqi cylinders tested in saturation condition under atmospheric and 5.0 bars water pressure. Parts B & D are for different UK and Iraqi thin layers tested in saturation condition under atmospheric pressure. Part C is for the white/Bantycock small four-point bending bars tested in saturation condition under atmospheric pressure. Part E is for white/Bantycock large four-point bending bars tested in saturation condition under atmospheric pressure. Part F is for the white/Bantycock and Iraqi cylinders for one year loaded cylinders in saturation condition under atmospheric pressure (for white/Bantycock cylinder) and under 5.0 bar water pressure (for Iraqi cylinder).

4.8.5 Box Model photos

It can be seen that a notable height of the artificial gypseous soil settled down as shown in Figure 4.92/B (about 55 mm). The soil surface lost the fine materials and in general coarser materials were left. Dissolution is quite visible as many white gypsum particles are found especially coarse ones. Dissolution and settlement happened together more at the boundary zone, which might be increased by the plastic internal surface. This shows that gypseous soils' boundaries with other layers may face more problems of dissolution. The erosion took place on the top surface of the model soil left it rough, with many other changes on geotechnical properties as shown in Figure 4.92/B below.

Fig. 4.92: Presents the box model experiment. Part A is for the model before 50 weeks of water flooding and part B is for the box after the 50 weeks (more details on this model work is in Section 3.9 of Chapter 3).

4.9 Summary

The major key themes of the results can be summarized as following:

A. Key points of gypsum rock:

- Analysis of the effects of water pressure is crucial for determining a dam's stability.
- All types and shapes of gypsum rocks are influenced by the dissolution process.
- Dissolution characteristics of gypsum rocks samples are influenced by impurities existing in those samples.
- Thick layers of gypsum rocks are prone to failure much more than thin layers.

- Increasing the roof length of cavities, simulated by the four-point bending test, decreases the time to failure and increases the value of vertical deflection due to applied axial stresses.
- The Iraqi gypsum rocks samples are stronger than the UK gypsum rock samples.
- The modified devices for compression and bending tests are successful. They are suitable to be used for the application of various real conditions of dams and to be used for testing other substrates from dams' area.

B. Key points of gypseous soils:

- The methods and techniques applied to gypsum rocks are suitable for application on gypseous soils.
- Artificially-prepared gypseous soils provide a successful method for simulating real gypseous soils.
- The presence of soil particles within gypseous soil has a significant impact on the engineering properties of the gypseous soil.
- There are measurable influences of gypsum content of gypseous soil samples on the behaviour of these samples under axial stresses with dissolution over time.
- The geotechnical properties of gypseous soil samples are noticeably influenced by the continuous dissolution process of gypsum in long term tests.

C. Key points of box Model:

- The continuous dissolution process due to water flooding for 50 weeks showed a significant effect in increasing surface settlement, and causes variations in particle size distribution inside gypseous soil strata.
- The boundary sides of gypseous soil strata are notably influenced by flooding for 50 weeks and showed larger settlement compare to the other surface soil areas.
- The geotechnical properties of gypseous soil strata are notably influenced by flooding for 50 weeks.
- Flooding during a period of 50 weeks leads to significant washing-out of the gypseous soil fine particles. Also, water movements inside the vertical layers of gypseous soil strata are important.

CHAPTER FIVE: DISCUSSION

5.1 Introduction to discussion

The overall purpose of this thesis is stated in Chapter 1 and repeated here for clarity:

A. **To understand stability issues of dams built on gypsum-rich substrates in the Mosul area of northern Iraq & other areas.**
B. **To develop new methods to assess impact of dissolution on mechanical properties of gypsum substrates.**
C. **To consider the extent to which the findings presented in this thesis can be applied to other areas.**

The following major features of the data were identified from the results presented in Chapter 4:

1. Dissolution under atmospheric pressure causes variable loss of material resulting in weakening of the physical strength of the sample, compared to its original condition.

2. Water pressure speeds up the dissolution process and results in weaker specimens compared to saturated specimens tested under lower pressure, such as atmospheric pressure.

3. Time is the third key point and may cause gypsum rock failure. The results show that: **a)** gypsum rock is not prone to failure in a short time period such as two months; **b)** The time factor may increase the rate of propagation of cracks during continuous dissolution and cause rock collapse even where lower stress is used in creep tests compared to the rock's original compressive strength.

These three key points are underpinned by a strong set of evidence which shows that gypsum present in the foundations of dams may cause collapse due to constant applied stress from the dam's weight and overburden pressure located over gypsum substrates.

The discussion in this chapter is based around the three key aims and major findings stated above. In order to focus the discussion, this chapter is divided into four major sections,

which deal with an explanation and understanding of the results. The first three sections deal specifically with each of the aims statements repeated above in terms of the results of gypsum rocks. The fourth section looks specifically at the findings of gypseous soils in relation with the stated aims, which will be discussed in **Section 5.5**. In each section, the issues regarding gypsum dissolution are considered.

5.2 Stability issues of dams built on gypsum-rich substrates in Mosul-Northern part of Iraq & other areas.

The experimental data in **Chapter 4** show clearly that gypsum under pressure of overburden is subject to dissolution at a greater rate and to a greater extent than without overburden. Since dams built on gypsum-rich substrates exert a significant additional load, it is logical to assume that they are at risk of dissolution enhanced collapse. However, to what extent do these data reflect real situations in dams? The following text assesses the degree to which the experimental data assembled in this thesis can be applied to real dams.

Since the dissolution increases due to the application of water pressure for a long time, there must be a role of water level from the reservoir (as the reservoir water level is simulated through water pressure in the experiments) and from the ground. An integral component of this is the potential impact of existing gypsum layer thickness and karstic features, discussed below, along with stresses from overburden aspects.

Soluble substrates like gypsum and anhydrite are present in the foundation of Mosul Dam (Kelley et al., 2007) (**Figure 2.15**). The presence of these soluble rocks could make the dam prone to collapse. The realization of this potential is indicated by published evidence of continuous dissolution and propagation of karstic features in the foundation of this dam (Abbas et al., 1990; CENWD, 2003; Kelley et al., 2007; MESF, 2007; SIGIR, 2007; Johnson, 2008; Al-Taiee and Rasheed, 2009; see **Figures 2.14, 2.15** and **2.16** in **Chapter 2**). More focused work on the Mosul Dam area specifically and on gypsum rocks generally have revealed the following information:

- US Army Corps of Engineers report on geological setting of Mosul Dam (Kelley et al., 2007) records that dissolution is happening at a faster rate in the Mosul Dam foundation than before construction, possibly due to the presence of the reservoir.

Therefore, the faster dissolution rate is probably related to water pressure from the reservoir level.

- Evidence collected in this study (**Section 4.3**) shows that water pressure speeds up the dissolution process and reduces rock resistance to compression.
- The data that have been collected in this study, **Figures 4.26** to **4.29** and **4.38** have revealed the role of macro-cracks and impurities in the dissolution process and the decrease in rock resistance to compression in both short and long term tests. This supports the study of Misra (1962) who found evidence for the creep rate in evaporates to be related to impurities.
- Data collected in this study (e.g. **Section 4.3** and **Figures 4.20-4.25**) have established the role of gypsum particle size, shape and orientation to characterize dissolution process. This is recognized from the differences in dissolution values among samples and connects this to the data from *SEM* photos of those samples particle sizes and shapes.

Transferring the understanding gained from this project's experimental work and published sources to the situation at Mosul suggests that there are 5 major destabilizing factors which present a risk to the dam: **1)** gypsum dissolution processes characteristics, **2)** karstic features, **3)** gypsum layer thickness, **4)** reservoir water depth (water pressure) and **5)** time.

The sum of these points shows that an increase of water pressure due to the presence of the reservoir speeds up the dissolution process. The presence of gypsum rock as thin layers or lenses and thick layers show the possibility of gypsum layer thickness controlling ground stability due to the higher dissolution of thicker layers. Karstic areas are also evidence of dissolution underneath Mosul Dam and therefore the dam may be prone to collapse. Note however that the development of those karstic areas may be enhanced by axial stresses resulting from the dam's weight and overburden. Overall, this analysis leads to the deduction that there is good evidence that the stability issue of Mosul Dam is mainly controlled by the impacts of water pressure over time (water pressure from reservoir water quantity), then the possibility of an effect of gypsum layer thickness (dissolution of various thickness over time) and karstic features development (increase dissolution through these karstic features over time).

In this section, three kinds of datasets are cross-compared in order to test this deduction. Short and long term testing datasets represent the first kind. Data that was collected through field observation on gypsum rock in the UK and Iraq is the second kind. The US Army Corps of Engineers' report on the geological setting of Mosul Dam (Kelley et al., 2007) and the Special Inspector General for Iraq Reconstruction (SIGIR, 2007) report on Mosul Dam represent the third kind of datasets. Further down follows a detailed discussion for each factor in turn to evaluate them according to their role to control stability issue of Mosul Dam.

5.2.1 Water Pressure over time

Short term testing on samples showed the impact of water pressure on the speed of dissolution, with weakening of the samples' mechanical properties.

Mechanical parameters such as compressive strength, time to failure and load at failure, mass and volume reduction and dissolution are strongly influenced by exposure to higher water pressure as can be seen in **Tables 4.4-4.8** and **4.11**. The decreasing values of compressive strength, load at failure and time to failure in addition to decreases in mass and volume, and dissolution in these samples strongly supports the hypothesis that the main factor controlling gypsum dissolution beneath the Mosul Dam is a combination of water pressure and time. Other parameters such as Poisson's ratio, shear modulus and bulk modulus reflect the materials ability to resist loading before failure in the elastic zone. It is worth in this stage to note that the increasing values of Poisson's ratio mean that the tested sample is weaker reflecting the formation of new micro-cracks or the extension of existing cracks (Gercek, 2007).

Long-term testing, completed on similar samples to short-term testing (**Section 4.4.3**) also provides strong evidence of how increased water pressure speeds up the dissolution process and weakens the gypsum rock samples. Values of strain percent, maximum dissolution, cumulative conductivity, mass and volume reductions, velocity and elastic modulus reductions (ultrasonic observations) are strongly related to water pressure on time (white cylinder in **Figures 4.58**, **4.59/B**, **4.60/A** and **Figure 4.61/A & B**). The increasing constant *B* of creep equations (*B* represent the secondary stage of creep) (**Tables 4.21** and **4.22**), gave valuable evidence of the samples' behaviour changes due to water pressure.

Values of strain percent, dissolution of one-year loaded samples (**Figure 4.62/A & B**) and the collapse of the sample (**Figure 4.91/F**) under water pressure after 4000 hours are very strong evidence of water pressure impacts on time progress on gypsum rock stability.

Kelley et al. (2007) show that the foundation of Mosul Dam includes apparently un-weathered gypsum and anhydrite. While this intact and saturated material reportedly has a low permeability, the presence of karstic features, including cavities (SIGIR, 2007) (**Figure 2.14**) indicates that some significant dissolution must be taking place.

The cavities existing in the foundation of Mosul Dam (see **Figure 2.14**) (SIGIR, 2007) probably reflects the accumulation of reservoir water enhancing the soaking process and increasing pressure.

As fully saturated samples were used for the water pressure experiment, the applied pressure will push the surrounding water inside the closed triaxial cell (see **Figures 3.23-3.25**). The modification of the standard triaxial cell means that the water pressure could be maintained at a stable level for long periods. There is a clear difference between the dissolution characteristics of samples tested at different water pressures. There may be two possible explanations:

1. Static pressure controls the rate of chemical dissolution. In this explanation, water pressure exerts a force on the sample, similar to a static axial load. However, the exact process remains unclear.
2. Changes in water pressure during the experimental test, which occurred regularly when the water was changed, may have induced small elastic oscillations within the samples. These could have weakened cementing bonds between gypsum crystals created a larger surface area.

During this stage, the dissolution characteristics of gypsum crystals probably play a role; the semi-circular/semi-elliptical crystals may dissolve (or allow smooth surface to dissolve) more than angular shapes, and hence, the pressure will push the water to act more on the weaker area and probably on internal cementing bonds. Regular changing of saturation water will speed up this process due to new amount of fresh water provided. Therefore, both of water pressure and fresh water will act and possibly the more important is the pressure, which will

weaken the cementing bonds among gypsum crystals due to the combination impacts of pressure and dissolution. Furthermore, when axial stress is applied, this will add an extra factor on water pressure to enhance dissolution pressure. In theory, the impacts of axial stress and water pressure will concentrate in/around weak places, such as voids and cracks. Then, because of the process of dissolution of gypsum rock is not very quick; the re-crystallization process will take place. Therefore, above process from axial load and dissolution under water pressure together, the re-crystallization process will speed up by the applied water pressure.

Over all, the evidence for weakening of the gypsum due to water pressure support the hypothesis of water pressure impacts over time as the main factor controlling the Mosul Dam stability issue.

5.2.2 Gypsum dissolution processes characteristics

Preliminary tests showed that the initial chemical characteristics of the water had an influence on the amount and rate of dissolution that could take place. In particular, distilled water was shown to be particularly aggressive (**Figures 4.14-4.16**). This is due to the absence of calcium or sulphate ions in the water which leads to the destruction of the bonds between minerals and produces more dissolution. It is worth noting here that Kelley et al. (2007) reported relatively small amounts of total dissolved solids and equilibrium in calcite percent in the water of reservoir of Mosul Dam. This means the relatively pure water in the reservoir was in contact with the gypsum rock beneath the dam. Although the choice of distilled water was logical because of the need to maintain constant chemical characteristics of the immersion water, the dissolution is more aggressive with distilled water (as shown in **Figures 4.13-4.15**).

The factors influencing dissolution characteristics like gypsum crystal size and shape, existing cracks, impurities and saturation water purity, recognized with tested gypsum rocks will be discussed in this section in order to explore the possibility of dissolution under atmospheric pressure causing the Mosul Dam failure.

The *SEM* photographs of UK and Iraqi gypsum rock (**Figure 4.20-4.25** and for more details see **Table 4.1**) show that there is a variety of particle sizes and shapes. The larger dissolution

values of Iraqi samples under atmospheric pressure than white/Bantycock samples in short-term datasets (see **Section 4.3.1**) were correlated with the effects of particle size and shape in characterizing the dissolution process i.e. larger particles dissolve less quickly than smaller particles. Shapes of semi-circular/semi-elliptical in tested samples may be more soluble than shapes with angular ends/edges due to their smaller sizes. In addition, the value of greater dissolution of fine particle size, semi-circular and semi-elliptical shape (Iraqi gypsum) in short-term testing, is also verified by the dissolution values of Iraqi thin layers tested in long term (**Figure 4.49/A & B)**. Although saturation water under atmospheric pressure caused dissolution, the white/Bantycock sample showed increased rates of dissolution during short-term tests under 1.75, 3.25 and 5.0 bar water pressure (**Table 4.4**).

The differences among values of dissolution of gypsum rock samples with macro and/or micro cracks (e.g. samples with cracks compare to intact white/Bantycock gypsum) shown in **Chapter 4** suggest that these cracks control the gypsum dissolution process. The increasing value of dissolution of samples with macro-cracks without any axial loading during short-term testing may be due to existing impurities. Some minerals in these impurities may react with calcium or sulphate of gypsum and probably affects dissolution, though the exact influence is not clear. However, the lower value of dissolution of similar samples under axial loading during long-term testing may result from the axial loading causing the cracks to close, so effectively reducing the surface area exposed to unsaturated water. Hence, due to no significant water pressure here, the water is unable to penetrate the existing cracks and cause dissolution. While it is not possible to determine the exact impact of the existing cracks on the dissolution experienced by the samples, it seems likely that they, and the impurities that they contain, play a role. Impurities may also work as cementing bonds and possibly change the dissolution values.

Impurities present within the gypsum, such as those shown in **Table 4.2**, influence the dissolution process, and thus there must be interplay of these minerals in gypsum dissolution process. Values of dissolution for samples tested in the short and long term (**Chapter 4**) suggest that the impurities within micro-cracks could have a dominant effect on dissolution. This is supported by the increasing value of dissolution for samples with impurities in their macro-cracks (shown in **Table 4.4-4.6, Table 4.8** and **4.11**) without axial

loading (short-term testing) (these impurities shown in **Table 4.2**). The exact role of impurities is an area for future research.

To sum up, the previous data in this section show that there are notable roles for particle size and shape, existing cracks, impurities, and saturation water purity in controlling dissolution characteristics and the probability of all of them control together the dissolution process. It is worth at this stage to say that saturation with the condition discussed in this section is under atmospheric pressure. Then, from the fact that ***Pressure = Load/Area*** (assume that the area is fixed for similar samples used for saturation condition with applied water pressures), the saturation water force here is less-able to penetrate inside micro-cracks smoothly. So, it is also less-able to overcome cementing bonds between particles. From the values of saturation under atmospheric pressure, discussed above, show the less possibility of dissolution characteristics under atmospheric pressure to cause failure of the Mosul Dam and support the hypothesis of combination of time and water pressure factor is the main factor controlling Mosul Dam stability issue.

5.2.3 Gypsum layer thickness

Information collected from field observations in the UK and Iraq revealed that gypsum strata may occur as lenses, thin layer and thick layers which can be horizontal, vertical or at various other angles of dip (**Figures 1.3, 1.4, 1.7** and **1.8** and **Section 3.2**). This variability is present at the Mosul Dam (Kelley et al. 2007), where the gypsum of the Fatha (Lower Fars) Formation is inter-bedded with a variety of other rock types. The experiments in this thesis provide controlled and simplified representations of this variability, using two main sample types-thick layer as cylinders (54 mm diameter x 135 mm height) and thin layers as small discs (54 mm diameter x 20 mm thickness) examined under short and long term conditions.

The results of the short-term tests (for dissolution at atmospheric pressure) (**Tables 4.4, 4.6** and **4.11** and **Figure 4.63**) show that the possibility of dam failure due to thick layers is higher than thin layers. However, the possible influences of un-confinement process and longer sample height exhibited to axial loading (cylindrical/thick layer samples).

The difference between compressive strength values (long-term testing) of thin layers and cylinders shown in **Figure 4.63** indicates the higher possibility of failure in the case of thick

layers. Increasing values of constant *A* and *B* of creep equations support the higher possibility of failure of cylinders (see **Table 4.15** and **4.22**). Increasing value of constant *B* for thicker layer, which represents secondary stage of creep (before the third stage failure of creep) established the increase likelihood of thicker gypsum layer to cause failure.

To sum up, the previous data in this section show that there are important role of gypsum rock layer thickness in causing failure.

5.2.4 Karstic features

Information collected from UK and Iraq field observation (**Figures 1.3-1.4** and **1.7**, **1.8**, **Section 3.2**), from Kelley et al. (2007), from Figures **1.3**, **1.4** and **1.7**, **1.8**, Figures **2.1-2.7**, **2.11-2.12**, **2.14-2.15** (for Mosul Dam) and **2.16** and **Figure 2.5** shows that gypsum rock may experience the development of karstic features, including voids. To simulate the possible response of gypsum around these cavities, a range of gypsum types were prepared as bar samples and subjected to four-point bending tests (**Sections 3.6.1**, **4.3.5**, **4.3.6**, **4.3.7** and **4.3.8** for the method and results).

As dissolution weakens the gypsum rock (**Figures 4.53-4.57** and **Tables 4.7**, **4.8** and **4.17** to **4.20**) the load required for failure and the time to failure is reduced. The differences in the results between small and large four-point bending bars shows that as a cavity grows and the surrounding rock is weakened, the potential for collapse is significantly increased.

The risk of cavity collapse is further increased by the presence of macro-cracks in the overlying gypsum rock. However, the exact contribution of these cracks to cavity instability requires further work.

Over all, the previous data in this section show that there are important role of karstic features existing in gypsum rock layer in causing failure.

5.2.5 Summary of the key factors influencing the stability of dams built on gypsum-rich substrates

The key point to check the deduction of combination of time and water pressure factor is the main factor controlling Mosul Dam stability issue is the water pressure datasets for short and long term tests.

Increasing values of compressive strength, time to failure, load at failure, mass and volume reductions, and maximum modulus and velocity reduction for short-term testing of thick and thin layers (**Section 4.3**) greatly support the proposed deduction. In addition, the failed pressurized white/Bantycock gypsum cylinder by 5.0 bars after 4000 hour shown in **Figure 4.62/A** is greatly support the hypothesis of combination of time and water pressure factor is the main factor controlling the Mosul Dam stability issue.

Decreasing values of flexural stress at failure, time to failure, load at failure and increasing value of mass and volume reductions and dissolution for small and large bending bars shown in **Table 4.7-4.8** and **Figure 4.31-4.36** support the proposed deduction. Other parameters such as flexural modulus and vertical deflection values in general follow similar pattern of the aforementioned parameters and their values in the samples we analysed correlation with them and they support the hypothesis of combination of time and water pressure factor is the main factor controlling the Mosul Dam stability issue.

Hence, as these key points, ultrasonic measurement was attempted for rock stiffness detection. Ultrasonic measurements (**Table 4.13**) indicate that rock stiffness changed over time in response to loading and dissolution. This was probably due to the creation of new cracks, or the propagation of existing cracks within the gypsum.

The discussion in this section showed the possibility of Mosul Dam failure due to the combination of water pressure and time progress. Although of these good indications on water pressure influences, more extend study is needed in this field in the future.

5.3 New methods to assess the impact of dissolution on the mechanical properties of gypsum substrates.

This thesis has developed experimental techniques to assess the degree of susceptibility of gypsum to dissolution and pressure, which exceed previous methods of testing. This section assesses the extent to which the methods applied here are an improvement on standard methods published in the literature.

5.3.1 Assessment of the modified compression (cylinder testing) device

The experimental datasets of long-term (creep) testing in **Section 4.4.3** show that the modified device for cylindrical samples is capable to examine creep of gypsum rock successfully. This can be done for samples in an air-dry and saturated state with various levels of water pressure.

Potential factors that may influence the success of the device include the impacts of humidity, temperature and chemical influences from gypsum salt.

It has been previously established that a lever system is an appropriate way to apply creep stress on rock samples (Griggs, 1939; Griggs, 1940; Price 1964; Drescher and Handley, 2003). While, alternative methods have been used (see **Section 2.7.1**).

There are 4 possible factors to consider when assessing the validity of the compression experimental method (developed conventional oedometer device): **1)** Accuracy, **2)** Replicability of results, **3)** Constraints imposed by real world conditions, and **4)** Environmental impacts.

A variety of systems exist for rock creep testing. While electrical or hydraulic systems could be used to apply stress over prolonged periods, these would be costly to run. Furthermore, given the duration of the long-term tests, there is a risk of interference in performance, for example by power failure or a ruptured pipe or seal. The simplicity and reliability of the new design shown in **Figures 3.23-3.26** therefore seem a significant methodological improvement in the study of long-term creep.

The equipment (see **Figure 5.1**) was calibrated (see **Figure 3.29**) to ensure that the results were accurate. The data from similar samples show that the modified oedometer yielded replicable results (see **Section 4.4.3**, **Figure 3.23-3.26** and **Figure 4.58-4.62**).

The design of the modified oedometer meant that it was easy for one person to operate. There was no risk due to failure of power or hydraulic pressure as stable loading was achieved by weights and a lever arm (**Figure 3.28**). Furthermore, the process of changing the water and of applying water pressure using a hand pump also shows that this is a simple and robust device.

The specifications for the device in terms of load and pressure capacity were determined with reference to real world conditions (**Figures 3.23-3.26** and **Figure 5.1**) so the results can be compared with real world situations. The possibility of using the modified system for testing different sizes of cylinders means that the device can be used in the future to simulate a range of scenarios where larger samples needed to be tested. The existing capability to add or extract water smoothly at any time means that the modified device can potentially be used to simulate both low and high permeability materials. The small and simple vent system to apply/release pressure internally means that the water pressure within the cell can be carefully controlled.

The stainless steel used to manufacture the modified parts (see **Figure 3.23-3.26** and **Figure 5.1**) of the conventional oedometer device means that the problems associated with corrosion are limited. Variability in environmental conditions could potentially have affected the performance of the modified device during the long term tests. Monitoring of the test room showed that environmental variability was limited and is not thought to be significant. In addition, once pressurised, the triaxial cell (**Figure 3.23-3.26** and **Figure 5.1**) maintained constant pressure.

As a result, it is possible to say that the modified device represents an improvement on standard methods used to assess the creep of rock.

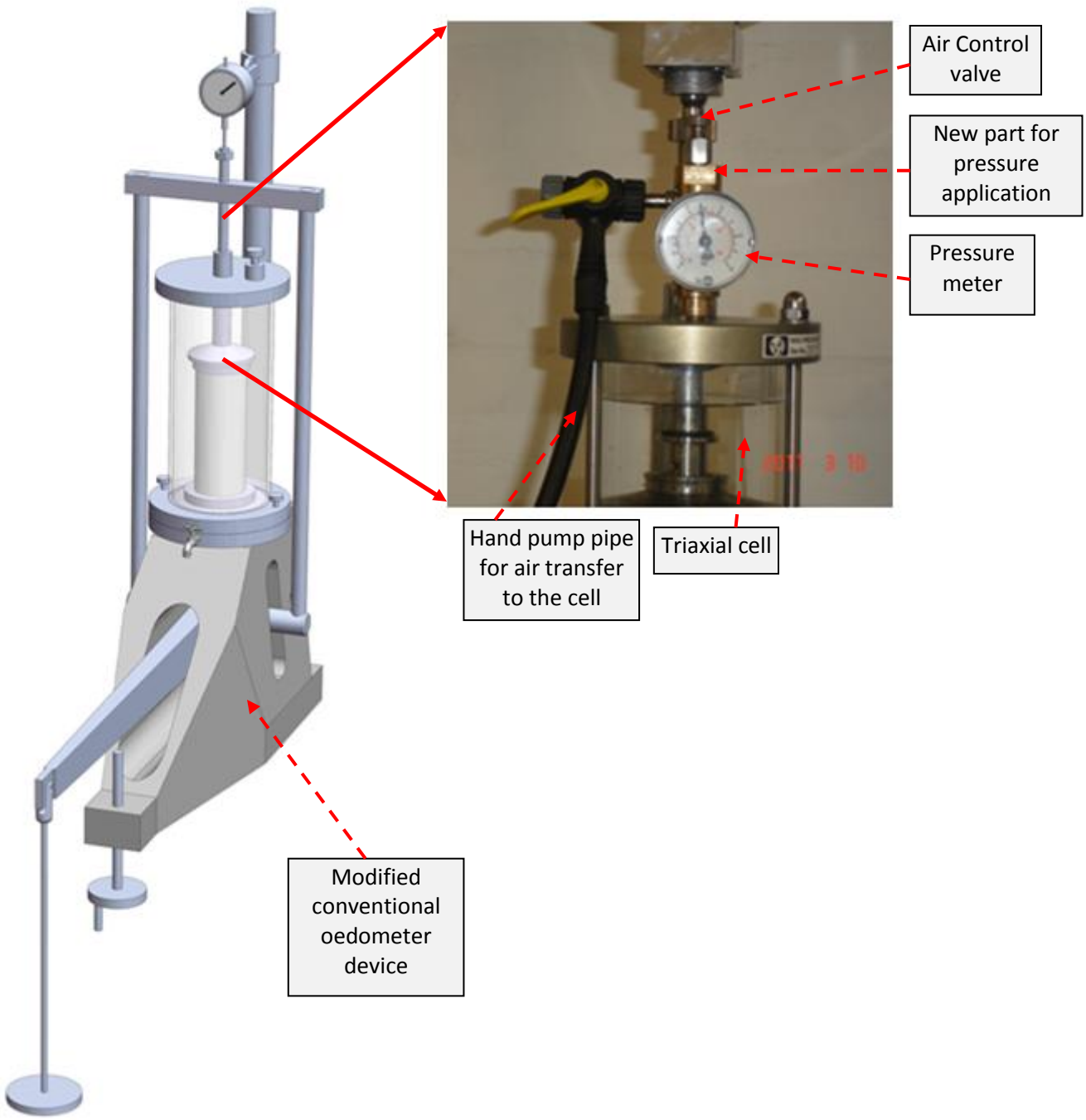

Fig. 5.1: Triaxial cell showing the modifications for pressure application.

5.3.2 Assessment of the modified bending (four-point bending) device

The experimental datasets of long-term (creep) testing in **Section 4.4.2** show clearly that the modified conventional oedometer system designed for four-point bending can successfully be used to examine creep behaviour in both air-dry and saturated gypsum rock at atmospheric pressure.

It has been previously established that a lever system is suitable to be used in the application of creep stress on rock sample (see **Section 2.7.1**) and can be used for bending (Price, 1964).

There are 4 possible ways to assess the validity of the bending experimental method: **1)** Accuracy, **2)** Flexibility of repeating experiments, **3)** Real world conditions simulation, and **4)** Environmental impacts.

In term of accuracy and precision, repeated tests on similar samples produced similar results.

Photographs of parts of developed conventional oedometer device **(Figures 3.30-3.31)** show the simple design. Experience has shown that the device is easy to operate by one person for analysis of both air-dry and saturated samples and small and large test bars. The manual loading system (**Figure 3.28**), small area required, none reliance on electrical or hydraulic systems and the process of changing water also strongly support the simple and robust way of testing creep by the developed device.

One of the aims of this experimental device was to be able to simulate conditions where dissolution, or another erosive process, had formed a cavity in gypsum (**Figure 3.30-3.31** and **Figure 5.2-5.3**). The possibility of using the developed system for testing two sizes of four-point bending bars allows some appreciation of the impact of cavity size.

Variability in environmental conditions could have affected the performance of the modified device during the long-term tests. Monitoring of the test room showed that environmental variability was limited and is not thought to be significant. The stainless steel used to manufacture the modified parts (**Figure 3.30-3.31** and **Figure 5.2**) of conventional

oedometer device means that the problems associated with corrosion are limited and successfully control the surrounding environmental effects on modified device.

The simplified method to convert the modified device between small sample form and large sample form reveal the simplicity of this device to test various measurements of rock bars.

All these conditions greatly support the improvement of the modified conventional oedometer device for four-point bending creep of rock compared to published methods.

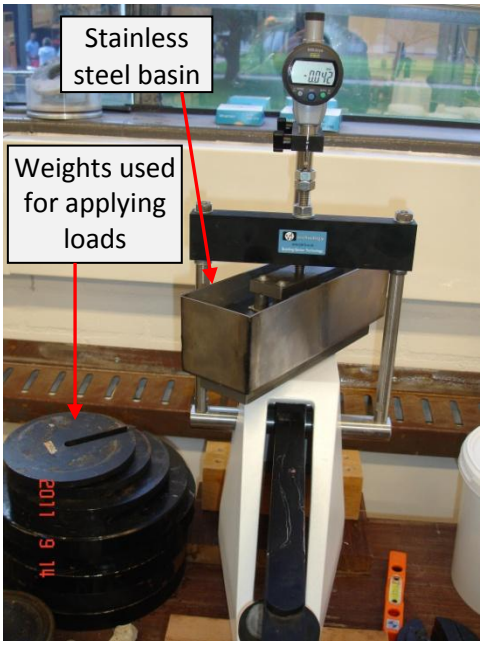

Fig. 5.2: Modified oedometer device for testing four-point bending bars in two sizes of 240 x 40 x 20 mm and 140 x 40 x20 mm. This system can be used for testing dry and soaked bars under atmospheric pressure inside the stainless steel basin.

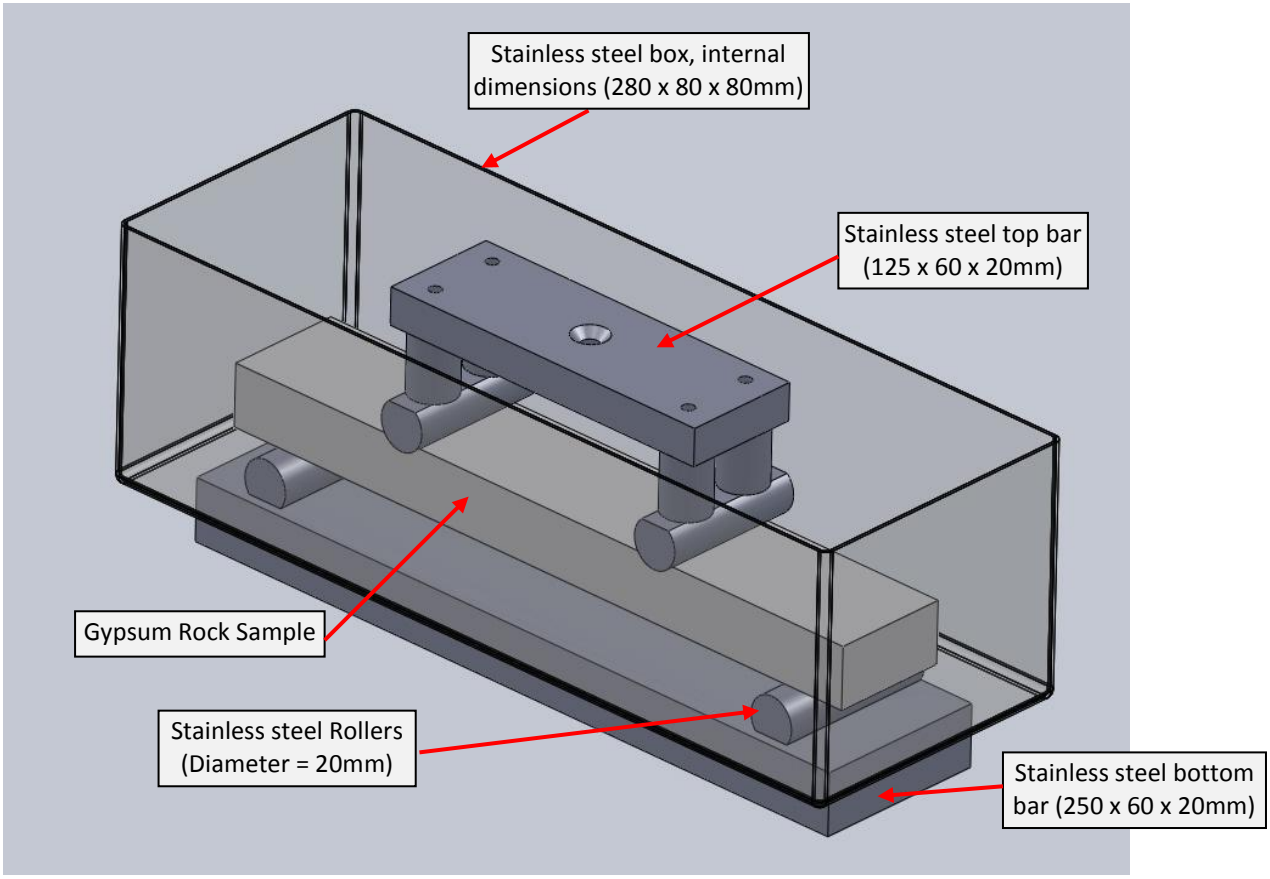

Fig. 5.3: Plan of modified oedometer device for testing four-point bending bars in two sizes of 240 x 40 x 20 mm and 140 x 40 x 20 mm, same system of testing in above Figure 5.2. Solid works program used to draw this sketch.

5.4 The extent to which the findings presented in this thesis can be applied to other areas?

This thesis presents the results of experimental work that uses the conditions at Mosul Dam as experimental constrain. This section addresses the extent to which the outcomes of this work may be applied to other dams.

There are 4 possible factors can be assess in order to find the suitability of this thesis work to other areas: **1)** transmitted stress from the Mosul Dam, **2)** problematic layer features of the Mosul Dam, **3)** volume of the reservoir of the Mosul Dam (Implications of water pressure as a control at different sites) and **4)** Dam's dimensions.

Similar to Mosul Dam, other dams of various sizes built on gypsum substrates also suffer from dissolution (see **Section 2.11-2.14**). Overall, this analysis leads to the conclusion that there is good evidence that the approach and findings of the Mosul Dam case study are applicable to other similar sites of dams constructed on soluble substrates.

It has been previously established that the Mosul Dam embankment is 113 metres high and the total volume of material in the embankment is reported to be approximately 37.7 million cubic metres. The embankment has a crest elevation of 340 m and upstream and downstream slopes measuring 1:2.5. One metre thick riprap covers the entire upstream slope. The active storage is over 8.1 billion cubic meters and total storage at maximum operating pool volume is 11.1 billion cubic metres (CENWD, 2003; Al-Faraj, 2005; SIGIR, 2007; Al-Taiee and Rasheed, 2009).

Evidence collected from various studies on dams built on soluble rocks show that gypsum rocks are distributed in the foundation and/or area of dams in various thicknesses as intact or inter-bedded with other minerals. Those studies on various dams' features were compared with Mosul Dam features shown as following in **Table 5.1** and **Figures 5.4-5.8**:

Table 5.1: Comparison among Mosul dam features with other dams constructed on problematic substrates.

Dam Name	Dam Type	Height of Dam (m)	Length of Dam (m)	Size of Dam (km^3)	Volume of Reservoir (km^3)	Problematic Layer Thickness or Features	Problematic Layer Depth	Reference
Mosul Dam, Iraq	Earth dam	113	3400	37700	8100000	Lenses, thin layers and thick layers of gypsum, anhydrite, marl and limestone inter-bedded with other minerals	Near and under the dam	CENWD (2003), SIGIR (2007)
Sanford Dam, USA	Earth dam	70	1954	Not given	17144	1-1.5m veins of gypsum in the abutment, at 30m depth large thicknesses of gypsum and anhydrite	Shallow and at 30m	Calcano (1967); Canadian River Project (2012)
A dam on the border line of lower Fars formation, Middle East	Earth dam	20	1500 m crest length	Not given	80000	First gypsum bed is about 4 m, the second gypsum bed is about 16 m	first bed is very shallow, second bed is at 12-25m depth	Calvino et al. (1981)
Keban Dam, Turkey	Concert and rock fill dam	211	1097m crest length	15585.5	30600	200-500m karstic marble and limestone	At the surface (outcrop)	Ozbek (1975); Ertunc (1999)
Ataturk Dam, Turkey	Rock fill dam	184	1820	84500	48.5	Dolomatic and bituminous and plaquette lime stone	From the surface to deep	Ertunc (1999)
Red Rock Dam, USA	Earth dam	30	2000	Not given	31080	Up to 6 m	3-12m beneath the surface rock in the cut-off wall	Calcano (1967)
Lower Kafirnigan Dam, Tadzhik SSR	Earth dam	70	210	Not given	Not given	35cm gypsum	at top	Nedriga and Dem'yanova (1986)
Tbilisi Dam, USSR	Concrete Dam	Not given	Not given	Not given	Not given	10-15m contain 7-21% gypsum	Upper zone of the foundation	Nedriga and Demyanova (1986)
Chamshir Dam, Iran (Designed and under study)	Concrete Dam	155	Not given	Not given	1800000	Gachsaran Formation in the area of the Dam, this formation has seven members, three of them in contact with the dame site(5, 6 and 7) are 324, 258 and 139m thick, each of these them has gypsum inter-bedded with other minerals	Not given	Kaveh et al. (2011); Kaveh et al. (2011)
San Juan Reservoir, Spain	Earth dam	3	700	31.5	850	4m of loose sand and silt with 37-40% gypsum	Under the dam	Gutierrez et al. (2003)

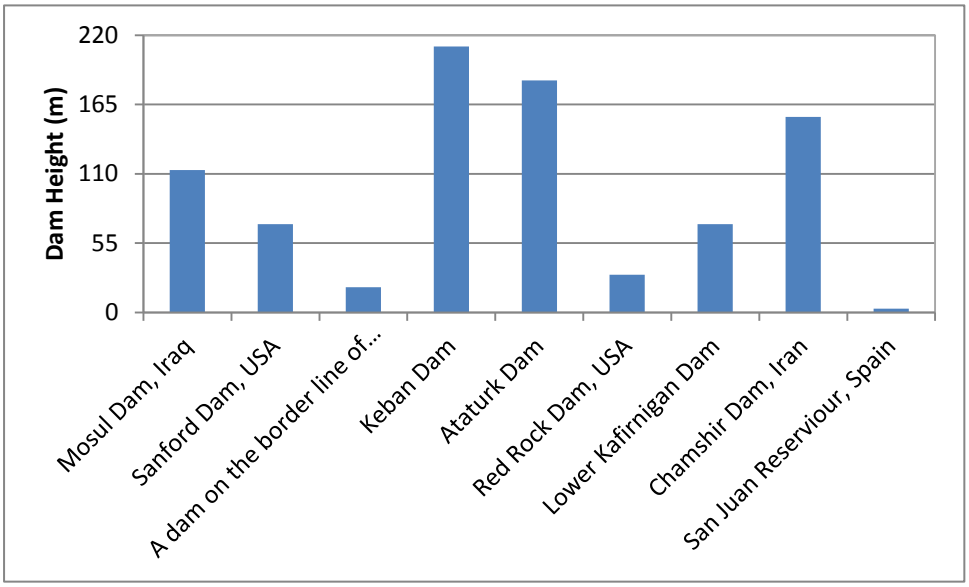

Fig. 5.4: Comparison of the Mosul Dam height and other dams constructed on problematic substrates.

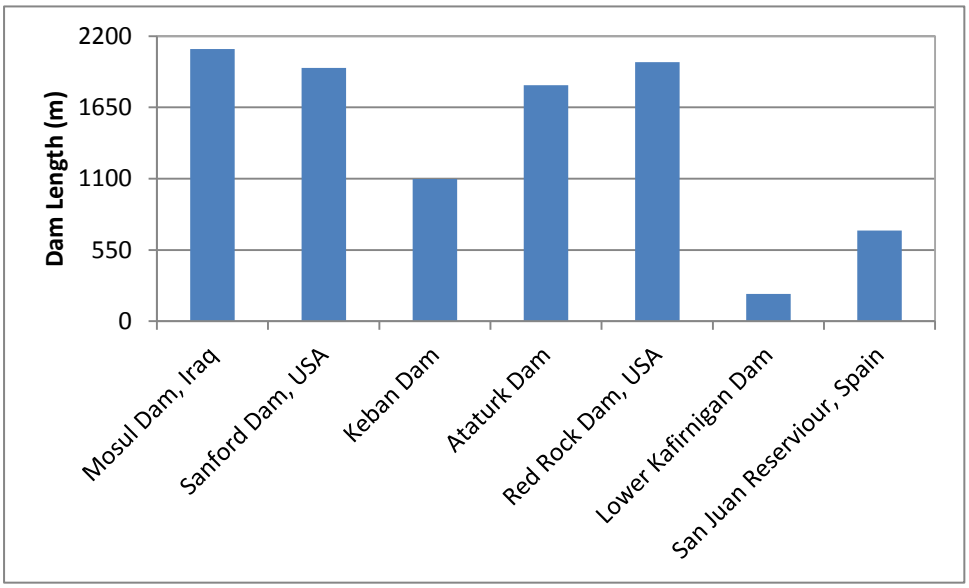

Fig. 5.5: Comparison of the Mosul Dam length and other dams constructed on problematic substrates.

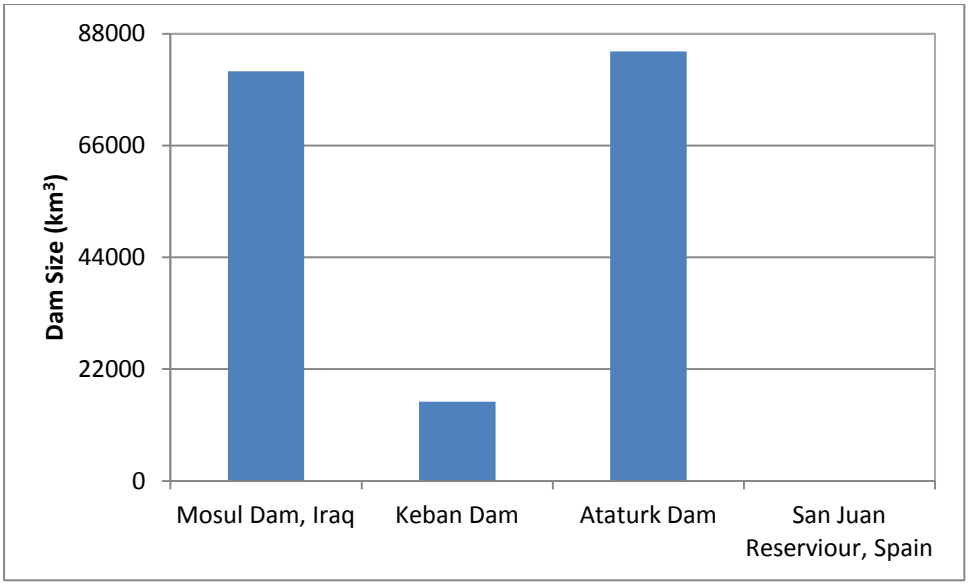

Fig. 5.6: Comparison of the Mosul Dam size and other dams constructed on problematic substrates.

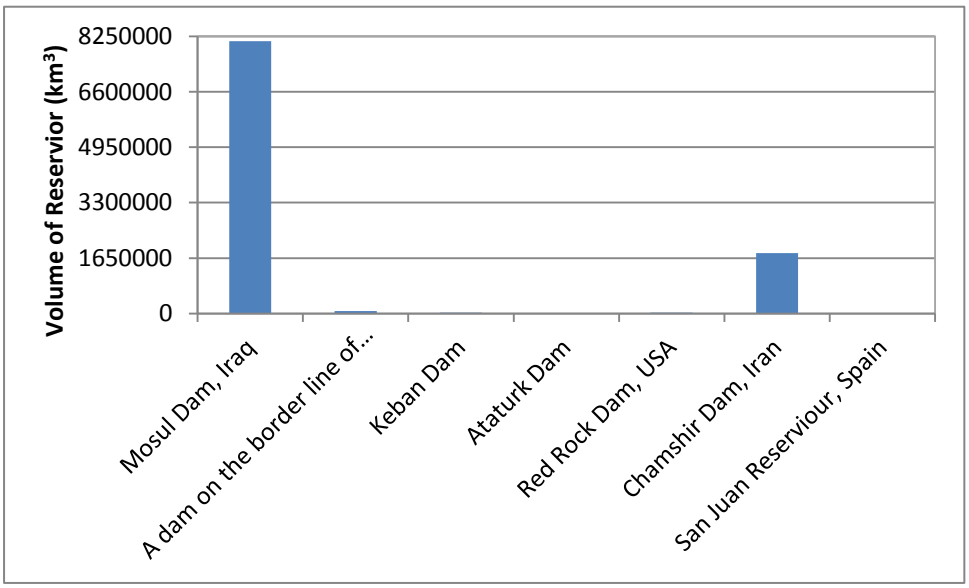

Fig. 5.7: Comparison of the Mosul Dam volume of reservoir and other dams constructed on problematic substrates.

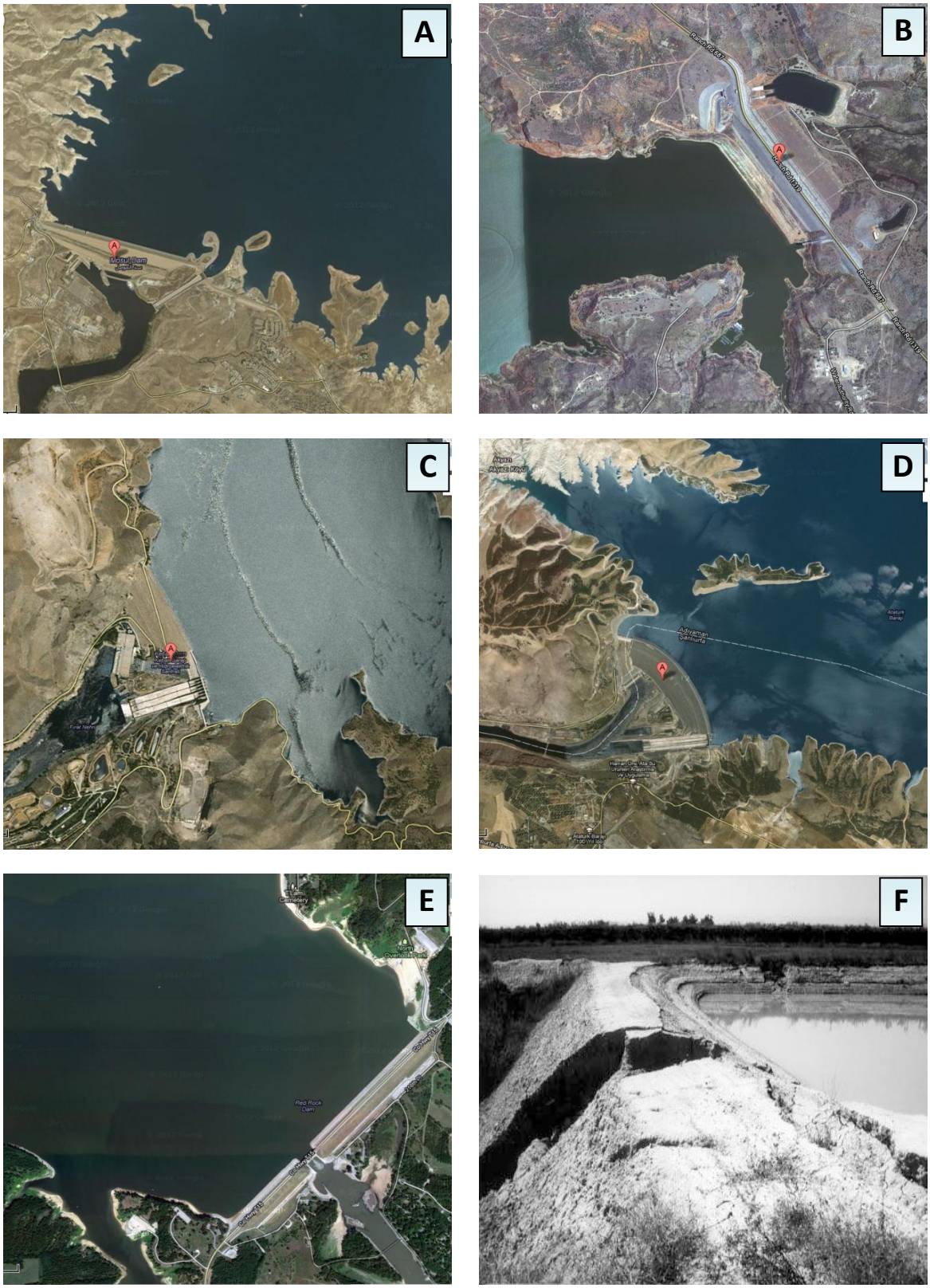

Fig. 5.8: Photographs of some of the dams listed in Table 5.1. Part A is Mosul Dam, Iraq. Part B is Sanford Dam, USA. Part C is Keban Dam, Turkey. Part D is Ataturk Dam, Turkey. Part E is Red Rock Dam, USA. Part F is San Juan Reservoir, Spain (Gutierrez et al., 2003, Figure 1), the dam failed because of gypsum dissolution and piping creating a large collapse scar).

The long-term tests shown in **Section 4.4** which were based on previous information of the Mosul Dam, yielded notable strain values after the application of axial stresses of 1792 and 2688.35 kPa. Although these stresses are not high they are about quarter of the compressive strength values they caused two cylinders' failure (see **Figure 4.62/A** and **4.91/F**).

The sum up of these points shows that the Mosul Dam is quite large and as a barrier it is impounding a massive quantity of fresh water from the Tigris River. Other large, medium and small dams store different amounts of water in their reservoirs and are still stable despite the presence of soluble layers underneath. There are also areas proposed to build dams also rich with soluble layers of rock. The experience from Mosul Dam and the results of this study indicate that it would be wise to implement a very detailed site investigation before any other dams are constructed in areas underlain by gypsum.

In this section, two kinds of datasets are cross-compared in order to test the deduction that there is good evidence that the case study of Mosul Dam (the findings in this study experimental works) is servant when considering similar sites of dam constructed on soluble substrates. Short and long terms testing with sub-major datasets for each one are the first kind. Data collected on the dams mentioned in **Table 5.1** and **Figure 5.4-5.8** represent the second kind. Further down follows a detailed discussion for each factor in turn to evaluate them according to their role to assess the possibility of this study's outcome to be applied to other similar dam sites.

5.4.1 Transmitted stress from the Mosul Dam

Values of applied stress stages shown in **Figure 4.49/C & D**, **Figure 4.51-4.52** and **Figure 4.58-4.62** yielded valuable information on the duration and amount of applied stresses on various gypsum rock samples (thin and thick layers as cylinders) in order to simulate the real size condition of the Mosul Dam. The time-strain percent relationship which is shown in **Figure 4.51/A & B** and **Figure 4.58/A** revealed the response of thin and thick layers of gypsum rock for the 1792 kPa axial stress, which is slightly higher than the stress transmitted from the Mosul Dam to the gypsum layers in the foundation. The increasing value of applied stress to 2688.35 kPa which is shown in **Figure 4.51/A & B**, **Figure 4.58/B** and **Figure 4.62/A** showed the response of thin and thick layers of gypsum rock to this high

stress, which is much higher than the Mosul Dam stress. This high examined stress (2688.35 kPa) increase the possible cases of application of the current study data on other larger dams compare to the condition of the Mosul Dam.

For comparison, the transmitted stresses from Keban and Ataturk Dams in the Turkey and San Juan reservoir dam in Spain (see **Table 5.1** and **Figures 5.6** and **5.8**) which are lower than 2688.35 kPa (applied stress in this study) due to their smaller sizes. The Ataturk Dam is larger than Mosul Dam, the conducted experiments of 2688.35 kPa in long-term condition of thin and thick layers (**Section 4.4**) is much higher than transmitted stresses from the Mosul Dam, they possibly cover the state of the Ataturk Dam.

5.4.2 Problematic layer features of the Mosul Dam

Results of short-term tests, shown in **Section 4.3,** confirm that the experimental approach using a variety of experimental parameters (such as thick and thin layers of gypsum rock and two different sizes of caves roofing simulated by small and large four-point bending tests, cases simulated from the Mosul Dam site), is valid. The results of long-term tests, which are shown in **Section 4.4,** verified the applied conditions of the short-term tests and showed the possibility of applying various cases of long-term tests in the laboratory.

The context of the Mosul Dam was used in the research reported here to establish laboratory test parameters. While the Mosul Dam is a particular case, conditions there are comparable with many other dams sites (**Table 5.1**) which means that the results are likely to indicative of processes and behaviour at those sites.

5.4.3 Implications of water pressure as a control at different sites

The results of short-term tests shown in **Section 4.3** show the multiple water pressure levels used in this part of the research for immersion gypsum rock samples. Values of those short-term results reveal the role of water pressure as a significant factor.

The results of long-term tests using real world conditions based on the Mosul Dam site, shown in **Section 4.4**, also showed the role of water pressure to be significant. The experiments showed that long-term tests can be successfully executed and provide a useful insight into the influence of prolonged dissolution under pressure on mechanical properties.

The parameters assessed during the long-term tests showed that water pressure is positively correlated with dissolution-induced weakening of gypsum rock. For example, when water pressure was applied at atmospheric and 5.0 bar pressure on thick layer/cylindrical samples, thin layer samples in air-dry and saturation state under atmospheric pressure and on small and large four-point bending bars in air-dry and saturation state under atmospheric pressure, the time to failure was shorter.

The information from **Table 5.1** and **Figure 5.7** revealed the importance of the large size of Mosul Dam reservoir compared with the rest of the other dams' reservoir in the table. This information shows the large size is taken into account in this study as 5.0 bars water pressure, which caused the failure of the white/Bantycock cylinder after 4000 hours as shown in **Figure 4.91/F**. Through this it can be seen the significant role of water pressure from the Mosul Dam reservoir contributed to failure, which is greater than the pressure of the water of the other dams' reservoir. The water pressure transmitted from the reservoir of other dams may cause failure, but this needs further study to assess the role of lower than 5.0 bar water pressure to cause failure of gypsum rocks.

5.4.4 Dam's dimensions

The Mosul Dam is larger than most other dams (**Figure 5.4**, **5.8**, **Table 5.1**). The information derived from the **Figures 5.4** and **5.5** shows that the Mosul Dam is the largest dam compared to the other dams mentioned in those two figures.

The use of the Mosul Dam specifications in this research (**Section 4.4**) in some parts of the long-term tests of the laboratory work (the simulation of 1792 kPa stress) and, in other parts of the long-term tests, of a load greater than at Mosul Dam (the simulation of 2688.35 kPa) shows that the work completed in this research is relevant to other sites.

Overall, that the following observations can be made:

5.4.5 Summary of the extent to which the findings presented in this thesis can be applied to other area

- The maximum loading stress used in the experiments (2688.35 kPa) is higher than the transmitted stress from the Mosul Dam and possibly is comparable to maximum stress at any of the dams listed in **Table 5.1**.

- The range of experiments conducted as part of the current research simulates a range of ground conditions which reported evidence shows exists at Mosul and many other dam sites.
- Simulated cases used to study the effect of water pressure from the Mosul dam reservoir are significant.

All those conditions support the conclusion that the finding of this experimental study can be applied to enable better understanding of processes occurring at other dam sites.

5.5 To what extent can the methods applied on gypsum rock samples be applied to gypseous soils?

It has been established previously that any gypseous soils with more than 2% gypsum content is unsuitable for foundations of hydraulic structures (Alphen and Romero, 1971). More focused work on gypseous soils has revealed the following information:

- Prolonged soaking causes a drop in gypsum content and a serious decrease in both the CBR (California Bearing Ratio) and the M_R (Resilient Modulus) (Razouki and Kuttah, 2004; Razouki et al., 2008).
- Compressibility increases with the addition of clay (Azam, 2000) or sand to calcium sulphate (Tran et al., 2012).
- The presence of gypsum content increases collapse potential and decreases peak shear strength, angle of internal friction and void ratio (AlNouri and AlQaissy, 1990; Fattah et al., 2008; Tran et al., 2012). An increase in gypsum content also decreases compression index, swelling index, cohesion and increases angle of internal friction.
- Long-term saturation can cause localised settlement, depending on the type of soil, initial gypsum content, relative amount of leached salts, soil properties and the acting load (Petrukhin and Boldyrev, 1978; Salih, 2003).
- Increasing the pressure applied on gypseous soil in long-term tests revealed that it can cause an increase in the recorded settlement values (Salih, 2003).
- Evidence collected on the seepage of flooding water through gypseous soil strata show that it causes a reduction in soil gypsum content and this reduction increases

with depth. The seepage of flooding water affects the distribution of soil grains associated with gypsum in the gypseous soil as following; gravel percent is not affected, sand percent decreased, while silt and clay percents were exhibited to appreciably increase. It also causes a decrease in cohesion in the first 50 cm of 150 cm depth while, for 125 to 150 cm depth, a marginal increase was observed. The reduction value (24%) of angle of internal friction remained fairly constant with depth due to dissolution (Salih, 2003).

- Evidence collected using the oedometer and permeability-leaching equipment for gypseous soils tests revealed that they can be successfully used to calculate the soaking and washing properties of gypseous soils through Long-term experiments. The study showed that the washing time increased soil settlement linearly, volumetric strain-time curves consist of sudden collapse and creep occurrence, and collapsibility may be considered as time dependent. Most of the compression process occurs during the first weeks of washing period and secondary compression at the later stages (Al-Neami, 2000).
- The data that have been collected in this study (**Figure 4.75-4.76**) showed that gypsum content increases the amount of dissolution and decreases the maximum soil strain percent.
- The chemical aggressivity of the water used to saturate the samples affects the rate of dissolution over time (**Figure 4.74 and 4.78/B**).
- Continuous water flooding over a 50 weeks time period has a significant role in the weakening of the geotechnical properties of gypseous soil strata and in the gypseous soil resistance to compression as tested in both short and long term tests (**Section 4.7**).
- The data that have been collected in this study (**Figure 4.76**) show that the dissolution process weakens the gypseous soil samples and decreases their response to axial stresses. This role may result from an increase of void ratio due to dissolution, which weakened the soil structure.

The work carried out during the current study suggest that there are 5 major variables that can be controlled to examine the mechanical response of gypseous soils to dissolution: **1)** Maintenance of the aggressivity of saturation water over time, **2)** Quantity of gypsum

(gypsum content) in examined samples, **3)** Influences of non-gypsum minerals in the soil samples, **4)** Duration of soaking and frequency of the water changes, and **5)** Gypsum particle sizes.

The sum of these points shows that the purity of the saturation water plays a notable role to keep regular dissolution process. Gypsum content has a significant role in the geotechnical properties of gypseous soil. Dissolution over time progress also play a significant role in disturbing and changing the chemical and geotechnical properties of gypseous soil strata. Note however that the mentioned change in the geotechnical properties of gypseous soil due to dissolution of its gypsum mineral may be influenced by the type and percent of accompanies minerals (non-gypsum minerals) to the gypsum in the bulk gypseous soil strata and/or the methods of tests in the laboratory. Overall, this analysis leads to the deduction of that there is good evidence that the simulated conditions, based on the context of the Mosul Dam can be applied on gypseous soils.

5.5.1 Maintenance of the aggressivity of saturation water over time

The process of repeated replacement of the saturation water during long-term tests maintains it aggressively. This replacement simulated slow flow of under-saturated groundwater through natural soils (**Section 4.6**). The impact of the water replacement on dissolution is shown by the stepwise segments shown in the time-strain percent relationships (see **Figure 4.73**). This is also shown by the increasing values of axial strain percent observed in **Figure 4.76/C** and the decreasing values of gypsum content due to long term dissolution shown in **Figure 4.75/A** and **4.76/A & B**.

The decreasing values of conductivity readings due to gypsum dissolution process are strongly related to the presence of regular changes of pure water with time (**Table 4.26** and **Figure 4.75/A**). This is similar to the findings of Razouki and Kuttah (2004) and Al-Farouk et al. (2009), whose studies showed a link between dissolution and both the regularity of water changing and the water's aggressivity.

Thus, the information derived from both above studies confirmed the importance of aggressivity of water of saturation for the studies on gypseous soil.

5.5.2 Quantity of gypsum (gypsum content) in the examined samples

Short-term tests on gypseous soil samples yielded valuable evidence of the impact of gypsum content on the variation of geotechnical properties of these samples.

Values of these geotechnical parameters are closely related to gypsum content, as can be seen in **Figure 4.67/D** and **4.68-4.69**. The increasing values of compression index, expansion index and cohesion (for consolidated un-drained shear test) revealed the significant role of gypsum content in controlling gypseous soil properties. Other parameters such as initial void ratio, natural water content, specific gravity and angle of internal friction typically decrease with a certain level of gypsum content increase and then tend to increase with more increase in the gypsum content. Such behaviour may be attributed to the role of other minerals in the bulk gypseous soil samples (see below). The particle size distribution of non-gypsum soil minerals is likely to play an important role in causing variations of bulk gypseous soil samples geotechnical properties such as expansion index, initial void ratio, natural water content, specific gravity, cohesion and angle of internal friction (**Figure 4.68-4.69**).

Long-term tests of gypseous soil samples (see **Section 4.6.1-4.6.2**) showed that decreasing values of instantaneous strain percent due to increase of axial stresses are related to the increase of gypsum content values (**Figure 4.70-4.73**). However, those decreasing values of instantaneous strain percent may relate to non-gypsum minerals contained in the bulk gypseous soils samples (these will be discussed in the next section). The increasing values of creep strain of samples, and the decreasing value of strain percent with large gypsum contents (**Figure 4.73/B** and **4.76/A & C**) show the important influence of gypsum quantity on gypseous soil mechanical properties.

The increasing values of dissolution over time revealed the role of gypsum content to change also the chemical properties of gypseous soil through the dissolution values, the higher gypsum content soil records the higher dissolution value (**Figure 4.74**). Dissolution is greater for coarse sand-coarse gypsum samples. This is probably related to the larger area in contact with the water. The increased dissolution of coarse materials compared to fine materials seems unexpected. However, in the context of the soil finer particles would produce lower permeability rates, whereas coarse particles would lead to initially high flow rates. In addition, coarse gypsum particles are vulnerable to fracturing under loading,

creating fresh un-weathered surfaces. The mentioned role of gypsum quantity was verified by the increasing value of dissolution with the increasing value of gypsum content, as can be seen in **Figure 4.75/B**.

Fattah et al. (2008) and Tran et al. (2012) showed that an increase in gypsum content leads to a decreased angle of internal friction, as well as lower expansion indices and cohesion. Azam (2000) reported that compressibility increases with the addition of clay to calcium sulphate, while Tran et al. (2012) showed that compressibility decreased with decreasing salt percent and increasing sand percent. Furthermore, AlNouri and AlQaissy (1990) also showed that a gypsum content increase decreases compression index, swelling index, and cohesion. Their study, however, suggested an increase in the angle of internal friction over time for an artificially-prepared gypseous soil. This contrasts with a more variable, both positive and negative, change in angle of internal friction found in the current study. This may reflect the much finer, silty clay gypseous soil with very low gypsum content (1%) used by AlNouri and AlQaissy (1990) and that their samples were submerged in water with different percents of soluble gypsum which was also heated.

5.5.3 Influence of non-gypsum minerals in the soil samples

Short-term tests for gypseous soil samples demonstrated the impact of non-gypsum minerals (soil minerals) percent in the gypseous soil samples. These minerals affected geotechnical properties such as initial void ratio, settlement, specific gravity, angle of internal friction, cohesion, compression index and expansion index (**Figures 4.66-4.67**).

Long-term tests for various gypseous soil samples (**Section 4.6.1-4.6.2**) showed that these non-gypsum minerals influence soil mechanical properties such as instantaneous strain percent. The variety of increasing values of instantaneous strain percent due to axial stress increase is controlled by the soil particle size distribution as coarse soil particles show immediate settlement within loading. This causes immediate settlement when axial stress is applied (sandy Soils). However, differences in the values of instantaneous strain percent for tested samples may relate to the increase of gypsum content, discussed in **Section 5.5.2**, which changes the characteristics of the bulk gypseous soils samples. The variety of values of constant *A* of creep equations (as can be seen in **Tables 4.24-4.25**), which is related to the primary creep, suggest that soil particles have a role in how the soil samples behavior

changed with axial stresses application. As a result, following the work of Azam (2000) and Tran et al. (2012) as well as the current research, it seems likely that the exact mineralogical composition of the soil influences a range of geotechnical responses in the soil. The precise nature of this response, however, remains unclear and merits further investigation.

5.5.4 Duration of soaking and frequency of the water changes

Geotechnical parameters of gypseous soil samples were found to have been modified by soaking for 50 weeks, as can be seen in **Table 4.30** and **Figure**s **4.81-4.84** and **4.92**. These parameters showed that prolonged exposure to dissolution significantly weakened gypseous soil's resistance to axial stresses in addition to change the soil particle distribution in the examined gypseous soil strata. Other parameters such as specific gravity also follow in a generally similar pattern which verified the role of dissolution on gypseous soil strata. Moreover, the increasing values of other parameters such as angle of internal friction, water content, sand percent, wet density and dry density revealed the role of dissolution over 50 weeks to change the geotechnical properties of gypseous soil strata.

It is worth noting the change in the structure of gypseous soil strata due to 50 weeks flooding. The increasing cohesion values in the top layer (**Figure 4.81/C**) showed that the top layer compacted due to water flooding (**Figure 4.92**). The decreasing value of cohesion in the bottom layer showed that the dissolution leaves a weak and permeable layer due to water seepage at the bottom surface due to changing the flooding water each week. The decreasing values of silt percent in the bottom layer (**Figure 4.83/C**) also revealed the role of prolonged dissolution to change the particle size distribution of gypseous soils due to losses of clay and fine silt particles and redistributing other non-gypsum particles due to flooding. Moreover, the decreased values of specific gravity in the top and bottom surfaces of gypseous soil strata in general verified the role of 50 week flooding to change the structure of gypseous soil strata through dissolving more gypsum minerals from the top and bottom of the soil strata.

Long-term tests of various gypseous soil samples (see **Sections 4.6.3-4.6.4**) yielded valuable evidence of the impact of prolonged saturation on dissolution. The existing value of constant *B* of the creep equations shown in **Tables 4.24-4.25** revealed the dissolution increase over time and influence on the mechanical properties of those gypseous soil

samples. The variety among values of constant *B* relates to the applied axial stress and the soil samples' particle sizes, which can be supported by the differences of values of dissolution due to the differences in particle sizes and gypsum content of soil samples as shown in **Figure 4.76**.

Decreasing values of instantaneous and maximum strain and increasing values of creep strain due to leaching over 50 weeks of gypseous soil (**Figures 4.77/A & B** and **4.77/C & D**) showed how prolonged dissolution changes the mechanical response to axial stresses. The increasing values of conductivity readings shown in **Figure 4.78/B** and the differences among those readings (for gypseous soils samples before and after 50 weeks of flooding) also revealed the important role of prolonged dissolution on gypseous soil. The prolonged dissolution decreased the original soil gypsum content and thus lower conductivity readings were established for those samples after flooding for 50 weeks compared to original sample conductivity readings. The increasing values of constant *B* of creep equations (**Table 4.27**) also revealed the role of dissolution after 50 week to weaken gypseous soils samples, resulting in a higher creep rate. The information derived from the decreasing values of the dissolution-strain percent relationship shown (**Figure 4.79, Table 4.29**) and maximum creep strain due to loading stages (**Figure 4.80**) also showed that significant role of dissolution on gypseous soils over time.

The new experimental results, together with previous studies (Petrukhin and Boldyrev, 1978; Al-Neami, 2000; Salih, 2003; Razouki and Kuttah, 2004; Razouki et al., 2008) showed the significant role of dissolution over long time to be a control factor to change the geotechnical properties of gypseous soil. Furthermore, the new results show that a series of notable outcomes such as increases in permeability, changes of the original particle size distribution of gypseous soil strata, losses of very fine non-gypsum particles like clay takes place.

5.5.5 Gypsum particle sizes

Values of a variety of geotechnical parameters assessed by short-term tests are probably related to gypsum particle sizes as can be seen in **Table 4.23** and **Figures 4.67/D** and **4.68-4.69**. Although the variations of those parameters are related with other factors such as overall soil texture, gypsum content and continuous dissolution, they are likely to be

influenced by differences among gypsum particle sizes for each gypseous soil sample. Note however, those changed geotechnical parameters, were calculated from short-term tests so there was not sufficient time for slow dissolution to have an influence.

Long-term tests of gypseous soil samples (**Sections 4.6.1-4.6.2**) showed the impact of gypsum particle sizes on mechanical properties such as creep strain. In fine sand-fine gypsum samples the increasing values of creep strain due to increasing axial stresses are related to the gypsum particle sizes. The fine gypsum particles need less time to dissolve and thus cause higher creep strain due to constant stress applied over time. Other samples such as fine sand-(fine, medium and coarse gypsum) and medium sand-(fine, medium and coarse gypsum) also followed similar modes of behaviour under 1792 and 2688.35 kPa axial stresses.

Notable increases of creep strain values occurred in the coarse sand-coarse gypsum sample (**Figure 4.73/B**) under 2688.35 kPa axial stress, which may be due to the impact of high axial stress crushing gypsum particles and thus causing higher creep strain on time progress. The increasing value of constant *B* (**Tables 4.24-4.25**) of the creep equation of coarse sand-coarse gypsum sample shows influence of higher axial stress. Moreover, the reduction in gypsum content and the highest dissolution-maximum strain percent relationship of coarse sand-coarse gypsum sample (**Table 4.26**, **Figure 4.75/A** and **4.76**) after creep test also verified the influence of higher axial stress.

5.5.6 Summary of the extent to which can the methods applied on gypsum rock samples be applied to gypseous soils

Overall, the previous conditions discussed in this section (maintenance of the aggressivity of the saturation water over time, quantity of gypsum (gypsum content) in samples, presence of non-gypsum minerals in the samples, saturation over long time duration and gypsum particle sizes) show that:

- Maintaining the aggressivity of the water of immersion of gypseous soil samples is significant for dissolution process for both short and long term tests.

- Quantity of gypsum (gypsum content) in gypseous soil samples plays an important role in the samples' response to axial loading due to the continuous dissolution process.
- Non-gypsum minerals in the gypseous soil samples influence the behaviour of the bulk soil sample.
- Saturation over a long time has a significant role in the behaviour of gypseous soil samples. It provides weaknesses and voids due to the amount of gypsum that is being continuously removed by dissolution.
- Gypsum particle sizes play a notable role in gypseous soils behaviour. They contribute to soil collapsibility and compressibility through particle break down and dissolution.

The results from short and long term experiments discussed above, together with the comparison with published research on gypseous soils and how they are influenced by some environmental factors, show that the experimental approach applied in this research on gypsum rocks can also be successfully applied to gypseous soils.

5.6 Comparison between gypsum rock and gypseous soil

The experimental works on gypseous soils have revealed the significant role of vertical stress and continuous immersion to weaken them in a similar way to gypsum rocks. When the two types of gypsum-rich substrates are compared, there are a number of similarities and differences in their behaviour which can be summarised as follows:

A. Similarities:

1. There is a remarkable similarity between the gypseous soil and gypsum rocks in their respective dissolution as the weekly solubility rates are similar for each type.
2. Instantaneous and creep strain percents over time have been established in both cases, which result from the continuous dissolution of gypsum in addition to the axial loading effect.
3. The surface roughness of both gypsum rocks and gypseous soils was increased after the dissolution process (see **Figures 4.87-4.88** and **4.92/B**). At the start of the tests, the samples were smooth, but by the end of the tests, their surfaces were rough. For

the rock, dissolution created surface roughness amplitude of +/- 0.5 mm. For the soil, dissolution created a residual surface with coarse particles.

4. The whole settlement value of all gypseous soil and gypsum rock samples is the combination of the process of compaction and the process of compressibility enhanced by dissolution.
5. Both gypsum rocks and gypseous soils showed a range of responses, reflecting where they came from and their detailed characteristics.

B. Differences:

1. Permeability of gypseous soils is much higher than permeability of gypsum rock and this may lead to differences in the response of each type to soaking and axial loading.
2. Significant and very clear stepwise behaviour was obtained in the creep curves of gypseous soil samples, while lower visibility in the case of gypsum rock samples.
3. Instantaneous strain is higher in the case of gypseous soils than in the case of gypsum rocks. This is because of weak cohesion between gypsum with soil particles and strong cohesion between gypsum particles in gypsum rock.
4. The dissolution process in gypseous soils with soil grains appears to be influenced by impurities. In contrast, the dissolution process in intact clean gypsum rocks is semi-regular because of the lack of impurities present.
5. In the case of gypseous soils, the final behaviour of the tested sample is the combination of soil particles' reaction to vertical stress during immersion and the enhanced compressibility due to gypsum dissolution. However, in the case of gypsum rock, a small part of the behaviour results from the compaction while the larger part is from the enhanced compressibility after gypsum dissolution. Crushing of gypsum particles due to axial stress may also contribute to the bulk behaviour of gypsum rock sample.
6. The known gypsum content of a gypseous soil limits its reaction to a vertical load which is limited by the end of the dissolution process. Gypsum rock reaction to vertical load can be continuous either to the point of failure or ongoing creep adjustment to the continued dissolution with vertical load.

The outcomes of this study are presented in the conclusions chapter, Chapter 6.

CHAPTER SIX: CONCLUSIONS AND RECOMMENDATIONS

The conclusions of this research using evidence from the data assembled during the work for this thesis, demonstrate the following points:

6.1 Gypsum Rock

1. Water pressure applied to gypsum rock samples causes failure after a period of time and under the influence of axial stresses. Water pressure of 5.0 bars causes failure after a short time, 5.0 bars is equivalent to fifty metres of height of water column above the sample, simulating conditions in the reservoir of the Mosul Dam, which directly affects the gypsum-rich substrates near the surface underneath the Mosul dam and in the dam area.
2. Experiments demonstrate that the properties of dissolution under the influence of atmospheric pressure also caused significant changes in the samples of gypsum rock and also may cause failure; however this occurred after a long time of immersion and under applied vertical stresses on the samples (see **Figures 4.62/A**, **4.87** and **4.91/A & F**) with the amount of dissolution controlled in part by impurities inside gypsum rock samples on the solubility properties.
3. Experiments demonstrate the influence of the thickness of gypsum rock layers to cause the failure of dams built on them. Due to the lower amount of gypsum in thin layers, lower amounts of dissolution are obtained in addition to less deformation compared to the thick layers. Thick layers are more prone to failure than thin layers.
4. Comparisons between UK and Iraqi samples show that there are no substantial differences in the behaviours of at least two different rock formations of gypsum. Both have substantial numbers of highly visible fractures that facilitated failure. Differences are almost certainly due to impurities in gypsum rock samples. However, the Iraqi gypsum rock samples are stronger than the UK gypsum rock samples.
5. An increase of the size of the caves' roof causes a decrease in the time required for failure, causes also decrease of deflection ratio and deflection values required for failure.

6. Ultrasound can proved extra evidence (in addition to experimental results) on the importance of immersion under water pressure to reduce the compressive strength of gypsum rock samples more than immersion under atmospheric pressure.
7. Finally, this work emphasizes that the application of a lever system to simulate of long-term dam real situations through the modified devices shown in **Figures 5.1-5.3** is successful. The reliability of the data, the ease of preparation and testing, no requirement for electricity or hydraulic systems, the fast data gathering, the simple way to change and add the water of saturation needs only one person to do all the requirements of the test. These attributes make this modified device excellent equipment for long-term testing of uniaxial compression and four-point bending test.

6.2 Gypseous Soils

1. Evidence obtained through tests on gypseous soils proves that the grains of soil associated with gypsum in the soil samples have an effective role in the behaviour of the samples and their recorded settlement. The soil grains may exhibit immediate settlement and/or consolidation settlement, which depend on the grains particles sizes, coarse or fine grains.
2. Experiments prove that the recorded settlement of gypseous soils is from the compaction of soil particles in addition to the compressibility resulting from the dissolution of gypsum. It is likely that crushing of larger gypsum particles under weight added to the settlement of the gypseous soil.
3. Evidence shows that geotechnical properties were affected by the loading process on both short and long term timescales, but that the dissolution process acts over a long-term progression of time.
4. The approach of using several tests on gypseous soil demonstrates correlations between the findings of those methods. Strain of gypseous soils is clearly related to gypsum content and the dissolution process is clearly related to aggressivity of water of saturation.
5. Evidence shows that a layer of gypseous soil is subject to three separate but interacting influences, which are: 1) particle size distributions of gypsum and soil; 2) depth of burial of the soil; and 3) amount of water passing through the soil causing

dissolution. These processes are in addition to the recorded settlement that occurs due to dissolution of gypsum over time in the gypseous soil layer surface, mainly and notably in the areas adjacent to the walls of the box model. Dissolution of gypsum of gypseous soil strata changed the original particle size distribution along the soil layer.

6.3 Contribution to Knowledge

In relation to the research questions identified in Chapter 1, this thesis offers three contributions to knowledge:

A. To understand:

- A practical demonstration that water pressure has a significant role in causing dam failure over time.
- A new set of comparisons between short and long term test characteristics of UK and Iraqi gypsum rock, providing useful knowledge of similarities and differences.

B. To develop:

- New simple, easy to use and robust devices for compression and four-point bending test, which are very suitable for long-term tests.
- A practical demonstration of successful artificial preparation of Iraqi gypseous soil depending on UK soil and gypsum for resources.

C. To consider a practical demonstration of various conditions of the Mosul Dam site and foundation has established the applicability of the experimental work of this study to many other dams' sites or foundations.

6.4 Recommendations

Although this study reaches powerful conclusions from the scientific point of view, further work in the future is required and will be useful to discover the further aspects after this research. Some suggestions concerning work on both gypsum rock and gypseous soils are given as following.

6.4.1 For Gypsum Rock

A. The research work cannot determine the influence of water pressure on the four-point bending test; therefore further study is required for water pressure application during creep tests of four-point bending bars. Thus, examination of water pressure influences on four-point bending bars has not been established in the experimental work of this study and the application of it will help to understand more about the real conditions underneath dams built on soluble substrates and minimize the uncertainty factors of those dams' in terms of stability issues.

B. Tests were conducted at atmospheric pressure and at 5.0 bars. To fully understand the role of water pressure, and simulate conditions at other dams and reservoirs, further study using other pressures is needed.

C. The research has identified that impurities play a role in dissolution but further work to clarify the mechanisms and full impact of this control are required.

D. The research did not focus on the impacts of multiple problematic substrates present together underneath dams. Study of multi-problematic layers, joints impacts, simulations of karstic features, reservoir volume influences and the deteriorations after seepage of those layers, can all be done in future work.

6.4.2 For Gypseous Soil

A. Gypsum content is significant and clearly is a problem in gypseous soils. Therefore, further study is required on artificially-prepared gypseous soils with various gypsum contents and various accompanying soil particles distribution.

B. It may be that water pressure controls some properties of gypseous soils. Therefore, water pressure application on gypseous soils using different levels of pressure, may reveal further characteristics of gypseous soils of importance in dam stability. Only

saturation state with atmospheric pressure was considered in this study regarding gypseous soil samples.

C. The research work cannot determine the impacts of soil mineral types on the geotechnical properties of gypseous soils flooded for long time duration. Therefore, further study is required on physical soil strata models, different gypsum content and particle sizes and different non-gypsum mineral particle sizes.

To sum up, gypsum rock and gypseous soil samples tested robustly in short and long-term experiments, showed some similarities and differences. So, the results of this thesis can help to determine controls on failure of dams constructed on soluble substrates and therefore find solutions in order to achieve a long term protection for these dams against failure.

References

Abbas, M.K., Sedek, I.A. and Yahya, A.M. (1990) 'Study of Natural Conditions of the Reservoir Watershed of Saddam Dam, Natural Characteristics of Surrounding Lands' *2nd Sci, Conf, of Saddam Dam Research Centre.* Mosul University, Mosul-Iraq, 18-20 March 1990.

Abid-Awn, S.H. (2004) *Improvement of Gypseous Soils Using Locally Manufactured Reinforcement Materials*. PhD Thesis: University of Technology, Iraq.

Abou-Sayed, A.S., Brechtel, C.E., Tek, T. and Inc. (1976) 'Experimental Investigation of the Effects of Size on the Uniaxial Compressive Strength of Cedar City Quartz Diorite', *The 17th U.S. Symposium on Rock Mechanics (USRMS)*, August 25-27, Snow Bird, UT.

Afrouz, A. and Harvey, J.M. (1974) 'Rheology of Rocks within the Soft to Medium Strength Range', *Int. J. Rock Mech. Min. Sci.*, 11, pp. 281-290.

Agarwalk, K.B. and Joshi, D.K. (1979) 'Problems of Earth Dam Construction in the Deccan Trap of India', *Bulletin 20 of the International Association of Engineering Geology*, pp. 29-32.

Agustawijia, D.S. (2007) 'The Uniaxial Compressive Strength of Soft Rock', *Civil Engineering Dimension*, 9 (1), pp. 9-14.

Akram, M. and Bakar, M.Z.A. (2007) 'Correlation between uniaxial compressive strength and point load index for salt-rang rocks', *Pak. J. Engg. & Sci.*, 1.

Alainachi, I.H. and Alobaidy, G.A. (2009) 'Engineering Geological Study, in Part of Mohamed Bin Zayed City-Abu Dhabi-UAE', *EJGE*, 14 (bundle D).

Al-Alawee, A.B.G. (2001) *Treatment of Al-Therthar Gypseous Soil by Emulsified Asphalt Using Model Tests*. MSc Thesis: University of Technology, Iraq.

Al-Ani, M.M. and Seleam, S.N. (1993) 'Effect of Initial Water Content and Soaking Pressure on the Geotechnical Properties of Gypsiferous Soils', *Al-Muhandis*, 116.

Al-Dabbagh, T.H., Elias, E.M. and Khaleel, M.S. (1990) 'Determination of the Rate of Dissolution of Gypsum and Anhydrite from Saddam Dam Foundation', *Proceeding of the 2nd*

Sci Conf of Saddam Dam Research Centre. Mosul University, Mosul-Iraq, 18-20 March 1990, pp.341-353.

Al-Dabbas, M.A., Schanz, T. and Yassen, M.J. (2010) 'Proposed Engineering of Gypsiferous Soil Classification', *Arab J Geosci*, 5, pp. 111-119.

Al-Emami, O.H.F. (2007) *Collapsibility of Gypseous Soil under Fluctuation of Ground Water Table*. MSc Thesis: University of Technology, Iraq.

Al-Faraj, F.A.M. (2005) 'Iraqi Country Water Resources Assistance Strategy', *Water Resources and Hydraulic Engineering, National Consultant-Iraq, FAO/WB*.

Al-Farok, O., Al-Damloji, S., Al-Obaidi, A.L.M., Al-Omari, R.R., Al_Ani, M.M. and Fattah, M.Y. (2009) 'Experimental and Numerical Investigations of Dissolution of Gypsum in Gypsiferous Iraqi Soils', *Proceedings of the 17th International Conference on Soil Mechanics and Geotechnical Engineering*, M. Hamza et al. (Eds.), 2009 IOS Press.

Ali, S.A. (1979) *Creep Properties of Evaporite Rocks with Particular Reference to Gypsum*. PhD Thesis: University of Sheffield, UK.

Aliha, M.R.M., Ayatollahi, M.R. and Kharazi, B. (2009) 'Numerical and Experimental Investigations of Mixed Mode Fracture in Granite Using Four-Point-Bend Specimen', *Damage and Fracture Mechanics: Failure Analysis of Engineering Materials and Structures*, pp. 275-283.

Al-Layla, M. T. and Thabet, K. M. (1990) 'Formation of Cavities in the Alluvial Deposits in Mosul City' *Proceeding of the 2nd Sci, Conf, of Saddam Dam Research Centre*. Mosul University, Mosul-Iraq, 18-20 March 1990, pp. 172-185 (In Arabic Language).

Al-Mufty A.A. and Nashat I.H. (2000) 'Gypsum Content Determination in Gypsum Soils and Rocks', *3rd International Jordanian Conference on Mining*, pp.500-506.

Al-Neami, M.A.M. (2006) *Evaluation of Delayed Compression of Gypseous Soils with Emphasis on Neural Network Approach*. PhD Thesis: University of Technology, Iraq.

AlNouri, I.A. and AlQaissy, F.F. (1990) 'Gypsum Migration and its Effect on Compressibility and Shear Strength', *Symposium on Recent Advances in Geotechnical Engineering*, Singapore 6 July 1990.

Alphen, J.G. and Romero, F.R. (1971) 'Gypsiferous Soils, Notes on their Characteristics and Management', *Bulletin 12 of International Institute for Land Reclamation and Improvement*. Wageningen-The Netherlands, Available at: http://edepot.wur.nl/60171 (Accessed: 17 July 2012).

Al-Saigh, N.H. and Toffeq, A.N. (1990) 'Geological and Geophysical Study of the Southern Part of Saddam Dam Reservoir', *Proceeding of the 2nd Sci. Conf. of Saddam Dam Research Centre*. Mosul University, Mosul-Iraq 18-20 March 1990.

Al-Taiee, M.T. and Rasheed, A.M.A. (2009) 'Simulation Tigris River Flood Wave in Mosul City Due to a Hypothetical Mosul Dam Break' *Proceeding of Thirteenth International Water Technology Conference*. IWTC 13: Hurghada, Egypt.

Al-Zubaydi, J.H.A. (1998) *Engineering Geological Study of Selected Areas in Bahr Alnajaf, Middle Iraq*. MSc Thesis: University of Baghdad, Iraq.

Ameen, B. M. and Karim, K. H. (2007) 'Evidence of Tempestite and Possible Turbidite in the Middle Miocene Lagoonal Deposits of Lower Fars Formation, Kurdistan Region, NE-Iraq', *Germenal*, II, pp. 745-756.

Andrejchuk, V. and Klimchouk, A. (1996) 'Gypsum Karst of the Eastern-European Plain', *Int. J. Speleol*., 25 (3-4), pp. 251-261.

Aoki, H. and Matsukura, Y. (2008) 'Estimating the Unconfined Compressive Strength of Intact Rocks from Equotip Hardness', *Bull Eng Geol Environ*, 67, pp. 23-29.

Arakelyan, E.A. (1986) 'Characteristics of the Determination of the Physical Properties of Gypsum Soils', Translated from: *Osnovaniya, Fundamenty I Mekhanika Gruntov*, (1), pp. 20-21, January-February 1986.

ASTM (1996) 'Standard Test Method for Measurement of Collapse Potential of Soils', *ASTM Standards D5333-92*, (Reapproved 1996).

ASTM (2006) ‘Standard Test Method for Flexural Strength of Soil-Cement Using Smpile Beam with Third-Point Loading’, *ASTM Standards D1635-00*, (Reapproved 2006).

ASTM (2010) ‘Standard Test Method Compressive Strength and Elastic Moduli of Intact Rock Core Specimens under Varying States of Stress and Temperatures’, *ASTM Standards D7012-10*, (Approved 15/01/2010).

Auvary, C., Homand, F. and Hoxha, D. (2008) ‘The Influence of Relative Humidity on the Rate of Covergence in an Undergroud Gypsum Mine’, *International Journal of Rock Mechanics & Mining Sciences,* 45, pp. 1454-1468.

Azam, S. (2000) ‘Collapse and compressibility behaviour of arid calcerous soil formations’, *Bull Eng Geol Env,* 59, pp. 211-217.

Azam, S. (2008) ‘Engineering Behaviour of Clay-Bearing Calcium Sulphate in Dammam Dome, Eastern Saudi Arabia’, *Bull Eng Geol Environ*, 67, pp. 521-528.

Azam, S., Abduljauwad, S.N., Al-Shayea, N.A. and Al-Amoudi, O.S.B. (1998) ‘Expansive Charecterstics of Gypsiferous/Anhydritic Soil Formations’, *Engineering Geology*, 51, pp. 89-107.

Bashour, I.I. and Sayegh, A.H. (2007) ‘Methods of Analysis for Soils of Arid and Semi-arid Regions’, *Food and Agricultural Organization of the United Nations*, FAO Publication, Rome 2007.

Behnamtalab, E. (2012) ‘Experimental Evaluation of Solubility of Gypsum’, *Journal geological Society of India*, 80, pp. 262-266.

Bell, F.G. (1981) ‘Geotechnical Properties of Some Evaporitic Rocks’, *Bulletin 24 of the International Association of Engineering Geology*, pp. 137-144.

Bell, F.G. (1994) ‘A Survey of the Engineering Properties of Some Anhydrite and Gypsum from the North and Midlands of England’, *Engineering Geology*, 38, pp. 1-23.

Bell, F.G. (2007) *Engineering Geology*. 2nd edition. Butterworth-Heinemann: Elsevier.

Bieniawski, Z.T. (1967) 'Stability Concept of Brittle Fracture Propagation in Rock', *Engineering Geology*, 2 (3), pp. 149-162.

Bieniawski, Z.T., Denkhaus, H.G. and Vogler, V.W. (1969) 'Failure of Fractured Rock', *Int. J. Rock Mech. Min. Sci.*, 6, pp. 323-341.

Bieniawski, Z.T., Franklin, J.A., Bernede, M.J., Duffaut, P., Rummel, F., Horibe, T., Broch ,E., Rodrigues, E., Van Heerden, W. L., Vogler, U.W., Hansagi, I., Szlavin, J., Brady, B.T., Deere, D.U., Haweks, I., Milovanovic, D. (1978) 'Suggested Methods for Determining the Uniaxial Compressive Strength and Deformability of Rock Materials', *International Journal of Rock Mechanics and Mining Sciences & Geomechanics Abstracts*, 16 (2), pp. 135-140. Known by ISRM.

Biolzi, L., Cattaneo, S. and Rosati, G. (2001) 'Flexural/Tensile Strength Ratio in Rock-Like-Materials', *Rock Mech. Rock Engng*, 34 (3), pp. 217-233.

Biolzi, L., Labuz, J.F. and Muciaccia, G. (2011) 'A Problem of Scaling in Fracture of Damaged Rock', *International Journal of Rock Mechanics & Mining Scinces*, 48, pp. 451-457.

Bonetto, S., Fiorucci, A., Fornaro, M. and Vigna, B. (2008) 'Subsidence Hazards Connected to Quarrying Activities in a Karst Area: The Case of the Moncalvo Sinkholes Event (Piedmont, NW Italy)', *Estonian Journal of Earth Sciences*, 57 (3), pp. 125-134.

Boyadgiev, T.G. and Verheye, W.H. (1996) 'Contribution to a Utilitarian of Gypsiferous Soil', *Geoderma*, 74, pp. 321-338.

Bradshaw, R.L., Boegly, W.J. and Empson, F.M. (1964) 'Correlation of Convergence Measurements in Salt Mines with Laboratory Creep Data', *Proc. 6th Sym. Rock Mech.* Univ. Missouri, Rolla, pp. 501-513.

Brady, B.H.G. and Brown, E.T. (2004) *Rock Mechanics for Underground Mining*. 3rd edition. Springer Publication: The Netherland.

BS EN 12390-5 (2009) 'Testing Hardened Concrete-Part 5: Flexural Strength of Test Specimens', *British Standards*.

BS EN 13161 (2008) 'Natural Stone Test Methods-Determination of Flexural Strength under Constant Moment', *British Standard*.

BS EN 14614-2 (2008) 'Agglomerated Stone-Test Methods-Part2: Determination of Flexural Strength (Bending)', *British Standards*.

BS EN 15216 (2007) 'Characterization of Waste-Determination of Total Dissolved Solids (TDS) in Water and Elutes', *British Standards*.

BS EN 1926 (2006) 'Natural Stone Test Methods-Determination of Uniaxial Compressive Strength', *British Standards*.

BS ENV 1997-2 (1999) 'Uniaxial Compressive Strength and Deformability', *British Standard ENV 1997-2: A.15.2*, Page 95.

BS ISO 11277 (2009) 'Soil Quality-Determination of Particle Size Distribution in Mineral Soil Material-Methods by Sieving and Sedimentation', *British Standards*.

Buringh, P. (1960) *Soils and Soils Conditions in Iraq*. The Ministry of Agriculture, Baghdad. Veenman & Zonen, Wageningen: Netherlands.

Calaforra, J.M. and Pulido-Bosch, A. (1996) 'Some Examples of Gypsum Karst and the More Important Gypsum Caves in Spain', *Int. J. Speleol.*, 25 (3-4), pp. 225-237.

Calcano, C.E.F. and Alzura, R.A. (1967) 'Problems of Dissolution of Gypsum in some Dam Sites', *Bulletin of Venezuelan Society of Soil Mechanics and Foundation Engineering*, July-September 1976.

Calvino, F., Costantino, F. And Mirri, F.C. (1981) 'Design Criteria for a Dam, Reservoir and Irrigation System on a Middle East Evaporite Formation' *Bulletin 24 of the International Association of Engineering Geology*, pp. 53-55.

Canadian River Project (2012) *Sanford Dam*. Available at: http://www.usbr.gov/projects/Project.jsp?proj_Name=Canadian+River+Project (Accessed: 04 November 2012).

Cardani, G. and Meda, A. (1999) 'Flexural Strength and Notch Sensitivity in Natural Building Stones: Carrara and Dionysos Marble', *Construction and Building Materials*, 13, pp. 393-403.

Cardani, G. and Meda, A. (2004) 'Marble Behaviour under Monotonic and Cyclic Loading in Tension', *Construction and Building Materials*, 18, pp. 419-424.

Castellanza, R., Gerolymatou, E. and Nova, R. (2009) 'Experimental Observation and Modeling of Compaction Bands in Oedometric Tests on High Porosity Rocks', *Strain*, 45 (5), pp. 410-423.

CENWD (2003) 'Inspection of Mosul Dam (Formerly Saddam Dam), Tigris River, Iraq'. *Report*, 31 May-1 June 2003, [Online]. Available at: http://www.envirozan.info/EZ_Docs/Dams/Mosul_dam.pdf (Accessed: 17 July 2012).

Chardon, M. and Nicod, J. (1996) 'Gypsum Karst of France', *Int. J. Speleol.*, 25 (3-4), pp. 203-208.

Chen, Y.L. and Azzam, R. (2007) 'Creep Fracture of Sandstones', *Theoretical and Applied Fracture Mechanics*, 47, pp. 57-67.

Cho, N., Martin, C.D., Sego, D.C. and Jeon, J. (2010) 'Dilation and Spalling in Axially Compressed Beams Subjected to Bending', *Rock Mech Rock Eng*, 43, pp. 123-133.

Cogan, J. (1976) 'Triaxial Creep Tests of Opohonga Limestone and Ophir Shale', *Int. J. Rock Mech. Min. Sci. & Geomech. Abstr.*, 13, pp. 1-10.

Cooper, A.H. (1996) 'Gypsum Karst of Great Britain', *Int. J. Speleol.*, 25 (3-4), pp. 195-202.

Cooper, A.H. (1998) 'Subsidence Hazards Caused by the Dissolution of Permian Gypsum in England: Geology, Investigation and Remediation', in Maund, J. G and Eddleston, M. (eds.) *Geohazards in Engineering Geology*. Geological Society, London, Engineering Geology Special Publications, 15, pp. 265-275.

Cooper, A.H. (2006) 'Gypsum Dissolution Geohazards at Ripon, North Yorkshire, UK', *Field Trip Guide Ripon*, IAEG 2006.

Cooper, A.H. and Calow, R. (1998) 'Avoiding gypsum geohazards: guidance for planning and construction', *British Geological Survey Technical Report WC/98/5* [Online]. Available at http://www.bgs.ac.uk/dfid-kar-geoscience/database/reports/colour/WC98005_COL.pdf (Accessed: 15 November 2010).

Cooper, A.H. and Waltham, A.C. (1999) 'Subsidence Caused by Gypsum Dissolution at Ripon, North Yorkshire', *Quarterly Journal of Engineering Geology*, 32, pp. 305-310.

Cooper. A. H. and Saunders. J. M. (2002) 'Road and Bridge Construction across Gypsum Karst in England', *Engineering Geology*, 65, pp. 217-223.

Coviello, A., Lagioia, R. and Nova, R. (2005) 'On the Measurement of the Tensile Strength of Soft Rocks', *Rock Mech. Rock Engng*, 38 (4), pp. 251-273.

Daoxian, Y. (1997) 'Sensitivity of Karst Process to Environmental Change along the PEP II Transect', *quaternary International*, 37, pp. 105-113.

Day R.W. (2000) *Geotechnical Engineer's Portable Handbook*. McGraw-Hill: New York, USA.

Drescher, K. and Handley, M.F. (2003) 'Aspects of Time Dependent Deformation in Hard Rock at Great Depth', The Journal of the South African Institute of Mining and Metallurgy, pp. 325-335.

Dreybrodt, W., Romanov, D. and Gabrovsek, F. (2002) 'Karstification below Dam Sites: a Model of Increasing Leakage from Reservoirs', *Environmental Geology*, 42, pp. 518-524.

Dusseault, M.B. and Fordham C.J. (1993) 'Time-Dependent Behaviour of Rocks', in Hodson, J.A. (ed.) *Comprehensive Rock Engineering*. 3rd vol. Oxford: Pergamon Press, pp. 119-149.

Efimov, V.P. (2009) 'The Rock Strength in Different Tension Conditions', *Journal of Mining Science*, 45 (6), pp. 569-575.

Elizzi, M.A.S. (1976) *The Time Dependent Behaviour of some Evaporite Rocks*. PhD Thesis: University of Sheffield, UK.

El-Sayed, M.I. (1993) 'Gypcrete of Kuwait: Field Investigation, Petrography and Genesis', *Journal of Arid Environments*, 25, pp. 199-209.

Ertunc, A. (1999) 'The Geological Problems of the Large Dams Constructed on the Euphrates River (Turkey)', *Engineering Geology*, 51, pp. 167-182.

Eslami, J., Grgic, D. and Hoxa, D. (2010) 'Estimation of the Damage of a Porous Limestone from Continuous (P-and S-) Wave Velocity Measurements under Uniaxial Loading and Different Hydrous Conditions', *Geophys. J. Int.*, 183, pp. 1362-1375.

Fabre, G. And Pellet, F. (2006) 'Creep and Time-Dependent Damage in Argillaceous Rocks', *International Journal of Rock Mechanics & Mining Sciences*, 43, pp. 950-960.

FAO (1990) 'Management of Gypsiferous Soils', Food and Agricultural Organization of the United Nations Rome, [Online]. Available at: http://www.fao.org/docrep/t0323e/t0323e02.htm (Accessed on 09-03-2012).

Farid, A. and Habibagahi, G. (2007) 'Dissolution-Seepage Coupled Analysis through Formations Containing Soluble Materials', *Journal of Engineering Mechanics*, 133 (6), pp. 713-722.

Fattah, M.Y., Al-Shakarchi, Y.J. and Al-Numani, H.N. (2008) 'Long-Term Deformation of some Gypseous Soils', *Eng & Tech.*, 26 (12), pp. 1461-1485.

Fengxianga, C. and Mingjiang, W. (1983) 'Investigation of the Engineering Properties of a Dam Foundation Containing Gypsum Seams', *Rock Mechanics and Rock Engineering*, 16, pp. 275-280 (Technical Note).

Ford, D.C. and Williams, P.W. (1989) *Karst Geomorphology and Hydrology*. Chapman & Hall: London.

Forti, P. and Sauro, U. (1996) 'The Gypsum Karst of Italy', *Int. J. Speleol.*, 25 (3-4), pp. 239-250.

Fratta, D., Aguettant, J. and Roussel-Smith, L. (2007) *Introduction to Soil Mechanics Laboratory Testing*. CRC Press: Taylor & Francis Group.

Fu, Z., Zheng, Y. and Liu, Y. (2008) 'Rock Bending Creep and Disturbance Effects', *J. Cent. South Univ. Technol.*, 15, pp. 438-442.

Gao, H., Liang, W., Yang, X., Zhang, G., Yue, G. and Zhang, P. (2011) 'Experimental Study of Mechanical Property of Gypsum Rock Soaked in Hot Saturated Brine', *Chinese Journal of Rock Mechanics and Engineering*, 30 (5), pp. 935-943.

Garcia-Guinea, J., Morales, S., Delgado, A., Recio, C. and Calaforra, J. M. (2002) 'Formation of Gigantic Gypsum Crystals', *Journal of the Geological Society, London*, 159, pp. 347-350.

Garcia-Ruiz, J. M., Ayora, R. V. C., Canals, A. and Otalora, F. (2007) 'Formation of Natural Gypsum Megacrystals in Naica, Mexico', *Geology*, 35, (4), pp. 327-330.

Gercek, H. (2007) 'Poisson's Ratio Values for Rocks', *International Journal of Rock Mechanics & Engineering Sciences*, 44, pp. 1-13.

Google maps (2012). Available at: http://maps.google.co.uk (Accessed: 05 October 2012).

Griggs, D. (1939) 'Creep of Rocks', *The Journal of Geology*, 47 (3), pp. 225-251.

Griggs, D.T. (1936), 'Deformation of Rocks under High Confining Pressures', *J. geol.*, 44, PP. 541-577.

Griggs, D.T. (1940) 'Experimental Flow of Rocks under Conditions Favouring Recrystallization', *Geol. Soc. Am. Bull.*, 51, pp. 1001-1022.

Gutierrez, G., Desir, G. and Gutierrez, M. (2003) 'Causes of the Catastrophic Failure of an Earth Dam Built on Gypsiferous Alluvium and Dispersive Clays (Atorricon, Huesca Province, NE Spain)', *Environmental Geology*, 43, pp. 842-851.

Hadjicharalambous, K. and Michaelides, P. (2007) *Karstic Phenomena-Problems in Gypsum Rocks of Cyprus*. Presentation. Available at: http://www.moa.gov.cy/moa/gsd/gsd.nsf/All/A20BA100E44BE710C2257545003CBAEA/$file/KarsticPhenomena_EN.pdf?OpenElement (Accessed: 17 July 2012).

Halferdahl, L. B. (1965) Kananaskis Gypsum Deposit. *Alberta Research Council Open File Report*, 1965-5. Available at: http://www.ags.gov.ab.ca/publications/OFR/PDF/OFR_1965_05.PDF (Accessed: 17 July 2012).

Hawkins, A.B. (1998) 'Aspects of Rock Strength', *Bull Eng Geol Env*, 57, pp. 17-30.

Hawks, I. and Mellor, M. (1970) 'Uniaxial Testing in Rock Mechanics Laboratory', *Eng. Geol.*, 4 (3), pp. 177-285.

Head, K.H. (2006) *Manual of Soil Testing*. 3rd Edition, Volume 1: Soil Classification and Compaction Tests. Whittles Publishing: CRC Press, Taylor & Francis Group.

Head, K.H. and Epps, R. (2011) *Manual of Soil Testing*. 3rd Edition, Volume 2: Permeability, Shear Strength and Compressibility Tests. Whittles Publishing: CRC Press, Taylor & Francis Group.

Heidari, M., Khanlari, G.R., Mehdi, T.K. and Kargarian, S. (2011) 'Predicting the Uniaxial Compressive and Tensile Strength of Gypsum Rock by Point Load Testing', Rock Mech Rock Eng, 45, pp. 265-273, [Online]. Available at: http://www.springerlink.com/content/pm6n834g177t2435/fulltext.pdf (Accessed: 17 July 2012).

Herrero, J. and Porta, J. (2000) 'The Terminology and the Concepts of Gypsum-Rich Soils', *Geoderma*, 96, pp. 47-61.

Hobbs, D.W. (1970) 'Stress-Strain Time Behaviour of Number of Coal Measure Rocks', *Int. J. Rock Mech. Min. Sci.*, 7, pp. 149-170.

Hofer, K.H. and Knoll, P. (1971) 'Investigation into the Mechanism of Creep Deformation in Carnallitite, and Practical Applications', *Int. J. Rock Mech. Min. Sci.*, 8, pp. 61-73.

Holiday, D.W. (1978) 'The origin of gypsum and anhydrite, some effects of its solution', *Summaries of Papers Read at The Engineering Group of the Geological Society, Jl Engng Geol*, 11, pp. 325-333.

Hoxha, D., Homand, F. and Auvray, C. (2006) 'Deformation of Natural Gypsum Rock: Mechanisms and Questions', *Engineering Geology*, 86, pp. 1-17.

Hudson, J. A. (1971) 'Effect of Time on the Mechanical Behaviour of Failed Rock', *Nature*, 232, pp. 185-186.

Hudson, J., Hardy, M.P. and Fairhurst, C. (1973) 'The Failure of Rock Beams-Part II Experimental Studies', *Int. J. Rock Mech. Min. Sci.*, 10, pp. 69-82.

Ingebritsen, S.E. and Sanford W.E. (1998) *Ground Water in Geologic Processes*. Cambridge University Press: UK.

James, A.N. (1978) ‘Calcium Sulphate in the Foundation of Major Embankment Dams’, *Summaries of Papers Read at The Engineering Group of the Geological Society, Jl Engng Geol*, 11, pp. 325-333.

James, A.N. and Kirkpatrick, I.M. (1980) ‘Design of Foundations of Dams Containing Soluble Rocks and Soils’, *Q. J. Eng. Geol. London*, 13, pp. 189-198.

James, A.N. and Lupton, R.R. (1978) ‘Gypsum and Anhydrite in Foundations of Hydraulic Structures’, *Geotechnique*, 28 (3), pp. 249-272.

James, A.N., Cooper, A.H. and Holliday, D.W. (1981) ‘Solution of the Gypsum Cliff (Permian, Middle Marl) by the River Ure at Ripon Parks, North Yorkshire’, *Proceeding of the Yorkshire Geological Society*, Vol. 43-Part 4, No. 24.

Janeiro, R.P. and Einstein, H.H. (2010) ‘Experimental Study of the Cracking Behaviour of Specimens containing inclusions (Under Uniaxial Compression)’, *Int J Fract*, 164, 83-102.

Jassim, S. Z. and Goff, C. J. (2006) *Geology of Iraq*. Dolin: Prague and Moravian Museum, Brno.

Jassim, S. Z., Jibril, A. S. and Numan, N. M. S. (1997) ‘Gypsum Karstification in the Middle Miocene Fatha Formation, Mosul Area, Northern Iraq’, *Geomorphology*, 18, pp. 137-149.

Jeschike, A.A., Vosbeck, K. and Dreybrodt, W. (2001) ‘Surface Controlled Dissolution Rates of Gypsum in Aqueous Solutions Exhibit Nonlinear Dissolution Kinetics’, *Geochimica et Acta*, 65 (1), pp. 27-34.

Johnson, K.S. (2005) ‘Subsidence Hazards due to Evaporite Dissolution in the United States’, *Environ Geol*, 48, pp. 395-409.

Johnson, K.S. (2008) ‘Gypsum-Karst Problems in Constructing Dams in the USA’ *Environ Geol*, 53, pp. 945-950.

Jones, C.J.F.P. and Cooper, A.H. (2005) 'Road Construction Over Voids Caused by Active Gypsum Dissolution, with an Example from Ripon, North Yorkshire, England' *Environ Geol*, 48, pp. 384-394.

Kanagawa, T. and Nakaari, K. (1970) 'Restraint of Swelling Creep and Effect of Absorption of Water on Triaxial Strength and Deformability of Rocks', *Rock Mech. In Japan*, 1, pp. 74-76.

Karacan, E. and Yilmaz, I. (1997) 'Collapse Dolines in Miocene Gypsum: an Example from SW Sivas (Turkey)', *Environmental Geology*, 29 (3/4), pp. 263-266.

Karacan, E. and Yilmaz, I. (2000) 'Geotechnical Evaluation of Miocene Gypsum from Sivas (Turkey)', *Geotechnical and Geological Engineering*, 18, pp. 79-90.

Kaveh, M.T., Heidari, M. and Miri, M. (2011) 'Karstic Features in Gypsum of Gachsaran Formation (case study; Chamsir Dam Reserviour, Iran)', *Carbonates Evaporites*, 27, pp. 291-297.

Kaveh, M.T., Heidari, M., Behzad, H.R.M. and Miri, M. (2011) 'Effect of Dissolved Sodium Chloride Content in Water on the Dissolution of Gypseous Rock (Case Study; Chamshir Dam Reservoir, SW Iran)', *Australian Journal of Basic and Applied Sciences*, 5 (9), pp. 1418-1424.

Kelley, J.R., Wakeley, L.D., Broadfoot, S.W., Pearson, M.L., McGrath, C.J., McGill, T.E., Jorgeson, J.D. and Talbot, C.A. (2007) 'Geologic Setting of Mosul Dam and its Engineering Implications', *Engineering Research and Development Center VICKSBURG MS* [Online]. Available at: http://oai.dtic.mil/oai/oai?verb=getRecord&metadataPrefix=html&identifier=ADA472047 (Accessed: 17 July 2012).

Kempe, S. (1996) 'Gypsum Karst of Germany', *Int. J. Speleol.*, 25 (3-4), pp. 209-224.

Khademi, H. and Merut, A.R. (2003) 'Micromorphology and Classification of Arid and Associated Gypsiferous Arid soils from Central Iran', *Catena-Elsevier*, 54, pp. 439-455.

Klimchouk, A. (1996) 'The Dissolution and Conversion of Gypsum and Anhydrite' *Int. J. Speleol.*, 25 (3-4), pp. 21-36.

Klimchouk, A. (1996) 'The Typology of Gypsum Karst According to its Geological Geomorphological Evolution', *Int. J. Speleol.*, 25 (3-4).

Klimchouk, A. and Andrejchuk, V. (1996) 'Sulphate Rocks as an Arena for Karst Developement', *Int. J. Speleol.*, 25 (3-4), pp. 9-19.

Klimchouk, A., Forti, P. and Cooper, A. (1996) 'Gypsum Karst of the World: a Brief Overview', *Int. J. Speleol.*, 25 (3-4), pp. 159-181.

Kourkoulis, S.K., Exadaktylos, G.E. and Vardoulakis, I. (1999) 'U-notched Dionysos-Pentelicon Marble Beams in Three Point Bending: The Effect of Nonlinearity, Anisotropy and Microstructure', *International Journal of Fracture*, 98, pp. 369-392.

Lee, R. and De souza, E. (1998) 'The Effect of Brine on the Creep Behaviour and Dissolution Chemistry of Evaporites', *Canadian Geotechnical Journal*, 35 (5), pp. 720-729.

Li, Y. and Xia, C. (2000) 'Time-Dependent Tests on Intact Rocks in Uniaxial Compression', *International Journal of Rock Mechanics and Mining Sciences*, 37, pp. 467-475.

Liang, F., Zheng, Y. and Liu, Y. (2008) 'Rock Bending Creep and Disturbance Effects', *J. Cent. South Univ. Technol.*, 15 (s1), pp. 438-442.

Liang, W., Xu, S. and Dusseault, M.B. (2008) 'Dissolution and Seepage Coupling Effect on Transport and Mechanical Properties of Glauberite Salt Rock', *Transp Porous*, 74, pp. 185-199.

Liang, W., Zhang, C., Gao, H., Yang, X., Xu, S. and Zhao, Y. (2012) 'Experiments on Mechanical Properties of Salt Rocks under Cyclic Loading', *Journal of Rock Mechanics and Geotechnical Engineering*, 4 (1), pp. 54-61.

Liang, W.G., Xu, S.G. and Zhao, Y.S. (2006) 'Experimental Study of Temperature Effects on Physical and Mechanical Characteristics of Salt Rock', *Rock Mech. Rock Eng.*, 39 (5), pp. 469-482.

Liguori, v., Manno, G. And Mortellaro (2008) ' vaporite Karst in Sicily', *Environ Geol*, 53, pp. 975-980.

Lin, Q., Fakhimi, A., Haggerty, M. and Labuz, J.F. (2009) 'Initiation of Tensile and Mixed-mode Fracture in Sandstone', *International Journal of Rock Mechanics & Mining Scinces*, 46, pp. 489-497.

Lomnitz, C. (1956) 'Creep Measurements in Igneous Rocks', *J. Geol.*, 64, pp. 473-504.

Lundborg, N. (1967) 'The Strength-Size Relation of Granite', *Int. J. Rock Mech. Min. Sci.*, 4, pp. 269-272.

Ma, L. and Daemen, J.J.K. (2006) 'An Experimental Study on Creep of Welded Tuff', *International Journal of Rock Mechanics & Minning Sciences*, 43, pp. 282-291.

Maksimovich, N.G. and Sergeev, V.I. (1984) 'Effect of Chemical Injection Stabilization on Gypsum Stability in the Foundation of Hydraulic Structures', *Translated from Gidrotekhicheskoe Stroitel'stvo*, 7, pp. 30-32.

Mancino, N. (2008) 'Gypsum in the Middle East; From Antiquity to Modern Day', *Global Gypsum Magazine*, May 2008 [Online]. Available at: http://www.docstoc.com/docs/41307002/Gypsum-in-the-Middle-East-from-antiquity-to-modern# (Accessed: 17 July 2012).

Maranini, E. and Brignoli, M. (1999) 'Creep Behaviour of a weak Rock: Experimental Characterization/Technical Note', *International Journal of Rock Mechanics and Mining Sciences*, 36, pp. 127-138.

Martin, R.J., Noel, J.S., Boyd, P.J. and Price, R.H. (1997) 'Creep Properties of the Paint Brush Tuff Recovered from Borehole USW NRG-7/7A: Data Report', *SANDIA Report*, SAND95-1759, UC-814.

Maximovich, N.G. and Meshcheryakova, O.Y. (2009) 'The Influences of Gypsum Karst on Hydro Technical Constructions in Perm Region', *Proceedings of the International Symposium and the 7th Asian Regional Conference of IAEG*, 9-11 September 2009 [Online]. Available at: http://nsi.psu.ru/misc/china/stat.pdf (Accessed: 09 March 2012).

MESF (2007) 'The Mosul Dam Issue File', *The Middle East Seismological Forum Special Reporting* [Online]. Available at: Http://www.meseisforum.net (Accessed: 25 January 2012).

Milanovic, P. (2011) 'Dams and Reservoirs in Karst', in van Beynen, P.E. (ed.) *Karst Management*. Springer Science & Business Media.

Mirza, U.A. (1974) *A Study of the Mechanism of Creep in Evaporite Rock Materials*. MSc Thesis: University of Newcastle upon Tyne, UK.

Misra, A.K. (1962) *An Investigation of Time-Dependant Deformation or-Creep-in Rocks*. PhD Thesis: University of Sheffield, UK.

Mitchell, J.K. and Soga, K. (2005) *Fundamental of Soil Behaviour*. 3rd edn. John Wiley & Sons.

Moonen, P. (2009) *Continuous-Discontinuous Modelling of Hydrothermal Damage Processes in Porous Media*. PhD Thesis: Delft University of Technology, Netherlands.

Mortimore, R.N., Stone, K.J., Lawrence, J. and Duperret, A. (2004) 'Chalk physical properties and cliff instability', in: *Coastal Chalk Cliff Instability*. Geological Society Engineering Geological Special Publication, Geological Society, London, UK, pp. 75-88.

MP (2007) 'Test Method for Unconfined Compressive Strength of Rock Core Specimens'. *West Virginia Department of Transportation Division of Highways, Materials Control, Soils and Testing Division, Materials Procedure* [Online]. Available at:

http://www.transportation.wv.gov/highways/mcst/Material%20Procedures/M2120121.pdf (Accessed: 18 July 2012).

Mulder, M.A. (1969) *The Arid Soils of the Balikh Basin (Syria)*. PhD Thesis: University of Empire, Germany.

Muller N.S., Kilikoglou, V., Day, P.M. and Vekinis, G. (2010) 'The Influence of Temper Shape on the Mechanical Properties of Archaeological Ceramics', *Journal of the European Ceramic Society*', 30, pp. 2457-2465.

Munsell (2010) *Soil Colour Charts*.

Nedriga, V.P. and Dem'yanova, E.A. (1986) 'Construction of Dams on Soils Containing Soluble Salts', *Translated from Gidrotekhnicheskoe Stroitel'stvo*, (2), pp. 44-47.

Nonveiller, E. (1982) 'Treatment Methods for Soluble Rocks', *Bulletin 25 of the International Association of Engineering Geology*, pp. 165-169, Paris: France.

Nuri, T.M., Ali, A.Y. and Ahmed, S. (2012) 'Correlation Study between Point Load Test and Uniaxial Compressive Strength and Tensile Strength of Some Sedimentary Rocks in Mosul City', *Eng & Tech. Journal*, 30 (1), pp. 155-166.

Obret, L., Windes S.L. and Duvall W.I. (1946) *Standardized Test for Determining the Physical Properties of Mine Rock*. Report of Investigations, R.I. 3891, United States Department of Interior-Bureau of Mines, [Online]. Available at: http://babel.hathitrust.org/cgi/pt?id=mdp.39015078487306;seq=4;view=1up (Accessed: 03 December 2012).

OUGS (2008) 'OUGS feild visit to Bantycock opencast gypsum mine near Newark, Notts'. *Open University Geological Society, East Midlands Branch [Online]*. Available at: http://www.emgs.org.uk/files/gallery/Bantycock%20Mine%20%20OUGS%20Field%20Trip.pdf (Accessed: 21 November 2012).

Ozbek, E. (1975) 'Cavity at Keban Dam, Turkey', *Bulletin of the International Association of Engineering Geology*, (12), pp. 45-48.

Ozkan, I., Ozarslan, A., Genis, M. and Ozsen, H. (2009) 'Assessment of Scale Effects on Uniaxial Compressive Strength in Rock Salt', *Environmental & Engineering Geosciences*, XV (2), pp. 91-100.

Padevet, P., Tesarek, P. and Plachy, T. (2011) 'Evolution of Mechanical Properties of Gypsum in Time', *International Journal of Mechanics*, 5 (1), pp. 1-9.

Pando, L., Pulgar, J.A. and Gutierrez-Claverol, M. (2012) 'A Case of Man-Induced Ground Subsidence and Building Settlement Related to Karstified Gypsum (Oviedo, NW Spain), *Environ Earth Sci*, [Online]. Available at: http://www.springerlink.com/content/5134343hl8q35328/fulltext.pdf (Accessed: 18 July 2012).

Panu, M. And Gautheryrou J. (2006) *Handbook of Soil Analysis, Mineralogical, Organic and Inorganic Methods*. Springer-VerlagBerlin Heidelberg.

Papadopoulos, Z., Kolaiti, E. and Mourtza, N. (1994) 'The Effect of Crystal Size on Geotechnical Properties of Neogene Gypsum in Crete', *Quarterly Journal of Engineering Geology and Hydrogeology*, 27, pp. 267-273.

Pearson, R. M. and Hurcomb, R. D. (2002) 'Gypsum Karst of the Lykins Formation and Effects for Colorado Front Range Water Project, Horsetooth and Carter Lake Reservoirs'. Denver Annual Meeting October 27-30 [Online]. Available at: https://gsa.confex.com/gsa/2002AM/finalprogram/abstract_44387.htm (Accessed: 17 July 2012).

Peng. S.S. (1973) 'Time-Dependant Aspects of Rock Behaviour as Measured by a Servocontrolled Hydraulic Testing Machine', *Int. J. Rock Mech. Min. Sci.*, 10, pp. 235-246.

Petrukhin, V.P. and Boldyrev, G.B. (1978) 'Investigation of the Deformability of Gypsofied Soils by a Static Load', *Translated from Osnovaniya Fundamenty I Mekhnika Gruntov*, (3), pp. 20-23.

Pires, V., Amaral, P.M., Rosa, L.G. and Camposinhos, R.S. (2011) 'Slate Flexural and Anchorage Strength Considerations in Cladding Design', *Construction and Building Materials*, 25, pp. 3966-3971.

Price, N.J. (1964) 'A Study of the Time-Strain Behaviour of Coal-Measure Rocks', *Int. J. Rock Mech. Mining Sci.*, 1, pp. 277-303.

Rauh, F., Spaun, G. and Thuro, K. (2006) 'Assessment of the Swelling Potential of Anhydrite in Tunnelling Projects'. *IAEG 2006 Paper number 473* [Online]. Available at: http://iaeg2006.geolsoc.org.uk/cd/PAPERS/IAEG_473.PDF (Accessed: 17 July 2012).

Razouki, S.S. and El-Janabi, O.A. (1999) 'Decrease in the CBR of Gypsiferous Soil Due to Long-Term Soaking', *Quarterly Journal of Engineering Geology and Hydrology*, 32, pp. 87-89.

Razouki, S.S. and Kuttah, D.K. (2004) 'Distress of Light Structures and Pavements over Swelling Gypsiferous Soils', *Proceeding of International Conference on Geotechnical Engineering*, 3-6 October 2004. Sharjah, UAE.

Razouki, S.S. and Kuttah, D.K. (2004) 'Effect of Soaking Period and Surcharge Load on Resilient Modulus and California Bearing Ratio of Gypsiferous Soil', *Quarterly Journal of Engineering Geology and Hydrology*, 37, pp. 155-164.

Razouki, S.S., Kuttah, D.K., Al-Damluji, O.A. and Nashat, I.H. (2006) 'Strength Erosion of Fine-Grained Gypsiferous Soil during Soaking', *The Arabian Journal for Science and Engineering*, 32, (1B), pp. 147-152.

Razouki, S.S., Kuttah, D.K., Al-damluji, O.A. and Nashat, I.H. (2008) 'Using Gypsiferous Soil for Embankments in Hot Desert Area', *Proceedings of the institution of Civil Engineers, Construction Materials*, 161 (2), pp. 63-71.

Robertson, E.C. (1960) 'Creep of Solenhofen Limestone under Moderate Hydrostatic Pressure', *Mem. Geol. Soc. Amer.*, 79, pp. 227-244.

Romanov, D., Gabrovsek, F. and Dreybrodt, W. (2003) 'Dam Sites in Soluble Rocks: a Model of Increasing Leakage by Dissolution Widening of Fractures beneath a Dam', *Engineering Geology*, (70), pp. 17-35.

Saini, G.R. (1971) 'Comparative Effect of Gypsum and Limestone on Drainage and Salt Removal from Coastal Alluvial Soils of New Brunswick', *Plant and Soil*, (34), pp. 159-164.

Salih, N.B. (2003) *Field Models on Gypseous Soils Reinforced with Stone Columns Stabilized with Asphalt and Lime*. MSc Thesis: University of Technology, Iraq.

Sangha, C.M., Talbot, C.J. and Dhir, R.K. (1974) 'Microfracturing of Sandstone in Uniaxial Compression', *Int. J. Rock Mech. Min. Sci. & Geomech. Abstr.*, 11, pp. 107-113.

Sargent, C. (2009) *An Examination of Subsidence in North-East England due to the Dissolution of Sub-Surface Gypsum Using the Shallow Seismic Reflection Technique*. PhD Thesis: Durham University, UK.

Schwartz, A.E. (1964) 'Failure of Rock in the Triaxial Shear Test', *Prod. 6th Symp. Rock Mech*. University of Missouri at Rolla, pp. 109-151.

Shafiei, A., Dusseault, M.B. and Baghdardokht, Z. (2008) 'Geotechnical Properties of Soluble Rocks from a Dam Site in Iran', *The 2nd US Rock Mechanics Symposium and Us-Canada Rock Mechanics Symposium*. 29 June-2 July, San Francisco, US.

Sherard, J.L. and Singh, S. (1992) *Embankment Dams: James L. Sherard Contributions*. American Society of Civil Engineers, Geotechnical Special Publication, no.32: New York.

Shih, T.M. (1965) *The Physical Properties of a Gaspe Skarn*. MSc Thesis: McGill University, Canada.

SIGIR (2007) 'Relief and Reconstruction Funded Work at Mosul Dam, Mosul-Iraq', *Special Inspector General for Iraq Reconstruction*, 29 October 2007. [Online]. Available at: http://www.sigir.mil/files/assessments/PA-07-105.pdf (Accessed: 17 July 2012).

Singh, D.P. (1975) 'A Study of Creep of Rocks', *Int. J. Rock Mech. Min. Sci.*, 12, pp. 271-275.

Singh, V.K. and Singh, D.P. (1993) 'Correlation between Point Load Index and Compressive Strength for Quartz Rocks', *Geotechnical and Geological Engineering*, 11, pp. 269-272.

Sonnenfeld, P. (1984) *Brines and evaporates*. Academic Press, London.

Spiegel, Z. (1969) 'Engineering Geology Problems at Dam and Reservoir Sites in East-Central New Mexico', *Guidebook*. Santa Fe, New Mexico [Online]. Available at: http://nmgs.nmt.edu/publications/guidebooks/downloads/23/23_p0184_p0186.pdf (Accessed: 17 July 2012).

Stacy, F.D. (1963) 'The Theory of Creep in Rocks and the Problem of Convection in the Earth', *Mantle I CARUS*, 1, pp. 304-313.

Stevanovic, Z. and Markovic, M. (2003) 'Hydrogeology of Northern of Iraq', *Climate, Hydrology, Geomorphology and Geology*, 1, 2nd edition (FAO Publication).

Summaries of Papers Read at the Engineering Group Regional Meeting-Cardiff (1977) 'Engineering Geology of Soluble Rocks', *Quarterly Journal of Engineering Geology and Hydrology 1978*, 11, pp. 325-333.

Swift, G.M. and Reddish, D.J. (2005) 'Underground Excavations in Rock Salt', *Geotechnical and Geological Engineering*, 23, pp. 17-42.

Taminskas, J. and Marcinkevicius, V. (2002) 'Karst Geoindicators of Environmental Change: The Case of Lithuania', *Environmental Geology*, 42, pp. 757-766.

Thanoon, H. A. (1990) 'Geomorphology and Instability of Slops along the Eastern Bank of Regulating Lake at Saddam (Mosul) Dam', *2nd Sci. Conf. of Saddam Dam Research Centre*, Mosul University: Mosul-Iraq. 18-20th of March 1990.

Thuro, K., Plinninger, R.J. and Schutz, S. (2001) 'Scale Effects in Rock Strength Properties, Part 1: Unconfined Compressive Test and Brazilian Test', *ISRM Regional Symposium, Eurock 2001, Rock Mechanics, A Challenge for Society*. Espoo: Finland, 3-7th of June, pp. 169-174.

Tran, M.K., Shin, H., Byun, Y. and Lee, J. (2012) 'Mineral Dissolution Effects on Mechanical Strength', *Engineering Geology*, 125, pp. 26-34.

Trzcinski, Y. (1996) 'Gypsum Karst in the South of the Siberian Platform, Russia', *Int. J. Speleol.*, 25 (3-4), pp. 293-295.

Tuncay, E. And Hasancebi, N. (2009) 'The Effect of Length to Diameter Ratio of Test Specimens on the Uniaxial Compressive Strength of Rock', *Bull Eng Geol Environ*, 68, pp. 491-497.

Ulker, R. and Gumusoglu, M.C. (1982) 'The Investigation of the Effect of Gypsum on Foundation Design', *Bulletin 25 of the International Association of Engineering Geology*, pp.99-105.

Urushadze, T.F. and Urushadze, T.T. (2011) 'Soils of Georgia: Condition and Persepectives', *Екологія та ноосферологія*, Т. 22 (1-2), pp. 58-63, [Online]. Available at: http://www.nbuv.gov.ua/portal/chem_biol/ein/2011_1-2/Urushadze.pdf (Accessed: 13 January 2013).

Varo, L. and Passaris, E.K.S. (1977) 'The Role of Water in the Creep Properties of Halite', *Proceeding Conference of Rock Engineering British Geological Society*, Vol. 1, pp. 85-100, University of Newcastle upon Tyne: UK.

Vasarhelyi, B. and Van, P. (2005) 'Influence of Water Content on the Strength of Rock', *Engineering Geology*, 84, pp. 70-74.

Waltham, A.C. and Fookes, P.G. (2005) 'Engineering Classification of Karst Ground Conditions', *Speleogenesis and Evolution of Karst Aquifers,* 6 (1), [Online]. Available at: http://www.speleogenesis.info (Accessed: 05 February 2010).

Waltham, T. (2009) *Foundations of Engineering Geology*. 3rd edn. Tayler & Francis.

Watson, A. (1985) 'Structure, Chemistry and Origins of Gypsum Crusts in Southern Tunisia and the Central Namib Desert', *Sedimentology*, 32, pp. 855-875.

Wawersik, W.R. (1972) 'Time-Dependent Rock Behaviour in Uniaxial Compression', *Rock Mechanics*, pp. 85-106.

Wawersik, W.R. and Fairhurst, C. (1970) 'A Study of Brittle Rock Fracture in Laboratory Compression Experiments', *Int. J. Rock Mech. Min. Sci.*, 7, pp. 561-575.

Whittles, D.N., Kingman, S., Lowndes, I. and Jackson, K. (2006) 'Laboratory and Numerical Investigation into the Characteristics of Rock Fragmentation', *Minerals Engineering*, (19), pp. 1418-1429.

Woodward R. (2005) *The Dam Site*. Available at: http://members.Optusnet.com.au/~engineeringgeologist/page18.html (Accessed: 18 January 2010).

Worley, N. and Reeves, H. (2007) 'Field Guide, Application of Engineering Geology to Surface Mine Design, British Gypsum, Newark Nottinghamshire'. *Field Guide* [Online]. Available at: http://nora.nerc.ac.uk/3225/1/Keyworth_Field_Trip.pdf (Accessed: 21 November 2012).

Xeidakis, G.S., Samaras, I.S., Zacharopoulos, D.A. and Papakaliatakis, G.E. (1996) 'Crack Growth in a Mixed-mode loading on Marble Beams under Three Point Bending', *International Journal of Fracture*, 79, pp. 197-208.

Yaoru, L. and Cooper, A.H. (1996) 'Gypsum Karst in China', *Int. J. Speleol.*, 25 (3-4), pp. 297-307.

Yilmaz, I. (2001) 'Gypsum/Anhydrite: Some Engineering Problems', *Bull Eng Geol Env*, 59, pp. 227-230.

Yilmaz, I. (2007) 'Differences in the Geotechnical Properties of Two Types of Gypsum: Alabastrine and Porphyritic', *Bull Eng Geol Env*, 66, pp. 187-195.

Yilmaz, I. (2011) 'On the Value of Dolines in Gypsum Terrains as a "Geological Heritage": an Example from Sivas Basin, Turkey', *Environ Earth Sci* [Online]. Available at: http://www.springerlink.com/content/p7h325330864m6x2/fulltext.pdf (Accessed: 20 February 2012).

Yilmaz, I. and Sender, H. (2002) 'Correlation of Schmidt Hardness with Unconfined Compressive Strength and Young's Modulus in Gypsum from Sivas-Turkey', *Engineering Geology*, 66, pp. 211-219.

Yu, X., da-Gama, C.D., Na, Y., Wang, Q. and Xie, Q. (2005) 'Deformation Behaviour of Rocks under Compression and Direct Tension', *The Journal of the South African Institute of Mining and Metallurgy*, pp. 55-62.

Zatonskikh, A.T., Volkova, G.I. and Krivoshchekova, N.P. (1965) 'The Effect of Scale Factor on the Strength of Ugle-Plast', *Translated from Fiziko-Tekhicheskie problemy Razrabotki Iskopaemykh*, (3), pp. 144-145.

Zhao, X., Chen, B., Zhao, H., Jie, B. and Ning, Z. (2012) 'Laboratory Creep Tests for Time-Dependent Properties of a Marble in Jinping II Hydropower Station', *Journal of Rock Mechanics and Geotechnical Engineering*, 4, pp. 168-176.

Zheng, H.F., Duan, T.Y., Liu, Y. and Sun, Q. (2009) 'Abrupt Solubility of Gypsum in Water at High Pressure and Ambient Temperature and its Implication', *Acta Petrologica Sinica*, 25 (5), pp. 1288-1290.

Zuo, Y., Li, X., Zhou, Z., Ma, C., Zhang, Y. and Wang, W. (2005) 'Damage and failure rule of rock undergoing uniaxial compressive load and dynamic load', *J. Cent. South Univ. Technol.*, 12 (6), pp. 742-748.

APPENDICES

Contents

APPENDIX A: PILOT STUDIES

A.1 Cylinders Loading Rates

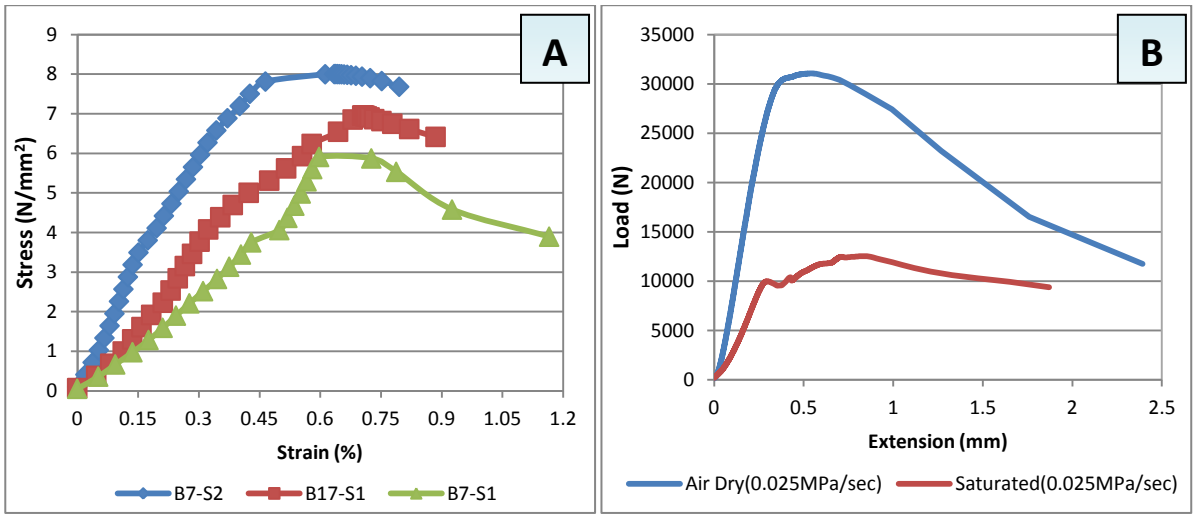

Fig. A.1: Air-dry cylinders trial experiments-different loading rates, A is on 0.05 MPa/sec and Plate B is on 0.025 MPa/sec loading rates.

A.2 Thin Layers Loading Rates

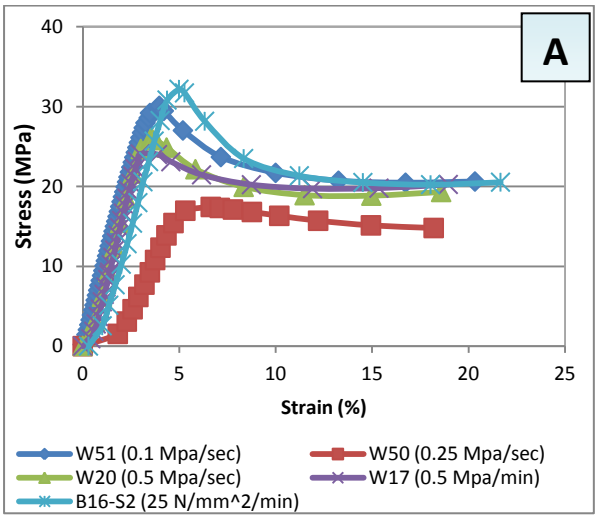

Fig. A.2: Air-dry thin layers trial experiments-different loading rates as shown on the figure.

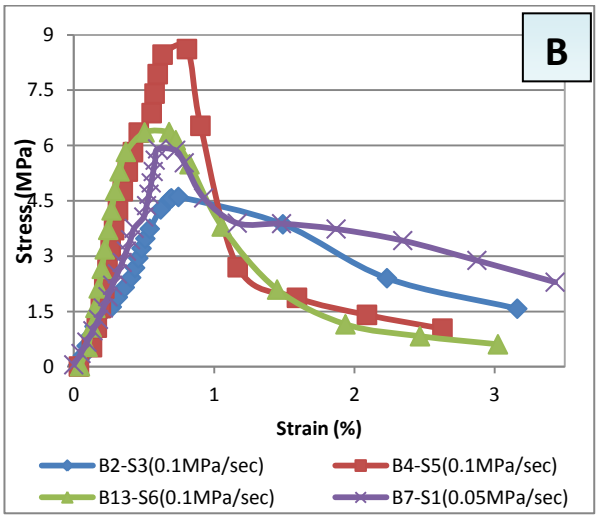

Fig. A.3: Air-dry thin layers trial experiment (0.01MPa/sec and 0.05MPa/sec).

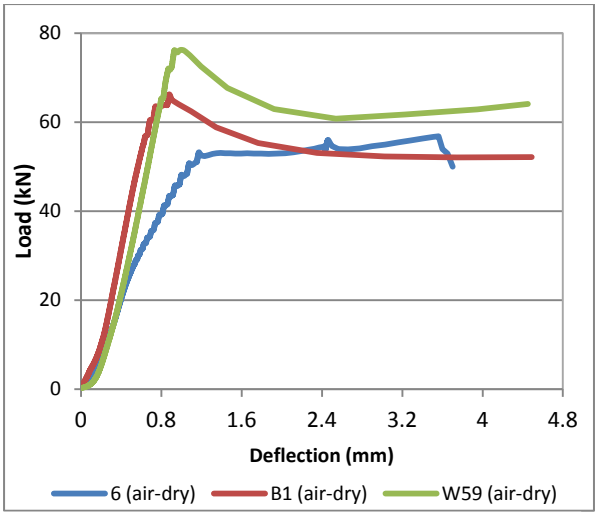

Fig. A.4: Air-dry thin layers trial experiments (0.075MPa/sec).

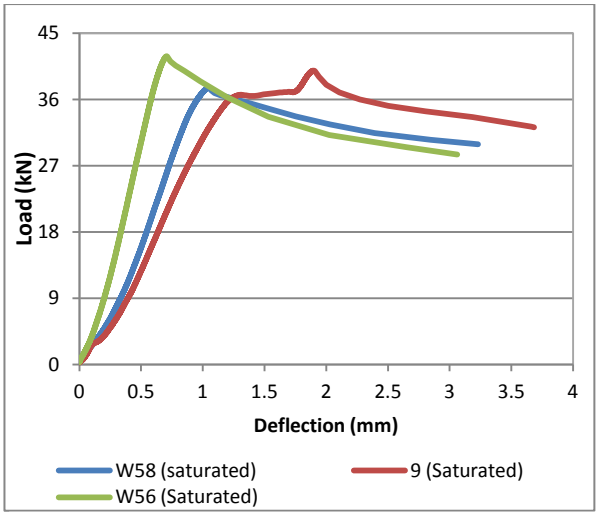

Fig. A.5: Saturated thin layers trial experiment (0.075MPa/sec).

A.3 Small Four-Point Bending Loading Rates

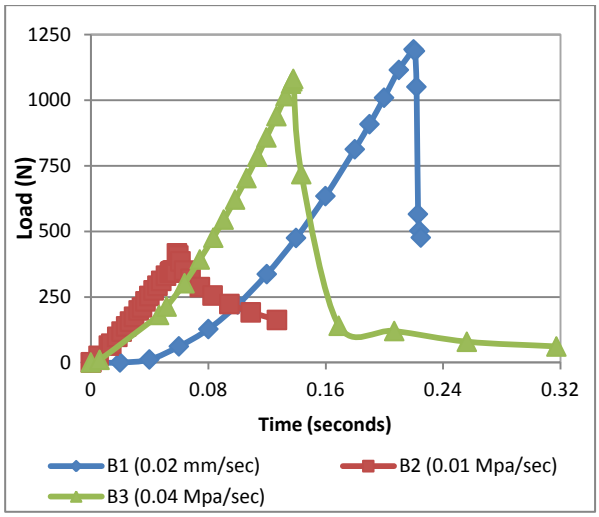

Fig. A.6: Air-dry small bending trial experiments-Different loading Rates.

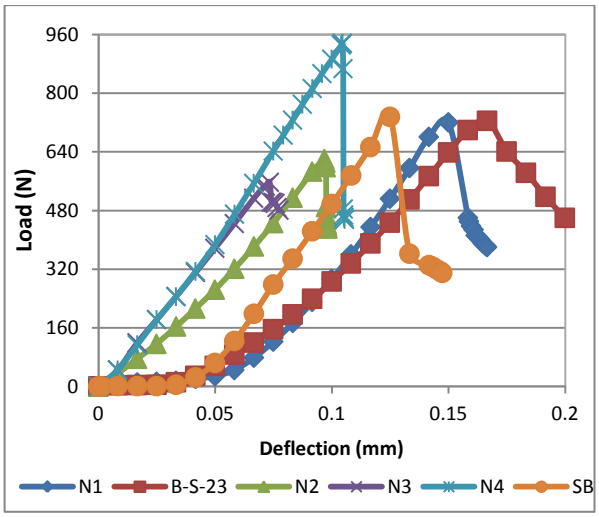

Fig. A.7: Air-dry small bending trial experiment (0.01mm/min).

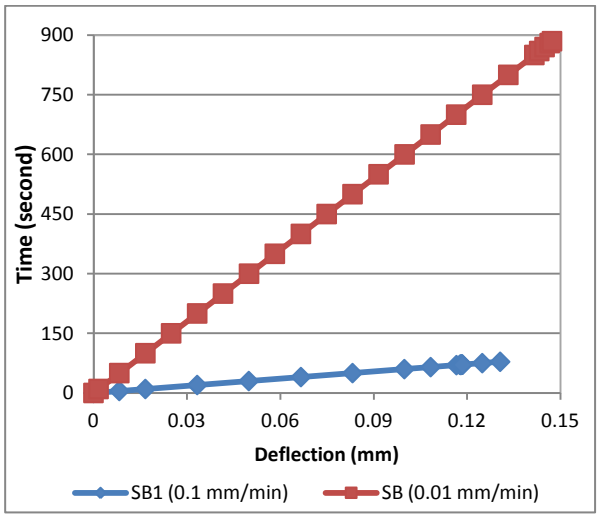

Fig. A.8: Air-dry small bending trial experiments-different loading rates.

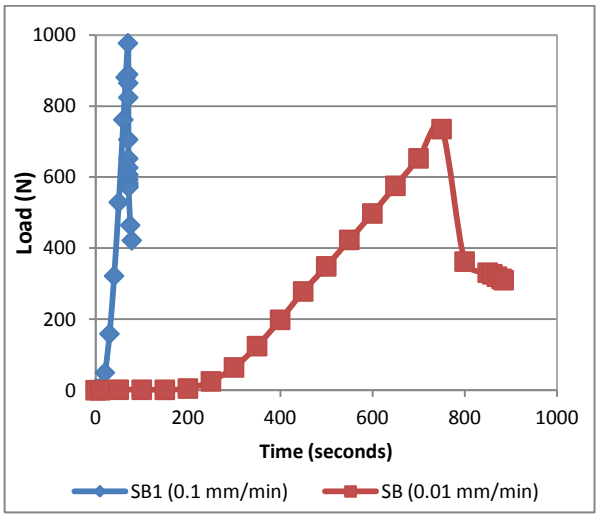

Fig. A.9: Air-dry small bending trial experiment-different loading rates.

A.4 Loading-Unloading Experiment

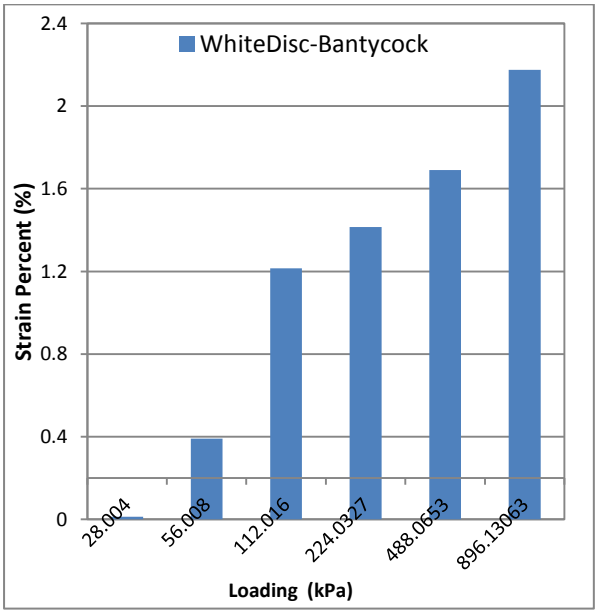

Fig. A.10: Loading stages for white/Bantycock thin layer.

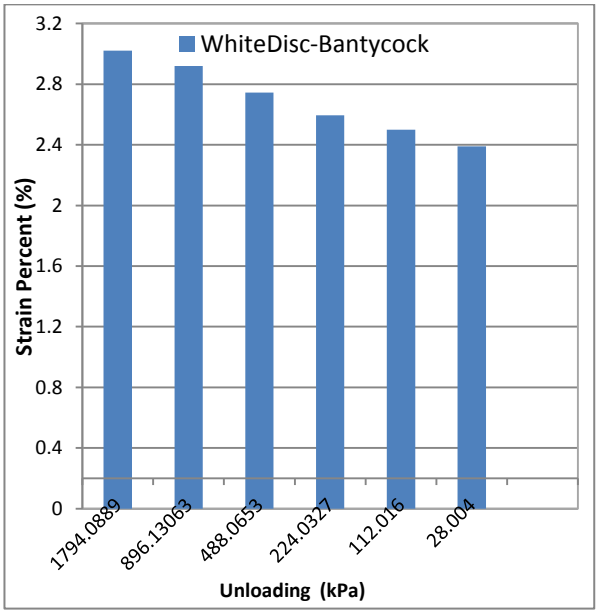

Fig. A.11: Unloading stages for white/Bantycock thin layer.

APPENDIC B: GYPSUM ROCK WORK (SHORT-TERM)

B.1 Thin Layers:

Different kinds of abbreviations were used in below tables, which represent properties such as: *Eα* = Axial Modulus (GPa), *Ec* = Circumferential Modulus (GPa), *PR* = Poisson's ratio, *SM* = Shear Modulus (GPa), $б_c$ = Compressive Strength (MPa), *P* = Load at failure (N), *T* = Time to failure (seconds), *MAD* = Maximum axial deflection (mm), *MHD* = Maximum horizontal deflection (mm), *MWR* = Maximum weight reduction (%), *MVR* = Maximum volume reduction (%), *MD* = Maximum dissolution (US/cm) *MDR* = Maximum diameter reduction (%), *MLR* = Maximum length reduction (%).

Table B.1: Short term uniaxial compression tests results of air-dry gypsum thin layers from different origins.

Thin Layer No.	*Ea* (GPa)	*Ec* (GPa)	*PR*	*SM* (GPa)	$б_c$ (MPa)	*P* (N)	*T* (seconds)	*MAD* (mm)	*MHD* (mm)	Density (gm/cm^3)
White/Bantycock (Air-Dry)										
N1	0.86101	1.625	0.529852	10.57143	32.34545	74078.4	429.85	1.03115	2.69399	2.2581
N2	0.9918	1.6297	0.608578	10.75701	34.607	79257.9	459.8	0.99893	2.63894	2.2568
N3	1.02083	0.9599	1.063475	9.29022	38.34028	87807.9	510.55	1.08286	3.02568	2.28624
W1	1.458	9.3473	0.155981	18.71273	43.26312	99082.3	574.65	0.69894	1.09545	2.295
W57	1.07196	2.927	0.366232	9.158579	25.02548	57314	332.75	0.83033	2.94871	2.289
Pink/Bantycock (Air-Dry)										
PS1	1.275	2.2608	0.56396	13.67018	42.75921	97928.3	568.95	0.94049	1.71668	2.2913
PS2	1.50173	2.4694	0.608136	13.10503	42.14933	96531.5	560.7	0.69939	0.90667	2.3001
PS3	1.0659	2.4694	0.431643	12.45107	35.65098	81648.8	473.85	0.83182	1.86537	2.273
PS4	0.9193	1.7796	0.516577	11.04377	33.49745	76716.7	445.25	1.41619	5.79915	2.258
PS5	0.6548	0.9825	0.666463	15.16288	50.53677	115741	672.3501	0.72973	0.85414	2.247
Aust Cliff (Air-Dry)										
1	0.788	1.0171	0.774752	10.08328	35.79065	81968.7	475.7	1.09841	3.0911	2.27801
3	1.0997	1.9144	0.574436	13.70749	43.16312	98853.3	574.1001	1.04699	2.55038	2.2537
5	1.1052	4.073	0.271348	15.96574	40.59601	92974.1	539.95	0.84094	1.37752	2.0955
6	0.90573	1.399	0.647412	12.29629	40.51412	92786.5	538.75	1.1437	4.04115	2.3188
8	0.6357	0.68882	0.922883	8.650481	33.26772	76190.6	442.15	1.39863	4.41991	2.307
Iraqi (Air-Dry)										
I1	1.2	2.7333	0.43903	28.64826	82.45139	188832.3	1100.05	1.17909	2.11635	2.2745
I2	1.664	9.69231	0.171682	35.83008	83.96295	192293	1121.05	1.02515	1.40957	2.218
I3	1.47333	7.2655	0.202784	36.86482	88.68087	203099.3	1182.5	1.13246	1.43955	2.216
I4	1.573	5.617	0.280043	34.40759	88.08637	201737.7	1174.3	1.44091	2.1002	2.314
I5	1.37514	7.004	0.196336	36.0059	86.15034	203098.1	1182.2	1.1324	1.43954	2.26742
White & Clay/Bantycock (Air-Dry)										
1	1.01904	1.9688	0.517594	12.16287	36.9166	84547.3	491.05	1.02023	2.1691	2.25611
2	0.93292	1.1697	0.797572	10.77968	38.75449	88756.6	515	1.06612	3.14558	2.2619
5	0.5787	0.8783	0.658886	7.108398	23.58405	54012.8	313.3	1.18241	4.51598	2.265
B21,S2	1.5641	6.5463	0.238929	21.42801	53.09556	121601	706.45	0.84722	1.04879	2.287
B21,S3	1.425	6.2308	0.228703	24.24913	59.58993	136474	793.3	0.95372	1.34174	2.2959

Table B.2: Short term uniaxial compression tests results of white/Bantycock gypsum thin layers. These samples tested after saturation under atmospheric pressure for 5, 10, 15, 30 and 50 week time durations.

Thin Layer No.	*Ea* (GPa)	*Ec* (GPa)	*PR*	*SM* (GPa)	$б_c$ (MPa)	*P* (N)	*T* (seconds)	*MAD* (mm)	*MHD* (mm)	*MD* (%)	*MWR* (%)	*MVR* (%)	*MDR* (%)	*MLR* (%)
White/Bantycock (Saturated under atmospheric pressure-5week)														
X3	0.31415	0.35454	0.886078	0.083281	28.86023	65222.1	378.5	3.49911	9.34699	6693.1	2.3097	1.641	0.664	0.322
W8	0.445152	1.048713	0.424475	0.156251	30.56275	69138.1	401.15	1.20693	3.87342		2.3941	2.862	0.614	1.662
W15	0.72111	3.08144	0.234017	0.29218	27.22766	61635.8	357.5	0.69558	1.64826		2.2014	1.38	0.58	0.202
White/Bantycock (Saturated under atmospheric pressure-10week)														
W4	0.49122	0.62133	0.79059	0.13717	25.41038	57208.2	331.75	1.17897	5.0227	13293.9	4.5311	3.05	0.852	1.38
W3	0.762	1.70053	0.4481	0.2631	25.60117	57695.3	334.55	0.84012	3.01522		4.359	2.784	0.8	1.3
W7	0.5458	6.0065	0.09087	0.25017	28.80803	64273.3	373.1	1.09654	4.19958		4.635	3.94	1.3	1.37
White/Bantycock (Saturated under atmospheric pressure-15week)														
B16S3	0.6136	0.4854	1.264112	0.13551	26.9899	59792.1	346.55	1.37531	6.18823	20159.4	6.92	5.52	1.65	2.33
B2S4	0.371	0.3335	1.112444	0.08781	27.0194	60173.6	348.55	3.40554	9.63714		6.5631	4.47	1.39	1.763
B11S2	0.7576	0.4573	1.656681	0.14258	24.64665	54920.1	318.05	1.26403	5.27301		6.708	5	1.361	2.372
White/Bantycock (Saturated under atmospheric pressure-30week)														
X1	0.2616	0.2422	1.080099	0.062882	28.8684	60842.3	352.978	3.58782	9.65761	40657.2	13.6	26.56	3.98	5.261
X2	0.3815	0.34844	1.09488	0.091055	23.73704	49622.7	274.9	3.23289	10.26002		13.13	13.73	4.64	5.29
W11	0.4674	0.8619	0.54229	0.151528	21.69899	46183.7	267.35	1.03331	4.00383		12.44	11.12	3.46	4.67
White/Bantycock (Saturated under atmospheric pressure-50week)														
1	0.0957	0.09205	1.03965	0.02346	9.287887	18564.3	106.876	1.50139	5.17263	67030	23.13	22.01	6.53	10.75
2	0.1455	0.12097	1.20299	0.03303	13.54806	27168.5	156.73	1.50042	5.55299		21.57	19.88	6.43	8.484
3	0.1533	0.1344	1.140625	0.035807	16.52909	33059	191.026	2.00123	8.8353		22.61	20.9	6.404	9.69

Table B.3: Short term uniaxial compression tests results of white/Bantycock gypsum thin layers. These samples tested after saturation under 1.75 and 3.25 water pressure for 5, 10 and 15 week time durations.

Thin Layers No.	*Ea* (GPa)	*Ec* (GPa)	*PR*	*SM* (GPa)	$б_c$ (MPa)	*P* (N)	*T* (seconds)	*MAD* (mm)	*MHD* (mm)	*MD* (%)	*MWR* (%)	*MVR* (%)	*MDR* (%)	*MLR* (%)
White/Bantycock (Saturated under 1.75bar water pressure-5week)														
W9	0.1953	0.2073	0.942113	0.05028	23.64358	52968.92	287.95	3.26981	10.30515	9611	7.181	6.967	1.701	0.5134
W21	0.1744	0.19905	0.876162	0.046478	24.54359	52955.5	292.9	3.31346	9.3906		7.1502	7.21	1.51	1
W2	0.1685	0.1876	0.898188	0.044384	22.96641	46237.5	269.2	1.442508	5.10942		7.053	7.01	0.97	1.81
White-Bantycock (Saturated under 1.75bar water pressure-10week)														
W1	0.2298	0.30783	0.746516	0.065788	21.48184	39976.7	231.274	2.04532	9.68115	19842	13.88	14.174	3.05	6.57
W2	0.302234	0.50645	0.59677	0.094639	25.6357	55126.3	320.85	1.3771	4.87597		12.63	13.8	3.1	8.19
W16	0.2716	0.401552	0.676375	0.081008	23.1608	50543.2	294.1	1.33211	4.38088		8.88	7.58	2.39	3.01
White-Bantycock (Saturated under 1.75bar water pressure-15week)														
W13	0.4155	0.5125	0.810732	0.114733	21.7272	48267	279.5	1.27232	6.25346	29339	18.72	22.253	4.579	13.5724
X	0.27807	0.38744	0.717711	0.080942	19.95939	44366	258.2	1.30939	5.01818		18.58	18.814	4.651	9.8713
2	0.363	0.528	0.6875	0.107556	19.8898	44409.4	257.25	1.2014	4.6245		18.67	16.0664	3.86032	8.6112
White-Bantycock (Saturated under 3.25bar water pressure-5week)														
W3	0.2903	1.272212	0.228185	0.118182	26.58166	58810.1	342.25	1.56611	5.79548	10043.7	7.024	6.942	1.71	2.56
W4	0.37242	0.46913	0.793852	0.103805	20.15941	44229.5	257.3	0.94938	3.3279		6.997	8.251	2.142	2.24
W10	0.27002	0.4708	0.573534	0.0858	24.63095	54310.3	316.2	1.52523	4.9725		7.03	6.574	2.07712	2.313
White-Bantycock (Saturated under 3.25bar water pressure-10week)														
3	0.4463	0.8154	0.547339	0.144215	21.62347	46421	268.6	0.97995	3.83894	19849.8	15.099	13.816	3.532	8.1697
4	0.425013	0.79784	0.532705	0.138648	21.6499	46137.5	267.65	1.08309	4.6271		14.77	13.759	3.6097	7.197
W12	0.4953	1.121	0.441838	0.17176	23.05203	48934.7	283.7	0.96052	3.51514		14.632	11.9634	3.124	6.2023
White-Bantycock (Saturated under 3.25bar water pressure-15week)														
Y	0.1956	0.2863	0.683199	0.058104	20.047	40962.2	238.24	2.04069	9.55099	29852.5	21.669	21.825	5.4971	12.439
A4	0.4052	1.10662	0.36616	0.148299	21.347	43430.5	251.6	0.90805	2.7239		21.605	21.223	5.4895	11.939
A2	0.5056	1.09375	0.462263	0.172883	20.2939	41903	242.6	0.76254	2.42718		21.447	19.671	4.9895	11.02463

Table B.4: Short term uniaxial compression tests results of white/Bantycock gypsum thin layers. These samples tested after saturation under 5.0 water pressures for 5, 10 and 15 week time durations.

Thin Layers No.	*Ea* (GPa)	*Ec* (GPa)	*PR*	*SM* (GPa)	σ_c (MPa)	*P* (N)	*T* (seconds)	*MAD* (mm)	*MHD* (mm)	*MD* (%)	*MWR* (%)	*MVR* (%)	*MDR* (%)	*MLR* (%)
White/Bantycock (Saturated under 5bar water pressure-5week)														
1	0.244	0.23478	1.039271	0.059825	24.22668	53408.2	309.5	2.11707	9.76932	10114.7	7.887	8.242	3.17	2.99
2	0.4434	0.7597	0.583651	0.139993	21.10048	46505.9	269.2	0.97838	3.85971		7.3665	8.632	2.99	3.27
3	0.4932	0.70417	0.700399	0.145025	25.62249	5744.6	331.3	1.27516	6.16403		7.808	8.14	3.39	2.96
White-Bantycock (Saturated under 5bar water pressure-10week)														
W6	0.3249	0.405	0.802222	0.090139	22.91773	49128.6	280.65	2.02716	9.11632	20350.3	16.156	15.57532	3.0614	10.2032
W22	0.3911	0.6122	0.638844	0.119322	23.64766	50449.7	286.9	1.78464	9.31516		15.865	14.2423	3.474	7.824
W1	0.2341	0.33471	0.699411	0.068877	19.4317	39976.7	231.274	2.04532	9.68115		16.291	14.71	4.67	6.253
White/Bantycock (Saturated under 5bar water pressure-15week)														
A3	0.35854	0.735	0.48781	0.120493	19.75169	40277.5	198.05	4.08288	14.13873	30855.4	23.822	22.262	6.002	12.0775
1	0.36444	0.6287	0.579672	0.115353	21.709	43769.6	253.2	1.14093	4.88324		24.938	22.4923	5.9408	12.2903
Z	0.158997	0.17395	0.914039	0.041534	14.68011	29578.6	169.25	1.74854	8.28792		24.93	24.6637	6.225	13.963

Table B.5: Short term uniaxial compression tests results of pink/Bantycock gypsum thin layers. These samples tested after saturation under atmospheric pressure for 5, 10, 15, 30 and 50 week time durations.

Thin Layers No.	*Ea* (GPa)	*Ec* (GPa)	*PR*	*SM* (GPa)	$б_c$ (MPa)	*P* (N)	*T* (seconds)	*MAD* (mm)	*MHD* (mm)	*MD* (%)	*MWR* (%)	*MVR* (%)	*MDR* (%)	*MLR* (%)
Pink/Bantycock (Saturated under atmospheric pressure-5week)														
A1	0.955593	1.456933	0.655894	0.288543	42.98821	95982.8	557.5501	1.07188	3.81218	7081.3	2.2933	1.93	0.67	0.601
A2	0.599454	1.059184	0.565958	0.191402	27.95529	63231.8	366.3	1.07539	1.02365		2.252	1.98	0.761	0.47
A3	0.668361	1.42726	0.468283	0.2276	28.24378	63551.6	368.45	0.92539	2.9901		2.163	2.04	0.77	0.52
Pink-Bantycock (Saturated under atmospheric pressure-10week)														
P8	0.56893	1.09976	0.517322	0.187478	30.00022	67471.1	391.7	1.0085	3.33274	14516	3.78	3.51	0.904	1.17
P10	0.504692	1.05438	0.478662	0.170658	28.73327	64283.8	373.3	1.14871	3.92566		4.54	3.452	1.163	1.19
P9	0.633164	1.0494	0.603358	0.197449	34.44503	77267.8	448.05	1.15409	4.36001		4.35	3.631	1.032	1.61
Pink-Bantycock (Saturated under atmospheric pressure-15week)														
P1	0.52834	0.750725	0.703773	0.15505	30.26458	67603.2	392	1.27105	4.9384	20236.8	6.285	3.87	1.241	1.43
P2	0.45963	0.4944	0.929672	0.119095	25.73386	56870	329.7	1.29243	5.9822		7.347	6.2	1.77	2.73
P6	0.494396	0.660192	0.748867	0.141348	25.67812	56968.2	330.05	1.12741	4.50745		6.632	5.273	1.58	2.213
Pink-Bantycock (Saturated under atmospheric pressure-30week)														
P3	0.27636	0.27	1.023556	0.068286	26.79905	56462.1	327.05	1.96154	8.52293	40686.4	14.204	13.795	4.09	6.2992
P7	0.23996	0.215863	1.111631	0.056819	21.7672	45651.3	264.6	1.74847	8.11125		12.78	12.94	4.003	4.93
P5	3.2641	62.262	0.052425	1.550751	21.7672	48736.7	282.4	1.39287	6.50808		12.923	12.803	4.306	5.3821
Pink-Bantycock (Saturated under atmospheric pressure-50week)														
X1	0.2044	0.15862	1.288614	0.044656	20.99797	42361.9	247.304	2.83455	10.76	66517.4	20.77	19.502	8.828	6.037
X2	0.208294	0.1916	1.087129	0.0499	25.83139	52232.4	298.508	3.42026	10.58156		22.312	20.354	9.592	6.144
X3	0.18807	0.1274	1.476217	0.037975	20.69598	40715	238.494	2.77991	11.97511		26.862	25.6363	13.43	8.32

Table B.6: Short term uniaxial compression tests results of Aust Cliff gypsum thin layers. These samples tested after saturation under atmospheric pressure for 5, 10, 15, 30 and 50 week time durations.

Thin Layers No.	*Ea* (GPa)	*Ec* (GPa)	*PR*	*SM* (GPa)	$б_c$ (MPa)	*P* (N)	*T* (seconds)	*MAD* (mm)	*MHD* (mm)	*MD* (%)	*MWR* (%)	*MVR* (%)	*MDR* (%)	*MLR* (%)
Aust Cliff (Saturated under atmospheric pressure-5week)														
4	0.75072	1.6195	0.46355	0.256472	25.51419	57695.3	334.55	0.84012	3.01522	6928.7	3.962	4.9443	0.688	5.885
12	0.4705	1.01362	0.464178	0.16067	30.84553	69138.1	401.15	1.20693	3.87342		3.8452	4.063	1.162	1.3142
A6	0.636	1.0014	0.635111	0.194482	30.93262	69138.12	389.698	1.17981	3.4869		3.7148	4.11256	1.09878	1.21546
Aust Cliff (Saturated under atmospheric pressure-10week)														
A1	0.2919	0.49333	0.591693	0.091695	14.08097	31960.1	184.7	1.90669	9.03194	12928.7	4.35	2.88	0.491	1.8
14	0.76172	3.416	0.222986	0.311418	27.2944	61635.8	357.5	0.69558	1.64826		5.92	11.36	0.7564	1.59
10	0.16579	0.0976	1.698668	0.030717	30.39107	69369.7	403.7	4.08108	9.39025		4.4	2.151	0.181	2.39
Aust Cliff (Saturated under atmospheric pressure-15week)														
11	0.2201	0.3661	0.601202	0.06873	17.94657	39904.8	231.2	2.16804	9.38633	21453	9.63	6.0331	1.512	2.642
12..	0.2066	0.2124	0.972693	0.052365	23.15113	49602.34	282.12	2.38845	9.22145		10.74	7.75	2.185	2.899
13	0.16021	0.156	1.026987	0.039519	11.75014	49602.3	287.75	2.49778	10.30043		12.66	9.568	3.325	3.241
Aust Cliff (Saturated under atmospheric pressure-30week)														
A3	0.135	0.18223	0.740822	0.038775	11.80508	23959.2	137.5	2.6412	10.27606	41695.2	20.55	21.05	5.96	10.141
7	0.1678	0.138713	1.209692	0.037969	4.948323	10000	57.952	0.43093	1.10658		18.9	20.12	5.55	9.98
50	0.4751	1.0508	0.452132	0.163587	33.8963	69138.22	387.698	1.18982	3.8869		18.9154	20.3321	5.25511	10.1245
Aust Cliff (Saturated under atmospheric pressure-50week)														
A4	0.1711	0.17432	0.981528	0.043174	13.6591	25776.4	148.5	2.2368	9.5761	68298.1	27.099	27.7	9.39	9.9342
A5	0.0957	0.0911	1.050494	0.023336	11.87133	23935.3	137.8	2.12933	8.26437		19.84	22.561	6.321	9.711
A2	0.17362	0.1916	0.906159	0.045542	16.19862	30948.8	178.3	2.75637	12.6411		29.84	27.69	8.606	13.431

Table B.7: Short term uniaxial compression tests results of Iraqi gypsum thin layers. These samples tested after saturation under atmospheric pressure for 5, 10, 15, 30 and 50 week time durations.

Thin Layers No.	*Ea* (GPa)	*Ec* (GPa)	*PR*	*SM* (GPa)	$б_c$ (MPa)	*P* (N)	*T* (seconds)	*MAD* (mm)	*MHD* (mm)	*MD* (%)	*MWR* (%)	*MVR* (%)	*MDR* (%)	*MLR* (%)
Iraqi (Saturated under atmospheric pressure-5week)														
3	0.7432	1.22733	0.605542	0.231448	65.64152	147059	856.1001	1.90878	6.10966	7070.7	1.58	3.141	1.085	1.005
1	0.5571	0.85977	0.647964	0.169027	37.30857	85255.4	496.3	1.26619	4.44374		1.842	1.82	0.111	2.038
IS6	0.6377	0.8066	0.790603	0.178069	38.27048	86886.7	505.65	1.38921	5.51774		1.998	1.09	0.42	0.251
Iraqi (Saturated under atmospheric pressure-10week)														
IS1	0.59154	1.0507	0.562996	0.189233	38.57826	86629.1	504.3	1.39384	4.88682	14047.7	3.41	5.99	0.973	0.25
IS2	0.5932	0.89699	0.661323	0.178532	28.7121	63914.3	371.9	1.04968	3.34699		4.67	4.74	1.373	2.07
4	0.47184	0.648774	0.727279	0.136585	37.27849	84384	491.1	1.45655	4.77597		2.7133	2.591	0.579	1.38
Iraqi (Saturated under atmospheric pressure-15week)														
IS5	0.5695	0.55	1.035455	0.139895	43.21345	96119.2	559.45	1.54586	5.77875	21227	6.465	4.634	1.44	1.835
5	0.46342	0.59197	0.782844	0.129967	31.26669	69309.3	403.35	1.58031	6.3242		6.399	5.613	1.602	2.38
IS4	0.5688	1.0728	0.530201	0.185858	24.36515	53510.9	311.4	0.89161	3.61937		7.08	6.903	2.0534	2.96
Iraqi (Saturated under atmospheric pressure-30week)														
IS3	0.56614	0.716114	0.790572	0.158089	25.02108	52731.1	306.65	1.15618	5.4414	41994.2	12.85	13.59	4.032	6.172
2	0.4648	0.4875	0.953436	0.11897	23.1984	47423.6	275.85	1.09176	5.30956		16.242	17.721	5.2397	8.3711
9	0.2772	0.2384	1.162752	0.064085	35.08996	72161.2	408.65	3.26802	9.4776		17.399	17.797	5.404	7.78
Iraqi (Saturated under atmospheric pressure-50week)														
7	0.29673	0.335045	0.885642	0.078681	35.37271	65029.1	338.4	3.66719	10.02217	69607.9	23.79	30.858	10.3022	11.931
8	0.29091	0.38098	0.763583	0.082477	17.47239	33177.4	179.45	1.51783	6.4213		28.69	30.0261	8.85	15.78
6	0.1724	0.3015	0.571808	0.054841	13.20448	25534.4	143.75	2.06745	8.90375		22.87	25.44	8.03	11.7223

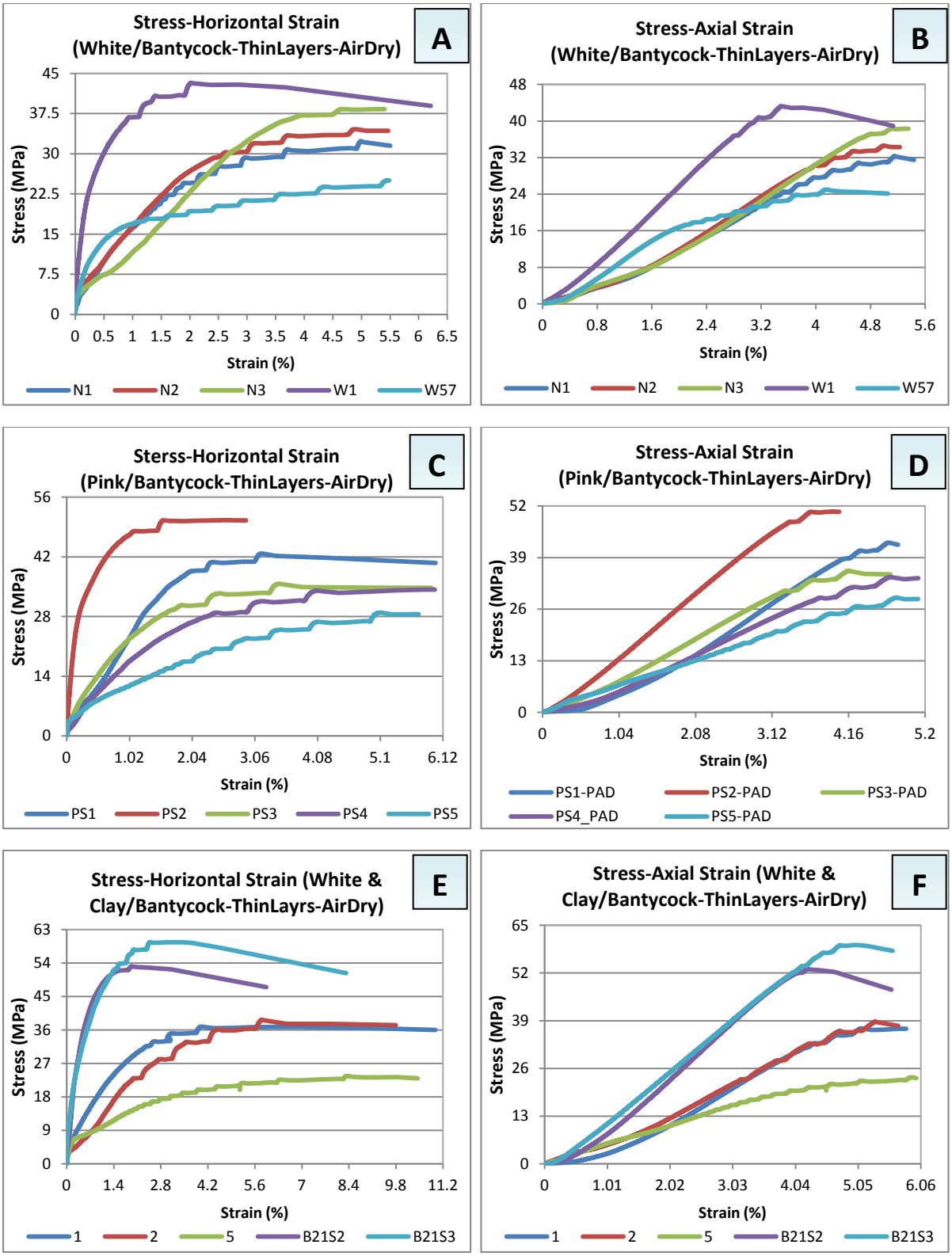

Fig. B.1: Presents short-term uniaxial compression tests results for thin layers of different Bantycock gypsum types. These samples tested in air-dry state for different types of gypsum as shown on each plate.

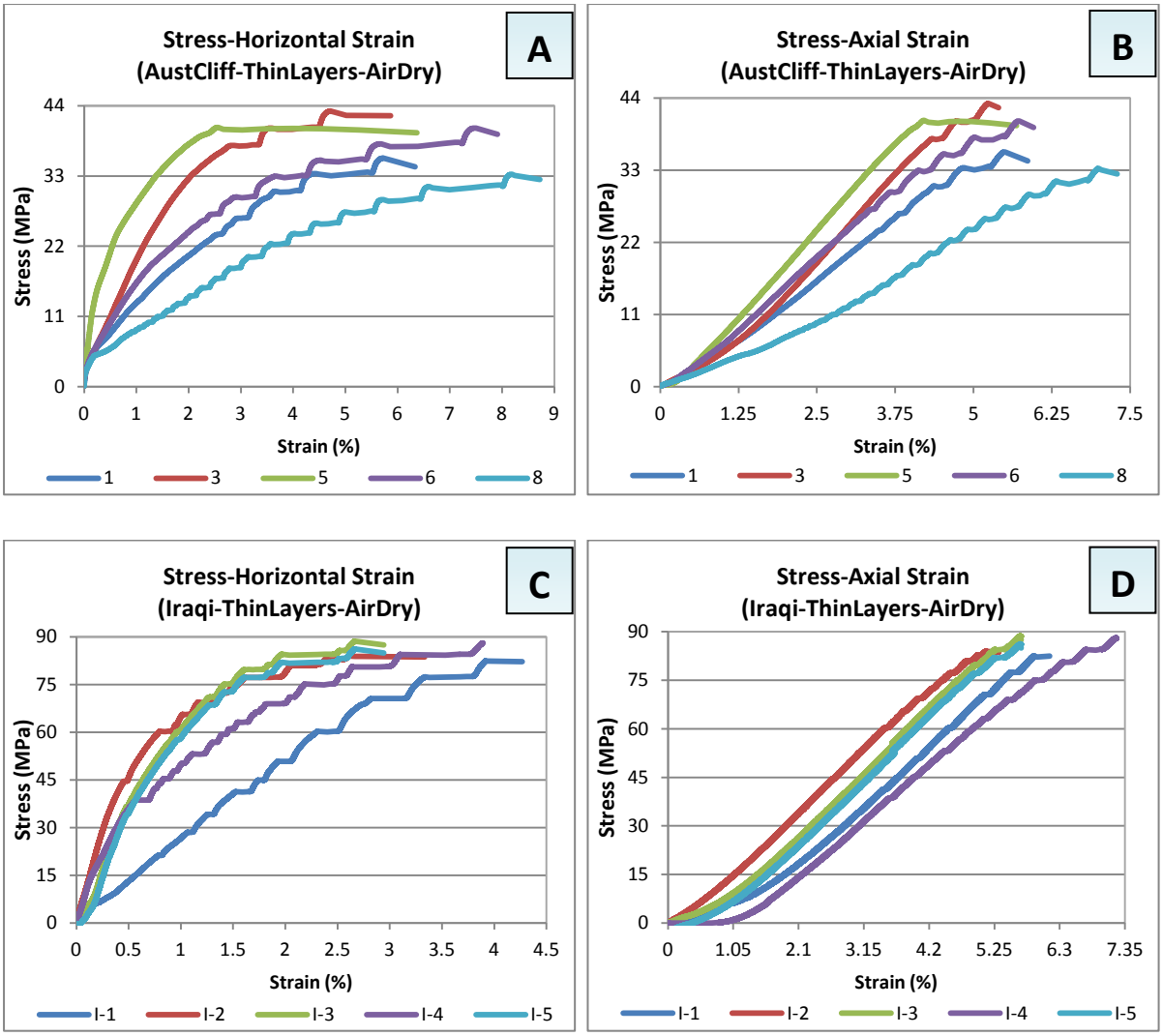

Fig. B.2: Presents short-term uniaxial compression tests results for Aust Cliff and Iraqi thin layers. These samples tested in air-dry state.

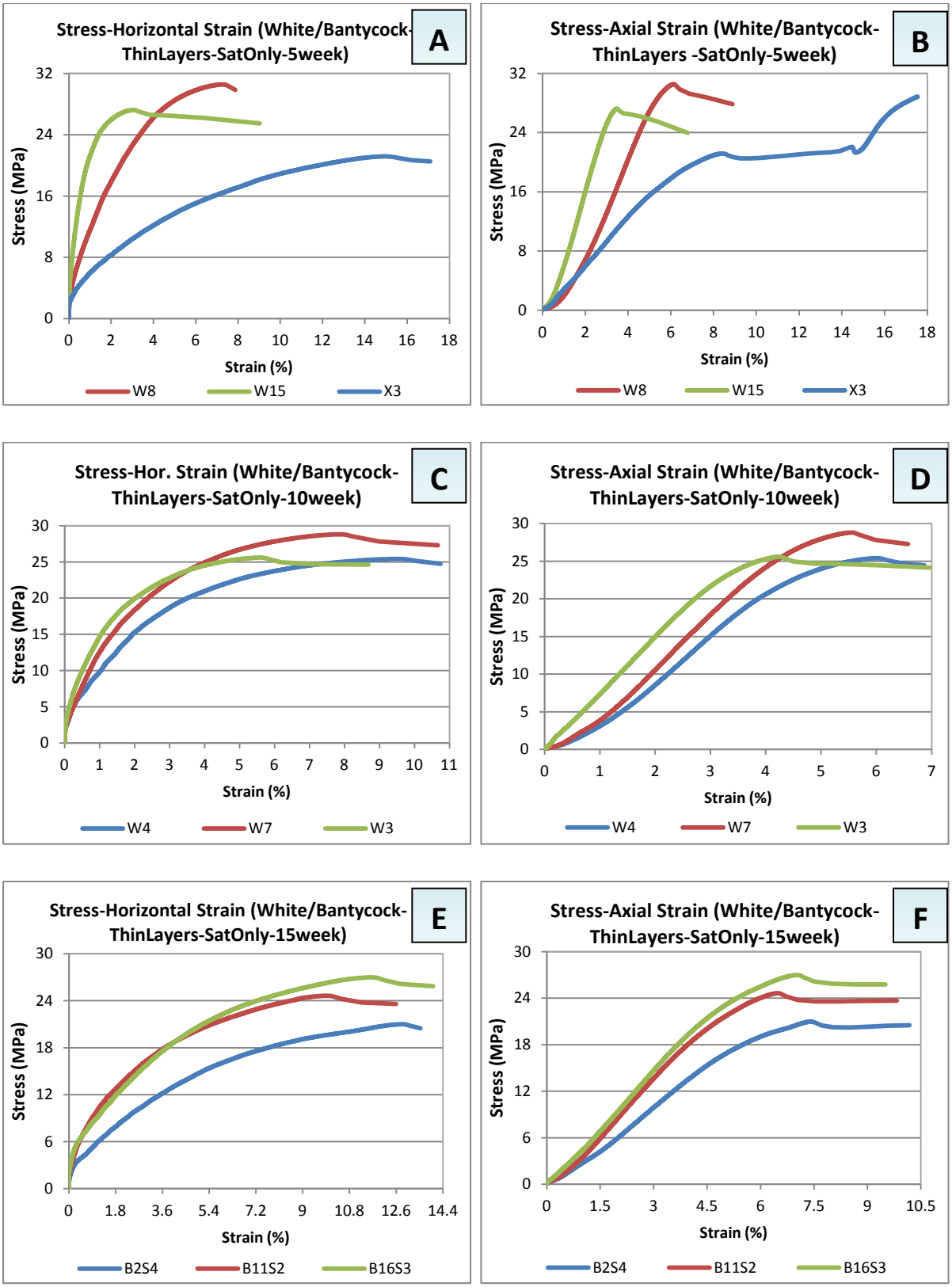

Fig. B.3: Presents short-term uniaxial compression tests results for white/Bantycock thin layers. These samples tested after saturation under atmospheric pressure for 5, 10 and 15 week time durations as shown on each part.

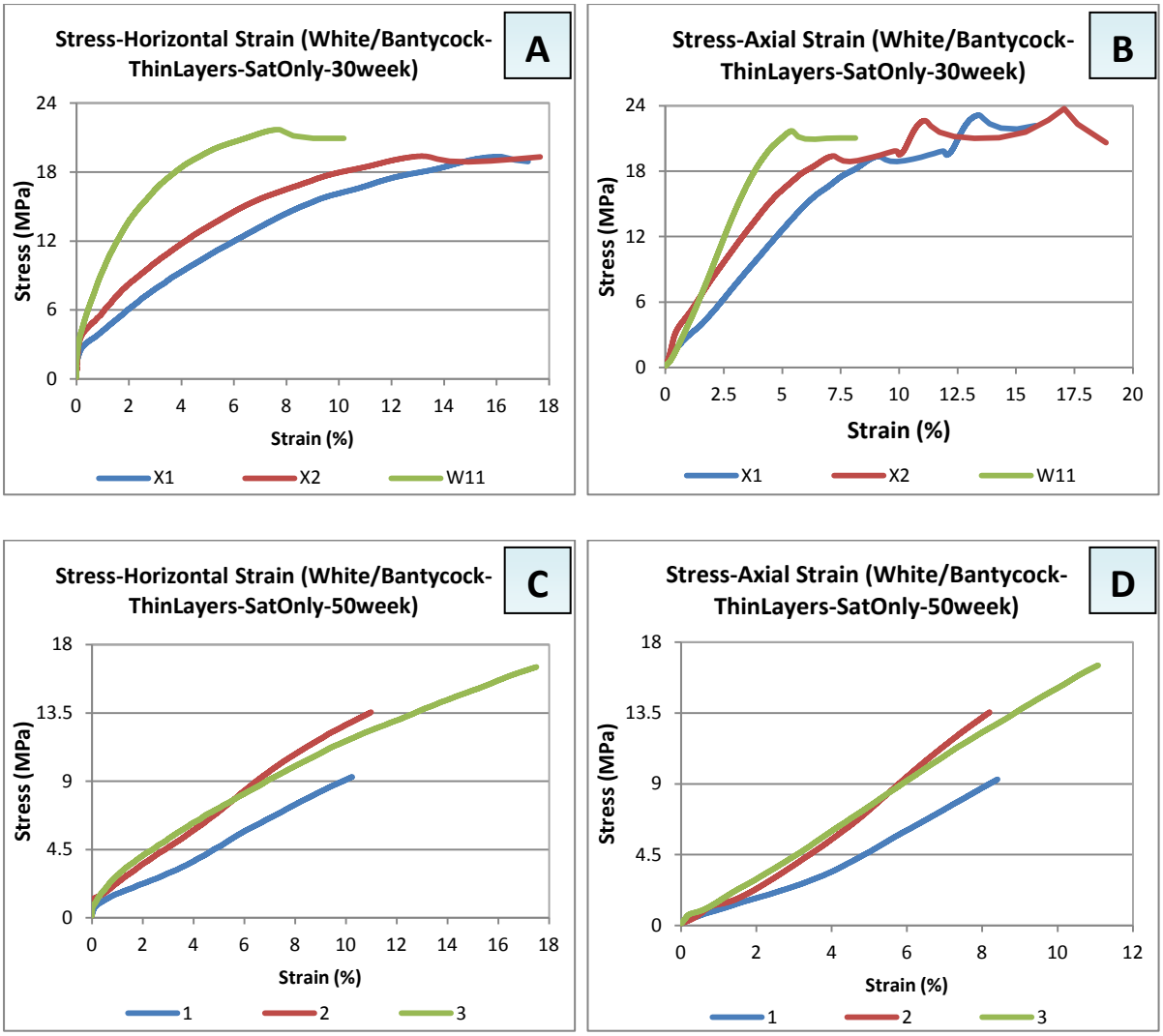

Fig. B.4: Presents short-term uniaxial compression tests results for white/Bantycock thin layers. These samples tested after saturation under atmospheric pressure for 30 and 50 week time durations as shown on each part.

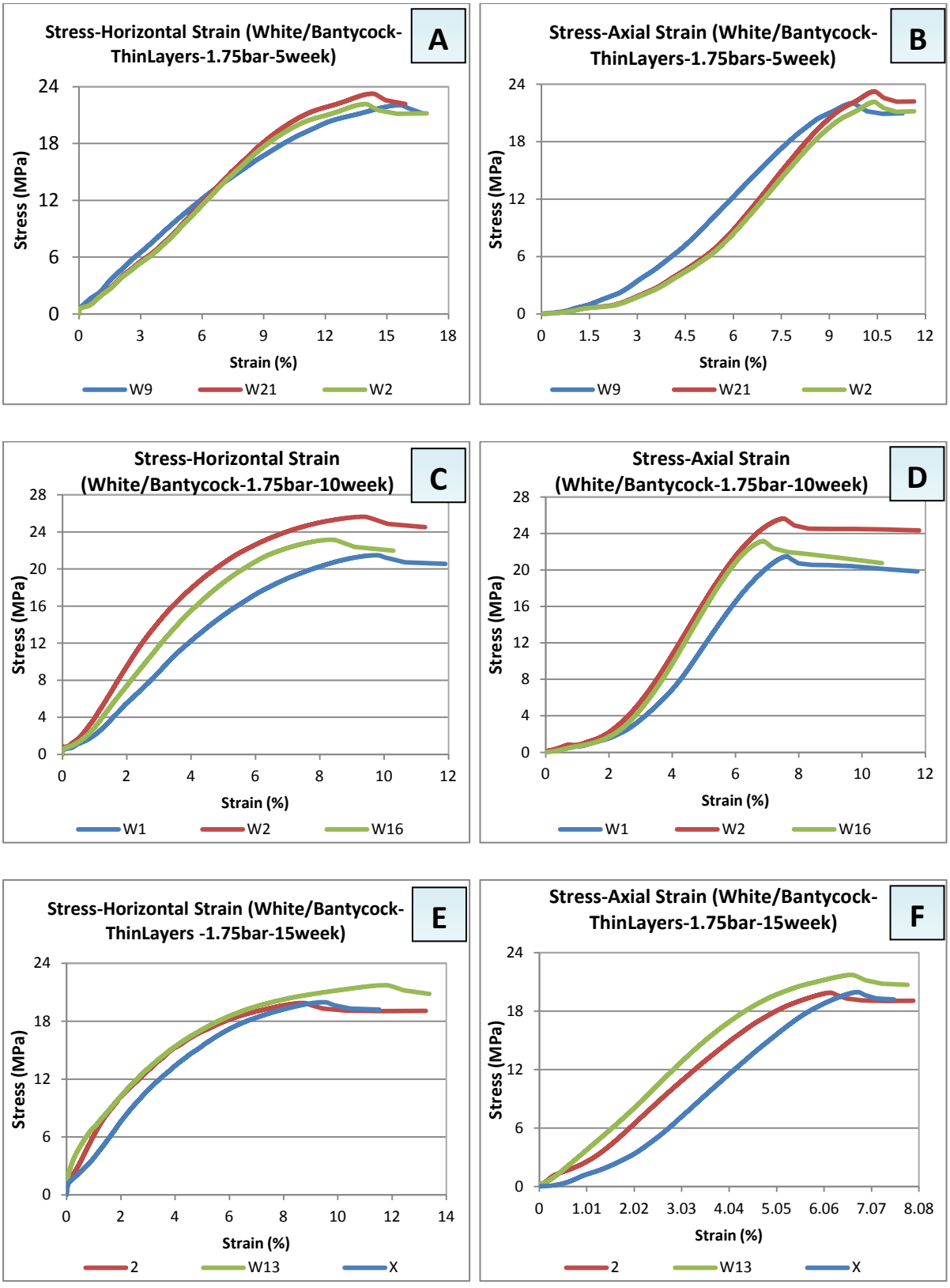

Fig. B.5: Presents short-term uniaxial compression tests results for white/Bantycock thin layers. These samples tested after saturation under 1.75 bar water pressure for 5, 10 and 15 week time durations as shown on each part.

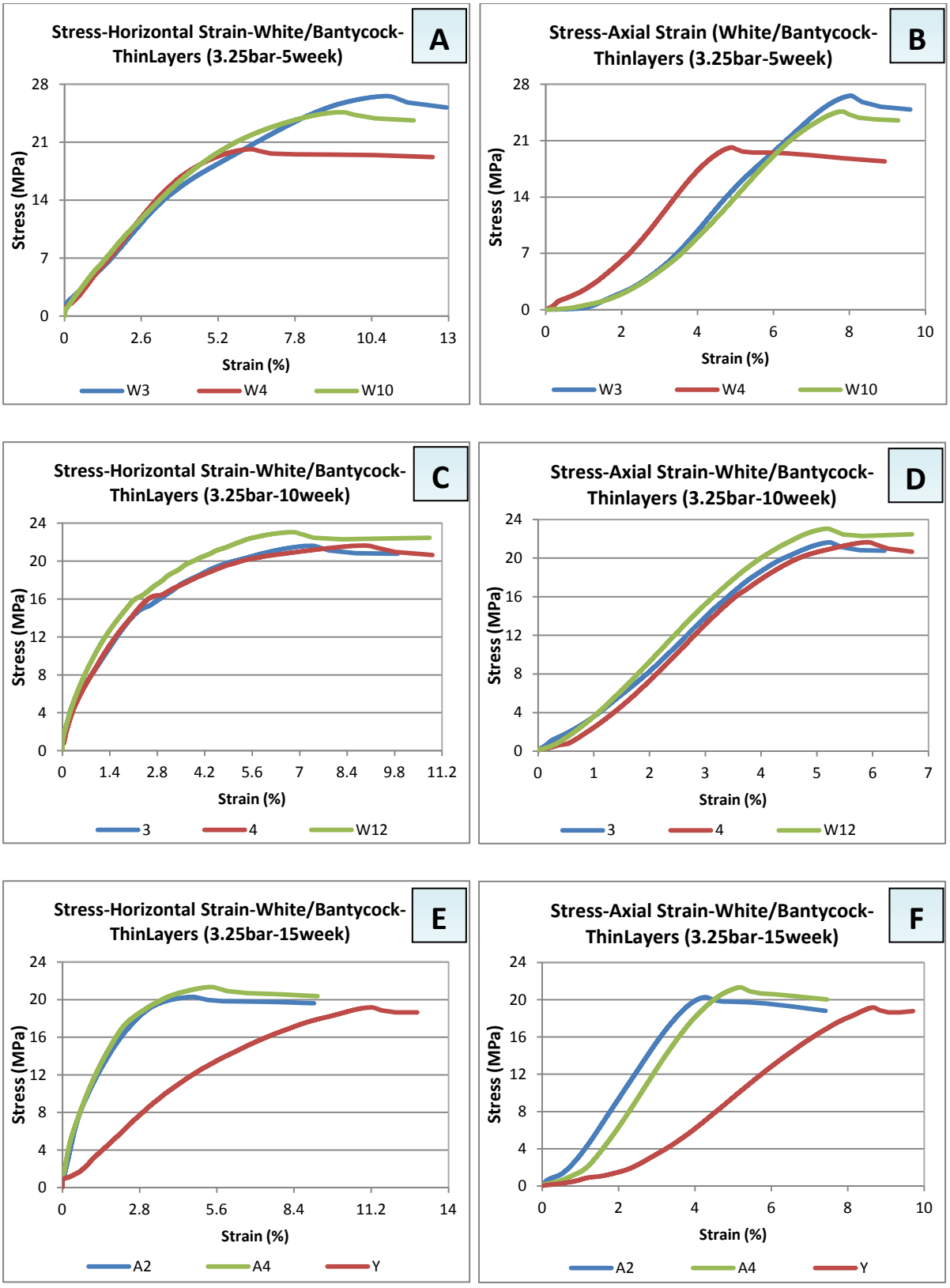

Fig. B.6: Presents short-term uniaxial compression tests results for white/Bantycock thin layers. These samples tested after saturation under 3.25 bar applied water pressure for 5, 10 and 15 week time durations as shown on each part.

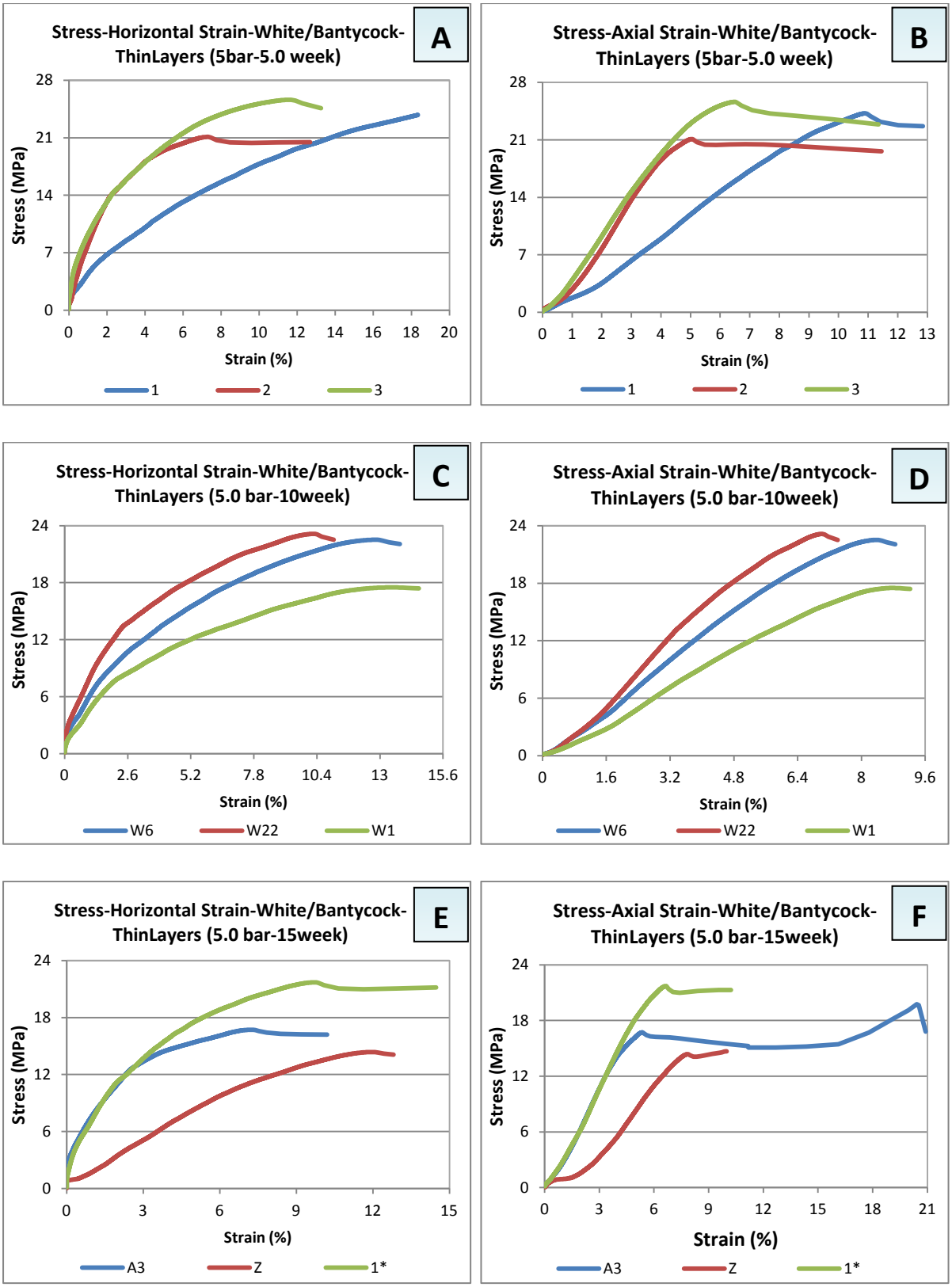

Fig. B.7: Presents short-term uniaxial compression tests results for white/Bantycock thin layers. These samples tested after saturation under 5.0 bar applied water pressure for 5, 10 and 15 week time durations as shown on each part.

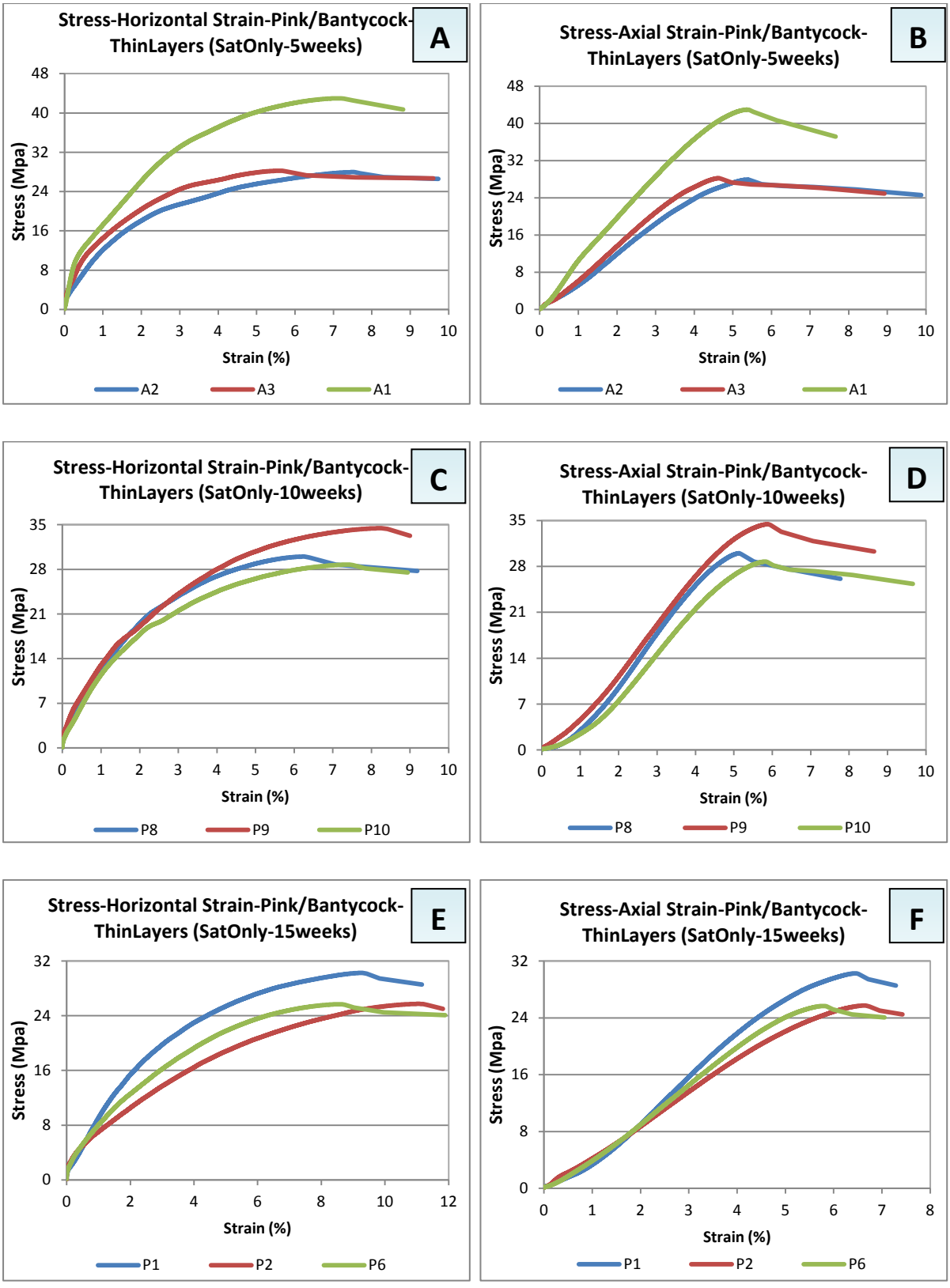

Fig. B.8: Presents short-term uniaxial compression tests results of pink/Bantycock thin layers. These samples tested after saturation under atmospheric pressure for 5, 10 and 15 week time durations as shown on each part.

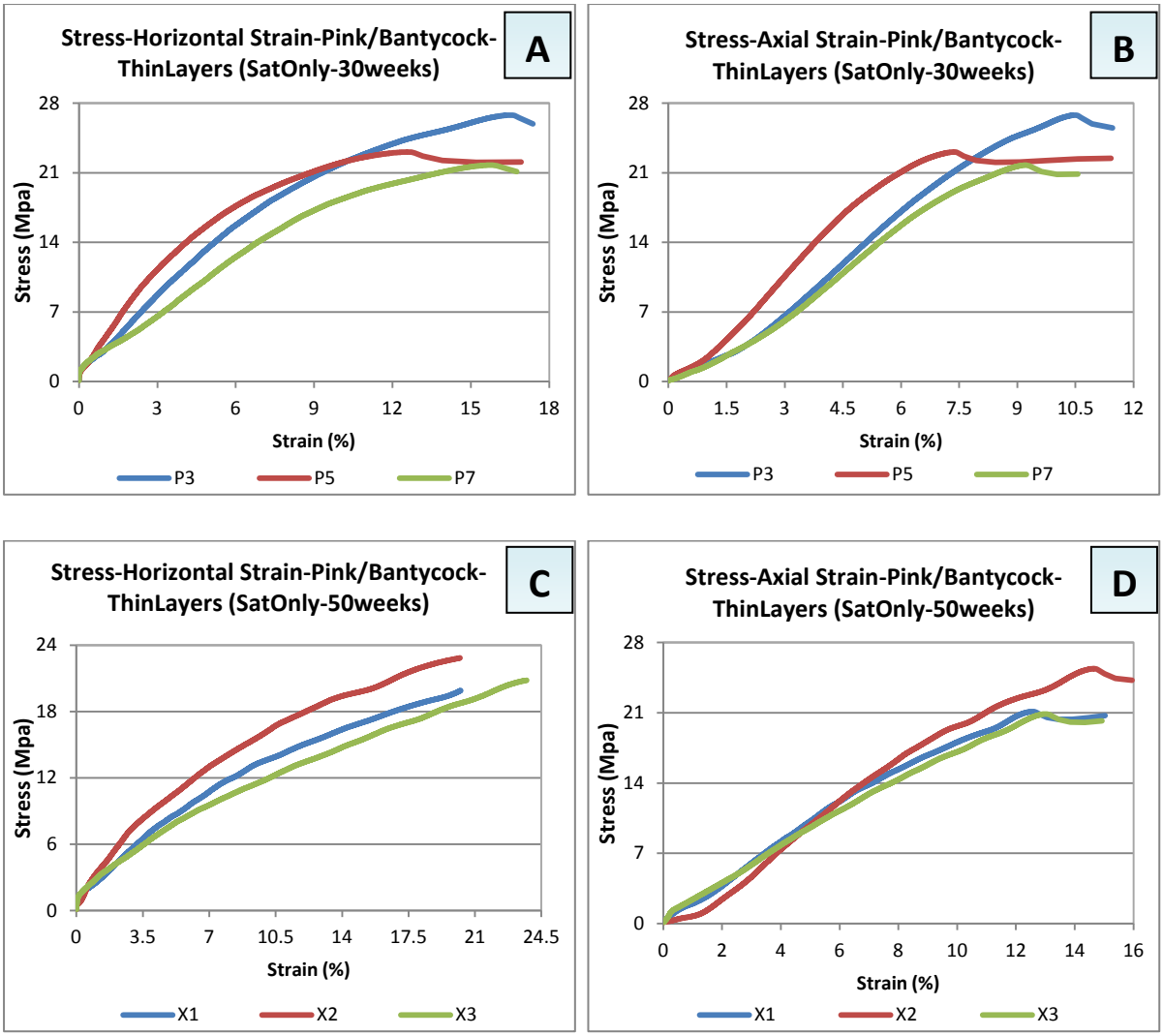

Fig. B.9: Presents short term uniaxial compression tests results for pink/Bantycock thin layers. These samples tested after saturation under atmospheric pressure for 30 and 50 week time durations as shown on each part.

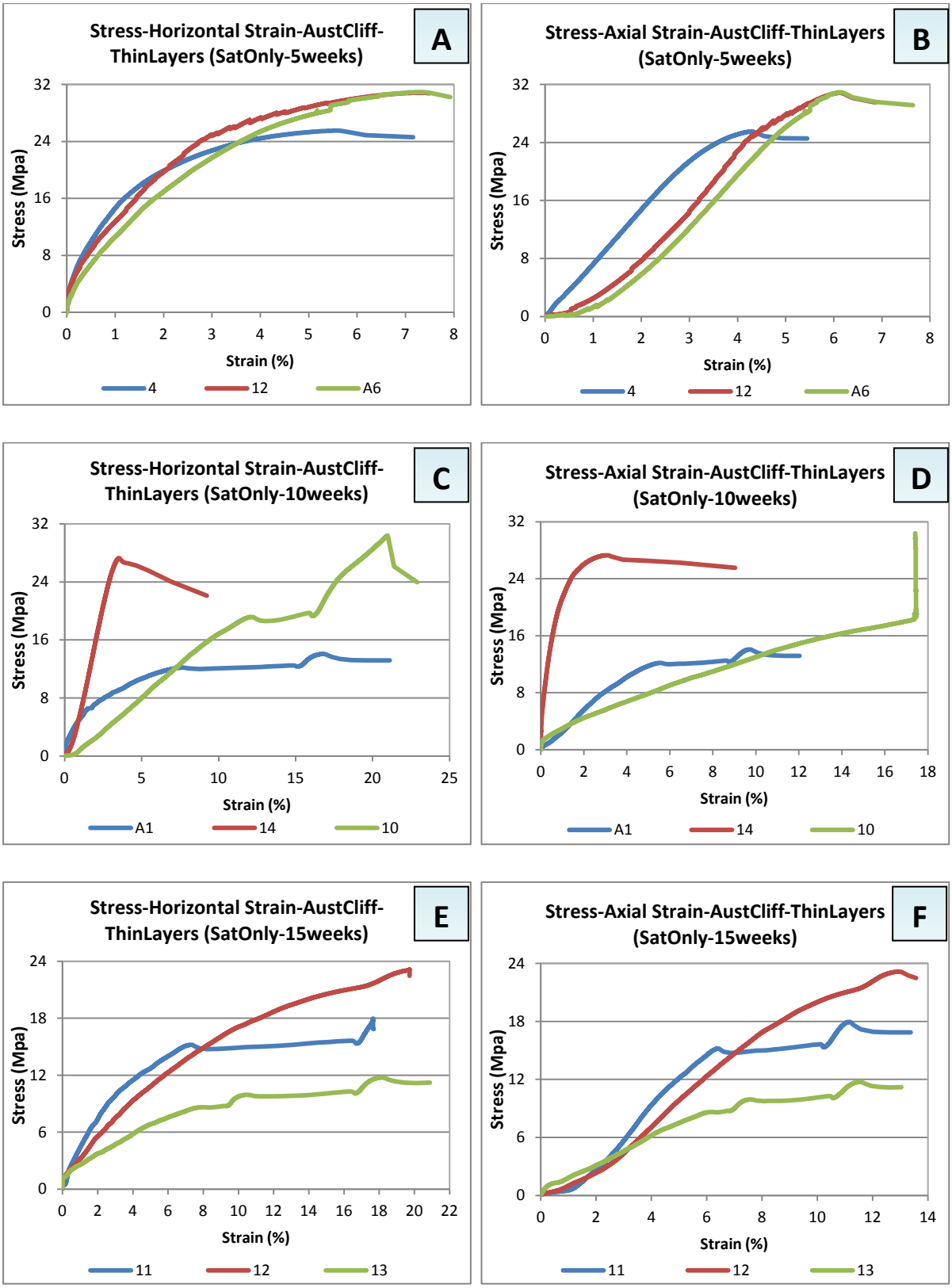

Fig. B.10: Present short-term uniaxial compression tests results of Aust Cliff thin layers. These samples tested after saturated under atmospheric pressure for 5, 10 and 15 week time durations as shown on each part.

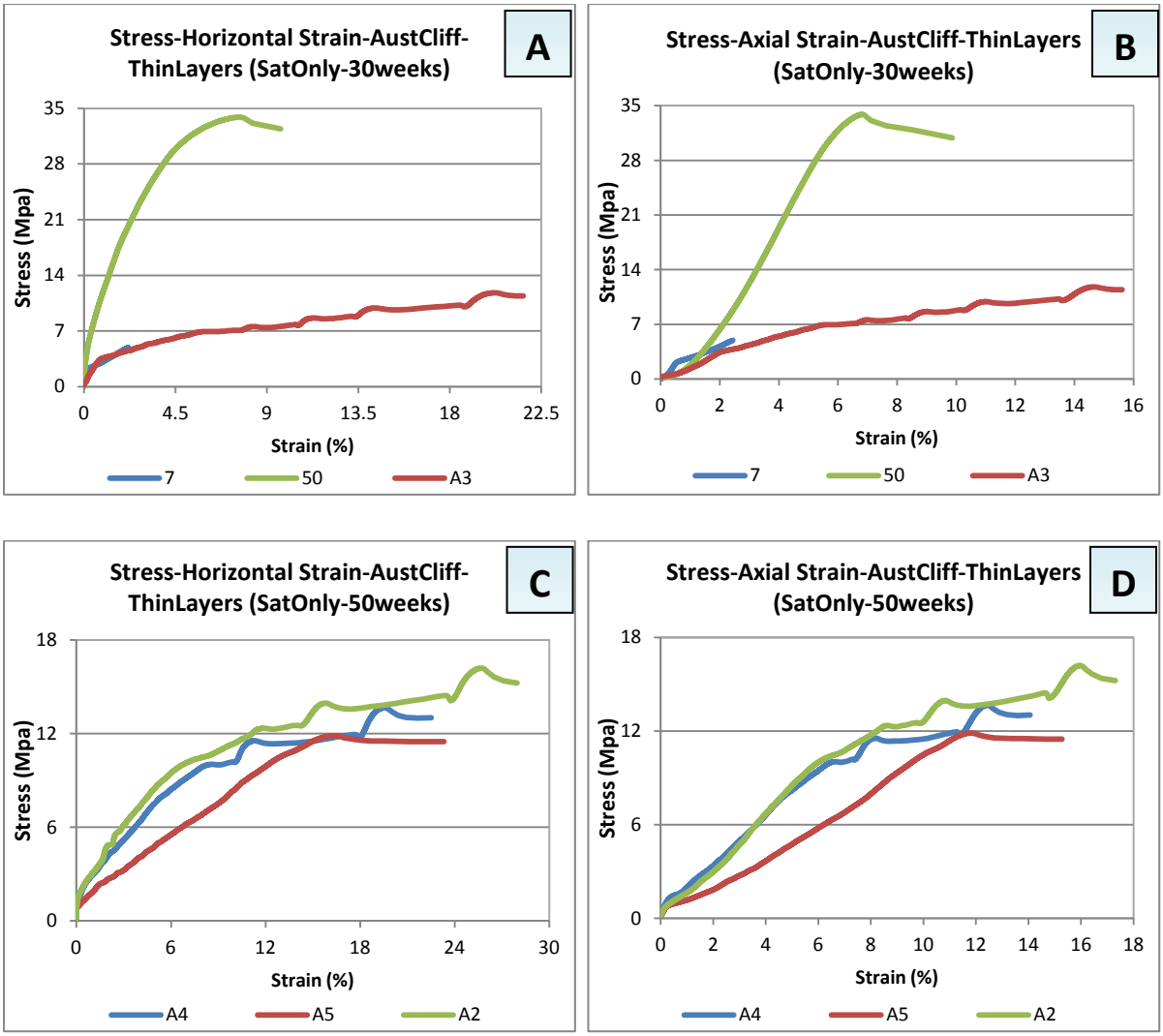

Fig. B.11: Present short-term uniaxial compression tests results of Aust Cliff thin layers. These samples tested after saturation under atmospheric pressure for 30 and 50 week time durations as shown on each part.

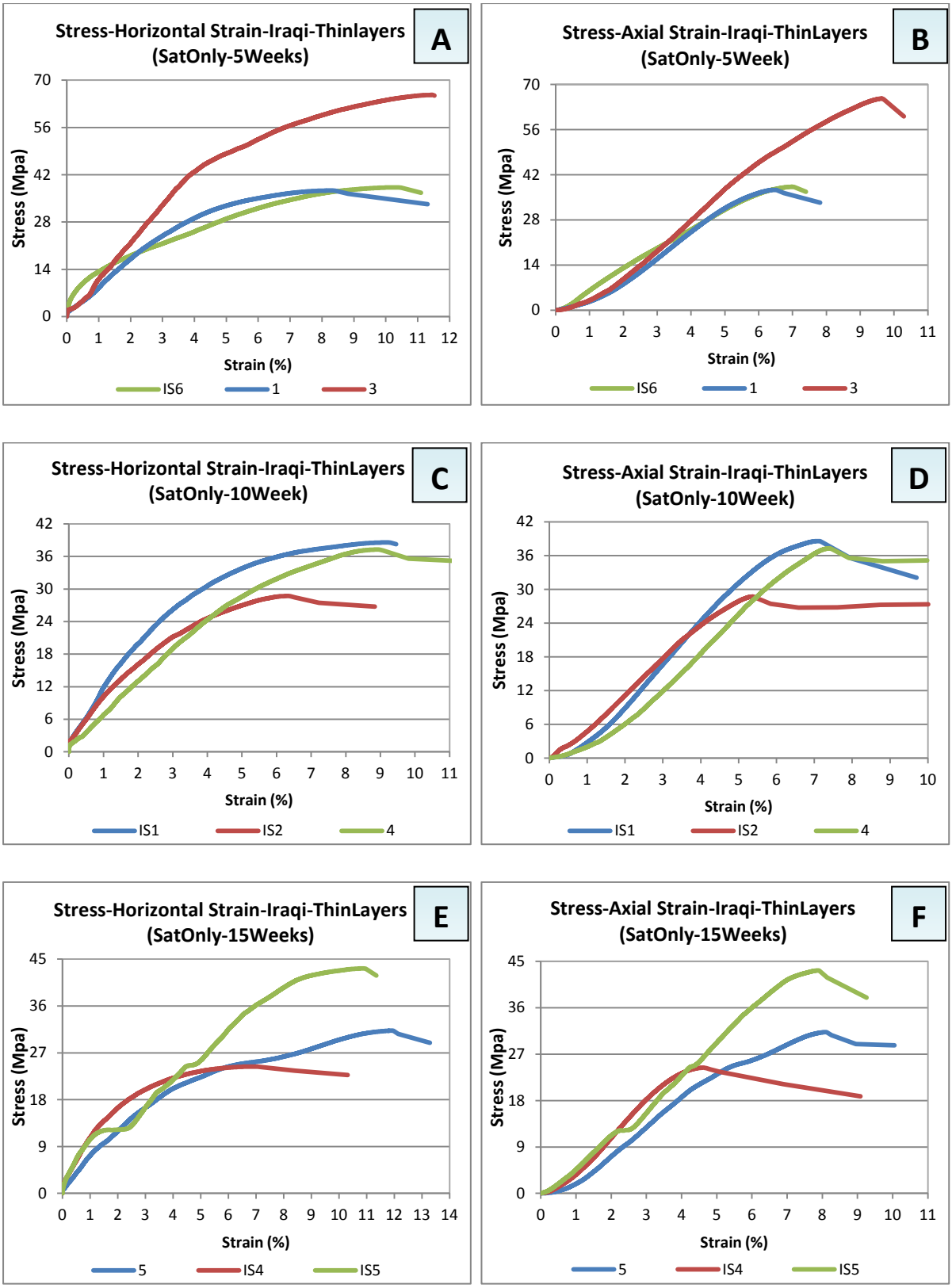

Fig. B.12: Present short-term uniaxial compression tests results of Iraqi thin layers. These samples tested after saturation under atmospheric pressure for 5, 10 and 15 week time durations as shown on each part.

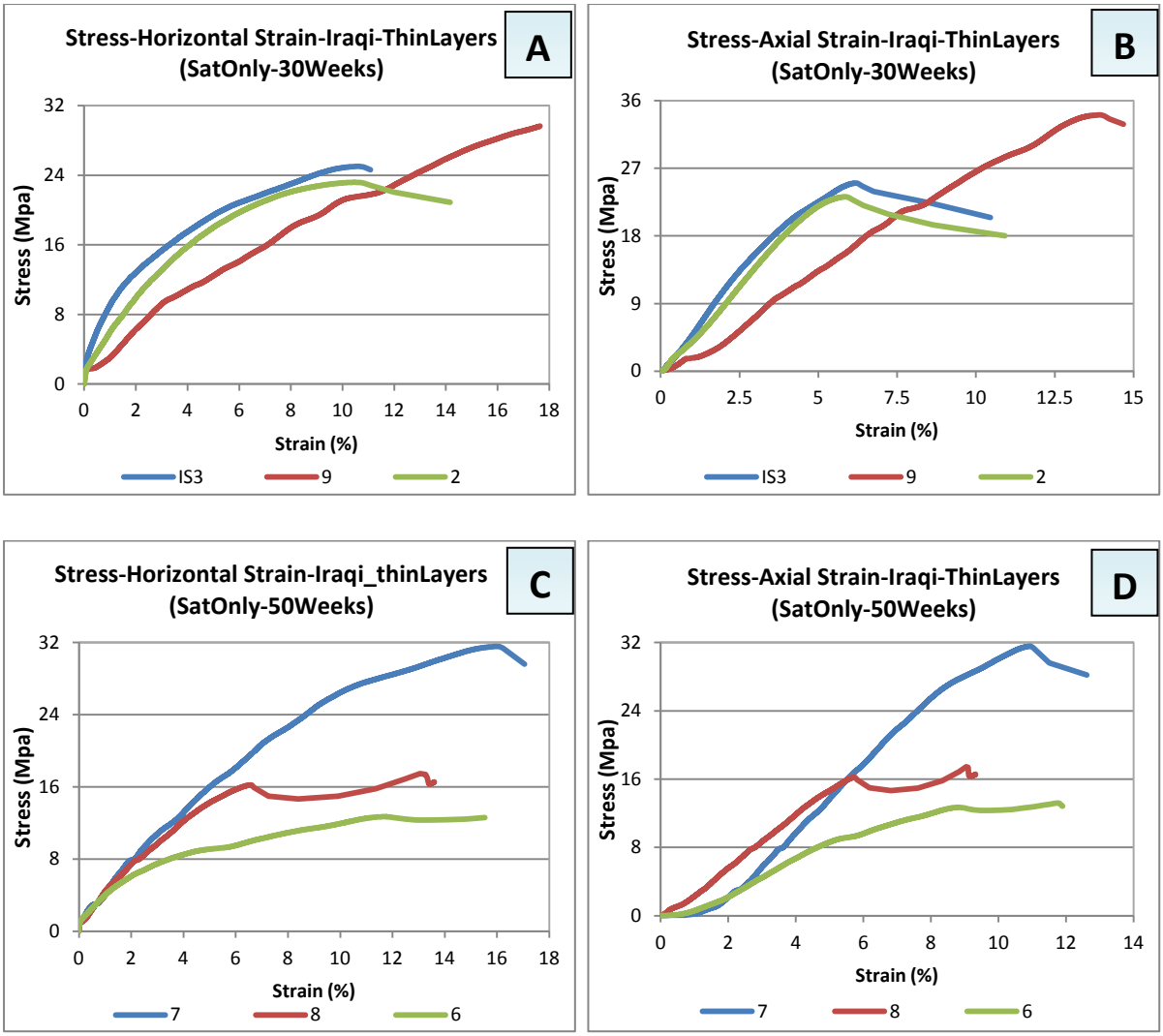

Fig. B.13: Present short-term uniaxial compression tests results of Iraqi thin layers. These samples tested after saturation under atmospheric pressure for 30 and 50 week time durations as shown on each part.

B.2 Large Four-Point Bending

Different kinds of abbreviations were used in below tables, which represent properties such as: *Ea* = Flexural Modulus (GPa), $F\sigma_c$ = Flexural Stress at failure (MPa), *P* = Load at failure (N), *T* = Time to failure (seconds), *MAD* = Maximum vertical deflection (mm), *MD* = Maximum dissolution (US/cm), *MWtR* = Maximum mass reduction (%), *MVR* = Maximum volume reduction (%), , *MLR* = Maximum length reduction (%), *MWR* = Maximum width reduction and *MDeR* = Maximum depth reduction (%).

Table B.8: Short-term flexural tests results of white/Bantycock large bars tested in air-dry state.

Large Bending Kind	Axial Modulus (*Ea*)(GPa)	Time to Failure (*T*) (seconds)	Compressive Strength (σ_c) (MPa)	Load at Failure (*P*) (N)	Max Axial Deflection (*MAD*) (mm)
White/Bantycock (Air-Dry)					
B1	17.051	295	5.99165	479.3323	0.12705
B2	19.6	280.9	5.83541	466.8325	0.11502
B3	22.2877	320.6	6.56947	525.5579	0.21382
B4	18.5514	400.1	8.13151	650.5204	0.16166
B5	19.234	304.2	6.13466	505.1727	0.12451

Table B.9: Short-term flexural tests results of white/Bantycock large bars. These samples tested after saturation under atmospheric pressure for 5, 10, 15, 30 and 50 week time durations.

Large Bending No.	*Ea* (GPa)	*T* (seconds)	σ_c (MPa)	*P* (N)	*MAD* (mm)	*MD* (US/cm)	*MWtR* (%)	*MVR* (%)	*MLR* (%)	*MWR* (%)	*MDeR* (%)
White/Bantycock (saturated under atmospheric pressure-5Week)											
1	8.0738	106.5	2.25705	180.564	0.13049	7533.6	2.6912	2.234	0.018	1.772	0.452
2	3.0511	105.8	2.18353	174.682	0.23266		2.77	0.4554	0.082	3.2221	0.445
BB10	0.3485	163.1	3.56706	285.3648	0.2121		2.724	2.669	0.259	1.749	0.679
White/Bantycock (saturated under atmospheric pressure-10Week)											
1	10.364	102.3	2.20713	176.5707	0.13124	14997.9	5.704	4.8271	0.3396	1.596	2.9544
2	10.64	102.2	2.31241	184.9932	0.1207		5.65	5.34	0.334	2.993	2.1
3	15.94759	112.4	2.37063	189.6501	0.09477		5.96	5.17	0.486	2.902	1.86
White/Bantycock (saturated under atmospheric pressure-15Week)											
3	8.51183	100.8	2.21476	177.1807	0.11988	23328.6	7.412	5.774	0.397	2.973	2.5
BB-3	6.12469	63.2	1.44796	115.8365	0.07862		8.4513	3.44	0.669	2.052	3.238
2	8.4569	116.6	2.51943	201.554	0.12974		7.844	6.632	0.949	4.661	1.1294
White/Bantycock (saturated under atmospheric pressure-30Week)											
B-B-7	1.7685	52.1	1.17236	93.78864	0.22219	43316.4	15.7	23.2199	0.961	9.73	14.217
B-B-8	8.133	80.4	1.85659	148.5274	0.12361		16.73	24.541	0.805	9.181	16.239
B-B-9	4.5899	66.4	1.40328	112.2622	0.13677		15.5	23.3762	1.384	9.236	14.3944
White/Bantycock (saturated under atmospheric pressure-50Week)											
B-B-1	3.5396	65.10001	1.40524	112.4196	0.19133	70372.4	26.39	21.24	1.2612	12.8974	22.2
B-B-2	6.4367	71.60001	1.60721	128.5768	0.12077		24.3797	34.263	1.152	13.03	23.537
B-B-3	9.355	54.4	1.30965	104.7718	0.08161		27.389	41.1581	1.714	16.84	24.2664

Table B.10: Short-term flexural tests results of white/Bantycock large bars. These bars tested after saturation under 1.75 and 3.25 applied water pressure for 5, 10 and 15 week time durations.

Large Bending Kind	*Ea* (GPa)	*T* (seconds)	σ_c (MPa)	*P* (N)	*MAD* (mm)	*MD* (US/cm)	*MWtR* (%)	*MVR* (%)	*MLR* (%)	*MWR* (%)	*MDeR* (%)
White/Bantycock (saturated under 1.75 bar water pressure-5Week)											
BB-7	5.02973	85.3	1.88958	151.1663	0.12862	10724.7	4.001	7.41	0.17	2.391	1.693
N1	4.5434	144	3.04528	243.6225	0.32787		3.75	6.911	0.0743	2.052	4.94
N2	12.59171	141.2	3.0255	242.0399	0.14118		4.112	8.01	0.129	2.361	5.68
White/Bantycock (saturated under 1.75 bar water pressure-10Week)											
1	7.525	91.10001	1.93791	155.0328	0.13639	21582.2	7.89	11.203	0.595	3.83	7.1862
2	17.46924	97.4	2.12639	170.1113	0.09469		8.04	10.883	0.663	3.67	6.918
1	6.9678	113.7	2.43831	195.0648	0.12466		7.98	11.28	0.896	2.439	8.238
White/Bantycock (saturated under 1.75 bar water pressure-15Week)											
BB-6	0.670133	57.9	1.56642	125.3134	0.05119	32056.1	11.71	11.56	0.5213	4.155	7.7
BB-8	0.9036	88.00001	2.1779	174.2297	0.0793		11.58	11.04	0.482	3.79	7.452
BB-10	0.6978	64	1.78255	142.6042	0.06121		11.763	12.152	0.61	4.2732	8.09
White/Bantycock (saturated under 3.25 bar water pressure-5Week)											
4	6.51143	107.9	2.31535	185.2279	0.16076	10974.7	4.094	8.16	0.817	2.37	5.8
5	18.4416	131.2	2.81096	224.877	0.10082		4.3899	8.41	0.091	2.659	5.821
6	26.95088	121.3	2.63933	211.1468	0.0997		4.2634	7.3704	0.274	2.71	4.57
White/Bantycock (saturated under 3.25 bar water pressure-10Week)											
BB-9	7.8132	86.9	1.91439	153.1509	0.09977	21825.1	8.8333	15.2332	0.90977	5.0144	9.993
BB11	0.43877	77.60001	1.94187	155.3492	0.12586		8.65	15.824	0.73574	6.271	9.557
3	20.06667	82.8	1.80849	144.6792	0.06883		6.81	10.115	0.8412	3.9033	5.713
White/Bantycock (saturated under 3.25 bar water pressure-15Week)											
3	5.68417	76.20001	1.76161	140.9286	0.12571	32944.8	12.54	14.1804	0.814	5.0132	9.49
BB-3	6.12469	63.2	1.44796	115.8365	0.07862		13.2222	13.34	0.714	4.5434	9.06794
BB12	0.64017	61.3	1.61626	129.3007	0.07287		13.222	14.636	0.768	4.992	9.967

Table B.11: Short term four-point flexural tests results of white/Bantycock large bars. These samples tested after saturation under 5.0 applied water pressure 5, 10 and 15 week time durations.

Large Bending Kind	*Ea* (GPa)	*T* (seconds)	σ_c (MPa)	*P* (N)	*MAD* (mm)	*MD* (US/cm)	*MWtR* (%)	*MVR* (%)	*MLR* (%)	*MWR* (%)	*MDeR* (%)
White (5bar-5Week)											
7	5.91113	124.9	2.64792	211.8332	0.15485	11316.1	4.54	8.6332	0.429	2.21	6.14
8	2.61198	112	2.33159	186.5271	0.2343		4.6721	7.9683	0.37	1.572	5.7
9	19.08144	115.9	2.54638	203.7105	0.07847		4.68	8.1	0.172	2.151	5.09
White (5bar-10Week)											
1	0.8955	86.9	1.85907	148.7257	0.55313	22578	9.11	14.17	0.8	5.1	9.253
2	2.06604	88.8	1.87959	150.3668	0.27309		9.63	17.01	0.905	4.99	10.559
3	4.4156	76.70001	1.62398	129.9184	0.13423		9.003	15.2	0.91	5.252	10.054
White (5bar-15Week)											
B-B-4	7.05223	71.2001	1.61079	128.8631	0.10045	33911	13.574	14.82	0.7531	5.55	9.562
B-B-5	4.698	84.10001	1.82846	146.2769	0.24701		13.762	14.644	0.89	5	9.86
B-B-6	20.36541	83.20001	1.88802	151.0415	0.06046		14.464	17.4142	0.997	6.31	11.64

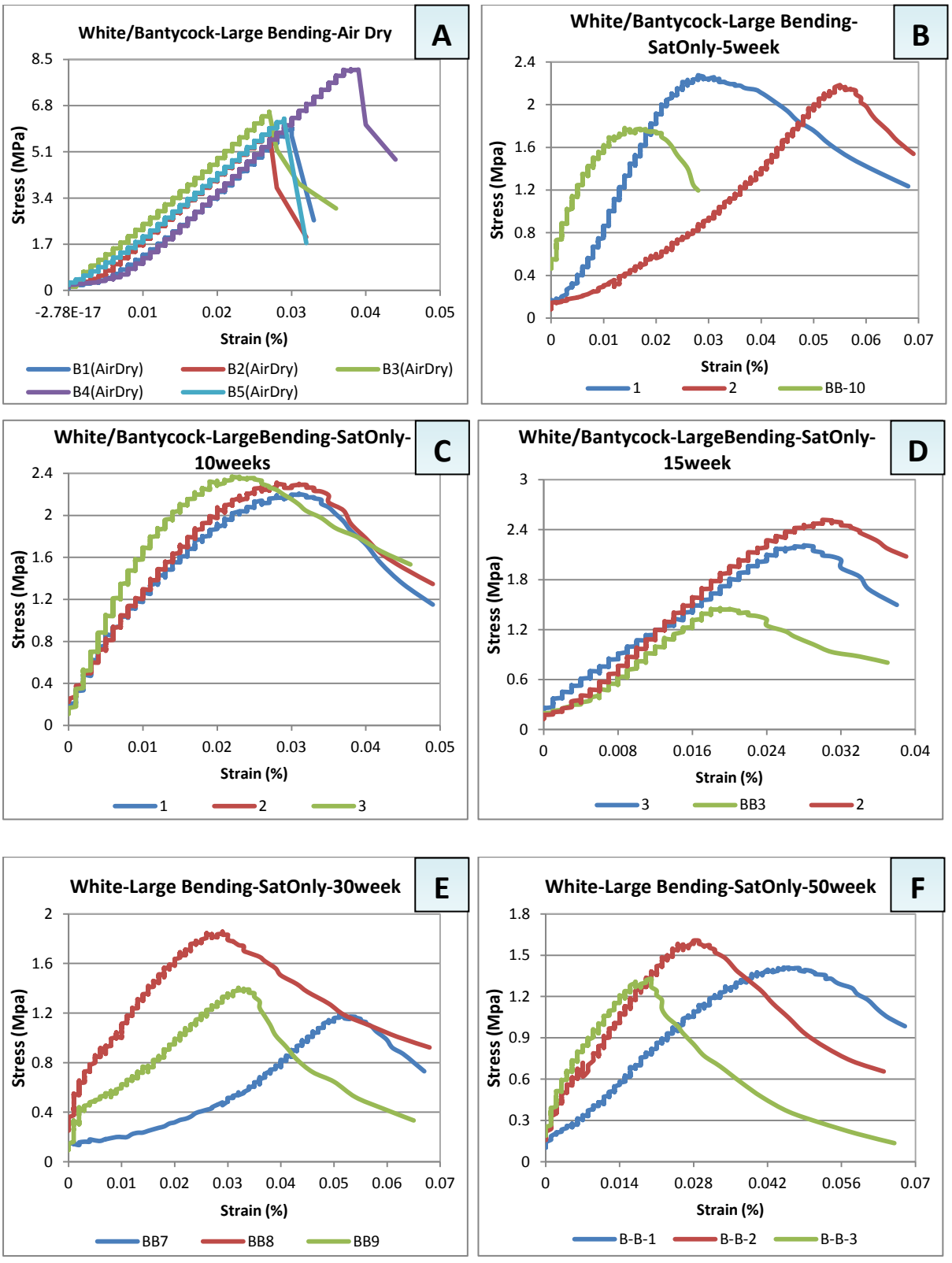

Fig. B.14: Present short-term four-point flexural tests results of white/Bantycock large bars. These samples tested in air-dry/part A and saturation state (other parts) under atmospheric pressure for 5, 10, 15, 30 and 50 weeks time durations as shown on each part.

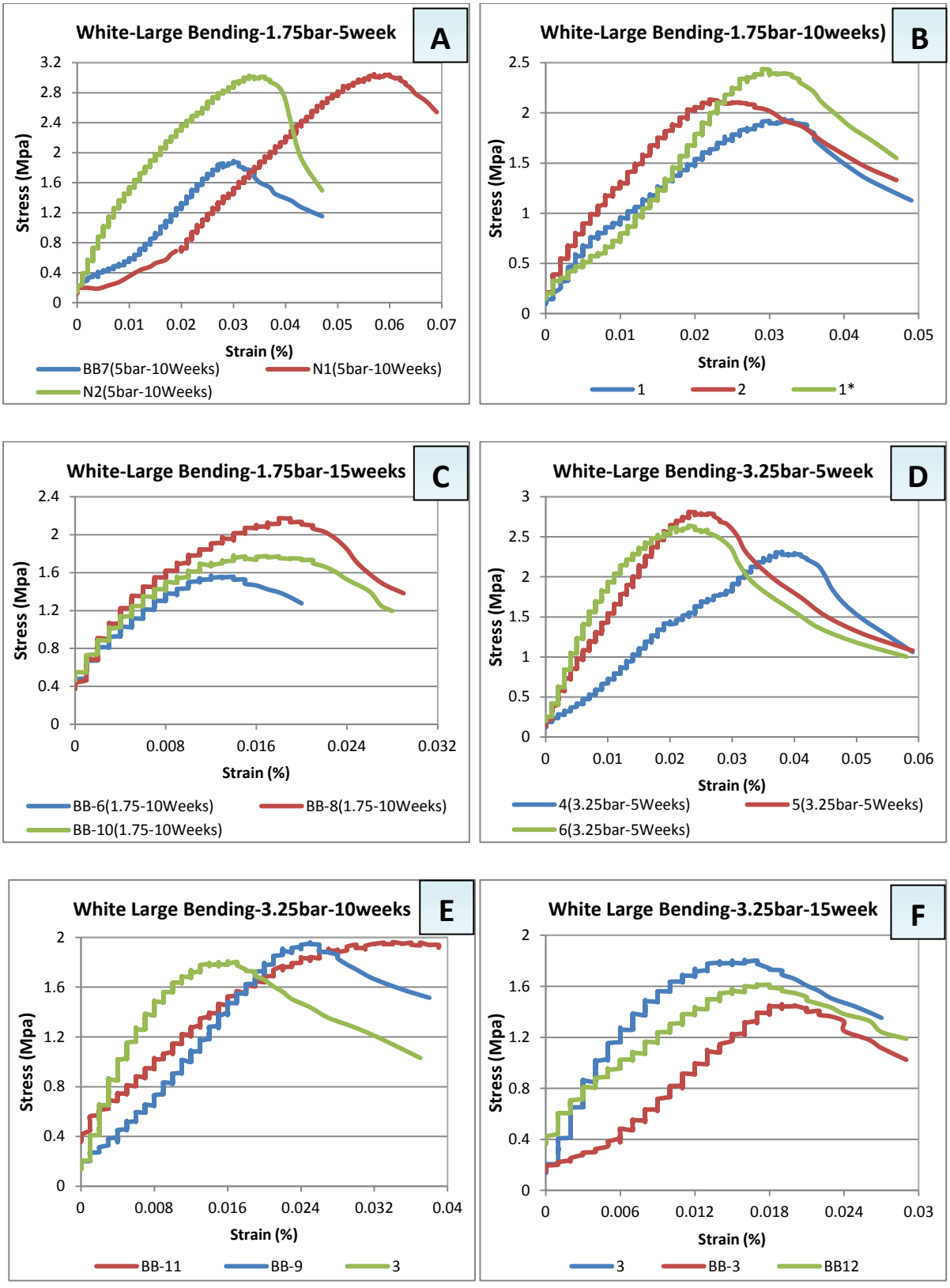

Fig. B.15: Present short-term four-point flexural tests results of white/Bantycock large bending. These samples tested after saturation under 1.75 and 3.25 bar applied water pressure for different time durations shown on each part.

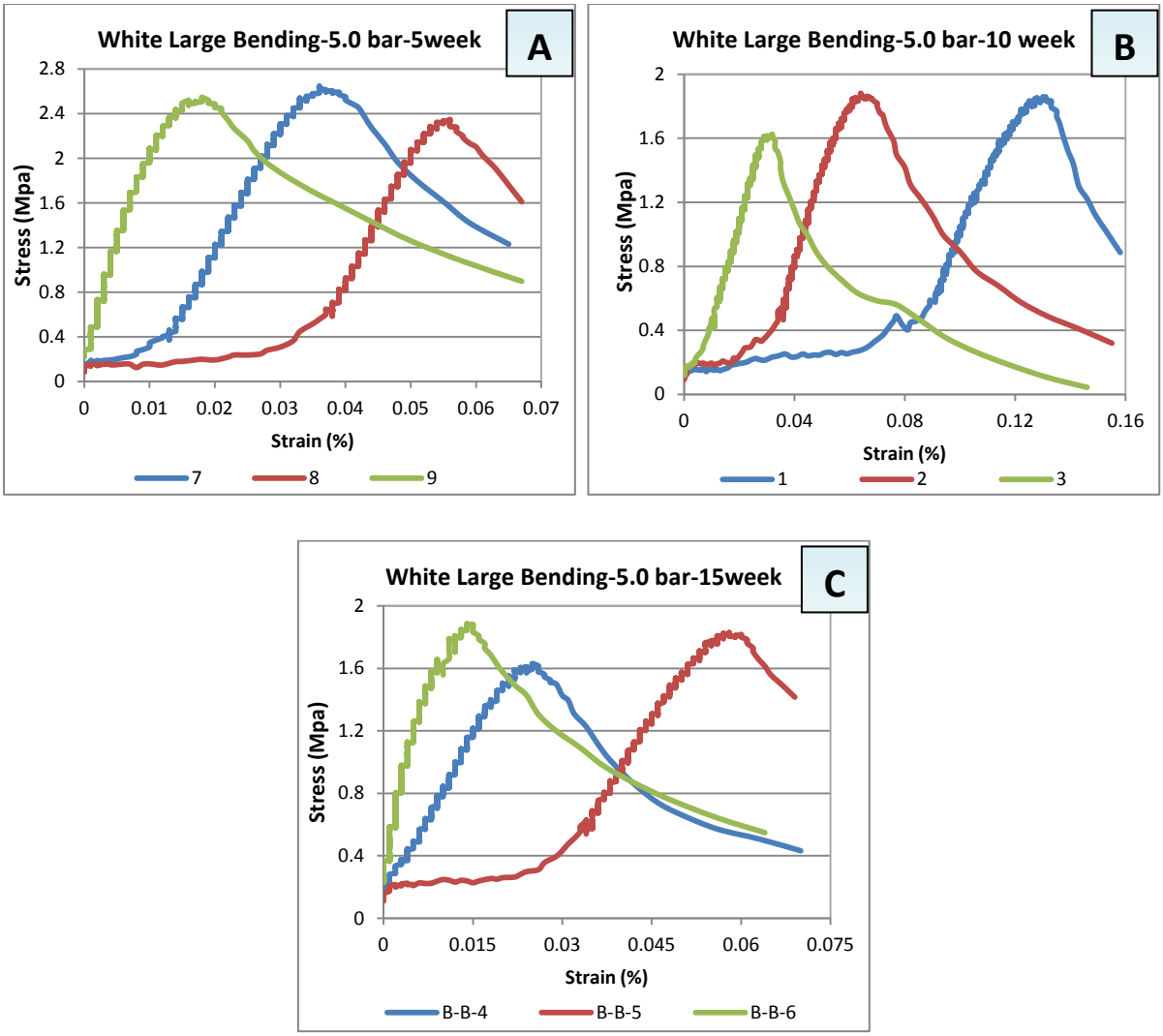

Fig. B.16: Present short-term four-point flexural tests results of white/Bantycock large bars. These samples tested after saturation under 5.0 bar applied water pressure for 5, 10 and 15 week time durations.

B.3 Small Four-Point Bending

Different kinds of abbreviations were used in below tables, which represent properties such as: *Eα* = Flexural Modulus (GPa), $F\sigma_c$ = Flexural Stress at failure (MPa), *P* = Load at failure (N), *T* = Time to failure (second), *MAD* = Maximum vertical deflection (mm), *MD* = Maximum dissolution (US/cm), *MWtR* = Maximum mass reduction (%), *MVR* = Maximum volume reduction (%), , *MLR* = Maximum length reduction (%), *MWR* = Maximum width reduction and *MDeR* = Maximum depth reduction (%).

Table B.12: Short-term four-point flexural tests results of different four-point bending bars. These bars tested in air-dry state.

Small Bending Kind	*Eα* (GPa)	*T* (seconds)	$F\sigma_c$ (MPa)	*P* (N)	*MAD* (mm)
White/Bantycock (Air-Dry)					
1	8.5584	404.7	8.11586	1298.537	0.09021
2	7.63684	359.9	7.41761	1186.817	0.09589
3	10.84667	319.6	6.45437	1032.7	0.06405
4	13.56706	327.5	6.74952	1079.922	0.04903
5	9.65962	497.4	10.07803	1612.485	0.10187
White & Clay/Bantycock (Air-Dry)					
SC1	3.32729	316.1	6.39797	1023.676	0.15725
SC2	9.36622	261.4	5.24074	838.5188	0.07519
SC3	5.944081	325	6.61434	1058.294	0.08229
SC4	10.72915	255.1	5.35061	856.0974	0.05456
SC5	8.753523	215.9	4.34668	695.469	0.0784
White & Cracks/Bantycock (Air-Dry)					
WK1	4.70269	268.2	5.42454	867.9256	0.10037
WK2	6.66256	158.4	3.34779	535.6458	0.07272
WK3	9.62625	383.4	7.75045	1240.071	0.08184
WK4	7.426392	154.2	3.08229	493.1665	0.05097
WK5	3.65239	171.5	3.46581	554.5297	0.07533
White & Marl/Bantycock (Air-Dry)					
MS1	14.36658	317.8	6.59852	1055.763	0.05471
MS2	7.423503	383.1	7.73159	1237.054	0.09671
MS3	8.203491	67.7	1.5596	249.5353	0.03804
MS4	11.91888	308.8	6.27642	1004.227	0.09977
MS5	8.113893	331.6	6.73502	1077.604	0.0778
Pink/Bantycock (Air-Dry)					
1	9.053254	250.5	5.18106	828.9692	0.05516
2	10.60934	321.2	8.21984	1315.174	0.08154
3	9.197593	233.6	4.9093	785.4886	0.06001
4	12.22353	255.1	5.36188	857.9	0.05321
5	14.2704	353.9	7.39293	1182.869	0.05448
Iraqi (Air-Dry)					
1	8.19867	318.8	6.52001	1043.201	0.07272
2	6.27534	267.3	5.54136	886.6178	0.07862
3	9.623521	395.2	8.00649	1281.039	0.07698
4	9.36374	230.3	4.87232	779.5717	0.04985
5	4.621671	295.1	6.07055	971.2887	0.11323
Aust Cliff (Air-Dry)					
AB1	2.91852	114.8	2.48074	396.9184	0.07548
AB2	6.05821	126	2.64612	423.3784	0.04895
AB3	1.80268	73.3	1.6093	257.4886	0.09962
AB4	6.70982	87.4	2.02536	324.0578	0.0438
AB5	3.520125	153.5	3.1544	504.7036	0.08572

Table B.13: Short-term four-point flexural tests results of white/Bantycock small bending bars. These bars tested after saturation under atmospheric pressure for 5, 10, 15, 30 and 50 week time durations.

Small Bending Kind	*Ea* (GPa)	*T* (seconds)	$F\acute{o}_c$ (MPa)	*P* (N)	*MAD* (mm)	*MD* (US/cm)	*MWtR* (%)	*MVR* (%)	*MLR* (%)	*MWR* (%)	*MDeR* (%)
White/Bantycock (Saturated under atmospheric pressure-5 week)											
BP1	3.417889	156.7	3.23405	517.4485	0.12885	6214.1	2.329	2.5524	0.383	1.65	0.5374
BP2	5.695341	105	2.20611	352.977	0.06502		2.232	1.5742	0.6	0.97	0.01
B-S-20	2.98066	150.4	3.04952	487.9226	0.13071		2.1351	1.584	0.5434	1.078	0.032
White/Bantycock (Saturated under atmospheric pressure-10 week)											
O1	2.625	94.8	2.03921	326.2741	0.18	12194	4.0622	2.26	0.371	2.338	0.449
O2	2.00635	120.9	2.60233	416.3735	0.17518		4.85	3.671	0.701	2.009	1.002
B-S-26	2.500014	113	2.39311	382.8981	0.14275		5.21	3.813	0.703	1.92	1.239
White/Bantycock (Saturated under atmospheric pressure-15 week)											
BS1	2.311642	107.6	2.34957	375.9316	0.13064	19089.4	6.78	5.28	0.569	2.56	2.22
BS2	5.664482	83.7	1.98731	317.9701	0.0506		7.36	6.467	1.2553	2.572	2.792
BS3	1.55601	104.2	2.35456	376.7301	0.23288		7.6013	5	0.399	2.829	1.829
White/Bantycock (Saturated under atmospheric pressure-30 week)											
B-S-5	1.530094	98	2.02106	323.3699	0.23206	37357.8	14.96	19.882	1.453	7.014	12.63
B-S-7	1.76304	109	2.28964	366.3424	0.1491		15.423	18.503	1.198	7.1214	12.275
B-S-10	1.43472	69.1	1.42073	227.3171	0.14514		14.96	19.221	1.052	6.56	11.061
White/Bantycock (Saturated under atmospheric pressure-50 week)											
B-S-6	6.3855	38.7	0.80341	128.5452	0.02257	62105	23.103	29.184	1.954	11.7994	18.102
B-S-8	1.77971	69.5	1.40851	225.3613	0.09245		25.51	32.864	2.725	12.88	20.8
B-S-9	2.228581	92.4	2.01224	321.9591	0.10314		25.16	33.67	1.824	12.884	22.36

Table B.14: Short-term four-point flexural tests results of white/Bantycock small bending bars. These bars tested after saturation under 1.75 and 3.25 bar applied water pressure for 5, 10 and 15 week time durations.

Small Bending Kind	*Ea* (GPa)	*T* (seconds)	$F\acute{o}_c$ (MPa)	*P* (N)	*MAD* (mm)	*MD* (US/cm)	*MWtR* (%)	*MVR* (%)	*MLR* (%)	*MWR* (%)	*MDeR* (%)
White/Bantycock (Saturated under 1.75bar water pressure-5Week)											
BS7	3.03453	119.5	2.73259	437.214	0.1201		5.795	7.722	0.41	2.47	5.025
BS8	2.658231	140.5	3.12949	500.7184	0.16016	10844.7	5.6	8.6702	0.553	2.55222	5.768
BS9	4.745975	83.6	2.00687	321.0985	0.07212		5.26	8.126	0.8703	2.453	4.99
White/Bantycock (Saturated under 1.75 bar water pressure-10 week)											
BS4	6.36292	99.1	2.38937	382.2997	0.06689		10.35	10.81	1.03944	3.698	6.931
BS5	2.995713	117.9	2.62622	420.196	0.11651	21632.5	10.66	11.03	1.022	3.814	6.532
BS6	6.408361	63	1.5767	252.2717	0.0645		10.662	10.4941	1.0533	3.77	5.9983
White/Bantycock (Saturated under 1.75 bar water pressure-15 w eek)											
D	1.68381	82.6	1.67642	268.2277	0.17533		15.181	19.614	1.762	7.052	11.48
E	2.68167	99.3	2.02586	324.137	0.09641	32967.6	15.013	20.266	1.8224	6.921	12.11323
F	2.968662	104.3	2.2196	355.1355	0.07793		14.665	22.6261	1.812	7.1122	14.347
White/Bantycock (Saturated under 3.25 bar water pressure-5 week)											
B-S-28	7.952875	150.2	3.11905	499.0477	0.08826		5.55	7.724	0.6922	3.004	5.821
B-S-29	3.9543	79.1	1.72971	276.7536	0.05971	11054.7	5.95	9.0653	0.7014	2.77	5.8094
B-S-30	5.44	129.5	2.66237	425.98	0.16808		5.89843	9.3383	0.767	2.74841	6.00514
White/Bantycock (Saturated under 3.25 bar water pressure-10 week)											
B-S-2	2.96711	120.9	2.55719	409.15	0.10792		11.9713	16.684	1.52	5.81912	10.089
B-S-3	1.74492	120.9	2.49334	398.9351	0.13789	21846.7	11.557	16.5715	1.6645	5.126	10.5754
B-S-11	1.3125	69.1	1.42062	227.2994	0.0985		11.411	16.945	1.7092	5.1298	10.932
White/Bantycock (Saturated under 3.25 bar water pressure-15 week)											
B-S-27	2.38836	73.3	1.47998	236.797	0.08303		23.897	23.3434	2.307	7.9805	13.8985
B-S-24	7.110979	115.7	2.32993	372.7889	0.07137	33036.9	17.93	20.12053	2.0297	7.977	11.529
B-S-22	3.254891	100.6	2.11162	337.8591	0.08288		17.851	22.229	2.193	7.9424	13.6597

Table B.15: Short-term four-point flexural tests results of white/Bantycock small bending bars. These bars tested after saturation under 5.0 bar applied water pressure for 5, 10 and 15 week time durations.

Small Bending No.	*Ea* (GPa)	*T* (seconds)	$F\acute{o}_c$ (MPa)	*P* (N)	*MAD* (mm)	*MD* (US/cm)	*MWtR* (%)	*MVR* (%)	*MLR* (%)	*MWR* (%)	*MDeR* (%)
White (saturated under 5.0 bar water pressure-5 week)											
A	2.86062	85.7	1.77916	284.6649	0.08116	11204.7	6.345	9.6599	0.77514	3.12844	6.1724
B	2.524189	93.9	1.93169	309.071	0.07653		6.483	10.003	0.7876	3.0422	6.6353
C	4.11886	123.5	2.6274	420.3846	0.07519		7.001	9.844	0.8771	3.04981	6.0841
White (saturated under 5.0 bar water pressure-10 week)											
1	2.216383	136.3	2.78098	444.9561	0.11592	22571	13.0631	18.2192	1.66123	5.6492	11.965
2	3.923973	42.8	0.90921	145.4734	0.05994		13.003	17.409	2.55122	5.4195	11.355
3	8.461352	123.9	2.54431	407.0898	0.0426		12.95	18.50614	1.211	6.787	11.9919
White (saturated under 5.0 bar water pressure-15 week)											
B10	2.194391	106	2.35242	376.387	0.13602	33732.2	18.058	26.0353	2.943	8.022	17.341
B11	2.31903	69.6	1.63267	261.2276	0.18288		19.19	25.887	2.2542	9.7012	15.7301
B12	1.335851	75.8	1.71041	273.6661	0.20986		19.409	26.088	3.0843	8.4813	17.107

Table B.16: Short-term four-point flexural tests results of pink/Bantycock small bending bars. These bars tested after saturation under atmospheric pressure for 5, 10, 15, 30 and 50 week time durations.

Small Bending No.	*Ea* (GPa)	*T* (seconds)	$F\sigma_c$ (MPa)	*P* (N)	*MAD* (mm)	*MD* (US/cm)	*MWtR* (%)	*MVR* (%)	*MLR* (%)	*MWR* (%)	*MDeR* (%)
Pink/Bantycock (saturated under atmospheric pressure-5 week)											
A4	8.06452	198.4	4.0161	642.576	0.1429	6537.3	2.64	3.0042	0.2207	1.377	1.434
A5	7.01992	163.3	3.3391	534.2557	0.08146		2.303	2.378	0.2048	0.846	1.3433
A6	4.76017	19.3	0.61527	98.44248	0.01981		1.8	1.5672	0.0458	0.46	1.0054
Pink/Bantycock (saturated under atmospheric pressure-10 week)											
P4	5.11424	62.6	1.39189	222.7027	0.05396	11646.07	5.27	8.797	0.7329	2.66	5.415
P5	2.552813	93.8	1.94954	311.9263	0.11412		5.48	8.211	0.529	3.161	4.722
P6	1.23848	83.4	1.67799	268.4778	0.2343		5.27	7.599	0.5308	2.573	4.591
Pink/Bantycock (saturated under atmospheric pressure-15 week)											
P1	2.275883	70.5	1.4476	231.6153	0.12414	19443.4	7.73	12.407	0.907	7.08	4.2032
P2	3.22792	71.6	1.26695	202.7117	0.55239		8.63	12.141	0.6502	3.947	7.932
P3	1.61264	111.9	2.28168	365.0682	0.16195		6.93	9.527	0.863	2.828	6.084
Pink/Bantycock (saturated under atmospheric pressure-30 week)											
B-S-6	3.704206	76.3	1.57769	252.4301	0.11943	37137.6	13.31	17.12731	1.235	6.618	11.703
B-S-2	1.99065	62.3	1.28851	206.162	0.13737		14.87	21.804	1.503	7.885	13.816
B-S-1	1.863053	60.6	1.23624	197.7977	0.12249		15.6	23.353	1.543	7.601	15.6383
Pink/Bantycock (saturated under atmospheric pressure-50 week)											
BS3	1.165743	33.9	0.80967	129.5473	0.08072	61857.8	23.57	31.4999	2.09	13.321	19.29
BS4	2.154974	56.7	1.36806	218.89	0.21285		25.151	33.01	1.951	14.37	20.202
BS5	3.826473	29.1	0.9037	144.5919	0.03423		25.21	32.914	2.31	14.29	19.89

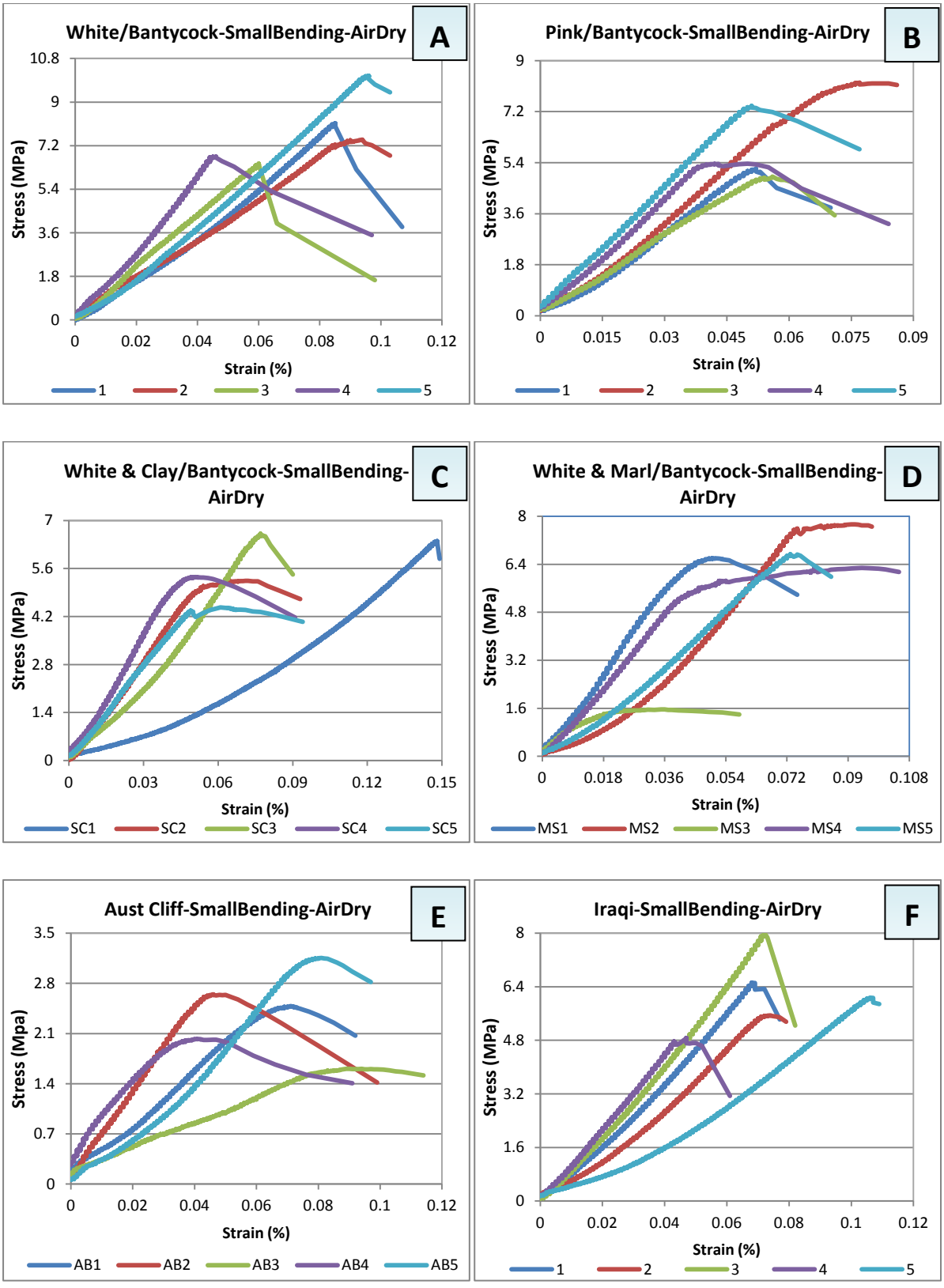

Fig. B.17: Presents short-term four-point flexural tests results of air-dry small bending bars; parts A, B, C & D for Bantycock gypsum samples/UK; part E for Iraqi gypsum samples and part F for Aust Cliff/UK gypsum samples.

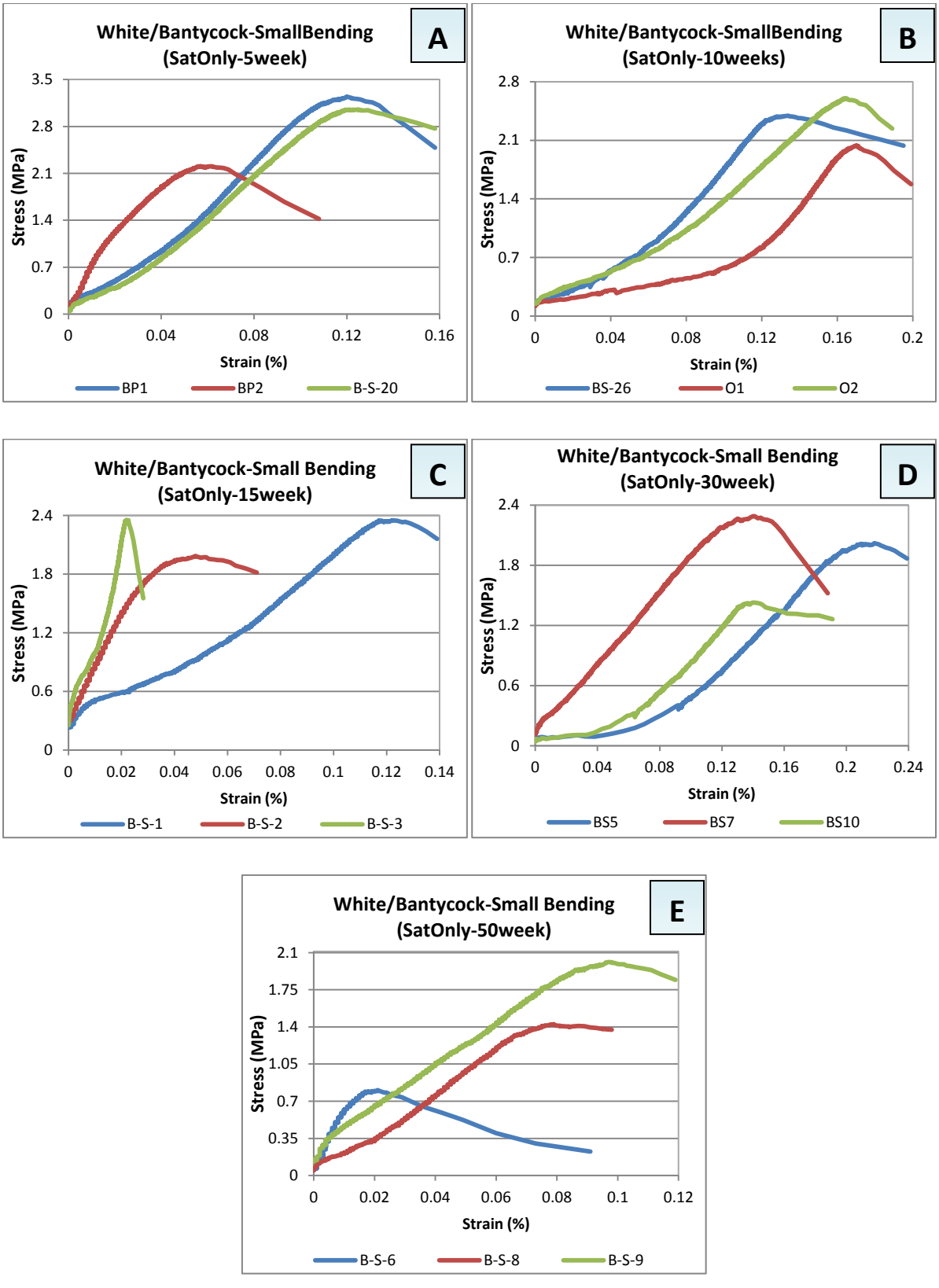

Fig. B.18: Presents short-term four-point flexural tests results of white/Bantycock, UK small bending bars. These bars tested after saturation under atmospheric pressure for 5, 10, 15, 30 and 50 week time durations.

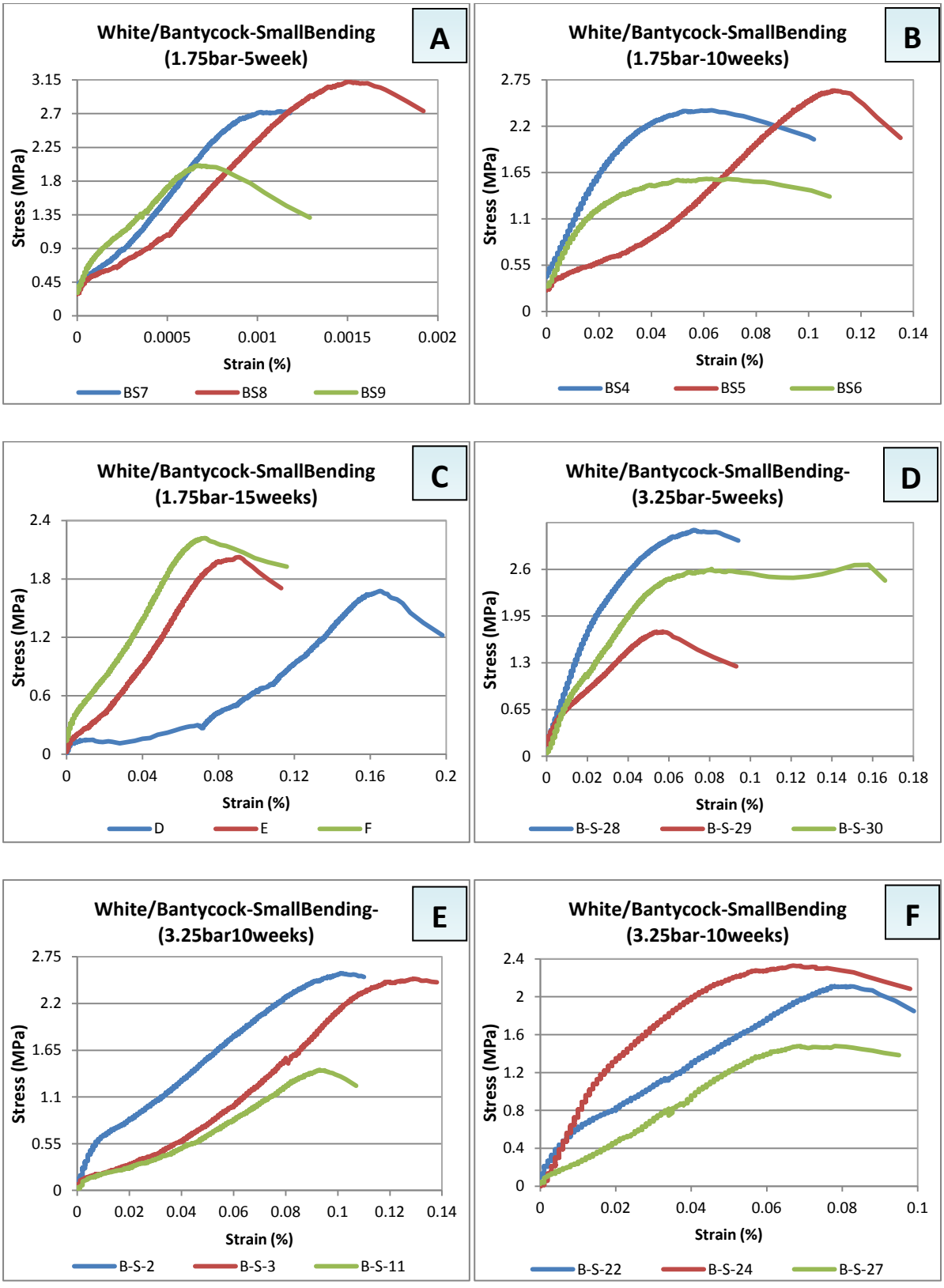

Fig. B.19: Presents short-term four-point flexural tests results of white/Bantycock small bars saturated under applied water pressure; parts A and B for 1.75 bar; parts C, D and E for 3.25 bar and part F for 5.0 bar.

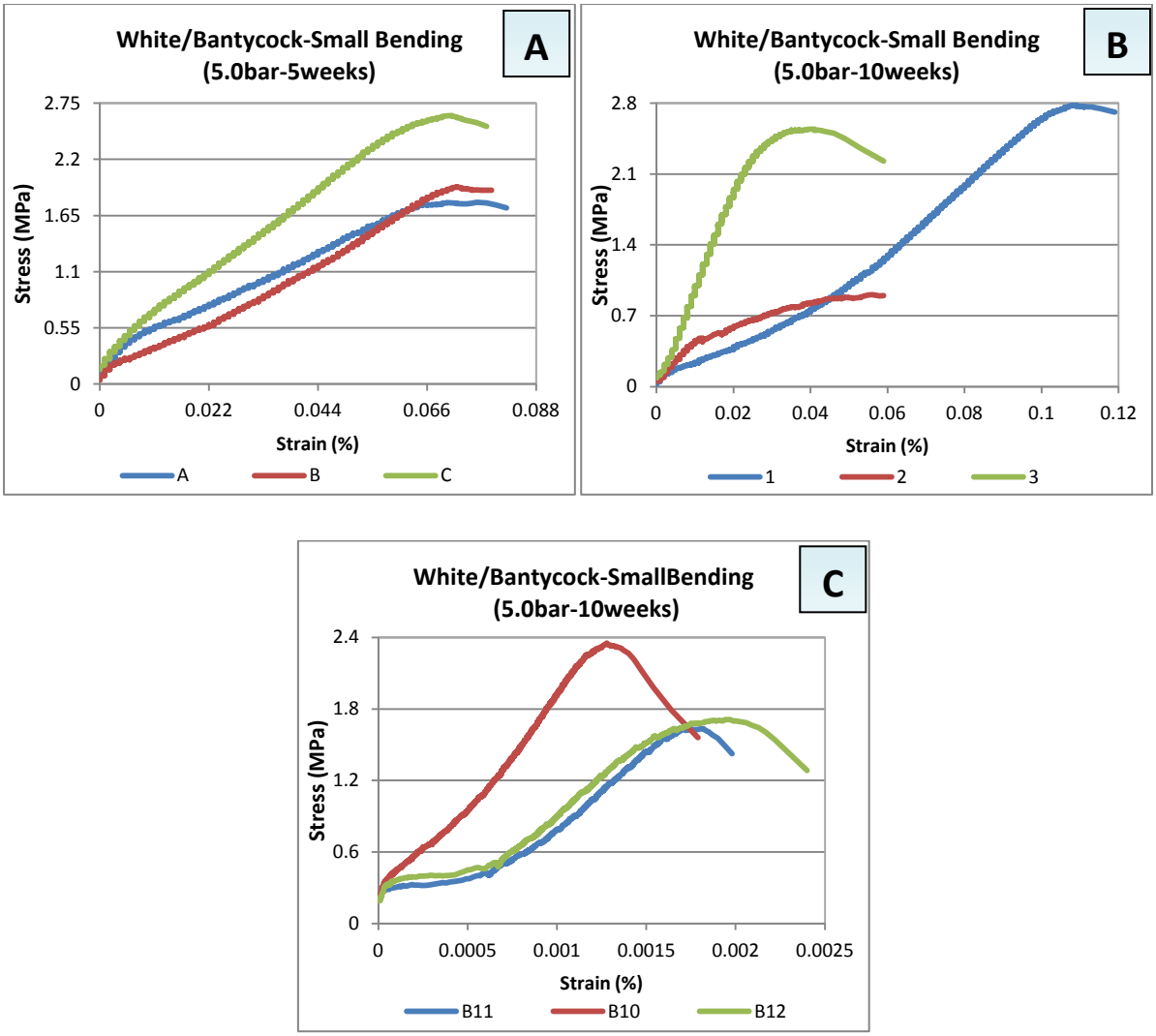

Fig. B.20: Presents short-term four-point flexural tests results of white small bars. These bars tested after saturation under 5.0 bar applied water pressure for 5, 10 and 15 week time durations.

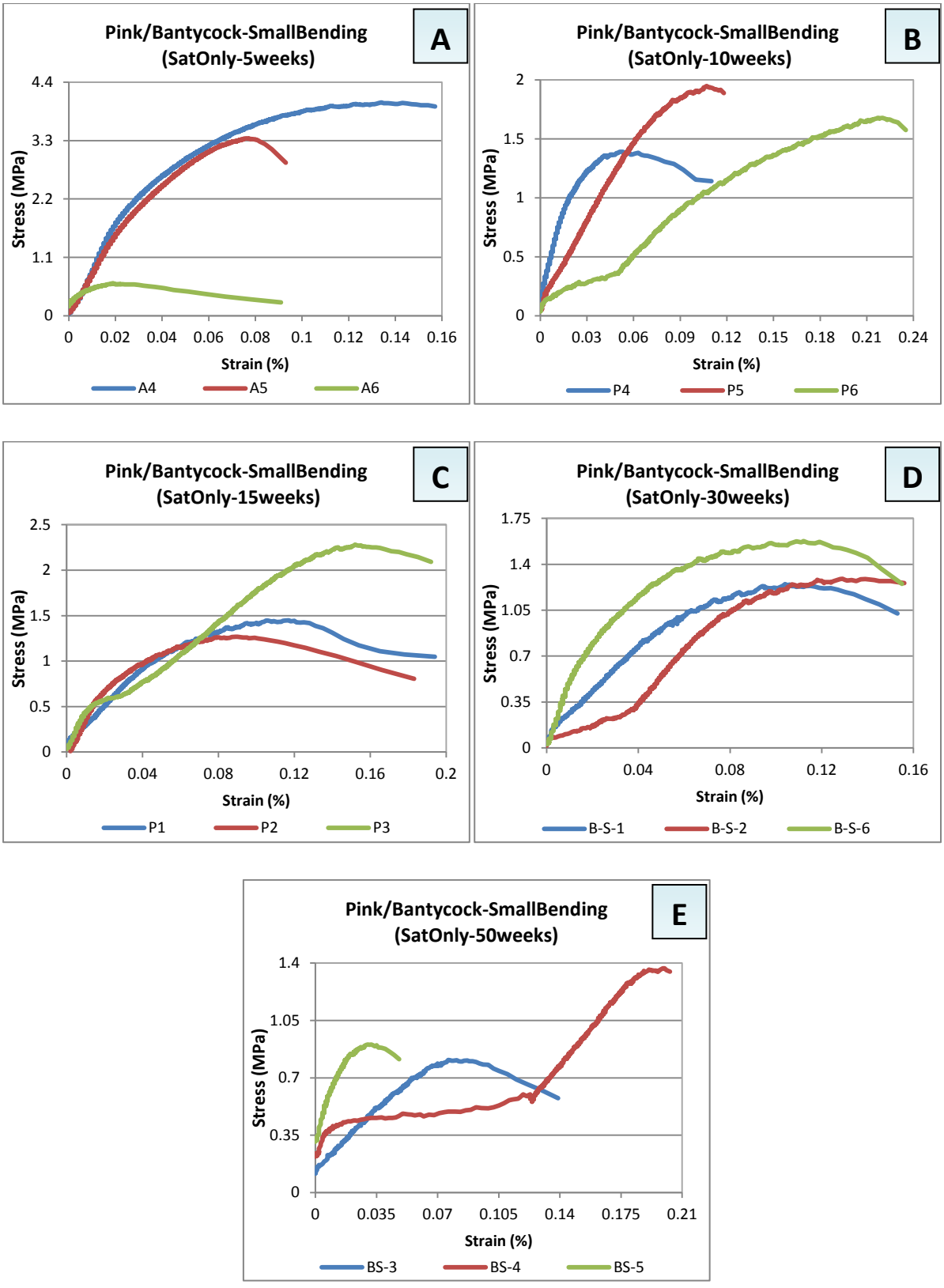

Fig. B.21: Presents short-term four-point flexural tests results of pink/Bantycock small bars. These samples tested after saturation under atmospheric pressure for 5, 10, 15, 30 and 50 week.

B.4 Cylinders:

Different kinds of abbreviations were used in below table, which represent properties as list: *Ea* = Axial Modulus (GPa), *Ec* = Circumferential Modulus (GPa), *PR* = Poisson's ratio, *SM* = Shear Modulus (GPa), *BM* = Bulk Modulus (GPa), $б_c$ = Compressive Strength (MPa), *P* = Load at failure (N), *T* = Time to failure (seconds), *MAD* = Maximum axial deflection (mm), *MHD* = Maximum horizontal deflection (mm), *MR(U)* = Modulus reduction from ultrasound observations (%), *VR(U)* = Velocity reduction from ultrasound observations (%), *PLR(U)* = Path length reduction from ultrasound observations (%), *TTR(U)* = Transit time reduction from ultrasound observations (%).

Table B.17: short-term uniaxial compression tests results of different gypsum cylinders. These cylinders tested in air-dry state.

Cylinder No.	*Ea* (GPa)	*Ec* (GPa)	*PR*	*SM* (GPa)	*BM* (GPa)	σ_c (MPa)	*P* (N)	*T* (seconds)	*MAD* (mm)	*MHD* (mm)	*MR(U)* (%)	*VR(U)* (%)	*PLR(U)* (%)	*TTR(U)* (%)	Density (gm/cm^3)
White/Bantycock (Air-Dry)															
B1-S1	3.9586	44.224	0.08951	1.816684	1.607276	13.92204	31884.6	556.4	0.53355	0.03661	19.9	2952	1084	27.1	2.29905
B4-S3	2.3024	43.1	0.05342	1.092822	0.859271	10.75154	24623.5	422.7	1.09759	2.17818	20.8	3018	106	26.5	2.3006
B10-S3	2.0427	38.8036	0.05264	0.970273	0.761024	13.2756	30404.1	530.1001	1.01463	0.00430	19.8	2941	108	27.2	2.2957
B16-S4	1.8516	33.124	0.0559	0.876788	0.694887	9.547315	21865.5	378.15	1.32949	1.86346	21.5	3065	1044	26.1	2.3002
B23-S2	1.6287	36.2964	0.04487	0.779378	0.596426	10.25757	23492.2	407.5	0.99303	0.74671	19.2	2898	110	27.6	2.298
White & Clay/Bantycock (Air-Dry)															
B1-S6	1.3544	30.0686	0.04504	0.648011	0.496165	13.50788	30936.1	535.75	1.11171	0.03266	21.7	3076	104	26	2.30414
B11-S1	2.8082	25.4615	0.11029	1.264622	1.200985	13.01062	29797.3	515.25	0.75679	0.09778	19.5	2919	109	27.4	2.3026
B11-S2	4.5864	21.5932	0.2124	1.891455	2.65786	13.06335	29918	519.4	0.45859	0.07978	20.3	2973	107	26.9	2.303
B21-S3	3.28	23.575	0.13913	1.439695	1.514859	11.88204	27212.6	470.7	0.94438	1.28173	20.4	2985	107	26.8	2.305
B23-S1	2.94872	33.6389	0.08766	1.355536	1.191859	11.12381	25476	440.7	0.82495	0.57584	18.3	2826	113	28.3	2.3
Pink/Bantycock (Air-Dry)															
B14-S4	1.7898	21	0.08523	0.824619	0.719191	15.04481	34456	596.9	0.92995	0.0535	17.8	2797	114	28.6	2.2872
B15-S3	2.2218	48.79	0.04554	1.062515	0.81481	14.08285	32252.9	558.300	0.9458	0.08851	15	2564	124	31.2	2.28724
B15-S5	2.2083	7.0439	0.31351	0.840613	1.973515	13.47592	30862.9	534.050	0.94086	0.48616	12.1	2318	138	34.5	2.2867
B18-S1	2.2667	37.6	0.06029	1.068911	0.859154	11.88768	27225.5	469.8	0.57547	0.04534	15.3	2597	123	30.8	2.2849
CP1	1.6239	21.5322	0.07542	0.755009	0.637449	12.55495	28753.7	495.1	1.48711	2.16055	18.7	2867	111	27.9	2.292
Iraqi (Air-Dry)															
I4	2.8581	49.5475	0.05768	1.351112	1.076945	10.26843	23517	405.7	0.45261	0.03133	16.9	2758	113	29	2.234
I5	1.3605	0.7454	1.8252	0.24078	-0.17111	10.17763	23309.1	400.4	0.90074	0.88197	18.1	2846	112	28.1	2.2474
I6	3.2443	17.0924	0.18981	1.36337	1.743176	13.25521	30357.4	525.15	0.38577	0.57615	19.1	2888	110	27.7	2.2978
I7	1.4172	29.12	0.04867	0.675715	0.523339	11.0052	25193.7	438.2	1.26305	1.52867	23.2	3200	100	25	2.2743
I8	2.7019	20.935	0.12906	1.196525	1.213992	7.904181	18102.4	309.3	0.0528	0.33407	25.6	3347	95	23.9	2.2933

Table B.18: Short-term uniaxial compression tests results of white/Bantycock gypsum cylinders. These cylinders tested after saturation state under atmospheric pressure for 5, 10, 15, 30 and 50 week time durations.

Cylinder No.	*Ea* (GPa)	*Ec* (GPa)	*PR*	*SM* (GPa)	*BM* (GPa)	σ_c (MPa)	*P* (N)	*T* (seconds)	*MAD* (mm)	*MHD* (mm)	*MR(U)* (%)	*VR(U)* (%)	*PLR(U)* (%)	*TTR(U)* (%)	Density (gm/cm^3)	*Ea* (GPa)	*Ec* (GPa)
White/Bantycock (saturated under atmospheric pressure-5week)																	
B1	1.492	33.413	0.04465	0.71411	0.54610	7.56765	16446.7	282.6	1.03578	0.24789		81.38	1.82	2.6744	5.53	2.38	0.87
B2	2.2519	36.67	0.06141	1.06081	0.85573	9.74494	21387.1	369.7	0.68354	0.10744	10277	72.22	1.094	2.39	4.474	1.796	0.944
B3	3.309	52.0212	0.06361	1.55555	1.26377	9.32032	20559.8	354.45	0.4772	0.18704		17.42	0.76	2.39	3.91	1.78	0.398
White/Bantycock (saturated under atmospheric pressure-10week)																	
B6S4	4.08697	53.68	0.07614	1.89891	1.60703	6.85518	14796.3	254.5	0.29984	0.02692		55.492	1.84	4.204	5.59	2.463	0.76
B13S4	2.43	43.3096	0.05611	1.15045	0.91238	7.28836	15834.1	271.4	0.5127	0.06802	19643.6	57.455	3.731	4.6023	6.02	2.92	0.274
B16S3	3.240741	59.306	0.05464	1.53641	1.21279	8.10554	17660.3	305.4	0.75566	0.04102		26.37	1.51	4.38	5.83	2.604	0.73
White/Bantycock (saturated under atmospheric pressure-15week)																	
B2S5	2.64407	25.2471	0.10473	1.19671	1.11487	7.38537	15804.7	271.85	0.56374	0.0166		23.844	1.53	6.972	8.044	3.222	1.44
B1S5	2.2422	23.0519	0.09727	1.02172	0.92791	8.25315	17703.1	304.85	0.61411	0.22752	29139	28	1.12	6.77	8.096	3.34	1.18
6	1.6399	27.124	0.06046	0.77320	0.62182	6.37747	13472.7	230.75	1.06134	0.05852		31.871	1.499	7.1222	9.51	3.96	1.33
White/Bantycock (saturated under atmospheric pressure-30week)																	
B2S1	2.3672	14.9132	0.15873	1.02146	1.15608	3.19428	6099.79	100.5	0.60477	1.53757		75.98	32.63	13.59	18.752	8.69	2.56
B8S2	2.44342	30.58995	0.07988	1.13134	0.96933	10.2611	19525.6	335.1	0.7106	0.07003	57648.9	36.95	1.87	15.35	19.998	8.85	3.712
B16S2	3.2489	57.025	0.05697	1.53689	1.22224	4.8227	9063	154.5	0.24775	0.02277		23.51	8.3	14.8	20.042	9.414	2.56
White/Bantycock (saturated under atmospheric pressure-50week)																	
B2S4	2.6448	100.9008	0.02621	1.28862	0.93037	5.3454	8688.81	148.25	0.74909	0.05947		82.06	80.129	23.997	32.22	15.8	4.396
B4S2	1.7636	53.5272	0.03295	0.85367	0.62934	2.31290	3801.49	55.75	3.04284	3.77933	96445.4	83.27	84.604	22.94	31.56	15.32	4.493
B6S1	2.6341	58.746	0.04484	1.26053	0.96453	4.39931	7193.89	122.3	0.60447	0.00471		54.701	83.6996	23.583	31.832	15.611	4.28

Table B.19: Short-term uniaxial compression tests results of white/Bantycock gypsum cylinders. These cylinders tested after saturation state under 1.75 and 3.25 bar applied water pressure for different time durations as shown in the table below.

Cylinder No.	*Ea* (GPa)	*Ec* (GPa)	*PR*	*SM* (GPa)	*BM* (GPa)	$б_c$ (MPa)	*P* (N)	*T* (seconds)	*MAD* (mm)	*MHD* (mm)	*MR(U)* (%)	*VR(U)* (%)	*PLR(U)* (%)	*TTR(U)* (%)	Density (gm/cm^3)	*Ea* (GPa)	*Ec* (GPa)
White/Bantycock (saturated under 1.75 bar water pressure-5week)																	
B1S1	2.99201	63.378	0.04721	1.42856	1.10132	9.86986	21500.2	371.25	0.6238	0.0279	10851.2	50.611	83.584	3.09	5.09	2.422	0.856
B1S5	2.8013	51.1261	0.05479	1.32789	1.04869	7.78513	16956.4	290.75	0.6156	0.022		49.633	83.82	3.19	4.99	2.49	0.644
B15S3	1.1713	47.7041	0.02455	0.57162	0.4106	8.858	19294.9	332.3	0.3697	0.0254		54.274	83.571	3.124	4.86	2.4774	0.893
White/Bantycock (saturated under 1.75 bar water pressure-10week)																	
B5S2	1.63212	59.8234	0.02728	0.79439	0.57544	7.34778	15497.4	266.8	0.8497	0.0331	21843.4	76.07	55.135	6.164	7.916	3.524	1.241
B13S1	1.4459	19.944	0.0725	0.67408	0.56370	6.67476	14153.3	242.65	0.7752	0.0250		59.962	83.761	6.213	7.329	3.202	1.242
4	1.1262	53.5684	0.02102	0.55151	0.39188	8.23790	16814	289.9	1.0162	0.0215		65.993	84.183	6.14	7.312	3.251	1.12
White/Bantycock (saturated under 1.75 bar water pressure-15week)																	
B13S2	3.4166	58.8291	0.05808	1.61453	1.28853	7.13743	13101.9	224.55	0.7265	0.0286	32971.9	25.024	1.523	9.239	10.805	4.8243	1.884
5	1.482	34.648	0.04277	0.71061	0.54021	8.02509	14904.5	256	1.1226	0.1144		25.024	1.523	9.24	11.0154	4.8543	2.096
B8S1	2.30456	20.343	0.11329	1.03503	0.99322	5.51700	10202.9	172.25	0.7659	1.5285		37.1341	1.49	9.26	11.02	4.96	1.864
White/Bantycock (saturated under 3.25 bar water pressure-5week)																	
C4	4.03812	51.2925	0.07873	1.87171	1.59759	8.95293	19608.3	337.05	0.5684	0.0411	11151.2	66.5131	83.627	3.422	4.26	2.179	0.603
C5	3.0303	56.7222	0.05342	1.43831	1.13094	10.5819	22935	396.25	0.5392	0.0253		65.902	83.34	3.28	4.884	3.406	0.963
C6	3.9	45.2297	0.08623	1.79521	1.57091	6.06103	13072.8	223.05	0.3267	0.0855		29.452	83.702	3.318	6.77	2.909	0.98
White/Bantycock (saturated under 3.25 bar water pressure-10week)																	
B12S1	1.843	71.395	0.02581	0.89831	0.64778	7.35391	14669.2	251.85	0.9342	0.019	22433.4	60.234	83.522	6.41	8.355	3.684	1.416
B12S2	1.106	47.9556	0.02306	0.54053	0.38649	7.12785	14292.8	246.05	1.0554	0.0933		69.33	83.695	6.91	8.811	3.952	1.33
B19S3	1.1778	61.7295	0.01908	0.57787	0.40818	6.59379	13285.2	228.85	0.9172	0.0473		67.42	83.73	6.405	8.17	3.6	1.36
White/Bantycock (saturated under 3.25 bar water pressure-15week)																	
B22S4	2.024	22.712	0.08912	0.92919	0.82099	8.39198	15504.8	266.55	1.2033	0.0082	33871.8	58.99	2.582	9.655	11.834	5.341	1.984
2	2.49602	47.0455	0.05306	1.18513	0.93077	7.76694	14130	242.55	0.5771	0.0662		76.996	2.553	9.731	13.04	5.7874	2.449
3	1.0902	143.631	0.00759	0.54099	0.36900	5.66631	10598.9	181.45	0.8031	0.0032		67.14	2.941	9.7	11.23	5.068	1.87

Table B.20: Short-term uniaxial compression tests results of white/Bantycock gypsum cylinders. These cylinders tested after saturation under 5.0 bar applied water pressure for 5, 10 and 15 week time durations.

Cylinder No.	*Eα* (GPa)	*Ec* (GPa)	*PR*	*SM* (GPa)	*BM* (GPa)	σ_c (MPa)	*P* (N)	*T* (seconds)	*MAD* (mm)	*MHD* (mm)	*MR(U)* (%)	*VR(U)* (%)	*PLR(U)* (%)	*TTR(U)* (%)	Density (gm/cm^3)	*Eα* (GPa)	*Ec* (GPa)
White/Bantycock (saturated under 5.0 bar water pressure-5week)																	
C1	3.4336	33.03	0.103954	1.555137	1.44495	8.869686	19440.1	335.95	0.55358	0.12729	11449.1	65.365	84.002	3.53	6.282	2.794	0.8182
C2	2.455	140.1375	0.017519	1.206366	0.848046	5.81976	12455.4	213.35	0.69737	0.57892		62.76	83.64	3.53	5.74	2.47	0.91
C3	2.25	44.984	0.050018	1.07141	0.833366	8.796224	19204	332	0.80828	0.77468		71.89	83.82	3.563	5.313	2.282	0.839
White/Bantycock (saturated under 5.0 bar water pressure-10week)																	
A1	1.39904	80.7813	0.017319	0.687611	0.483079	5.868623	12126.5	208.05	1.02405	0.00518	23018	28.014	36.434	7.227	10.566	4.402	1.231
A2	2.8551	56.1	0.050893	1.358416	1.059547	5.994655	12280.8	208.05	0.6331	0.09382		13.584	40.75	7.14	10.3195	4.5141	1.63634
A3	2.68824	184.632	0.01456	1.32483	0.922956	8.490664	17556.4	301.2	0.78302	0.03229		14.19	0.762	7.2564	10.2934	4.3463	2.027
White/Bantycock (saturated under 5.0 bar water pressure-15week)																	
B1S4	2.73953	44.987	0.060896	1.29114	1.039818	5.057944	9520.73	162.65	0.81164	0.00564	34578.9	16.195	0.76	8.71	12.353	5.5301	2.12
B22S3	2.0419	24.71711	0.082611	0.943044	0.815346	5.596201	11085.8	188.45	0.84901	0.04597		40.51	1.48	10.76	10.6933	4.8734	1.4902
1	2.3457	57.7193	0.04064	1.127047	0.851075	7.934682	9072.88	154.65	0.39932	0.00996		6.455	0.39	10.86	13.742	6.3613	1.964

Table B.21: Short-term uniaxial compression tests results of pink/Bantycock gypsum cylinders. These cylinders tested after saturation under atmospheric pressure for 5, 10, 15, 30 and 50 week time durations.

Cylinder No.	*Ea* (GPa)	*Ec* (GPa)	*PR*	*SM* (GPa)	*BM* (GPa)	$б_c$ (MPa)	*P* (N)	*T* (seconds)	*MAD* (mm)	*MHD* (mm)	*MR(U)* (%)	*VR(U)* (%)	*PLR(U)* (%)	*TTR(U)* (%)	Density (gm/cm^3)	*Ea* (GPa)	*Ec* (GPa)
Pink/Bantycock (saturated under atmospheric pressure-5week)																	
10	2.1275	46.5756	0.04568	1.01728	0.78047	8.47122	18444.6	318	0.60455	0.06281		46.281	0.37	1.96	4.37	2.037	0.351
11	1.7128	26.8571	0.06378	0.80506	0.65440	5.459	12075.4	206.1	1.57964	0.02101	10126.3	47.93	6.129	2.16	3.296	1.39	0.5482
12	2.3604	24.8719	0.09490	1.07790	0.97112	6.35446	13983	237.75	0.43646	0.16479		48.15	4.809	2.072	3.75	1.498	0.278
Pink/Bantycock (saturated under atmospheric pressure-10week)																	
7	1.5117	33.06	0.04573	0.7228	0.55462	4.6719	9827.53	166.15	0.55858	0.00701		74.56	4.244	4.753	7.86	3.537	0.9764
8	3.2456	13.9608	0.23248	1.3167	2.02203	6.31936	13474.8	229.85	0.50627	1.09895	19907.6	37.34	61.396	4.393	6.57	3.0394	0.621
9	2.2964	27.5709	0.08329	1.05992	0.91847	6.07305	12500.8	159.85	1.19273	0.01525		101.3	59.095	4.82	7.259	3.271	0.88022
Pink/Bantycock (saturated under atmospheric pressure-15week)																	
1	3.9891	31.4313	0.126915	1.76992	1.78203	5.75655	10759.2	187.4	0.6529	0.80715		9.694	84.002	6.674	10.489	4.741	1.36
2	3.1872	28.1096	0.113385	1.43131	1.37398	4.31292	8112.3	141.9	0.35552	0.10306	30076.3	36.082	84.004	7.007	10.353	4.5164	1.672
3	2.4563	36.501	0.067294	1.15071	0.94610	6.35421	11951.83	208.4	0.53145	0.09827		49.14	83.82	6.46	10.2597	4.6371	1.32
Pink/Bantycock (saturated under atmospheric pressure-30week)																	
4	1.5464	15.5733	0.099298	0.70336	0.643205	5.69198	11716.4	201.05	0.57263	0.11618		91.41	57.02	13.79	20.7	9.58	3.008
5	2.2622	13.8964	0.16279	0.97275	1.118098	5.49745	11466	196.1	0.88855	0.15756	59429.1	18.27	60.64	13.47	20.194	9.358	2.8
6	1.8393	12.7021	0.144803	0.80333	0.863042	5.20964	10736.1	183.8	0.86874	0.42049		57.062	36.697	13.96	20.21	9.412	2.77
Pink/Bantycock (saturated under atmospheric pressure-50week)																	
B15,S1	2.4999	94.716	0.026394	1.21781	0.879739	5.31386	9026.08	156.2	0.44551	0.06446		88.93	93.8	22.85	29.584	13.98	4.86
B15,S2	2.0229	67.8163	0.029829	0.98215	0.71708	5.141965	8717.23	151.95	1.55057	0.0054	97273.3	2.603	59.49	22.79	29.844	13.999	5.146
B20,S2	2.76	63	0.04381	1.32208	1.008351	5.318149	9039.95	157.5	0.43138	0.06831		13.18	28.26	22.391	29.321	13.871	4.825

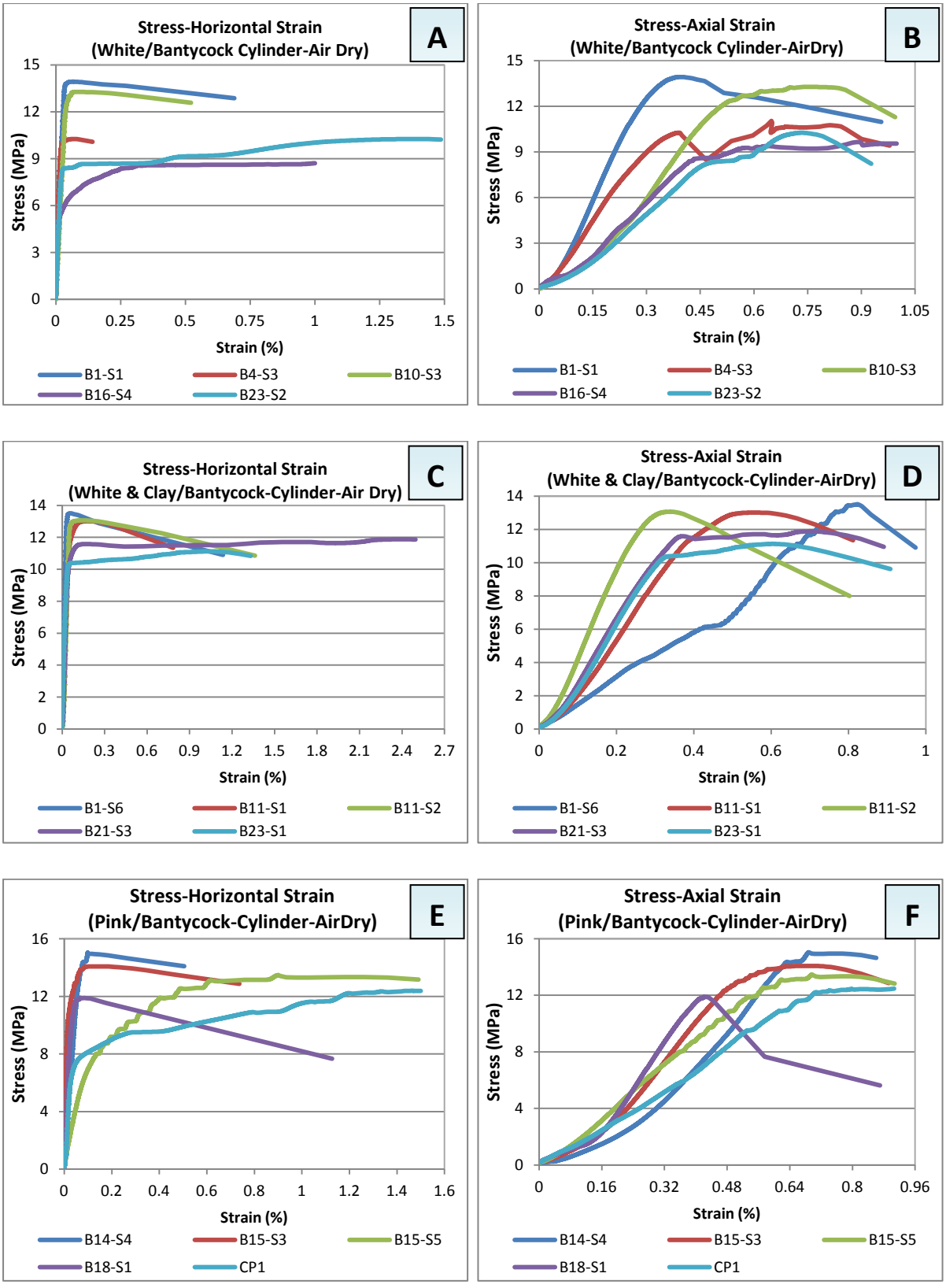

Fig. B.22: Presents uniaxial compression tests results of different gypsum rock cylinders from various origins. These cylinders tested in air-dry condition.

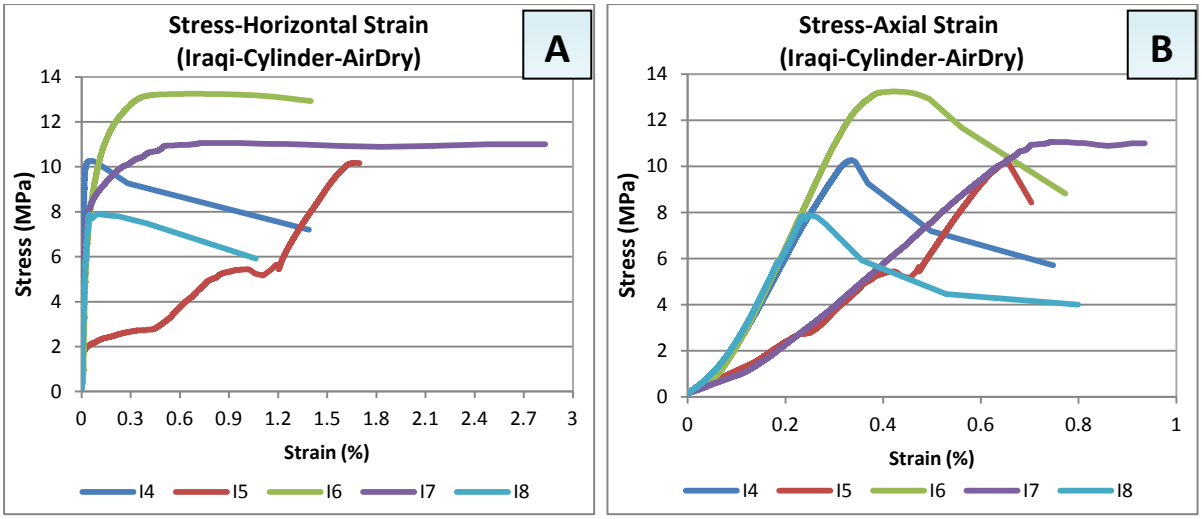

Fig. B.23: Present uniaxial compression tests results of air-dry Iraqi gypsum cylinders.

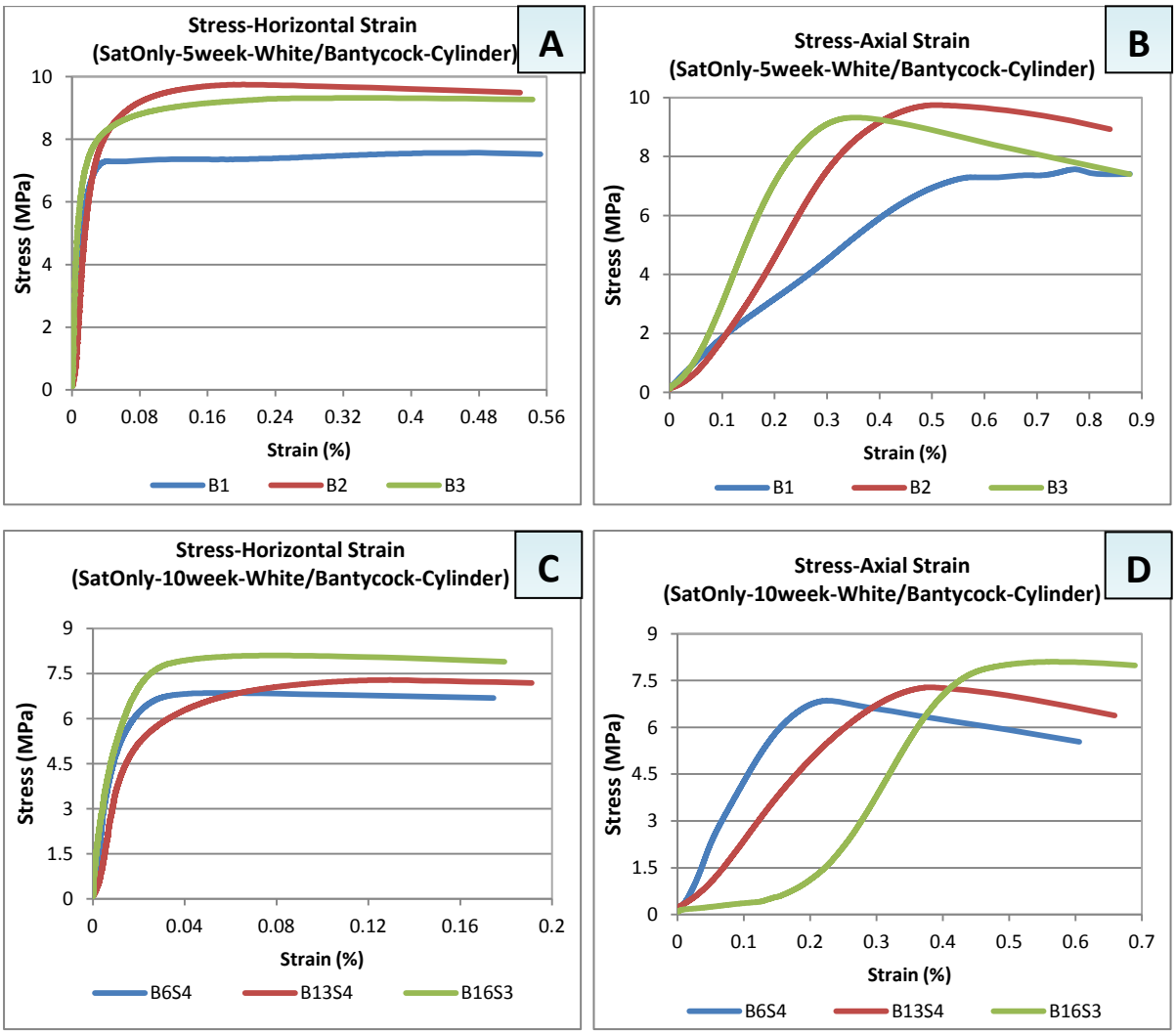

Fig. B.24: Presents uniaxial compression tests results of white/Bantycock gypsum cylinders. These cylinders were tested after saturation under atmospheric pressure for 5 and 10 week time durations.

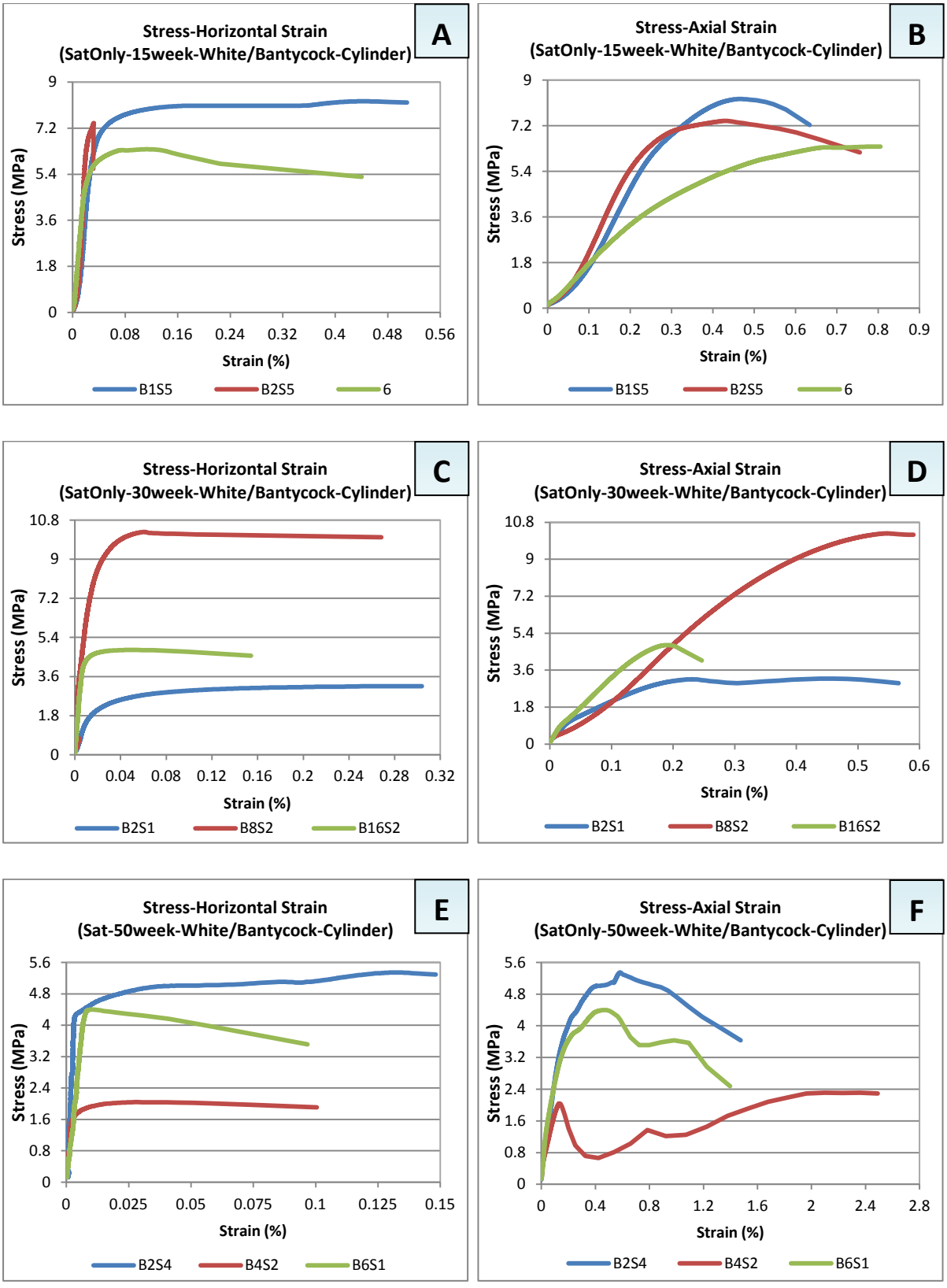

Fig. B.25: Present uniaxial compression tests results of white/Bantycock gypsum cylinders. These cylinders were tested after saturation under atmospheric pressure for 15, 30 and 50 weeks time durations.

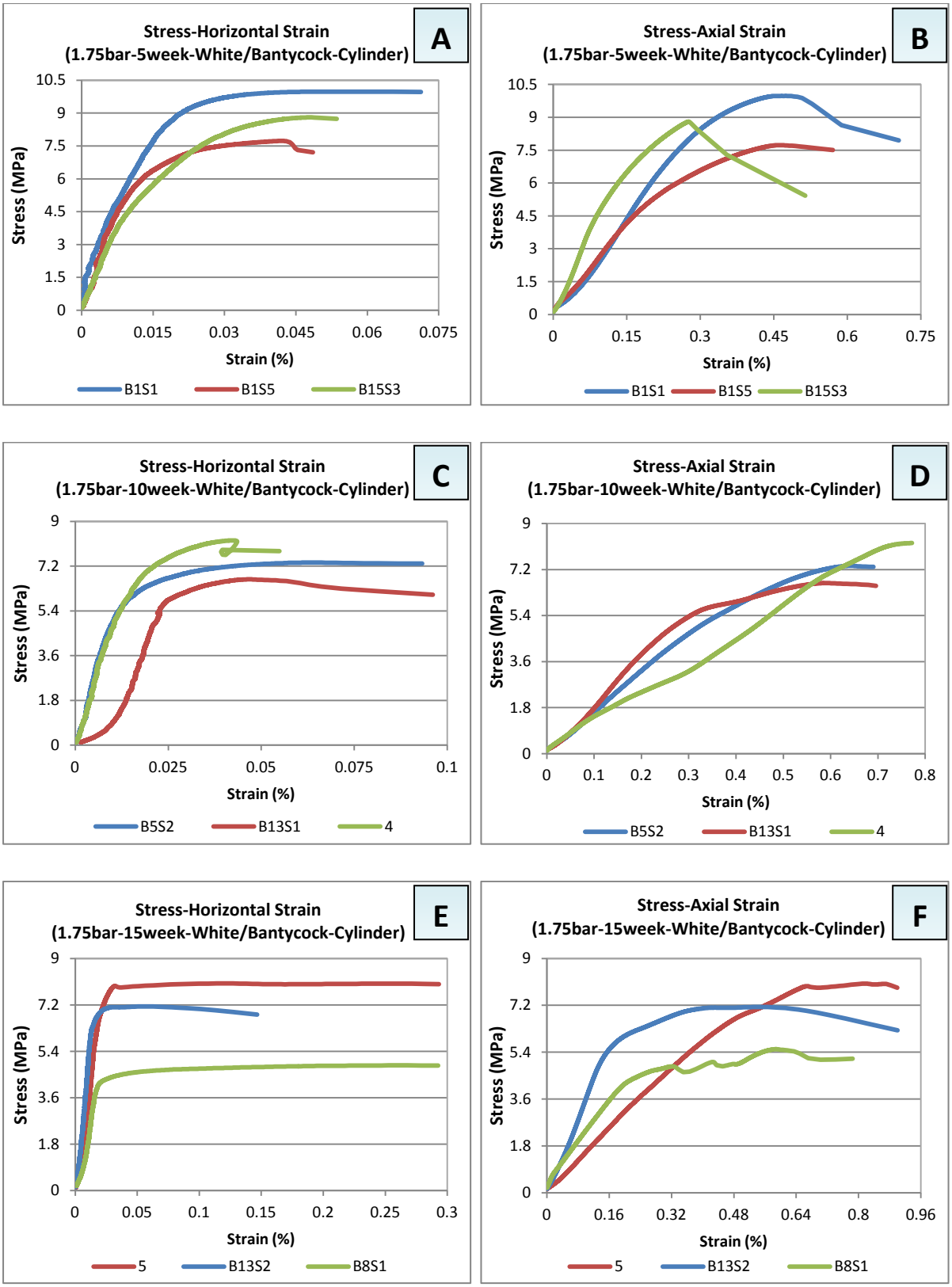

Fig. B.26: Present uniaxial compression tests results of white/Bantycock gypsum cylinders. These cylinders were tested after saturation state under 1.75 bars applied water pressure for 5, 10 and 15 week time durations.

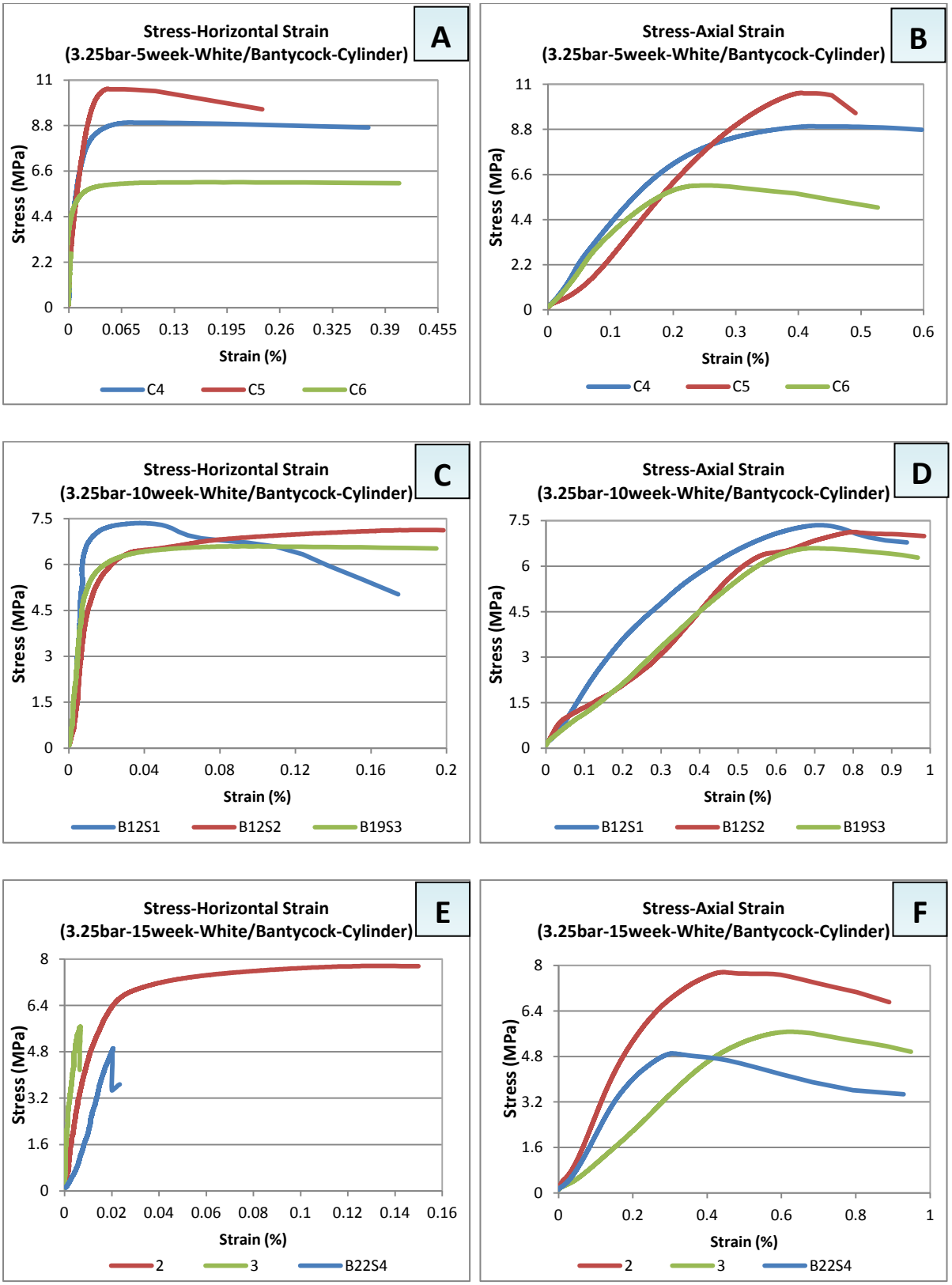

Fig. B.27: Present uniaxial compression tests results of white/Bantycock gypsum cylinders. These cylinders were tested after saturation under 3.25 bar applied water pressure for 5, 10 and 15 week time durations.

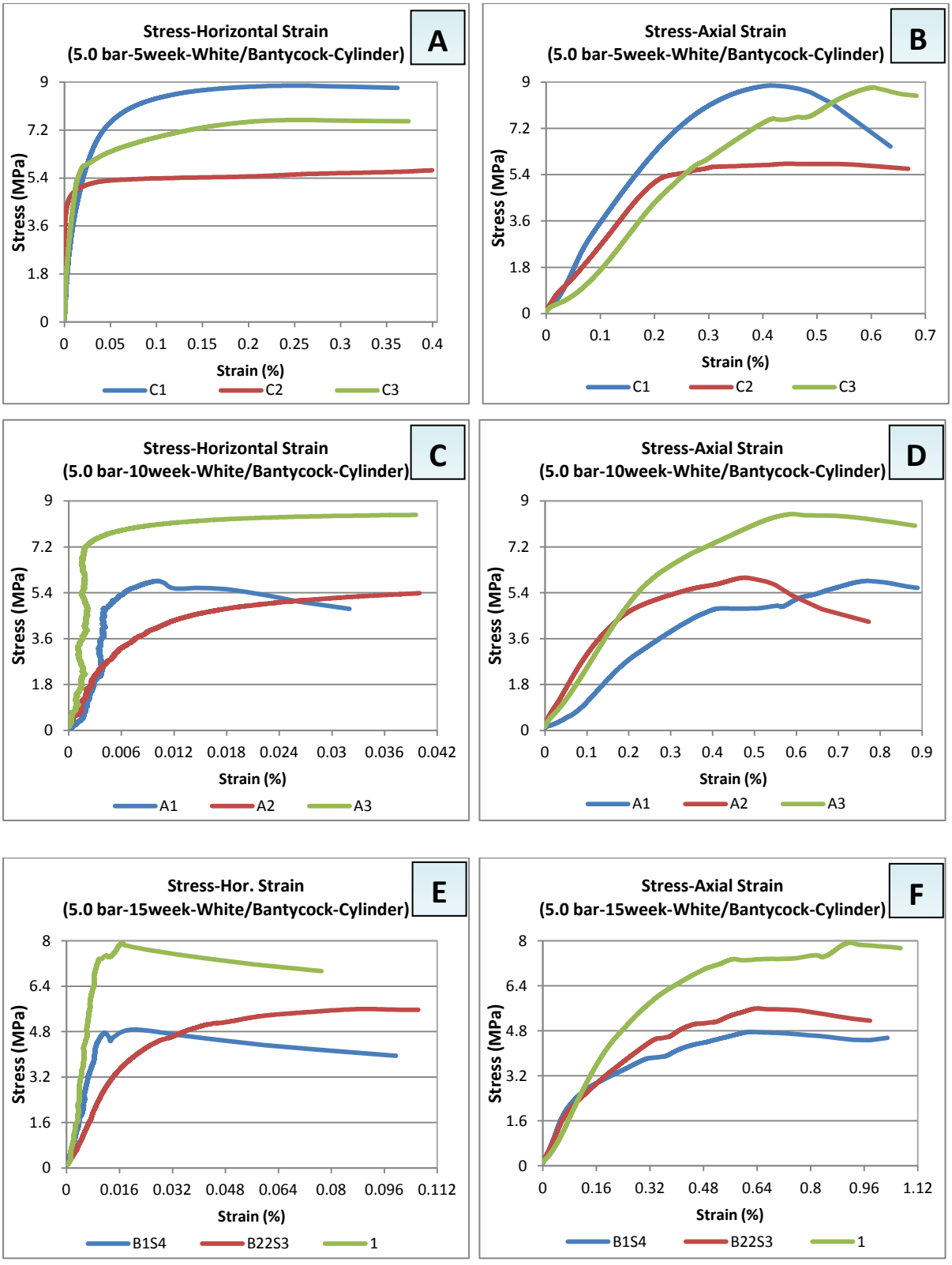

Fig. B.28: Present uniaxial compression tests results of white/Bantycock gypsum cylinders. These cylinders were tested after saturation under 5.0 bar applied water pressure for 15, 30 and 50 week time durations.

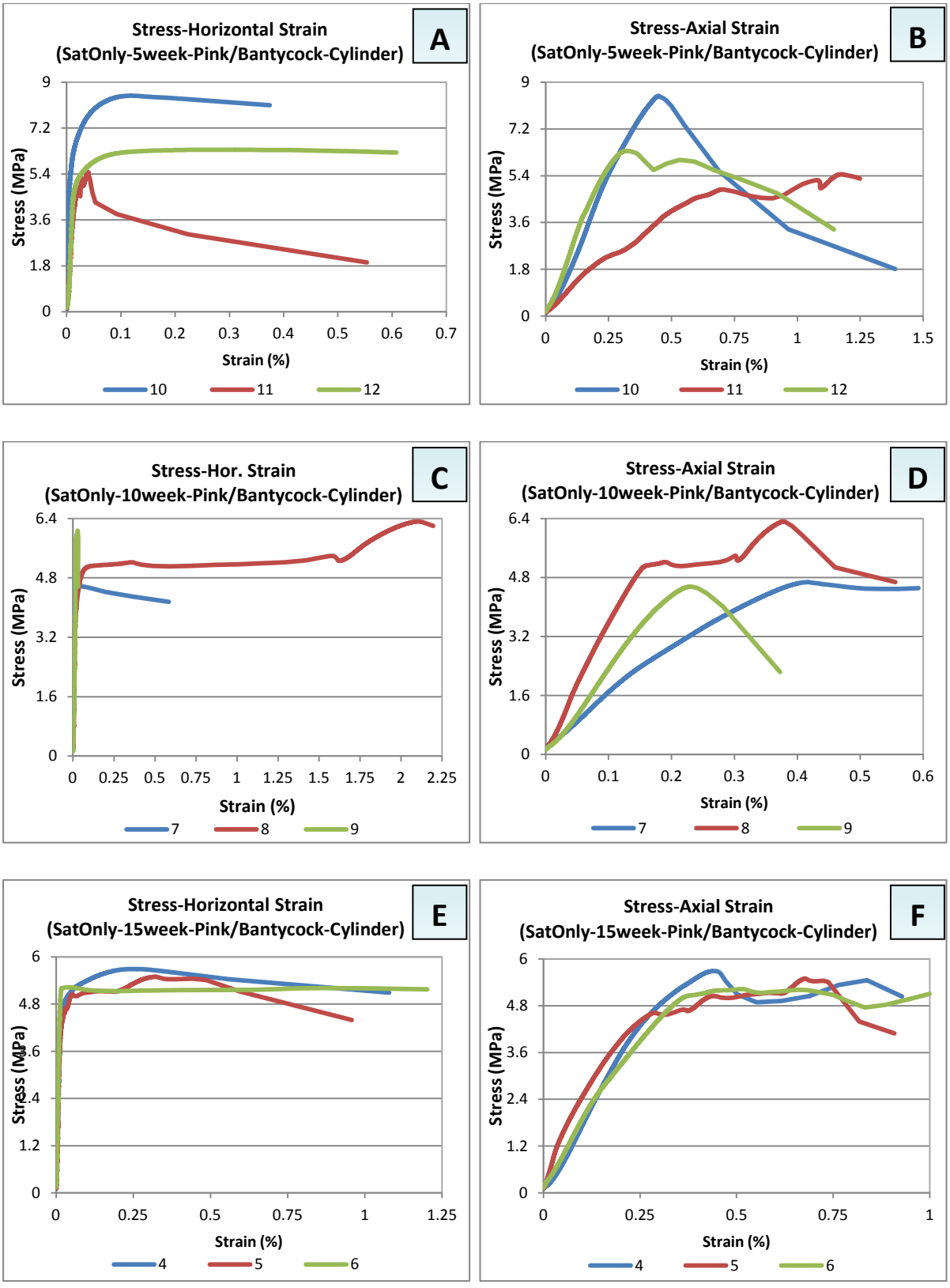

Fig. B.29: Present uniaxial compression tests of pink/Bantycock gypsum cylinders. These cylinders were tested after saturation state under atmospheric pressure for 5, 10 and 15 week time durations.

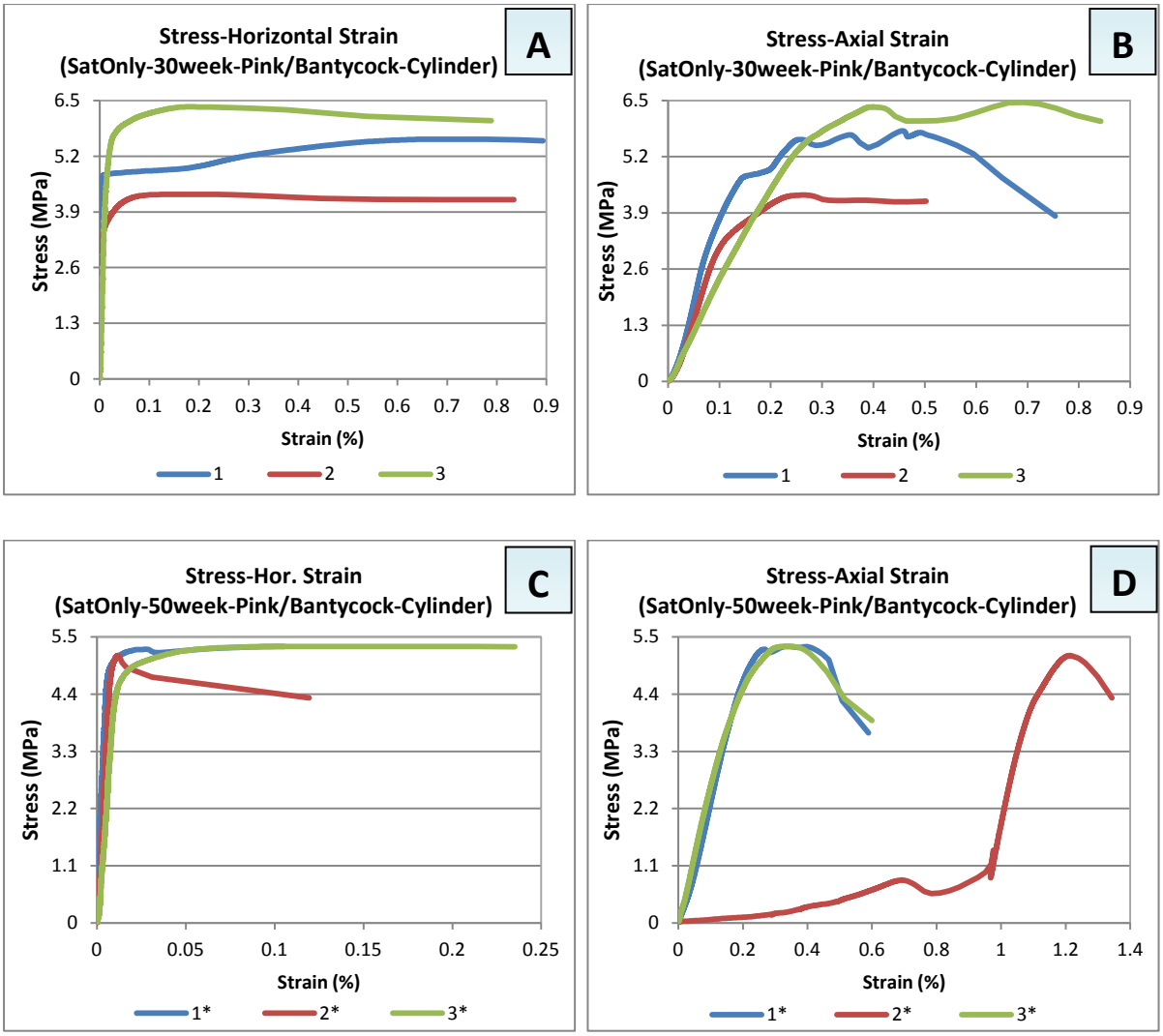

Fig. B.30: Presents uniaxial compression tests results of pink/Bantycock gypsum cylinders. These cylinders were tested after saturation state under atmospheric pressure for 30 and 50 week time durations.

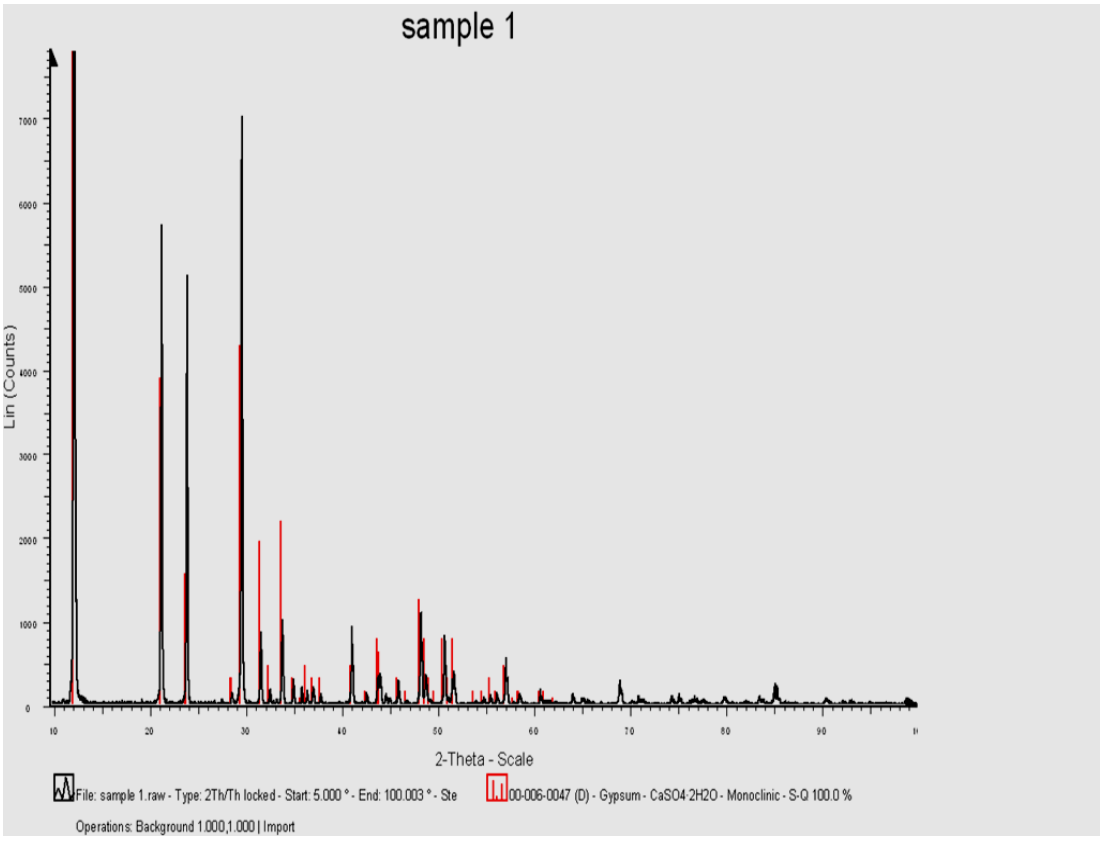

Fig. B. 31: *XRD* analysis of white/Bantycock gypsum rock sample.

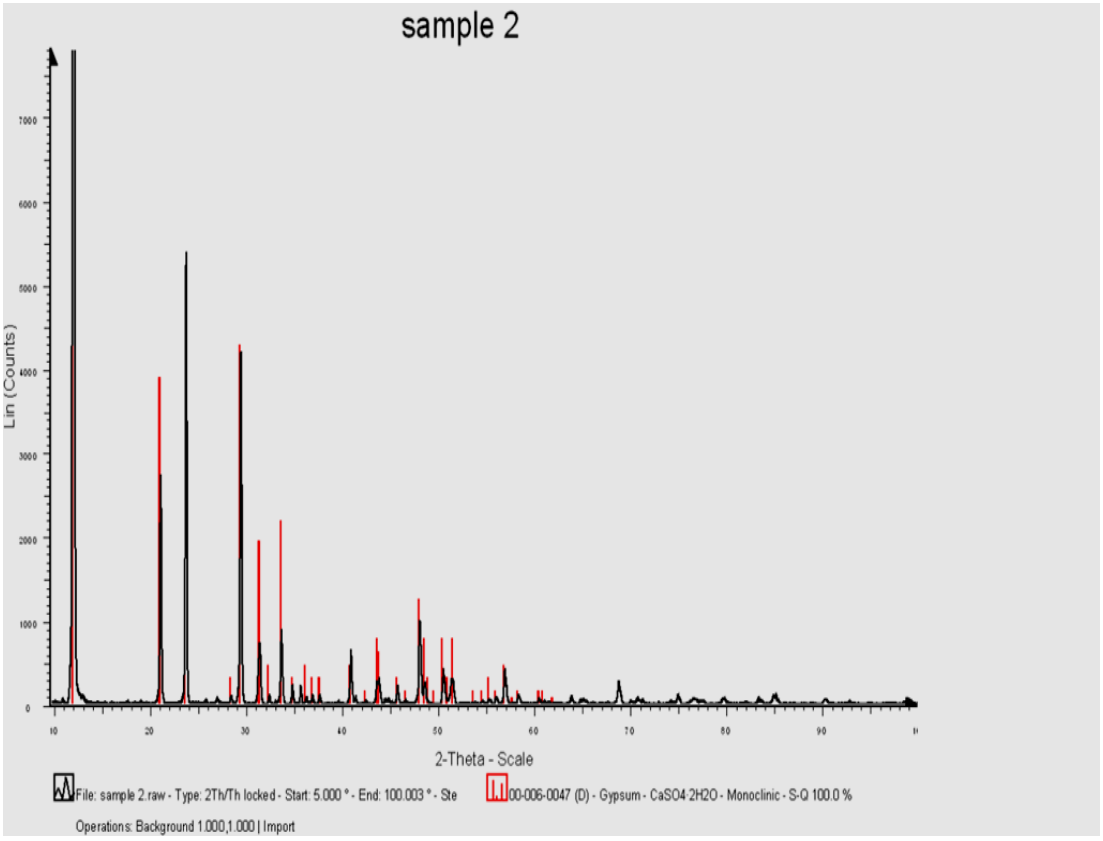

Fig. B.32: *XRD* analysis of pink/Bantycock gypsum rock sample.

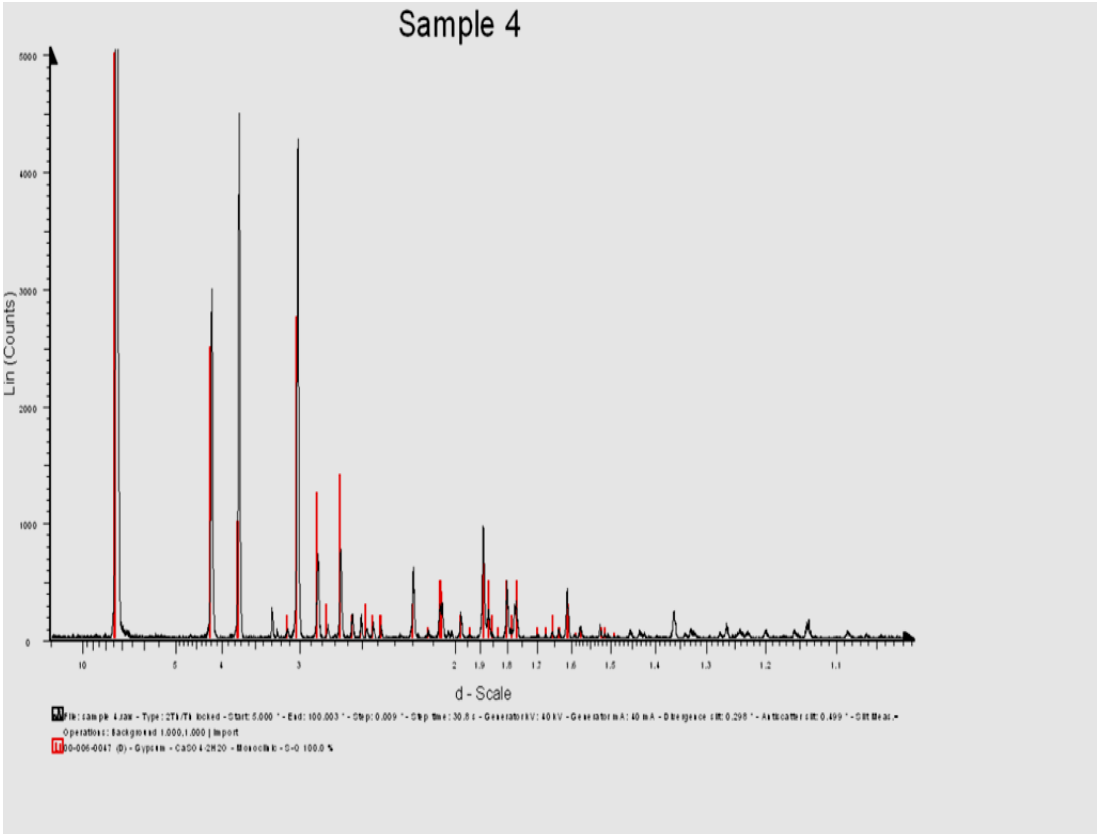

Fig. B.33: *XRD* analysis of white with marl/Bantycock gypsum rock sample.

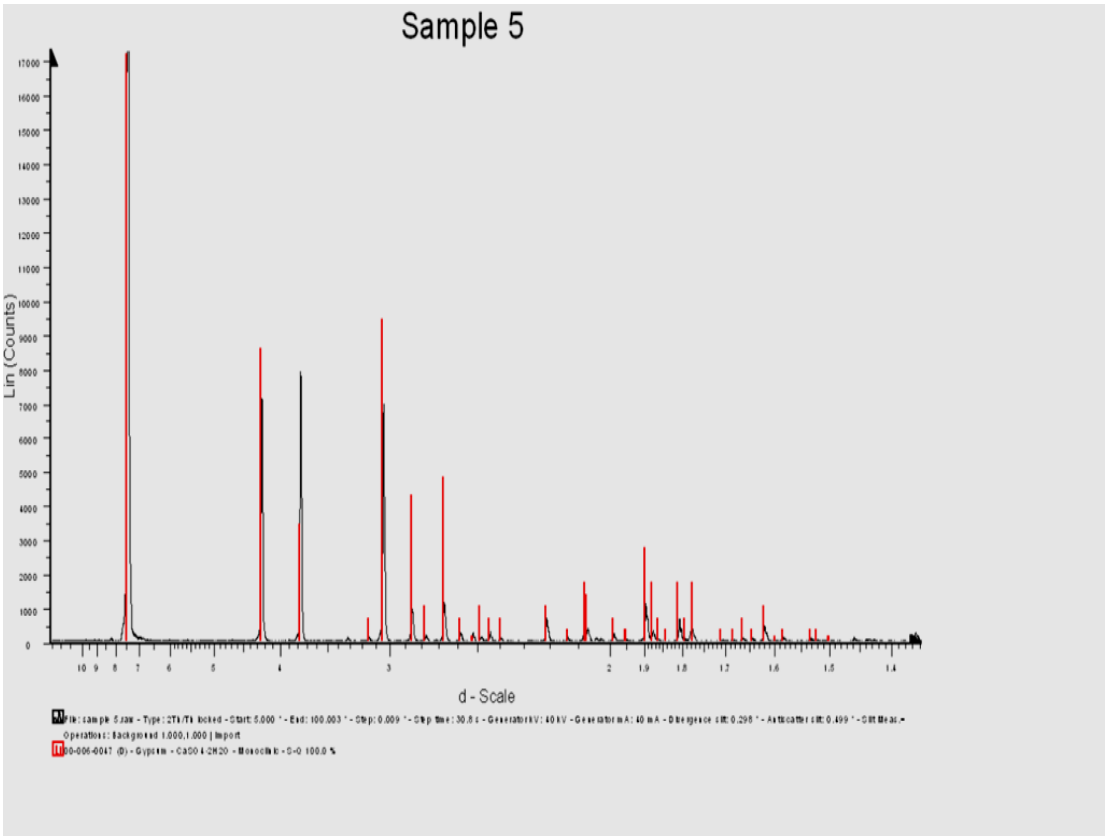

Fig. B.34: *XRD* analysis of white with clay/Bantycock gypsum rock sample.

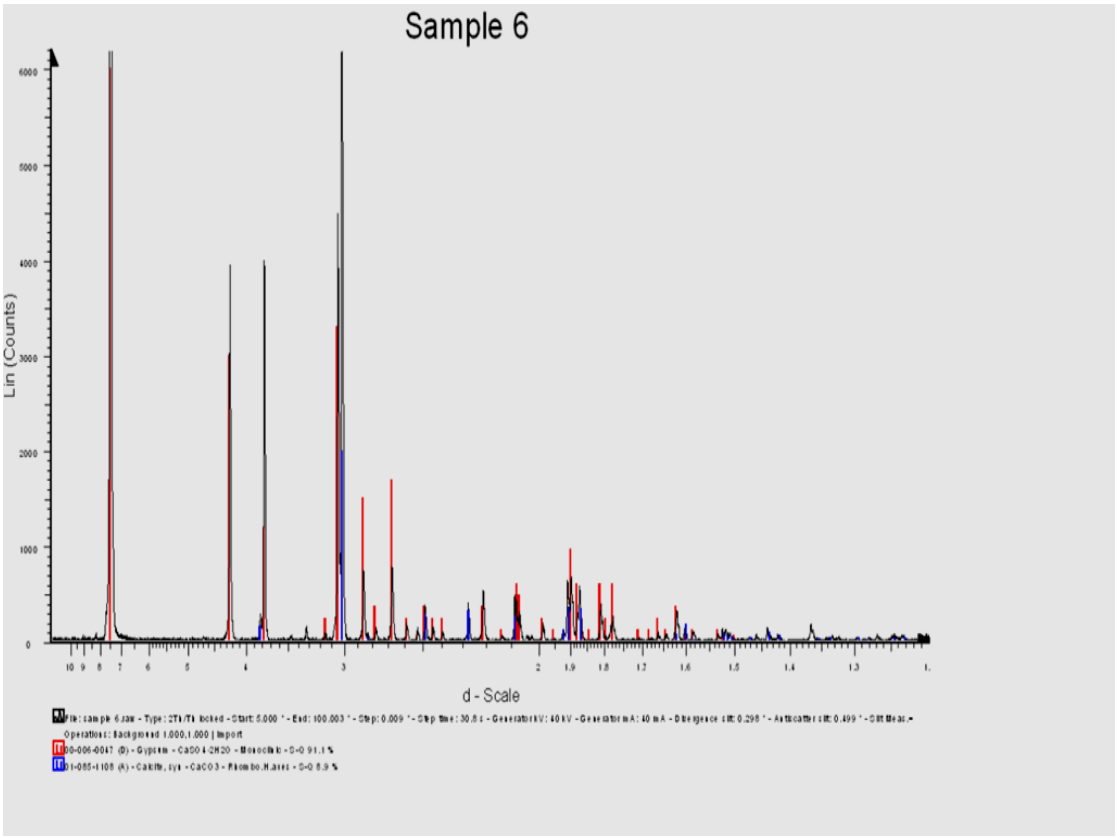

Fig. B.35: *XRD* analysis of Aust Cliff gypsum rock sample.

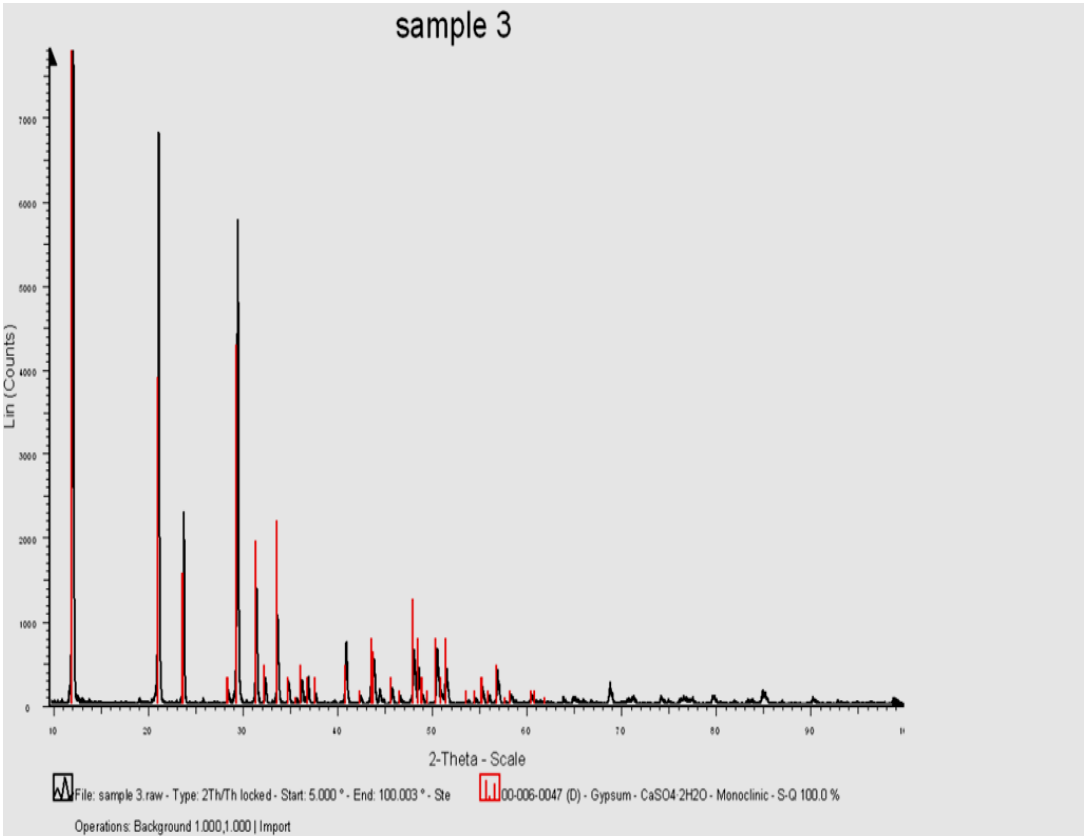

Fig. B.36: *XRD* analysis of Iraqi gypsum rock sample.

APPENDIX C: GYPSUM ROCK WORK (LONG TERM)

C.1 Thin Layers

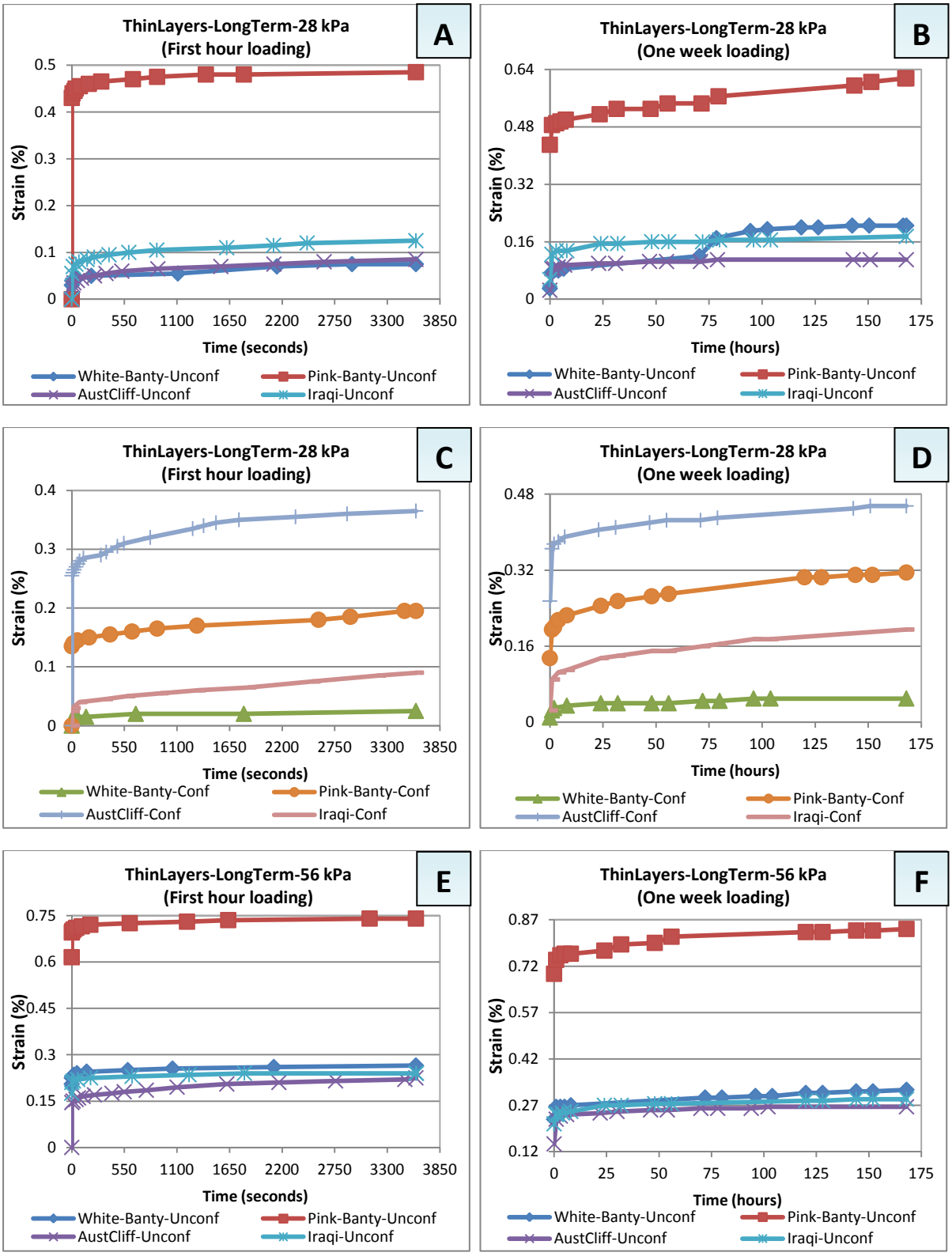

Fig. C.1: Present stages of loading of long-term tests of different gypsum thin layers. It shows first hour and one week creep results of 28 and 56 kPa loading stages for confined and unconfined samples.

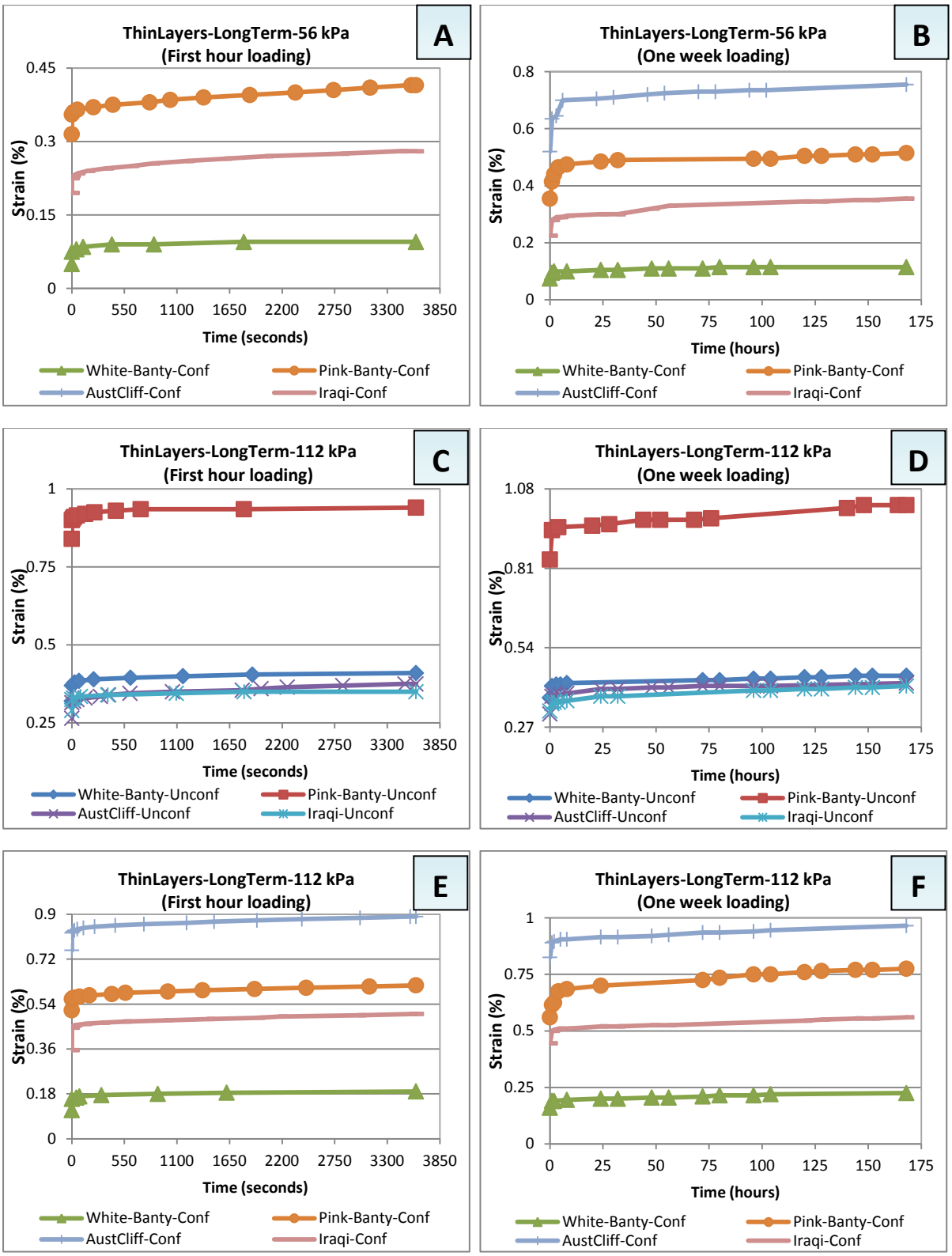

Fig. C.2: Present stages of loading of long-term tests of different gypsum thin layers. It shows first hour and one week creep results of 56 and 112 kPa loading stages for confined and unconfined samples.

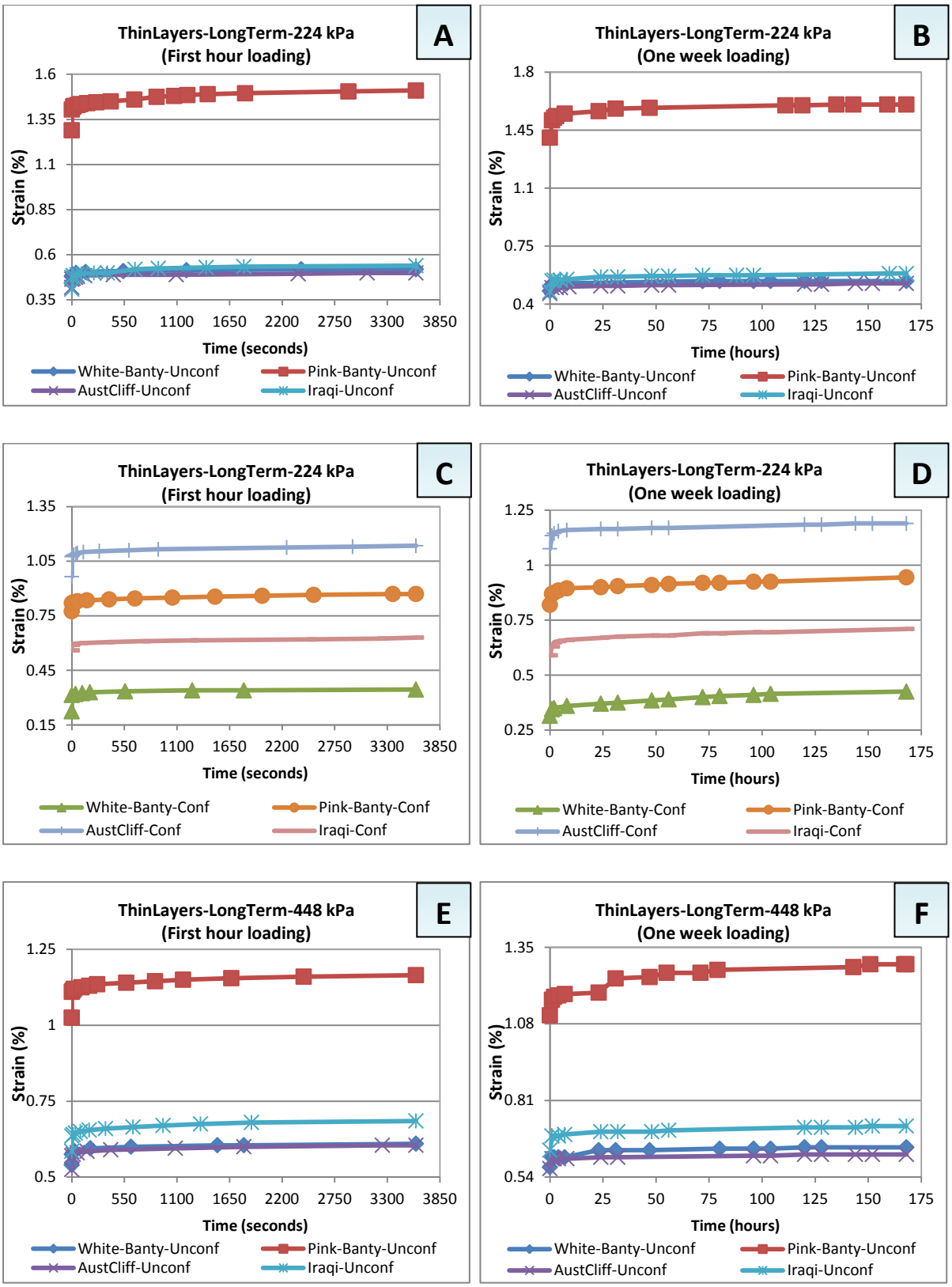

Fig. C.3: Present stages of loading of long-term tests of different gypsum thin layers. It shows first hour and one week creep results of 224 and 448 kPa loading stages for confined and unconfined samples.

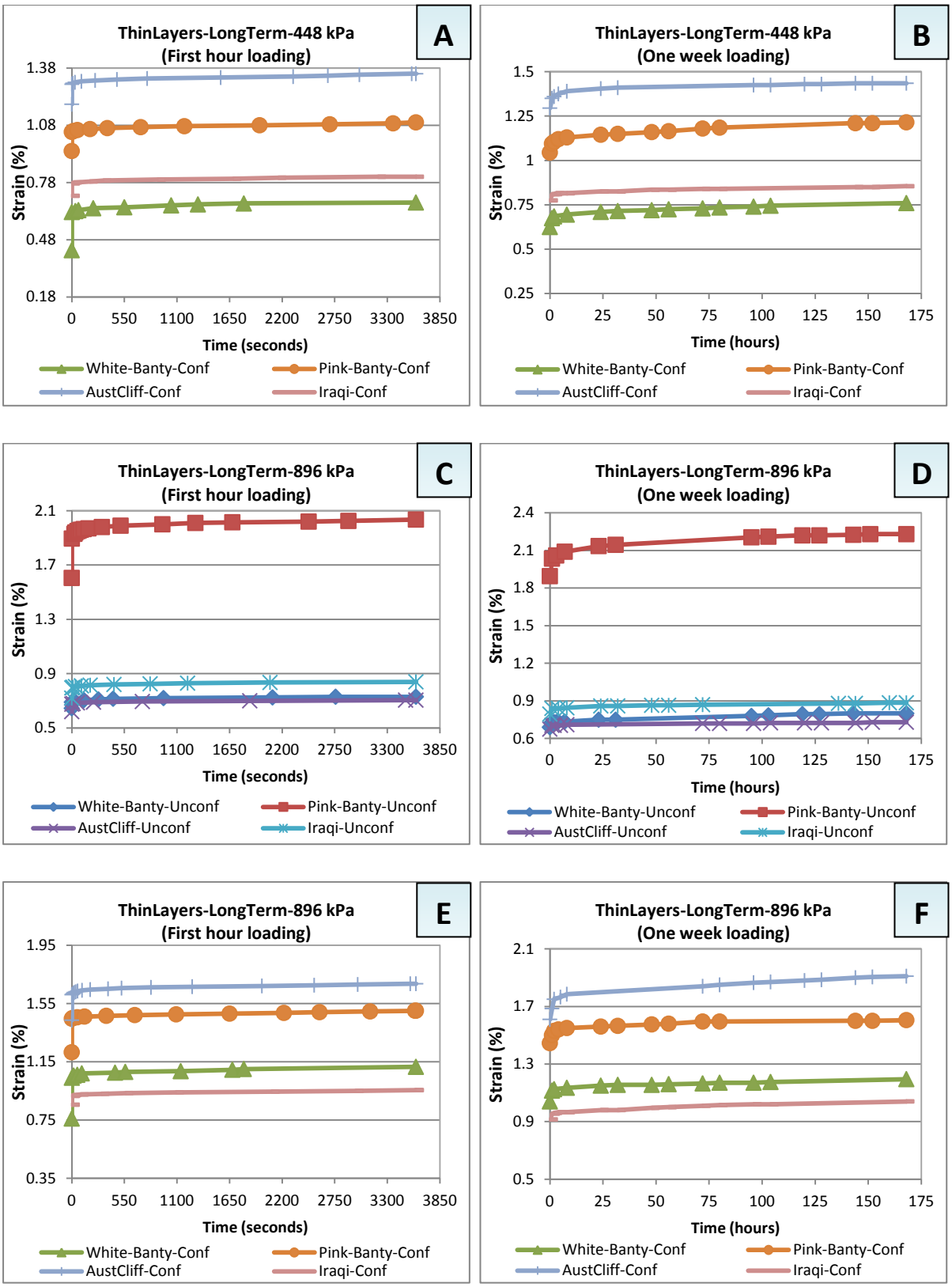

Fig. C.4: Present stages of loading of long-term tests of different gypsum thin layers. It shows first hour and one week creep results of 448 and 896 kPa loading stages for confined and unconfined samples.

C.2 Cylinders

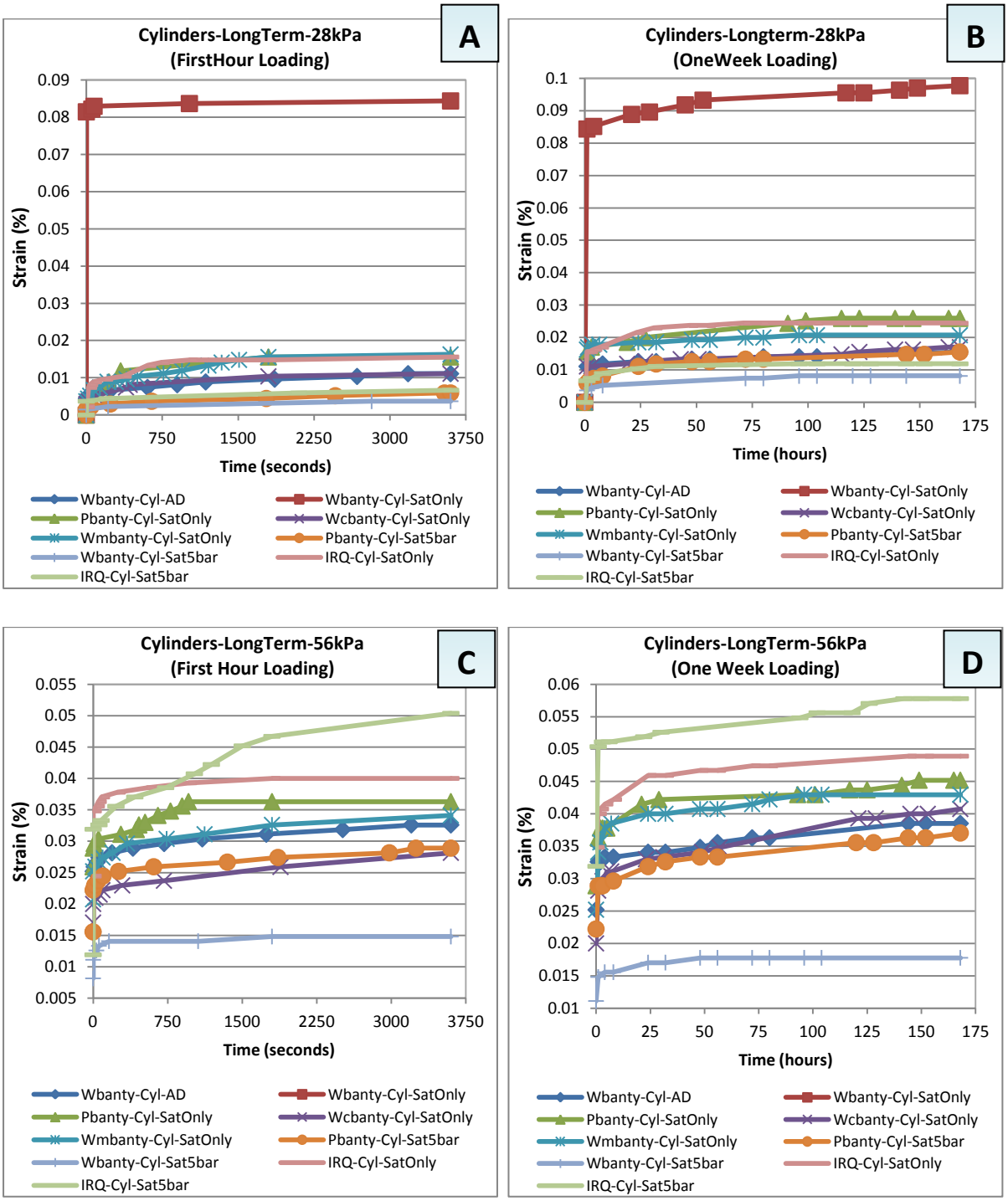

Fig. C.5: Present stages of loading of long-term tests of different gypsum cylinders. It shows first hour and one week creep results of 28 and 56 kPa loading stages.

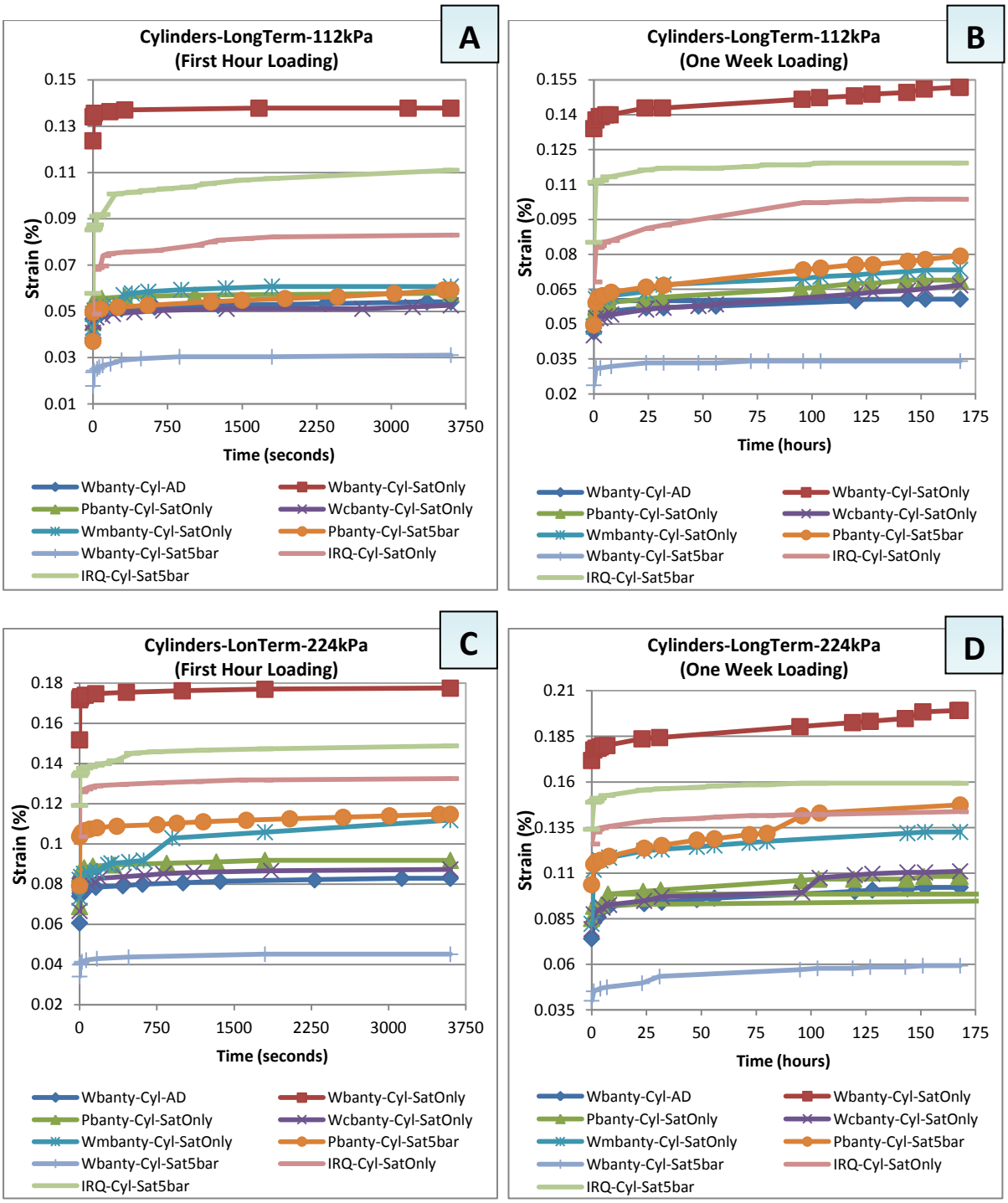

Fig. C.6: Present stages of loading of long-term tests of different gypsum cylinders. It shows first hour and one week creep results of 112 and 224 kPa loading stages.

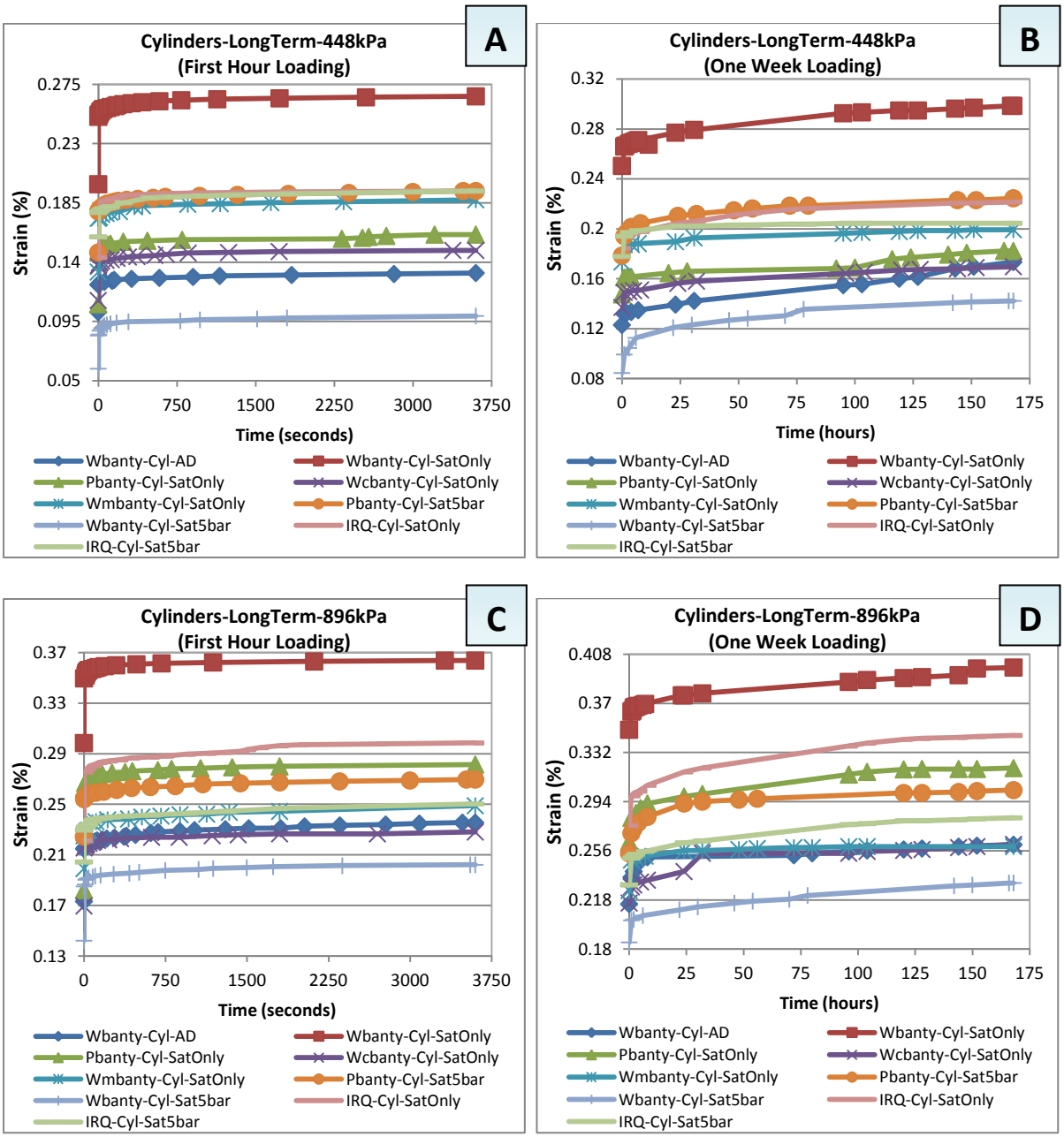

Fig. C.7: Present stages of loading of long-term tests of different gypsum cylinders. It shows first hour and one week creep results of 448 and 896 kPa loading stages.

APPENDIX D: GYPSEOUS SOIL WORK (SHORT-TERM)

Table D.1: Iraqi real gypseous soils chemical analysis/XRD (*Mg* = Magnesium, *Al* = Aluminium, *Si* = Silicon, *S* = Sulfur, Ca = Calcium, *pb* = Lead, O = Oxygen, K = Potassium, *Fe* = Iron, *Na* = Sodium, *Cl* = Chlorine, *Ba* = Barium and *Ti* = Titanium).

Chemical Analysis-Iraqi Gypseous Soils														
Sample Name	**Spectrum No.**	***Mg***	***Al***	***Si***	***S***	***Ca***	***Pb***	***O***	***K***	***Fe***	***Na***	***Cl***	***Ba***	***Ti***
Tar Al-Najaf	1	1.25	-	21.93	9.44	15.12	2.3	46.83	1.14	1.15	0.35	0.5	-	-
	2	0.97	1.25	21.44	9.53	14.96	2.2	47.15	0.59	1.11	0.39	0.43	-	-
	3	1.12	-	20.92	10.13	15.36	2.48	46.76	0.82	1.39	0.41	0.6	-	-
Badosh soil	1	2.39	-	12.89	1.9	40.13	-	36.6	1.18	3.85	-	-	1.06	-
	2	2.34	-	12.87	1.86	40.61	-	36.7	1.5	4.12	-	-	-	-
	3	2.6	-	13.49	1.78	39.76	-	37.04	1.19	4.14	-	-	-	-
Doz city	1	3.15	-	14.94	7.71	23.98	2.35	42.11	0.98	4.36	-	-	-	0.41
	2	2.9	-	14.02	8.85	24.82	-	42.82	1.24	5.34	-	-	-	-
	3	3.06	-	13.94	8.69	23.27	2.91	42.18	1.04	4.49	-	-	-	0.41

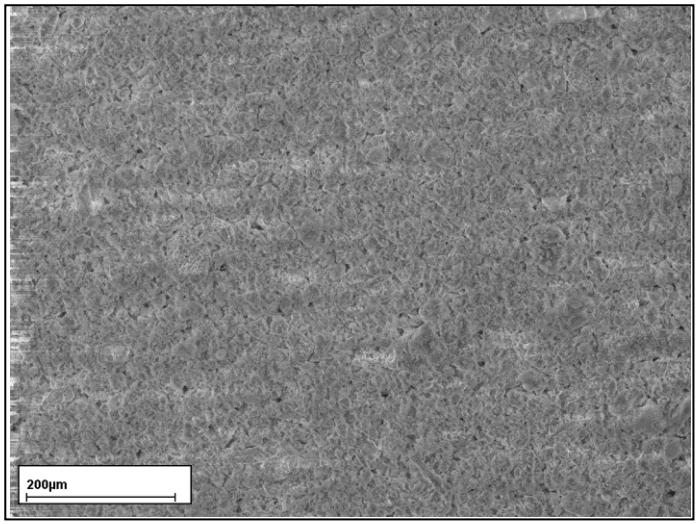

Fig. D.1: Badosh/Iraqi gypseous soil *SEM* photo.

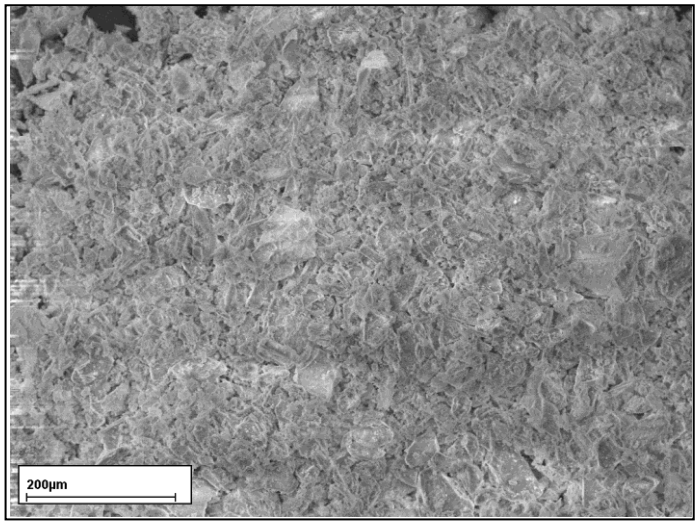

Fig. D.2: Tar Al-Najaf/Iraqi gypseous soil *SEM* photo.

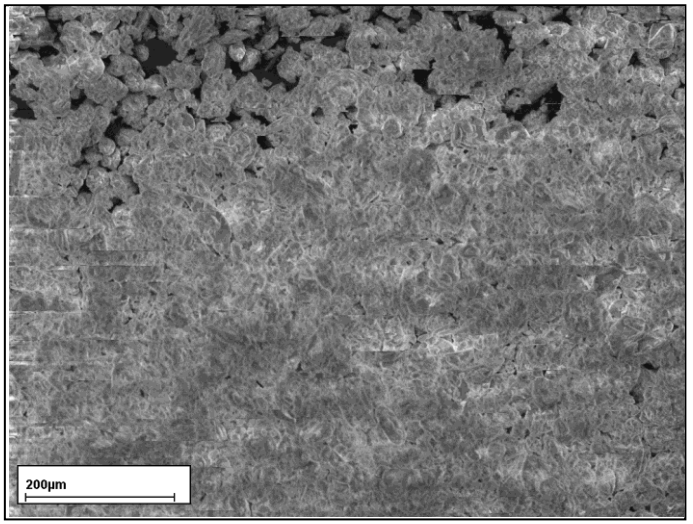

Fig. D.3: Doz/Iraqi gypseous soil *SEM* photo.

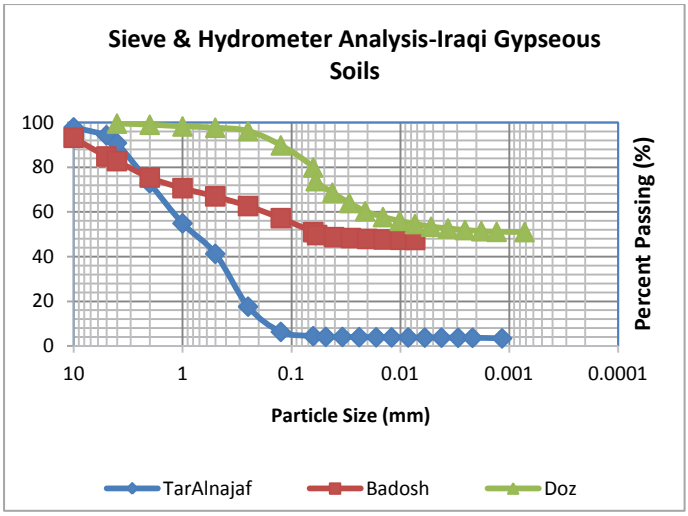

Fig. D.4: Sieve and Hydrometer Analysis (particle size distribution) for Iraqi real gypseous soils.

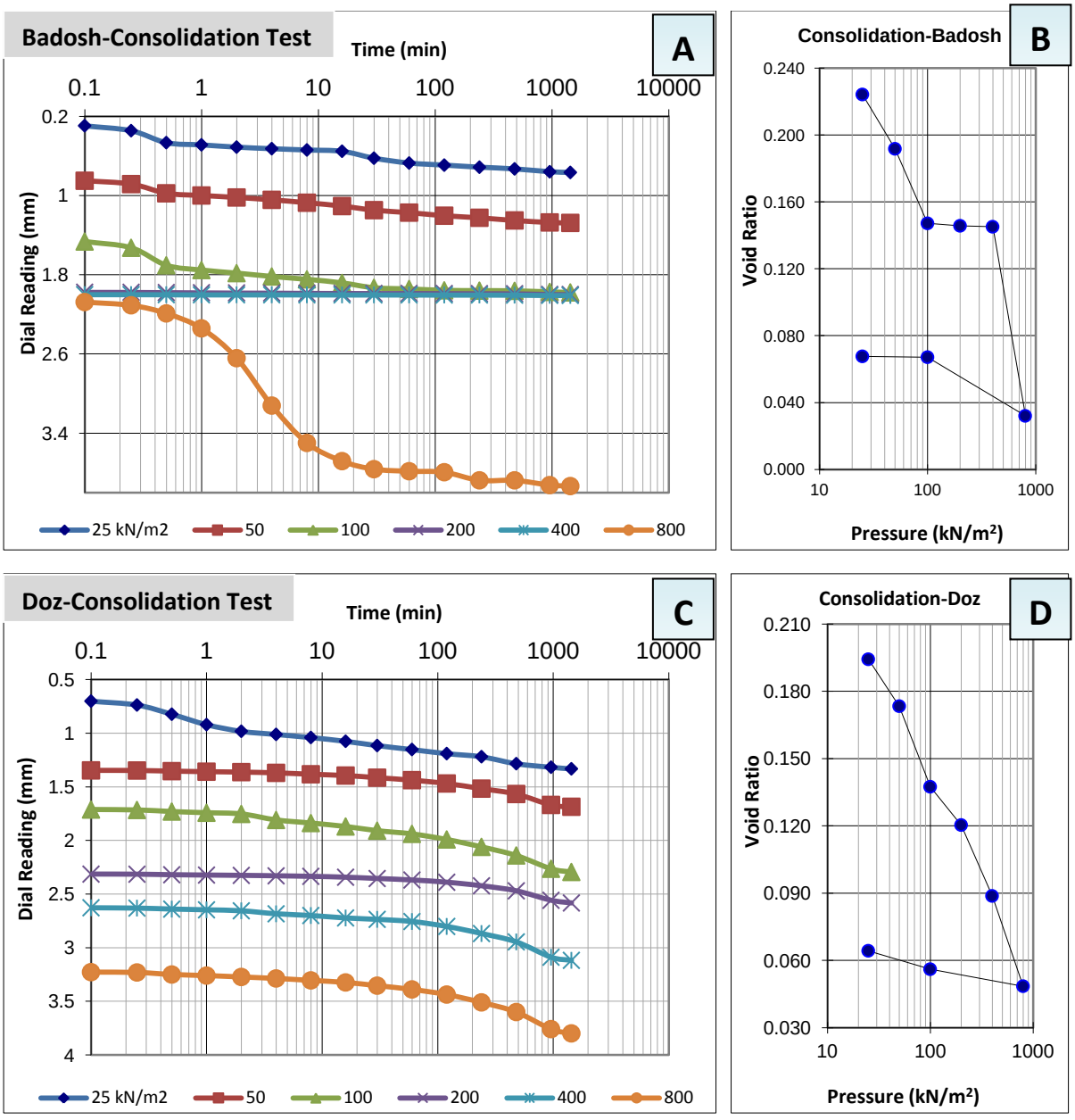

Fig. D.5: Parts A, B, C and D present consolidation test results for Badosh and Doz/Iraqi gypseous soils.

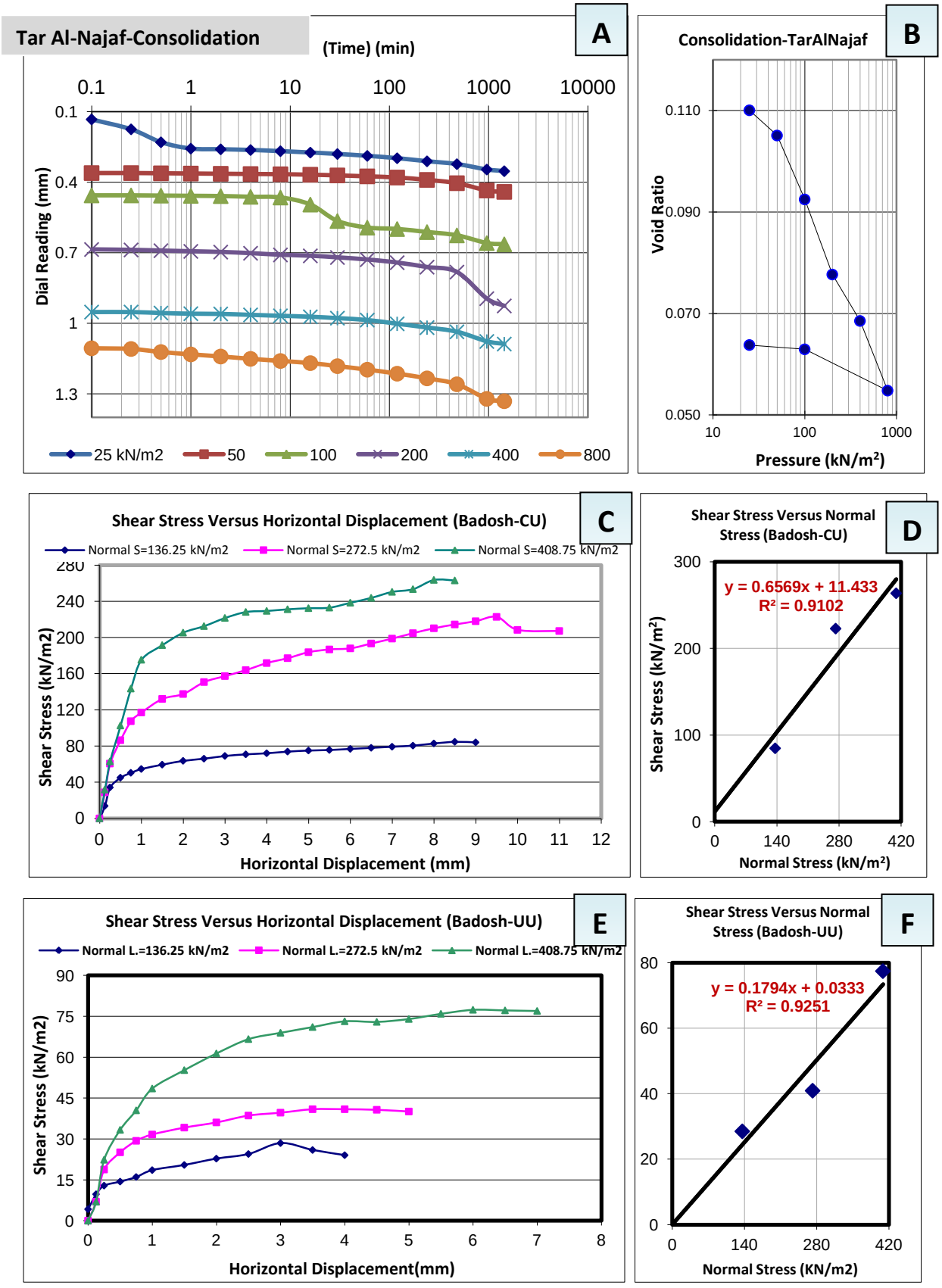

Fig. D.6: Parts A and B present consolidation test results for Tar Al-Najaf/Iraqi gypseous soils. Parts C and D present consolidated un-drained direct shear test. Parts E and F present unconsolidated un-drained direct shear test, all parts C, D, E & F for Badosh/Iraqi gypseous soil.

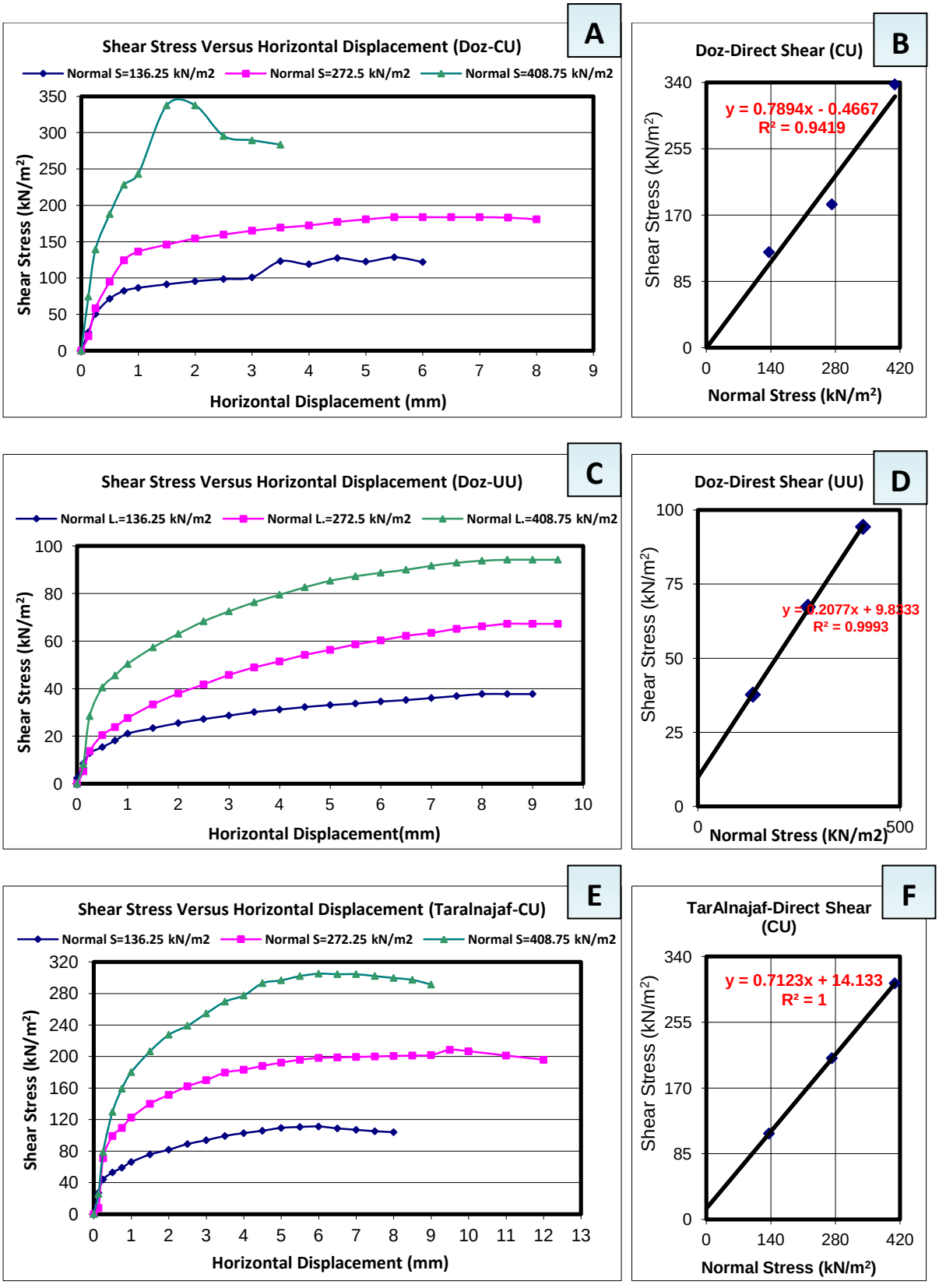

Fig. D.7: Part A and B present consolidated un-drained direct shear tests results for Doz/Iraqi gypseous soils. Part C and D present unconsolidated un-drained direct shear tests results for Doz sample. Part E and F present unconsolidated un-drained direct shear test for Tar Al Najaf/Iraqi gypseous soil.

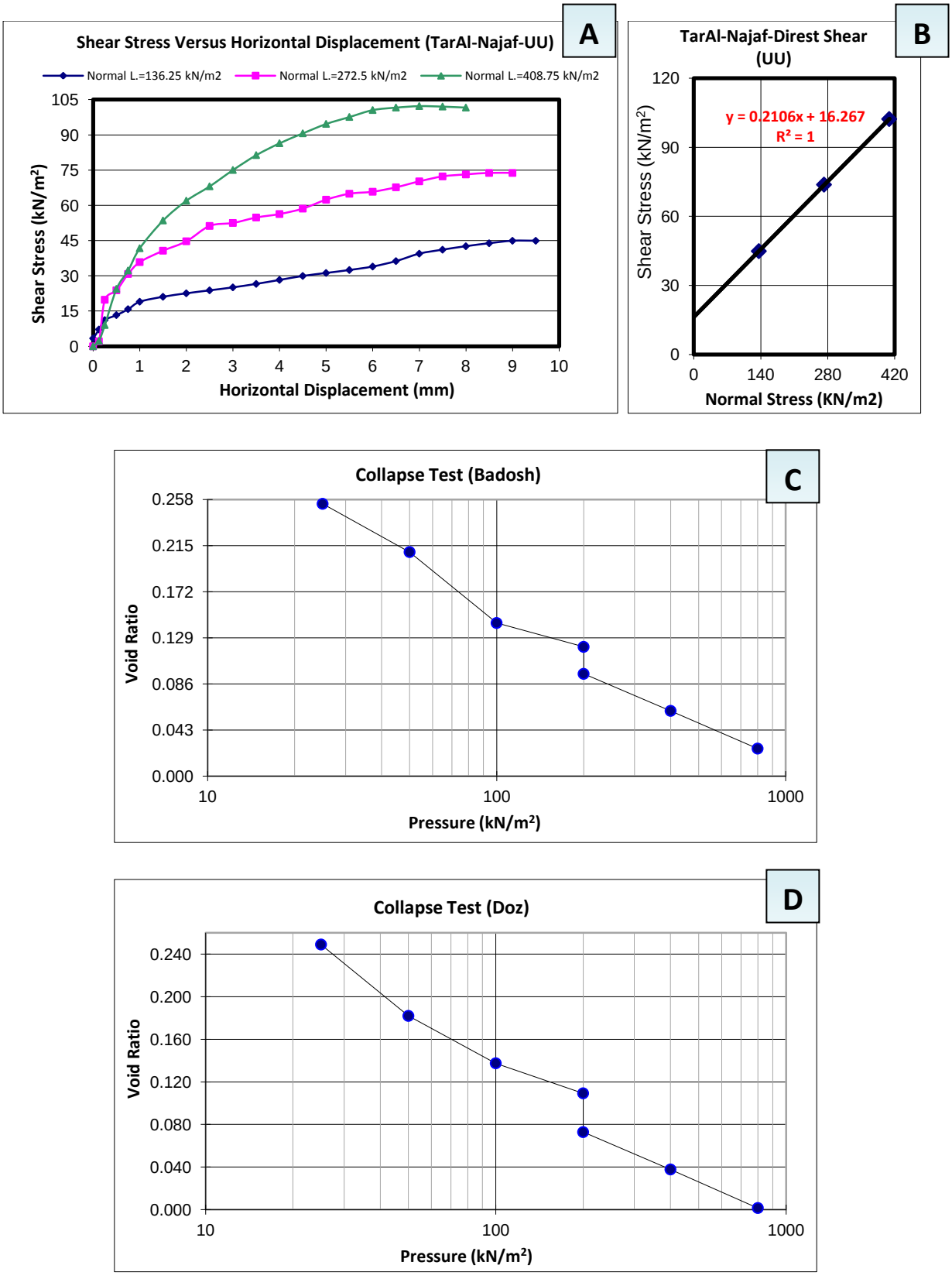

Fig. D.8: Part A and B present unconsolidated un-drained direct shear tests results for Tar Al-Najaf/Iraqi gypseous soil. Part C presents Badosh/Iraqi gypseous soil collapse test result. Part D presents Doz/Iraqi gypseous soil collapse test result.

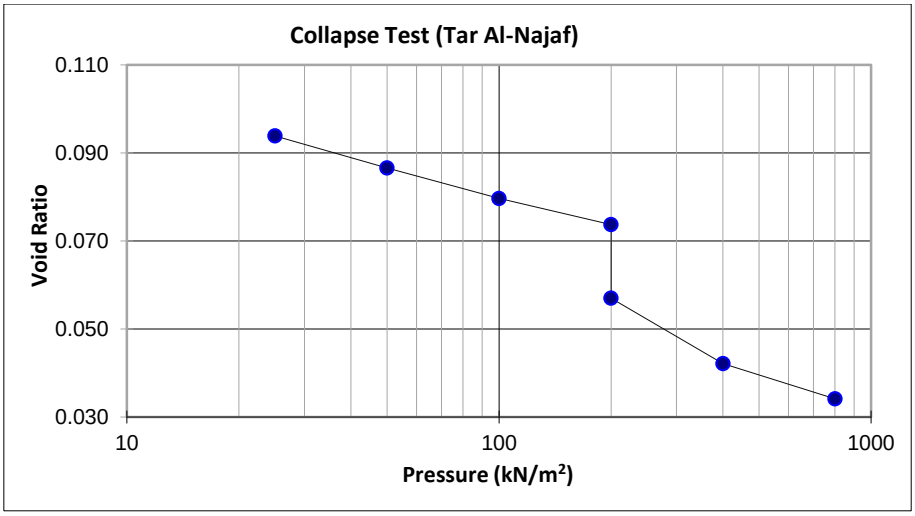

Fig. D.9: Presents Tar Al-Najaf/Iraqi gypseous soil collapse test result.

APPENDIX E: BOX MODEL

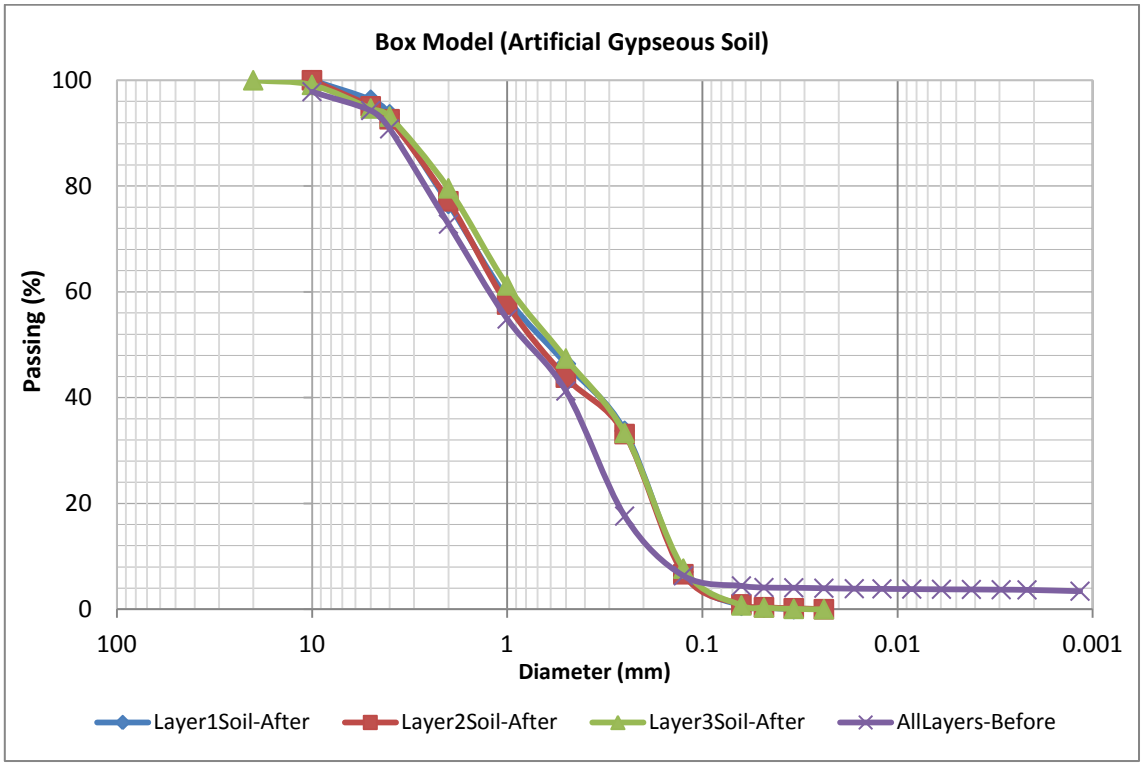

Fig. E.1: Presents sieve and hydrometer analysis for box model soil before and after 50 week of water flooding.

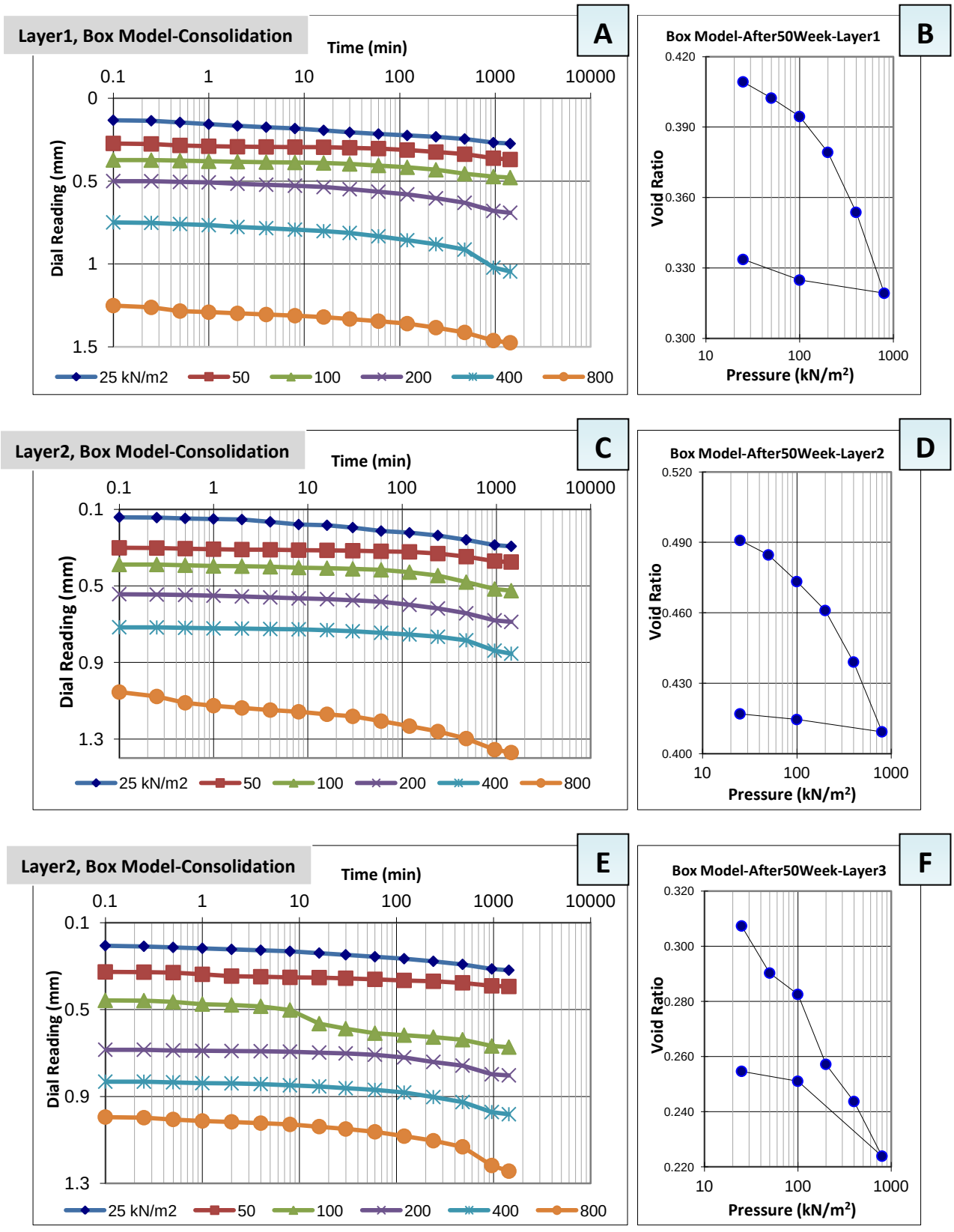

Fig. E.2: Presents consolidation tests results for box model soil after 50 week of saturation. Part A and B for layer 1, part C and D for layer 2 and part E and F for layer 3.

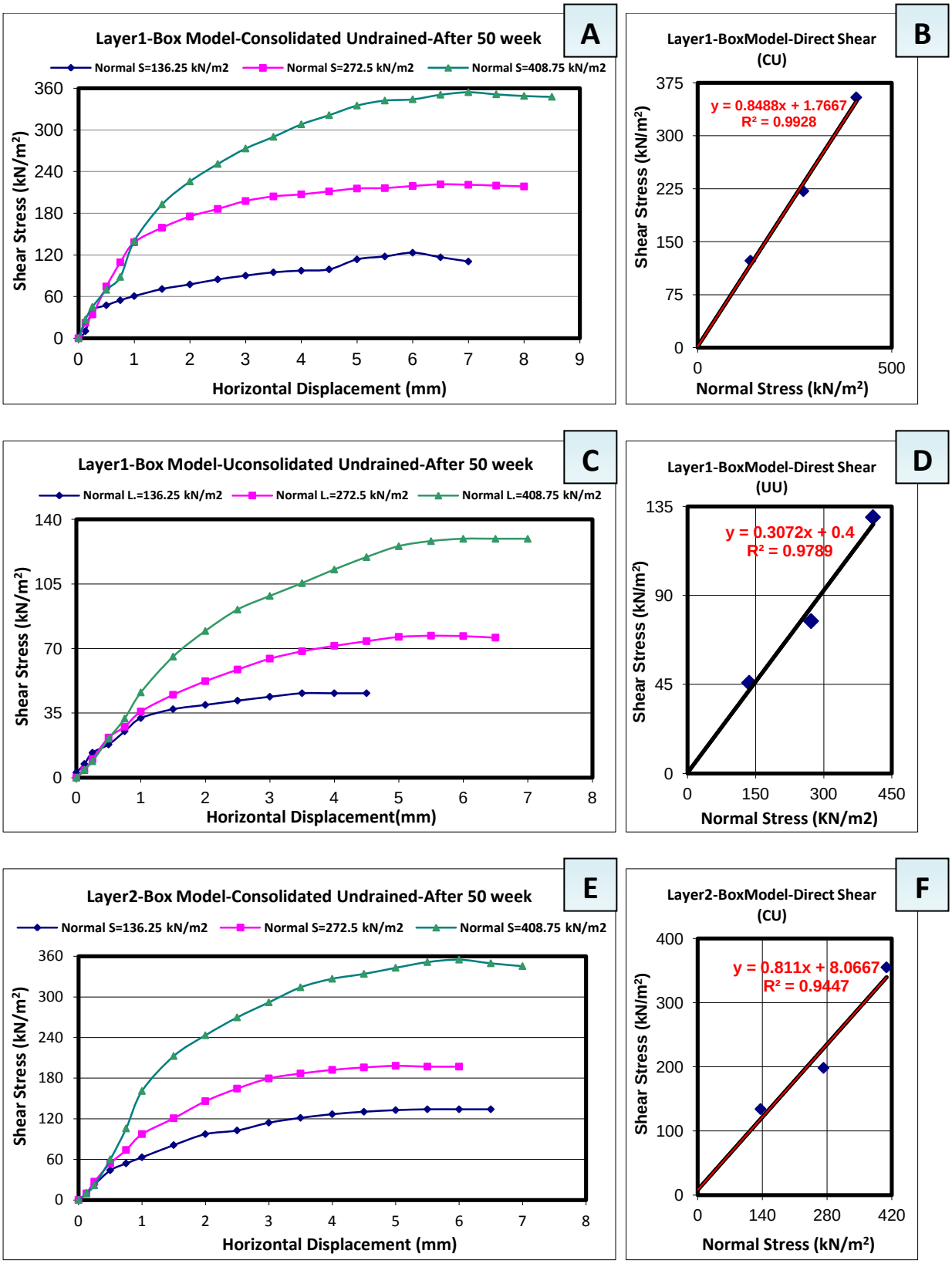

Fig. E.3: Presents direct shear tests results for box model soil after 50 week of saturation. Part A and B for layer 1/consolidated un-drained, part C and D for layer 1/unconsolidated un-drained (UU) and part E and F for layer 2/consolidated un-drained (CU).

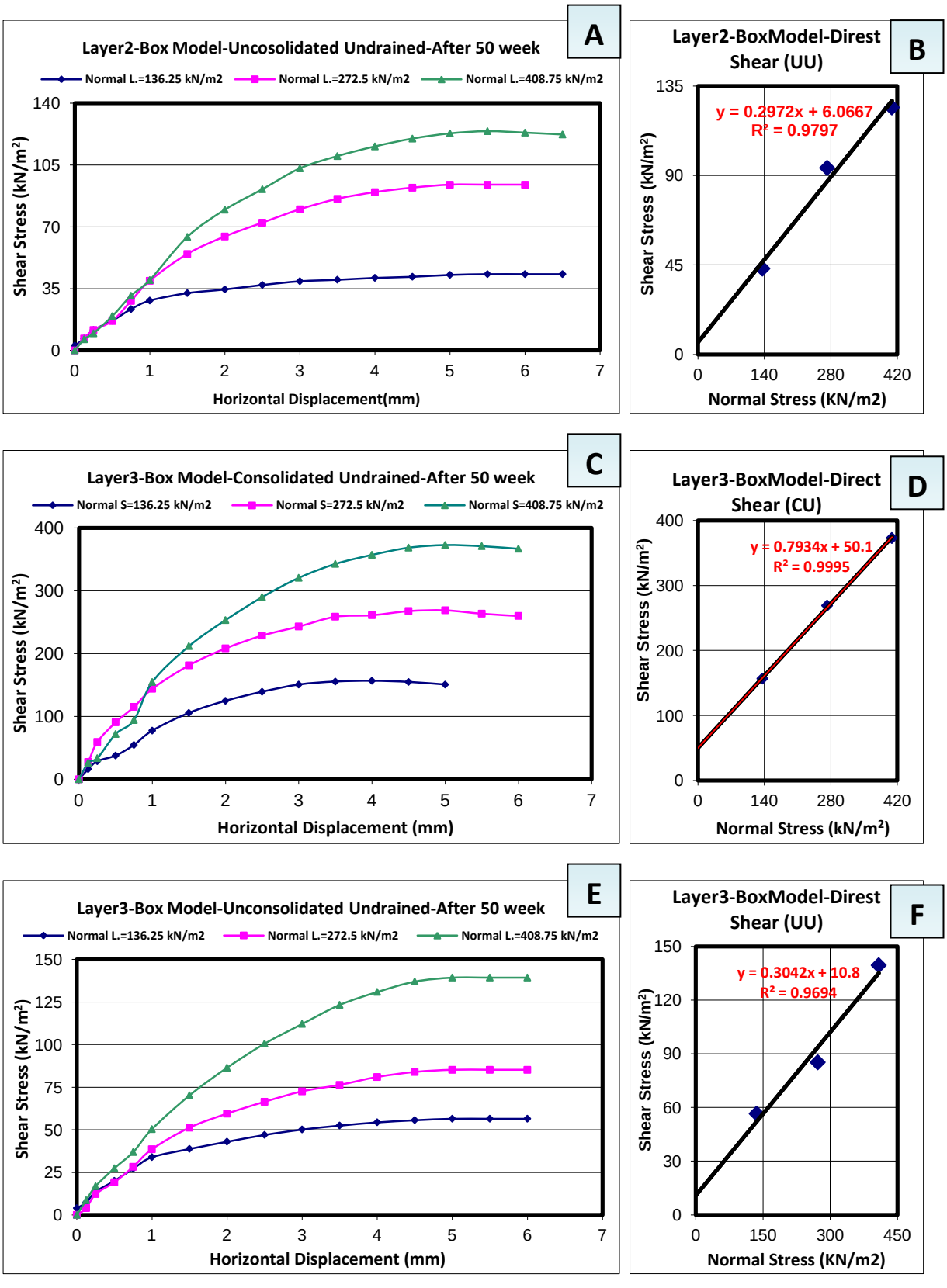

Fig. E.4: Presents direct shear tests results for box model soil after 50 week of saturation. Part A and B for layer 2/unconsolidated un-drained, part C and D for layer 3/consolidated un-drained and part E and F for layer 3/unconsolidated un-drained.

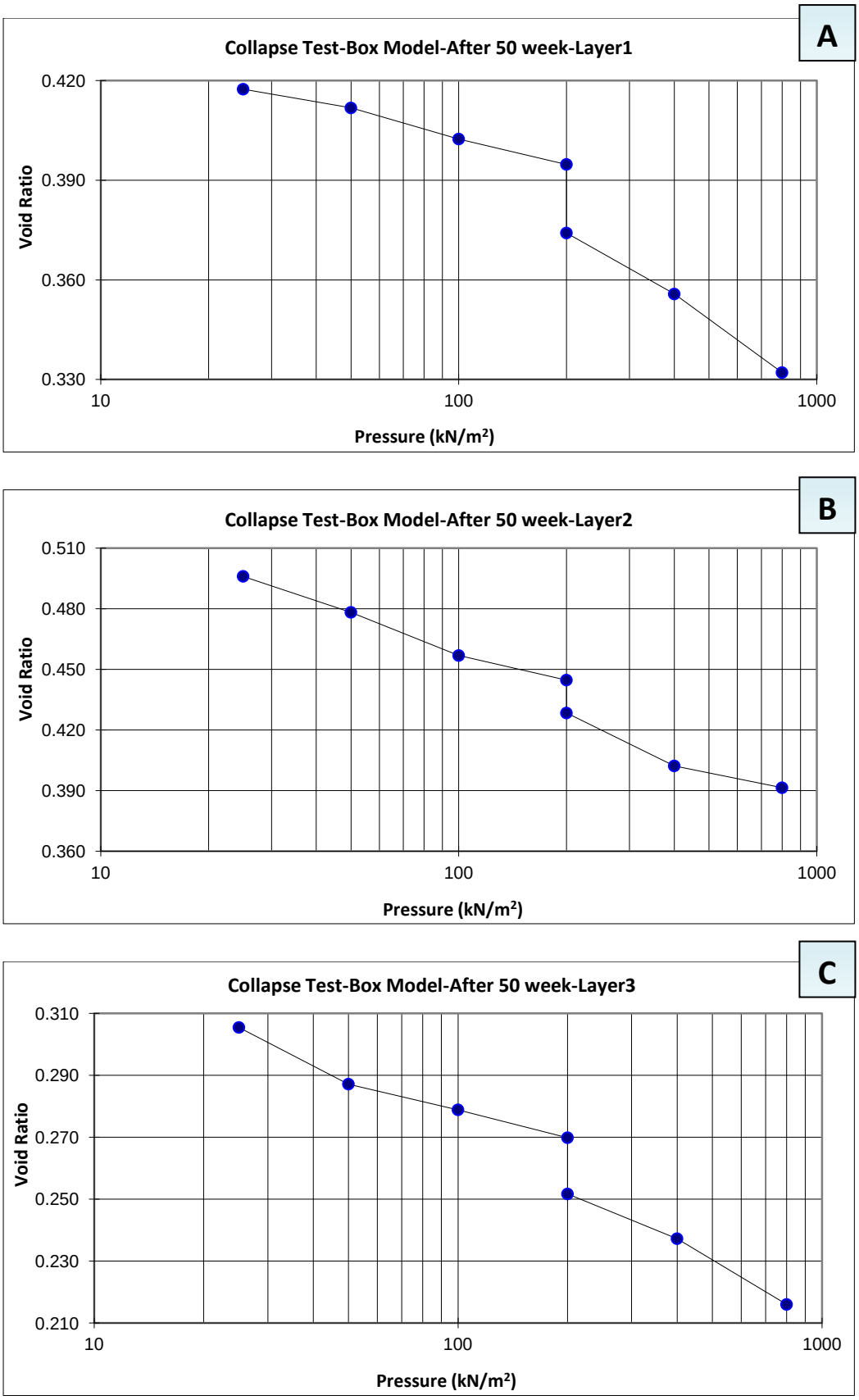

Fig. E.5: Presents collapse tests results for box model soil after 50 week saturation. Part A for layer 1, part B for layer 2 and part C for layer 3.